AGARD-CP-443

AGARD-CP-443

AGARD

ADVISORY GROUP FOR AEROSPACE RESEARCH & DEVELOPMENT

7 RUE ANCELLE 92200 NEUILLY SUR SEINE FRANCE

AGARD CONFERENCE PROCEEDINGS No.443

Energy Absorption of Aircraft Structures as an Aspect of Crashworthiness

NORTH ATLANTIC TREATY ORGANIZATION

DISTRIBUTION AND AVAILABILITY ON BACK COVER

COMPONENT PART NOTICE (CON'T)

AD#: TITLE:

AGARD-CP-443

NORTH ATLANTIC TREATY ORGANIZATION

ADVISORY GROUP FOR AEROSPACE RESEARCH AND DEVELOPMENT

(ORGANISATION DU TRAITE DE L'ATLANTIQUE NORD)

AGARD Conference Proceedings No.443

ENERGY ABSORPTION OF AIRCRAFT STRUCTURES AS AN ASPECT OF CRASHWORTHINESS

Papers presented at the 66th Meeting of the Structures and Materials Panel of AGARD
held in Luxembourg, 1—6 May 1988.

THE MISSION OF AGARD

According to its Charter, the mission of AGARD is to bring together the leading personalities of the NATO nations in the fields of science and technology relating to aerospace for the following purposes:

- Recommending effective ways for the member nations to use their research and development capabilities for the common benefit of the NATO community;
- Providing scientific and technical advice and assistance to the Military Committee in the field of aerospace research and development (with particular regard to its military application);
- Continuously stimulating advances in the aerospace sciences relevant to strengthening the common defence posture;
- Improving the co-operation among member nations in aerospace research and development;
- Exchange of scientific and technical information;
- Providing assistance to member nations for the purpose of increasing their scientific and technical potential;
- Rendering scientific and technical assistance, as requested, to other NATO bodies and to member nations in connection with research and development problems in the aerospace field.

The highest authority within AGARD is the National Delegates Board consisting of officially appointed senior representatives from each member nation. The mission of AGARD is carried out through the Panels which are composed of experts appointed by the National Delegates, the Consultant and Exchange Programme and the Aerospace Applications Studies Programme. The results of AGARD work are reported to the member nations and the NATO Authorities through the AGARD series of publications of which this is one.

Participation in AGARD activities is by invitation only and is normally limited to citizens of the NATO nations.

Published December 1988

ISBN 92-835-0485-2

Printed by Specialised Printing Services Limited
40 Chigwell Lane, Loughton, Essex IG10 3TZ

PREFACE

Considerable effort has hitherto been devoted to crash avoidance, but relatively little to crash survivability. In certain regimes the risk of accident remains high, e.g. the low-altitude low-speed regime. There is a strong incentive to increase the prospects for occupant survival through improvements in airframe design. Information about structural behaviour and characteristics under these conditions is very sparse and an exchange of information between the NATO nations is long overdue.

To facilitate an exchange of experience and development results, the AGARD Structures and Materials Panel sponsored a Specialists' Meeting in the Spring of 1988 in Luxembourg. The Meeting included five sessions:

Session I: Accident Scenarios and Crash Safety Requirements.
Chairman: Dr W.Elber, NASA, Hampton, US

Session II: Crashworthy Design Procedures and Limitations.
Chairman: R.Labourdette, ONERA, Châtillon, France

Session III: Materials and Structures Testing and Evaluation Related to Crashworthiness.
Chairman: Professor W.G.Heath, BAe, Manchester, UK

Session IV: Analytical Modelling and Crash Response Prediction.
Dipl-Ing. Ch.Kindervater, DFVLR, Stuttgart, Germany

Session V: Interaction Structure-Seat-Occupant.
Chairman: C.L.Petrin Jr, ASD/ENFS, Dayton, US

On behalf of the Structures and Materials Panel, I would like to express my thanks to all authors and session chairmen for their outstanding contributions which were instrumental in making this meeting such a success.

G.Grüninger
Chairman, Sub-Committee on
Aircraft Structural Crashworthiness

STRUCTURES AND MATERIALS PANEL

SUB-COMMITTEE MEMBERS

PANEL EXECUTIVE

ABSTRACT

Considerable effort has hitherto been devoted to crash avoidance, but relatively little to crash survivability. In certain regimes the risk of accident remains high, e.g. the low-altitude low-speed regime. There is a strong incentive to increase the prospects for occupant survival through improvements in airframe design. Information about structural behaviour and characteristics under these conditions is very sparse and an exchange of information between the NATO nations is long overdue.

At its sixty-sixth meeting, the Structures and Materials Panel held a conference of Specialists, the aim of which was to simulate an exchange of experience and development results. A further aim was to act as a focus for the discussion of those novel design philosophies which may be needed to provide the balance between survivability and function. This document contains the papers presented at that Meeting.

* * *

Jusqu'ici des efforts considérables ont été consacré à l'étude du problème de l'évitement de l'écrasement mais il existe relativement peu d'informations sur la survivabilité en cas d'impact. Le risque d'accident reste toujours élevé en certains régimes de vol et dans certains configurations, par exemple le vol à basse altitude et à vitesse reduite, on remarque une tendance très nette vers une accroissement des chances de survie de l'équipage grâce à des perfectionnements apportés à la construction des cellules d'avion. Il existe très peu d'informations concernant le comportement et la modification des caracteristiques structurales des cellules d'avion en cas d'écrasement, et le besoin d'une échange de vue à ce sujet entre les nations membres de l'OTAN se fait sentir depuis longtemps.

A l'occasion de sa soixante sixième réunion, le Panel AGARD des Structures et Matériaux a organisé une conférence de spécialistes, afin d'encourager une echange de vues et une mise en commun des résultats des différents travaux de developpement en cours. La conférence a également servi de forum en ce qui concerne les nouvelles stratégies de conception qui pourraient s'avérer nécessaires pour asurer l'équilibre entre les aspects de survivabilité et les aspects fonctionnels.

Le présent document regroupe toutes les communications présentées lors de cette conference.

CONTENTS

*Not available at time of printing.

*Not available at time of printing.

ASPECT REGLEMENTAIRE DU CRASHWORTHINESS

par

P.J.Rabourdin
Ingénieur à la Direction des Constructions Aeronautiques
Paris, France

En ce début de réflexion sur les capacités des structures à participer au traitement du problème du crash, je voudrais brièvement rappeler le contexte général technique et réglementaire dans lequel évolue la navigabilité des aéronefs sur cet aspect particulier de la sécurité.

D'abord quelques précisions sur les limites de cet exposé :

Trois questions peuvent être posées en préliminaire :

- pourquoi le crash ?

- pourquoi nous limiterons-nous aux avions de transport ?

- pourquoi réglemente-t-on cet aspect de la navigabilité ?

. Pourquoi le crash ? Tout simplement parce que depuis et pour longtemps le retour d'une machine volante vers le sol peut revêtir un caractère brutal et dramatique pour de multiples raisons dont la planche 1 donne une illustration.

Au passage, je rappelle qu'une cause non explicitée ici est la combinaison de l'imprudence de l'homme et de la défaillance de la machine volante, tel cet exemple illustre d'Icare voulant s'échapper du labyrinthe par la voie des airs et qui se termina par la mort du premier homme-oiseau à la suite de la désintégration de sa voilure assemblée à la cire dont l'ardeur du soleil eut raison.

. Pourquoi nous limiterons-nous aux avions de transport ? pour plusieurs raisons :

- d'abord il faut limiter le sujet compte tenu du temps imparti,

- ensuite l'avion de transport ayant pour mission d'emporter une charge payante vers une destination connue, c'est sa mission même qui est mise en question, si un crash survient, mettant en cause l'intégrité de sa charge,

- par ailleurs, la notion de sécurité est à l'évidence beaucoup plus développée dans cette catégorie de transport, et le crash est l'une des situations d'urgence pour laquelle, comme nous allons le voir, des précautions et des règlements existent,

- enfin la longue expérience acquise en service, basée malheureusement sur de trop nombreux cas de crash (estimés à 583 dans une période prise comme exemple : 1959 à 1979) permet de faire divers commentaires sur les différents aspects du crash.

Pourquoi réglemente-t-on cet aspect de la navigabilité ? Rappelons que ce n'est pas en additionnant des règlements que l'on construit et fait voler des avions, mais qu'il revient aux Autorités de Navigabilité de tous pays, en concertation ou non, de définir le niveau minimal de sécurité d'un tel moyen de transport afin qu'en aval, les populations survolées soient protégées et que les usagers puissent intégrer ce facteur de sécurité dans la gamme de ceux qui leur permettent de retenir ou de refuser ce mode de transport.

Généralement basé sur un objectif à tenir, le règlement évolue pour tenir compte des carences découvertes en service, ou de l'évolution des techniques et des conditions d'utilisation du produit ; le but reste, en Europe du moins, d'évaluer le niveau d'exigence à requérir techniquement et économiquement, en face de toutes nouvelles hypothèses techniques et opérationnelles.

C'est ainsi que nous allons successivement voir comment les règlements ont jusqu'ici évolué, et ce qu'il est souhaitable d'entreprendre pour que cette situation d'urgence qu'est le crash, soit de plus en plus souvent survivable, admettant que le but ultime est de protéger les passagers, que la machine soit détruite ou non ; nous verrons au passage, sur la base d'exemples, les corrélations entre les règlements et l'expérience, ainsi que les conséquences sur les machines des exigences réglementaires ; nous ne parlerons pas ici des conditions d'amerrissage d'urgence, considérant qu'il s'agit là d'un autre sujet par ailleurs tout aussi digne de retenir votre attention.

Rappel sur l'évolution passée des règlements :

Le règlement CAR 4b, qui est à l'origine des règlements actuels, établit les exigences en condition d'atterrissage d'urgence pour lesquelles la sécurité des passagers doit être assurée : § 4b.260. Il s'agit d'un crash mineur au cours duquel, si les équipements utilisés par les passagers (sièges, ceintures, etc,...) le sont correctement, il doit y avoir une probabilité raisonnable d'éviter les blessures graves, quand l'avion se pose train haut (s'il est équipé d'un train rétractable), et les structures entourant les passagers, à savoir les sièges, soumises aux forces d'inertie extrêmes suivantes, exprimées en accélération :

- "upward" : 2 g,
- "forward" : 9 g,
- "sideward" : 1,5 g,
- "downward" : 4,5 g.

Il était acceptable d'utiliser une valeur, en "downward", plus faible, si le constructeur montrait que la structure de l'avion pouvait absorber des charges à l'atterrissage résultant d'un impact à une vitesse de descente extrême Vz max de 5 ft/sec, à la masse de calcul à l'atterrissage, et sans dépasser la valeur d'inertie "downward" choisie (au niveau des sièges).

Naturellement toutes les masses, i.e. meubles, racks à bagages, équipements de sécurité divers, etc,..., dont la projection est susceptible de blesser les passagers ou l'équipage, doivent répondre aux mêmes facteurs d'accélération, quant à leur liaison avec la structure de l'avion.

Outre ce § 4b.260, existaient des § s'y rapportant directement :

- 4b.358 (a) (justification des sièges et des ceintures),

- 4b.359 (c) (protection des passagers vis-à-vis du chargement des soutes et compartiments à bagages),

- 4b.420 (e) (à partir de l'amendement 12) (protection des réservoirs de fuselage : inertie et frottement),

- 4b.643 (points d'accrochage des ceintures),

ou d'autres comme le 4b.356 traitant des conséquences du crash mineur sur les portes, mais sans précisions sur les facteurs d'accélération à prendre en compte.

C'est sur ces bases qu'ont été certifiés en France des avions du type MYSTERE 20 et CARAVELLE dans les années 1958 à 1965.

L'expérience en service a démontré la bonne adaptation de ces avions aux exigences réglementaires, comme le prouvent les exemples suivants empruntés à l'histoire de CARAVELLE (voir planche 2) ; ceci peut être complété par les exemples tirés du document britannique "World Airline Accident" publié par la CAA(voir planche 3), pour la même période, et pour d'autres avions.

Les nouvelles rédactions de ces exigences, apparues dans la première édition de la FAR 25 en 1965 (règlement américain publié par la FAA) n'ont pas modifié l'objectif poursuivi (crash mineur, pas de blessures graves, réduction du risque de feu) ni modifié la valeur des facteurs d'accélération.

Il faut attendre 1970, époque des grands programmes développés en France (CONCORDE, AIRBUS, MERCURE) et aux Etats-Unis (BOEING 747, DC 10) pour voir apparaître d'une part l'amendement 23 à la FAR 25 ajoutant au § 25.561 b3 la notion de l'action séparée des facteurs d'accélération, et d'autre part la condition spéciale française CC 12 applicable aux programmes AIRBUS et MERCURE, introduisant un facteur de 1,5 g vers l'arrière, élevant le facteur latéral de 1,5 à 2,25 g et envisageant toutes les combinaisons de facteurs dans la limite d'une résultante inférieure ou égale à 9 g ; par ailleurs, dans cette condition, était ajoutée une exigence relative à la projection vers l'avant des moteurs et de l'APU (fixations justifiées à 12 g vers l'avant) pour éviter de blesser les

passagers et l'équipage, une exigence relative aux conditions et aux conséquences de la rupture du train d'atterrissage (si sorti) en cas d'atterrissage dur à Vz > 12 ft/sec vis-à-vis des réservoirs de carburant, enfin l'application des nouveaux facteurs d'accélération aux pieds des sièges et à leurs liaisons avec la structure du plancher.

Depuis 1970, la FAR 25 n'a que peu évolué : introduction en 1972 du § 25.789 (fixation de toutes masses en poste, cabine et galley), tandis que le règlement européen JAR 25 apparaissait en 1974 ; celui-ci a modifié profondément les exigences applicables et fourni aux constructeurs des données sur les moyens de conformité acceptables. C'est ainsi que la comparaison des § FAR 25.561 et JAR 25.561 montre les additions suivantes apportées par le JAR, illustrées en partie par la planche 4 :

- les facteurs d'accélération/décélération sont rapportés à l'avion et non pas, comme pour la FAR, à la structure environnant le passager, c'est-à-dire le siège,

- un facteur de 1,5 g est introduit en "rearward",

- la combinaison des facteurs avec une valeur maximale de 9 g pour la résultante, est introduite. Toutefois une variante française et allemande permet de supprimer cette exigence pour les sièges et autres équipements commerciaux,

- la possibilité de réduire le facteur de 4,5 en "downward" est supprimée,

- des précisions sur la rétention des masses, notamment des masses élevées, telles que moteurs et APU, pouvant blesser les passagers, sont ajoutées,

- des exigences concernant la conception et l'installation des réservoirs dans ou au voisinage du fuselage ou près des moteurs, en ce qui concerne les risques de feu, sont ajoutées.

Le texte du JAR 25.561 a évolué au "change" 11 par suppression de cette dernière exigence, laquelle est reportée en JAR 25.963, en complément de celle qui y figurait déjà , comme dans le règlement FAR. A noter que ce § 963, comme d'autres tels que les § 783, 785, 787, 789, 809, 812, 963 et 1413 se rapportent aux facteurs d'accélération précisés en 561, mais de façon hétérogène quant à la prise en compte ou non de leur combinaison ; on voit donc là des différences importantes de traitement de ces paragraphes périphériques en JAR et en FAR, puisque rapportés à des § 561 différents.

En conclusion de cette première partie, nous voyons que nous disposons d'une panoplie d'exigences telles que le montre la planche 5 ; ces exigences sont rapportées à des crash mineurs, mais en quelques années et par quelques amendements aux règlements, la sévérité s'est accrue, et le souci de protéger les passagers durant et après le crash s'est affirmé.

Qu'en est-il à ce stade de l'expérience en service ?

En cette matière, je ne dispose pas de statistiques récentes et je ferai état de nouveau de l'étude de la NASA de 1982 (Commercial Jet Transport Crashworthiness NASA-CR-165849) commandée par la FAA. Elle fait apparaître que sur 583 accidents, 153 sont déclarés survivables quand l'un au moins des critères suivants existent :

- volume survivable maintenu,
- facteurs d'accélération non mortels,
- possibilité réelle d'évacuation,
- bonne tenue de la structure ou des systèmes démontrée lors de l'accident.

Parmi ces 153 cas, 29 ont été retenus comme significatifs à cause du nombre de passagers à bord et du nombre de rescapés, et vous sont présentés sur la planche 6 ; il apparaît sur ce tableau que pour le plus grand nombre (25 sur 29), il y a eu feu ; d'autre part les accidents ont eu lieu, dans la même proportion, en phase d'approche finale ou d'atterrissage. Mais les cas cités ne représentent qu'à peine 20 % des 153 cas survivables ; les cas non retenus représentent des accidents avec fort peu de survivants, ce qui montre la nécessité de travailler dans de nouvelles voies :

a) ne plus considérer que le seul objectif est le crash mineur, par ailleurs démontré en service comme non critique,

b) renforcer le niveau des exigences périphériques, notamment en matière de feu, fumée et toxicité, permettant au passager de survivre après le crash et d'évacuer correctement.

Puisque le crash n'est pas extrêmement improbable, au niveau d'une flotte d'avions, il doit être prouvé que les conséquences ne sont pas catastrophiques.

Evolution prévisible des règlements :

La NASA a défini le crash survivable comme un évènement à la suite duquel les occupants n'ont pas tous subis des blessures mortelles consécutives à l'impact lié à la séquence de crash ; la première évolution sera donc d'étendre la notion de crash à celle de survie pour le plus grand nombre de passagers, en considérant d'abord tous les moyens qui peuvent atténuer les facteurs d'accélération, et notamment les pics au moment de l'impact, et ensuite toutes les causes qui peuvent contrarier l'évacuation.

Rappelons, pour éclairer cette 2ème partie de l'exposé, les résultats de l'essai effectué le 1er décembre 1984 par la FAA et la NASA sur un BOEING 720 dans le cadre du programme CID (Controlled Impact Demonstration) : l'avion, télépiloté, a touché le sol à 150 kt avec une Vz de 17,3 ft/sec, les accélérations verticales et horizontales au niveau de certains sièges, atteignant en pic 40 g ; je laisse à d'autres conféren-

ciers le soin de développer l'aspect physiologique lié à de telles accélérations. Malheureusement l'essai ne fut pas concluant sur l'un des points essentiels, à savoir le système dit "fuel inerting" prévu pour retarder l'inflammation du carburant.

Mais revenons à l'examen des 2 aspects cités ci-dessus :

1 - Atténuation des facteurs d'accélération au niveau du passager :

Plusieurs moyens sont envisageables :

1.1 - Modification des standards de sécurité des sièges :

Cette voie, proposée par la FAA, probablement sous la pression des fabricants de sièges, conduit aujourd'hui à la NPRM 86-11 (Notice of proposed rulemaking) ; cette proposition diffusée, pour consultation, à différentes Autorités et Constructeurs, contient de nouvelles exigences pour le maintien du passager sur le siège et de nouveaux critères de blessures à l'impact, que l'on peut résumer comme suit :

- Nouveaux facteurs d'accélération (extrêmes) appliqués aux sièges :
  - "upward" : 3,5 (au lieu de 2 en FAR 25),
  - "forward" : 9 (inchangé),
  - "sideward" : 4,5 (au lieu de 1,5 en FAR 25),
  - "downward" : 6,5 (au lieu de 4,5 en FAR 25),
  - "rearward" : 1,5 (au lieu de 0 en FAR 25),
- Création du § 25.561 (d) relatif aux structures retenant les sièges et toutes masses pouvant blesser passagers et équipage, ou pouvant retarder l'évacuation ; ce paragraphe a le même objectif que le § 25.561 (c) du JAR, bien que moins précis,
- Création d'un § 25.562 prévoyant des exigences propres aux sièges et notamment les conditions des essais dynamiques permettant de les justifier au crash ; prévoyant également des valeurs de charges extrêmes pour les baudriers et ceintures, ainsi qu'un critère HIC (Head Injury Criterium) pour les blessures à la tête et un critère de protection des fémurs.

Ce document, particulièrement quantifié, a fait l'objet de la part des Autorités du JAR, au début 1987, des observations suivantes :

- si la notion de système global d'absorption d'énergie constitué par le passager attaché, le siège et sa structure de liaison, est acceptable,

par contre la rédaction présentée de l'exigence et du moyen de conformité est arbitraire et imprécise, par exemple :

. faut-il renforcer les planchers et les structures d'attache des sièges, quand on impose un désalignement des rails ?,

. où sont les limites des structures-supports de sièges ?,

. quelles sont les relations entre les § 561 et 562 de même qu'entre le § 561 et les § périphériques cités plus haut ?.

- il est nécessaire d'inclure une alternative pour la justification des sièges ; la FAR 25 prévoit généralement la possibilité "analyse et/ou essais", laissant à l'Autorité le soin de vérifier que le postulant dispose de données et d'un savoir-faire corrects.

Ces observations font l'objet d'un examen de la part de la FAA qui sera probablement conduite à amender sa proposition.

1.2 - <u>Absorption d'énergie par l'avion</u> :

La principale critique faite par les Européens à la FAA au sujet de la NPRM 86-11 est d'un autre ordre : en limitant l'application des facteurs d'accélération au siège, la déformation et donc l'absorption d'énergie par l'avion ne sont pas prises en compte, et la relation entre l'ensemble siège/passager et la structure environnante n'est pas claire. Les Européens souhaitent que la FAA ne limite pas son projet aux seuls sièges, mais les considèrent comme inclus dans un système global d'absorption d'énergie ; il est évident qu'il est difficile, à ce sujet, de comparer un "large body" dont la structure est déformable, à un avion d'affaire de masse réduite et dont la structure est rigide ; faudra-t-il dans ce dernier cas, comme on le prévoit pour les hélicoptères, prévoir des sièges équipés de système d'absorption d'énergie ?.

Tout ceci est dans la ligne de réflexion des Autorités du JAR qui continuent à rechercher une corrélation entre les facteurs d'accélération appliqués à l'avion, et ceux appliqués aux sièges ; c'est dans ce but qu'un essai sera entrepris en 1988 sur une cellule de FALCON 10 dans un laboratoire officiel : cet essai connu sous la référence "crash FALCON 10" entre dans le cadre des études réglementaires financées en partie par l'Etat, en partie par l'Industrie.

Dans ce chapitre d'absorption d'énergie, il y a lieu de signaler le dilemme bien connu du crash avec ou sans train d'atterrissage (sorti) ; je citerai à ce propos le cas du FALCON 900 dont la justification au § 25.561 est faite train rentré, avec impact sur les quilles de crash et absorption d'énergie par usure de ces quilles,

lesquelles protègent également les réservoirs de fuselage ; mais on trouve dans le Manuel de Vol et le Manuel d'Exploitation la consigne, en cas d'atterrissage forcé, de sortir le train même dissymétriquement ; ce train, dont la rupture est prévue par la disposition de fusibles a pour rôle d'absorber de l'énergie en quantité difficile à définir.

Il y aura donc lieu de faire évoluer la réglementation sur cet aspect, afin de tenter de s'approcher de la réalité, c'est-à-dire de prendre en compte l'effort des Industriels dans la conception des structures prévues pour absorber de l'énergie durant la séquence de crash.

2 - <u>Précautions relatives à l'évacuation et vis-à-vis du feu</u> :

Nous avons fait état plus haut de cet important problème, abordé ici sous 3 aspects : les moteurs, le train d'atterrissage et les réservoirs de carburant ; ces éléments font l'objet d'exigences réglementaires en cas de crash, afin d'éviter le développement d'un feu préjudiciable à l'évacuation des passagers.

2.1 - En ce qui concerne les moteurs, notamment ceux installés sous les voilures basses, seul le JAR 25.561 et son ACJ (méthode acceptable de conformité = Acceptable means of compliance and interpretation) prévoit que les réservoirs doivent être installés de façon, en cas d'atterrissage d'urgence, à n'être pas endommagés par le train (si sorti), les moteurs et le sol, si l'avion glisse sur celui-ci ; ceci a conduit notamment, et a contrario, certains constructeurs à concevoir des fusibles sur les attaches moteurs, comme il vient d'être dit pour les attaches de train, afin que ces moteurs, avion en configuration train rentré, prennent à l'impact une position minimisant le risque de perforation des réservoirs de voilures et favorisent le glissement sur le fuselage ; je rappelle qu'une telle disposition existe sur le MERCURE et sur l'AIRBUS. La FAA serait bien avisée de suivre ici l'exemple du JAR.

2.2 - En ce qui concerne de nouveau le train d'atterrissage, et bien que les règlements considèrent le crash train rentré, il a été rappelé ci-dessus que ce n'est pas toujours la pratique. Se posent alors les problèmes d'impact avec train dissymétrique.

Quelle énergie le train peut-il absorber avant rupture, et quelles sont les conséquences de cette rupture ?. Si le § 25.721 prévoit que le train soumis à une surcharge puisse rompre, il exige que toute fuite de carburant provenant de l'endommagement des réservoirs voisins ne soit pas telle qu'un risque de feu important existe ; cette rupture, justifiée jusqu'ici par des essais statiques, a montré sur la base d'accident récent, que la méthode de justification était insuffisante ; seule une justification par essai et analyse dynamiques peut approcher la

réalité, et c'est dans ce but qu'une étude réglementaire est lancée en France, en vue d'améliorer le Règlement.

2.3 - Un autre domaine, enfin, conduit à une proposition d'amendement au règlement JAR : il s'agit du cas particulier des réservoirs d'empennage non considérés dans le § 25.963, ; ces réservoirs, outre l'augmentation de carburant qu'ils permettent, assurent une fonction de variation de centrage sur les nouveaux avions.

Toutefois l'intégrité structurale de tels réservoirs devra être assurée pour les facteurs d'accélération du § 25.561 avec un chargement en carburant à définir par les Autorités, afin d'éviter que leur endommagement ne provoque un feu par écoulement du carburant sur l'APU ou les moteurs installés à l'arrière du fuselage, ou un feu au sol remettant en question l'évacuation des passagers dans la zone arrière de l'avion.

Permettez-moi de terminer ce chapitre par la planche 7 relative à l'"interpretative material" rédigée pour la certification de l'AIRBUS A 320, et qui résume en tant qu'application pratique, les exigences actuelles des autorités européennes.

Je terminerai cet exposé par un commentaire sur l'évacuation des passagers : considérant la notion de crash survivable, non encore écrite en clair dans la réglementation, l'ultime souci des Constructeurs, Exploitants et Autorités est d'assurer aux survivants de l'impact, des conditions d'évacuation telles qu'ils échappent à l'asphyxie et au feu ; la protection des réservoirs, les précautions prises au niveau de systèmes sensibles tels que l'oxygène et l'électricité, la lutte contre la fumée, la multiplication des issues,leur répartition et leur dimension satisfaisantes, les aides à l'évacuation telles que les toboggans, font l'objet de beaucoup d'études et d'essais dûs à l'importance de l'édifice réglementaire en constante évolution ; ceci est capital pour les avions gros porteurs, dans lesquels tout évènement classé situation d'urgence a tendance à devenir rapidement critique, du fait des réactions imprévisibles d'une foule. Il est souhaitable que tous les aspects touchant à la sécurité des passagers dans de telles situations, soient mieux regroupés dans les règlements afin d'être traités de façon homogène.

Selected impact survivable accidents
all operation 1959-1979 world wide air carriers

Probable cause	Number of accidents
Cockpit crew	110
Airplane	16
Weather	7
Airport/Atc.	3
Misc.	2
Maint.	1
Sabotage	1
Total	140
Unknown	13
Total	153

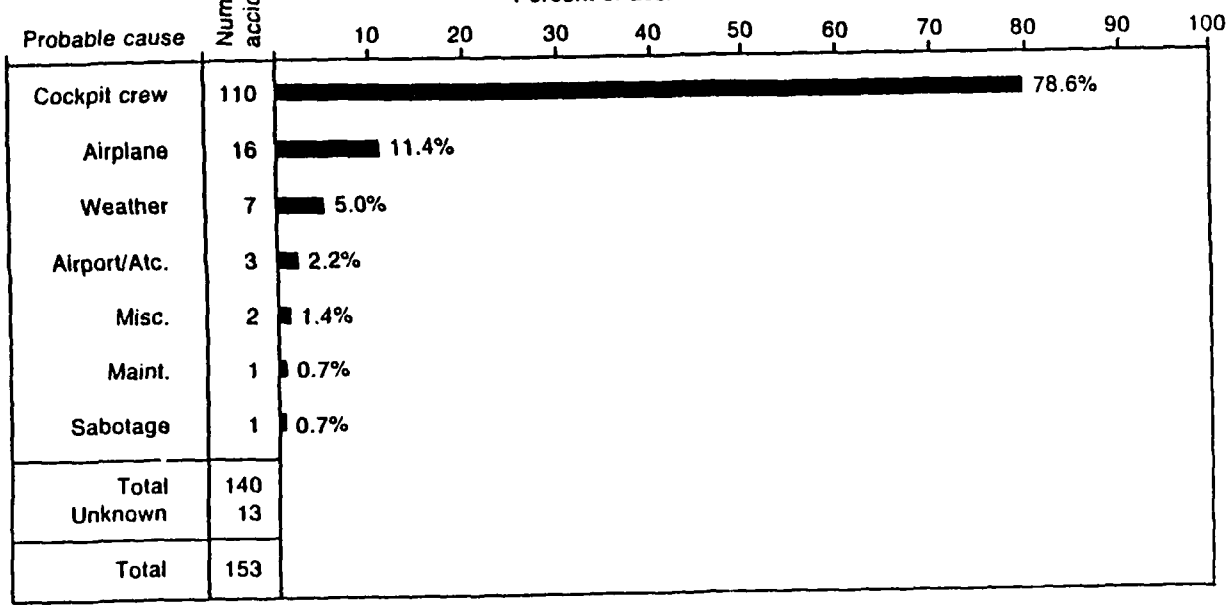

Probable Cause of Accidents

Planche 1

Crash Mineurs

Caravelle

DATE	LIEU	OCC.	SURV.	FEU	
09/61	BRASILIA	70	70	X	
07/63	CORDOBA	70	70	X	
02/66	DELHI	80	79	X	
07/69	BISKRA	36	2	X	EN VOL
08/69	RIO	46	46		
08/69	MARIGNANE	94	94		
04/70	BERRECHID-MAROC	62	20		
02/71	LAS PALMAS	42	42		
12/73	MANAOS	66	66	X	
07/79	BOGOTA	57	57	X	
06/82	DAMAS	80	80		REPARÉ
04/83	GUYAQUIL	101	93		
01/87	STOCKHOLM	27	27		

Source: Aérospatiale

Planche 2

Crash Mineurs

Autres Avions
(Avion Considéré Perdu)

DATE	TYPE	LIEU	OCC.	SURV.	FEU	
01/69	BAC 111	MILAN	33	33		
02/69	VISCOUNT	EAST MIDLAND	53	53		
07/07	B 737	PHILADELPHIE	61	61		
12/70	B 727	SAINT THOMAS	55	53	X	
02/72	FALCON 20	SAINT MORITZ	5	5		
07/73	B 707 (VARIG)	PARIS	134	11	X	EN VOL
11/73	DC 9	CHATTANOOGA	79	79		
12/73	B 707	DELHI	109	109	X	
12/75	B 707	MILAN	125	125		
05/78	B 727	PENSACOLA	58	58		
08/78	B 707	EZEIZA	63	63	X	
12/78	B 737	HYDERABAD	132	131	X	
07/80	VISCOUNT	EXETER	62	62		
08/80	TU 154	NOUADHIBOU	168	166		

Source: CAA World Accident Report Summary

Planche 3

Ultimate inertia forces (g)				
	CAR 4b + FAR 25	C.C. 12	JAR 25	NPRM 86-11 (FAR 25)
Upward	2	2	2	3.5
Forward	9	9	9	9
Sideward	1.5	2.25	1.5	4.5
Downward	4.5	4.5	4.5	6.5
Rearward	–	1.5	1.5	1.5

Planche 4

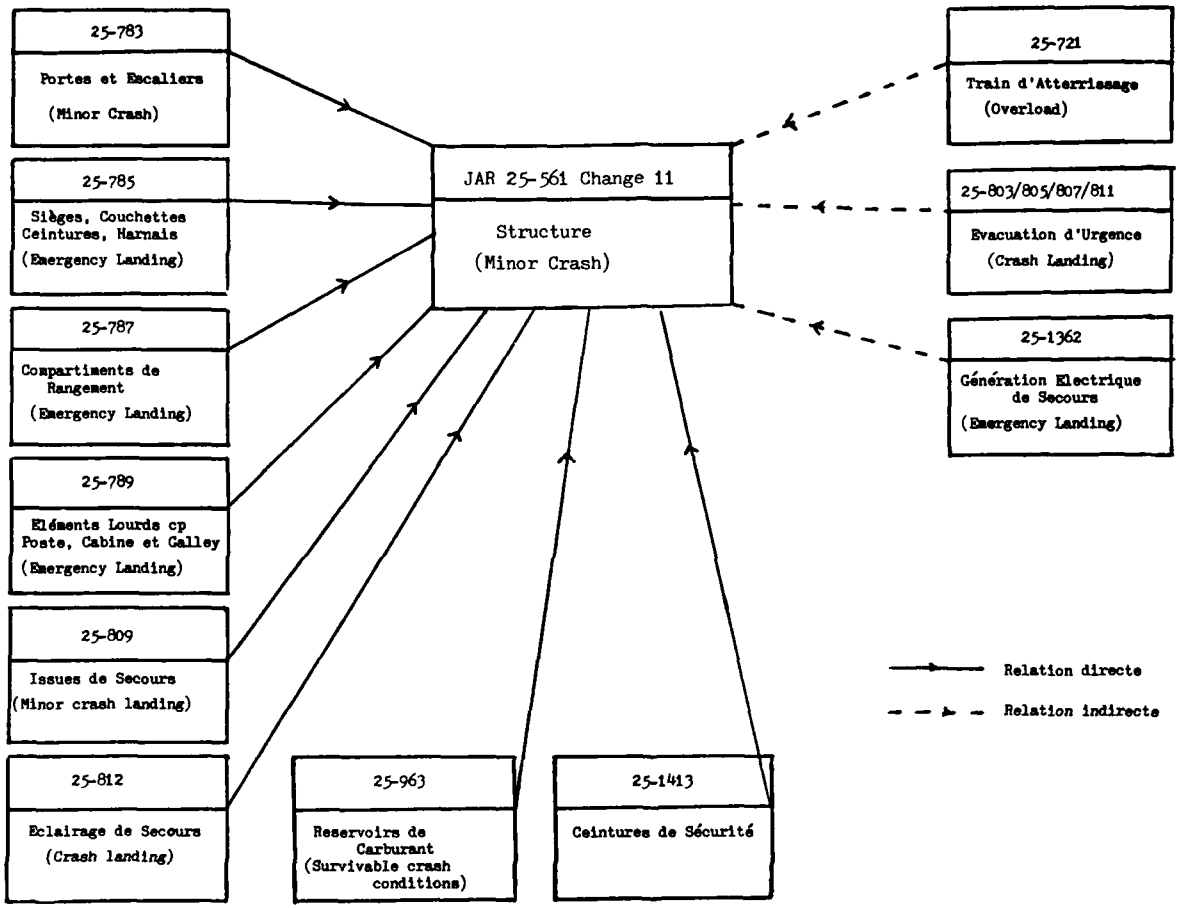
25-783
Portes et Escaliers
(Minor Crash)
25-785
Sièges, Couchettes
Ceintures, Harnais
(Emergency Landing)
25-787
Compartiments de
Rangement
(Emergency Landing)
25-789
Eléments Lourds cp
Poste, Cabine et Galley
(Emergency Landing)
25-809
Issues de Secours
(Minor crash landing)
25-812
Eclairage de Secours
(Crash landing)
JAR 25-561 Change 11
Structure
(Minor Crash)
25-963
Reservoirs de
Carburant
(Survivable crash
conditions)
25-1413
Ceintures de Sécurité
25-721
Train d'Atterrissage
(Overload)
25-803/805/807/811
Evacuation d'Urgence
(Crash Landing)
25-1362
Génération Electrique
de Secours
(Emergency Landing)
Relation directe
Relation indirecte

Planche 5

Crash Survivables

DATE	TYPE	LIEU	OCC.	VICT.	FEU
08/62	DC 8	RIO	105	15	X
11/64	B 707	ROME	73	48	X
11/65	B 727	CINCINNATI	62	58	X
11/65	B 727	SALT LAKE CITY	91	43	X
03/66	DC 8	TOKYO	71	63	X
11/67	CV 880	CINCINNATI	82	70	X
04/68	B 707	WINDHOEK	128	123	X
01/69	B 727	LONDRES	65	50	X
01/69	DC 8	LOS ANGELES	45	15	
09/69	B727	MEXICO	118	28	
09/69	BAC 111	MANILLE	47	45	X
11/70	DC 8	ANCHORAGE	229	47	X
03/70	CVL	CASABLANCA	82	61	X
05/70	DC 9	ST CROIX	63	25	
07/70	DC 8	TORONTO	108	108	X
12/72	B 737	CHICAGO	61	43	X
12/72	DC 9	CHICAGO	45	10	X
07/73	DC 9	BOSTON	89	89	X
01/73	B 707	KHANO	202	172	X
05/73	B 737	NEW DELHI	65	52	X
01/74	B 707	PAGO-PAGO	101	97	X
09/74	DC 9	CHARLOTTE	82	71	X
11/74	B 747	NAIROBI	157	59	X
06/75	B 727	NEW YORK	124	112	X
04/76	B 727	ST THOMAS	88	37	X
04/77	DC 9	NEW HOPE	85	62	X
02/78	B 737	CRANBROOK	49	42	X
12/78	DC 8	PORTLAND	186	10	
03/79	B 727	DOHA	64	45	X

Source: DOT/FAA-CT-82-86
DOCT NASA CR 165849

Planche 6

STRUCTURE

References :

INTERPRETATIVE MATERIAL
IM - A 3.7
Status : CLOSED
Date : 09.10.1985

1. CRI : A 3.7

2. JAR : ACJ 25.561 (a), (c) and (d)
25.721

EMERGENCY LANDING CONDITIONS (JAR 25.561)

AND LANDING GEAR (JAR 25.721)

In showing compliance with JAR paragraphs 25.561 and 721 the following interpretative material is applicable :

1. The aircraft has to be designed to avoid ruptures that would be catastrophic for the safety of the occupants, including ruptures leading to fuel spillage under the following conditions :

   1.1 Impact at 5 fps vertical velocity at maximum landing weight :

   - with all gears retracted,
   - with any one or two gears retracted.

   1.2 Sliding on the ground :

   - with all gears retracted up to a yaw angle of 20°,
   - with any one or two gears retracted with zero yaw angle.

   1.3 Failure of the landing gear under overload, assuming the overload conditions to be any reasonable combination of drag and vertical loads.

2. Consideration should also be given to :

   2.1 The possible separation of an engine pod (or pod + pylon) under predominantly drag loads or under predominantly vertical (upward or downward) loads.

   2.2 The possible failure of the landing gear under overload conditions including side loads.

3. In all the above justifications involving failures of part of the aircraft structure, the dynamic behaviour of the different parts at rupture should be taken into account.

EVOLVING CRASHWORTHINESS DESIGN CRITERIA

by

C. Hudson Carper
Chief, Safety and Survivability Technical Area

and

LeRoy T. Burrows
Chief, Ballistic and Crash Protection Team
Safety and Survivability Technical Area

Aviation Applied Technology Directorate
U.S. Army Research and Technology Activity (AVSCOM)
Fort Eustis, Virginia 23604-5577

SUMMARY

Although significant strides have been made in recent years toward improving aviation safety, mishaps involving all classes of helicopters presently are and will continue to be a major, expensive U.S. Army problem in terms of casualties, materiel loss, and reduction in mission effectiveness. Modernday training and tactical employment requirements for the U.S. Army helicopter dictate that a large percentage of operations occur in the low-speed, low altitude flight regime, which contributes to the problem by reducing critical margins of safety normally associated with higher airspeed and higher altitude operations with accompanying greater time for response in case of an emergency. This increased probability of accident occurrence, coupled with the lack of an in-flight egress capability, makes design for crashworthiness essential for Army helicopters.

This paper discusses the evolution of crash survival design criteria for rotary-wing aircraft and its application to current and new generation Army helicopters. Emphasis is given to the need for a total systems' approach in design for crashworthiness and the necessity for considering crashworthiness early in the design phase of a new aviation weapon systems development effort. The actual app ication of crashworthiness to Army helicopters is presented with statistics that show dramatic reductions in fatalities and injuries with implementation of a crashworthy fuel system. The cost effective aspects of designing helicopters to be more crash survivable are also discussed.

INTRODUCTION

Research investigations directed toward improving occupant survival and reducing materiel losses in aircraft crashes have been conducted by the Army for more than 20 years. However, up until approximately 10 years ago the principal emphasis within Army aviation survivability was placed on accident prevention. Although this is indeed the ultimate objective deserving priority effort, past experience clearly shows that accident prevention alone simply is not sufficient. Mishaps of all natures involving Army aircraft have been, are, and will continue to be a major, expensive problem. Research has been accomplished on accidents worldwide involving Army aviation, and accident histories are routinely disseminated throughout the Army. Unfortunately, many lessons learned from these accident histories are not applied and hazardous design features remain and operational errors are repeated. Too many Army aircrewmen are still being fatally injured in potentially survivable accidents, and the percentage of major injuries and rate of materiel losses are still unacceptably high. There is no easy solution to the problem. Significant gains can be made, however, toward reducing these unacceptable accident losses, but to do so we must aggressively pursue a program that addresses key issues of both accident prevention and crashworthiness design. Since the helicopter's potential for accident is great due to its mission and the environment in which it must accomplish that mission, it is imperative that it be engineered to minimize damage and enhance occupant survival in crashes. In designing helicopters to be more crash survivable, two subissues then become paramount: establishing viable crashworthiness design criteria, and the more difficult task, applying these crashworthiness criteria to Army aircraft design.

To help establish the severity of the problem within U.S. Army aviation, Table 1 provides a summary of accident statistics for Army helicopters for the period of time from 1972 to 1986. During the period reviewed there were over 5,000 helicopter Class A, B, C, and D mishaps (an average of one a day) and over 550 occupant fatalities. The number of fatalities would, without question, have been much greater had not Army aircraft been retrofitted in the early to mid 70's with crashworthy fuel systems. The cost of these mishaps considering casualties and materiel were nearly 600 million dollars. These costs primarily reflect relatively low cost helicopter losses (i.e. OH-58, UH-1, AH-1) as compared to the higher cost modern helicopter (UH-60, AH-64). Also, they do not reflect the potentially greater costs that are associated with loss of mission capability. Further, these statistics are based on current peacetime

experience which reflects a total cumulative flight time of approximately 1½ million hours per year for Army aviation with a fatality rate of approximately 2.5 per 100,000 hours of flying time. The severity of the problem increases severalfold during periods of combat, as demonstrated in Vietnam when, during the height of the conflict, total helicopter flight time was in excess of 5 million hours per year with the fatality rate of 10 per 100,000 hours.

Table 1. Army Helicopter Accident History 1972-1986

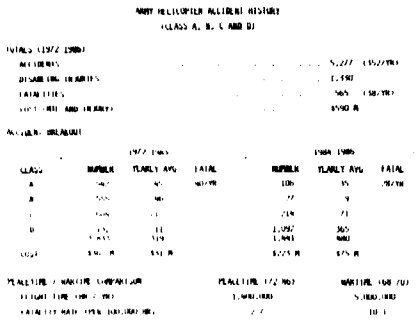

Data from these accident and crash injury investigations (reference 1) have revealed deficiencies in the crashworthiness of the older, existing Army helicopters. Key deficiencies include:

- *Structural collapse (roof downward* and floor upward) causing loss of occupiable volume.
- Inward buckling of frames, longerons, etc., causing penetration wounds to personnel.
- Lethal internal structure causing head, chest and extremity injuries from occupant flailing.
- Floor breakup permitting seats to tear out and occupants to become flying missiles.
- Landing gear penetration into occupied areas and fuel systems causing contact injuries and fires.
- Landing gears not designed for sufficiently high sink rates and insufficient deformable airframe structure permitting excessive acceleration (G) forces to be transmitted to the occupants and causing excessive materiel damage.
- Intrusion of the occupied area by the main rotor gearbox and other high mass items causing crushing and contact injuries to the occupants.
- Insufficient structural stiffness permitting inward crushing and entrapment of occupants in rollover accidents.

CRASHWORTHINESS DESIGN CRITERIA

General

In-depth assessment of available crash data was first accomplished in the mid-60's by a joint Government/industry review team. The product of that team was the world's first crash survival design guide (CSDG) for light fixed- and rotary-wing aircraft, published in 1967. Revisions to this guide were made in 1969, 1971, 1980 (reference 2) and a current effort is scheduled for completion in 1989. Figures 1a and 1b depict the many facets of crashworthiness research and development that have directly helped to support the evolution of crashworthiness design criteria. Continual component development programs, full scale crash testing, and structural analyses efforts are being conducted which increase the knowledge base and provide new technology applicable to crashworthiness design, thus dictating the need for periodic revisions of the CSDG. In 1974, the CSDG was converted into a military standard (MIL-STD-1290)(reference 3). Although a draft revision to this MIL-STD exists (1290A), this revision will not be finalized until the completion of the current CSDG update effort. In addition, an Aeronautical Design Standard, *ADS 36, entitled "Rotary Wing Aircraft Crash Resistance"* (reference 4) was formulated to be specifically applied to the U.S. Army's Light Helicopter (LHX) development program. This will be discussed in more detail later in the paper.

Figure 1a

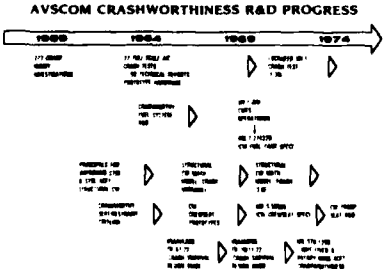

Figure 1b

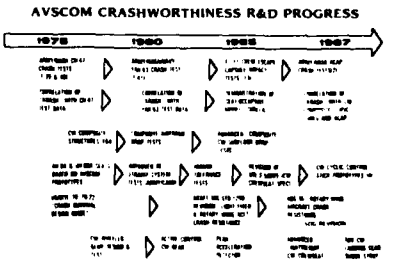

MIL-STD-1290 addresses five key areas that must be considered in designing a helicopter to conserve materiel and provide occupant protection in a crash:

- Crashworthiness of the structure--assuring that the structure has proper strength and stiffness to maintain a livable volume for the occupants and prevent the seat attachments from breaking free.
- Retention strength--assuring that the high mass items such as the transmission and engine do not break free from their mounts and penetrate occupied areas.
- Occupant acceleration environment--providing the necessary crash load absorption by using crushable structures, load limiting landing gears, energy-absorbing seats, etc., to keep the loads on the occupants within human tolerance levels.
- Occupants environment hazards--providing the necessary restraint systems, padding, etc., to prevent injury caused by occupant flailing.
- Postcrash hazards--after the crash sequence has ended, providing protection against flammable fluid systems and permitting egress under all conditions.

Typical Army Crash Impacts

In the Army, typical crash impact conditions are depicted in Figure 2. Roll, pitch, and forward velocity is usually present along with vertical and forward velocity components. Some level of yaw attitude is also frequently present. This dictates the need for impact design criteria involving longitudinal, vertical and lateral velocity components.

About 95% of Army helicopter mishap crash impacts have been in the potentially survivable range. Accordingly, helicopter crash resistance requirements given in Figure 3 were adopted by the Army in the early 1970's. Specifically, the aircraft structure shall provide a protective shell for occupants in crash velocity changes of the severity cited in Figure 3. Moreover, the structure and equipment shall allow deformation in a controlled, predictable manner so that forces imposed upon the occupants will be tolerable while still maintaining the protective shell. The forces imposed on occupants is governed by the stopping distance and pulse duration. Figure 4 illustrates this relationship and indicates the importance of controlled energy absorption in a crash.

Systems Approach

For maximum effectiveness, design for crashworthiness dictates that a total systems approach be used and that the designer consider such survivability issues with at least equal priority as other key design considerations such as weight, load factor, and fatigue life during the initial design phase of the helicopter. Figure 5 depicts the system's approach required relative to management of the crash energy for occupant

ATTITUDE: RELATIVELY LEVEL (± 10° ROLL; +15°/−5° PITCH)
VELOCITY: FORWARD SPEED — 10 FPS (7 MPH)
VERTICAL SINK SPEED — 15 FPS (10 MPH)
SURVIVABILITY: >90%

Figure 2. Typical Crash Impact Condition U.S. Army Helicopters (Existing Fleet)

- IMPACT VELOCITY/G LANDING

DIRECTION	TOTAL SYS (FT/SEC) (± 10° ROLL; +15°/−5° PITCH)	LANDING GEAR (FT/SEC)
VERTICAL	42	20
LONGITUDINAL	50	(NO FUSELAGE DAMAGE)
LATERAL	30	
RESULTANT	50	
PLOWING & SCOOPING (G)	10 UP/4 AFT	
ROLL-OVER (G)	4 SIDE/4 ROOF	
HIGH-MASS ITEM RETENTION (G)	20 LONG/20 VERT/18 LAT	

- *OCCUPANT RETENTION*
- CARGO & EQUIPMENT RETENTION
- POST CRASH FIRE PREVENTION
- VALIDATION TEST METHODS

Figure 3. Key Crash-Resistant Design Requirements for Army Helicopters

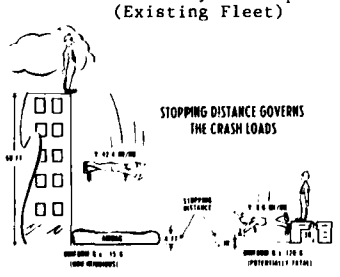

Figure 4. Impact Accelerations

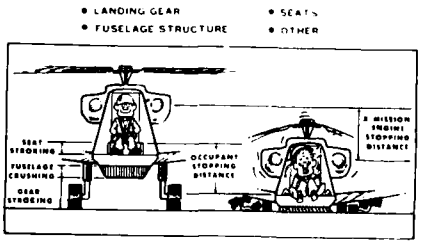

Figure 5. Systems Approach to Crashworthiness

survival for the vertical velocity crash design condition. The crash G loads must be brought to within human tolerance limits in a controlled manner to prevent injury to the occupants. This can be accomplished by using the landing gear, floor structure, and seat to progressively absorb crash energy during the crash sequence. That is, the occupant is slowed down in a controlled manner by stroking/failing the landing gear, crushing the floor structure, and stroking the seat at a predetermined load before being subjected to the crash pulse which by then has been reduced to within human tolerance limits. In addition, the large mass items such as the overhead gearbox are slowed down by stroking/failing of the landing gear or fuselage structure, and in some cases, by stroking of the gearbox within its mounts. With the advent of airframes constructed from composite materials (fiberglass, Kevlar, graphite) the need for a systems approach to crashworthiness, coupled with innovative design, becomes more urgent due to the characteristically nonductile behavior of these materials.

Crash Impact Design Conditions

A survivable crash is generally defined as one wherein the impact conditions inclusive of pulse rate onset, magnitude, direction and duration of the acceleration forces that are transmitted to the occupant do not exceed the limits of human tolerance for survival, and in which the surrounding structure remains sufficiently intact during and after impact to permit occupant survival. Inasmuch as the crew must stay with the helicopter in an impending crash, a high level of what constitutes a survivable or non-injurious crash impact velocity change is desirable and is a key objective of design for crashworthiness. The Army's crash impact velocity change design conditions for longitudinal impacts against a rigid barrier are 6.1 m/s (20 ft/s) for the cockpit and 12.2 m/s (40 ft/s) for the cabin. There has been little disagreement with this design requirement. The vertical velocity change crash impact design condition however, has continually been the subject of controversy. It is becoming evident that one set of crashworthiness design criteria is not necessarily practical for all rotary-wing aircraft, military and commercial, large and small. Factors such as the following must also be considered in future development of crashworthiness design criteria.

- Helicopter size and transportability requirements (space available for energy absorbing seats and crushable subfloor structure).
- Performance of the aircraft (e.g. disk loading, autorotational sink rate, flight velocity capability).
- Basic aircraft configuration.
- How the aircraft is to be employed.

Obviously, the smaller the aircraft the larger percent of weight empty that is devoted to crashworthiness for a given set of design impact conditions. This could lead to an impractical design. Also, commercial helicopter operations are generally less perilous than military operations indicating that commercial helicopter crash impact design requirements could be less stringent than for military systems. Ballistic tolerance is not a consideration in designing a crashworthy fuel system for commercial helicopters.

The following is a summary of vertical velocity crash impact vs. pitch and roll design criteria that have evolved over the past few years. It should be noted that this is for impact on a rigid surface without (1) reducing the height of the cockpit and passenger/troop compartments by more than 15% or (2) allowing the occupants to experience injurious accelerative loading.

Table 2. Vertical Velocity Crash Impact Design Criteria

	Velocity Change V (m/s)	Roll	Pitch
MIL-STD-1290 (Ref 3)	12.8 (42 ft/sec)	± 30°	± 15°
CSDG (Ref 2)	12.8 (42 ft/sec)	± 20°	+ 25° to - 15°
ADS-36 (Ref 4)	11.6 (38 ft/sec)	± 10°	+ 15° to - 5°
MIL-STD-1290A Draft	12.8 (42 ft/sec)	± 10°	+ 15° to - 5°

The original MIL-STD-1290 contained an impractical requirement for roll since a 30 degree attitude would result in only half the landing gear absorbing energy in a crash before fuselage contact, assuming it would stroke at all with such severe side loadings. The current published CSDG (reference 2) also specifies a too severe roll and negative pitch impact attitude requirement. This criteria is not substantiated by accident history data of roll and pitch values and designing to meet it has an adverse effect on aircraft system design and weight.

ADS-36 (reference 4) is based upon that level of crashworthiness that has been demonstrated by the UH-60 helicopter. Since Army aviation leaders have been pleased, for the most part, with the UH-60 crashworthiness, they have dictated their desire that the LHX have at least this level. ADS-36 and the draft MIL-STD-1290A are essentially the same except for the vertical velocity change requirement. The roll and pitch attitude values selected are derived from analysis of accident historical data presented in Figures 6 and 7. The attitude envelop specified in ADS-36 is presented in Figure 8 and it illustrates how the airframer can be relieved from having to design for the extreme corners of the combined roll and pitch conditions which rarely occur.

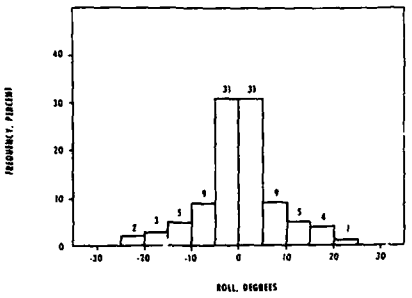

Figure 6. Aircraft Roll Angle at Impact for Survivable and Partially Survivable Army Helicopter Mishaps, 1972-1982

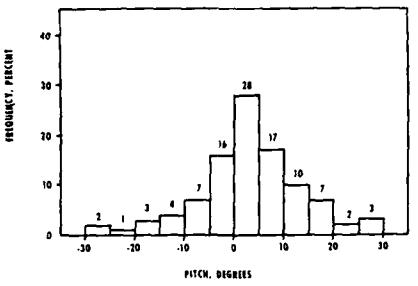

Figure 7. Aircraft Pitch Angle at Impact for Survivable and Partially Survivable Army Helicopter Mishaps, 1972-1982

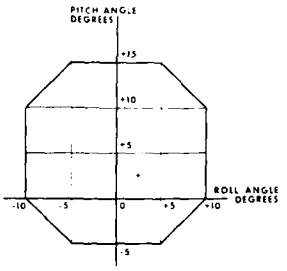

Figure 8. Roll and Pitch Attitude Envelope

Landing Gear

As a minimum, the landing gear shall be capable of decelerating the aircraft at normal gross weight from an impact velocity of 6.1 m/s (20 ft/sec) onto a level rigid surface within an attitude envelope of ±10 degrees roll and +15 degrees to -5 degrees pitch without allowing the fuselage to contact the ground and without gear penetration into an occupied area. Plastic deformation of the landing gear and its mounting system is acceptable in meeting this requirement; however, with the possible exception of the rotor blades, the remainder of the aircraft structure shall be flightworthy after impact. Prior to the 1970's, helicopter landing gear (usually skids) had relatively little energy absorbing capability and very limited capability to withstand lateral loads without failing. Skid gears were designed, typically to withstand an 8 ft/sec vertical impact speed without collapse at basic structural design gross weight (BSDGW). Too often in the past, a certain accident scenario has repeated itself in the Army's skid gear equipped aircraft. The helicopter will touch down with some roll attitude angle (out of an autorotation, perhaps) at a vertical sink speed slightly exceeding the skid capability. One skid fails, causing the helicopter to roll right or left, bringing the main rotor into contact with the ground. The reactive torque loads then exceed the capability of the transmission mounts and the rotor system/transmission departs the aircraft during the post impact gyration. Accidents such as described usually result in complete loss of the aircraft, serious injuries to the occupants and often fatalities. It is possible to totally avoid this type of accident for impacts involving sink speeds of 6.1 m/s (20 ft/sec, or 1200 ft/min) (or even greater), through use of a landing gear designed to absorb this amount of energy.

A high performance landing gear is the key component in the system approach to crashworthiness as well as in mishap prevention. Future helicopter systems will include very expensive mission equipment to the point that the airframe part of the system will be less than half the system cost. The 6.1 m/s (20 ft/sec) landing gear (or better) will help protect the airframe and expensive subsystems from damage, resulting in the major factor in substantiating the cost effectiveness of design for crashworthiness.

CRASHWORTHY FUEL SYSTEM (CWFS)

The crashworthy fuel tank specification, MIL-T-27422, was originally a joint services specification that was modified to require a crashworthy, ballistically tolerant (self-sealing) tank material that was developed during the mid and late 1960's. The modification, MIL-T-27422B (reference 5), was published in 1971. In addition to the 19.8 m/s (65 ft/sec) full-scale tank drop onto concrete requirement, the specification includes important puncture, cut and tear resistance tests that the tank wall material must pass.

If fuel is allowed to spill during survivable crashes, a postcrash fire is often the result due to the multitude of ignition sources available. Prior to the advent of crashworthy fuel systems, the Army studied 2382 survivable rotary-wing accidents occurring between 1967-69. Postcrash fires were present on 10.5 percent of the accidents and contributed to 39.3 percent of the fatalities. Through an intensive effort, the Army developed a CWFS consisting of self-sealing breakaway valves/couplings; frangible attachments; self-sealing fuel lines; cut, tear and rupture resistant bladders; and a means of preventing fuel spillage at all postcrash attitudes. The military specification, MIL-T-27422B, was developed with specific test requirements and pass/fail criteria for the CWFS. Though brute strength has some importance, the cut and tear resistance of the fuel tank material are key issues for successful fuel containment in deforming aircraft structure. The Army specification fuel tank material is also designed to be self-sealing for small caliber ballistic hits.

All Army helicopters now have a CWFS and postcrash fire statistics have been altered dramatically. During the period April 1970 to June 1976, a time when retrofit of the CWFS was in progress, for helicopter not CWFS equipped there were 65 thermal fatalities. This compares with only one fatality for helicopters equipped with the CWFS. Since 1976, there have been no thermal fatalities in potentially survivable accidents of Army helicopters.

Field evidence has shown that aircraft with the CWFS have experienced fuel system failures and resulting fires in severe accidents slightly above the human survival limit. This has verified the validity of current design criteria. No reduction in drop height, or of cut- and tear-resistance values should be considered, especially in light of the more severe crash impacts being experienced with higher performance helicopters such as the UH-60A.

RELATIONSHIP TO CIVIL AVIATION

In the civil aviation community, prevention of accidents has always been a high priority. However, even with technological advancements, increased mechanical reliability, improved pilot training, and intensive studies of accident causal factors, accidents do occur. Statistics indicate that for one decade (1967-1976) the number of general aviation aircraft involved in accidents was equivalent to at least 38 percent of the total U.S. aircraft production during that period. Estimates that an aircraft will be involved in an accident over a 20-year life range are as high as 60-70 percent.

Recognizing this accident probability, it makes sense to apply a worthwhile degree of crashworthiness to contemporary design philosophy. Because of differences in mission profiles, civil aircraft are normally flown somewhat differently than Army helicopters. The civil helicopter crash environments may not be sufficiently severe to justify using all of the MIL-STD-1290 crashworthiness design techniques that have been addressed in this paper. From a cost viewpoint the easiest to justify might be the use of state-of-the-art restraint and energy absorbing seat systems, although the crashworthy fuel system should perhaps be at the top of the priority listing of needed crashworthy features. As composite airframe structures become more attractive from a cost/weight standpoint, their demonstrated potential to act as good energy absorbers should not be overlooked. Usually, however, design innovations to benefit crashworthiness will equate to a design in excess of the Federal Air Regulations (FAR's), which are intended as minimum requirements only rather than design goals. FAA Order DA 2100.1 clearly states, "Such standards do not constitute the optimum to which the regulated should strive."

Finally, not to be overlooked in the civil area is the very real economic savings that can be gained (in concert with crashworthiness) from the inclusion of an energy absorbing (EA) landing gear. The potential Army savings were addressed earlier and would certainly, to a degree, apply in the civil market. Avoided materiel damage from hard landings alone should go a long way toward justifying an EA gear.

Some design practices such as excellent protective structure around the occupant along with adequate restraint in agricultural aerial application airplanes are now standard procedure. In time, it is hoped that a variety of meaningful crashworthiness improvements will be providing increasingly higher levels of occupant protection and damage avoidance.

NEW REQUIREMENTS OF MIL-STD-1290A AND ADS-36

Hundreds of changes have been made to MIL-STD-1290 since its initial publication, the vast majority of which were to correct typographical errors and to enhance clarification. Nevertheless, a number of significant new requirements did evolve and some of the more important ones, not already mentioned are as follows:

- Type II aircraft have been expanded to include tilt prop/rotor aircraft.
- If system testing is not conducted, then analysis shall be required to show the individual crashworthy components and subsystems function together effectively to achieve the desired overall level of crashworthiness.
- For vertical impacts calculations should include a 1 W rotor lift factor. This is also true for the retracted gear condition.
- For the case of retracted landing gear the seat/airframe/landing gear pod combination shall have a vertical crash impact design velocity change capability of at least 7 m/s (23 ft/sec) at an impact attitude within $\pm$ 10° roll and + 15 to - 5° pitch.
- Figure 8 applies for all impact conditions which include an attitude envelope of $\pm$ 10° roll and + 15° to - 5°, pitch.
- Neither seats nor litters should be suspended from the overhead structure unless the ceiling is capable of sustaining, with minimum deformation, the downward inertial loads from occupied seats or litters under crash conditions.
- It is desired that in a 15.25 m/s (50 ft/sec) vertical impact that the height of occupiable areas not be reduced by more than 50% and that the surrounding structure not fracture.
- For head impact protection, frangible items, such as optical relay tubes, shall break away at a total force not exceeding 300 pounds.
- It is desired that the landing gear continue to absorb energy even after fuselage contact has been made to maximize the protection afforded by the gear.
- Type II aircraft wings used to support external stores prevent roll over in many accidents and should not be frangible, but should allow the stores to separate under G loads while maintaining the structural integrity of the wing. However, the wing should break off before the fuselage itself collapses in order to maintain fuselage structural integrity.

CONCLUSIONS

- Many helicopter occupants are still being fatally injured in potentially survivable accidents, and the percentage of major injuries and rate of materiel losses are still high, even though the technology and design criteria presently exist to significantly reduce these losses.
- Army aviation mission effectiveness can be significantly enhanced through the application of crashworthiness design to Army helicopters.
- Life-cycle costs can be significantly reduced through the application of crashworthiness design to Army helicopters early in their life cycle.
- MIL-STD-1290A/ADS-36 is a practical, viable, and cost effective requirements document.
- Although higher levels of crashworthiness can be achieved in a complete new helicopter system design, significant improvements can be made in the crashworthiness of existing helicopters through retrofit programs.
- The need exists to continually improve/update helicopter crashworthiness design criteria and standards.
- Military crashworthiness features and technology have direct application to the civil/commercial fleet.

REFERENCES

1. Haley, Joseph L., Jr., "Helicopter Structural Design for Impact Survival,' presented at the Symposium on Environmental Effects on VTOL Designs, sponsored by the AHS, AIAA, and the University of Texas at Arlington, November 1970.

2. Desjardins, S. P., et al, "Aircraft Crash Survival Design Guide," USARTL Technical Report 79-22, 5 Vols., Applied Technology Laboratories (AVRADCOM), Ft Eustis, VA., 1980.

3. Military Standard MIL-STD-1290 (AV), "Light Fixed- and Rotary-Wing Aircraft Crashworthiness," 25 January 1974.

4. Aeronautical Design Standard 36, "Rotary Wing Aircraft Crash Resistance," USAAVSCOM, May 1987.

5. Military Specification, MIL-S-27422B Amendment 1, Tank, Fuel, Crash-Resistant Aircraft, Department of Defense, Washington, DC, 13 April 1973.

CRASHWORTHINESS DESIGN METHODS APPLICABLE AT CONCEPT STAGE

by

M. M. Sadeghi, Cranfield Impact Centre, Cranfield Institute of Technology, Cranfield, Bedford, MK43 0AL, England.

ABSTRACT.

For the effective incorporation of the secondary safety into structures developed for Aircraft, Cars etc. it is essential to tackle crashworthiness in the early stage of the development. For a set of defined loading conditions (crash or crush) to which the structure must comply, it is of great benefit to specify necessary guidelines for defining collapse zones, as well as structural properties concerning non-linear behaviour of constituent components and joints of the overall structure.

This paper describes a hybrid approach to predicting the crash behaviour of an impacting structure which is tailored to velocities which do not exceed 30-40 miles/h. The method involves using component and joint test data (as data base) in conjunction with coarse finite element idealisation to determine collapse mechanism sequence of the collapse and collapse speed of an impacting structure.

1. INTRODUCTION.

Transport and vehicle safety is governed by a number of factors. Such factors can be divided into two main categories of primary and secondary safety. Considerable effort is put into ensuring that vehicles are designed to perform to the required standard and the operator is well trained to understand the vehicle's limitations, as well as his own ability to operate the vehicle. Despite all the efforts to ensure compatibility between operator, vehicle and operating environment, accidents do occur. For such occasions secondary safety is designed into the vehicle to ensure a more survivable crash. Secondary safety is, in the main, concerned with the structural behaviour during an impact. Designing crashworthiness into a structure will provide the mechanism by which a proportion of impact energy is absorbed by the vehicle structure and a very small portion of initial deceleration is transferred to the occupant. To design crashworthiness into a structure effectively it is important to incorporate the work at the early stages of the concept design.

There are two methods of ensuring crashworthiness. One is by trial and error through the testing of prototype structures, the other is using a detailed mathematical model of the structure in a finite element analysis. To incorporate this type of purely theoretical simulation in the early stage of designing when detailed structural data is limited is found to be very difficult, on the other hand manufacture and testing of prototype structures is a very costly exercise. It is however, necessary to provide the engineers with a system or tool which can be used to study alternative design ideas for compliance with the required loading conditions.

Since plate elements do not contribute to energy absorption significantly and the majority of such contributions are due to beam type components, the finite element modelling can be simplified accordingly. Additionally, the difficulties encountered in the use of a fine finite element idealisation is overcome by combining any known experimental structural data with the limited available information on the design configuration to generate a much simpler model. The method aids the continuous assessment of the structural integrity for crash requirements throughout the development stage of a design. The parameters assessed are load carrying capabilities, energy absorption ability and general collapse properties of individual structural components as well as those of the overall structure.

Such information is then used to compute the dynamic behaviour of the complete structure as well as the speed of the collapsing structure relative to a fixed set of axis. In the case of a vehicle this dynamic information is subsequently used in a crash victim simulation program to evaluate the effect of structural collapse and vehicle body dynamics on the occupant injury level. An example of this method's application is the side impact studies carried out by CIC (Ref. 1.)

2. ANALYSIS TECHNIQUE.

In general the path taken by this technique is shown in Fig. 1 and includes the following steps:-

2.1) Component data base - since it is developed to be used at the start of a design project, this system requires component and joint data which is to be obtained through test or analysis. At such an early stage of the design the detailed information required for adequate analysis is not available and therefore, the non-linear data for components and joints is obtained through testing. Such data, once obtained, is stored in a data base to be accessed when necessary. Acquisition or manipulation of information from the data base constitutes the first step in this design technique.

2.2) Acquisition of component data by test or analysis - if for a particular design the data base cannot be used, the required component or joint is manufactured and tested to obtain the necessary non-linear properties. During the test the collapse mechanism and sequence of collapse for the section or joint is noted so that the failure of the section can be delayed or prevented by stablising the area where the fold lines or separation is initiated. The non-linear data acquired from such tests is added to the data base for future use.

2.3) Overall collapse analysis - once all non-linear properties of all constituent components and joints (strength and energy absorption ability) have been acquired, a quasi-static analysis of the complete structure or sub-structure is performed resulting in the total non-linear load carrying capability of the structure.

It is important to point out that this step (step 3) can only be taken when the following assumptions hold:-

a) The mass of the collapsing structure is negligible when compared to the retarding mass.

b) The direction of the loads on the collapsing structure during impact can be predicted in advance.

Such assumptions can be justified in a variety of crash situations such as a bus rollover, passenger car side impact, aircraft heavy landing and many other types of vehicle crashes.

If such assumptions could not be justified step 3 of this system is by-passed.

2.4) Structural optimisation - in addition to the load carrying capability curve resulting from step 3 the individual component's contribution towards strength and energy absorption is also computed. Such information aids the designer to single out incompatible components or joints for modification. The criteria examined is whether each and every component can transmit impact load throughout the structure and in the process absorb an appropriate portion of impacting energy. The design which ensures the maximum use of material to absorb energy will ensure distribution of deformation and thus avoid gross localised deflection. If step 3 cannot be carried out it is still possible to check the compatibility of individual components within the structure (step 2) be comparing their general load carrying capability rather than the specific one computed through step 3.

2.5) Improvement in components strength and energy absorption ability - once the incompatible components are singled out the extent and type of improvement is decided upon. In this step the analysis is to result in the choosing of the properties to be improved (bending, compression etc.) and by what percentage to bring incompatible components into line with the requirement.

2.6) Bending collapse calculation - having decided on the required properties (strength and energy absorption ability) the necessary calculation is carried out to determine the simplified section dimension (metal gauge, section dimensions) which under bending or compressive load would reach and maintain the necessary internal load.

2.7) Component and joint design - although the simplified section resulting from step 6 is adequate in the initial stages of design, it is only a guideline on the general section dimension

for the detailed design at the final stages of a project. In the design of passenger car components for instance, the simplified section required for crashworthiness is determined at the concept stage but due to various other requirements the section is turned to a complex configuration using simplified shapes as the datum data. On completion of the section design which may involve steps 2, 6 and 7, step 3 could be carried out to check the effect of the component's new section on the overall collapse property of the structure.

2.8) Dynamic analysis - in analysing for crashworthiness it is necessary to study the effects of individual mass initerias on the collapse mechanism. In general this problem can be studied in one of two ways.

If the mass of the collapsing structure compared to the retarding mass is negligible and the speed if impact is not very high (i.e. collapse due to bus rollover, car side impact etc.) the load carrying capability curve resulting from step 3 can be used as a non-linear spring property in a mass spring system of equations set up in step 8, to compute the speed of the collapsing structure. If however, there are significant masses within the collapsing structure the information obtained from steps 1, 2, 6 and 7 are directly used in step 8.

2.9) Occupant simulation - completion of step 8 where the velocity of the vehicle and the collapsing structure is known it may be necessary to consider the occupant or content safety during impact. This is of prime importance in the cases of bus and car rollovers as well as passenger car side impacts. Whilst step 4 ensures that load and deformation are distributed so that every structural component is used to disipate the energy, in this step timing or maximum structural speed in relation to the occupant is computed and the effect of structure - occupant impact on the occupant is determined.

2.10) Dynamic optimisation - if the results from step 9 show unacceptable levels of injuries on the occupant the complete analysis system is utilised again, modifying the appropriate structural components until the required crashworthy standard is achieved.

Such a method of design for crashworthiness can be used in any concept design stage where detailed structural information is not available or relatively quick and cost effective study is required. Fig. 2 represents one such circumstance.

3. APPLICATION.

The method described above has been applied to a variety of projects which are as diverse as vehicles, motorway safety barriers and offshore structures. The following three examples describe application of the method to automotive related crashworthy design.

a) Passenger car side impact.

This study, which can be part of the overall design (Fig. 2) involves steps 1 and 2 (Fig. 1), to generate the non-linear properties of components likely to absorb energy during a side impact. Using a collapse analysis model (Fig. 3), the load carrying capability curves were obtained and used in step 8 to check the validity of the method. The procedure to carry out this part of the analysis is reported in Ref. 2.

Fig. 4 shows the comparison between test and simulated side frame velocity. Using this information in step 9, occupant behaviour was simulated showing good correlation between test and simulation (Fig. 5 and 6). Having proved the validity of the system the structure was theoretically improved using a loop containing steps 2, 3, 4, 5 and 6 followed by steps 8, 9 and 10 (Figs. 7 and 8). Figs. 7 and 8 show the improvement achieved.

b) Passenger car seat.

The problem concerning the fitting of a three point belt in a rear centre seat of a passenger car where the seat back is a folding 2/3 - 1/3 arrangement is in two parts. Firstly the seat back must be strong enough to carry the required load through the belt (Fig. 9). Secondly the vehicle floor must be capable of carrying the transfer load through the seat mountings. The

requirements to comply with were, load due to a belted occupant in a vehicle experiencing 20g forward acceleration, 20g rearward acceleration as well as the load due to a 100kg of luggage behind the seat back. The criteria for the design is that the forward deformation at point 2 (Fig. 9) must not exceed 100mm. Having decided on the load path due to belt loading (Fig. 10) the appropriate joint and component were tested to determine their total load carrying capability curve. Each of the components were then redesigned to carry the extra load using material where required. Typical redesigned seat back behaviour is shown in Fig. 11. The occupant behaviour as a result of such a seat structure is shown in Fig. 12. The seat structure which could carry 4kN was modified to carry 16kN with an extra metal content of 2kg.

c) Bus rollover.

In a similar process the component data obtained by test or analysis (Ref. 3) was used in the collapse analysis of the super structure (Ref. 4) resulting in good correlation between test and analysis. In line with this project objective, steps 8, 9 and 10 were not utilised.

d) Aircraft structures.

The application of the methodology to aircraft structures has been on the possible loading of the underbody structure in heavy landing or crash landing situations. In such a crash case the behaviour of an aircraft seat and its lap belted occupants were also analysed aiming at a seat structure which reduces the acceleration level on the occupant to a specified low level.

In this analysis a number of different types of seat (metal or composite material) were considered. Typical structural finite element model used is shown in Fig. 13. The case study here has a Sierra dummy representing the centre seat occupant with equivalent weight bags representing the two side occupants. Results such as those shown in Figs. 14 and 15 are used in designing energy absorbers to be incorporated into the seat legs to reduce occupant acceleration levels.

e) Motorway safety fence impact.

In this project steps 2 and 3 were used to obtain a laod carrying capability curve of the barrier (Fig. 16). A simple dynamic model of a lorry (Fig. 17) was developed and impacted through a non-linear spring representing the fence against a solid stop simulating the barrier restraint. The simulated trajectory of a 15 degree angle impact of 50m/h velocity is shown in Fig. 18. Despite the simplicity of the model and lack of data to model the lorry, reasonably good correlation between test and simulation was achieved (Fig. 19). Step 9 was also carried out to predict the drivers movement during impact (Fig. 20). A number of modifications were tried to examine the impact situation involving lorry, articulated lorry and passenger car against metal and concrete motorway barriers for the impact speed of 50m/h, the angle of impact was 15 or 20 degrees. A comparison between simulation and test for passenger car is shown in Fig. 19).

CONCLUSIONS.

Through applications to numerous problems it is shown that if within each step, the necessary code is developed and tailored to a given impact condition, this system of design for crashworthiness can be cost effectively applied at the early stages of the design enabling engineers to take the necessary steps in the design sequence and avoid unnecessary and often difficult analysis, made more difficult due to lack of data.

REFERENCES.

1. SADEGHI, M.M., SUTHURST, G.D., NG, P., Inclusion of Crashworthiness in Concept Design, 10th Int. Conf. on Experimental Safety Vehicle, Oxford, 1985.

2. SADEGHI, M.M., SUTHURST, G.D., Test Aided Computer Prediction of Passenger Car Side Impact, ISATA Conference, Wolfsburg, 1982.

3. KECMAN, D., Bending Collapse of Rectangular and Square Section Tubes, 4th Int. Conf. on Vehicle Structural Mechanics, Detroit, Michigan, 1981.

4. TIDBURY, G.H., SADEGHI, M.M., KECMAN, D., Alternative Methods of Evaluating a Bus structure for the Proposed Rollover Safety Regulation, Int. Conf. of Bus Experts, Budapest, 1981.

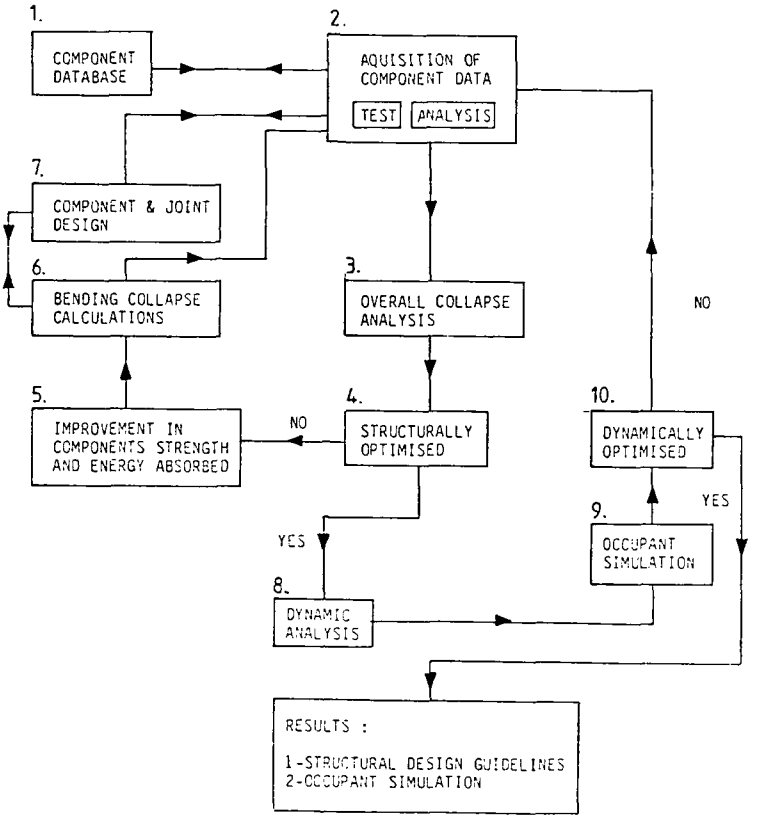

FIG. 1. DESIGN FOR CRASHWORTHINESS

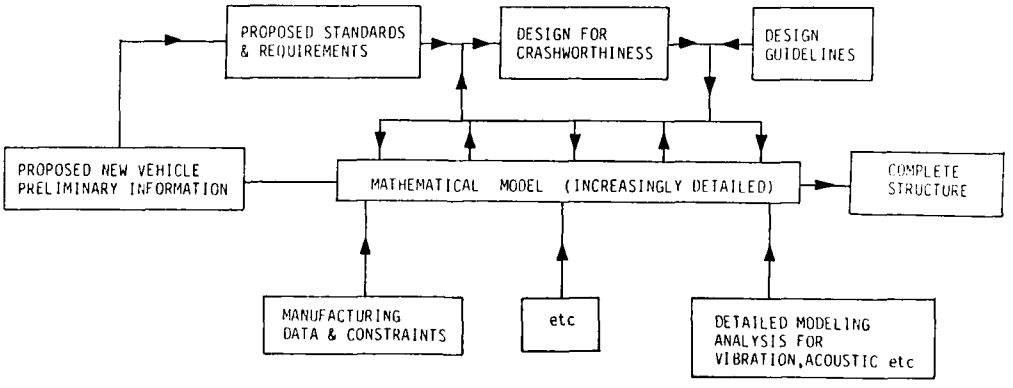

FIG. 2. INCLUSION OF CRASHWORTHINESS IN THE DESIGN OF STRUCTURE AT CONCEPT STAGE

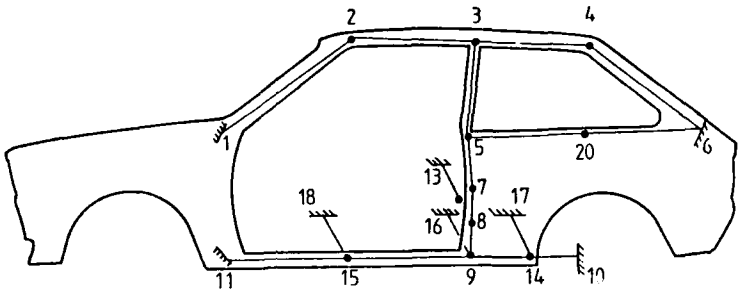

FIG. 3. IDEALIZATION OF BASELINE STRUCTURE (MODEL 1 & 2)

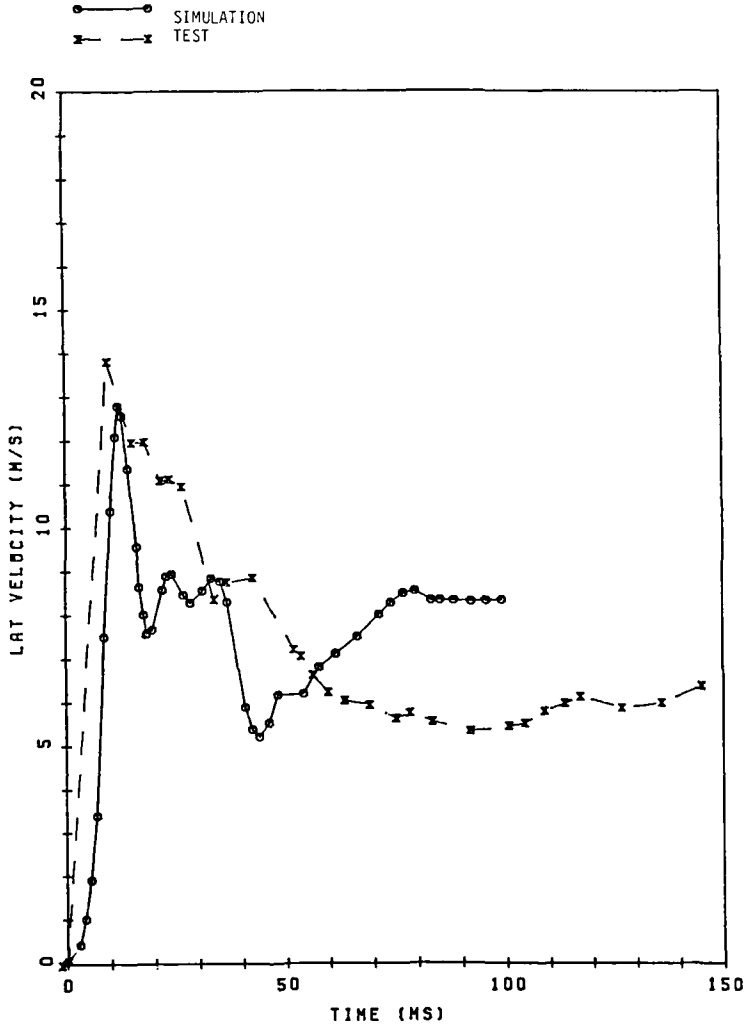

FIG. 4. SIDEFRAME VELOCITY

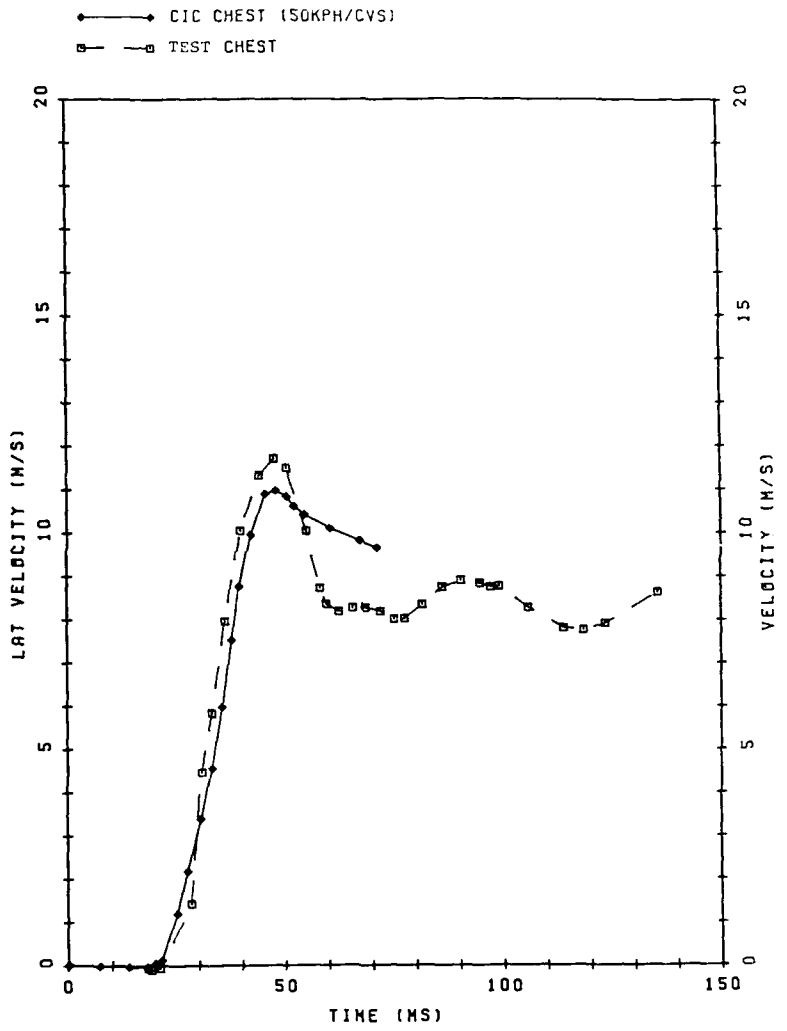

FIG. 5. SIDE IMPACT COMPARISON

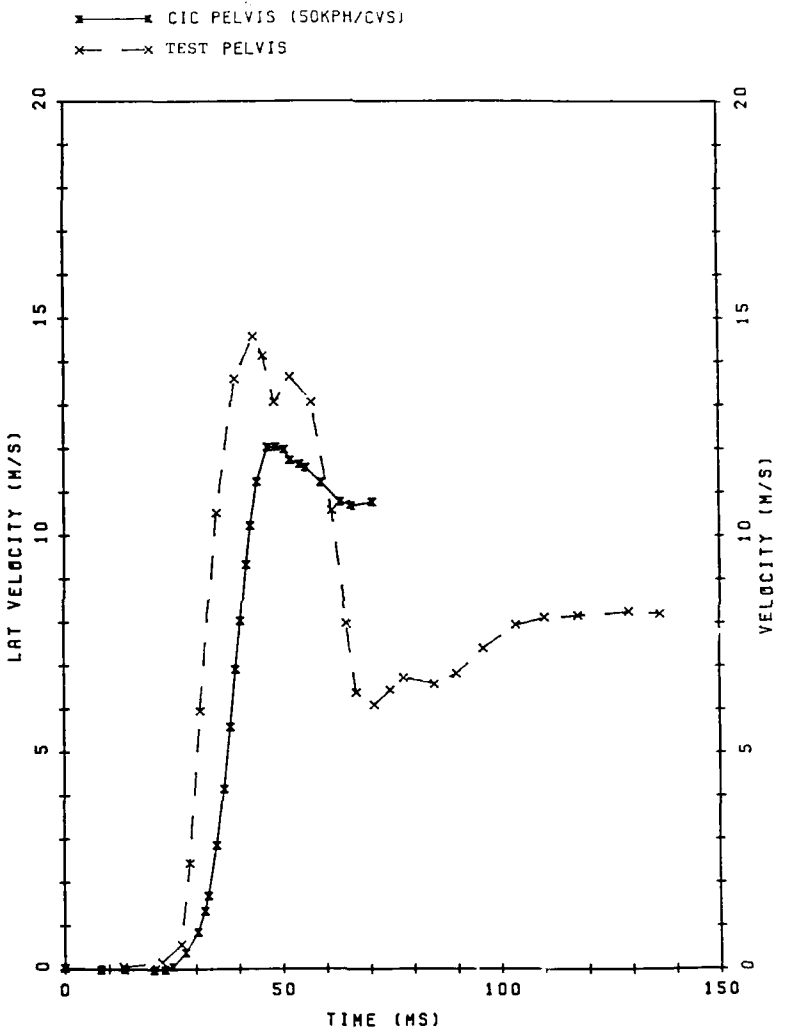

FIG. 6. SIDE IMPACT COMPARISON

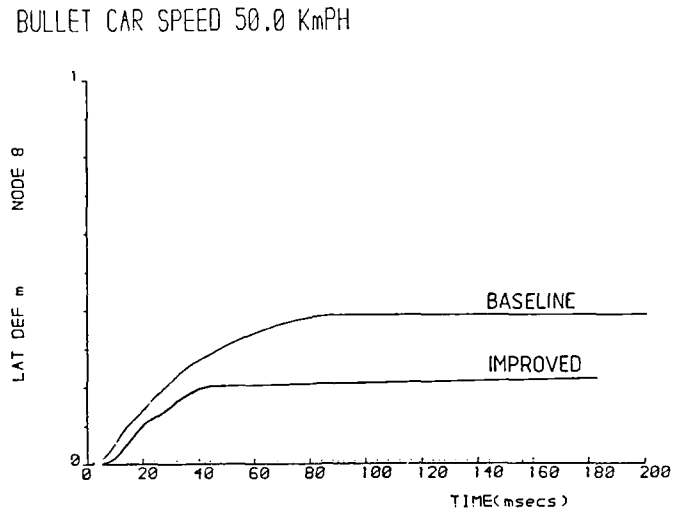

FIG. 7. SIDE IMPACT ON 3-DOOR BASELINE

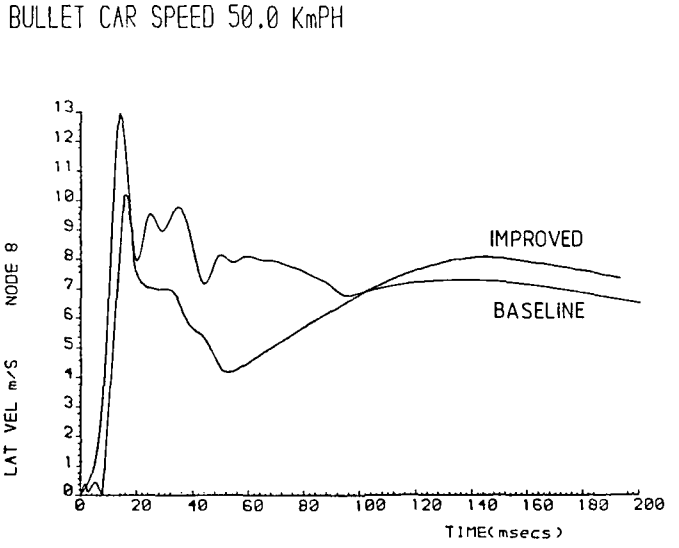

FIG. 8. SIDE IMPACT ON 3-DOOR BASELINE

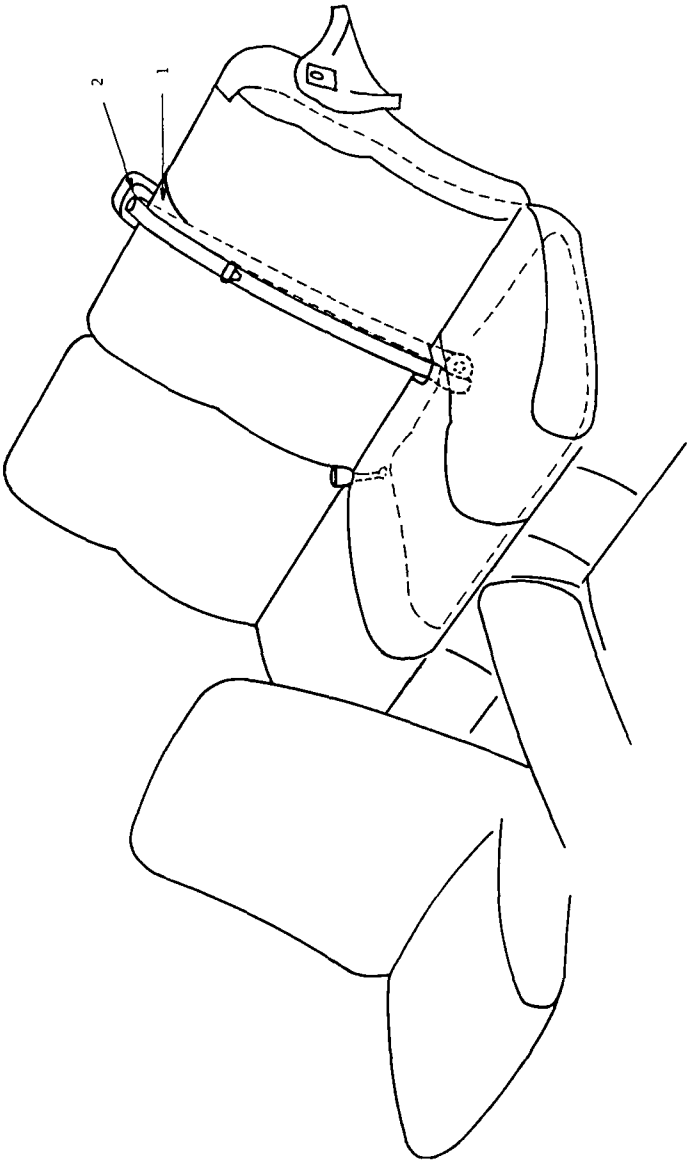

FIG. 9. SEAT LAYOUT

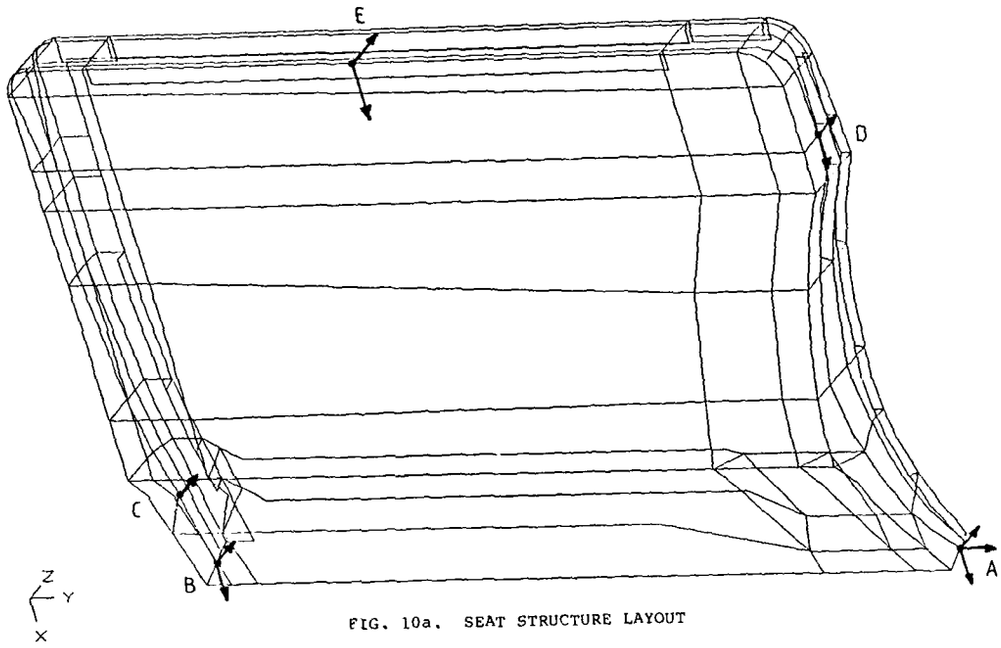

FIG. 10a. SEAT STRUCTURE LAYOUT

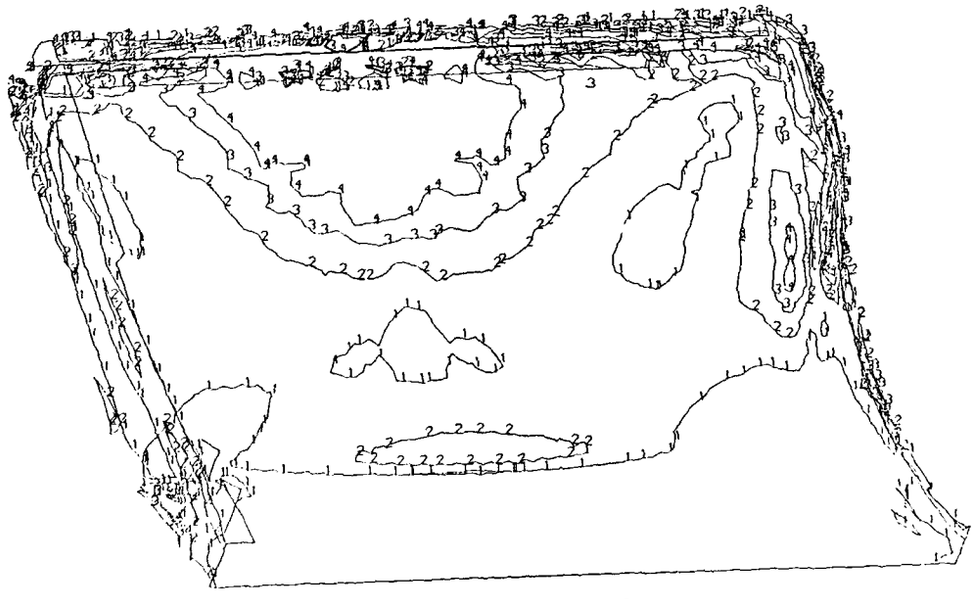

FIG. 10b. STRESS PATTERNS

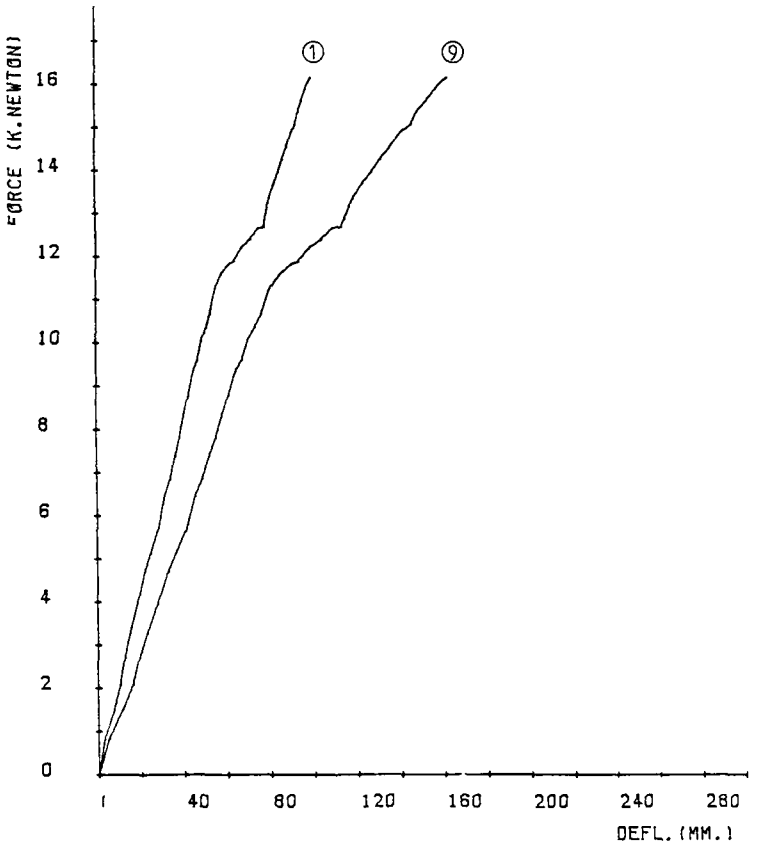

FIG. 11. LOAD IN LINE WITH POINT 1

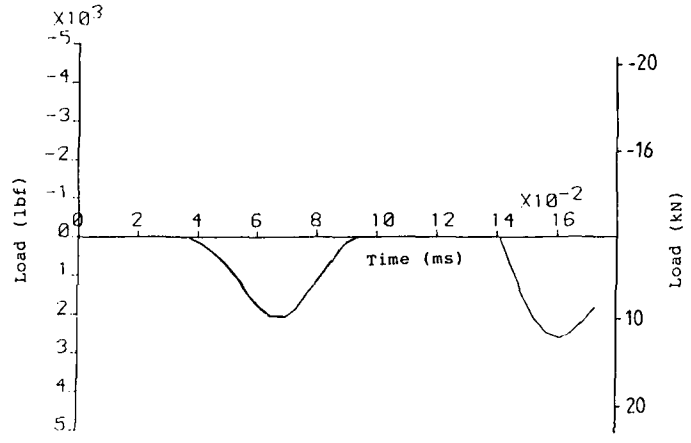

FIG. 12a. LAP BELT LOADS (RIGHT AND LEFT)

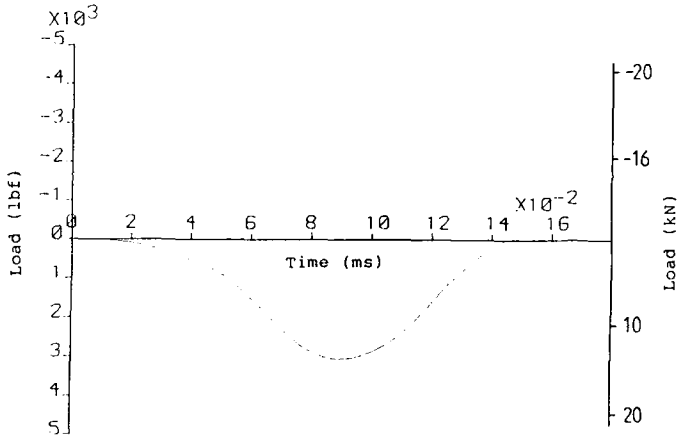

FIG. 12b. SHOULDER BELT LOAD

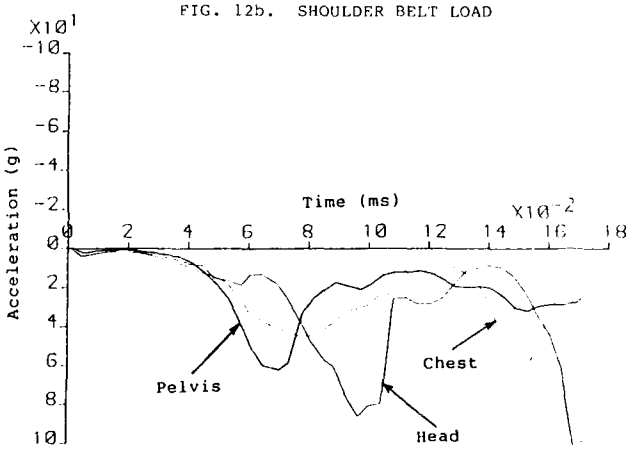

FIG. 12c. RESULTANT ACCELERATIONS

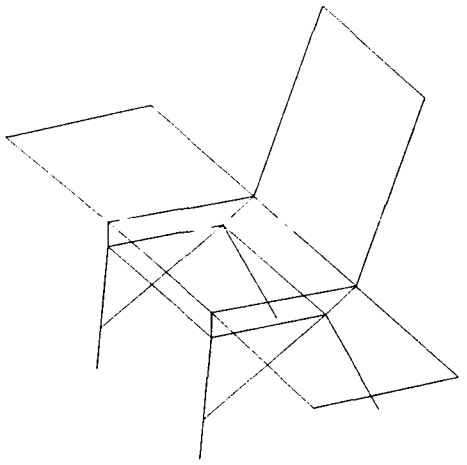

FIG. 13. TRIPLESEAT "A" CIC SIMULATION - TIME = 3ms

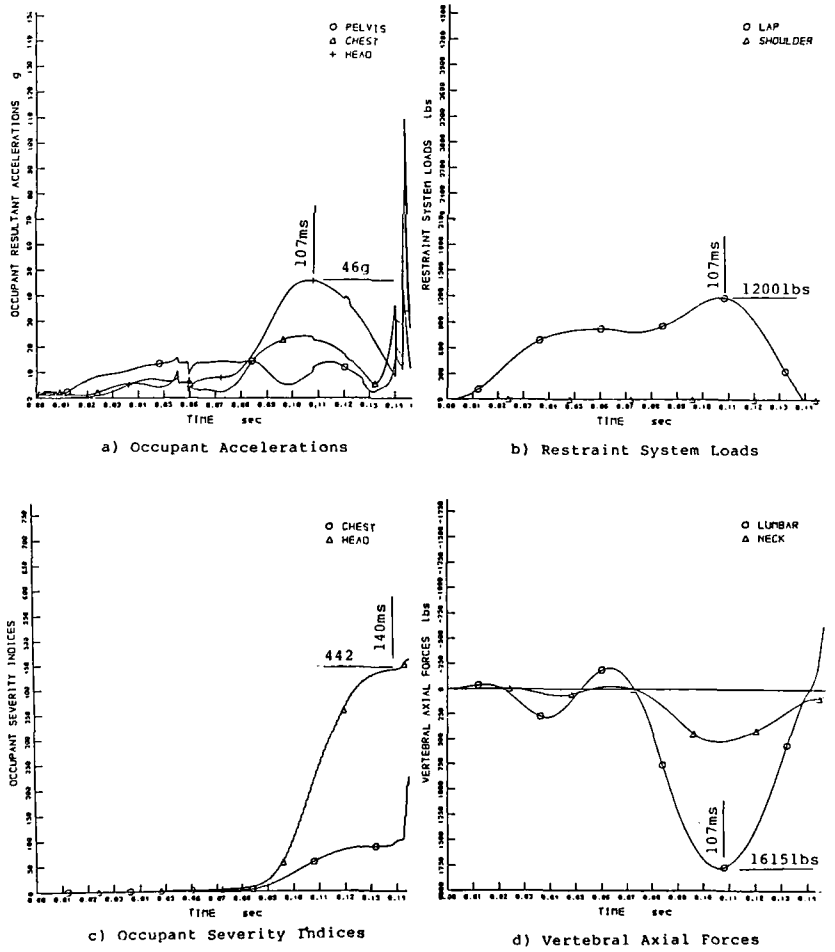

a) Occupant Accelerations

b) Restraint System Loads

c) Occupant Severity Indices

d) Vertebral Axial Forces

FIG. 14. TRIPLESEAT "A" CIC SIMULATION - TIME = 3ms

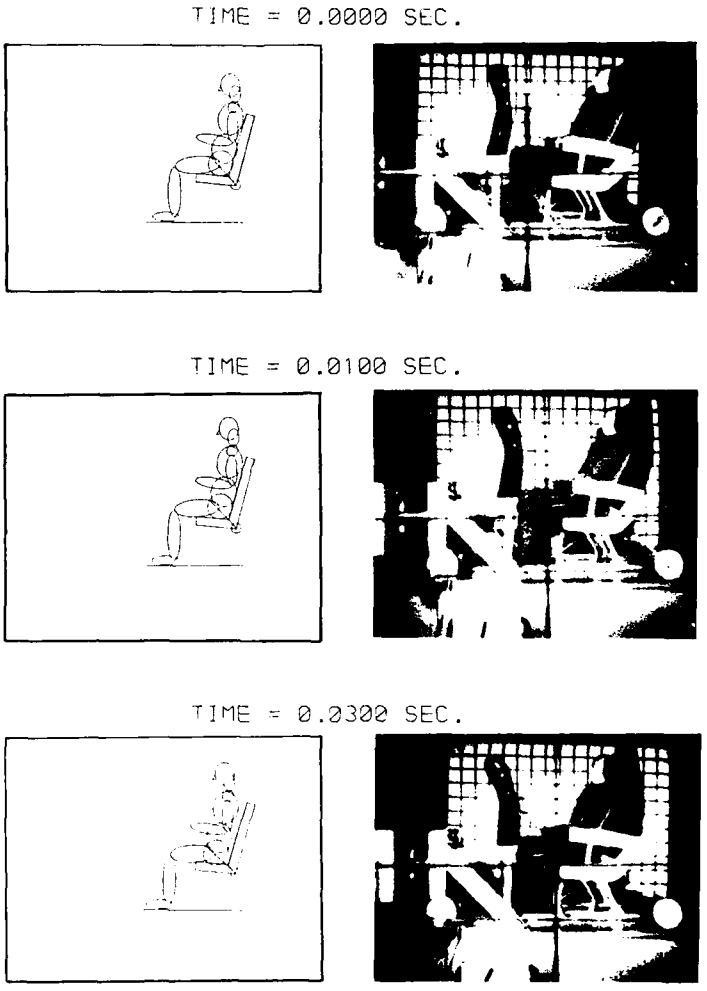

FIG. 15. COMPARISON OF SIMULATION AND TEST

TIME = 0.0600 SEC.

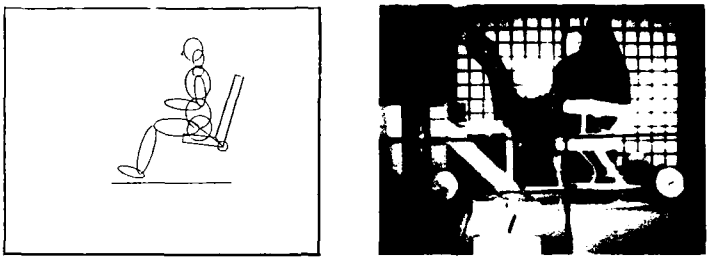

TIME = 0.0900 SEC.

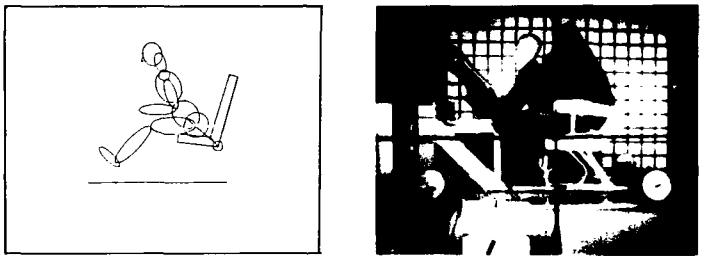

TIME = 0.1200 SEC.

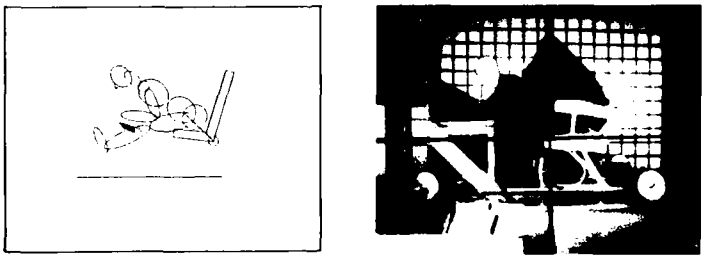

FIG. 15. COMPARISON OF SIMULATION AND TEST (CONT.)

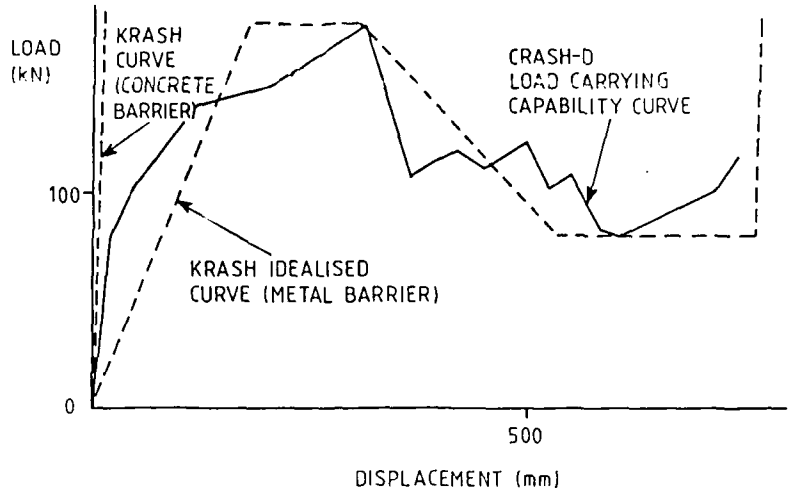

FIG. 16. BARRIER/EXTERNAL SPRING LOAD CARRYING CAPABILITY CURVE

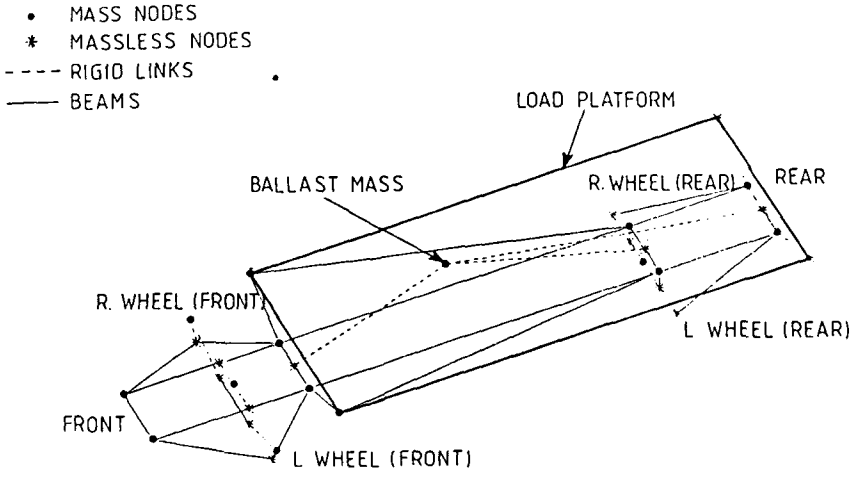

FIG. 17. RIGID CHASSIS LORRY MODEL

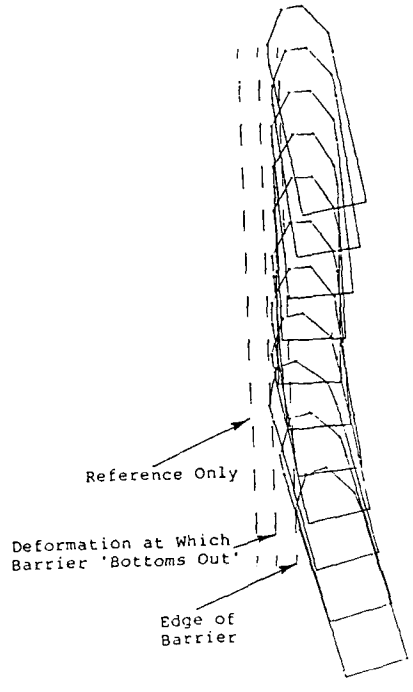

FIG. 18. VEHICLE TRAJECTORY BASELINE RUN

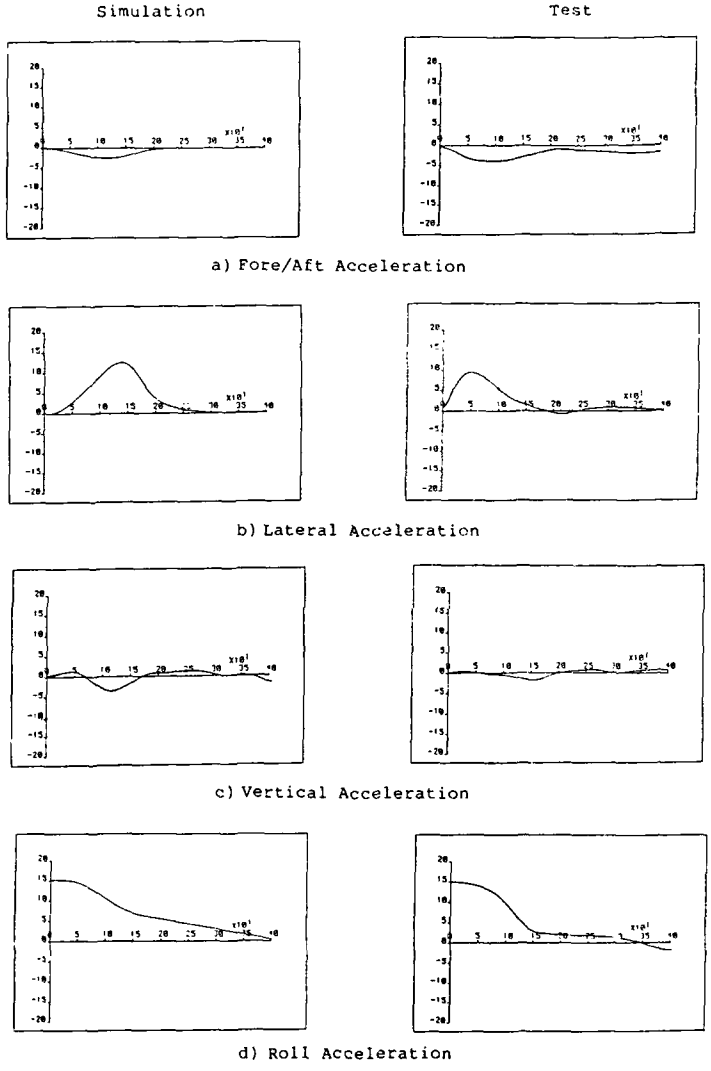

FIG. 19. ACCELERATION (G) VS TIME (MILLISECONDS)

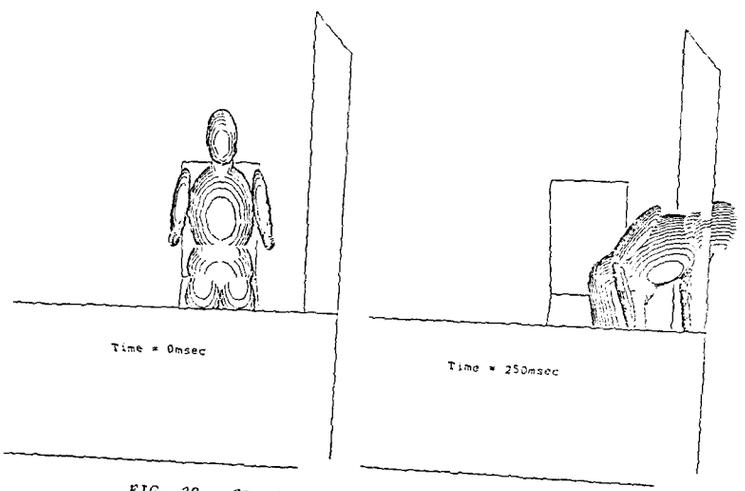

FIG. 20. CRASH VICTIM SIMULATION (FRONT VIEW)

CRASHWORTHINESS ACTIVITIES ON MBB HELICOPTERS

by
F.Och
Messerschmitt-Bölkow-Blohm GmbH
Postfach 80 11 40
8000 München 80, Germany

SUMMARY

Crashworthiness activities at MBB date back to the late sixties, when during BO 105 development crash protection systems such as seats, fuel systems, and landing gears were developed which are integrated in the military versions of the BO 105 for the German Army.

In February 1974 a BO 105 was crash tested to show compliance with the Crash Survival Design Guide (TR 71-22) under an impact condition of 15 m/s longitudinal and 8 m/s vertical velocity.

Since the mid seventies theoretical studies were conducted with the aid of the computer programme KRASH and nonlinear finite element codes, supported by the German Ministry of Defence, and partly verified by component tests.

The experience with the crash behaviour of the BO 105 was successfully used for the development of the BK 117 which has been shown by a full-scale crash test, conducted in 1985 by Kawasaki, MBB's partner of the BK 117 development.

Effective design tools, both in house and at subcontractors and experience with helicopters in service are used at MBB to contribute significantly to fulfill the crash requirements in European helicopter programmes and in joint developments with foreign partners.

Although crash protection techniques and crashworthiness prediction methods are already fairly well established, there remain still a lot of tasks, mainly when using advanced materials and in improving the analytical methods from an economic point of view.

1. INTRODUCTION

Of course, MBB helicopters like all others, are designed and built to safely fly and not to crash. Accident prevention, i.e. active safety, therefore is treated with high priority [1], e.g. by

- improving manoeuvrability through application of hingeless rotor systems, like "System Bölkow", with which MBB's BO 105 and BK 117 are equipped, or MBB's rigid rotor with elastomeric bearing (FEL), with which the German-French antitank helicopter PAH2 and the Indian Advanced Light Helicopter ALH will be equipped;

- installing redundant vital systems, such as the twin-engine design with single-engine capabilities or dual hydraulic for primary flight controls;

- applying damage-tolerant structures, like glass/carbon fibre rotor blades which are an essential design feature of MBB's hingeless rotor systems, or rotor shafts and hubs made from materials with high fracture toughness, such as high purity steel or titanium alloy.

But nevertheless there will be technical failures and/or human errors that may result in varying degrees of accidents. Especially military helicopters, to reduce detectability, often will operate at extremely low altitude, below tree level if possible, taking advantage of cover afforded by the landscape and thus exposing the occupants to high-risk situations where accidents may occur.

Crashworthiness activities at MBB therefore date back to the late sixties, when during BO 105 development crash protection systems such as seats, fuel systems, and landing gears were developed with the aim of preventing or reducing occupant injury and hardware damage.

2. CRASHWORTHINESS DESIGN FEATURES

Crashworthiness engineering is designing to prevent occupant fatalities, to minimize the number and severity of occupant injuries, and to minimize, to the maximum extent practical, aircraft damage, when the helicopter is exposed to crash environments. This requires that the energy absorbing systems of the helicopter be designed so that the occupant will not be exposed to incapacitating injury prior to or after the various parts expend all of their required energy absorption capacity. The decelerative forces on the occupants must be reduced to levels that the human body is capable of withstanding. Large mass items, which would normally pose a hazard to personnel, must be located and the support structure designed so as to preclude their penetration into occupied areas. A habitable space must be maintained around the occupants when proper use is made of seats, belts and other safety design provisions. Postcrash hazards must be avoided by providing for sufficient size and number of exits to allow occupant escape after the crash sequence, including ditching, is over and by minimizing spillage of flammable fluids and by preventing their ignition to the maximum extent practical during and after all survivable crash impacts.

2.1 Seats

One major crash-protection function of the seat is to prevent the occupant from experiencing injurious accelerative loadings, primarily in the vertical direction for which the spinal column is the weakest, by energy attenuation.

The primary mechanism for absorbing crash energy is to apply a force over a distance. The larger the distance through which the force acts, the lower the average load on the occupant for a given energy to be absorbed and a given efficiency. The design aim is to dissipate kinetic energy irreversibly rather than convert and store it elastically and in particular restitution is to be avoided. Devices used should be of a load-limiting design with a more-or-less rectangular force-displacement characteristic.

From past experience we know that plastic deformation of metals fulfils the above described requirements and results in a reasonably efficient energy-absorbing process.

In aircraft design, where weight minimization is important, structural elements should directly be used in energy-absorbing systems, perhaps with slight modifications.

One such element, we have studied at MBB, is based upon tube expansion and seemed us to be easily applicable to an integral concept of lightweight seats in tubular design.

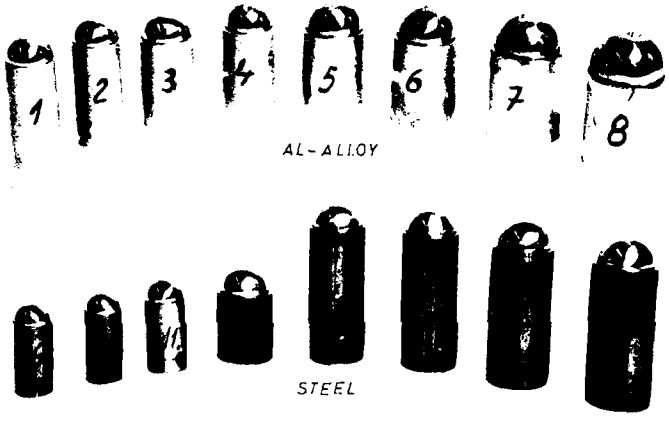

Figure 1. Tubes Expanded by Oversized Steel Balls

As shown in Figure 1, thin-walled, circular cross-section metal tubes of aluminium-alloy and mild steel have been expanded by pressing a hardened, oversized steel ball through them. The force required to expand the diameter and to overcome friction is used for energy absorption. A typical, almost ideal rectangular force-displacement characteristic is shown in Figure 2.

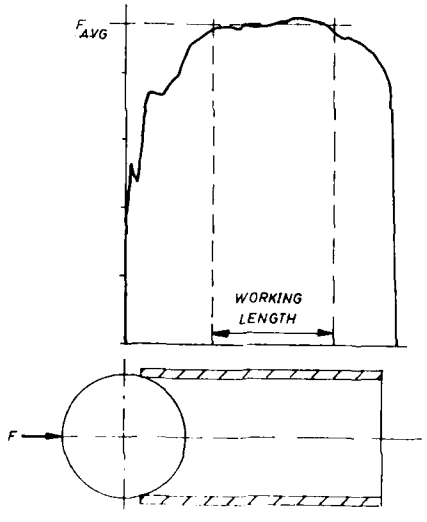

Figure 2. Tube Expansion Force-Displacement Characteristic

The tests have been conducted under quasi-static conditions with a loading velocity of 0.5 mm/sec and without lubrication.

Depending upon the tube material and the ratio of ball diameter to inner diameter of the tube, a boundary effect on a length of 0.4 to 1.0 times the ball diameter was noticed on both ends of the tube. The variation in the stroking load over the remaining (working) length generally was very small, with the exception of the tubes made of AlMg 5, which can be found from the test results shown in Table 1.

Table 1. Test Results from Tube Expansion

No.	Tube Material		Tube Cross Section mm	Ball Diameter mm	Stroking Load [1] kN F_{PEAK}	Stroking Load [1] kN F_{AVG}	Specific Energy Absorption [1] [2] kNm/kg	Remarks
1	Aluminium Alloy	3.1354T3 (W3125.5) S_y = 290 N/mm² S_{ult} = 440 N/mm²	25 x 1	24	3.40	3.30	16.2	
2					3.15	3.10	15.2	
3			30 x 2	27	9.60	9.40	19.8	
4					11.50	11.50	24.2	
5			35 x 2.5	32	34.20	-	-	no working length
6					27.20	27.20	39.5	
7		AlMg5 S_y = 200 N/mm² S_{ult} = 280 N/mm²	40 x 3	35	11.70	8.20	23.5	
8				38	20.20	-	-	tube failed
9	Mild Steel	1.7214.9 S_y = 520 N/mm² S_{ult} = 650 N/mm²	25 x 1	24	7.32	7.32	12.5	
10					7.50	7.50	12.6	
11			28 x 1	27	7.02	7.02	10.6	
12					6.80	6.80	10.3	
13			40 x 3	35	26.80	26.80	9.9	
14					25.80	24.50	9.0	
15					24.40	24.10	8.9	
16				38	62.50	60.50	22.2	
17					61.00	60.00	22.1	

Note: [1] Measured during working length
[2] Ball weight not considered

Besides being used on seat struts or support, this device can also be used as a load limiter in landing gears or in the supporting structures for heavy mass items.

Another element, which is well suited for energy absorption and which can be used to directly support the seat-pan, is a block of aluminium honeycomb. The relatively constant force required to crush honeycomb materials parallel to the longitudinal axis of the cells is used for energy absorption, as shown in Figure 3. The block length, i.e. the remaining thickness of the honeycomb when bottoming occurs, was found to be about 25% of the original thickness.

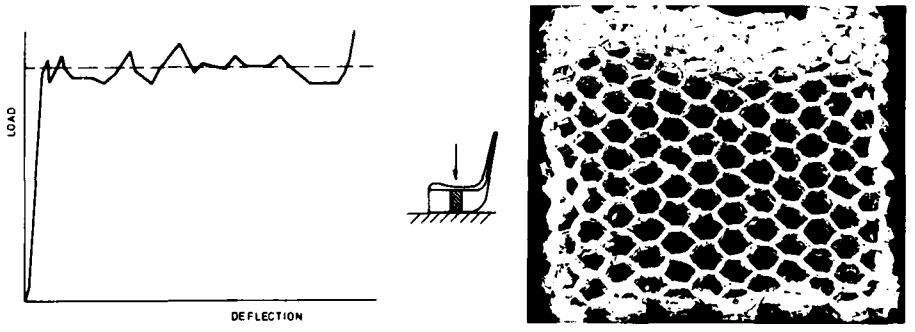

Figure 3. Load-Deformation Curve of Aluminium Honeycomb

In order to provide sufficient stability and transverse load resistance, we found that overall proportions must be chosen so that the thickness of the honeycomb block does not significantly exceed the width or the length of the block or parts of the piece, when not a parallelepiped, or when relatively large lightening holes are used, as shown in Figure 4.

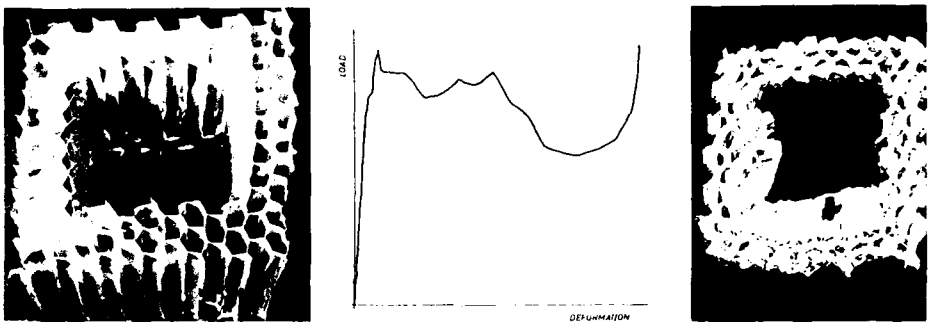

Figure 4. Load-Deformation Curve of Aluminium Honeycomb with Lightening Hole

As load limiter for the BO 105 crew seats we use an aluminium honeycomb energy absorption system, as shown in Figure 5.

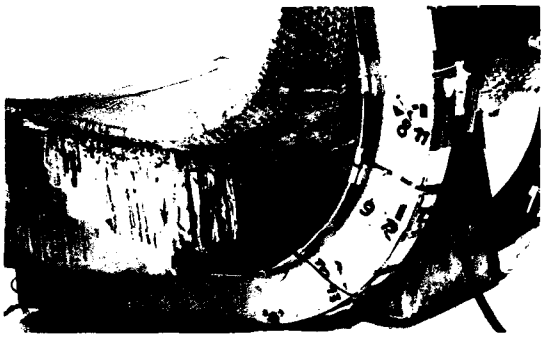

Figure 5. BO 105 Crew Seat with Aluminium Honeycomb Energy Absorption System

The crush load and thus the factor of deceleration rate can easily be varied for a given honeycomb system by just varying the impacting area, as shown in Figure 6.

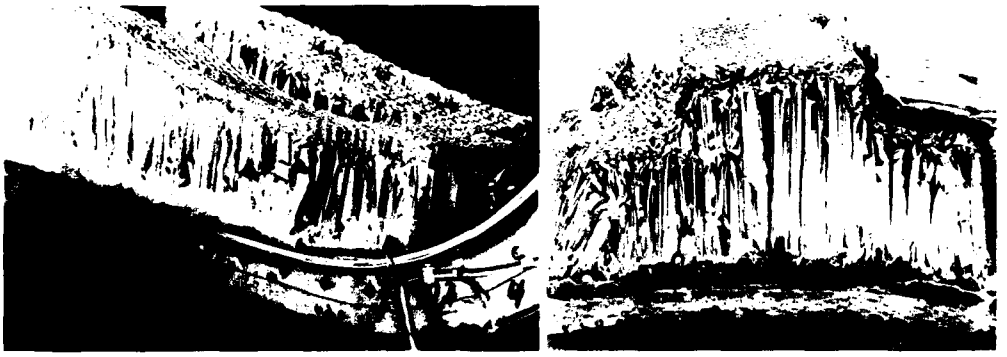

Figure 6. Crushable Seat Structures for Different Deceleration Rates

Although we did not notice during material testing an initial high load peak, as mentioned in the literature, we precrush the honeycomb about two millimeters to initiate buckling and to insure that instantaneous deceleration rates will not exceed those at the buckling load level.

2.2 Landing Gear

During most of the helicopter crash attitudes, the landing gear is the first element to come in contact with the ground.

Since the helicopter spends a large percentage of its operational life in the low-speed, low-altitude flight regime, accidents predominantly occur with high vertical descent rates and with the aircraft in a near normal attitude. The landing gear, including the skid-type, for improved crashworthiness must protect the fuselage against contact with the impact surface to as great an extent as possible and once its strength and its energy-absorbing capability is exceeded, it must be sure that the landing gear failure does not increase danger to occupants, either by penetrating the occupiable areas or by rupturing flammable fluid containers. Both during and after impact the landing gear must provide lateral stability to the fuselage and thus prevent it from overturning in the majority of cases.

At MBB's BO 105 and BK 117, skid-type landing gears use the plastic deformation of aluminium alloy cross tubes in bending as an energy absorption system. The BO 105 landing gear is capable of absorbing the energy developed for a 2,500 kg gross weight helicopter with 1 g rotor lift at about 4 m/sec sink rate. The capability of the cross tubes to bend vertically without failure until the fuselage contacts the ground provides lateral stability to the helicopters for higher sink rates and avoids danger to occupants.

To improve energy absorption in lateral direction during a vertical impact including a simultaneous fuselage angular alignment in roll, MBB has developed splitting tubes to attach the cross tubes to the fuselage, as shown in Figure 7.

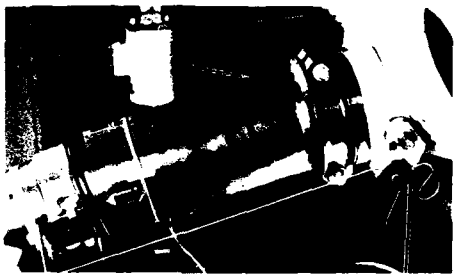

Figure 7. BO 105 Landing Gear with Splitting Tube

The energy is absorbed simultaneously in a combined mode of axial splitting and subsequent curling of the split ends of tubes and by friction when pressed axially against a die.

Figure 8. Split and Curled Tubes

Figure 8 shows steel and aluminium-alloy tubes that have been split and curled. To start splitting the tubes have been notched aequidistantly at the circumference.

A typical, almost ideal rectangular force-displacement characteristic for aluminium-alloy tubes is shown in Figure 9.

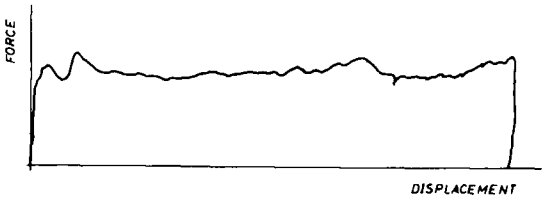

Figure 9. Force-Displacement Characteristic of Splitting Tube

The tests have been conducted under quasi-static conditions with a loading velocity of 0.5 cm/sec. The tubes made from steel 1.7734.4 showed after an initial high load peak with nearly twice the average load, an almost constant load-displacement curve. A similar behaviour was noticed on tubes made from steel 1.4544.9, of wall-thicknesses larger than 1.0 mm, with the exception that the initial peak was about 50% higher than the average load. No initial load peak was found with tubes made from steel 1.0333.5 and from aluminium-alloy. The variation in the stroking load after the initial peak generally was relatively small, especially for steel 1.7734.4 and aluminium 3.4335T6. The test results are shown in Table 2.

Table 2. Test Results from Welded Splitting Tubes

No.	Tube Material		Tube Wall Thickness mm	Number of Notches	Stroking load kN		Specific Energy Absorption kNm/kg
					F_{PEAK}	F_{AVG}	
1	Steel	1.7734.4	1.2	10	46.5	28.5	9.1
2		S_y = 540 N/mm²	1.5	12	>100	52	13.0
3		S_{ult} = 700 N/mm²	2.0	12	114	65	12.4
4		1.0333.5	1.5	10	51	42	10.3
5		S_y = 270 N/mm²	2.0	12	37	33	6.3
6		S_{ult} = 280 N/mm²	2.5	12	80	65	9.7
7		1.4544.9	1.0	10	26	24	8.9
8		S_y = 205 N/mm²	1.5	12	54	37	9.2
9		S_{ult} = 500 N/mm²	2.5	12	70	43	6.5
10	Aluminium Alloy	3.3214T6	2.0	16	20	15	8.2
11		S_y = 110 N/mm² S_{ult} = 210 N/mm²	2.5	16	33	29	12.6
12		3.4335T6	1.5	12	12.5	10	7.1
13		S_y = 280 N/mm²	1.6	16	11	8.5	5.8
14		S_{ult} = 360 N/mm²	2.0	16	17.5	15	8.0

Note: Tube Diameter 92 mm
Die Radius 20 mm

The BO 105 cross tubes are supported in the landing gear attachment fittings by pivoted bearing rings and conical elastomeric bushings that form an integral part with tightening clamps to prevent lateral movement.

The military versions of the BO 105 for the German Army have been equipped with splitting tubes, as shown in Figure 10, leading to a significant improvement of crashworthiness in lateral direction, as shown in Figure 11.

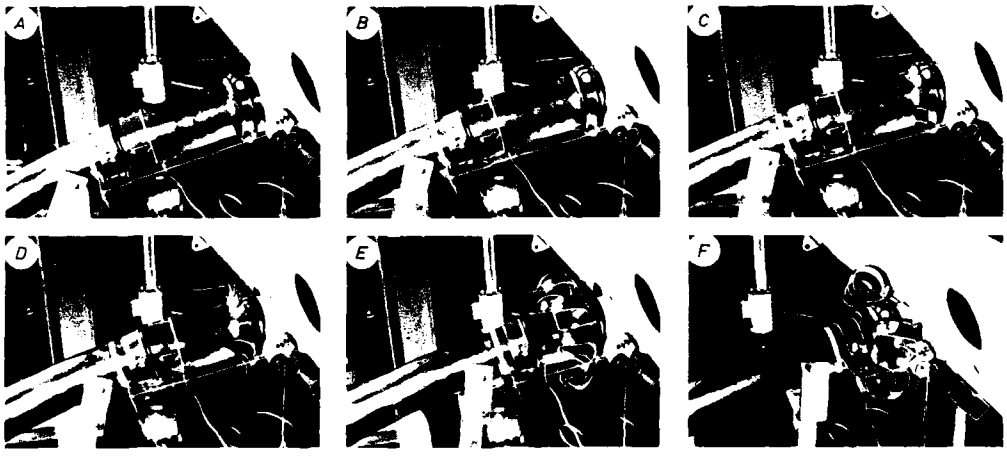

Figure 10. Behaviour of Splitting Tube at Lateral Displacement of Landing Gear

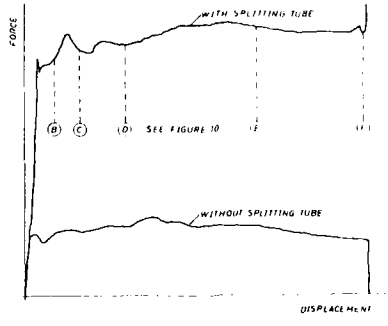

Figure 11. Force-Displacement Curve of Landing Gear with and without Splitting Tube under Lateral Loading

2.3 Airframe Structure

Besides carrying the normal flight and ground loads, the airframe structure should absorb a significant amount of impact energy and still maintain a protective shell when a crash occurs.

The MBB helicopters BO 105 and BK 117 are characterised, e.g. by a fuselage cross section, which is nearly ellipsoidal, to avoid inward buckling; by box-type main frames to ensure that premature failures due to local instability are minimized; by a continuous high strength structural floor, which in combination with rugged but deformable longitudinal subfloor beams minimize fuselage separation potential; and by extended crash load factors for heavy mass items to prevent hazards to personnel.

At MBB, the energy-absorbing capability of the structure beneath the floor is regarded to be extremely important because helicopter crashes typically involve a relatively high vertical deceleration component. Investigations started in the seventies, when a crash research programme, sponsored by the German Ministry of Defence, has been conducted at Vereinigte-Flugtechnische Werke (VFW), Bremen, now part of MBB.

The objective of these investigations is to develop crashworthy subfloor systems, which allow for controlled structural collapse to absorb energy and to limit the vertical loads to human tolerance levels over as much distance as possible.

Up to now, more than hundred specimens with various load-limiting concepts were constructed at MBB and tested statically and dynamically to evaluate their performance. The test specimens comprised flat panels as well as I-shaped and box-type structures, both in metal and in composite materials. The concepts included stiffened sheet panels with variations of the relevant parameters, sine-wave panels, corrugated panels, and sandwich panels. To arrive at nearly constant loads for a range of displacements, we investigated different triggering systems, A few examples of the test specimens are shown in Figure 12; more detailed information is given in another paper [2] presented at this AGARD meeting.

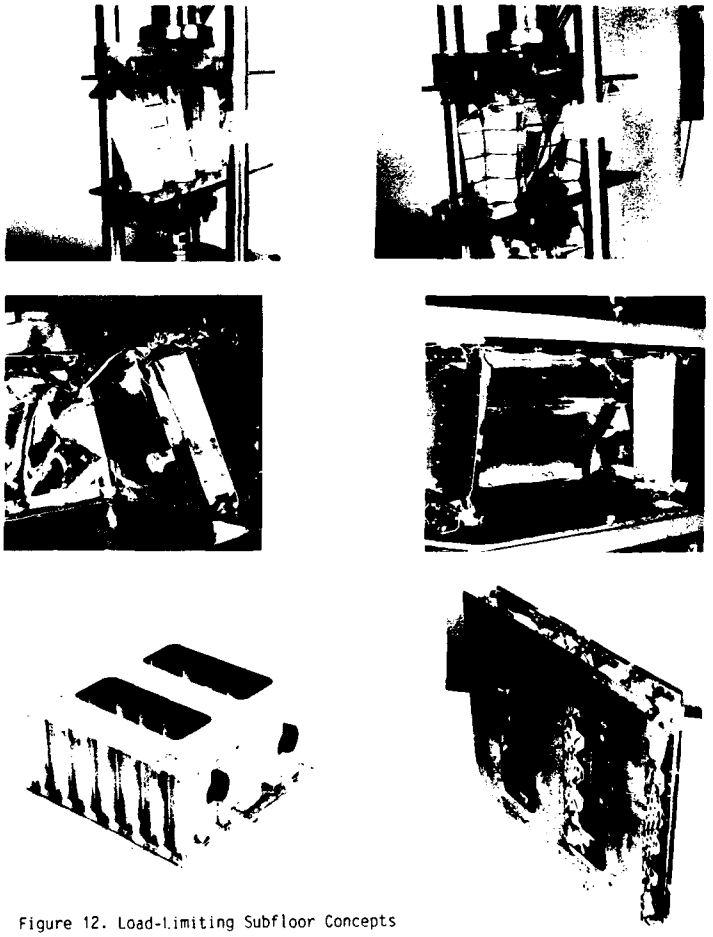

Figure 12. Load-Limiting Subfloor Concepts

2.4 Fuel System

Postcrash fire prevention is primarily to avoid or at least minimize spillage of flammable fluids during and after survivable crash impacts. Besides self-sealing breakaway couplings; frangible attachments; self-sealing fuel lines; and anti-spillage vent valves, particular attention must be given to the derivation of fuel tank bladder material that is cut, tear and rupture resistant while incorporating energy-absorbing ability to withstand internal pressure as well as perforation by broken structural components. Since the crash-resistant fuel tanks account for the largest weight penalty of any helicopter crash protection system components, weight saving is of special importance when deriving bladder material.

In the early seventies, MBB investigated tensile strength and strain of potential bladder material from several manufacturers. The tests have been conducted at room temperature, the results are shown in Table 3.

Table 3. Results of Strength Tests on Potential Bladder Material

No.	Loading Velocity	Material Type	Tensile Strength[1] N/mm²	Failure Strain %	Remarks
1	30 mm / min	A	8.8	39	Specimens in accordance with DIN 53504
2			9.6	40	
3		B	9.7	42	
4			9.3	43	
5		C	7.0	53	
6			7.4	55	
7		D	9.0	130	
8			8.8	102	
9	100 mm / min	E	12.3	1526	Length: 130 mm Width: 22 mm
10			12.2	1616	
11			12.3	1542	
12			11.9	1644	
13			11.4	1486	
14		F (PF 615)	10.7	1548	Length: 130 mm Width: 26 mm
15			10.6	1582	
16			9.3	1440	
17			11.0	1564	
18			11.2	1582	

Note: [1]) With reference to original cross section

For further material selection we conducted constant-rate-tear-tests, impact-penetration-tests and impact-tear-tests, as specified in the U.S. Military Specification MIL-T-27422B. The test setups and the test results are shown in Figure 13 to Figure 15 and in Table 4.

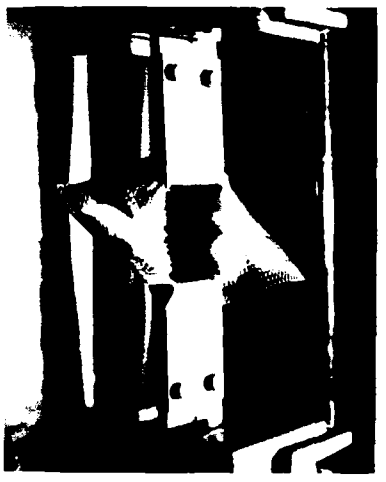

Figure 13. Constant Rate Tear Test Setup

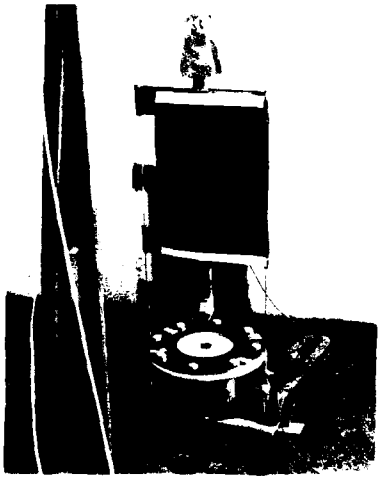

Figure 14. Impact Penetration Test Setup

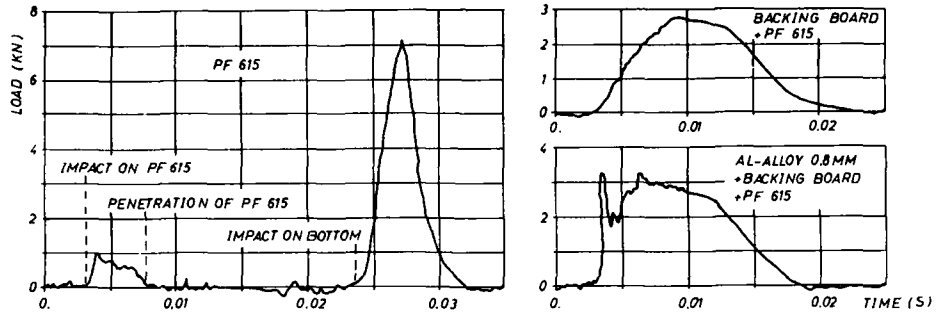

Figure 15. Load-Time Histories of Different Materials During Impact Penetration

Table 4. Results of Preproduction Tests on Potential Bladder Material

No.	Material	Constant-Rate-Tear-Test Energy Absorption Nm	Impact-Penetration Test Leakage after Impact?	Impact-Tear-Test Length of Tear mm
1	PF 615	27	yes	80[1]
2	MBB Backing-Board	73	not tested	110
3	MBB Backing-Board + PF 615	108	yes, when B-B clamped no, when B-B loose	60
4	ARM 062	655	not tested	5
5	ARM 063	608	no	5
6	0.8 mm Aluminium Alloy + MBB Backing-Board + PF 615	not tested	yes, when B-B clamped no, when B-B loose	not tested
7	0.3 mm Aluminium Alloy + 15 mm Aluminium Honeycomb + 0.2 mm Aluminium Alloy + PF 615	not tested	yes	not tested

Note: [1] 17 mm with series production type material

Several fullsize fuel tanks for the BO 105 have been fabricated out of the chosen material (PF615) and then crash impacted from different drop heights up to 20 m with and without a supporting structure to simulate their structural environment. The test results are shown in Figure 16 to Figure 18 and in Table 5.

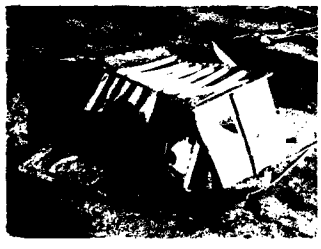

Figure 16. Impact from 20 m

Figure 17. Impact from 10 m on Obstacle

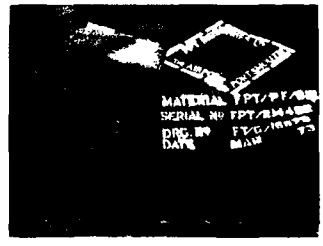

Figure 18. Impact of Bare Fuel Cell from 20 m

Table 5. Results of Impact Tests on Full Size Fuel Tanks

Test No.	Tank No.	Test Sample	Drop Height m	Result
1	1	PF 615 tank + MBB Backing-Board in a supporting structure with a honeycomb sandwich bottom plate	10	no leakage
2			15	no leakage
3		PF 615 tank in a supporting structure with a sheet metal bottom plate	10	no leakage
4			16	no leakage
5		PF 615 tank without a supporting structure	20	spillage, see Fig. 18
6	2	PF 615 tank with supporting structure	20	no leakage, see Fig. 16
7		PF 615 tank without supporting structure	20	spillage
8	3[1]	PF 615 tank with supporting structure	10	no leakage, see Fig. 17

Note: [1] Tank No. 3 was impacted on an obstacle (steel tube with 120 mm diameter), as can be seen from Figure 17

To prove the perforation resistance, one PF615 tank was filled with water and then impacted with the chisel from the impact-penetration-test. One half of the impacted area was covered by backing board and 0.8 mm aluminium-alloy, the other half was covered by 0.8 mm aluminium-alloy only. The part covered by backing board was impacted from 4.57 m; 7.5 m; and 11.25 m without any visible damage on the tank bladder. The part not covered by backing board was impacted from 4.57 m without leakage, however, the tank bladder was distinctly marked by the chisel. When impacted from 9.2 m, the aluminium-alloy and the tank wall were completely penetrated.

From the tests conducted at MBB, the following conclusions can be drawn:

- Drop tests on fuel tanks without a supporting structure to simulate their structural environment are far too conservative, as a fuel tank installed in a rigid structure that absorbs the stresses generated by the pressure increase is more representative of actual crash environment.

- High-flexible bladder material, such as PF615, in combination with a supporting structure and a backing-board material, is well suited for a crashworthy fuel tank to withstand internal pressure as well as perforation.

The military versions of the BO 105 for the German Army therefore have been equipped with crashworthy fuel tanks of the above mentioned construction, at a weight increase of nearly 20 kg.
During service with the crashworthy fuel system no crash-related fire has been reported.

3 FULL-SCALE CRASH TESTS

Without doubt, full-scale crash tests of complete helicopters are best suited for proof of compliance for fuselage and related structures such as landing gears, engines, transmissions, and seat tiedown provisions. But also to complement and substantiate analytic determination of airframe behaviour, the use of full-scale dynamic crash testing is highly recommended.

Data acquisition from full-scale crash tests is accomplished with extensive photographic coverage using low- and high-speed cameras and with onboard strain gauges and accelerometers. The accelerometers are the primary data generating instruments and are positioned to measure accelerations parallel to the helicopter axes in all interesting areas.

3.1 BO 105 Crash Test

In February 1974 a Bo 105, which had been damaged during a mishap to such an extent that it would not be economically viable to restore the helicopter to a flightworthy condition, was crash tested after repair of the fuselage, installing a crashworthy fuel system, and adding splitting tubes to the landing gear cross tube attachments. Main and tail rotor, hydraulic aggregate and horizontal stabilizer were replaced by dummies with equivalent weight. The fuel tanks were filled with 410 kg water and the pilot seat was occupied by an anthropomorphic dummy of 75 kg. The test helicopter, shown in Figure 19, was ballasted by lead ingots on the floor to a grossweight of 1,800 kg and a centre of gravity within the BO 105 centre of gravity range.

To realize a combined forward-downward impact velocity vector, the crash test was accomplished using the pendulum method with the aid of two cranes, as shown in Figure 20.

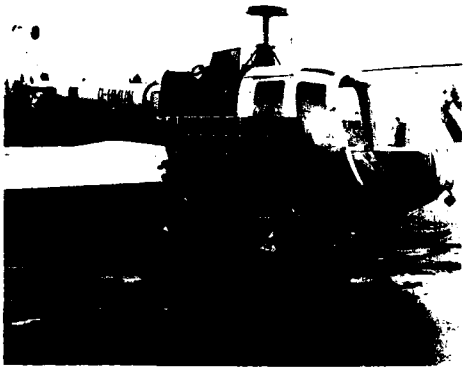

Figure 19. BO 105 Crash Test Helicopter

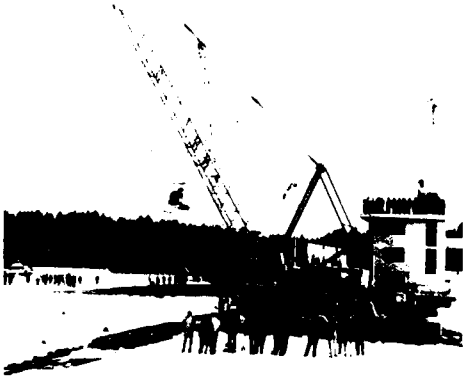

Figure 20. BO 105 During Movement in its Pull-Back Position

The helicopter was suspended from one crane by two swing cables and drawn back by a pull-back cable of a second crane to its release position. The cables were rigged to simulate at a flight attitude with *horizontal* skid tubes a vertical velocity of 8 m/sec and a longitudinal velocity of 15 m/sec, leading to a resultant impact velocity of 17 m/sec, which is just above the resultant impact vector of 95th percentile severity, as shown in Figure 21. The impact test arrangement can be seen in Figure 22.

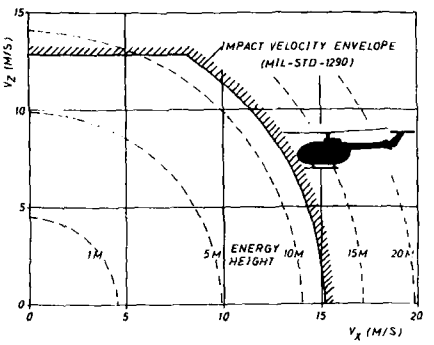

Figure 21. BO 105 Impact Velocity

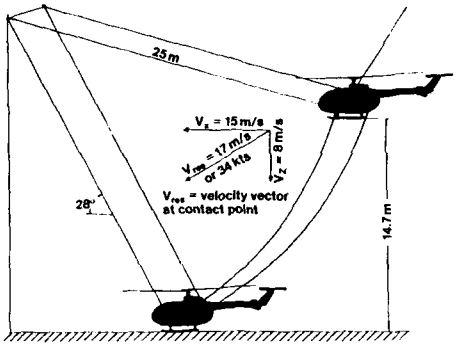

Figure 22. BO 105 Impact Test Arrangement

Thirteen acceleration pickups were installed on the floor, on the main transmission, and in the head and chest of the anthropomorphic dummy. Four strain gauges were applied to measure the loads in the four transmission struts. An umbilical cable, linking the onboard accelerometers and strain gauges to a data acquisition system located on the ground, hung from the rear door opening of the helicopter and had a length that did not restrain the movement of the helicopter even during skid-out.

The helicopter was released by electrically activating a load hook of the pull-back harness. The swing cable harnesses were separated also by electrically activated load hooks at impact. The impact surface was frozen sod, slightly covered with snow.

The helicopter contacted the impact surface with the skid tubes parallel to the ground. The landing gear cross tubes travelled through their entire 0.35 m of available stroke and the subfloor structure aft of the rotor axis was damaged by contacting the ground. The crew and passenger compartment did not show any damage and even the windshields remained completely in place and undamaged. Also the engine and transmission mountings were only slightly damaged and the self-sealing breakaway coupling between main and reserve fuel tank worked, and the fuel system did not show any leakage. The aluminium honeycomb crush structure in the pilot seat was 5 mm compressed by the anthropomorphic dummy. The splitting tubes on the landing gear came not into play, as virtually no lateral loads were developed. A still sequence photo taken approximately 100 milliseconds after impact is shown in Figure 23. The condition of the BO 105 after the crash test can be seen in Figure 24. The peak decelerations measured are shown in Table 6.

Figure 23. BO 105 about 100 ms after Impact

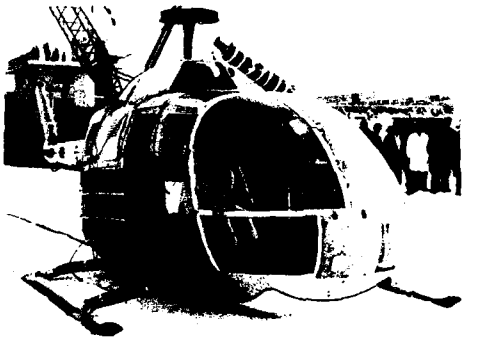

Figure 24. BO 105 after Crash Test

Table 6. Peak Deceleration Load Factors during BO 105 Impact

Direction	Forward Floor		Aft Floor		Trans-mission	Dummy	
	Left	Right	Left	Right		Chest	Head
x	-	4.5	-	-	4	14	7
y	-	-	-	-	-	4	2
z	19	14.5	27	27	16.5	-	36.5

From the full-scale crash test of a BO 105 helicopter the following conclusions could be drawn:

- The airframe structure is able to absorb the impact energy of a severe survivable crash and still maintains a protective shell.

- The forces and accelerations imposed upon occupants do not exceed the limits of human tolerance for survival, as the peak acceleration of 36.5 g, recorded on the anthropomorphic dummy, had only a duration of about 2 milliseconds. For a duration of 10 milliseconds an acceleration of 15 g was established.

- The mounts and the structural support of all heavy mass items which would pose a hazard to personnel are designed to withstand the loads occurring during a severe crash.

- The aluminium honeycomb crush structure of the crew seats works satisfactorily. The relatively small stroke observed was due to the relatively low input load of about 14-19 g measured on the floor beneath the crew seats.

- The crashworthy fuel system works excellent. The fuel cells in combination with the surrounding structure are able to withstand internal pressure occurring during a severe crash. The self-sealing breakaway couplings work with no spillage. A postcrash fire hazard therefore can be regarded as extremely remote.

3.2 BK 117 Crash Test

In March 1985, Kawasaki Heavy Industries (KHI), MBB's partner of the BK 117 development and amongst other parts responsible for the airframe structure except the tail boom with empennage, conducted the first full-scale helicopter crash test in Japan, using a BK 117 preproduction helicopter modified as close as possible to the series production type [3] . Main and tail rotor, hydraulic module, right-hand engine, and the forward passenger seats were replaced by dummies with equivalent mass and moment of inertia. The secondary structures such as doors, windows, and cowlings were not installed. The fuel tanks were filled with about 600 kg water and the copilot seat was occupied by an anthropomorphic dummy of 60 kg. Three NAS809 body blocks and four dummy masses, each with a weight of 80 kg, were used to simulate the pilot and the passengers. Additional masses in the cockpit and the baggage compartment were installed on the floor to adjust the grossweight to 2,850 kg and the centre of gravity within the range of normal operation. The configuration of the test helicopter is shown in Figure 25.

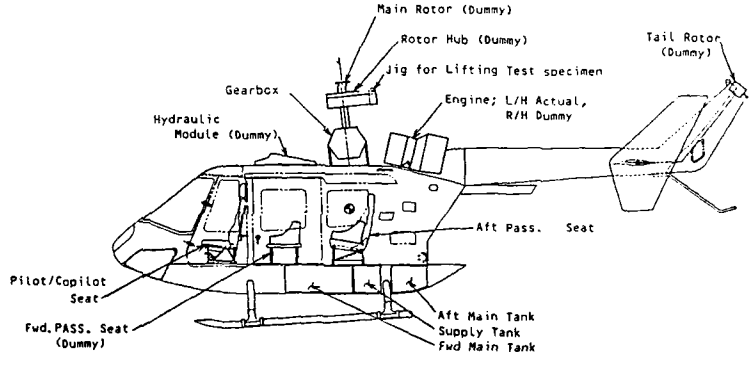

Figure 25. BK 117 Crash Test Helicopter

The impact conditions and the crash testing method were the same as for the BO 105, reported in the chapter before.

Fourteen acceleration pickups were installed on the floor, the main transmission, the left-hand engine, the body blocks, and in the chest of the anthropomorphic dummy.

The following impact sequence was established from the high-speed motion-picture data:

(1) The helicopter approached the ground in an attitude of 5.7 degree pitch up (3.5 degree corresponds to level landing), 0.9 degree roll right, and 2.2 degree yaw left. The impact angle was 35.5 degree instead of 28 degree.

(2) Rear part of right-hand skid tube first contacted the ground.

(3) Rear cross tube travelled through its entire 0.35 m of available stroke and the bottom of rear cabin contacted the ground.

(4) Cabin subfloor structure crushed, resulting in the burst of the forward main fuel tank and canted frame buckled.

(5) Bottom of the cockpit subfloor impacted on the ground and the upper connection of the centre pillar failed.

(6) Side panel structures under the forward mainframe collapsed.

(7) Horizontal stabilizer endplate contacted the ground and rebounded.

(8) Ceiling structure slightly moved forward relative to the cabinfloor and the door openings slightly deformed.

(9) The test helicopter came to rest after forward sliding of about 8 m.

The condition of the BK 117 after the crash test can be seen in Figure 26. The peak decelerations measured are shown in Figure 27, the deceleration-time histories in Figure 28.

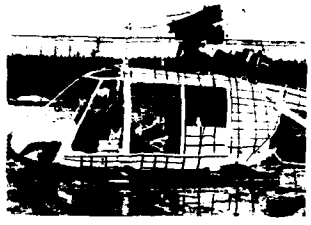

Figure 26. BK 117 after Crash Test

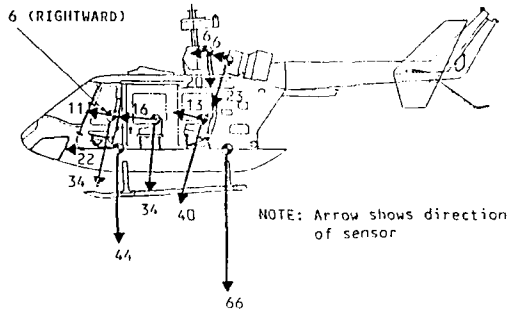

Figure 27. BK 117 Peak Decelerations

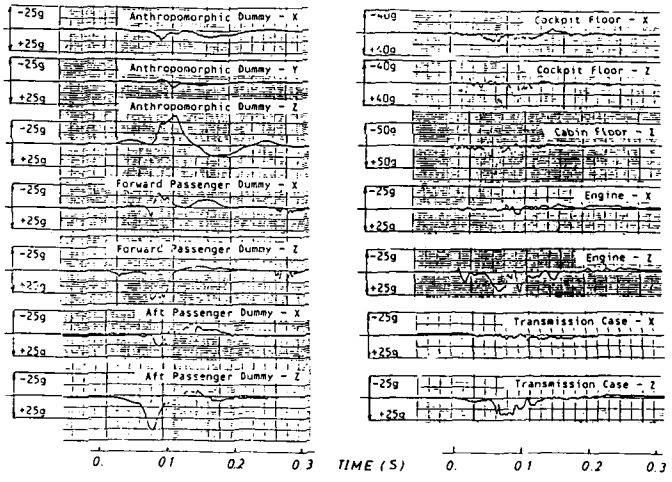

Figure 28. BK 117 Deceleration-Time Histories

From the full-scale crash test of the BK 117 helicopter the following conclusions could be drawn:

- The airframe structure is able to absorb the impact energy of a severe survivable crash and still maintains a protective shell. The reduction of the occupiable volume was just above 3% as against 15% allowed according to MIL-STD-1290.
- The mounts and the structural support of all heavy mass items which would pose a hazard to personnel are designed to withstand the loads occurring during a severe crash.
- The non-stroking seats are not able to prevent occupants from experiencing injurious accelerative loadings during a severe crash. A maximum dynamic response index (DRI) of 35 was established for the occupants against a desired value of not greater than 21.
- As expected, the noncrashworthy fuel system cannot avoid spillage during a severe survivable crash and therefore a certain hazard for a postcrash fire exists.
- The BK 117, equipped with crashworthy seats, has a good potential to prevent occupant fatalities and minimize the number and severity of occupant injuries during a severe survivable crash.

4. ANALYTICAL SIMULATION

In terms of fidelity, the dynamic testing of full-scale structures most closely approximates actual crash conditions, especially if velocity components and impact surface conditions can be realistically represented. However, during the early design stages of a new helicopter, full-scale testing is untimely and would be extremely expensive. Additionally there are several sets of crash conditions that must be investigated in support of the design process.

As a result of expanding computer capability, a number of digital computer codes for analysis of helicopter structures, subcomponents, and helicopter occupant dynamics in a crash environment have been developed.

These computer programmes can provide a means of evaluating the effectiveness of helicopter structures, energy absorbing systems, and occupant retention in satisfying a set of crashworthiness criteria.

4.1 Crash Impact

Crash impact simulation, i.e. predicting of the structural behaviour of a helicopter and the decelerations to which the occupants are subjected in a crash environment, must include extensive plastic deformations; large deflections and rotations; and the ability to handle nonlinear boundary conditions required by variable contact/rebound.

During the seventies, MBB selected as tool the computer programme KRASH, well-known in the helicopter community, which predicts the structural response of a helicopter to multidirectional crash environments. The programme solves the coupled Euler equations of motion for n interconnected lumped masses, each allowed six degrees of freedom. The interconnecting structural elements represent the stiffness characteristics, both linear and nonlinear, of the structure between the masses and must be defined by user input data.

The KRASH code has been implemented and tested using simplified models as well as more sophisticated models, as shown in Figure 29, taken from the literature [4].

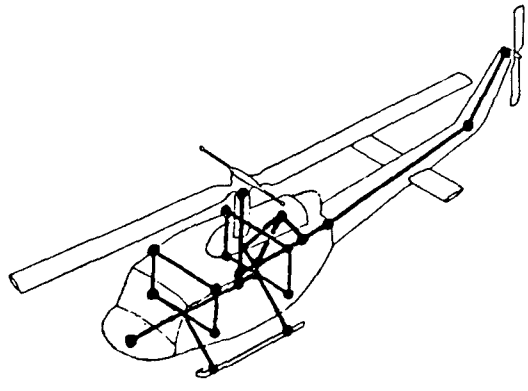

Figure 29. KRASH Helicopter Model

From working with KRASH we found that it enables the representation of a helicopter structure by a relatively small number of beams which facilitates data evaluation and result interpretation. The calculation of a measure of occupant injury potential (Dynamic Response Index) allows the evaluation of the probability of spinal injury. Computer time is reasonable for simple and intermediate models. The programme KRASH can be used for studies of structural design parameters and energy dissipation in subassemblies for two- and three-dimensional geometry and motions.

4.2 Subcomponent Crushing

The nonlinear stiffness behaviour of interconnecting beams in crash impact simulations are frequently found directly by experimental tests, but due to cheaper computing power the nonlinear properties of subcomponents will more and more be derived from separate refined finite element analyses, taking into account effects, such as section distortion, shell folding, and rivet popping.

During the crash research programme (see chapter 2.3) the load-carrying capability of a trapezoidal aluminium-alloy sheet in the pre- and post-buckling area under axial compression has been analysed with the finite element programme MARC parallel to quasi-static crushing tests [5].

A drawing of the test panel is shown in Figure 30 and the mathematical model of a repeating element can be seen in Figure 31.

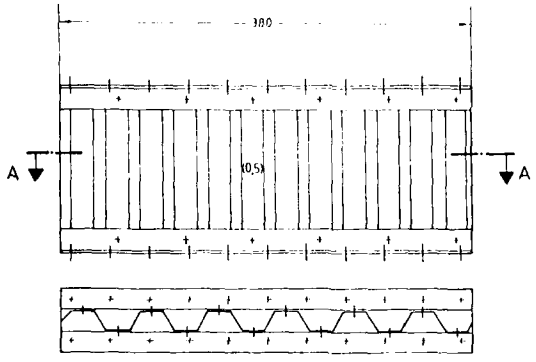

Figure 30. Trapezoidal Test Panel

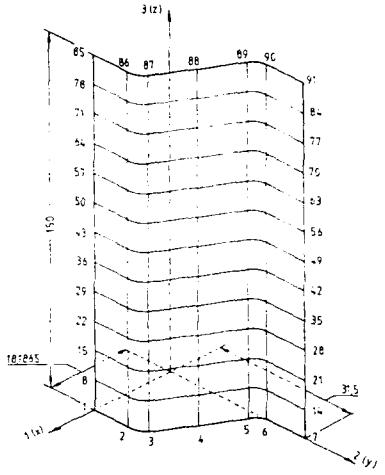

Figure 31. Mathematical Model of Trapezoidal Panel

Non-linearities due to large deflections and the elasto-plastic material behaviour have been taken into account. The analysis was conducted by using the dynamic Slow-Ramp solution method, where system damping and deformation velocity are the significant parameters. The load-deformation behaviour corresponds well with test result, however, the first crushing peak is strongly dependent on the deformation velocity, as shown in Figure 32.

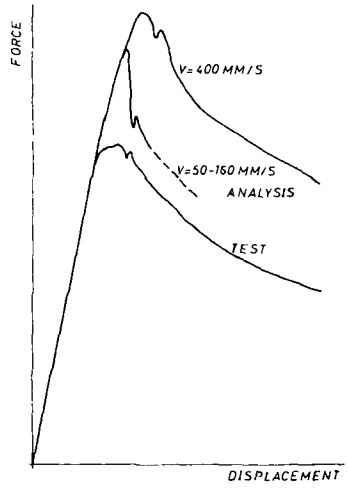

Figure 32. Load-Deformation Characteristic of a Trapezoidal Panel

For an aluminium-alloy sheet-stringer concept, in cooperation with Engineering System International (ESI), a mathematical model has been developed with shell elements and special rivet elements and ESI conducted a non-linear dynamic analysis using the explicit finite element code PAM-CRASH as given in another paper [6] presented at this AGARD meeting. Provisions were made for contact between the different parts of the structure.

The sheet-stringer structure has a vertical plane of symmetry. Therefore, only one symmetric half was considered in the finite element model, as shown in Figure 33.

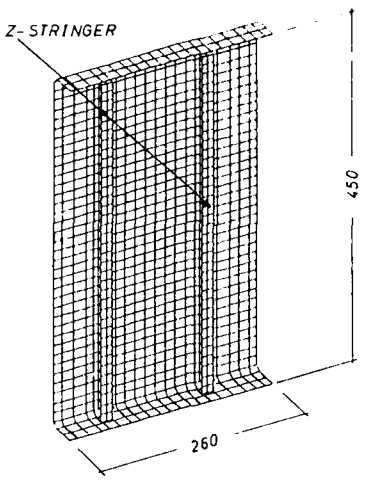

Figure 33. Mathematical Model of Sheet-Stringer Panel

Loading of the finite element model was applied by two moving rigid walls at top and bottom of the structure. Each wall travelled at 5 m/s axially toward the structure, thus producing a 10 m/s crushing velocity. The first 15 milliseconds of the crush were simulated. This corresponded to a 150 mm crushing of the 450 mm high structure.

A total of nine cases of the stringer reinforced panel were considered, differing with regard to:

- the boundary conditions at top and bottom of the structure,
- the number of rivets connecting the stringer to the panel,
- the rivet failure conditions (failure allowed/not allowed),
- the wall-thickness of the panel,
- the height of the z-stringers,
- time dependent lateral loads, representing fuel tank pressure loading.

The following results have been presented by ESI:

- Load versus deformation diagrams for the overall structure and the two stringers only, thereby giving an indication of the proportion of load transferred through the stiffeners (see Figure 34).
- Integrated energy absorption versus deformation diagrams (see Figure 35).
- Sequence of deformed shape plots (see Figure 36).
- Force versus time diagrams for rivets in the no-failure-condition.
- Time of rivet failure, when failed within the simulation time.

Figure 34. Load-Deformation Characteristic of Sheet-Stringer Panel

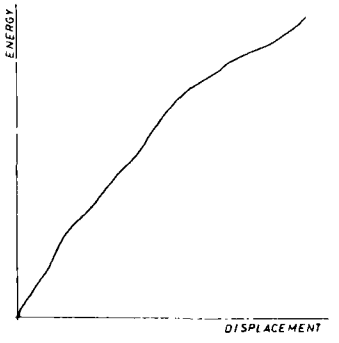

Figure 35. Integrated Energy Absorption of Sheet-Stringer Panel

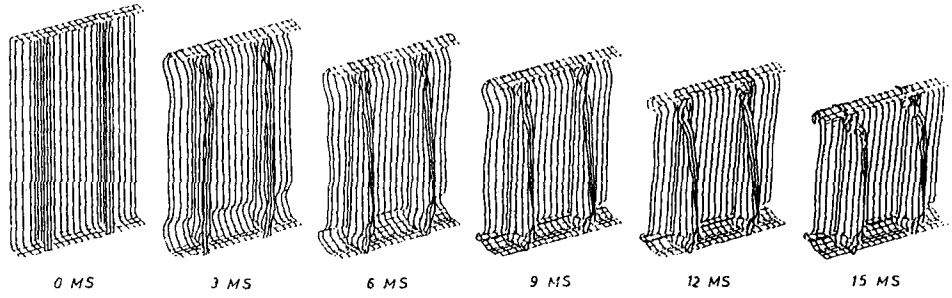

Figure 36. Crushing Sequence of Sheet-Stringer Panel

A comparison between analytical results and test results, conducted by MBB, is given in another paper [2] presented at this AGARD meeting.

For an aluminium-alloy sandwich concept, a mathematical model also has been developed in cooperation with ESI and a non-linear dynamic analysis using PAM-CRASH has been conducted by ESI, as given in another paper [6] presented at this AGARD meeting.

The sandwich panel analysed is shown in Figure 37 and the panel after a quasi-static test of 5 mm crushing which corresponds to 0.5 ms at 10 m/s is shown in Figure 38. A series of deformed shapes, illustrating the development of deformation during a crash can be seen in Figure 39.

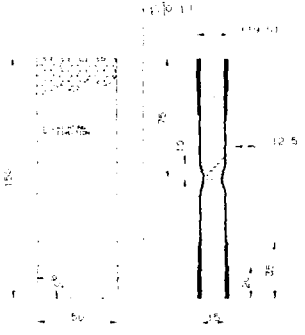

Figure 37. Sandwich Test Panel

Figure 38. Sandwich Test Result

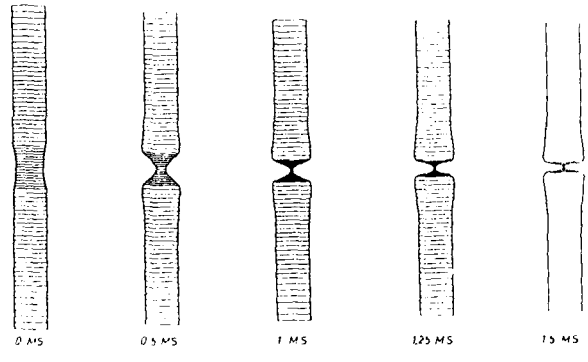

Figure 39. Crushing Sequence of Sandwich Panel

From the experience gained with analytical simulation of subcomponent crushing, using finite element programmes, we can conclude that these codes can be a viable tool to simulate realistically structural detail behaviour and thus reduce the amount of experiments required at reasonable computer time.

4.3 Occupant Dynamics

Injury assessment in a multiaxial acceleration environment must consider the compactness of the cockpits of modern military helicopters and the close proximity of mission equipment which pose serious crash impact hazards to the aircrew.

During the crash research programme (see chapter 2.3), the computer code MVMA 2-D, developed at the University of Michigan for the automotive industry [7] , was selected as an analytical tool to establish the movement of occupants relative to a surrounding structure and the loads acting on occupants under crash conditions.

The programme is based on a two-dimensional biomechanical model which reproduces the human response to impact and which is able to simulate contacts and contact forces when interacting with the restraint harness and the surrounding structure. The surrounding structure, such as seat, floor, instrument panel, windshield etc. can be specified in its time-dependent position, as shown together with the biomechanical model in Figure 40. Also several restraint systems, including air-bag are available.

To run a simulation, the programme needs information about the initial occupant position and the impact velocity components for the considered plane as well as the time dependent linear and angular decelerations of the occupant in tabular form.

The programme gives detailed information about the time-dependent position of the occupant relative to the surrounding structures, as shown in Figure 41 and the time-dependent loads acting during contact between the occupant and its restraint harness and surroundings. Biomechanical injury criteria, such as Severity Index (SI) and Head Injury Criterion (HIC) are established as well.

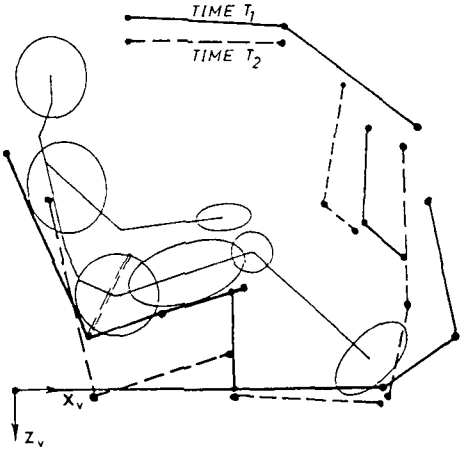

Figure 40. Occupant Dynamics Mathematical Model

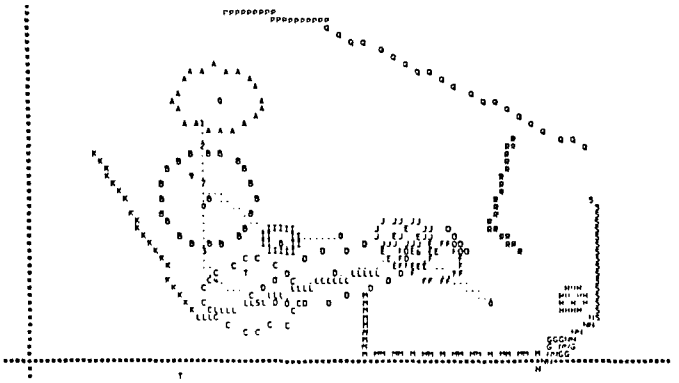

Figure 41. MVMA Stick Figure Printer Plot Frame

The programme MVMA 2-D can be regarded as a post-processor for KRASH, when considering a two-dimensional crash environment only. The quality of the results gained with this programme is of course strongly dependent on the biomechanical model used. The MVMA 2-D code has been developed more than ten years ago and it can be assumed that improved versions, perhaps with three-dimensional capabilities are available.

5. APPLICATION TO NEW PROJECTS

Crashworthiness improvements and other safety features are most efficiently included in a helicopter as integral system requirements in the conceptual design stage. The many benefits realized by enhancing helicopter crashworthiness are not obtained without some impact on the weight, on the initial acquisition costs and on operational costs due to weight/performance penalties for the crashworthy features.

The optimum protection level is found, when the total costs, i.e. the sum of accident costs and crash protection costs are minimum. This optimum depends on the type of helicopter, the mission to be performed, and the flying hours per year.

5.1 Advanced Light Helicopter (ALH)

The ALH, a multi-purpose helicopter in the 4,000 kg class, shown in Figure 42, is presently under development by Hindustan Aeronautics Limited (HAL), Bangalore (India), with the support of MBB.

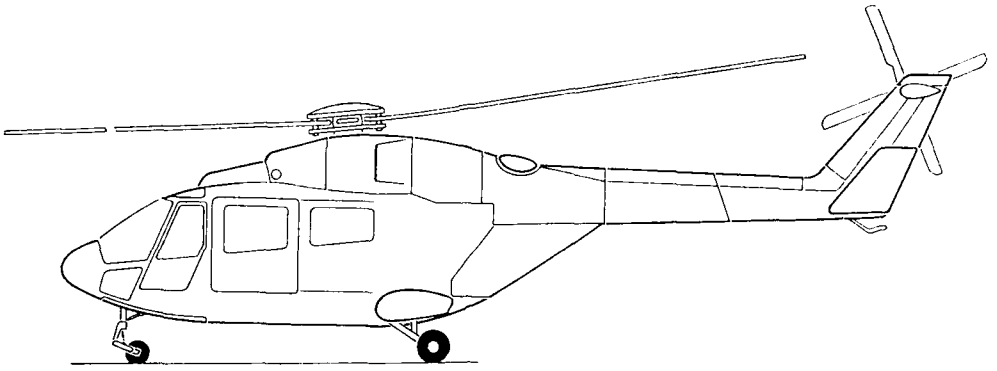

Figure 42. Advanced Light Helicopter ALH

Concerning crashworthiness the following requirements have been specified:

- Fulfillment of MIL-STD-1290 fully in the vertical direction, i.e. v_z = 12.8 m/s, at an all up weight of 4,000 kg.
- In the longitudinal and lateral directions, according to MIL-STD-1290 up to the maximum possible extent.
- Crew seats to withstand
  - 30 g longitudinal
  - 20 g lateral
  - 15 g vertical
- Engine and transmission mountings to withstand
  - + 20 g longitudinal
  - ∓ 18 g lateral
  - ∓ 20 g/-10 g vertical.

The vertical crash impact energy is to be absorbed primarily through stroking of the landing gear and crushing of the fuselage subfloor structure. During preliminary design phase the following crash protection systems have been defined:

- Main landing gear with 700 mm and nose landing gear with 545 mm energy-absorbing stroke. With a maximum deceleration of 6 g and a structural efficiency of 80% the landing gear units will withstand vertical speeds of about 8 m/s.
- At vertical speeds exceeding 8 m/s, the subfloor structure will be crushed in a controlled deformation. During a displacement of 150 mm the subfloor structure will absorb the energy equivalent to an impact velocity of 10 m/s, when developing a peak deceleration of 50 g and a structural efficiency of about 70%. The landing gear and the subfloor structure together thus will absorb the energy resulting from a vertical impact of 12.8 m/s.
- To protect the crew from injurious acceleration levels, the ALH will be equipped with crashworthy seats of 300 mm stroke.
- The fuel tanks, located under the floor, will be crash-resistant, and the fuel system equipped with self-sealing breakaway couplings.

Due to different reasons, a skid-type landing gear finally was chosen with an energy absorption capacity of about 5 m/s, leading to a total capacity of the helicopter of about 11 m/s and thus covering at least 90% of all survivable accidents. Sheet-stringer concepts have been designed for the ALH with efficiencies > 0.7 as shown both by analysis and static as well as dynamic tests. To check the overall behaviour of the helicopter during vertical crash impact, at present investigations are under way, based on simple one- and two-dimensional models using the KRASH code. A more detailed three-dimensional model is expected to be available at the end of this year.

5.2 German-French Antitank Helicopter (PAH2)

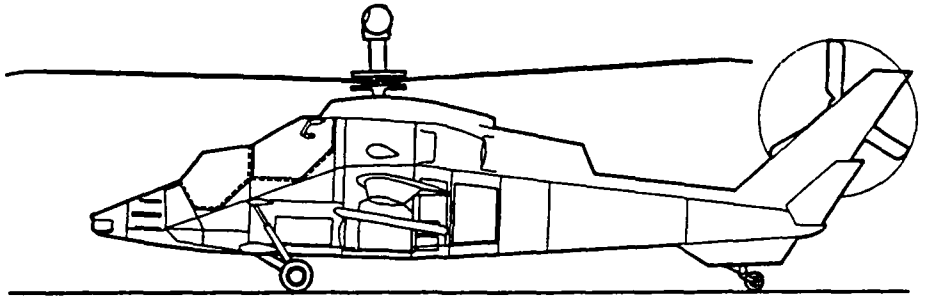

Figure 43. Antitank Helicopter PAH2

For the PAH2, shown in Figure 43, the crashworthiness requirements have been specified to fulfill a protection level which corresponds to 90% of MIL-STD-1290. The following impact velocities therefore must be considered:

- 10.5 m/s vertical
- 12 m/s longitudinal
- 7.2 m/s lateral.

To fulfill the requirements in the most critical, the vertical direction the following crash protection systems have been defined:

- Landing gear units to withstand a vertical velocity of about 6.5 m/s due to 700 mm energy absorbing stroke.
- At vertical speeds exceeding 6.5 m/s the bottom structure will be crushed during 100 mm controlled deformation and thus will absorb the energy equivalent to an impact velocity of about 8.5 m/s. Landing gear and subfloor structure together will absorb the energy resulting from a vertical impact of 10.5 m/s.
- Crashworthy seats with 200 mm stroke protect the occupants from injurious acceleration levels.
- The fuel tanks will be crash-resistant up to impact velocities of 14 m/s, and the fuel system will be equipped with self-sealing breakaway couplings.

Development work for the PAH2 has just started at Aerospatiale and MBB, including the design of an energy absorbing all composite subfloor structure.

5.3 NATO-Helicopter for the Nineties (NH 90)

The NH90 is a quattrolateral programme, comprising France, Italy, Germany and The Netherlands to develop a Common Helicopter, as shown in Figure 44 which will be the basis for a Tactical Transport Helicopter (TTH) and a NATO Frigate Helicopter (NFH). The Basic Helicopter is a multi-purpose, twin-engine helicopter in the 8-10 t class with a voluminous cabin and a retractable three-wheeled landing gear.

Concerning crashworthiness the following requirements have been specified:

- Vertical impact velocity

  6 m/s without fuselage/ground contact
  11 m/s with extended landing gear
  8 m/s with retracted landing gear

- Longitudinal impact velocity

  15 m/s with extended and retracted landing gear

- Lateral impact velocity

  8 m/s with extended landing gear
  7 m/s with retracted landing gear

- Impact attitude

  15 degrees nose up pitch and ± 10 degrees roll

The main objectives of the present Project Definition Phase (PDP) is a definition of the basic helicopter. Crash protection systems, such as landing gear units, subfloor structure of the all-composite airframe to allow deformation in a controlled and predictable manner as well as occupant retention and fuel systems will be defined in the PDP in a total systems approach to arrive at a cost-effective design that is best adapted to the level of risk.

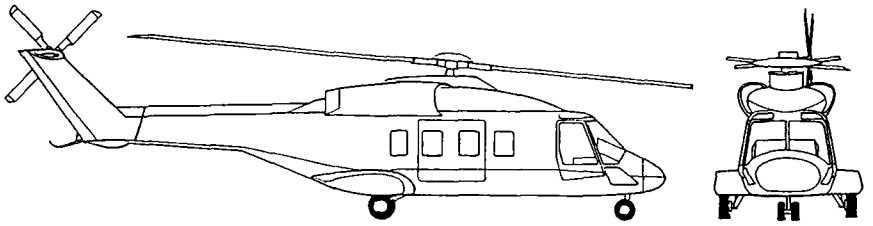

Figure 44. Common Basic Helicopter NH90

6. CONCLUSION

From more than twenty years activities in the crashworthiness field the following can be concluded:

- Load-limiting, energy absorbing seats are indispensable to prevent or reduce occupant injury in a severe survivable crash. There are several systems in use to provide a measure of load reduction by stroking.

- A crashworthy landing gear offers very real economic savings, as it avoids material damage from hard landings, however, a decrease in helicopter performance due to increased landing gear weight must be taken into account.

- Modern helicopters are characterised by an airframe structure which ensures that premature failures and a fuselage separation potential are minimized to maintain a habitable space for the occupants during and after impact. The subfloor structure shows energy absorption and force attenuation capabilities to prevent injury of the occupants and to lead to a low enough g environment for large mass items to reduce, in combination with a high static tiedown strength, the probability of breaking loose.

- The standard material for metal fuselage structure is at present a ductile aluminium-alloy that can tolerate rather large strains, deform plastically, and absorb a considerable amount of energy without fracture. Load-limiting concepts are available with virtually no additional weight, showing relatively high structural efficiencies. The use of advanced composite materials in helicopter fuselages will not prevent improvements in the crashworthiness of the structure if proper emphasis is placed on crashworthiness early in the design process, as shown in common DFVLR/MBB activities, given in another paper [8] presented at this AGARD meeting.

- Fire prevention is primarily to avoid or at least minimize spillage of flammable fluids. Self-sealing breakaway couplings and anti-spillage vent valves are state of the art for crashworthy fuel systems. Fuel cells in combination with the surrounding structure are shown to withstand internal pressure as well as perforation by broken structural components. Drop tests of fuel tanks without simulating their structural environment are far too conservative. In a total system's approach, considering energy absorption and force attenuation by the landing gear and the subfloor structure, it can be shown, that an impact velocity of 19.8 m/s, as specified in MIL-T-27422B, is too conservative. We consider an impact velocity of about 150% of the fuselage vertical impact velocity to be sufficient for fuel tank drop tests.

- During full-cale crash tests valuable information could be gained on the crash-behaviour of MBB helicopters. The test results also can be used to verify the modeling of these helicopters for an analytical simulation.

- A number of digital computer codes are available for the analysis of complete helicopters, structural subcomponents and occupant dynamics. These computer programmes can provide a means of evaluating the effectiveness of helicopter structures, energy absorbing systems, and occupant retention in satisfying a set of crashworthiness criteria. As a result of expanding computer capability and cheaper computing power an improvement of the analytical methods from an economic point of view is to be expected.

- The work accomplished so far at MBB and in cooperation with partners and subcontractors enables us to contribute significantly to fulfill the crash requirements in present and future helicopter and tilt rotor developments, such as ALH, PAH2, NH90 and EUROFAR.

7. REFERENCES

1. Och, F., "Helicopter Crashworthiness Problems and Promises", Keynote Address presented at the International Conference on STRUCTURAL IMPACT AND CRASHWORTHINESS, Imperial College, London, UK, 1984.

2. Frese, J., Nitschke, D., "Crushing Behaviour of Helicopter Subfloor Structures", AGARD Structures and Materials Panel Specialists' Meeting on "Energy Absorption of Aircraft Structures as an Aspect of Crashworthiness", May 1988, Luxembourg.

3. Onishi, M., Yoshimura, T., "Full Scale Crash Test of a BK 117 Helicopter", AHS National Specialists' Meeting on "Crashworthy Design of Rotorcraft", May 1986, Atlanta, Georgia, USA.

4. Wittlin, G., Gamon, M.A., "Experimental Program for the Development of Improved Helicopter Structural Crashworthiness Analytical and Design Techniques", Vol. I + II, USAAMRDL-TR-72-72, 1973.

5. Schneider, E., "Das Tragverhalten eines gedrückten Alu-Trapezträgers im Nachbeulbereich", Z. Flugwiss. Weltraumforsch. 5 (1981), Heft 5.

6. Ulrich, D., Pickett, A.K., Haug, E., Bianchini, J., "Crash Simulation and Verification for Metallic Sandwich and Laminate Structures", AGARD Structures and Materials Panel Specialists' Meeting on "Energy Absorption of Aircraft Structures as an Aspect of Crashworthiness", May 1988, Luxembourg.

7. Robbins, D.H., Bennett, R.O., Bowman, B.M., "MVMA 2-D Crash Simulation Version 3", HSRI, University of Michigan, Ann Arbor, UM-HSRI-BI-74.

8. Kindervater, Ch., Gietl, A., Müller, R., "Crash Investigations with Sub-Components of a Composite Helicopter Lower Airframe Section", AGARD Structures and Materials Panel Specialists' Meeting on "Energy Absorption of Aircraft Structures as an Aspect of Crashworthiness", May 1988, Luxembourg.

THE DESIGN OF HELICOPTER CRASHWORTHINESS

by

V.Giavotto, C.Caprile, G.Sala

Aerospace Engineering Department
Politecnico di Milano
Italy

Abstract

The extensive use of composite materials in helicopter structures has prompted new research activities in crashworthiness in the last dacade.

A rational design of crashworthy structures requires a great deal of data and experience to be collected and organized; in particular the most efficient mechanisms of energy absorbtion must be understood and carefully investigated and consequently the best structural concepts and detail design can be identified.

With this aim and in cooperation with Agusta Helicopters a research program has been undertaken, covering many of the basic aspects of crashworthy design, i.e. dynamic experimentation on subcomponents and subassemblies, hybrid and true finite element modeling, design and verification procedures.

The paper presents some preliminary results, together with the outline of the whole program.

1. INTRODUCTION

The idea of modern helicopter crashworthiness takes its origin from the observation, made from the end of the 60s, that a large part of the helicopter crashes could have been survived if some dangerous secondary events had been prevented; i.e. fire, the collapse of the cabin structure, and the collision of hard protruding objects with human bodies (1).

The first effort in crashworthiness was then aimed to design fuel systems, structures, cabin fitting out, seats and restraints able to prevent such secondary events, in order to make survivable what were been considered as potentially survivable accidents.

Potentially survivable accidents were spontaneously defined as the ones inside a velocity envelope such that, with current helicopter structures, peak accelerations were limited within human tolerance limits.

These early ideas and definitions have subsequently been developed and widened, following the development of crashworthiness technology.

2. THE ROLE OF REQUIREMENTS

In this scenario requirements have been issued, both in the form of military regulations (2), (3) and of customer's requirements (4); such requirements had a tremendous effect in forcing designers to work on specified crashworthiness aims and consequently in stimulating relevant research.

In the future, when crashworthy design technology will be more developed, crashwortiness will possibly become a performance, i.e. a measurable and saleable quality.

But nowadays the obtainement of good levels of crash safety both in automotive and in helicopter technology, strongly relies on the enforcement of suitable requirements or regulations. Requirements must contain a clear problem statement, and a correct definition of targets, the letter being significantly in advance, but still compatible, with the current technology. So appropriate requirements are very important and not easy to develop; they must be considered significant results, rather than a starting point for a research project.

On the other hand the application of crashworthiness requirements from the earliest stages of design, will lead to notable benefits, even if coupled with possible costs increase (5).

In automotive and also in helicopter technology such kind of requirements seems to have a tremendous effect in stimulating research and in improving knowledge; but as knowledge deepens, requirements likewise have to evolve, first of all from a quantitive

point of view (that is issuing clear, regular and unambiguous requirements), and also quantitatively (for instance continuously varying acceptable crash levels).

Relatively crude requirements may have a dramatic effect at the beginning, but they must be able to follow the evolving technology.

Anyway basic crashworthiness items have to define some foundamental targets: at least, the requirements must demand not to exceed survivable acceleration levels, not to produce too much severe impacts for the occupants against hard protruding objects, not to give rise to pieces projection.

In synthesis for light impacts nor occupants nor aircraft, except landing gear have to pay consequencies. Viceversa for severe impacts high probability to survive must be assured for occupants, with possible severe damage for aircraft.

The achievement of such target with minimum weight and cost increase demands a dynamic tuning and a design integration of the different energy absorbing mechanisms and components.

It has been already observed that it is quite difficult to obtain crashworthiness not starting from the first phase of the design, and the best way to obtain crashworthiness without any increse in weight and cost is to introduce crashworthiness from the conceptual design (6).

One of the most important and basic items of the crashworthiness requirements is the definition of the maximum survivable impact, that is the definition of the maximum impact that could be assumed as a test for the structure, taking into account that there is a physical human limitation.

Considering the simple energy balance:

$$1/2m(\Delta v)^2 (1-\eta_L) = \eta_S SmgD$$

if m is the mass of person to be survived, $(m(\Delta v)^2)/2$ is the kinetic energy and η_L is the amount of energy absorbed by the undercariage, the rest of the energy must be absorbed by the subfoor and seat restraint, characterized by a total stroke S.

Assuming a certain global stroke efficiency, related to subfloor plus seats, fixing D, maximum survivable peak acceleration, and knowing from ejection seats research (i.e. from the so called Eiband curve) that for pilot the maximum survivable vertical acceleration peak is of the order of 20 g's, assuming that the landing gear absorbs one half of the energy, a total stroke (seat plus subfloor) of 0.6 m, and a global stroke efficiency η_S of 0.7, a survivable impact velocity of 18.15 ms^{-1} is obtained.

Till now actual helicopter structures, have not allowed to reach such impact velocity level, surviving occupants: evidently the structures have not been designed considering suitable crashworthiness criteria, and consequenrly these levels must be regarded as target for the future.

3. STRUCTURAL CRASH SAFETY

A numerical crash simulation of a typical helicopter structure, made of a subfloor, a collapsable seat and a dummy has been worked out. The related results (figure 1) show that, having certain floor acceleration, that is acceleration of points were the seat is fixed, the effect of the seat itself and the dynamic interactions of the seat-pilot system is such that the acceleration of the pelvis region and the acceleration of the chest of the passenger is higher than the peak acceleration of the floor itself.

This means that it is very difficult to achieve a satisfactory decrease in occupant acceleration, because of the dynamic interactions of the components belonging to the system.

Lower acceleration levels could be obtained by performing a dynamic tuning of the seat and the passenger.

Anyway all this may lead to high increase in costs, so that it is necessary to take into account also economical aspects in defining the maximum survivable impact.

Considering Figure 2 one finds the increase in crashworthiness on the abscissa axis and increase in crashworthiness cost on the ordinate axis: the curve of the cost of safety becomes steeper and steeper having possibly a vertical asymptote.

The maximum survivable impact would be considered at the intersection of this curve with the maximum acceptable cost curve which is not a constant, but varies according to the required impact severity level.

In the future, thanks to improvement in technology, probably it will be possible to get higher survivable impaot levels with lower increase in cost.

A typical helicopter crash event, considering absorption mechanisms and main sequence of collapse for the energy absorbing structural elements is schematically represented in Figure 3. It is shown that firstly the landing gear than the subfloor, and finally the seat and the roof structure must collapse absorbing energy and meanwhile containing the heavy mass of the gearbox (7).

However it must be underlined that, dealing with the helicopter crashworthiness, one

has to take into account mainly the behaviour of each element (as for instance landing gear, subfloor, etc. (8), (9)) but also has to take care of the integration of the design, which must be very tight.

In order to accomplish this integration the following foundamental items must be taken into account: the structural design of components and subassemblies (paying particular care to joints and fitting), the choice of materials and their application, the definition of the dynamic behaviour of each element, capable to achieve a global well-matched tuning, so to avoid bad interactions.

4. DESIGN METODOLOGY

To fulfil crashworthiness requirements it is necessary to define a design procedure (10), (11); the sequence which may be considered in a first instance (not much different from the one used till now) (Figure 4) is based on preliminary design of the structure and contextual design of energy absorbing modes, subdivision of the total energy between the various modes according to the strokes available, and then on optimum structural design of the components separately, to obtain optimum stroke efficiency of every energy absorbing mode; this of course needs experience and data about the behaviour of details.

Then the verification of dynamic interaction is worked out; this must be done via hybrid simulation which is absolutely necessary to simulate crash with very simple models: in fact at this level of design the structure is not completely defined and so true finite elements analyses are useful (12) (13).

The study of this dynamic interaction may lead to non completely satisfactory results, and so a design modification may be necessary.

The detailed design needs experimental tests for some components, which are usually carried out parallelly to design procedure.

Besides special finite elements codes for crash analysis (that is complete finite elements as PAM-CRASH, DYCAST and ANCS) must be considered very important items to study structural components and to guide specific experimental research (14) (15).

But, in order to put into practice completely all the items previously listed, the design procedure must be optimized and rules somewhere changed, as shown in Figure 5.

After conceptual design, the first item consists in the identification of the hybrid model with undetermined control parameters and then optimization of the dynamic interaction of designed parts by obtaining the optimal dynamic behaviour of this deformable macro-element, and finally the structural design of actual component having the behaviour which has been specified by means of this optimization.

If this is not possible, a new feedback is need, and also a modification in design and/or design constraints to make this possible.

This is really something which is the best way of designing.

5. COMPOSITE MATERIALS

In modern helicopter structures composite materials are throughout used in place of conventional aluminium alloys, owing to their good specific strength and stiffness. So it is now mandatory to widen the knowledge of their crashworthiness capabilities (16) (17).

This fact demands new research activities, because these kinds of materials show higher brittleness, they are possibly more difficult to join, they are characterized by a decrease in mechanical properties in hot-wet conditions, post-crash integrity is less easy to achieve and a large amount of small fragments is projected in all directions during impact; but the real advantage offered by composites is that their specific energy is much higher so they really promise to reach higher crashworthiness standards (18).

In Figure 6 it is shown that the specific energy of carbon-epoxy specimens is more than twice with respect to aluminium specimens.

Besides in Figure 7 crushing behaviour of carbon-epoxy, kevlar-epoxy and aluminium alloy tube specimens are compared: it appears that composites guarantee a higher degree of energy absorption and an excellent load uniformity.

These results come from tube-test very simple, but however able to put into evidence some important aspects; even if there are some problems to solve, the promise to obtain good results is real.

6. FUTURE NEEDS

The aforementioned crashworthiness design procedures deserve the fulfilment of the following needs in the near future: to better understanding of energy absorbing mechanisms of composites, to increase post-crash integrity of composite structures, to

improve detail design, to develop a design procedure considering dynamic tuning between different energy absorbing mechanisms and joint behaviour, to widen and to deepen experience in the use of complete finite elements for crash analyses and to improve integration of experiments, hybrid simulation and true finite elements analyses.

7. CURRENT RESEARCH PROGRAM

Consequently, at Aerospace Engineering Department of Politecnico di Milano, a research program has started, sponsored by the Government within the frame of a "strategic project" and by Agusta Helicopters for the main technical aspects related to helicopter design.

The aims are: to improve knowledge on composites energy absorbing ability, to develop a reliable data base on crashworthiness detail design, to improve experience on crash testing and simulation, and finally to develop efficient procedures for crashworthy design of helicopter and aircraft structures.

The program of the research has scheduled first of all some component tests (namely beams and webs in compression, beam crossings in compression and beams in bending), using a drop test machine.

Beside, a larger horizontal crash machine has been developed, able to test subassemblies and large subfloor structures.

As far as finite elements crash analyses are concerned, to be used in conjunction with subcomponents experimental tests, a choice will be made between PAM-CRASH and ANCS codes.

At the end of this research program some drop tests of a full scale helicopter fuselage will take place.

In Figures 8, 9 the facilities existing in the Department are shown; the drop test machine has an height of 7 m, with a maximum velocity of 11 ms^{-1}, and a mass which can range from 55 to 180 kg; the bigger horizontal machine has a pneumatic drive, the plate is about 2 m^2 and the colliding mass may range from 350 to 1400 kg, while the maximum velocity is 15 ms^{-1} and the maximum impact energy is 80 kJ.

BIBLIOGRAPHY

(1) J.Mens, "Helicopter behaviour in crash conditions", IV European Rotorcraft and Powered Lift Aircraft Forum, Stresa, September 13-15, 1978.

(2) Military Standard, MIL-STD-1290 (AV), "Light fixed and rotary wing aircraft crashworthiness", January 25, 1974.

(3) Aircraft Crash Survival Design Guide, USARTL Technical Report 79-22, applied Technology Laboratory, U.S. Army Research and Technology Laboratories (AVRADCOM), Ft. Eustis, Va., 1980.

(4) G.Wittlin, "Aircraft crash dynamics research update", The Shock and Vib. Dig., vol.16, No.6, June 1984.

(5) J.L.Haley, J.E.Hicks, "Crashworthiness versus cost, based on a study of severe Army helicopter accidents during 1970 and 1971", J. of Am. Hel. Soc., April 1980.

(6) J.K.Sen, M.W.Votaw, "A skin stringer design for a crashworthy composite fuselage for the Hughes 500E helicopter", Hughes Helicopters Inc., Culver City, California.

(7) J.D.Cronkhite, L.T.Burrows, "Crashworthiness of helicopter composite structure", National Specialists' Meeting American Helicopter Society, March, 1983.

(8) J.K.Sen, M.W.Votaw, J.R.Downer, "Influences of two landing gear designs on helicopter crashworthiness and weights", XXXXI Annual Forum, Am.Hel.Soc., Forth Worth, Texas, May 1985.

(9) G.L.Farley, "Crash energy absorbing subfloor beam structure", J. of Am.Hel.Soc., October 1987.

(10) J.D.Cronkhite, T.J.Haas, R.Winter, R.R.Cairo, G.T.Singley, "Investigation of the crash impact characteristics of composite airframe structures", XXXXIV Annual Forum, Am.Hel.Soc., Washington, D.C., May 1978.

(11) J.Mens, J.C.Bianchini, "Computing codes for development of helicopter crashworthy

structures and test substantation", AHS/NAI International Seminar, Nanjing, November 6-8, 1985.

(12) R.J.Hayduk, R.G.Thomson, G.Wittlin, M.P.Kamat, "Non-linear structural crash dynamic analyses", Business Aircraft Meeting and Exposition Century II, Wichita, Aprile 3-6, 1979.

(13) B.L.Carnel, M.Pramanik, "ACAP crashworthiness analysis by KRASH", J. of Am.Hel.Soc., October 1984.

(14) R.Winter, J.D.Cronkhite, A.B.Pifko, "Crash simulation of composite and aluminium Helicopter fuselage using a finite element program", XX Structures, Dynamics and Materials Conference, St.Louis, April 1979.

(15) R.Hayduk, R.Winter, A.B.Pifko, E.C.Fasanella, "Application of DYCAST -A non-linear finite element computer program- to aircraft crash analysis", International Symposium on Structural Crashworthiness, Liverpool, September 15-16, 1983.

(16) J.K.Sen, "Designing for a crashworthy all-composite helicopter fuselage", XXXX Annual Forum, Am.Hel.Soc., Arlington, Va., May 1984.

(17) J.K.Sen, C.C.Dreman, "Design development tests for composite crashworthy helicopter fuselage", SAMPE Quar., vol.17, No.1, October 1985.

(18) D.C.Bannerman, C.M.Kindervater, "Crash impact behaviour of simulated composite and aluminium helicopter fuselage elements", Vertica, vol.10, No.2, 1986.

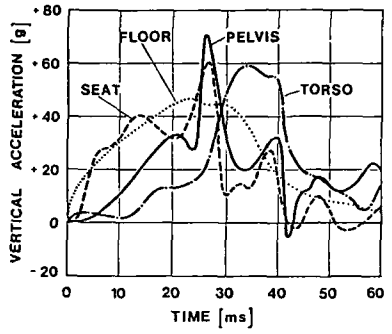

Figure 1: Results of numerical simulation

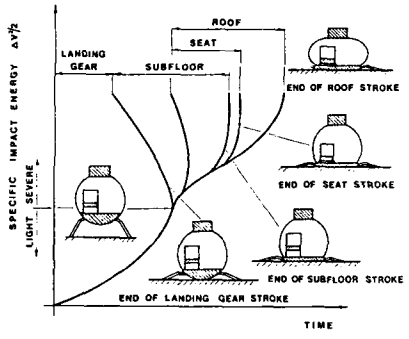

Figure 2: Economic constraint

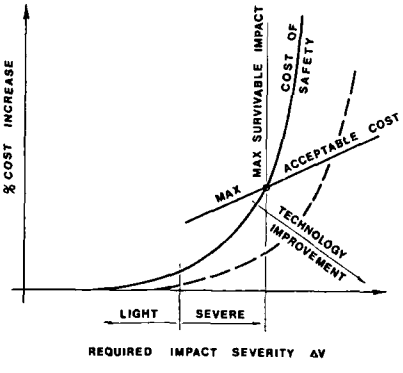

Figure 3: Intervention of the main energy absorbing elements (typical)

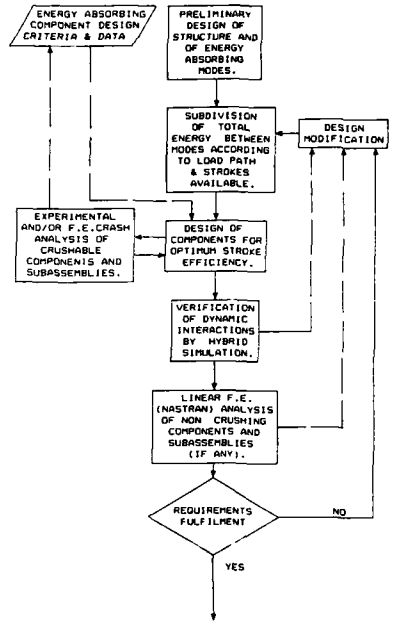

Figure 4: Non optimum design sequence

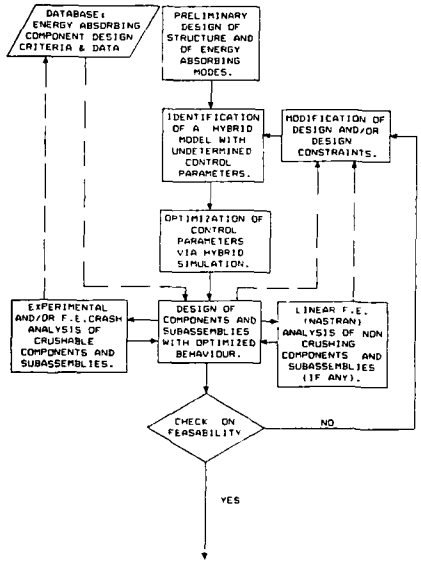

Figure 5: Optimum design sequence

MATERIAL : ALUMINUM ALLOY

MASS : 1.17 kg m^{-1}
ENERGY ABSORPTION : 29.9 kJ m^{-1}
SPECIFIC ENERGY : 25.5 kJ/kg
POST CRASH INTEGRITY : EXCELLENT

MATERIAL : GR/EPX $[\pm 45]_4$

MASS : .58 kg m^{-1}
ENERGY ABSORPTION : 40.4 kJ m^{-1}
SPECIFIC ENERGY : 69.6 kJ/kg
POST CRASH INTEGRITY : POOR

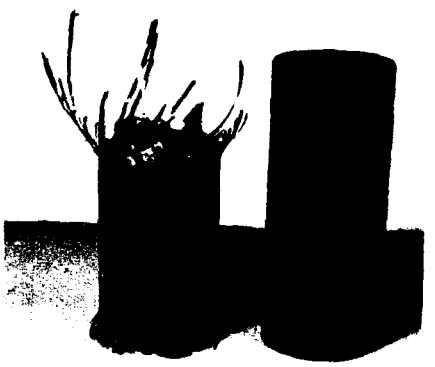

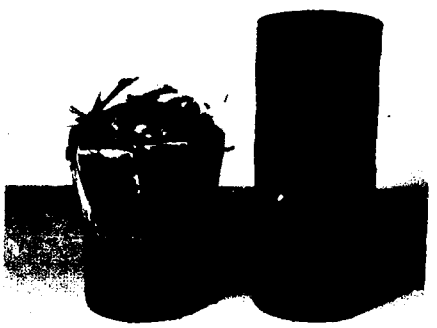

MATERIAL : GR/EPX $[\pm 45]_4$ + PTFE Peel Ply

MASS : .615 kg m^{-1}
ENERGY ABSORPTION : 43.2 kJ m^{-1}
SPECIFIC ENERGY : 70.2 kJ/kg
POST CRASH INTEGRITY : ACCEPTABLE

Figure 6: Energy absorption of tube specimens

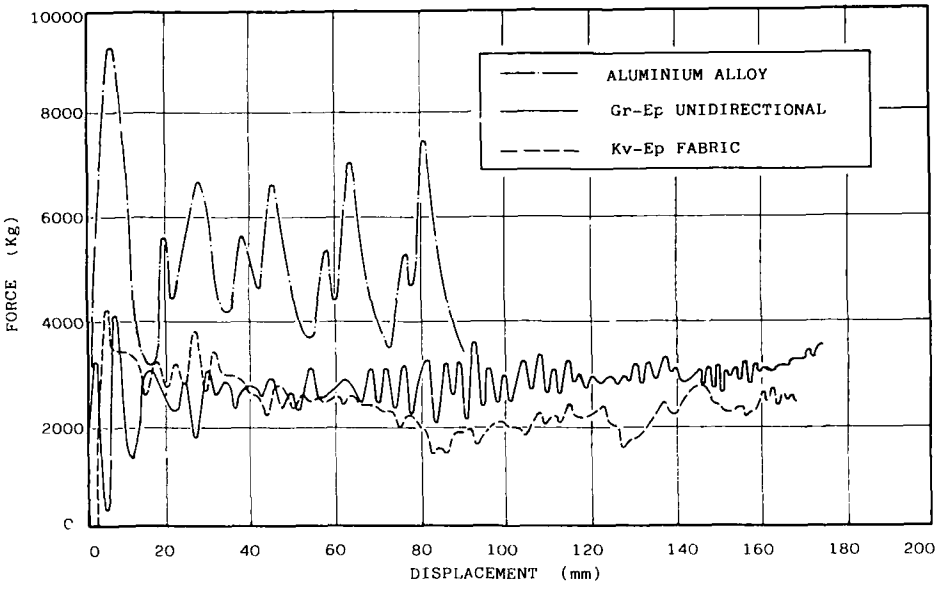

Figure 7: Typical crushing behaviour of tube specimens

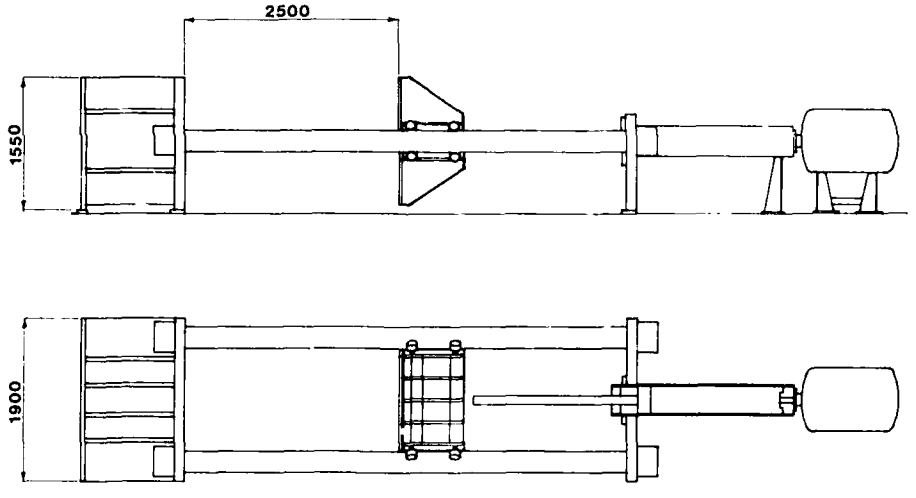

DRIVE : PNEUMATIC
MASS : 350 - 1400 KG
MAX VELOCITY : 15 ms^{-1}
MAX IMPACT ENERGY : 80 KJ

Figure 8: Horizontal crash machine

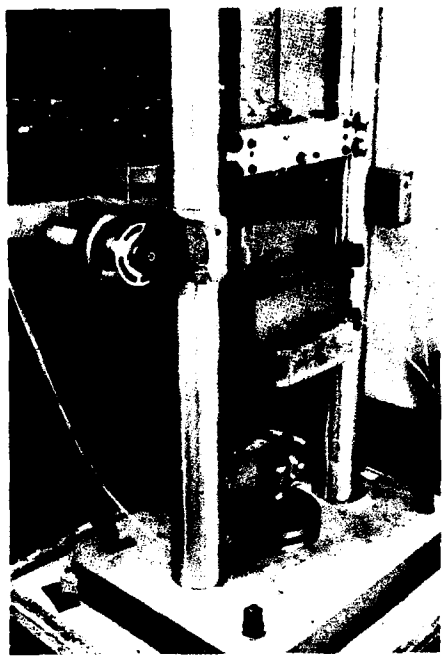

Figure 9: Drop test machine

MASS 55 ÷ 180 kg
HEIGHT 7 m

TRANSDUCERS:
3 load cells
1 accelerometer
1 encoder for velocity and displacement

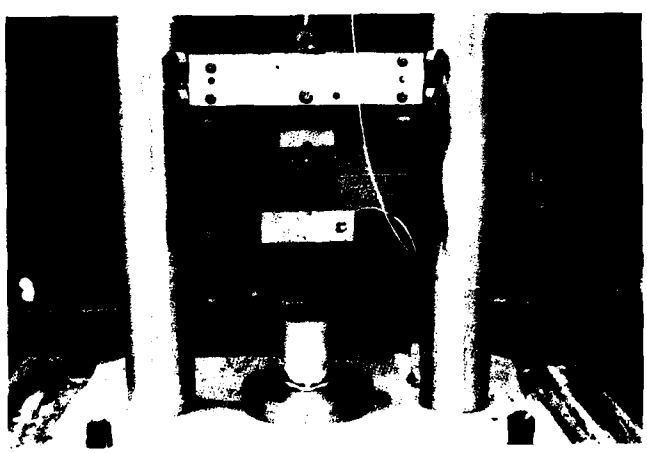

Développements et Perspectives dans le Domaine du Dimensionnement aux Impacts et au Crash aux AMD-BA

Y. MARTIN-SIEGFRIED

AVIONS MARCEL DASSAULT - BREGUET AVIATION

78, quai MARCEL DASSAULT - 92214 SAINT-CLOUD

ABSTRACT

Today we can solve efficiently the impact and soft crash sizing problems using a global ground-aircraft modeling.

Two illustrative examples are presented: hard landing of the MERCURE aircraft and soft crash of the FALCON 900 aircraft.

We are currently working on a research program dealing with hard crash problem for commuter-type aircrafts, funded by DGAC with technical support from STPAé and cooperation with FAA. This program includes study of actual crash cases, a crash demonstration experiment using a FALCON 10 aircraft. The data so gathered will be used to adjust our simulation model in order to determine the influence of various parameters. The final goal is to provide a sound basis to crashworthiness requirements.

In this paper we outline the main phases of this program.

1.0 INTRODUCTION.

Le dimensionnement des structures en dynamique présente des aspects complexes:

- le caractère aléatoire de nombreux paramètres, les conditions initiales par exemple, ce qui entraine un grand nombre de cas à envisager. Pour le crash il faut en outre fixer un seuil au delà duquel il est déclaré non survivable.

-la présence en général de nombreuses non-linearités au niveau de la géométrie, du contact et du comportement.

-la difficulté d'assurer une représentativité suffisante dans les essais et les calculs partiels.

Nous présentons deux exemples de dimensionnement aux impacts et au crash préparé qui illustrent une approche globale au moyen d'un outil de simulation efficace dont nous donnons les principes généraux.

Une action règlementaire, financée par la DGAC et supportée par le STPAé, est engagée en collaboration avec la FAA dans le domaine du crash survivable en conditions très sévères des avions de masse moyenne où il n'existe pas de données expérimentales.

AMD-BA assure la maitrise d'oeuvre de cette étude qui porte sur une analyse d'accidents, un programme d'essai de crash d'une cellule complète en vraie grandeur d'un MYSTERE-FALCON 10 et l'exploitation de simulations après recalage.

Nous décrivons les grandes lignes de cette étude en cours, en particulier les développements de nos méthodes de simulation pour répondre à ce genre de crash en conditions extrêmes.

2.0 REALISATIONS DANS LE DOMAINE DES IMPACTS ET DU CRASH.

2.1 Exemples de problèmes traités.

2.1.1 Atterrissage dynamique du MERCURE.

Bien que situé en deça du domaine du crash proprement dit, cet exemple illustre l'emploi d'un outil performant de dimensionnement en dynamique, élaboré dès le début des années 70 aux AMD-BA, selon une approche globale sol-atterrisseurs-avion.

Nous présentons, planche 1, une comparaison calcul-essai en vol d'un atterrissage dur du MERCURE, en particulier l'évolution des moments de flexion au droit des cadres principaux du fuselage.

Les principales caractéristiques du modèle utilisé sont:

- une schématisation par éléments finis de l'avion complet et de ses atterrisseurs.

- une linéarisation au voisinage du pas de temps précédent des non-linéarités "douces" (géométrie, aplatissement des pneumatiques etc ...).

- une condensation sur les degrés non-linéaires aigus (laminage et friction dans les amortisseurs) du système d'équations qui est résolu de façon exacte.

Des temps de calcul non prohibitifs ont permis de procéder à un grand nombre de simulations, rendant possible la prise en compte de l'aspect aléatoire de certaines entrées (conditions initiales, coefficient de frottement etc ...).

2.1.2 Dimensionnement des quilles du FALCON 900 à un crash préparé.

Le FALCON 900 est dimensionné pour une procédure d'atterrissage sévère trains rentrés à une vitesse verticale d'impact de 1,5 m/s.

Deux quilles en nid d'abeilles sous le fuselage absorbent une énergie suffisante pour assurer des efforts admissibles au niveau des cadres.

Outre la phase d'impact avec du roulis initial, les simulations effectuées comprennent la phase de glissement de l'avion jusqu'à son arrêt complet de façon à localiser et dimensionner des patins d'usure.

Quelques résultats d'un calcul sont regroupés planche 3 à 5.

Nous avons utilisé le module de dynamique quasi-linéaire de CATIA-ELFINI. Les étapes principales du calcul sont:

- une schématisation par éléments finis du demi-avion à 14000 degrés de liberté (planche 2).

- une condensation dynamique en base modale symétrique antisymétrique à 160 degrés de liberté.

- une intégration dynamique en base réduite par méthode implicite inconditionnellement stable.

Trois types de non-linéarités sont prises en compte:

- les grandes rotations du centre de gravité par linéarisation au pas de temps précédent.

- le comportement non-linéaire des éléments de nid d'abeilles (planche 6) traité de façon explicite.

- le contact sol-structure résolu par gradient conjugué projeté.

2.2 Principes des méthodes employées.

2.2.1 Degrés de liberté.

De façon générale les degrés de liberté Y sont issus d'un couplage de sous-structures discrétisées par éléments finis pouvant être traitées de deux manières:

- soit directement en base éléments finis X.

- soit en base réduite x par condensation dynamique pour les zones à comportement élastique linéaire prépondérant.

Dans ce dernier cas, le changement de base s'ecrit:

$$X = [\Phi]\, x$$

La base réduite est constituée:

- des modes rigides $[\Phi_r]$ s'il y a lieu.

- de modes élastiques fondamentaux $[\Phi_e]$.

- de déformées sous chargements unitaires $[\Phi_f]$ qui enrichissent la base au niveau des points de ccuplage, des points de contact etc ...

En pratique cette technique nous permet de réduire une structure de quelques milliers de d.d.l. à quelques centaines.

2.2.2 Intégration dynamique.

Nous avons à notre disposition toute une panoplie de méthodes d'intégration implicite et explicite programmées de façon unifiée par formule des résidus pondérés.

Pour les problèmes d'impacts et de crash, où les échelles de temps sont très supérieures à celles des propagations d'ondes, nous employons en général des schémas d'intégration implicite inconditionnellement stables de type Newmark notamment.

2.2.3 Non-linéarités.

Les cas de dimensionnement traités jusqu'à maintenant sont caractérisés par une intégrité d'ensemble de la structure dans le domaine élastique, les non-linéarités étant localisées.

Pour ce genre de problèmes, des éléments à comportement plastique simple sous forme scalaire se sont avérés suffisants et efficaces vis à vis des temps de calculs.

3.0 PERSPECTIVES.

3.1 Programme d'essai de crash d'une cellule de FALCON 10.

3.1.1 Objectifs et planning.

Un certain nombre d'essais dynamiques de crash ont concerné des avions de ligne de masse supérieure à 50 t, en particulier l'essai récent du BOEING 720 réalisé par la NASA pour la FAA.

Nous manquons par contre de données expérimentales pour les avions plus petits de la classe des "commuters" de masse comprise entre 6t et 50t.

Pour répondre à ce besoin, la DGAC et le STPAé nous ont chargés d'élaborer un programme d'essai de crash d'une cellule complète de notre avion d'affaire MYSTERE-FALCON 10 qui est représentatif de cette catégorie et dont nous donnons des caractéristiques générales planche 7 et un exemple d'aménagement intérieur planche 8.

L'objectif principal est de disposer d'éléments permettant d' orienter l'évolution des règlements.

L'étude engagée porte sur trois phases:

a) la préparation de l'essai.

Cette phase est en cours et sera terminée en Janvier 89.

Une collaboration engagée avec la FAA sera concrétisée au cours de cette phase.

Elle comprend:

- une étude d'accidents des avions de la classe des MYSTERE-FALCON afin d'évaluer les conditions initiales de l'essai de crash. Des conséquences structurales seront analysées afin de mieux évaluer les vitesses d'impact vertical.

- une étude des moyens d'essai.

- l'étude de l'aménagement de l'avion qui concerne l'instrumentation générale, les sièges et les mannequins.

b) l'essai et son analyse.

L'essai est prévu courant 89.

L'analyse portera sur les conséquences du crash au niveau structural depuis les zones de contact au sol jusqu'aux sièges, et au niveau des profils d'accélérations subis par les passagers eux-mêmes.

b) l'étude règlementaire.

Un modèle de simulation sera recalé sur l'essai. Il servira d'outil à une étude paramétrique.

Les résultats de ces travaux et de l'étude d'accidents seront analysés en vue d'en dégager des retombées réglementaires.

3.1.2 Scenario et moyens d'essais.

Le scénario envisagé d'ores et déjà correspond à un crash à forte vitesse d'impact vertical sans obstacle frontal, trains rentrés. Les conditions d'assiette et de roulis seront voisines de celles d'une présentation à l'atterrissage.

Deux moyens d'essai existants et susceptibles de remplir les conditions de crash sont actuellement à l'étude: l'aire de crash par pendulage du CEAT et le rail de catapultage du CEL. Le choix sera arrêté à l'issue de la phase préparatoire.

3.2 Développements dans le domaine des simulations.

Un développement des moyens d'analyse non-linéaire en dynamique fait l'objet d'une étude supportée par le STPAé. Il sera appliqué notamment à la simulation de l'essai de crash du FALCON 10.

Il s'agit d'une extension en dynamique du programme de flambement et post-flambement de notre logiciel ELFINI en y conservant la technique de super-éléments dynamiques décrite précédemment.

Ce développement comprend également la programmation d'éléments de flexion plastique, notamment pour la ruine en post-flambage multimode, et la prise en compte d'éléments de contact complexe et de frottement en grands glissements.

Le but est d'adapter le traitement de chaque type de non-linéarité , suivant des hypothèses simplificatrices raisonnables, afin d'aboutir à l'algorithme de résolution le plus économique possible.

4.0 CONCLUSION.

Nous couvrons aujourd'hui un grand nombre de nos besoins de dimensionnement aux impacts et au crash préparé.

L'exploration d'une approche globale du comportement au crash survivable extrême ,à laquelle nous participons au travers du programme d'essai du MYSTERE-FALCON 10, est une nécessité compte tenu de l'absence de données dans ce domaine et le manque de justification qui en résulte pour certaines règles de dimensionnement actuelles.

Elle requiert des développements supplémentaires dans nos techniques de simulation.

Il est encore trop tôt pour évaluer les conséquences au niveau des règles de dimensionnement pour les avions futurs.

MERCURE : ATTERRISSAGE DYNAMIQUE

Comparaison essais en vol - calculs

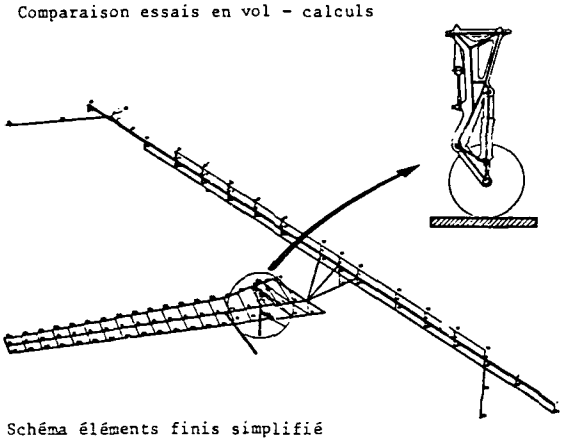

Schéma éléments finis simplifié

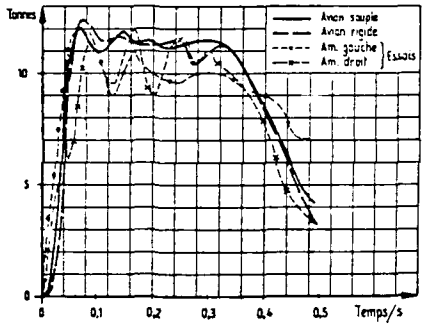

Effort amortisseur

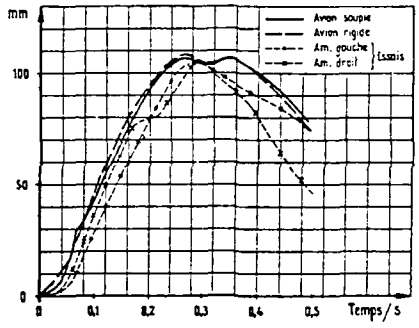

Enfoncement amortisseur

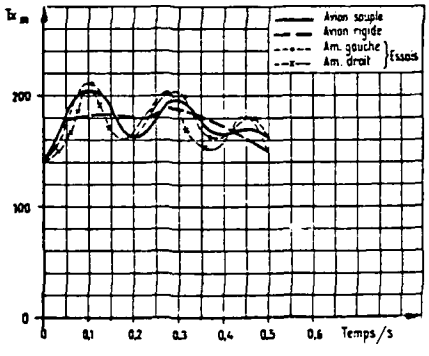

Moment de flexion au cadre
principal arrière

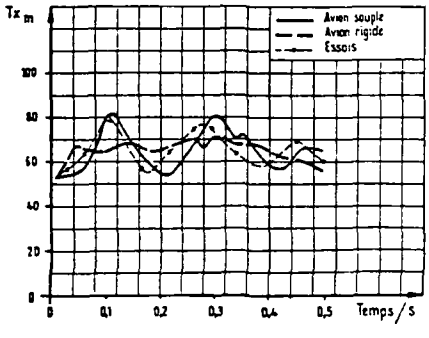

Moment de flexion fuselage
au cadre principal avant

Planche 1

MODELE PAR ELEMENTS FINIS DU FALCON 900

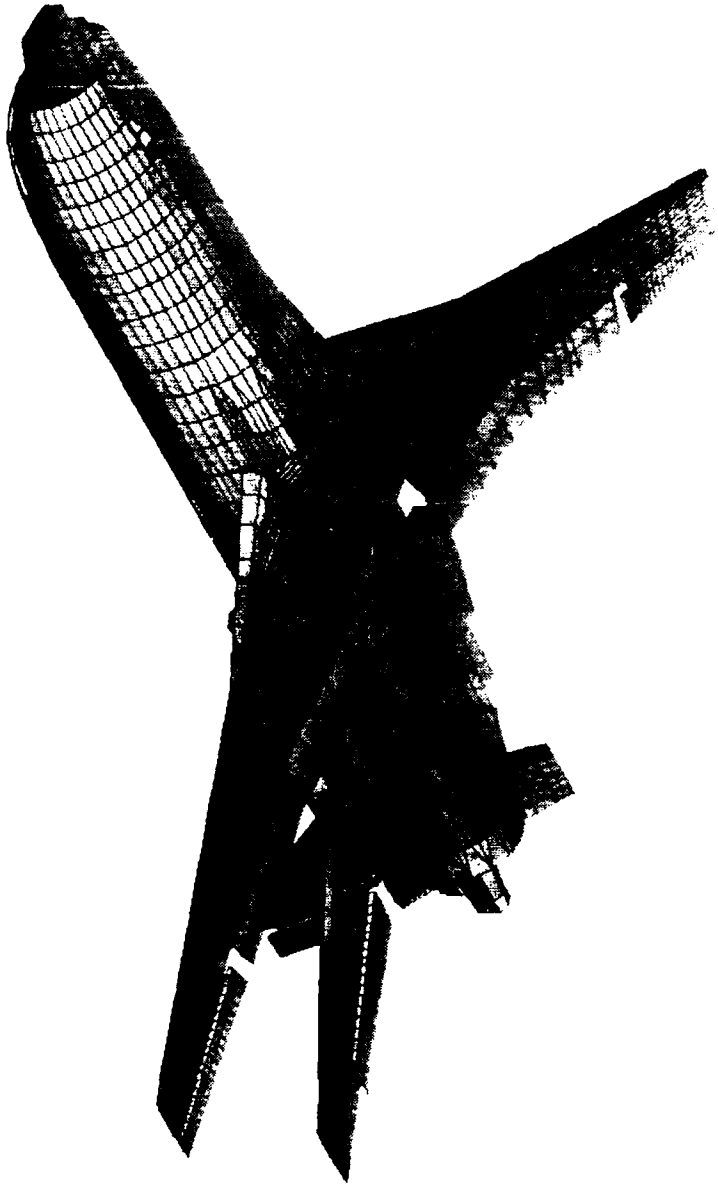

Planche 2

DIMENSIONNEMENT AU CRASH DU FALCON 900

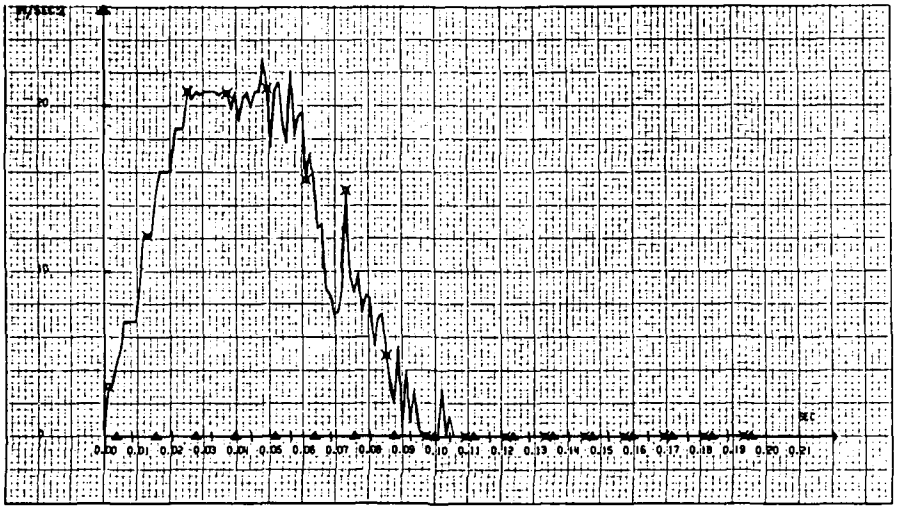

Accélération au C.D.G. dans la phase d'impact

Planche 3

DIMENSIONNEMENT AU CRASH DU FALCON 900

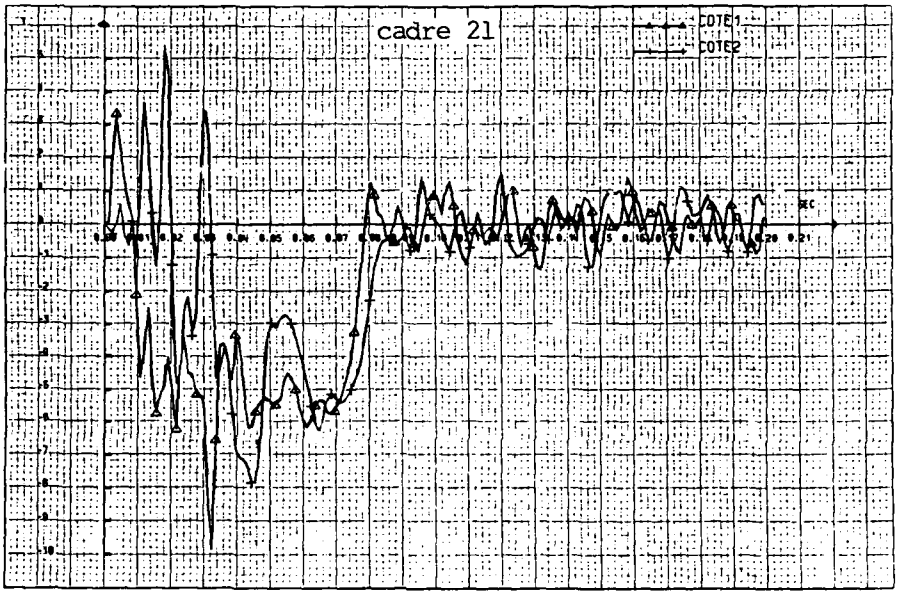

Efforts dans les cadres principaux
dans la phase d'impact

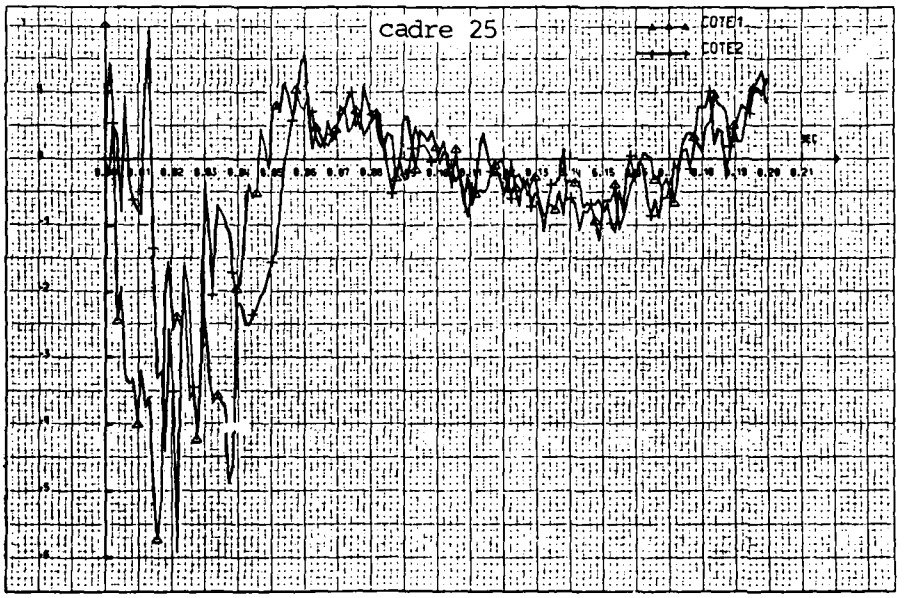

Planche 4

DIMENSIONNEMENT AU CRASH DU FALCON 900

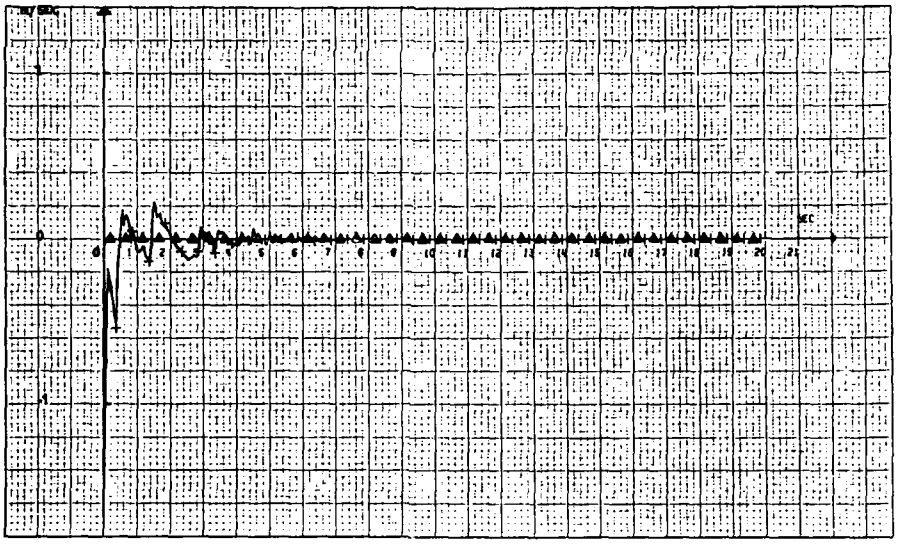

Vitesse verticale du C.D.G

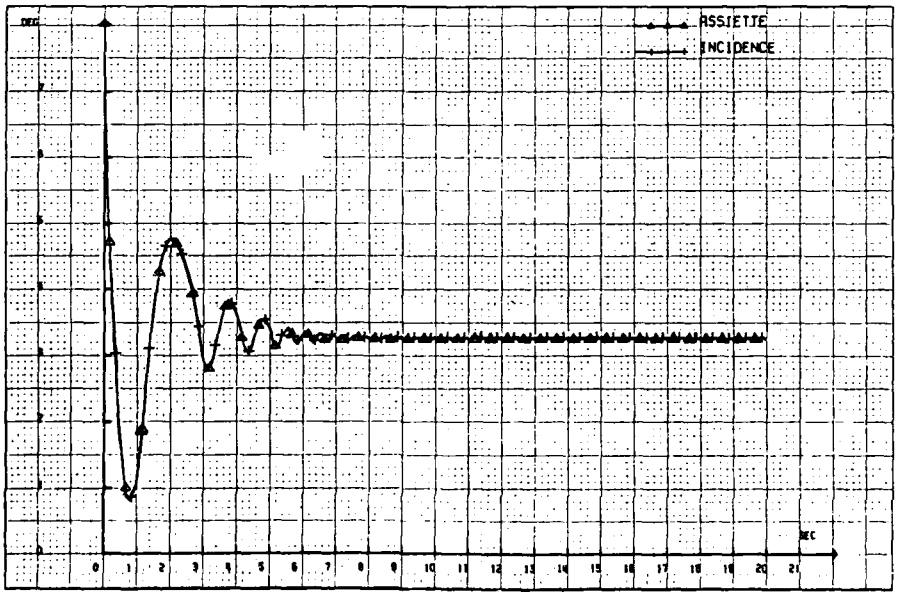

Assiette et incidence

Planche 5

HONEYCOMB CRUSH LAW

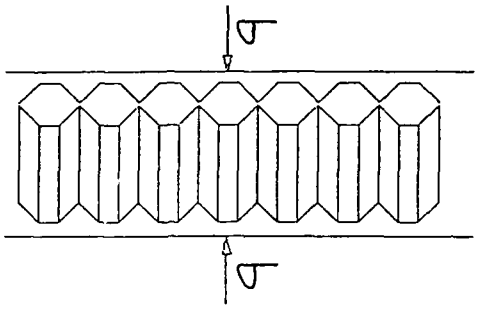

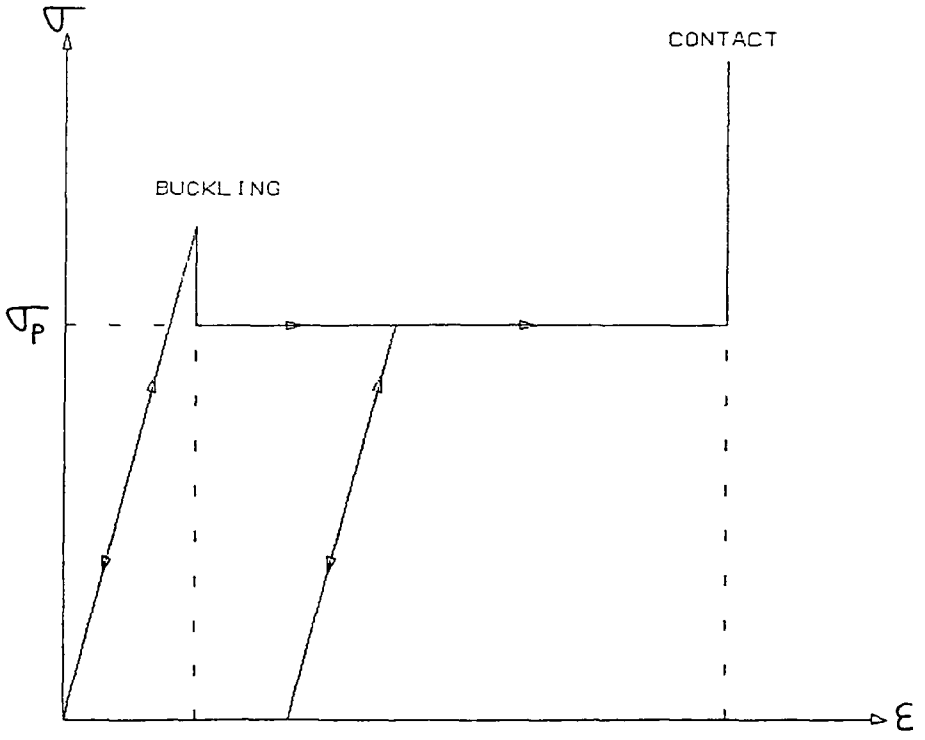

Planche 6

MYSTERE - FALCON 10

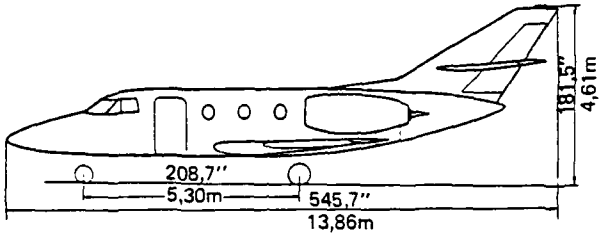

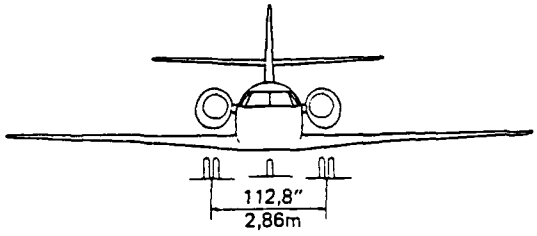

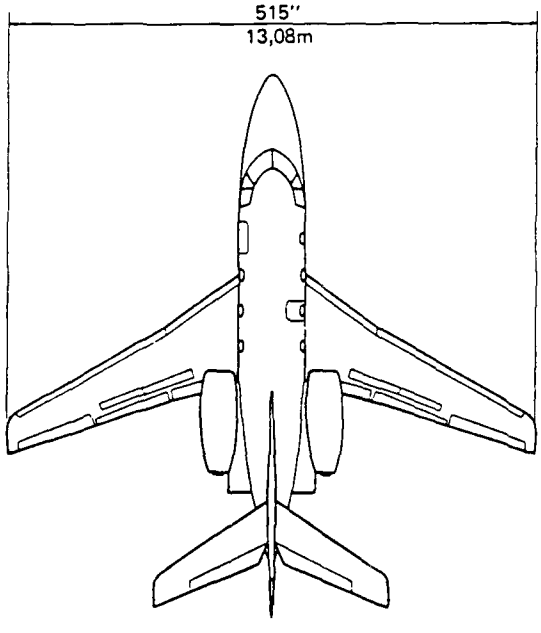

MASSES		WEIGHT
4 880 kg	10,760 lb	Equipped empty weight
2 680 kg	5,910 lb	Max fuel weight
1 090 kg	2,400 lb	Max Payload
8 085 kg	17,830 lb	Typical weight with 4 passengers, 2 pilots and max fuel
8 500 kg	18,740 lb	Max take-off weight
8 000 kg	17,640 lb	Max landing weight (≈ 94% of MTOW)
6 150 kg	13,560 lb	Max zero fuel weight

Planche 7

MYSTERE - FALCON 10

LAYOUT

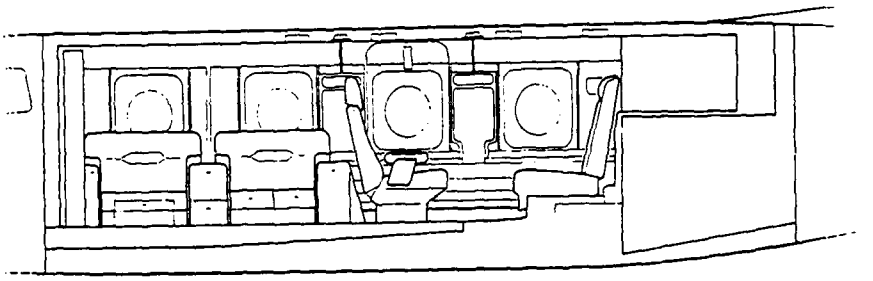

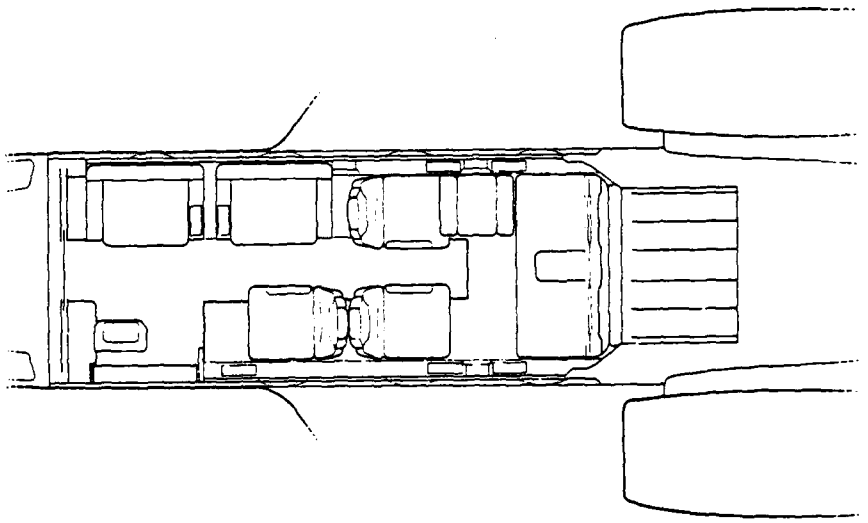

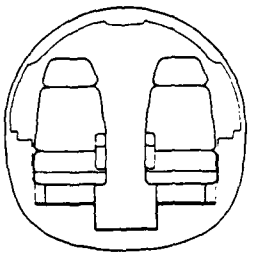

Planche **8**

FULL SCALE HELICOPTER CRASH TESTING

Harold Holland
Mechanical Engineer, Safety and Survivability Technical Area

Kent F. Smith
Aerospace Engineer, Safety and Survivability Technical Area

Aviation Applied Technology Directorate
U.S. Army Research and Technology Activity (AVSCOM)
Fort Eustis, Virginia 23604-5577

Introduction

Historically, whether one speaks of actual aircraft accident investigations or preplanned aircraft crash tests, a common objective exists: to gather as much pertinent information as is possible from a relatively complex and sometimes unpredictable dynamic event. The earliest aircraft accident investigations were for the purpose of merely establishing the primary accident cause. With aviation still in its infancy, those such as DeHaven (reference 1) began to learn far more from aircraft accident damage through a more sophisticated approach to accident investigation. Principles of energy absorption, human tolerance and structural integrity which contribute to occupant survival and injury reduction were gradually formulated based on astute observations. Eventually, the emphasis began to shift from merely determining the accident cause, to identifying a design philosophy which minimizes major injuries and fatalities in a crash. Consequently, more formal research activity was initiated.

Crash injury research began at Cornell University in the early 1940's with funding by the Office of Scientific Research and Development, a forerunner of the Office of Naval Research (reference 2). This work was later divided into two groups: one concerned with motor vehicle related problems (Cornell Aeronautical Laboratories in Buffalo, New York) and one concentrating on aircraft crashworthiness (Aviation Safety Engineering and Research (AVSER) in Phoenix, AZ).

Today, analytical math models are becoming more capable of predicting the dynamic behavior of aircraft structures and occupants subjected to crash loads. The engineering community still finds it necessary, however, to periodically perform full-scale crash tests for the purpose of validating math models, exploring new crashworthy component design concepts, defining synergistic effects or a variety of other valid goals.

The following sections will address aspects of full-scale aircraft crash testing based on almost 30 years experience by the U.S. Army Aviation Applied Technology Directorate (AVSCOM) and its predecessor organizations. Though each test is unique, certain principles and procedures have been found to provide a high degree of assurance of acquiring accurate data.

Background

The Army aviation crashworthiness development program was implemented in 1959 with award of a contract to Aviation Safety Engineering and Research (AVSER), Phoenix, AZ. Initial emphasis was on the in-depth accident investigation to acquire data on the kinematics and injury patterns associated with survivable accidents*. Concurrently with the accident investigation activities, an experimental testing program was undertaken to supplement the qualitative data derived from accident investigations with quantitative data derived from experimental testing.

During the ensuing 15 years, a total of 37 full-scale crash tests were conducted at AVSER for the Army for the purpose of evaluating a wide variety of experiments (seats, fuel tanks, modified fuels, atmospheric environment, cargo restraint, structural crashworthiness). The majority of these tests (18) utilized a moving crane drop method; however, other test methods utilized by AVSER were the track-rail method and the remote control drone system. A brief description of each of these crash test methods is presented as follows:

*Survivable accident - An accident in which the forces transmitted to the occupant through the seat and restraint system do not exceed the limits of human tolerance to abrupt accelerations and in which the structure in the occupant's immediate environment remains substantially intact to the extent that a livable volume is provided throughout the crash sequence.

a. Crane Drop Method - This method involves the suspension of the aircraft behind the elevated boom of a large crane at a predetermined height. The crane is then driven on a runway at a desired speed and as it passes over the impact site an automatic triggering mechanism releases the aircraft and it impacts on the target at predetermined vertical and longitudinal velocities. Data can be telemetered, however, the simplest procedure is to mount the recording device on the rear deck of the crane and connect the data recorder to the end instruments in the aircraft with an umbilical cable of sufficient length to permit the crane to stop after release of the aircraft without disconnecting the cable.

b. Track Rail Method - This method involves mounting the aircraft on a sled type device and accelerating the sled to the required velocity and impacting the aircraft into a barrier. The aircraft are mounted on the sled in such a way that, coupled with the design of the impact barrier, will provide the desired location and magnitude of forces imposed on the aircraft structure. Data can either be telemetered or transmitted through an umbilical cable. This method is utilized mostly for fixed wing aircraft as their gear and wheels can be used in moving the aircraft down the track.

c. Remote Control (Drone) Method - This method involves the use of a radio link, remote control flight system to guide the aircraft to the desired impact condition from powered flight. The interface controls actuating equipment is installed at the pilot seat location (pilot seat removed). Data from on-board instrumentation in the aircraft is transmitted to a data acquisition center near the impact area by means of FM telemetry.

After conducting 37 crash tests for the Army, AVSER started devoting more and more of their efforts to automobile crash testing and as a result removed themselves as the Army's foremost test facility for full scale testing and authority on aircraft crashworthiness. With this loss of AVSER as a test facility the Army had to find another source for the conduct of full scale crash testing. At approximately this same time period (early 1970's), the National Aeronautics and Space Administration's (NASA) Langley Research Center (LRC) converted their lunar landing research facility into an impact dynamics research facility for investigating structural crash effects on general aviation type aircraft. The Army has, since 1975, in cooperation with the NASA-LRC conducted five full-scale crash tests utilizing the impact dynamics research facility (Gantry swing method).

Gantry Swing Method involves suspending the aircraft above the ground under a gantry structure, then swinging it in pendulum fashion and releasing it to simulate free flight crash conditions at impact. Attitude of the aircraft at impact can be closely controlled by design of the cable suspension system. An umbilical cable used for data acquisition is suspended from the top of the gantry and is connected to the top of the aircraft. The swing cables which guide the aircraft into the desired impact conditions during the pendulum swing are separated from the aircraft by pyrotechnics just prior to impact, freeing the aircraft from restraint. The umbilical cable remains attached to the aircraft for data acquisition, but it also separates by pyrotechnics before it becomes taut during the slide, after impact.

Test Method Comparison

Utilizing the powered flight (drone) method of crash testing provides the most realism in that the dynamic (rotor) systems can be powered during the crash sequence thus providing more realistic test results for specified impact conditions. With respect to reliability, in terms of target impact velocities and aircraft attitudes at impact, the droned flight method is probably less reliable than the other methods due mainly to the remote control aspects of guiding the aircraft. More preparation time will be required to perform a droned crash due to installation of the interface equipment for actuating the aircraft controls upon command, and also precrash flight testing is required to assure proper control of the aircraft during the actual test flight. The drone test method also usually requires that the data be transmitted via telemetry or be recorded by onboard recorders. Telemetry data, using today's technology, is of approximately the same quality as that acquired over a hard wire. There is always the possibility, however, that interference may occur with the transmitted signal or that transmitting antennas may become blocked or damaged during the impact event, obscuring the data. Onboard recording of the data, of course, runs the inherent risk of loss due to unexpected damage to the recorders during the test.

The major cost element for each of the test methods, regardless of who performs the tests or where they are conducted, is the manpower required to prepare the aircraft, install the instrumentation, conduct the test, reduce and analyze the data, and prepare the test reports. The droned test method is generally more expensive due to the precrash flight testing and redundant instrumentation.

NASA - LRC Impact Dynamics Research Facility (IDRF)

The site of the five most recent U.S.. Army full-scale crash tests has been the IDRF at NASA Langley Research Center; Hampton, Virginia. The facility was originally constructed as a lunar lander training facility for the United States Apollo space

program. It consists of a 67 meter (220 foot) high by 122 meter (400 foot) long steel gantry structure and associated office, shop and control areas (see Figure 1). The gantry is supported by three sets of inclined legs spread 81.4 meters (267 feet) in width at ground level and 20.4 meters (67 feet) apart at the 66.4 meter (218 foot) level. A movable bridge with cable winches spans the gantry at the 66.4 meter (218 foot) level with the capability to traverse the length of the gantry. Along the centerline of the gantry, at ground level, a reinforced concrete strip 122 meters (400 feet) long, 9.1 meters (30 feet) wide and 20.3 cm (8 inches) thick is used as an impact surface.

The five full scale crash tests conducted at the NASA LRC Impact Dynamics Research Facility and the test objectives were:

- CH-47A (T-39) - To evaluate the airframe structural response, occupant and cargo loadings during a severe, nose-up crash impact of a cargo helicopter.

- CH-47A (T-40) - To evaluate the airframe structural response, occupant and cargo loadings during a severe, nose-down crash impact of a cargo helicopter.

- YAH-63 (T-41) - To assess the effectiveness of structural crashworthiness features designed into an Army attack helicopter during a severe but survivable accident and to evaluate the performance of several developmental crashworthy systems in an actual crash environment.

- D292-Bell Helicopter Textron Advanced Composite Airframe Program (ACAP) (T-42) To demonstrate the crash energy absorption capacity of the ACAP landing gear and advanced composite fuselage structure.

- S-75-Sikorsky Aircraft Advanced Composite Airframe Program (ACAP) (T-43) To demonstrate the crash energy absorption capacity of the ACAP landing gear and advanced composite fuselage structure.

As an example of what is required in terms of full scale helicopter crash testing equipment and procedure, much of this paper will examine the U.S. Army's Crash Test T-41, which occurred on 8 July 1981 at the NASA LRC IDRF. The test specimen was a YAH-63 attack helicopter and was the first full-scale test of a helicopter which, from inception, was designed with multiple crashworthiness features. The Army report on T-41 is shown as reference 3.

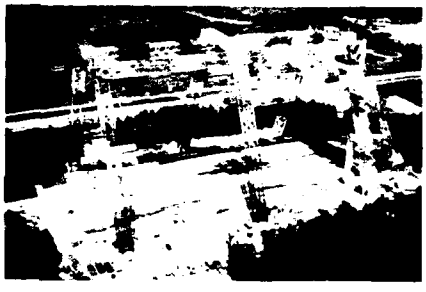

Figure 1. NASA-LRC Impact Dynamics Research Facility

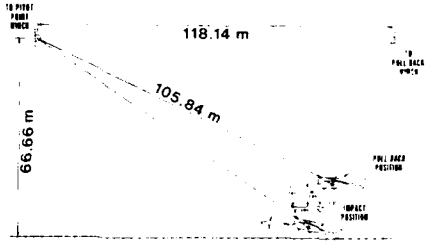

Figure 2. Facility and cable geometry for T-41 crash test at NASA-LRC

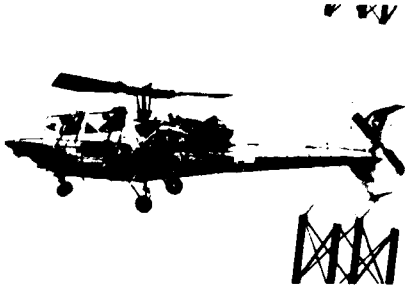

Figure 3. YAH-63 cable and data umbilical geometry for T-41 crash test

Figure 4. Guillotine type cable cutter for 11 mm (7/16 inch) diameter cable

The apparatus necessary to conduct the T-41 crash test is illustrated in Figure 2. Swing cable pivot-point platforms, located at the west end of the gantry, support the winches, sheaves, and pulley systems that control the length of the swing cables. A pull back platform, attached to the underside of the movable bridge (shown toward the east end of the gantry) supports the winch, sheave and pulley system that controls the length of the pull back cable. Swing and pull back cables are attached to a specially designed lifting harness, which supports the test article in the desired ground impact pitch, roll and yaw attitude. Each lifting harness configuration is unique to the particular test article and requires expert design to yield the desired results. For example, when properly rigged, both the swing cables and the pull back cable must project as imaginary lines through the aircraft center-of-gravity. Otherwise, upon pull back cable release, moments generated about the aircraft C.G. will cause unwanted attitude changes in the aircraft during the swing/drop event. In the case of T-41, the harness (Figure 3) was attached to special mounting bolts on steel support plates fabricated to place the mounting bolts at the aircraft's longitudinal and vertical C.G. The steel plates in turn were sandwiched in the stub wing mounting lugs. Each pull back cable was equipped with a pyrotechnic cable cutter (guillotine type), an example of which is shown in Figure 4. The part of the lifting harness attached to the swing cables was connected to the helicopter mounting bolts by pyrotechnic release nuts. The drop sequence begins when the pull back cable cutters are fired, allowing the aircraft to free-fall in a pendulum-like swing while still attached to the swing cables. At approximately 1.2 meters (4 feet) prior to impact, a lanyard connected to a pull pin near the rear of the aircraft is rigged to go taut, pulling the pin and activating a firing circuit. This circuit fires the swing cable pyrotechnic release nuts, releasing all suspension cables prior to impact. Therefore, except for the data umbilical cable(s), the aircraft impacts the surface in free flight at or near the preplanned impact attitude.

Cable Rigging for Typical Aircraft Test

The determination of cable lengths for a typical gantry swing crash test is by straightforward trigonometry. The desired ground impact angle is drawn through the aircraft C.G. as viewed in profile. This line is tangent to the flight path at the instant of impact and is also perpendicular to the swing cables. The angle thus formed between the swing cables and ground at the time of impact is 180° plus the flight path angle minus 90° = 90° plus the flight path angle, where the flight path angle is always a negative value. The height of the pivot point winch above the impact surface is a fixed distance of 66.7 meters (218.7 feet) (see Figure 2). The right triangle formed by the swing cables as the hypotenuse, the impact surface and the pivot winch height dimension is now solved to determine the required swing cable length. In the case of T-41, this length was 111.1 meters (364.5 feet). As this is the dimension from pivot winch to aircraft C.G., the distance consumed by the rigging harness, 5.26 meters (17.25 feet) must be subtracted to arrive at the actual swing cable length of 105.84 meters (347.25 feet).

Pull back height for any given test is determined by a simple potential-to-kinetic energy conversion process plus an additional height to account for aerodynamic drag. The appropriate equation is:

$$h = 0.5 \left(\frac{V_r^2}{g} \right) (1 + DF)$$

where: h = Vertical height above impact surface of aircraft component making initial contact (may be tail stinger for nose-up impact)

V_r = Resultant velocity desired at ground impact.

g = Gravitational constant

DF = Drag factor expressed as a percentage of total aircraft impact kinetic energy (usually 5% - 20%).

Figure 5 expresses this equation in graphical form. Care must be taken in estimating the drag factor for a given configuration. Aircraft geometry, wing loading and descent attitude must all be considered when making the estimate. In cases where additional accuracy is required, practice swings may be performed with the swing cable length appropriately adjusted to provide safe ground clearance. Actual peak velocities at the bottom of the pendulum swing can then be compared to theoretical (zero drag) predictions to establish a realistic drag factor. At the NASA-LRC facility, a tripod-mounted radar device is located in front of the aircraft during its swing. The electronic recording from this radar provides a continuous velocity (V_X) vs. time output during the swing.

Weight and Balance Considerations

It is never too early in the crash test preparation to begin planning a solution to the weight and balance problem. In most instances the test engineer has the test gross weight and sometimes the longitudinal C.G. position dictated by higher authority. The situation is often complicated by the fact that crash test articles are almost never flyable aircraft and are often received in pieces. The airframe may be devoid

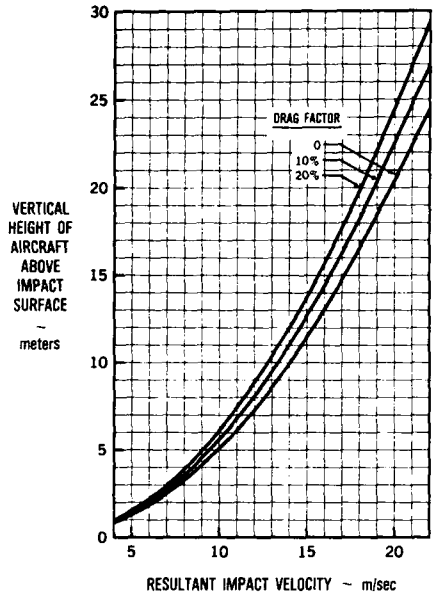

Figure 5. Pull back height/impact velocity relationship for gantry swing test method

of critical components whose absence would invalidate the test from a structural crashworthiness standpoint (e.g., engines and/or transmissions). In these cases, the missing items should be replaced with masses that closely approximate the inertial properties and attachment locations of the original components.

In helicopter crash tests, treatment of the main rotor blade deserves special attention, assuming the impact occurs with the rotor blade in a static (unpowered) condition. In most actual crash situations when the pilot is able to maintain attitude control until impact, a last-minute collective and cyclic flare maneuver is usually attempted. This is to cancel out forward speed and to minimize vertical sink speed. On impact lift being generated by the main rotor system is responsible for offsetting a certain percentage of the downward reactive inertial loads applied by the transmission to it's mounts. It would, therefore, be pessimistic to expect the airframe to be required to react 100% of the transmission/rotor hub/rotor blade inertial mass. In helicopter tests conducted by AATD, an attempt has been made to compensate for this by removing the outer 2/3 of the main rotor blades as part of the test preparation. This also assists in simplifying the cable rigging task in many cases.

As soon as the test specimen can be assembled (with seats, anthropomorphic dummies and high mass items) to the extent possible, it should be properly weighed in a level attitude and an initial gross weight and longitudinal C.G. determined. This information plus the center-of-gravity envelope for the aircraft will assist in planning the location and amounts of fuel, test equipment and ballast in order to achieve the target C.G. and gross weight. Care should be exercised in selection of ballast locations to avoid an inordinate and unrepresentative concentration at any single location. This will avoid localized structural failures during the test, caused by concentrated ballast dynamic loading.

The final weight and balance check should be in an "all-up" test condition and be accompanied by a detailed weight and balance sheet for test report purposes. The weight and balance summary for T-41 is shown in Table 1.

TABLE 1. WEIGHT AND BALANCE SUMMARY

ITEM	WEIGHT (lb)	LONGITUDINAL STATION (in)	MOMENT (in - lb)
Basic YAH-63	9,409	305.5614	2,875,027
Dummy T-700 Engines (2)	974	358.0000	348,692
CPG Crewseat (AH-64)	137	182.4000	24,989
CPG Dummy and Helmet	175	173.0000	30,275
CPG Cameras (2)	20	177.0000	3,540
Pilot Crewseat (YAH-63)	149	242.2000	36,088
Pilot Dummy and Helmet	175	234.0000	40,950
Pilot Camera (1)	10	244.0000	2,440
Camera Mounts (2)	120	210.0000	25,200
Stub Wing Lift Plates (2)	175	294.0000	51,450
Batteries (2)	60	232.0000	13,920
IBAHRS J-Box	35	193.0000	6,755
Navy FIR/CPL	14	494.0000	6,916
Nose Gun Turret	185	122.2000	22,607
Fuel (Water) - Fwd Tank	658	293.2500	192,959
Fuel (Water) - Aft Tank	859	324.1400	278,436
Tail Ballast (Removed)	-44	679.0000	-29,876
Nose Ballast	379	120.2000	45,556
Tailboom Ballast	278	417.0000	115,926
Totals at Test	13,768	297.2000	4,091,850

Photographic Coverage

Photographic coverage of the full-scale helicopter crash tests conducted at the Langley IDRF is provided by cameras located on the ground, on top of the gantry, and on-board the aircraft. There are three camera positions located on the gantry, two stationary and one movable, which view the crash from overhead and are used to measure yaw angle at impact. There are fixed ground cameras located on each side of the aircraft impact area and scanning cameras located to one side that, in addition to filming the crash from pull back cable release until impact, are used to determine roll and pitch angles, flight path angles, and velocity along the flight path. All fixed cameras are activated from the control room by an energizing circuit which is controlled from a pull back cable release circuit. Onboard cameras are used to film primarily onboard experiments and the reactions of seats, occupants, and selected structural areas of the aircraft. All of the cameras are 16 mm operating at speeds up to 400 ft/sec. In addition to these cameras, 70 mm still sequence cameras are used to film the crash. These cameras provide high resolution still photographs of the crash sequence at 50 ms intervals. In addition, real time film and video tape coverage of the test are taken. Extensive pre- and post- test still photographs are valuable in test documentation and analysis.

Instrumentation and Recording System

The test aircraft are heavily instrumented (100 data channels or more) with accelerometers, load cells, strain gages, displacement sensors, pressure sensors in order to obtain data to the maximum extent possible during the crash sequence. Some typical instrumentation functions are as follows:

a. Accelerometers - Used to provide accelerations of seat occupant head, chest, and pelvic positions, seat pan, transmission and engine tiedowns, and significant structural locations, such as seat input accelerations, throughout the airframe.

b. Load Cells - Provide the tension loads for the restraint system and to measure crew seat energy attenuator loads.

c. Strain Gages - Employed to measure axial load strain on such items as main transmission supports, seat energy attenuators, and main landing gear struts.

d. Displacement Sensors - Utilized to measure seat displacement, landing gear second stage displacement, and structural deflection at specific locations.

e. Pressure sensors - Used to measure fuel tank hydraulic ram pressure and oil pressure in landing gear struts.

f. Contact switches - Used as special purpose switches placed at specific locations to assist in determining precise timing of certain events, such as initial ground contact.

Data signals from the aircraft instrumentation during the crash sequence are transmitted through a junction box and umbilical cable into FM tape recorders and associated data conditioning equipment located in the control area.

Summary

The need for full-scale aircraft crash testing still exists as a means of demonstrating new crashworthiness concepts and improving the nonlinear predictive capability of current math models. The U.S. Army has conducted 43 full-scale crash tests over the past 29 years in a comprehensive effort to define occupant injury mechanisms, determine the upper limits of survivable loads and develop improved aircraft designs for crashworthiness.

Certain test methods and procedures for acquiring crash test data have been refined through the years and found to give reliable results. The gantry swing test method has been found to provide good impact vector control (aircraft attitude, flight path and velocity) while keeping the test confined to a relatively small area This aids greatly in acquiring good photographic and test data.

Instrumented full scale crash tests would prove very beneficial during the engineering development phase of a new aircraft development program to verify and substantiate the crashworthiness capability of the aircraft design. Comparison of the crash data with the design criteria will allow the designers to determine areas which are both overdesigned and inadequately designed so these areas can be corrected prior to aircraft production.

Enhanced or improved crashworthiness for Army helicopters in the future will result in (1) reduced loss of Army personnel and materiel as a result of aviation mishaps, (2) lower aircraft system weight devoted to crashworthiness thus reducing effects on operational performance, (3) reduction of aircraft system development, acquisition, and life cycle cost, (4) an earlier break even point where fleet life

cycle cost benefits of design for crashworthiness balance fleet cost, thereby enhancing the overall cost effectiveness of design for crashworthiness, and (5) improved Army aviation mission readiness.

The acquisition of a suitable aircraft test specimen remains a difficult task due to priorities and funding constraints. Given this fact, full-scale crash tests of the future must be performed using proven and reliable test methods having the capability to extract the maximum amount of data.

References

1. DeHaven, H., "Beginnings of Crash Injury Research," Speech at the 12th STAPP Conference in 1968 and published in the Proceedings of the 13th STAPP Conference 1969, Society of Automotive Engineers, New York, 1969.

2. Perrone, Nicholas, "An Overview of Aircraft Crashworthiness Research and Development," in Aircraft Crashworthiness, K. Saczalski, et. al., eds., University Press of Virginia, Charlottesville, Virginia, 1975, pp. 3-14.

3. Smith, K. F., Full-Scale Crash Test (T-41) of the YAH-63 Attack Helicopter, USAAVSCOM TR-86-D-2, Aviation Applied Technology Directorate, U.S. Army Research and Technology Directorate, U.S. Army Research and Technology Activity (AVSCOM), Fort Eustis, Virginia, April 1986.

4. Vanghan, Victor L. and Alfaro-Bon, Emilio, Impact Dynamics Research Facility for Full-Scale Aircraft Crash Testing, NASA TN D-8179, NASA Langley Research Center, Hampton, Virginia, April 1976.

CRUSHING BEHAVIOUR OF HELICOPTER SUBFLOOR STRUCTURES

by

J.Frese, D.Nitschke

Messerschmitt-Bölkow-Blohm GmbH

Postfach 80 11 40

8000 München 80, Germany

SUMMARY

Crash loads must be attenuated in the landing gear, the subfloor structure and the seat to values tolerable for the human body. In addition the remaining loads must not jeopardize a living space for the occupants.

A programme was undertaken to investigate, both analytically and experimentally, the crushing behaviour of helicopter subfloor structures.

Stiffened panels and honeycomb sandwich panels in metal were considered under quasistatic and dynamic conditions.

The primary intent of the investigations was to design subfloor structures with high efficiency for crash impact and to establish the nonlinear characteristics of subfloor structures as input data for the programme KRASH.

1. INTRODUCTION

With the growing importance of crashworthiness not only the loads envelope and system requirements have to be considered in designing the helicopter structure but also crashworthiness requirements according to MIL-STD-1290 (AV). This is also the case at the Indian ALH presently under design by Hindustan Aeronautics in cooperation with MBB. Numerous studies have shown that an improved crashworthiness can create economical benefits although additional costs are generated [e.g. 8]. Furthermore an improved crashworthiness is desirable from the humanitarian point of view.

In contrary to flight and landing loads the duties that are created by crashworthiness requirements are partially different or even contradicting. The traditional design principal of lightweight structures - - max. strength and stiffness at min.weight - has to be changed as it is necessary to design for controlled failures and stable crushing behaviour. Furthermore the designer has to distinguish between the different areas of the structure. While the underfloor structure as the first impact area has to fulfill primarily energy absorbing duties it is most important to keep the upper structure as a protective shell for the occupants.

This paper presents results from a running development program for an optimized underfloor structure considering the contraints of a real size structure as well as the system interfaces. As it is highly important to save additional weight not only a good absolute energy absorption has to be achieved but above all a good specific energy absorption (absorbed energy per mass of absorbing structure). Furthermore it is necessary to obtain a load level as constant as possible over the whole stroke. One reason for this requirement is the necessity that too high load factors have to be avoided and another is again the need to save additional weight.

Based on the results of previous work at the MBB Bremen plant we conducted numerous tests with sheet-stringer specimen as well as with sandwich specimen. Most of the tests with improved sandwich components are presently under way. Therefore no results of tests with this kind of structure will be presented. This paper deals primarily with sheet-stringer specimen. As those specimen were tested statically and dynamically a short overview of the test set-ups will be given too. Our tests comprised specimen with open section stiffeners and specimen with closed section stiffeners. It will be shown that closed sections are advantageous compared with open sections. Nevertheless it is possible to improve even open sections to a level that permits their use under certain conditions. Furthermore also first results with compound specimen with closed sections will be presented that show clearly that the effect of mutually supported edges is of great importance.

A comparison of test results and numerical calculations of panels under crash loads will be presented too as it was an important topic to investigate the possibility to replace expensive and timeconsuming tests by numerical simulations.

2. GENERAL REMARKS

The investigations summarized in this paper are related to cargo/utility helicopters in the 4 - 6 ton class with underfloor fuel tank systems as it is the Indian Advanced Light Helicopter (ALH. Figure 2-1.. This helicopter is presently in development by Hindustan Aeronautics Ltd. in cooperation with MBB.

The underfloor structure together with the landing gear are the main energy absorbing systems of a helicopter. The crashworthy seat although very important for the pilot himself takes only a negligible part of the total kinetic energy. Furthermore the structure is of great importance as the energy absorption of the landing gear may be hampered in a crash on muddy soil or in case of a retracted landing gear. In case of a skid type landing gear the structure is of primary importance as the energy absorbing capacity of the landing gear is limited.

For the assessment of structural concepts concerning energy absorption as well as for the optimization process there are a number of criteria on which these concepts should be checked for and compared between each other. The key parameters [4] are shown in figure 2-2. The parameter "load uniformity" has been exchanged from our side by the parameter "efficiency (η)" defined by the reciprocal

$$\eta = \frac{F_{AVG}}{F_{Peak}} \cdot 100\% = \frac{E}{s \cdot F_{Peak}} \cdot 100\% \qquad E = \text{absorbed Energy}$$

In our understanding this definition describes more clearly how far a load-deformation characteristic reaches the ideal of a rectangular shape.

The two objectives of the program were

- to make the adaptation development to the real size structure
- and to establish input data for the program KRASH.

The first goal means, that the specific requirements of this type of helicopter have to be fulfilled. Therefore to the above mentioned criteria additional aspects had to be regarded. Major constraints to be considered were the fuel tanks located in the underfloor structure, the structural dimensions e.g. the structure height of about 450 mm and of course other interfaces like the control system or the landing gear.

Simmilar to other helicopter programs the general system investigations concerning crashworthiness are performed with the program KRASH. As this is a so called hybrid program, contrary to e.g. a nonlinear Finite-Element-program (DYCAST, PAM-CRASH, CRASH-MASS etc.) the linear and nonlinear element behaviour has to be provided as input data.

One way of establishing these data is the component testing another way is to use one of the above mentioned FE-programs as a "preprocessor" for KRASH or to use a combination of both. The latter has been done by MBB in this project in a collaboration with Engineering Systems International (ESI) using the program PAM-CRASH. The objective was to test the maturity of such a program system for the application of typical aircraft structures with features like rivet connections, thin sheets, sandwich parts etc. instead of automotiv structures for which the quality has already been proved. To avoid any influence from test experience these simulations have been performed in advance thereby getting a feeling for this tool to presimulate unknown structures or structural features. With a program qualified in such a way we want to cover problems difficult and more expensive to investigate by tests. A comparison of the test results with the numerical results is given in chapter 6, a more comprehensive summary of the simulation results is given in another paper [6] of this AGARD-meeting as well as in [7].

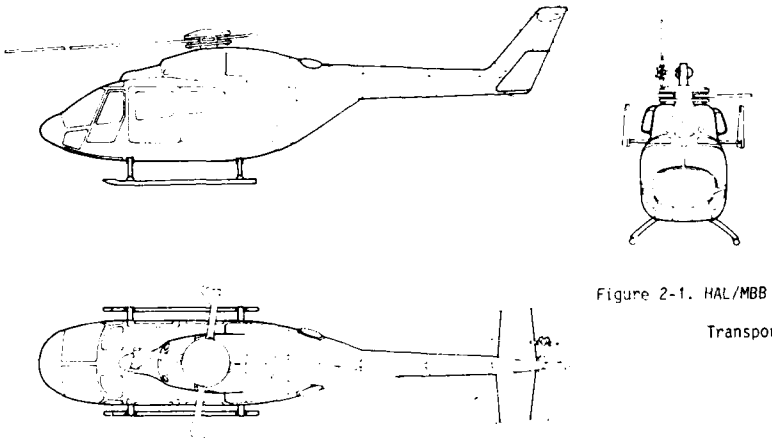

Figure 2-1. HAL/MBB Advanced Light Transport Helicopter ALH

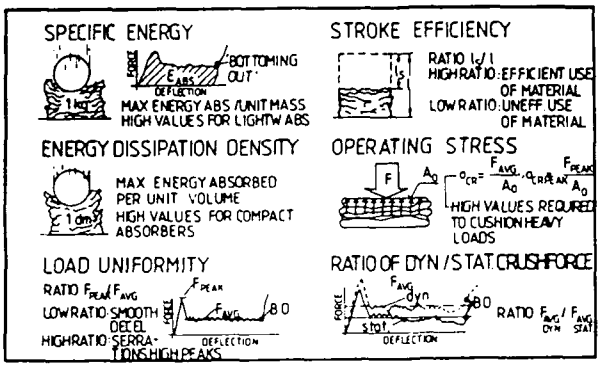

Figure 2-2. Key Parameter of Energy Absorption

3. PREVIOUS WORK AT MBB

As mentioned before this test program was not intended to be a basic investigation in structural energy absorption. A considerable amount of basic data were available from former crash research programs. These programs have been performed at the MBB-Bremen plant (the former VFW) in the years 1978 to 1981 under sponsorship of the German Ministry of Defence.

In these programs many possible structural concepts of energy absorption have been investigated. The following main different kind of metal structures have been tested statically and dynamically:

a) Sheet-stringer components with z-stringers (Figure 3-1 + 3-2) and sickle shaped stiffners

b) Sine wave components (Figure 3-3)

c) Trapezoidal shaped components (Figure 3-4)

d) Sandwich components with normal core and with crash core (length axis of the cells parallel to the sheets in direction of the stroke) (Figure 3-5)

For our development work the following main results could be extracted:

a) Trapezoidal shaped components have the best energy absorbing behaviour even better than sine wave components (Figure 3-6)

b) Sheet stringer components have a medium energy absorption with good potential for improvements

c) Sandwich components have the least promising behaviour but also there possibilities for improvements could be indentified

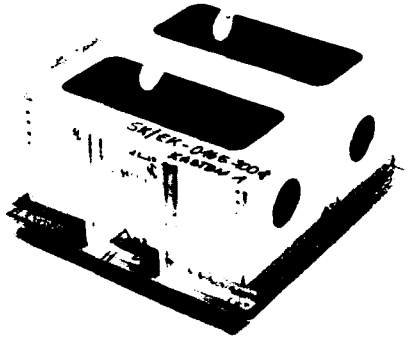

Figure 3-1. Sheet-Stringer Component with z-Stiffeners

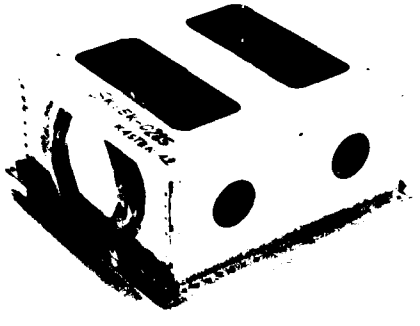

Figure 3-2. Sheet-Stringer Component with Sickle Stiffeners

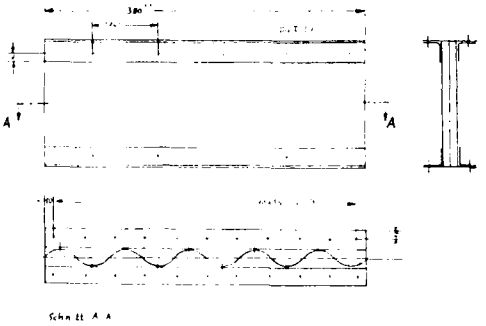

Figure 3-3. Sine Wave Component

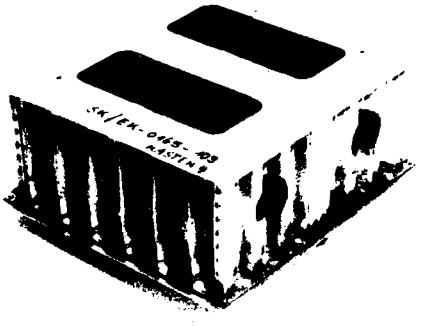

Figure 3-4. Trapezoidal Shaped Component

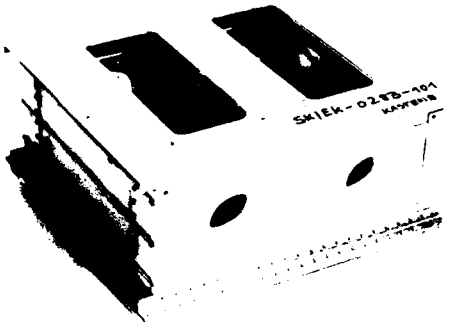

Figure 3-5. Sandwich Component

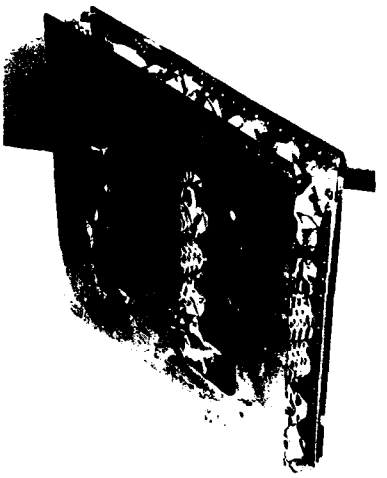

Figure 3-6. Trapezoidal Component after Crushing

4. MBB-PHILOSOPHY OF CRASHWORTHINESS-DESIGN

For the understanding of our work some explanations of our philosophy may be helpful. Under the isolated view of the crashworthiness requirements there are a large number of energy absorbing concepts (Figure 4-1).

But under considerations of the weight penalty as well as the impact on helicopter systems in weight and cost many of the concepts are not suitable for the individual helicopter type. The manufacturing aspects are a further factor to be regarded very carefully.

Therefore our approach is as follows:

- Definition of a structure which fulfills all requirements to be regarded. Some of the requirements often contradict to each other. Thus the result may not be optimal under certain considerations but an acceptable compromize.

- Dimensioning of that structure concerning flight and landing loads.

- Improvement of that structure concerning the crash requirements.

Following the above described guideline the most promising concept described in chapter 3 (Trapezoidal shaped elements) could not be used for this type of helicopter. To fulfill the fuel tank requirements (e.g. flat surface, sealing) would be extremely expensive. Therefore for the ALH the sheet-stringer design has been selected at areas with fuel on one side and sandwich design at areas with fuel on both sides. Thus these two types of structure were the matter of our investigation program.

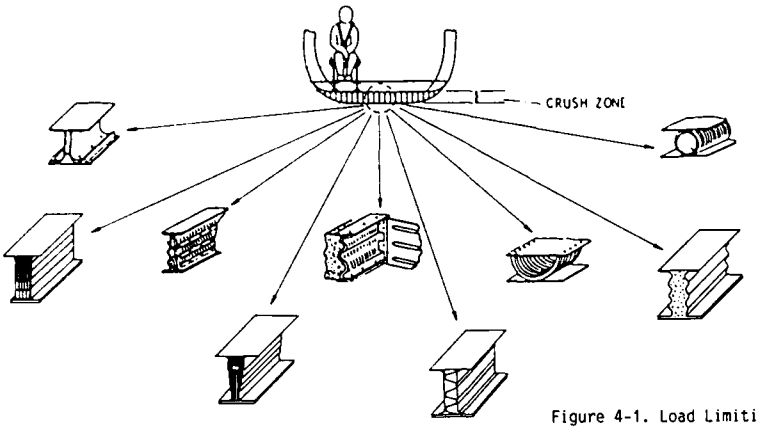

Figure 4-1. Load Limiting Subfloor Concepts

5. TEST SET-UP

5.1 Static Test

Up to now most of the tests were conducted with flat panels with various kinds of stiffeners to investigate and improve the basic behaviour of the crash elements. These tests were performed on an universal testing machine with one vertical hydraulic cylinder. The lower specimen support was rigidly mounted on a short steel cylinder which was provided with four strain gauges. The true compressive force was measured utilizing a compensating circuit (Figure 5-1). The stroke was given by an inductive displacement transducer which was connected with the upper specimen support. Three cylindrical rails guided this upper specimen support to prevent it and the specimen from rotational movement (Figure 5-1). The tests started with a slow feed to take into account the steep load increase at the beginning. During the tests the feed was accelerated. The force-stroke curves were directly recorded by a pen plotter.

As the specimens became bigger and more complex also the test set-up had to become more complex. For the compound components a new test rig was built. Three hydraulic cylinders were used to apply the necessary load vertically on a rectangular steel plate. To keep this moving upper support parallel to the lower rigid support the three cylinders were displacement-controlled. In addition the upper support was guided by two cylindrical rails to secure it against rotational and transversal movement. The applied loads of the cylinders were measured individually with three load cells and combined (tension and compression to ballance the support) in a computer. Due to the data processing by computer not only the load-stroke curves could be generated but also the energy-stroke curves by integrating the former ones.

The specimens were connected to both rigs with bolts. For that purpose the specimens were supplied with angles at the upper and lower end which would be used also in a real helicopter structure.

5.2 Dynamic Tests

As cooperation with DFVLR in Stuttgart has proved already very productive in the past we conducted the dynamic tests on their testing installation that existed already. The princinal set-up of the "drop tower" can be seen on Figure 5-2. The drop sleigh which can be loaded with additional weights is guided by two T-section rails. The specimen is mounted beneath the sleigh. This assembly can be hoisted to a maximum height of 14 m corresponding to 16,5 m/s drop speed. The sleigh can be released electromagnetically. At impact the specimen is secured against lateral and rotational motion by four protruding pins on the measuring plate which slip into four holes of an additional ground plate of the specimens. During the tests the following data have been recorded.

- The time history of the acceleration a_{zw} was given by a quartz acceleration pickup mounted on the sleigh above the specimen
- The time history of the stroke s_w was given by an inductive high speed displacement transducer
- The time history of the impact force F_{zp} was given by three piezoelectric load cells beneath the measuring plate
- The impact velocity was generated by measuring the time Δt which was necessary to pass a certain distance given by two infrared light barriers.

All time histories were collected by a transient recorder at a sample rate of 2 µs. Finally the time histories were processed to the force-stroke and energy-stroke curves. In addition all tests were filmed using a high speed camera with 3000 frames/sec.

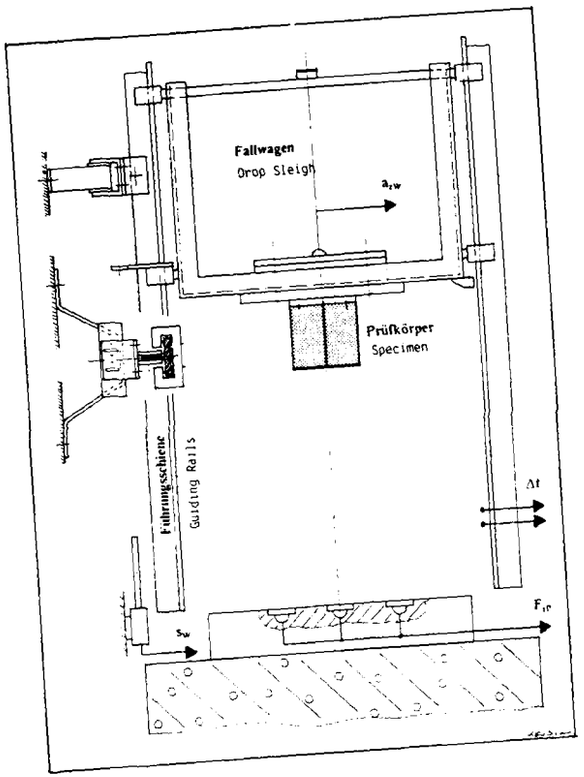

Figure 5-2. Principal Set-up of Dynamic Test Installation

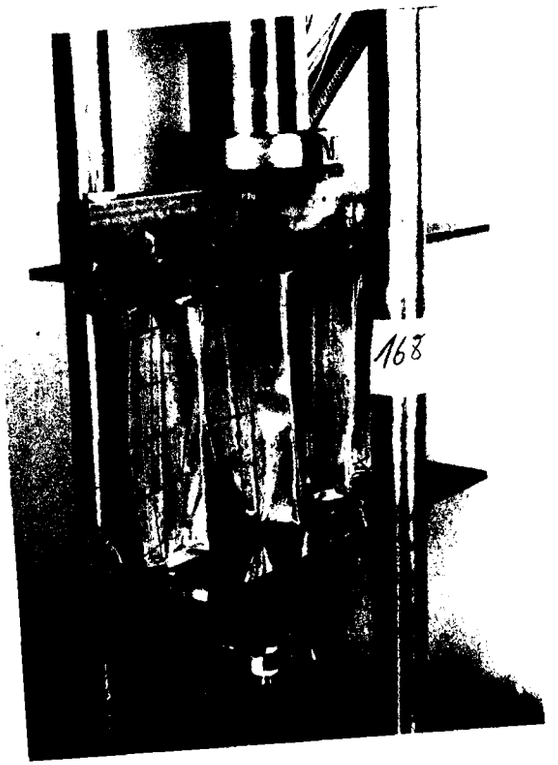

Figure 5-1. Static Force Measuring Device and Guiding Rails of Test Set-up

6. SHEET-STRINGER PANELS WITH OPEN SECTION STIFFENERS

The basic behaviour of thin sheet-stringer panels under compression is not very efficient in respect of energy absorption. Figure 6-1 to Figure 6-3 show a typical force deflection curve and the related failure modes of the component. Mainly the following instability modes are responsible for this deficiency

- Euler-buckling
- Combined Euler-buckling/crippling
- Torsional instability
- Combined torsional instability/crippling
- Insufficient sheet-stiffener connection

Figure 6-4 shows that the slenderness ratio is one major parameter which influences the instability behaviour. The Euler-region at the slenderness ratio of $\lambda > 50$ has in any case to be avoided. The region of $20 \leq \lambda \leq 50$ is the so called transition region in which local buckling and the elastic Euler-buckling occurs (Johnson-Euler). Below $\lambda = 20$ is the stable crippling region. Additionally to this the torsional instability has to be regarded very carefully as thin stringers with open cross section having a big i_x (radius of gyration parallel to the panel axis, transvers to the load direction) and a small i_y are very sensitive with this respect. Figure 6-5 shows that the torsional support of the sheet in the transition region ($20 < \lambda < 50$) is very important to keep the torsional instability stress above the crippling stress. This is reached at a ratio of sheet thickness to stringer thickness $S_H/S_p = 1$ and has been kept in almost all our test samples.

To avoid these instability modes the structural members have to be designed for the crippling stress region at $\lambda \leq 20$. This results in quite high stiffener sections at $b \geq 60$ mm at a stringer/component height of $l = 450$ mm. Regarding all these design features open section stiffeners have still a crippling failure mode resulting in plastic hinge formation around the y-axis and not in the desired short wave wrinkling. As described in chapter 2 there are major constraints to be regarded in the underfloor structure. The interface to the controls allowed a max. stringer height of 50 mm preferable 45 mm instead of the necessary height of 60 mm aiming to a slenderness ratio $\lambda = 20$. Considering all this the following means of improving the characteristics have been investigated:

1) Reducing the high force peak by introducing triggers for a controlled failure on a preselected force level. This can primarily be reached by the rivet pitch and rivet diameter in the load introduction region of the connection angles (Figure 6-6). Furthermore a suitable spacing between the stringer and the connection angle should give a smooth characteristic (Figure7-4). If the rivet failure at the connection angle is likely the uncontrolled spreading of the stiffeners off the sheet has to be avoided by e.g. clips (Figure 6-7).

2) Tuning of the stringers at the upper and lower end to get a first failure in this area without loss of load carrying capability. Thereby the remaining slenderness ratio is reduced after the first stroke. Investigated means are to shape the stringer end or to introduce cut outs in the stringer corners.

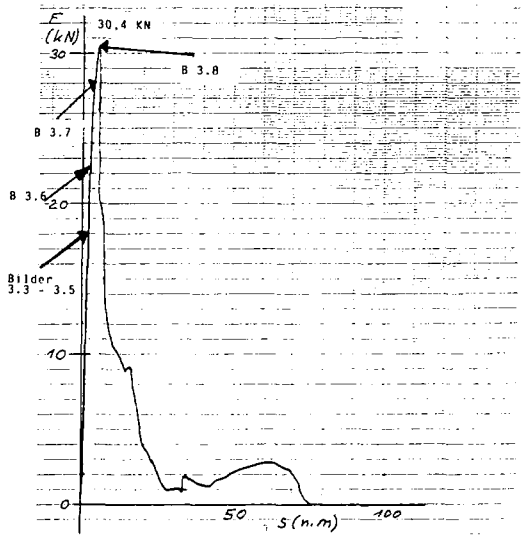

Figure 6-1. Force-Deformation Curve of Basic Sheet-Stringer Component

Figure 6-2. Component at Load Level B 3.7, see Figure 6-1

Figure 6-3. Component After Failure

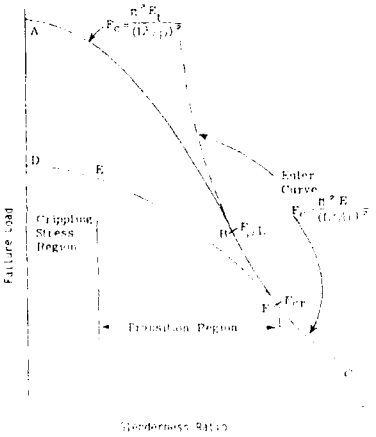

Figure 6-4. Johnson & Euler Column Curve [1]

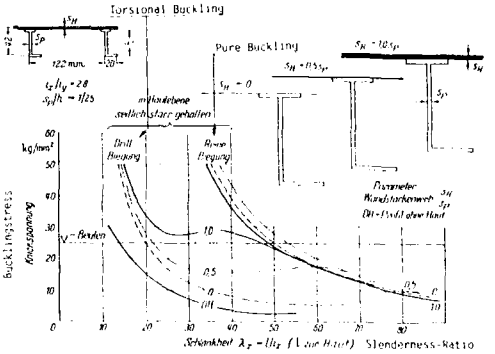

Abb. 171. Dünnwandiges Profil mit H. ist Knickspannungen. Bei L = 50 verschwindet praktisch der Drilleinfluß (nach H. Ebner, Z. f. Flugwiss. Bd. 4, H. 3/4 (1956) S. 118)

[1] Argyris: Flexure Torsion Failure of Panels, Aircraft Engineering 1954

Figure 6-5. Torsional Influence on Stiffened Panel Behaviour [3]

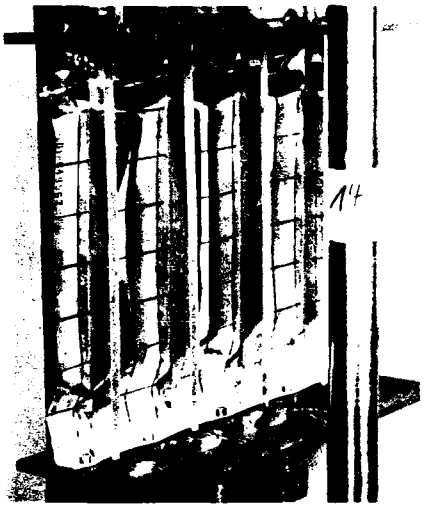

Figure 6-6. Sheet Buckling due to Triggers

Figure 6-7. Spreading of Stiffner off the Sheet

6.1 Test Results

In an iterativ development process of static tests the influence of the individual parameters as described before were studied and the best combination of trigger and tuning devices were selected. With these elements the behaviour has been improved considerably as a comparison of Figure 6-1 and Figure 6-10 may show. The trigger mechanisms work very reliable due to the induced sheet buckling as a result of the rivet pitch and the stringer distance to the connection angle (Figure 6-8). In the further process there is a drastic force fall due to a crippling resulting in a torsional instability collapse of about 50 mm stringer length. After this the system gets stabilized again with a reduced slenderness ratio and the force deflection curve shows a quite good characteristic. It should be noted that this crippling-torsional instability failure starts at the two outside stringers (Figure 6-9) and is mainly induced by the negativ influence of the free edges. This specific behaviour was very well reproducable for a slenderness ratio of $\lambda = 36$ as well as for $\lambda = 26$ but for the latter in the average of all test articles a better crushing behaviour could be reached (Figure 5-1 shows a sample with $\lambda = 26$ after test).

Due to obviously better behaviour of closed section stiffners only two basic samples without the full extend of triggers have been drop tested. The reason was to verify, the numerical simulations performed in advance with such a configuration [6]. One of the key impressions watching the high speed film is the high degree of torsional vibrations of the stringer subsequent to the impact (Figure 7-11). Due this a bending of the free flange occurs with the max. deformation in the middle of the stringer. Therefore these kind of structures are very sensitive to have the first failure there resulting in an overall instability of the stringer and often of the whole panel. The load deformation curves (Figure 6-11) show that with the reduced rivet diameter already a quite good triggering was reached. To summrize the findings of about 15 test articles the results are displayed in two parametric diagrams:

a) Efficiency over the slenderness ratio

$$\text{Efficiency} = \frac{\text{Energy absorbed}}{F_{peak} \quad \text{stroke}} \qquad \text{(Figure 6-12)}$$

b) Specific energy absorption over the slenderness ratio (Figure 6-13).

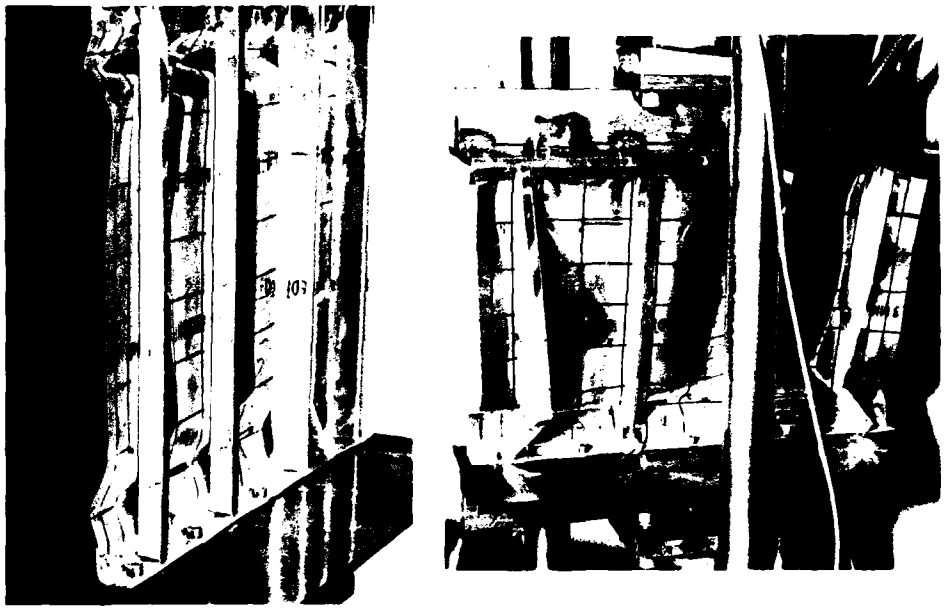

Figure 6-8 and 6-9. Failure Sequence at Load Levels B 5.6 & B 5.9 of Figure 6.10

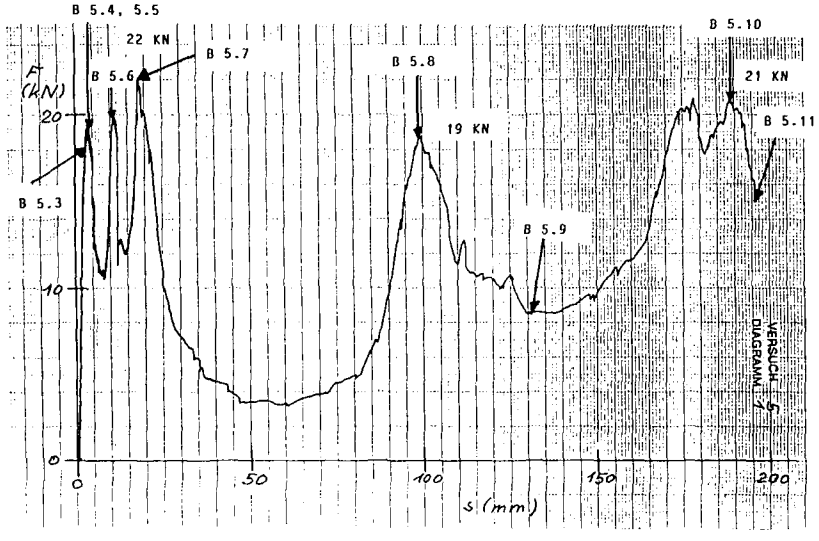

Figure 6-10. Load Deformation Curve

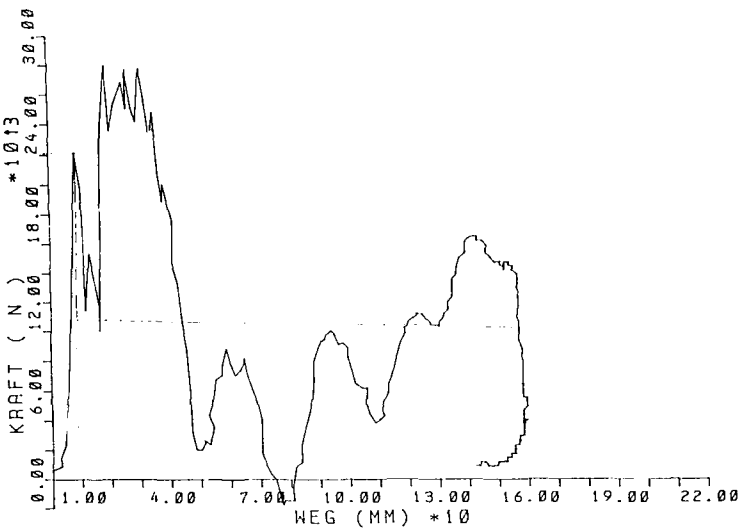

Figure 6-11. Crushing Characteristic of Panel with z-Stiffeners (Dynamic Test)

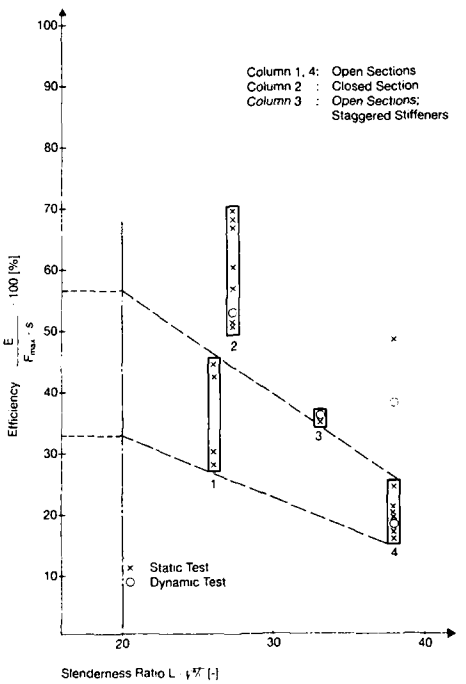

Figure 6-12. Efficiency Versus Slenderness Ratio of Various Sheet-Stringer Specimen

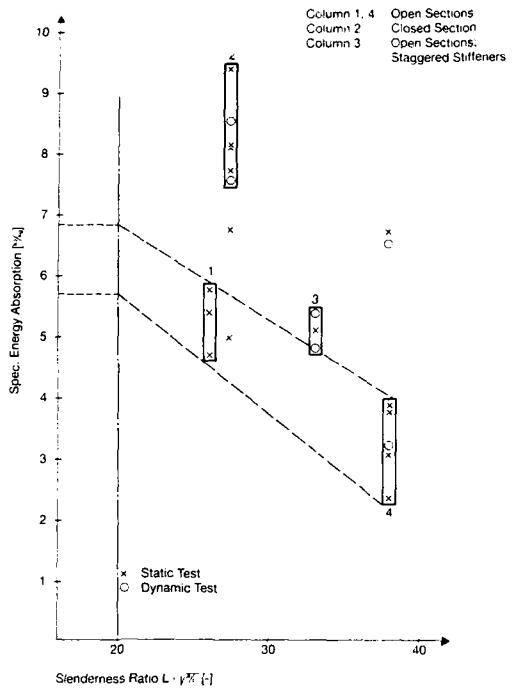

Figure 6-13. Spec. Energy Absorption Versus Slenderness Ratio of Various Sheet-Stringer Specimen

6.2 Comparison of Test Results with Numerical Results

As already mentioned in chapter 6-1 drop tests of stiffened panels with open cross sections have been performed which did not feature all the (triggering) details that may improved their behaviour. But the reason of these tests was to verify the results of numerical calculations performed with the program package PAM-CRASH in advance. The loading of the model has been applied by two moving rigid walls on top and bottom of the structure. Each wall travelled at a speed of constant 5 m/s producing a 10 m/s crushing velocity. That means the analysis time in ms relates to the stroke in mm. Special attention has been put to define the rivet behaviour.

The following results have been presented by ESI:

- Load versus time/deformation diagrams for the overall structure and the stringers only. This gives an indication of the load share between the structural members.
- Integrated energy absorption versus time/deformation.
- Sequence of deformed plots.
- Force versus time diagrams of rivet up to the failure.
- History of rivet failures.

Comparing the force-stroke curve of the drop test (Figure 6-11) with the corresponding curve of the calculation (Figure 6-14) it has to be noted that the simulated panel represented exactly one half of the tested one. Keeping that in mind both curves show a great resemblance not only in shape. Except the very high peak of the calculated curve which is originated by non-structural effects the first load levels at displacements up to 20-30 mm are quite comparable. Also a new load increase at the end of the total stroke was predicted very good. Although the similarity at medium stroke and the synchronism of events is not that good the general behaviour of the panel was predetermined very good again. The torsional warping of the stiffeners at the beginning of the stroke (Figure 6-15, Figure 7-10) as well as the buckling of the sheet between the first rivet spacing coincide extremely good (Figure 6-16, Figure 6-6, in this case the dynamic simulation has to be compared with a static test but the failure modes are similar).

A comparison of the absorbed energies gives the following surprizing result: Although there are some differences in the load-stroke characteristic especially in the range between 50-100 mm stroke the total energy at 150 mm deformation is with about 1580 nearly the same.

Finally it should be mentioned that in the numerical simulation additional 8 parameters were investigated too. For example it turned out that the energy absorption can be inproved by increasing the rivet pitch at the connection area of the stringer to upper and lower angle. A tendency which has also been proved by static tests.

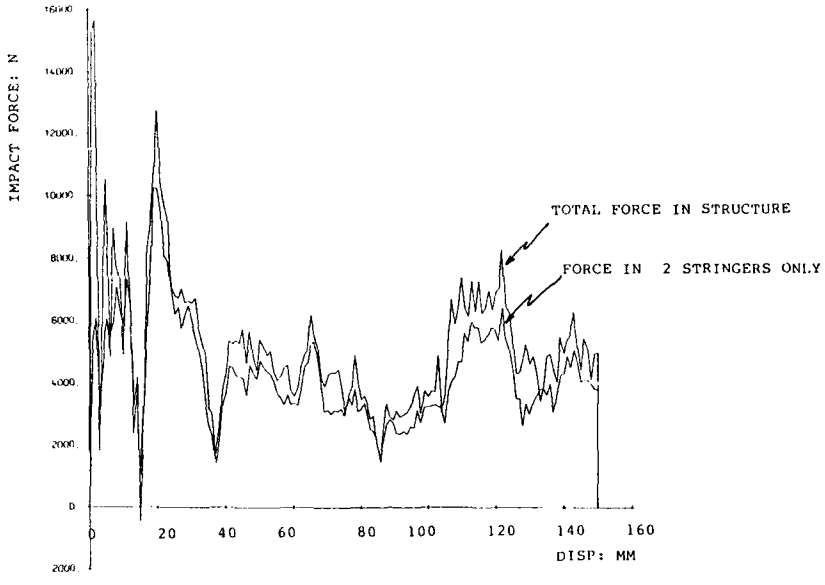

Figure 6-14. Force Versus Displacement Plots

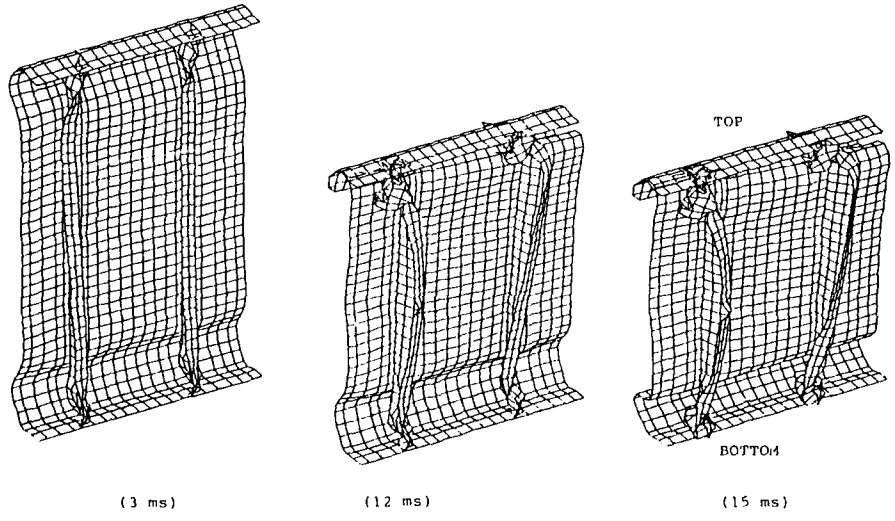

Figure 6-15. Deformed Shape Plots for Analysis 2

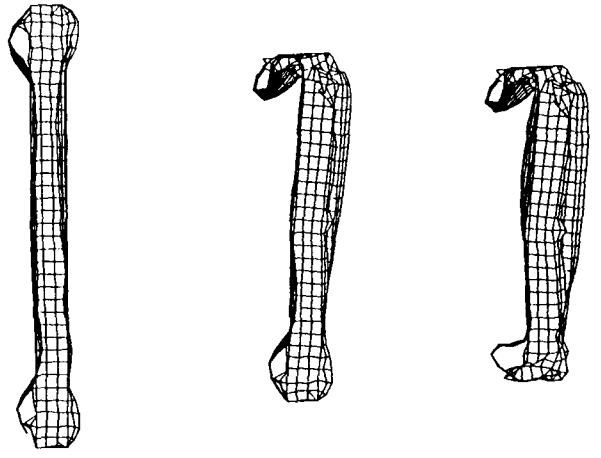

Figure 6-16. Deformed Shape Plots for Analysis 2

7. SHEET-STRINGER PANELS WITH CLOSED SECTIONS

As seen in paragraph 6.1 the crippling behaviour of flanges with free edges accompanied by a lack of torsional stiffness may only be improved up to an efficiency of max. 50% considering the restraint that a slenderness ratio of less than 26 was not feasible. As the very good experience with continuous trapezoidal sections could not be used (see chapter 4) it was decided to investigate stiffened panels with trapezoidal stiffeners (Figure 7-1 and Figure 7-4).

The experiences at the z-stiffened panels with different kind of triggers could be used also at the trapezoidal stiffeners. Special attention was again necessary to avoid the stiffener spreading off the panel (Figure 7-2). Al-straps at the top and bottom end of the stiffener were found to be one suitable means (Figure 7-3). Another possibility are improved connection rivets at the upper and lower stiffener end with an increased rivet diameter including washer and a slot aside (Figure 7-4, section A2-A2). These means allow a stringer travel after the first failure due to a shear out at the slot without loosing the connection to the upper and lower angle. Further tuning may be reached by weakening holes at the stiffener ends (Figure 7-5).

7.1 Test results

As expected the trapezoidal stiffeners proved to have a much more stable behaviour than stiffeners with open sections. The triggering of the first failure induced by interrivet buckling worked very reliable as it may be seen in the first 20 mm of the load-stroke plots (Figure 7-7 and 7-9). The pictures from the test samples show that now a real crushing with high degree of local plastic deformation occurs. It should be noted that the two samples (Figure 7-6 and 7-8) differ in the tuning devices therefore the results are not totally comparable. On the other side a certain degree of variation has always to be expected due to random influences. Thus the resulting load deformation curves are satisfactorily close to the ideal rectangular shape. Accordingly the specific energy-absorption (Figure 6-13) and the efficiency index (Figure 6-12) are much better than the results from z-stringer stiffened panels.

In the dynamic drop tests two samples according to Figure 7-4 have been investigated i.e. triggering with washers at the end rivets and slots aside. The results could demonstrate very impressively the significant difference between stiffeners with open and closed sections. Primarily due to the high torsional stiffness a very stable behaviour could be reached while at the open section stiffeners a high degree of torsional vibration is typical (see Figure 7-11 and 7-12). The trigger worked quite reliable although some more reduction of the failure load should be aimed for in the future (Figure 7-10). Furthermore the second peak loads should be avoided by suitable designed weakening holes (Figure 7-5) which proved to be very efficient. These features have not been incorporated in the samples due to the testing sequence. In the further deformation progress a satisfactorily good crushing behaviour was found.

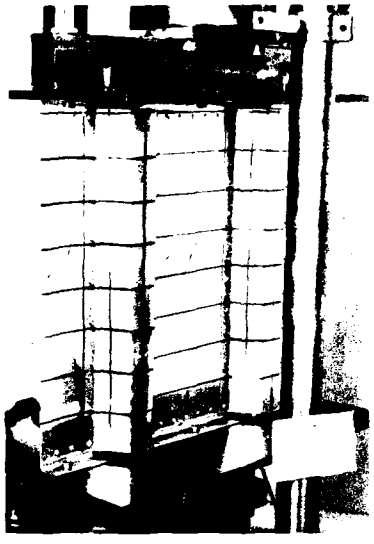

Figure 7-1. Panel with Trapezoidal Stiffeners

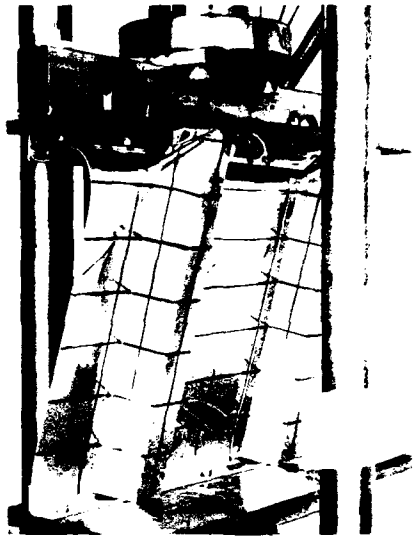

Figure 7-2. Spreading of the Stiffeners off the Panel

Figure 7-3. Trapezoidal Stiffeners with Al-Straps

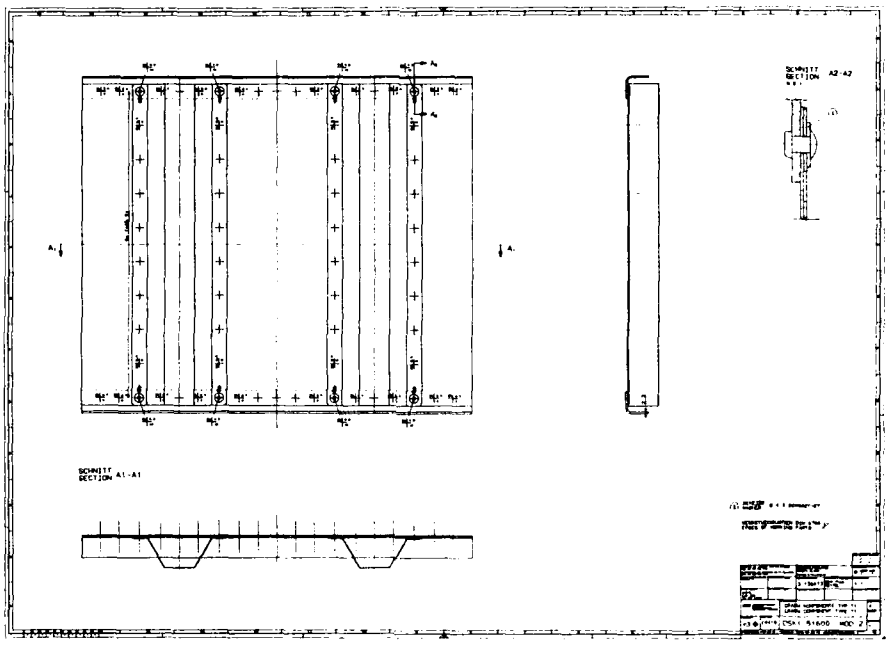

Figure 7-4. Trapezoidal Stiffeners with Washers and Slots

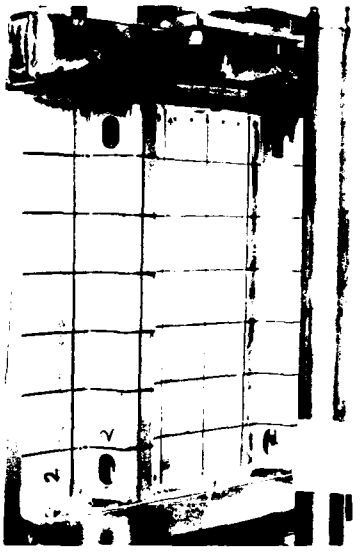

Figure 7-5. Trapezoidal Stiffeners with Weakening Holes

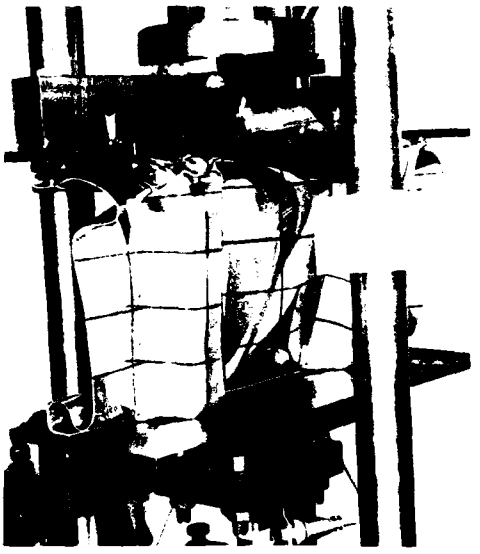

Figure 7-6. Panel after Test

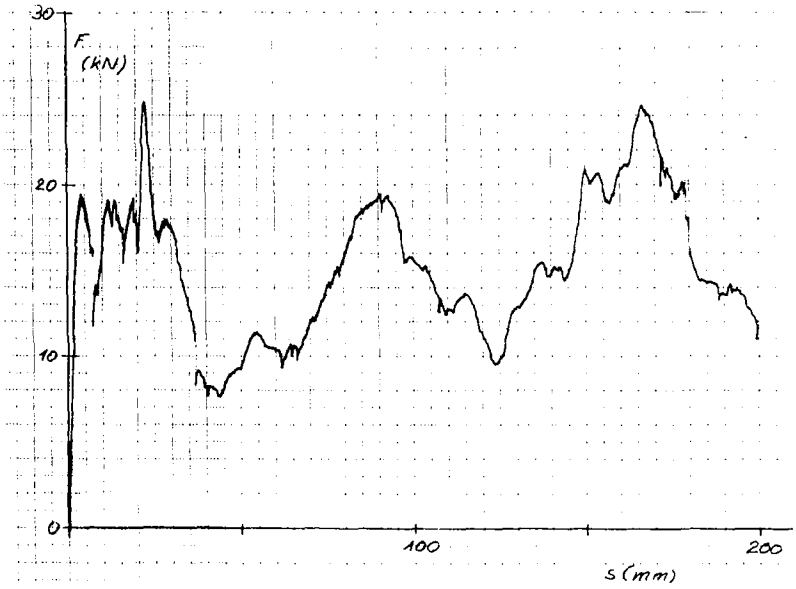

Figure 7-7. Static Load-Stroke Curve of Panel with Closed Section Stiffeners

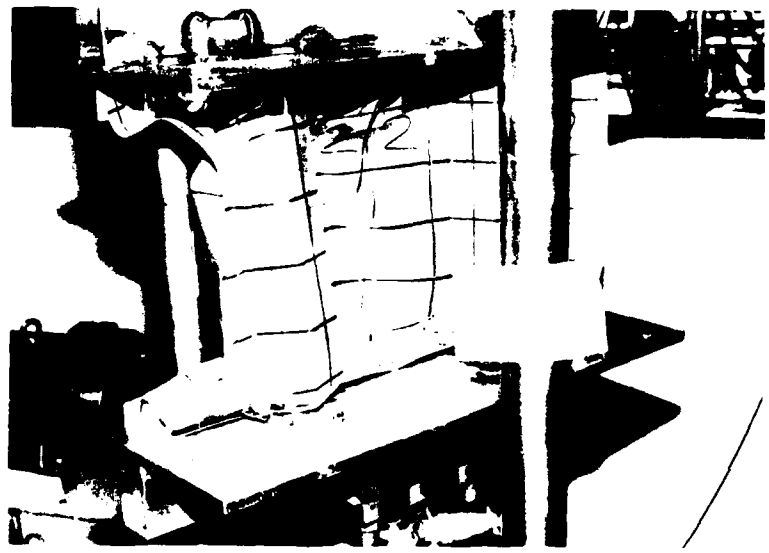

Figure 7-8. Panel after Test

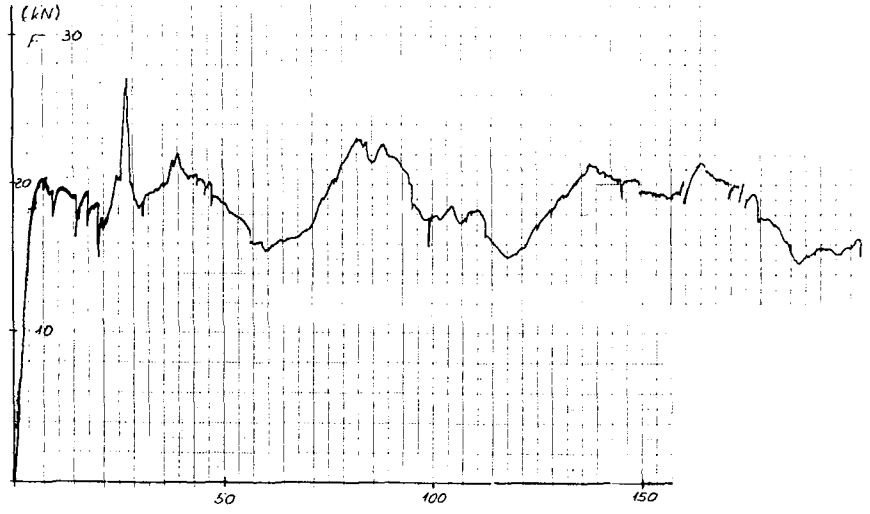

Figure 7-9. Static Load-Stroke Curve of Panel with Closed Section Stiffeners

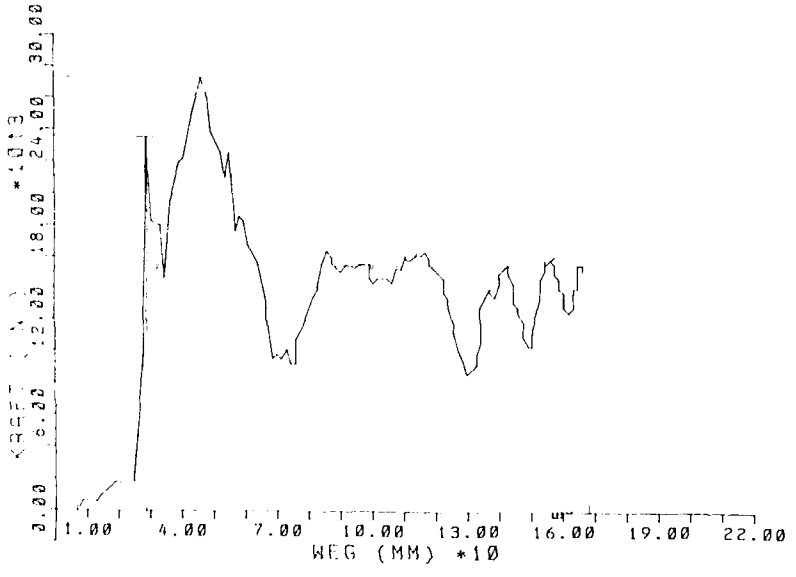

Figure 7-10. Dynamic Load-Stroke Curve of Panel with Closed Section Stiffeners

Figure 7-11. Panel with Open Section Stiffeners at Impact

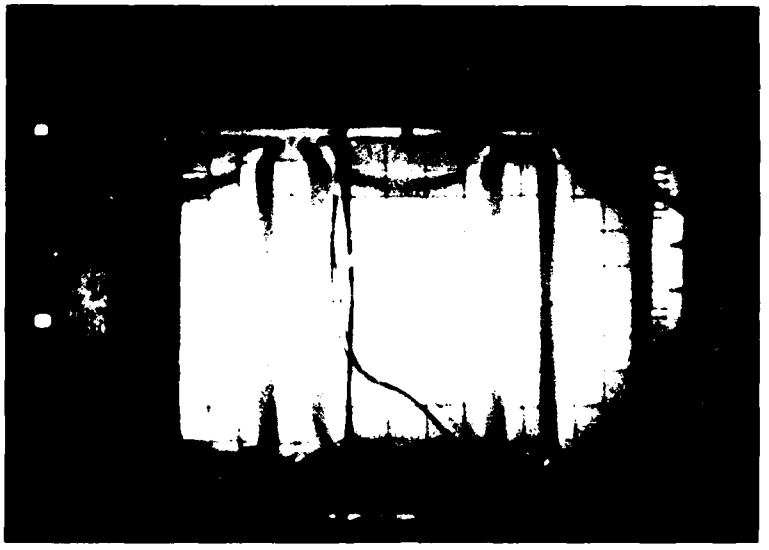

Figure 7-12. Panel with Closed Section Stiffeners at Impact

8. COMPOUND COMPONENTS INCLUDING CROSSPOINTS

In addition to the investigation and improvements of the behaviour of flat panels the behaviour of compound components representing the connection of frames and keelbeams in the lower structure is at least of equal importance. One advantage of these components e.g. an H-section in top view is the reduction of the influence of free edges. Another advantage is the opportunity to investigate and improve the behaviour of crosspoints. The goal was to attain a constant load level at good specific energy absorption utilizing the mutual edge support and to avoid simultaneously too high a load peak at the beginning of the load-stroke curve due to the stiff crosspoints.

Consequently when the investigations of flat panels with stiffeners had yielded good results in respect of efficiency (load uniformity), specific energy absorption and so on we started to test compound components utilizing proved features of the flat panels. From our engineering judgement we did not necessarily select details with the best results but those with good results and the prospect to be a feasible feature of a real helicopter subfloor structure. Therefore for example we avoided to trust on frictional load limiters. In addition our special attention was directed to the crosspoints. The connecting elements have to provide a stable support of the adjacent panels. Nevertheless they must not generate an unfavourable load peak. The conclusion of our reflections can be seen on Figure 8-1:

- The panels have trapezoidal stiffeners which proved most promising in the earlier tests
- The stiffeners have cut-outs at either end and the connecting angles have notches to avoid an initial load peak
- The panels are jointed with twin angles to provide a stable support of the edges.

8.1 Test Results

The force-stroke curve of the first compound specimen as described above can be seen on Figure 8-2. Except the one deep valley at the beginning the result is already quite promising. Although the general behaviour of the component is by far not optimum (Figure 8-3) the energy absorption capability in respect of efficiency and specific energy absorption is already among the best results of flat panels. The second test showed clearly that the result is reproducible (Figure 9-1).

Further improvements are necessary to avoid the seperation of the sheets from the upper or lower angle although the negative influence of the free edges is not representative for a real helicopter structure. Together with a modification of the cut-outs in the stiffeners and some additional tuning it is certainly possible to keep the load level nearly constant. To achieve this supplementary static and also dynamic tests are planed or even under way.

Figure 8-1. Compound Component with Triggers

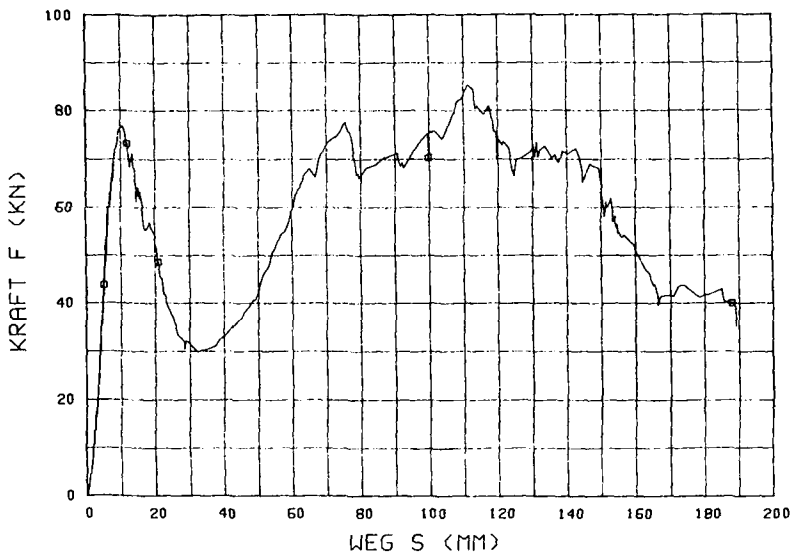

Figure 8-2. Static Load-Stroke Curve of Compound Component

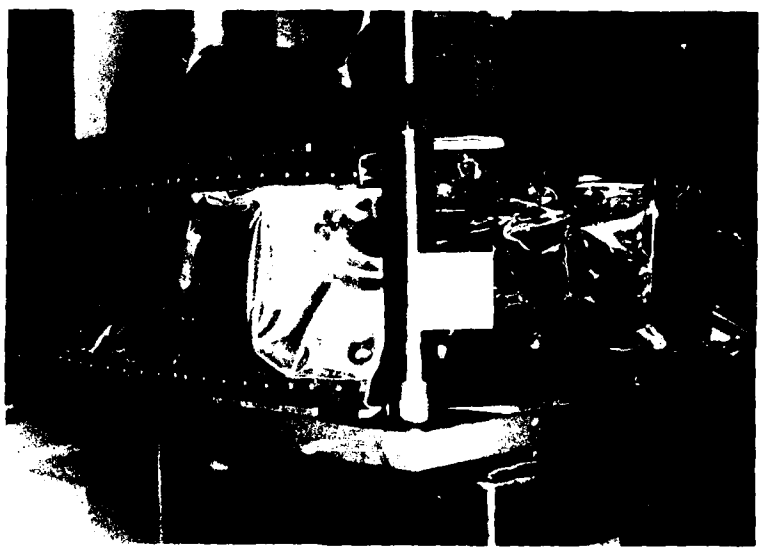

Figure 8-3. Compound Component after Static Test

9. CONCLUSIONS

During this development program the step from laboratory crash samples with the full range of possible concepts to the real size structure considering all the constraints due to system interfaces has been made. Maximum attention has been put to keep weight and cost penalties down. The objectives of these investigations were to optimize the statically dimensioned structure concerning crashworthiness requirements and to establish the necessary input data for the program KRASH. The results of these activities could demonstrate that even under the narrow constraints of system requirements there are still many possibilities to improve structural concepts which have basically a poor energy absorption behaviour. This is especially the case at the most often used stiffeners with open cross sections. With a slenderness ratio reduced as far as possible to $\lambda = 20$ as well as the incorporation of suitable triggers a considerable improvement may be reached. The maximum efficiency at $\lambda = 26$ was close to 50% and the specific energy absorption was between 5 to 6 kJ/kg (Figure 9-1). A certain improvement up to some 60% efficiency may be expected if tested in compound components.

As higher energy absorption is required closed section stiffeners have been selected. The higher torsional stiffness as well as the lack of free flanges resulted in an efficiency of $\eta \sim 70\%$ and an specific energy absorption of some 8 - 9 kJ/kg (Figure 9-1). With these data first system investigations using the program KRASH have been performed. The results show that the ALH design goals can be reached or even be exceeded. Presently further investigations with sandwich specimen are under way as this kind of structure is very attractive due to the superior specific load carrying capability as well as the easy interface to the fuel tanks. Similar to the sheet stringer specimen certain controlled weakening features have to be incorporated limiting the load carrying capability under axial pressure. For the design of crashworthy structures in general the traditional understanding of designers and stressmen aiming for max. strength and stiffness at minimum weight has to be corrected. Now somewhat contradicting requirements have to be considered aiming for controlled failures and deformations.

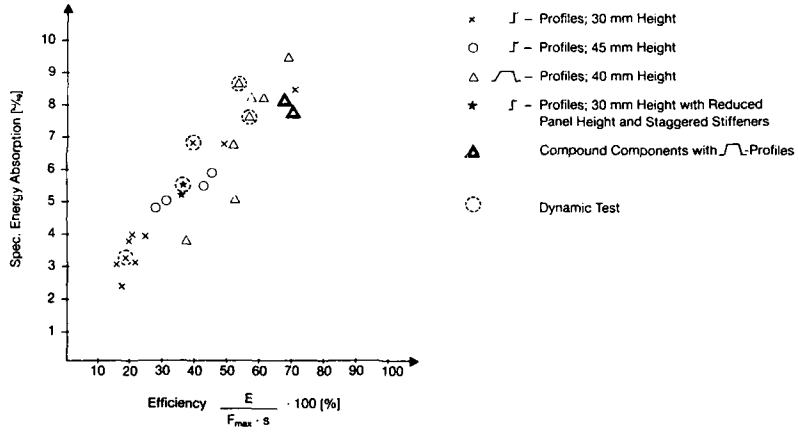

Figure 9-1. Specific Energy Absorption and Efficiency of Various Sheet-Stringer-Specimen

10. REFERENCES

[1] Bruhn, E.F., Analysis and Design of Flight Vehicle Structures. Jacobs Publishing Inc.

[2] Aircraft Crash Survival Design Guide, Vol. I-V, USARTL-TR-79-22

[3] Hertel, Leichtbau, Springer-Verlag, Berlin, Heidelberg, New York, 1980

[4] Kindervater, C.M., Energy Absorbing Qualities of Fiber Reinforced Plastic Tubes, AHS-National Composite Structures Specialists' Meeting, March 1983, Philadelphia, Pennsilvania.

[5] Och, F., Helicopter Crashworthiness, Problems and Promises, International Conference on Structural Impact and Crashworthiness, London, UK, 1984.

[6] Ulrich, D., Picket, A.K., Haug, E., Bianchini, J., Crashsimulation and Verification for Metallic, Sandwich and Laminate Structures., AGARD, 66th Structures and Material Panel Meeting, Luxembourg.

[7] Chedmail, J.F., Du Bois, P., Numerical Techniques, Experimental Validation and Industrial Applications of Structural Impact and Crashworthiness Analysis with Supercomputers for the Automotive Industries.

[8] Hicks, J.E., Economic Benefits of Utility Aircraft Crashworthiness, USAAAVS Technical Report 76-2, U.S. Army Agency for Aviation Safety, Fort Rucker, Alabama, July 1976.

CRASH INVESTIGATIONS WITH SUB-COMPONENTS OF A COMPOSITE HELICOPTER LOWER AIRFRAME SECTION

by

Ch. Kindervater
Institute for Structures and Design, DFVLR Stuttgart
Pfaffenwaldring 38-40, 7000 Stuttgart 80, Germany

and

A. Gietl

R. Müller

Messerschmitt-Bölkow-Blohm GmbH, Helicopter Division
P.O. Box 80 11 60, 8000 München 80, Germany

ABSTRACT

For the BK 117 helicopter a composite fuselage was designed, manufactured, and will be flight tested at MBB. Within the development programme evidence was given to the crashworthy design of the fuselage which was accomplished by a joint activity between MBB and DFVLR Stuttgart.

The crash investigations were focused on the lower airframe section under vertical crash loads. The task was performed by design support tests on the specimen level and by sub-component crush testing.

Sandwich panel specimens were statically and dynamically crushed to study various crush initiators at the panel-skin intersections, and to investigate the energy absorption capability.

Sub-component crush tests under quasi-static loading were concentrated on structural "node points" (intersections of keel beams and bulkheads) and on bulkheads located in the rear of the fuselage. The component's crush characteristics and the energy absorption performance were determined. Various designs with notched corners at the intersections of beams and bulkheads were considered with the aim to reduce the initial peak failure loads. Structural elements supporting the parallel panels of the landing skid frames were used to avoid global buckling and to initiate and stabilize efficient energy absorbing crush modes.

The generated load-deflection-characteristics of the sub-components are intended to be used as inputs for crash simulation calculations.

1. INTRODUCTION

Composite materials increasingly gain applications in primary aerospace structures due to their superior characteristics compared to conventional metal designs. Among others the advantages of composites are for example reduced weight and superior fatigue behaviour.

In helicopter design composite materials were used primarily for rotor blades and secondary structures for many years. But now also an increasing number of primary helicopter parts are intended to be designed and manufactured out of composites.

To investigate the impact of composite technology on future helicopter airframes MBB is developing a composite fuselage for a light transport helicopter. The project is funded by the German Ministry of Defence.

The composite fuselage is based on the MBB/Kawasaki BK 117 helicopter, Fig. 1. Composite parts replace most of the basic helicopter metal fuselage, Fig. 2. The experimen-

tal aircraft retains the engine deck, transmission deck, dynamic system and tail section of the standard basic helicopter.

One of the main design objectives for future helicopters will be an improved survivability of the occupants during crash landings.

During the development of the actual composite airframe some basic work concerning the crash behaviour of the composite subfloor structure was performed in cooperation between MBB and DFVLR.

Due to financial aspects some of the design features of the composite subfloor structure were restricted as, several systems, e.g. the tanks, the landing gear and the flight control system had to be taken from the existing BK 117 helicopter. The task for the common MBB/DFVLR activities was to investigate and establish the crushing behaviour of the composite airframe subfloor structure, Fig. 3, which could not be optimized for crashworthiness due to the restraints mentioned above. Considering mainly a vertical crash landing the crash-critical components of the subfloor were identified as shown in Fig. 4.

Quasi-static and selected dynamic crush tests with structural components of the crash-critical areas of the composite subfloor structure were performed in order to determine their failure behaviour and the energy absorption capability and to establish design recommendations and guidelines for future composite helicopters with the aim to balance properly between structural crashworthiness, load carrying capability and weight/cost effectiveness.

2. DESIGN ASPECTS

The aim of the investigations was to get a subfloor structure designed effectively for crashworthiness with respect to failure modes and energy absorption. In doing this, the following requirements had to be obeyed:

a) No additional weight impact; for weight reasons sandwich structures should be used wherever possible.

b) Single part geometry should be maintained in order not to cause changes in the tank system, the flight control system and other equipment details.

c) Main load paths should be unchanged.

d) Increase of manufacturing effort should be negligible.

The subfloor structure has to carry loads from the landing gear, the tank and the flight control system. Above mentioned requirement a) prohibited the use of additional crash elements such as load carrying profiles in the crash direction implemented into the sandwich bulkheads, frames and beams. Therefore, design effort was given to improve the inplane crush properties of sandwich structures with respect to a controlled failure mode. Because of the requirement d) on the specimen level separately machined - so called triggers - have been excluded in the final subfloor design, see Fig. 5.

By choosing the cost effective single shear bonding principle for subfloor assemblage, basically the design shown in Fig. 6 was finally selected for bulkheads, landing gear frames and keel beams.

Bulkheads, frames and beams consist of monolithic CFC-straps and sandwich webs with NOMEX-core and CFC-AFC-hybrid face sheets. The CFC-layers of the face sheet are adjacent to the NOMEX-core and have a $0^{\circ}/90^{\circ}$ fibre orientation to withstand the service loads which are mainly caused by hydrostatic tank pressure. The outer layers of the face sheets are AFC-fabric laminates with $+/- 45^{\circ}$ fibre orientation securing the rubber tank bag against splintering CFC-parts and giving a certain structural consistency in the case of a crash. To ease machining the NOMEX-core is bonded to the CFC- straps by a butt joint using splice adhesive; CFC-straps and sandwich webs are connected by CFC-angle layers. These angle layers have a fibre orientation of $+/- 45^{\circ}$ suitable for the mainly occuring shear loads during service. In case of crash loading the lower angle layers act as a predetermined failure zone separating the sandwich web from the CFC-strap. A satisfactory level of energy absorption can be realized by crushing the sandwich webs. Thereby the face sheets completely fold and smash together in a controlable manner.

At the intersection areas of bulkheads, frames and beams those parts are designed with monolithic shear webs and are bonded and riveted to each other. This design leads

to a major increase of the cross sectional area and is related to negative effects for crashworthiness. In order to investigate possible improvements in those areas for several components notched variants were designed. In the case of crash loading the reduction of initial peak failure loads and inititation of a controlled failure mode are intended by notching the structure, Fig. 7.

3. CRUSH TEST PROGRAMME

Fig. 8 overviews the crush test programme which was performed within the discussed limitations and taking into account the design aspects outlined in the previous section. The test programme was splitted into design support tests and structural component testing.

3.1 DESIGN SUPPORT TESTS

Energy Absorption of Sandwich Panels

The purpose of the sandwich panel crush test series was to extend the knowledge on the crushing and energy absorption behaviour of various sandwich designs and to investigate their weight effectiveness. In general, sandwich panel constructions show lower energy absorption capability under compression loads compared to integrally stiffened monolithic structures such as sine wave webs or hat-stringer stiffened panel designs /1-3/.

Typical sandwich failure modes under compression are general buckling, shear crimping, face wrinkling (adhesive bond failure or core compression failure) or intracell buckling (dimpling). None of those failure modes leads to efficient energy absorbing crushing. Various through the thickness stitching techniques with aramid fibre rovings were investigated in the past to improve the energy absorption behaviour of sandwich panels /1-3/. These techniques intended to initiate local face sheet folding and to avoid global face sheet debonding and failure of the core material. However, stitching techniques for the subfloor structure components had to be excluded due to their impact on manufacturing expense.

Sandwich panel joints

The sandwich panel joints of the keel beams, landing gear frames and bulkheads to the outer subfloor shell are very critical areas concerning crashworthiness. The joints are primarily designed for service load transfer. On the other hand, the joint areas must be designed for crush initiation, thereby a negative influence on the load transfer capability must be avoided. Crushing should preferably start at the intersections to the outer subfloor shell and progressive failure should continue from bottom to top of the panels.

3.2 SUB-COMPONENT CRUSH TESTS

Structural Intersections ("node point" areas)

Structural intersections of keel beams, landing gear frames and side shell frames represent structural "hard points" under crash loading within the framework of the subfloor. Those intersections are areas of high load transfer which correlates with increasing cross section areas. Crash simulation calculations with aircraft subfloors /4/ clearly indicate that "hard point" areas in subfloor frameworks generate high acceleration pulses at the cabin floor level and create dangerous inputs to the seat/occupant system. Structural elements at intersection areas which are designed to carry shear and bending loads react very stiff under compression crash loading. Investigations with metal aircraft subfloor structures /5/ have demonstrated the effectiveness of reducing the stiffness of "hard point" areas, which was accomplished among others by a "notched corner" concept. To study the peak failure load reduction, three simplified structural intersection components were quasi-statically crushed within a pretest series, one variant having a notched corner design. The fourth component of intersection structures was exactly manufactured as the original helicopter part, also including a notched corner concept. This component was also statically crushed and the failure and energy absorption behaviour was investigated.

Landing gear frame sections

The keel beams, the two landing gear frames and their intersections are very important components in the energy absorption concept of the subfloor structure. Therefore, the energy absorption performance of the landing gear frames was considered in a separate test series. The sandwich panels of the landing gear frames are loaded by

hydrostatic tank pressure, and in the case of a crash they are additionally loaded under compression. Those panels are consequently highly sensitive to global buckling. Therefore, the energy absorption concept has to take into account both - the initiation and the stabilization of energy absorbing crush modes. Within the test series two components were crushed, one component having a lightweight supporting element between the two panels of the frame.

4. CRUSH TEST SET UPS AND RESULTS

4.1 DESIGN SUPPORT TESTS

Sandwich Panel Crushing

Fig. 9 summarizes the results of the sandwich panel test series. Included in the test series were the finally selected basic sandwich design for keel beams, landing gear frames and bulkheads with CFC/AFC-NOMEX-core layup and other sandwich designs such as multi-layer CFC-NOMEX sandwich and CFC-NOMEX panels with integrated prefabricated CFC-crush profiles. As can be seen in Fig. 9, some sandwich panel configurations were provided with "crush initiators" (triggers) to reduce the peak failure loads (Fpeak) and to initiate stable crushing. All tested specimens had a height of 100 mm and were 180 mm long; the thickness of the panels varied depending on the design. For quasi-static and also for dynamic crush testing in a drop tower, the sandwich panels were clamped at the bottom and loaded at the unclamped top. The energy absorption performance of the crush specimens was evaluated on the basis of the load-deflection curves. Peak and average crush force levels (Fpeak and Favg) and the specific energy (Esp), i. e. the absorbed energy related to the crushed mass of the specimen, were determined. Progressive crushing of the face sheets starting at the top could be observed with CFC-Nomex, CFC/AFC-Nomex and all other triggered sandwich panels. Multi-layer CFC-Nomex sandwich and panels with integrated CFC-profiles which were not provided with a trigger failed catastrophically in the mid-sections of the panels by shear crimping or face sheet fractures and delaminations. Those failures resulted in poor energy absorption.

The specific energy absorption of the basic CFC/AFC-Nomex sandwich (weight factor = 1) was determined at 18 kJ/kg. As can be seen in Fig. 9 the specific energy absorption could be improved essentially with triggered multi-layer CFC-Nomex sandwich panels and panels with integrated CFC-profiles. The best result of the test series was gained with the integrated CFC-profile configuration having a concave tapered trigger at the top of the crush profiles. The specific energy absorption was determined at 51 kJ/kg which is an improvement by factor 2,8 compared to the CFC/AFC-Nomex sandwich, however, the weight factor doubled. From the energy absorption point of view, the advantage of the integrated crush profile configuration was obvious, however, the impact on total weight and manufacturing effort could not be accepted for the final subfloor design.

Sandwich specimens which were tested under quasi-static as well as dynamic crushing did show only small differences of specific energy absorption.

Sandwich Panel Joints to Outer Subfloor Shell

The results of various investigated designs for joints of sandwich shear webs of keel beams, landing gear frames and bulkheads to the outer subfloor shell are overviewed in Fig. 10. The manufacturing procedure for attaching the outer subfloor shell to the subfloor framework necessitated inclined CFC-straps at the bottom of the subfloor framework shear webs (see Fig. 10). All joint designs should fit for bonding as well as riveting the parts together.

As could be learned from the results of the sandwich panel crush test series a complete inplane progressive crushing, i. e. local symmetric folding of the face sheets could not be accomplished within the design limitations. Therefore, all joint designs were provided with predetermined failure zones - so called triggers - which were intended to initiate face sheet fractures localized at the bottom of the shear webs at a compression load level below the general buckling strength of the panels.

The geometrical dimensions of the sandwich panel joint specimens were also 180 x 100 mm, and the thickness was depending on design. For quasi-static crushing the specimens were clamped in the sandwich area, where the face sheets were reinforced by two GFC-straps to avoid failure in the clamping area (Fig. 10). The test set-up provided that the joint area couldn't slip sidewards during compression loading to simulate the bond to the outer subfloor shell.

The results of the test series clearly indicated the difficulty to initiate progressive energy absorbing fracture of the sandwich face sheets on the specimen level.

An effective crush initiation turned out to be highly sensitive to manufacturing parameters such as the distribution of splice adhesive in the butt joint area of the NOMEX-core. Most values of the specific absorbed energy (Esp) fell below 10 kJ/kg which is relatively low compared to the Esp-values of pure sandwich panel crushing. The "basic joint design" (weight factor = 1) had an Esp-value of 2.3 kJ/kg (pure sandwich: 18 kJ/kg) and the ratio of Fpeak/Favg was at 5.6. The best results of the test series were gained with the integrated CFC-crush profile concept (weight factor: 1.77). Those Esp-values were determined at 18.4 kJ/kg (pure sandwich: 51.3 kJ/kg) and the ratios of Fpeak/Favg were at 2.0. However, taking into account the weight factor and the increase of manufacturing effort, this joint concept could not be incorporated into the final subfloor design.

4.2 SUB-COMPONENT CRUSH TESTS

Structural Intersections ("node point" areas)

Within a pretest series three simplified structural assemblages (KN 1-3) of a keel beam, landing gear frame and side shell frame section were quasi-statically crushed between the parallel supports of a standard testing machine. Fig. 12 shows the test set-up for component KN3 which was provided with notched corners at the joints of the landing gear frame and side shell frame section. Components KN1 and KN2 did not have any notches. As can be seen in Fig. 11, at the intersection area the monolithic keel beam had a cutout for the landing gear tube. Landing gear tube dummies were used testing component KN2 and KN3. During the crush tests a force-deflection curve was recorded which was integrated to generate the absorbed energy versus deflection curve. Additionally 18 strain gage signals were recorded up to first failure to get detailed strain/stress informations. The failure sequences were recorded on video tapes and were documented by taking picture series.

Fig. 12 shows the force-deflection curves of the intersection components KN 1-3 up to a stroke of 50 mm. The two identical components KN1 and KN2 had the same initial compression stiffness and failed at the bottom of the keel beam at a load level of 85 KN and 99 KN, respectively. With both components first elastic buckling deformations were observed in the simplified monolithic landing gear frame and in the side shell frame section. Component KN3 failed at the notched corners to the left and to the right of the keel beam cutout at a load level of 54 kN. Also caused by the notched corners the initial compression stiffness was slightly reduced, and the absorbed energy up to a deflection of 50 mm was only 327 J compared to 850 J and 864 J for KN1 and KN2, respectively. However, looking at the force-deflection curves shown in Fig. 13, the notched corner component KN3 absorbed almost the same energy as KN2 (2015 versus 2178 J) at 100 mm stroke; up to 150 mm stroke the energy absorption of KN3 was even better. The energy absorption of KN1 which was tested without landing gear dummy was only 1560 J at 100 mm stroke. This test was interrupted at 105 mm stroke because the keel beam slipped sidewards and the crush force level dropped almost to zero.

Fig. 14 shows the crushed component KN3 with the landing gear dummy removed. In the area of the notched corners many controlled fractures of the keel beam, the angle joints of the landing gear frame and side shell frame sections did occur. Also the landing gear dummy played an important role in the energy absorption. After the contact of the upper edge of the keel beam cutout and the landing gear dummy, the keel beam laminate disintegrated completely, as can be seen in Fig. 14, which resulted in a high energy absorption up to 150 mm stroke.

The pretest series KN 1-3 demonstrated the effectiveness of the notched corner concept to reduce peak failure loads. Another outcome for the final design of structural intersections was that the number of four notches could be reduced to one or two with the aim to increase the crush force level up to 50 mm stroke. The low crush force level up to 50 mm stroke was mainly caused by the keel beam cutout and was further deteriorated by four notches in a row. For further intersection component testing it was obvious that the landing gear dummy had to be included in the test set up.

Fig. 15 shows the schematic test set-up for the intersection component KN4. The test procedure was equivalent to the test series KN 1-3. Additionally, two piezoelectric load cells (C1 and C2) were included in the test set-up (see Fig. 15) to get the flux of force in the keel beam/landing gear frame section and in the side shell frame section.

A simplified sketch of KN4 was already shown in Fig. 7 which also includes the locations of the notches, Fig. 16 shows the component prepared for quasi-static crush testing. The intersection component KN4 was manufactured identical to the original helicopter part. Only the cabin floor and the outer subfloor shell were substituted by 8 mm thick GFC-plates as can be seen in Fig. 16.

Fig. 17 shows the force-deflection characteristic and the absorbed energy versus deflection of component KN4. Fig. 18 shows the crushed component removed from the test machine after a vertical stroke of 150 mm. The first failure at the top of the keel beam occured at a peak load of 60 kN (stroke 1,5 mm) which was followed by a second peak at 85 kN and 4 mm stroke. After crush initiation the average crush force level dropped somewhat up to 50 mm stroke due to the keel beam cutout, and then further increased again due to the crushing of the keel beam after contact with the landing gear dummy. The average force level up to 150 mm stroke was at 40 kN which was high compared to the peak loads during crush initiation. The distribution of the flux of force up to maximum stroke is also shown in Fig. 17. Averaged over the total stroke, 57 percent of the crush force were contributed from the keel beam/landing gear frame section and 43 percent were provided by the side shell frame section.

The component KN4 absorbed about 7300 J at 150 mm stroke. As can be seen at the crushed component, Fig. 18, the energy absorption was provided by several fractures and crushing in the keel beam and by crushing in the upper part of the side shell frame and landing gear frame section. The areas where the metal fittings of the landing gear fixture were riveted to the side shell frame remained almost undamaged.

In order to minimize hazard to occupants for future civil helicopter crashworthiness it is recommended for the pure vertical impact, /6/, that the fuselage understructure and/or seats must attenuate the deceleration pulse which is created by a vertical flight path velocity of 7.9 m/s (26 ft/s). Thereby all the energy absorption capability of the landing gear is depleted. Taking into account that particular impact condition for the BK 117 composite fuselage, from the point of view of the energy absorption management about 30 percent of the initial kinetic energy could already be absorbed by the four intersection areas of keel beams, landing gear frames and lower side shell frame sections.

Landing Gear Frame Sections

The schematic set-up for the two tests of landing gear frame sections and a simplified sketch of the components are shown in Fig. 19. The component HUT1 was tested without a supporting structure between the parallel sandwich panels of the frame, and component HUT2 had a light weight AFC-cylinder built in, as can be seen in Fig. 19.

The two components represented mid-sections of the landing gear frame in the rear of the subfloor structure. Those frames under vertical crash conditions are loaded under compression and hydrostatic tank pressure (Fig. 19). Therefore the panels tend to buckle symmetrically towards the landing gear tube. The simulation of hydrostatic tank pressure couldn't be realized easily within the test set-up, however, side supports were provided to avoid at least outside buckling and to predetermine the inside buckling direction. The test set-up was also equipped with a landing gear dummy positioned between the panels of the frame section.

The AFC-supporting cylinder was thought to avoid any inside buckling and to guarantee crush initiation at the joints to the outer subfloor shell. The joint design of the two components was identical to that one shown in Fig. 6.

The force-deflection characteristics and the energy absorption versus deflection of the landing gear frame sections are shown in Fig. 20. The component HUT1 failed at a load level of 30 kN by buckling in the mid-section of one sandwich panel frame. The other panel also tended to buckle inside but then failed at the predetermined failure zone at the joint to the outer subfloor shell and crushed in a "rolling-up" action as can be seen in Fig. 21. Both CFC/AFC-face sheets of the panel locally folded and fractured at an average force level of about 9 kN and provided an energy absorption of 1375 J at 150 mm stroke. It was obvious that the energy absorption could be doubled if buckling failures could be avoided and both crush initiators at the panel joints would work.

The second component HUT2 with the AFC-supporting cylinder failed at 32 kN. One panel started to crush at the failure initiator at the bottom joint area, the other panel, however, failed at the butt joint of the upper connecting angle to the CFC-strap at the cabin floor level. Further crushing of the two panels was completely unsymmetric which finally resulted in debonding of the supporting cylinder and global buckling of one panel. The test was stopped at 105 mm stroke. The average force level up to 105 mm stroke was at 10.6 kN and the absorbed energy was determined at 1110 J.

5. CONCLUDING REMARKS

Within the development programme of a composite fuselage crash critical areas were identified and a test programme on the specimen and sub-component level was performed to study the structural crashworthiness of the lower airframe section under vertical crash loads.

Primarily, the composite fuselage was designed to fit the operational requirements and the load carrying capability of the metal baseline helicopter - the MBB/Kawasaki BK 117. Therefore, for the structural crashworthiness of the fuselage certain design limitations had to be obeyed. All design changes to improve the energy absorption performance of the fuselage had to be balanced properly between the impact on load-carrying capability, weight and manufacturing effort.

Within design support test series various sandwich configurations were investigated and variants with good inplane energy absorption performance could be found. However, sandwich configurations with better energy absorption than the finally selected basic sandwich design for shear webs of keel beams and bulkheads with CFC/AFC -face sheets and NOMEX - core, turned out to have a severe impact on weight and manufacturing effort.

Joints of keel beams, landing gear frames, and bulkheads to the outer subfloor shell were provided with predetermined failure zones and energy absorbing crushing after failure initiation at a load level below the general buckling strength of the shear web panels could be demonstrated within the test programme.

At structural "hard points", e.g. intersections of keel beams, landing gear frames and side shell frames, the feasibility of a "notched corner" concept with the aim to reduce peak failure loads under vertical crushing could be made evident. The notched corner concept did not affect very much the manufacturing efforts. However, it should be mentioned that this design concept, especially with composite structures, is not optimal. To "weaken" the "hard point" areas in composite subfloor structures other possibilities such as less stiff laminate layups or other geometrical shape variants at the intersection areas should be taken into account and further investigated. The tested structural "hard point" components, especially the component KN 4 which was manufactured equivalent to the original helicopter part, did show good energy absorption performance under vertical crush loads. The structural intersections are expected to contribute essentially to the energy absorption management of the lower airframe structure.

Also, at the landing gear frame sections good energy absorption capability could be demonstrated by predetermined failure initiation and stabilizing the energy absorbing crushing by light weight supporting structures to avoid glob buckling of the shear web panels under vertical crash loads and hydrostatic tank pressure acting in the lateral direction.

For the complete composite subfloor structure a favourable energy absorption performance was demonstrated by the crush test programme. Thereby the keel beams, the landing gear frames and their intersections play the most important role in the energy absorption management. About 150 mm stroke are available in the subfloor structure for energy absorbing crushing. It can be expected that the composite fuselage based on the BK 117 will be suitable for a vertical crash condition with 7.9 m/s impact velocity which is recommended for future civil helicopters. However, to guarantee a system crashworthiness for that particular impact condition, energy absorbing seats with about 100 mm stroke are highly recommended.

The system crashworthiness will be studied and demonstrated furtheron by crash simulation calculations. Thereby the various crush characteristics gained during the sub-component test programme will be used as inputs for the nonlinear behaviour of crush zones.

REFERENCES

/1/ FARLEY, G.L.
Energy Absorption of Composite Material and Structure.
43. Annual Forum of the American Helicopter Society,
June 1987

/2/ SEN, J.K.
Designing for a Crashworthy All-Composite Helicopter
Fuselage.
Journal of the American Helicopter Society, Volume 32 -
No 2, April 1987

/3/ KINDERVATER, C.M.; BANNERMAN, D.C.
Crashworthiness Investigations of Composite Aircraft
Subfloor Beam Sections.
Int. Conference on Structural Impact and Crashworthiness,
Imperial College, July 1984

/4/ HIENSTORFER, W.G.
Crashsimulationsrechnungen und Bauteilidealisierung für
einen Luftfahrzeugunterboden.
Zeitschrift für Flugwissenschaften und Weltraumforschung,
Band 11, Juli - Oktober 1987, Heft 4/5

/5/ CRONKHITE, J.D.; BERRY, V.L.
Crashworthy Airframe Design Concepts. Fabrication and
Testing.
NASA CR 3603 (1982)

/6/ COLTMAN, J.W:; BOLUKBASI, A.O.; LAANANEN, D.H.
Analysis of Rotorcraft Crash Dynamics for Development
of Improved Crashworthiness Design Criteria.
DOT/FAA/CT - 85/11, Final Report, June 1985

FIG. 1 MBB/KAWASAKI BK 117 LIGHT TRANSPORT HELICOPTER

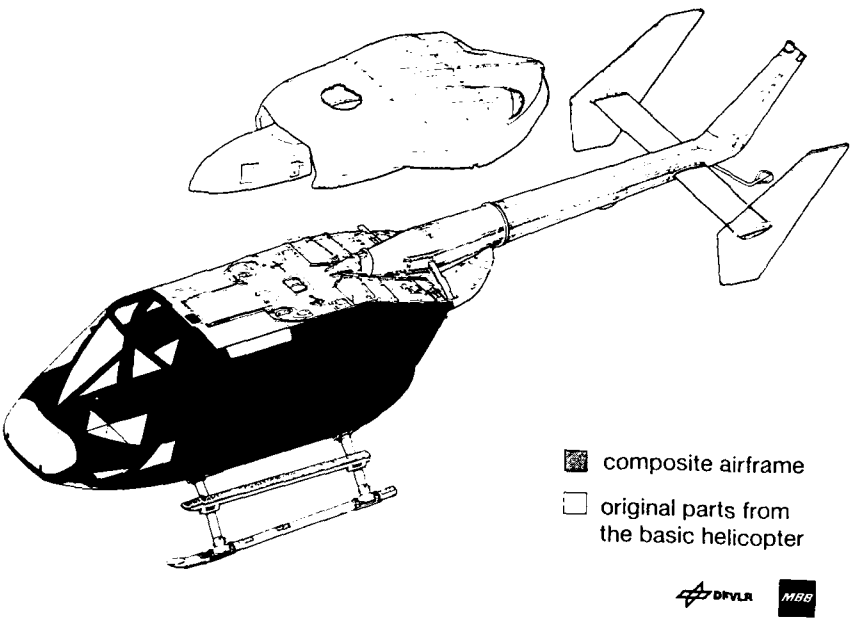

FIG. 2 THE COMPOSITE AIRFRAME

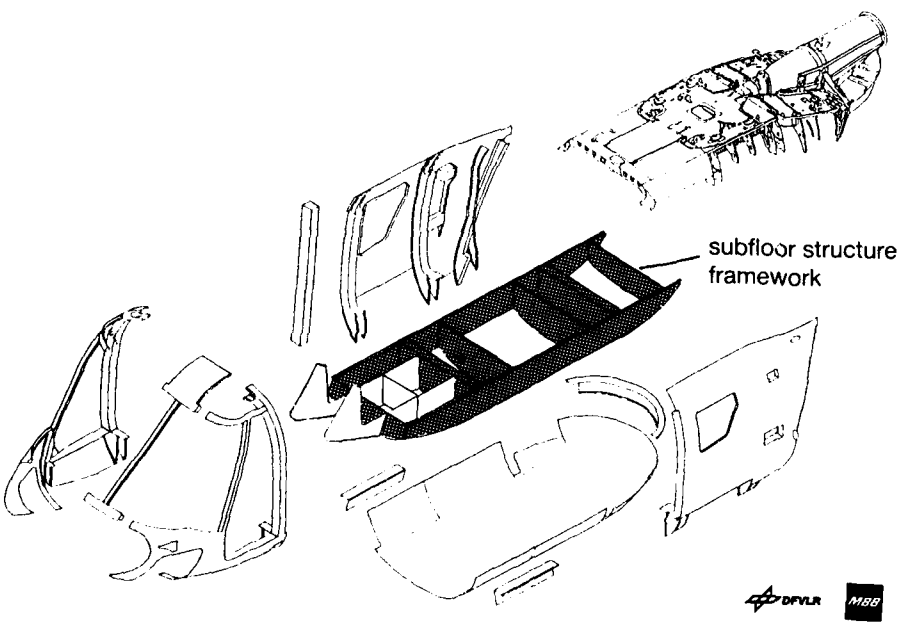

FIG. 3 STRUCTURAL BREAKDOWN OF THE COMPOSITE AIRFRAME

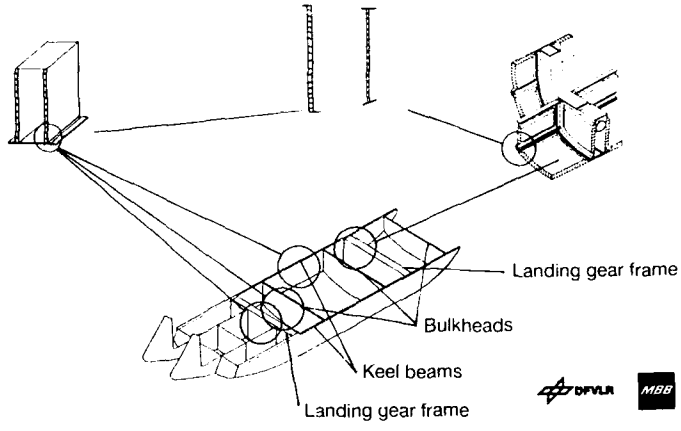

FIG. 4 CRASH – CRITICAL AREAS OF THE SUBFLOOR – STRUCTURE

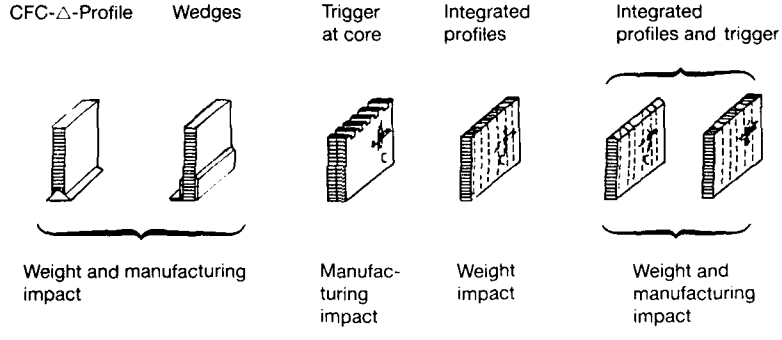

FIG.5 DESIGN VARIANTS NOT USED IN FULL – SCALE STRUCTURE WITH RESPECT TO IMPACT ON WEIGHT AND MANUFACTURING EFFORT

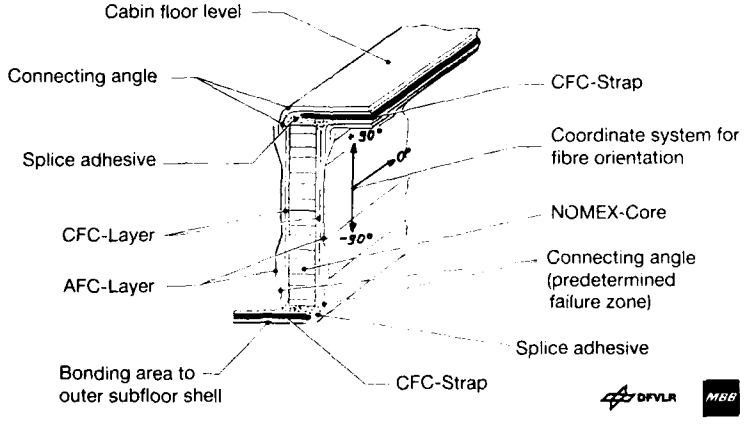

FIG.6 CROSS SECTION OF LANDING GEAR FRAME WITH SCHEMATIC LAY UP

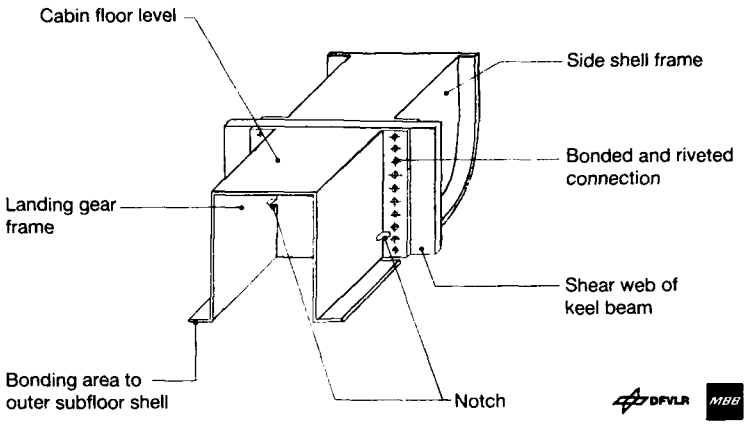

FIG. 7 NOTCHED STRUCTURE AT SUBFLOOR INTERSECTION AREA

DESIGN – SUPPORT TESTS	SUB – COMPONENT TESTS
* SANDWICH PANELS – Energy absorption performance	* STRUCTURAL INTERSECTIONS (Keel beams /landing gear frames /side shell frames) – Reduction of peak failure loads – Initiation of energy absorbing crushing
* SANDWICH PANEL JOINTS – Initiation of energy absorbing crushing	* LANDING GEAR FRAME SECTIONS – Initiation and stabilization of energy absorbing crushing

FIG. 8 CRUSH TEST PROGRAMME

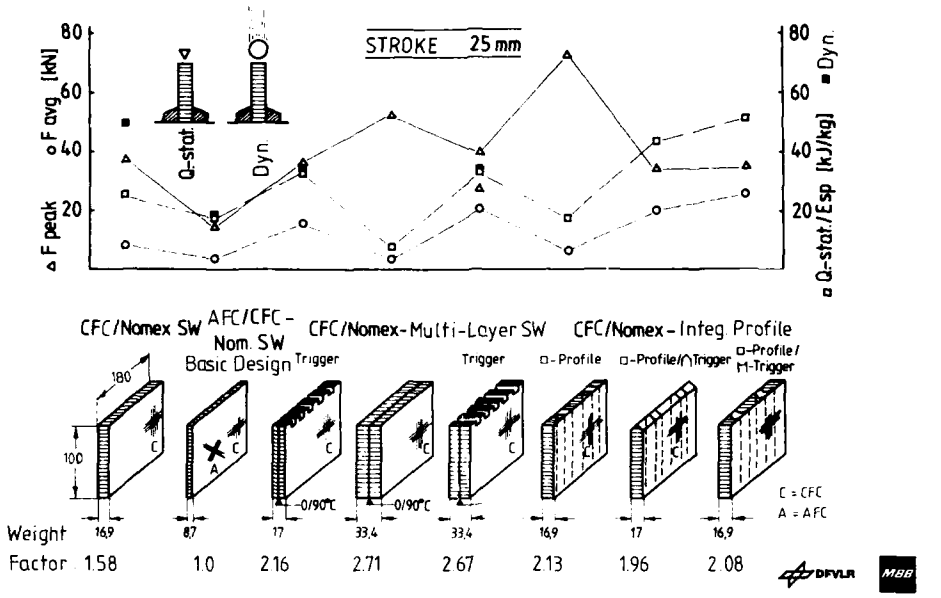

FIG. 9 DESIGN VARIANTS AND CRUSH TEST RESULTS OF SANDWICH PANELS

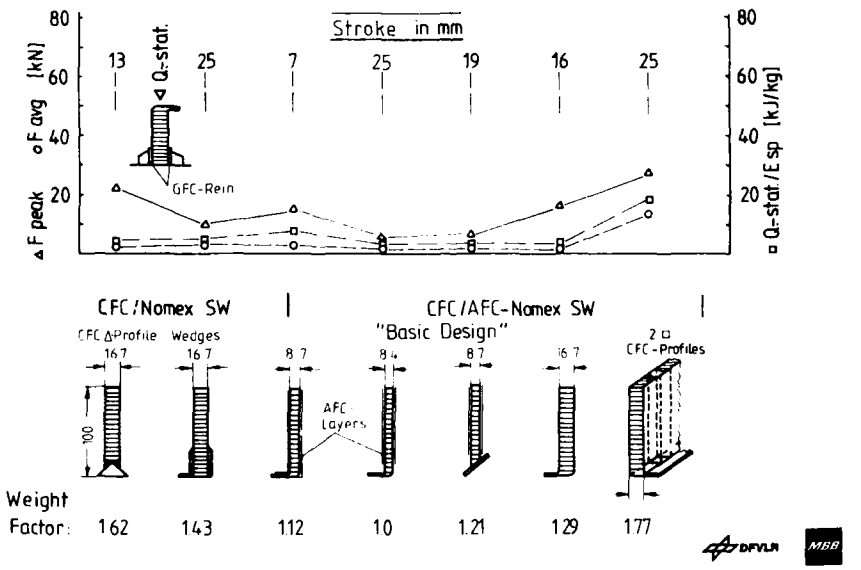

FIG. 10 DESIGN VARIANTS AND CRUSH TEST RESULTS OF SANDWICH PANEL JOINTS

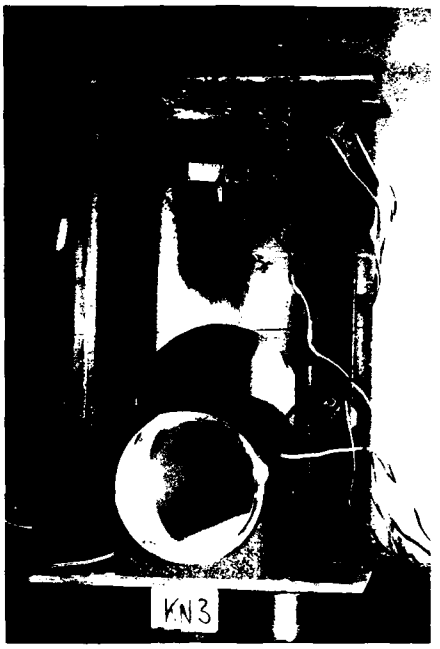

FIG. 11 TEST SET UP OF INTERSECTION COMPONENT KN 3 WITH "NOTCHED CORNERS"

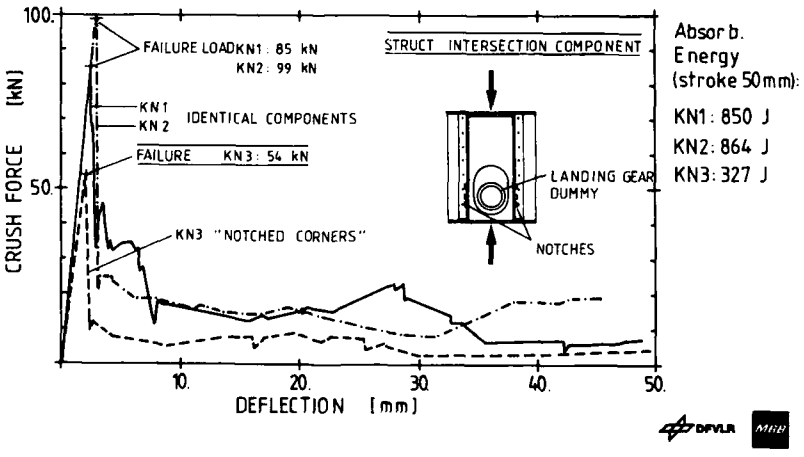

FIG. 12 CRUSH CHARACTERISTICS OF INTERSECTION COMPONENTS KN 1 – 3 UP TO 50 MM STROKE

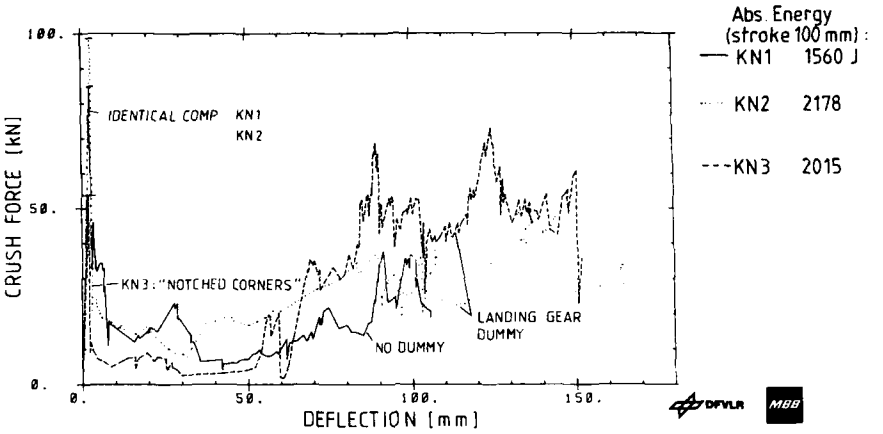

FIG.13 TOTAL CRUSH CHARACTERISTICS OF INTERSECTION COMPONENTS KN 1 – 3

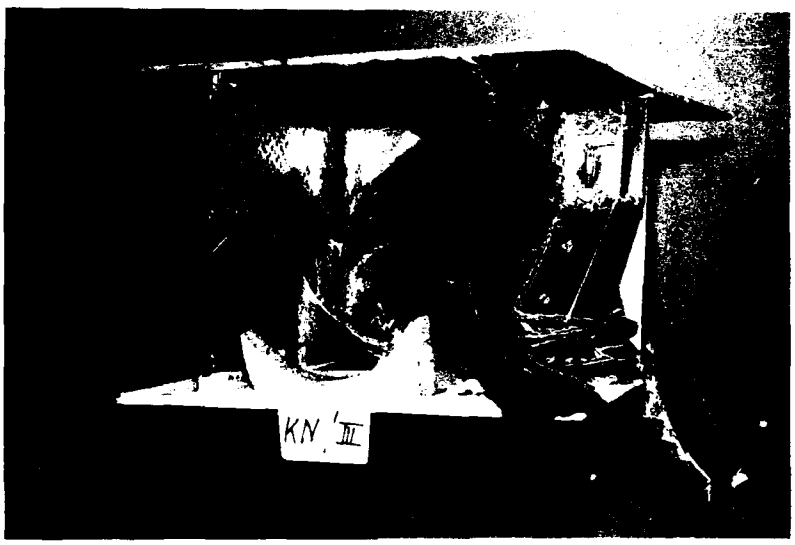

FIG.14 CRUSHED INTERSECTION COMPONENT KN 3

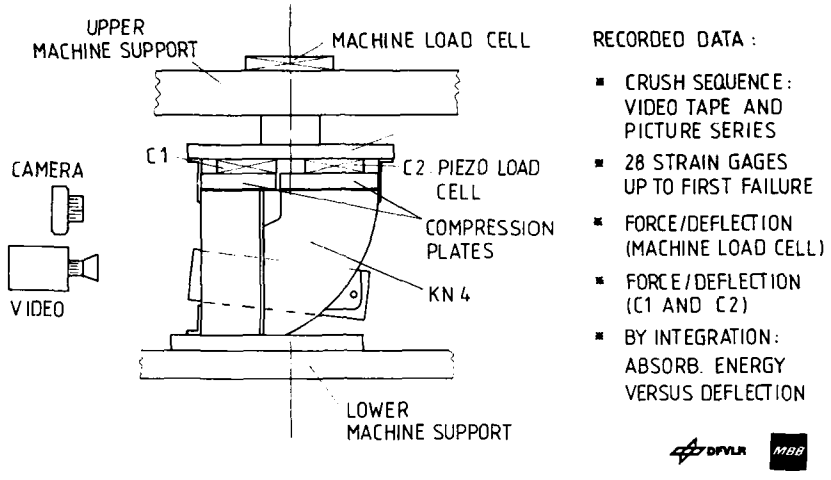

FIG.15 SCHEMATIC TEST SET UP FOR INTERSECTION COMPONENT KN 4

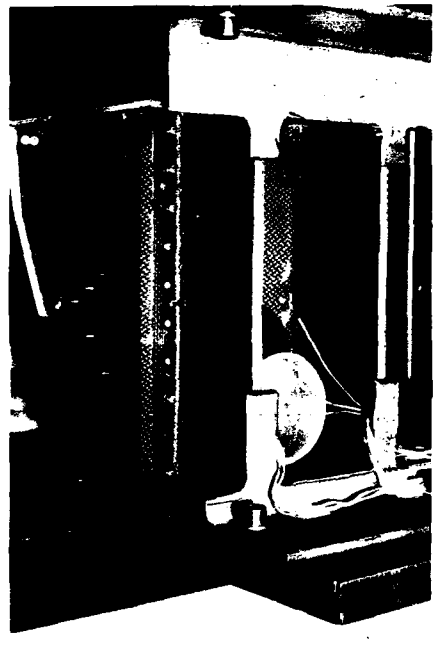

FIG. 16 INTERSECTION COMPONENT KN 4

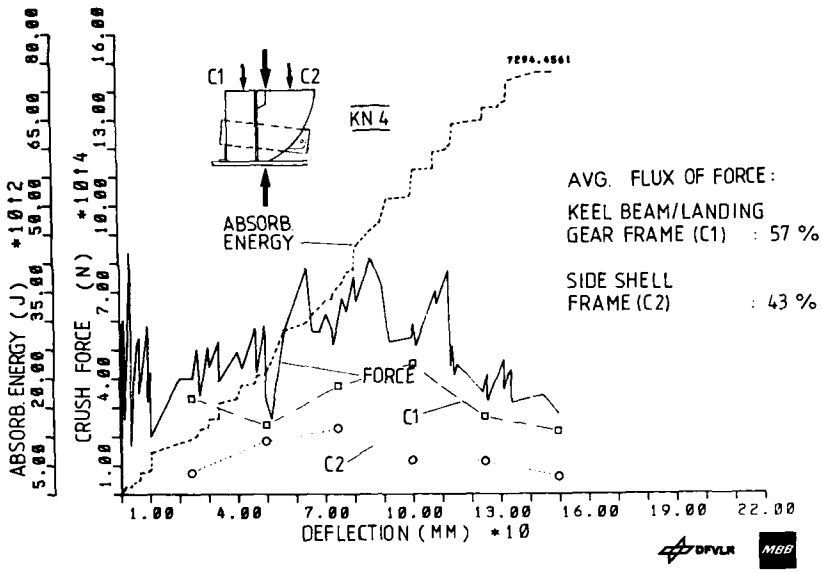

FIG. 17 CRUSH CHARACTERISTIC OF COMPONENT KN 4

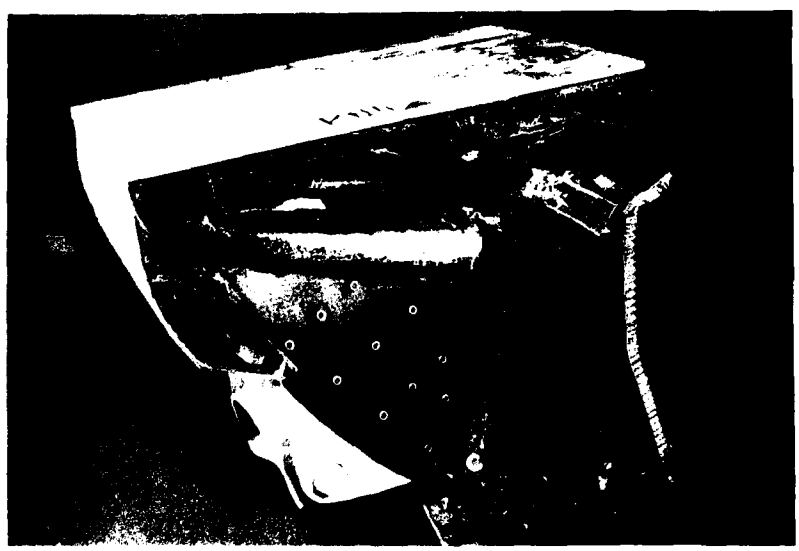

FIG. 18 CRUSHED COMPONENT KN 4

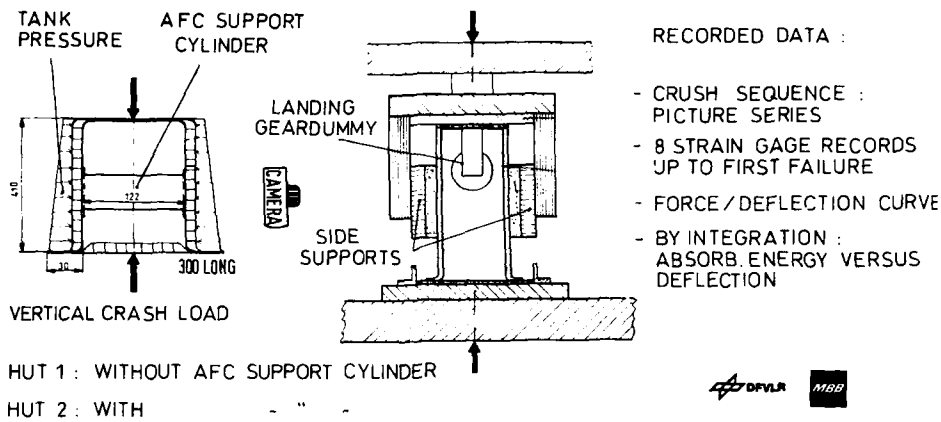

FIG. 19 SCHEMATIC TEST SET UP FOR LANDING GEAR FRAME SECTIONS

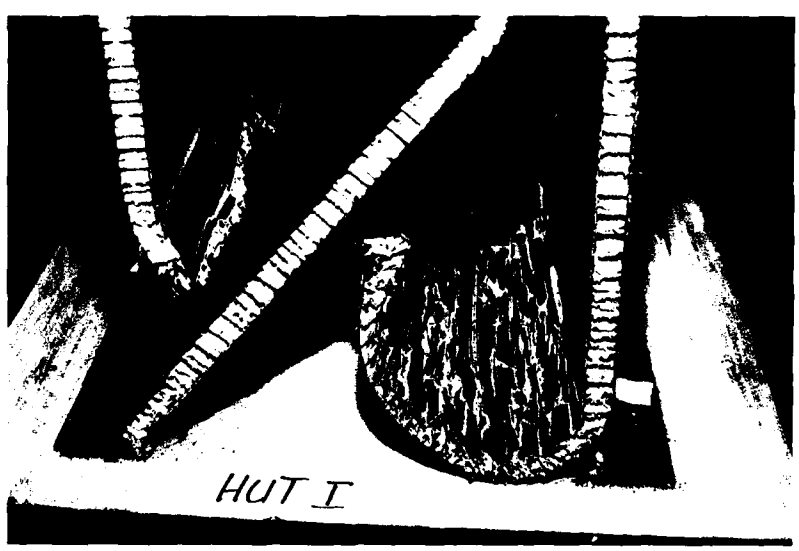

FIG. 21 CRUSH MODE OF LANDING GEAR FRAME SANDWICH PANEL

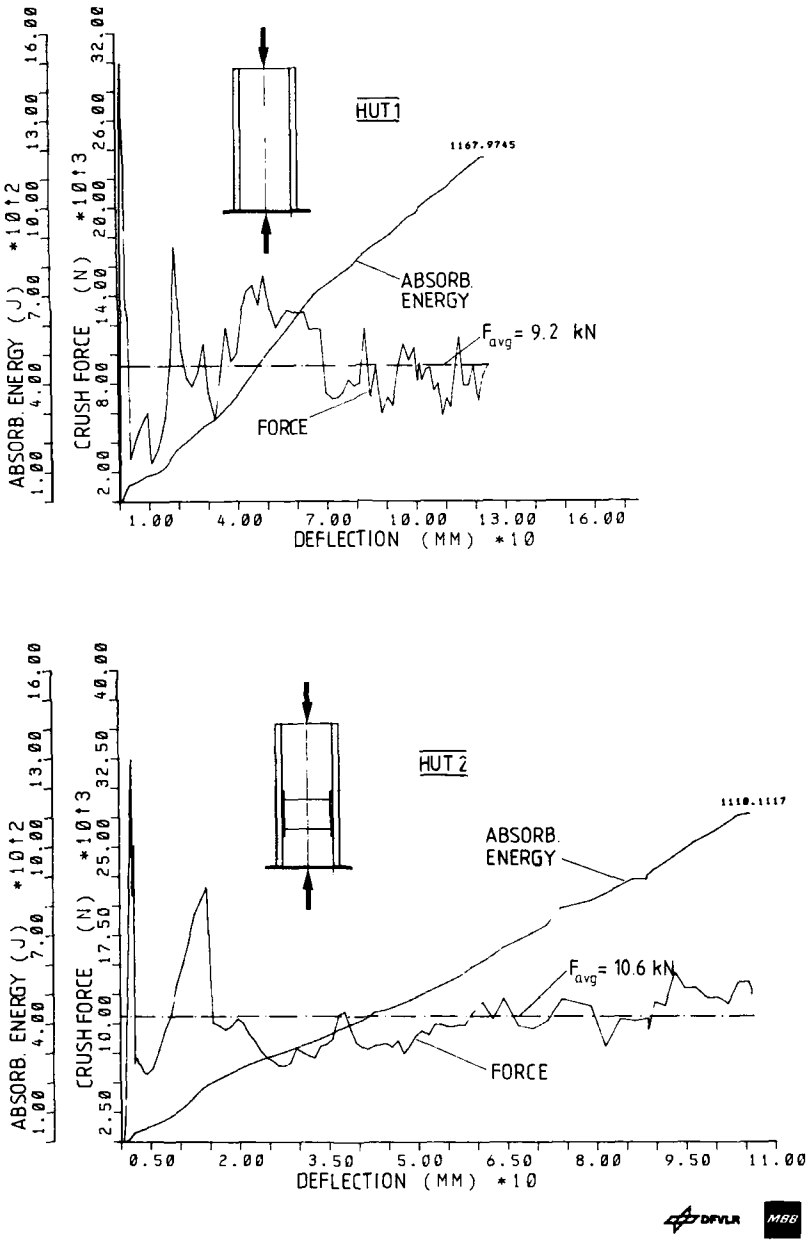

FIG. 20 CRUSH CHARACTERISTICS OF LANDING GEAR FRAME SECTIONS (HUT 1 AND 2)

CRASHWORTHY DESIGN OF AIRCRAFT SUBFLOOR STRUCTURAL COMPONENTS

by

Ch. Kindervater
H. Georgi
U. Körber

Institute for Structures and Design, DFVLR Stuttgart
Pfaffenwaldring 38-40, 7000 Stuttgart 80, Germany

ABSTRACT

Subfloor beams and bulkheads in aircraft structures are designed to carry longitudinal and shear loads resulting from fuselage bending and torsion. In crashes however, the subfloor is highly loaded in compression and shear. Especially the intersections of beams and bulkheads (cruciforms) represent stiff vertical "hard points", and the resulting high peak failure loads under compression can create life threatening crash pulses to the occupants.

For a commuter type aircraft subfloor aluminium as well as composite cruciforms were designed to match the same longitudinal stiffness of the floor beams and the same shear stiffness of the bulkheads. Various designs of the intersections including notched corners, corrugated and tapered edge joints, and less stiff laminate layups were investigated to reduce the initial peak loads, and to trigger efficient energy absorbing crush failure modes.

The cruciforms and sub-elements thereof such as angle stiffeners and angle stiffened plates were statically crush tested in order to gain informations about the complex collapse behaviour of subfloor constructions. Based on the load-deflection curves important energy absorption parameters were determined, and were compared to the aluminium baseline design.

For crash simulations with so called hybrid computer codes such as KRASH load-deflection-curves of structural elements are needed as input data. Those inputs can be created by tests or by analytical approaches. For the cruciforms and sub-elements thereof the prediction of load-deflection-curves are presented and discussed including plastic hinge formation and approximate mean crush load prediction as well as failure load and critical stress evaluations.

1. INTRODUCTION

Intensive investigations have been performed in the last decade to improve the structural crashworthiness of aircraft structures. Comprehensive accident statistics - mostly performed in the U.S.A - have shown that many fatalities occured in accidents which had a survivable crash envelope from the standpoint of human tolerance due to the lack of sufficient structural crash protection or non-crashworthy seat and restraint systems. Meanwhile, crashworthiness standards have been established for military helicopters and light fixed wing aircraft /1/. Also, for civil helicopters /2/, light fixed-wing aircraft, and large transport airplanes improved structural crashworthiness and crashworthy seat and restraint systems are recommended and appropriate requirements can be expected in the future.

In crashes with a high vertical component of the impact velocity the crash loads have to be absorbed by structural deformation. For the control of decelerative loads of seated occupants, the type of aircraft will affect the crashworthy design approach, Fig. 1. Light fixed-wing general aviation aircraft, small passenger airplanes and helicopters, expecially with retracted landing gear, having relatively little crushable airframe structure would require additional energy absorption in the seat system, to prevent injury to occupants in potentially survivable accidents.

The present investigation was oriented at a typical metal subfloor design of a commuter type aircraft, Fig. 2. The framework of the subfloor structure is composed of longitudinal keel beams and lateral bulkheads covered by the outer skin and the cabin floor. Structural cruciforms, Fig. 2, represent typical sub-elements of the subfloor framework connected to each other by keel beam and lateral bulkhead sections. Therefore, their crush-characteristics contribute essentially to the overall crash response of a subfloor assemblage. Under vertical crash loads structural cruciforms represent "hard point" stiff columns which do create high decelrative peak loads under compression at the cabin floor level and seat attachments, and cause dangerous inputs to the seat-occupant system.

For general aviation metal airframe structures crashworthy floor concepts have been already investigated intensively /3/. Those design variants included minimum modification concepts such as "notched corners" to weaken the intersections of keel beams and bulkheads, and other unconventional subfloor designs such as corrugated keel beams, corrugated half shell structures and foam-filled keel beam cylinders.

For future aircraft and helicopters a further increasing share of composite primary airframe structure can be expected due to the superior properties of composites . The present knowledge about the crash performance, viz. energy absorption capability and failure behaviour of composite airframes is very low. However, on the specimen and structural element level the efficient energy absorption performance of composites has been fairly demonstrated in the past. Also some knowledge is available on crashworthy designs of exemplary composite subfloor beam elements /4-6/. However, the incorporation of energy absorbing structural concepts into composite fuselage sections is limited up to now to a few helicopter projects.

The present work focuses on the experimental determination of crush characteristics and the energy absorption of aluminium and composite structural cruciforms and on design variants for crush initiation - so called trigger mechanisms - in this area. The aluminium baseline cruciform had the dimensions and the aluminium sheet material of a commuter type aircraft with a max. take-off weight of 5.7 t.

Up to date, the most reliable method for valuation of crashworthiness of structural elements or of composed structures is dynamic testing, and recording the load-deflection curve for determination of peak loads, average crush force levels and energy absorption capability. However, these tests may be too expensive to cover all informations needed about crash behaviour. Therefore, the second part of the present investigation was concentrated on analytical approaches for the determination of load-deflection-curves of structural elements such as cruciforms, angle stiffeners and angle stiffened plates. Those investigations include plastic hinge formation and approximative mean crush load prediction as well as failure load and critical stress evaluations.

Based on experimentally or analytically determined crush - characteristics design optimizations concerning the crash behaviour of complete subfloor structures can be performed by application of hybrid computer codes such as KRASH developed by Lockheed California Company.

2. DESIGN REQUIREMENTS FOR CRASHWORTHY SUBFLOOR CONCEPTS

The general design philosophy of crashworthy subfloor structures is outlined in /3/ and is shown in Fig. 3. The subfloor structure consists of a strong structural floor with a crush zone underneath. The structural floor is a platform designed to carry loads and moments imposed by the seats/occupants or cargo and to maintain seat-to-structure integrity without breaking up, heaving, or decreasing the cabin volume. The energy absorbing crush zone is designed to distribute the loads to the upper floor as uniformly as possible and to collapse in a controlled manner at loads at or near human tolerance levels and below the structural capability of the airframe. The "controlled load concept" curve for subfloor collapse is depicted in Fig. 3. This "ideal" crush characteristic can mainly be achieved by proper design of subfloor cruciforms which are manifold recurrent sub-elements of a subfloor assemblage.

Requirements for the crashworthy design of structural cruciforms following the "controlled load concept" are summarized as follows:

- Controlled stiffness and strength up to first failure.
- Constant, high crush force level after first failure and crush initiation to provide high energy absorption.
- Crushing by plastic deformation or controlled fractures to the highest extent of structural height.
- Provision of structural post crush integrity.
- Reproduceable crush-characteristics and energy absorption capability.

The lower airframe structure is primarily designed to carry operational airframe loads. The crash can be considered as an additional loading condition. The dual purpose subfloor design which provides load carrying capability and energy absorption in the crush zone would be an optimum. A crashworthy "minimum modification" concept should be achieved to minimize weight and manufacturing penalties.

The use of composite materials in airframe structures can provide structural weight savings between 20-30 percent. The crashworthy design of composite airframe structures, however, has to be treated very carefully. Especially CFC (carbonfibre composite) has very brittle failure behaviour and the micromechanical energy absorption mechanisms are quite different compared to aluminium which dissipates energy by plastic hinge formation and yielding. With composites different innovative design concepts have to be taken into account to achieve best results concerning load carrying capability and energy absorption performance.

3. CRUCIFORM DESIGNS AND CRUSH TEST PROGRAMME

3.1 DESIGN CRITERIA

Aluminium and composite cruciforms are primarily considered under the aspect of crushing and energy absorption behaviour. However, to achieve a basis of comparison to the aluminium baseline cruciform, Fig. 4, common design criteria concerning the load carrying capability have to be defined. Caused by the difficulty to design an isolated sub-element under service load conditions stiffness design criteria related to the structural function of the cruciform sub-elements, viz. keel beam and lateral bulkhead sections, are selected.

The keel beam in the subfloor assemblage has to carry longitudinal loads resulting from fuselage bending. Therefore, all keel beam sections are designed to match the same longitudinal stiffness $S_\sigma = E \cdot A$. The lateral bulkheads have to carry shear loads. Therefore, the shear stiffness criterion $S_\tau = G \cdot A$ is selected. The appropriate cross section A results from the sheet thickness s and the cruciform height h which is the same for all components. Thus, the design criteria reduce to:

$S_\sigma = E \cdot s$ keel beam section
$S_\tau = G \cdot s$ lateral bulkhead section

Although this is a simplified design approach the load carrying capability of the various designs is taken into account and the comparison of crush test results is based on common structural performance criteria.

3.2 CRUCIFORM DESIGN VARIANTS

The baseline aluminium cruciform (Al) was taken from a conventional design of a commuter aircraft subfloor structure where the aspect of improved structural crashworthiness was not taken into account.

Numerous design variants are possible to improve the crushing behaviour of cruciform elements. One way is the change of design at the cruciform straight junction. For aluminium cruciforms this was performed by the "notched corner" concept having single and multiple notches, Fig. 5. Also, for composite hybrid cruciforms (mixture of CFC and AFC (Aramid Fibre Composite) layers in the laminate) the multiple notches concept was used (HN), and also a corrugated edge joint design (HW) was investigated, as can be seen in Fig. 5, with the intent to initiate local failures at the joint.

Another possibility to influence the crushing behaviour of cruciforms is material selection. However, this tailoring capability is limited to composite configurations. In the present programme hybridization of CFC/AFC was used with the major intent to improve the post crush structural integrity of the cruciform elements. Fig. 6 gives a complete overview of the investigated design variants. For design details and the manufacturing procedure of the cruciform elements is referred to /7/.

3.3 CRUSH TEST PROCEDURE

All cruciform elements were quasi-statically crushed between the parallel supports of a standard testing machine. Two identical components were tested of each design variant. The specimens were clamped 10 mm at the top and bottom in a test fixture to simulate the connection to the cabin floor and outer subfloor shell. The vertical edges were not supported. This refers to the design of keel beams and lateral bulkheads in the

reference metal subfloor structure which have circular cutouts positioned at a distance of about 100 mm from the intersection. Therefore, the vertical unsupported edges simulated quite fairly realistic boundary conditions.

The rate of load application was set initially to 2 mm/min, and was increased during crushing up to 30 mm/min. During the tests a force-deflection-curve was recorded which was later integrated to the absorbed energy versus deflection curve. Both characteristics provided the basis for further data evaluation.

Up to now, only quasi-static crushing was performed within the test programme, however, dynamic cruciform crush tests are under preparation. Although crush components have to be designed to perform under dynamic loading, quasi-static crush tests have proved true in a first approach. Static tests offer a better possibility to study failure initiation and failure modes in great detail, and provide valuable information for dynamic testing. Based on our own experience and information taken out from the literature it is known that the differences of static and dynamic crush test results of composite as well as aluminium structures are not very large up to impact velocities of about 15 m/s. However, this fact holds only true if the static deformation behaviour will approximate the dynamic deformation behaviour.

Furtheron, the usefulness of statically determined crush data for dynamic analysis, i.e. crash simulation with hybrid computer codes, has successfully been demonstrated in the past /3/.

4. CRUCIFORM CRUSH TEST RESULTS

4.1 CRUSHING BEHAVIOUR VALUATION CRITERIA

The crushing behaviour and the energy absorption performance of a collapsing structure can be valuated by commonly used criteria which can be derived from the crush characteristic and the absorbed energy. Fig. 7 summarizes the valuation criteria which are used in the present investigation.

A very important valuation criteria for lightweight energy absorbing structures is the specific energy, i. e. the absorbed energy, which is the area under the force - deflection curve, is related to the structural mass of the absorber or structure. Often for absorber type structures only the crushed mass is taken into account, however, in the present work the total mass of the cruciform elements is related to the absorbed energy, because most of the elements did not show a clear crush front, and therefore the mass of the crushed structure was difficult to determine.

Another commonly used valuation criteria is the load uniformity which is the ratio of the peak failure load (Fpeak) to the average crush force level (Favg). The "ideal" absorber with a rectangularly shaped force-deflection-curve has a load uniformity value of one, and higher values do indicate unfavourable high peak loads. This is somewhat misleading, therefore, the inverse value of the load uniformity is defined as "crush force efficiency" A_E. Then the "ideal" absorber has an efficiency of 100 percent and lower percentages do indicate the deteriorating direction.

Additionally, the initial element compression stiffness K_{test} was determined which is an important input parameter for hybrid computer crash simulations.

4.2 FORCE-DEFLECTION-CHARACTERISTICS AND FAILURE MODES

The force-deflection curves of all tested cruciforms - aluminium as well as composite configurations - show basically similar shapes. After a first initial peak failure load, the crush force drops down in most cases to a much lower level. However, the average crush forces then remain almost constant or do even increase again up to a stroke of about 125 mm.

Fig. 8 shows crush characteristics of aluminium single and multiple "notched corner" cruciforms, and Fig. 9 shows the force-deflection curves of CFC/AFC-hybrid cruciforms with corrugated edge joints. Fig. 10 summarizes the initial peak failure loads and the initial stiffnesses (K_{Test}) of all tested variants.

The aluminium cruciform with a single notch in the middle of the angle joint of the lateral bulkhead sections turned out to be the best metal configuration with respect to the shape of the crush characteristic and energy absorption. The single notch created a drop of the peak failure load from 22,9 kN of the unnotched aluminium baseline to 15,8 kN. The initial stiffness was only slightly reduced. Multiple notches also caused a

significant peak load reduction (22,9 kN to 14,5), however, the average crush force levels and therefore the energy absorption was much lower compared to the single notch cruciforms.

At relatively low compression load levels first instabilities of the aluminium cruciform plate sections could be observed at the unclamped edges, whereas the plate junctions remained still straight. At further load increase, also the mid-sections buckled in the direction of the minor moment of inertia, and started to fold and to form plastic hinges, as can be seen looking at the failure mode of the aluminium baseline cruciform, Fig. 11. Lateron, also fractures in the lateral bulkhead angle joints to the keel beam section could be observed. Aluminium "notched corner" configurations started to fail and to form plastic hinges at the notched areas.

All composite cruciform elements showed an abrupt drop of the compression load after first failure, as can be seen looking at the crush characteristic of the corrugated edge joint CFC/AFC hybrid cruciform, Fig. 9. The peak failure loads of composite cruciforms, even with notched and corrugated edge joints, were much higher compared to the aluminium elements, and also higher initial stiffnesses could be observed. However, notches and corrugated edge joints with hybrid cruciforms resulted in remarkable drops of the peak failure load compared to the unnotched hybrid cruciform, Fig. 10.

Pure CFC-cruciforms failed abruptly at the bottom of the mid-section by laminate fractures, followed by brittle fractures of the cruciform plate sections which initially showed buckling instabilities comparable to those of aluminium elements. Most parts of the CFC-elements were completely destroyed at the crush front and showed no post crush structural integrity. However, caused by numerous local fractures and friction the energy absorption of the CFC-cruciforms was the highest of the whole test series, but large differences between the two tested identical components could be observed concerning average crush force levels and energy absorption.

Instability deflections with hybrid cruciform configurations were larger compared to the CFC-elements and were already extended at load onset more to the cruciform mid-sections. This behaviour was caused by the lower compression stiffness of the hybrid laminates of keel beam and bulkhead sections and of the bulkhead angle joints which had an AFC share of the laminate of about 60 percent. The failure behaviour of hybrid cruciforms on the macro level was more comparable to aluminium elements. Fig. 12 overviews crushed aluminium, CFC-, and CFC/AFC-cruciforms, and it can be seen that the hybrid element tended to fold in the plate as well as mid-sections, did not disintegrate and provided post crush structural integrity by the AFC share of the laminates. CFC-layers fractured along the folding lines and at the mid-section and partly delaminated from the AFC-layers. Those failure mechanisms contributed essentially to the energy absorption performance of hybrid cruciforms. The corrugated edge joint hybrid cruciforms turned out to be the best composite configuration with respect to the crush-characteristic, energy absorption performance and post crush structural integrity.

4.3 ENERGY ABSORPTION PERFORMANCE

The energy absorption performance of structural cruciforms is considered on the basis of the specific absorbed energy (Esp) and the crush force efficiency (A_E). The results shown in Fig. 13 are averaged values of two tests for each design variant.

Values of specific energies of all tested cruciforms vary between 4 and 7 kJ/kg. Esp-values of aluminium elements scatter between 4 and 5 kJ/kg and those of composite configurations between 4.4 and 7 kJ/kg. The best Esp-value of 7 kJ/kg is reached by the pure CFC-cruciform, however, the loss of post crush structural integrity has to be taken into account. Multiple notched configurations (AlN and HN) have lower energy absorption performance compared to other design variants intended for peak load reduction and crush initiation. The single notched aluminium cruciform (AlN I) is a "minimum-modification" concept and turns out as the best aluminium configuration with respect to specific energy (5 kJ/kg) and crush force efficiency (63 percent). The hybrid composite cruciform with corrugated edge joints (HW) can be considered as the overall best composite design variant. Although the specific energy is about 10 percent lower compared to the CFC-cruciform (C), the crush force efficiency is about 34 percent which is the highest value within the composite test series but, still below the aluminium elements. All other composite cruciforms reach crush force efficiencies of about 23 percent.

Fig. 14 shows the specific energy versus the related mass of the cruciform elements, thereby the mass of the aluminium baseline version (Al) is set to 100 percent. Fig. 14 does not include averaged Esp-values, both test results per design variant are depicted. Structural weight savings of almost 30 percent can be realized with CFC-elements compared to the aluminium baseline cruciform. The hybrid elements scatter between 15 and

25 percent weight savings. Although the corrugated edge joint concept (HW) shows favourable crush characteristics and energy absorption performance, only weight savings of about 15 percent can be realized, and also the increase of manufacturing effort has to be taken into account. Table 1 summarizes the results of the crush and energy absorption behaviour of the cruciform test series.

5. PREDICTION OF CRUSH LOAD-DEFLECTION CURVES

5.1 COMMENTS ON LOAD-DEFLECTION EVALUATIONS

This contribution deals with some trials of predicting load-deflection curves and compares the results with test data. Common methods which are predominately based on empirical experience are applied, and combined with some suggestions. The applicability of these approximations is due to the fact, that despite the complexity of crush behaviour of a collapsing structure qualitatively similar force-deflection characteristics are observed, independent of material and construction, Fig. 15.

The initial phase includes the fully elastic range and the buckling regime up to failure load, which lies as a rule of thumb above the critical buckling load, but beneath the yield load, respectively fracture load. The transition region is marked by partly elastic and plastic cross section portions, or with brittle materials by partly destroyed areas. The collapse regime is characterized by folding phases with formation of plastic hinges or by fracture and friction forces between broken parts. Bottoming out may occur if a structural deformation is no longer possible.

For simplification the real curve is substituted by a linear increase of force up to failure load; the rather complicated transition phase is neglected, and the collapse phase is directly connected at failure load.

5.2 ACCURACY REQUIREMENTS

For the quantitative prediction of force-deflection curves of a structure several uncertainties exist caused by different influences: material peculiarities, cross section, slenderness ratio, excentricities of structure or of load introduction, clamping effects, joints, failure mode, etc.. Fig. 16 illustrates for instance for two equal aluminium angles the measured differences in load-deflection curve and energy absorption under same conditions. The collapse sequences are sketched from a foto series taken during testing. While at specimen 1 after angle breakage one leg is bent laterally away, thus rendering only small crush loads, the broken parts of specimen 2 are furtheron axially compressed and rolled up, summing up to a more then twofold overall energy absorption. But note, too, that the same failure load and nearly the same energy absorption was measured up to an axial deflection of approximately 80 mm.

Due to those and other imponderables with the determination of structural crush behaviour a test program was initiated to gain reliable test values for elements of subfloor structures as a base for theoretical approaches. The still onrunning programme consists of aluminium elements (plates, angle stiffeners, stiffened plates, cruciforms, boxes); cruciforms of CFC and hybrid configurations of CFC/AFC have now been tested in quasi-static compression.

The tests showed that the measured differences of the failure loads at equal failure modes ranged within 10 %. Concerning the energy absorption capability the differences were larger: the best consistency was obtained for the hybrid cruciforms (10%), the largest divergence was measured with the CFC-cruciforms (28%). From these facts it is concluded that too high demands for prediction accuracy are unrealistic and sophisticated approach methods are unsuitable. Therefore, relatively simple but quick approximation procedures are preferable for the precalculations of force-deflection behaviour.

5.3 COMPARISON TEST/CALCULATION

From the test series two characteristic subfloor element configurations for comparing test results and calculations were selected:

- o Angle stiffened plate; aluminium
- o Cruciforms made of Al, CFC, and CFC/AFC

5.3.1 FAILURE LOAD

The same method was used for all calculations of failure load:

(5.1) $$P_V = \zeta \cdot \sigma_V \left[F_W + \lambda \cdot F_H \right]$$

$\zeta = .9$ rivet reduction factor
F_W stiffener area (angles)
$\lambda \cdot F_H$ effective plate area

The failure stress σ_V, related to yield stress σ_F, is taken from /8/

(5.2) $$\frac{\sigma_V}{\sigma_F} = c_1\left[\frac{c_2 \cdot t_W \cdot t_H}{F_W + F_H}\sqrt{\frac{E}{\sigma_F}}\right]^{0.85}$$

	c_1	c_2
	.55	5
	.583	7

The effective width of the plate can be calculated according to different relationships, one formula for a strip with one longitudinal side simply supported, proposed by Stowell, reads:

(5.3) $$\lambda = .44 + .56\frac{\sigma_{cr}}{\sigma_v} \quad ;$$

(5.4) $$\sigma_{cr} = K_c \frac{\pi^2 E}{12(1-\nu^2)} \cdot \left[\frac{t_H}{b_H}\right]^2 \quad ;$$ 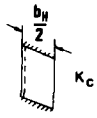 $K_c = 3$

σ_{cr} critical stress; E Young's modulus; ν Poisson's ratio

The buckling coefficient K_c depends on plate edge conditions and on aspect ratio. For the applied clamping device with the transversal edges clamped and one longitudinal side simply supported, one side free, K_c was derived from known values for similar clamping conditions.

For the composite cruciforms made of CFC re. CFC/AFC the continuous plate was matched to the same longitudinal stiffness as for the aluminium specimen; the riveted angles have the same shear stiffness as the aluminium cruciform. This results in different moduli in the two cruciform planes /7/. The calculations of the failure loads have shown that the best agreement of test and theory is found if for the critical buckling stress the low modulus of the composite cruciform, for the failure stress the high value is applied. Stiffness and strength were derived from classical laminate theory; instead of yield strength the compressive strength was introduced.

In Table 2 the experimental and predicted failure loads are listed, together with stress and modulus data.

With respect to the simple calculation procedure applied to failure loads, Tab. 2 shows an unexpected good agreement between test and theory for all cruciform configurations. This is not the case for the angle-stiffened plate (30 % difference). This may be contributed to the empirical factor $C_1 = 0{,}55$ in eq. (5.2) which seems to be too low (for $C_1 = 0{,}8 \rightarrow P_V = 9$ kN); additional tests are planned to clear this fact.

5.3.2 FOLDING OR FRICTION PHASE

This phase describes the structural collapse; the force drops down from failure load to a manifold lower level, e. g. by factor 10 for the stiffened plate, and by factor 4 for the Al-cruciforms. The magnitude of the residual force level is important with respect to the overall energy absorption capacity.

Due to the material's ductility aluminium elements form permanent folds in which yield stress is soon reached and thus the further endurable load is limited. This plastic hinge formation is the starting point for calculation of the load-deflection curve in the plastified state after failure.

The composite elements tested fail by fracture because of their fiber brittleness. Plastic hinge formation is not possible, but friction and fractures cause a residual force level, too.

Plastic moment

The maximum endurable pure bending moment is reached if the yield stress prevails all over the cross section. For a rectangular cross section the maximum plastic moment is known as:

$$M_{p\square} = \sigma_F \cdot b \cdot d^2/4 \qquad \text{(d = height, b = width)}$$

Other cross sections may be treated as composed of several rectangular parts; thus, the resulting plastic moment is the sum of the partial moments, related to the half area plane as neutral plane /9/.

If there acts an additional axial compression force P_A, then the plastic moment is reduced; if the axial stress equals the yield stress the moment carrying capacity of the cross section is depleted.

Different models exist to determine the reduced plastic moment under combined axial and bending loading. The usual method assumes fully plastified cross sections where the central parts about the neutral plane are successively occupied for compensating an increasing axial force /10/. The reduced plastic moment is in this case:

(5.5) $$M_{P\,red} = M_{P\square}\left[1 - \frac{P_A^2}{P_F^2}\right]$$

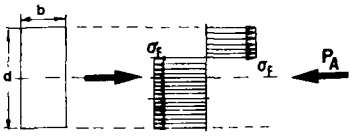

$P_F = \sigma_F \cdot b \cdot d$ yield load

Another model superimposes the axial stress $\sigma_A = P_A/bd$ to the maximum bending stress over the whole cross section. This means that the tension region is deloaded while the compression zone remains in the σ_F -state. Then a similar but linear expression results:

(5.6) $$M'_{P\,red} = M_{P\square}\left[1 - \frac{P_A}{P_F}\right]$$

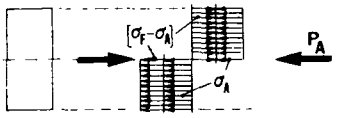

Plastic hinge model

The most simple plastic hinge model represents a plastic hinge positioned in the middle of a beam with straight beam halves connecting hinge and clampings. The folding radius at the plastic hinge and the elastic deformation of the beam are neglected. From moment balance results the endurable axial force:

(5.7) $$P_A = \frac{C}{v} M_{P\,red}$$

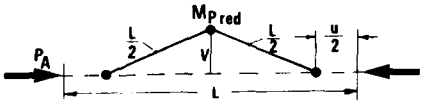

u axial deflection; $v = \sqrt{u\left[\frac{L}{2} - \frac{u}{4}\right]}$ transversal deflection

Coefficient C in eq. (5.7) regards to beam clamping: C = 2 for fixed ends, C = 1 for simply supported ends.

Thus, from (5.7) with (5.5) re. (5.6) the axial force P_A versus axial deflection u can be calculated.

Aluminium angle stiffened plate

Fig. 17 shows the comparison of test and theory for the angle-stiffened panel. Collapse figures at some distinct deflections were sketched according to foto sequences. Both measured curves for axial force and crush work exhibit after about 90 mm deflection an increasing tendency due to rivet collisions near the plastic hinge in the middle.

The calculations were based on the following presumptions, (Fig. 15):

- o Linear increase of axial force up to failure load
- o Transition phase near failure load neglected
- o Intersection of linear and collapse curves at failure load

The last point requires a correction of the force-deflection curve, which starts initially at $P_A = P_f$ for $u = 0$; on account of the steep slope of the curve in this region this correction is allowable and both curves are properly connected at $P_A = P_V$ and $u = s_V$. The axial deflection s_V at failure load ist roughly approximated by $s_V \approx \sigma_F \cdot l / \varepsilon_W \approx 1.7$ mm (ε_W = effective modulus at failure load). The experimental value is ca. 1,4 mm.

With increasing axial deflection the stiffening angle is subjected to a combined bending-torsional motion which causes the upright angle flange to rotate against the riveted flange. Thus, the plastic moment of the angle is decreased with increasing axial

deflection. This flange motion follows an exponential law not known particularly. The following approach was used:

(5.8) $$M_p(u) = M_{P\,max} \cdot \exp\left[\frac{u - s_v}{u_\zeta - s_v} \cdot \ln \frac{M_{P\,min}}{M_{P\,max}}\right]$$

For $u = s_v$: $M_p(s_v) = M_{P\,max}$; for $u = u_\zeta$: $M_p(u_\zeta) = M_{P\,min}$. In Fig. 17 $u_\zeta = L/2$ was engaged.

Following the described procedure the theoretical load-deflection curves in Fig. 17 are observed:

... upper curve: Quadratic law for $M_{P\,red}$, eq. (5.5);
fixed ends (C = 2);
$M_{P\,min}$ reached at $u = u_\zeta = 90$ mm

This case corresponds to a pragmatic proceeding, but renders a force drop too flat. If u_ζ would be smaller the slope in the initial collapse phase would be improved but at large axial deflections the axial force would become too small.

... lower curve: simply supported ends (C = 1);
No essential change of force-deflection curve.

+++ upper curve: Linear law for $M_{P\,red}$, eq. (5.6);
fixed ends (C = 2);
$M_{P\,min}$ reached at $u = u_\zeta = 90$ mm

Agreement test/theory deteriorated.

+++ lower curve: simply supported ends (C = 1).

This case delivers unexpectedly the best result, as the theoretical clamping influence does not agree with the test conditions.

Summing up, the described analytical approaches to the load-deflection curve of the angle-stiffened plate render useful approximations, but not fully satisfying results. There are several reasons: for aluminium no definite yield stress exists; at failure load the cross section is not yet fully plastified; stress distribution is not uniform; plastic hinge formation and plastic moments are more complicated as modelled, etc.

Aluminium cruciforms

Figs. 18 and 19 show the experimental and analytical load-deflection curves for two equal aluminium cruciforms, consisting of a continuous plate with long-flanged angles riveted on the plate. Deformation sketches illustrate the collapse sequence. Though the crush behaviour of both structural elements exhibits visually no remarkable differences there is for one specimen a stiffening with transitory force increase at a deflection of about 40 mm noticeable. Failure modes are identical, with a different number of plastic hinges in plate and angles; the buckling directions of those areas are not in the same sense.

The aluminium cruciforms have a different deformation behaviour than the angle stiffened panel, as from symmetry reasons global buckling and flange rotation is impossible. Thus, an according consideration concerning the plastic moment change with growing deflection is unnecessary.

It should be noted, that for this configuration the formal calculation of the plastic moment in the initial state cannot be carried out as for the stiffened plate; this would result in values too high. (Upper curve in Fig. 18). The reason is that the plastic moments of the four area sections act in two perpendicular planes with nonuniform stress distributions. If the four individual plastic moments are simply summed up to the maximum plastic moment of the cruciform there is a remarkable agreement with the test curve in the inital collapse phase. But at large deflection the calculated axial force becomes too small, as expected, because the resistance against folding in the cruciform corners is not accounted for (Fig. 18). Therefore, the calculation was supplemented by the demand for a prescribed mean crush load; this can be achieved by iteration, thus, that the two hatched areas in Fig. 18 are of equal size.

Premise to this procedure is the reliable predictability of the mean crush force. For cruciforms exist theoretical and experimental investigations /11, 12/, which include various folding mechanisms. Especially for large flange widths large differences occured for the mean crush load, depending on the applied folding model.

It was found that one of the proposed equations in /11/ agrees well with the mean crush force measured for the aluminium cruciforms:

(5.9) $$P_{m\,calc.} \triangleq 20 \sqrt{\frac{H}{h}} \cdot P_0 \quad ; \qquad P_0 = \frac{1}{4} \sigma_F h^2$$

Thus, for an arbitrary deflection $u=u_\zeta$ an axial force

$$P_A(u_\zeta) = \alpha \cdot P_{m\,calc.} \tag{5.10}$$

can be postulated and by variation of α the condition (5.9) can be fulfilled. Fig. 19 shows the force-deflection curves for different values of α .

Composite cruciforms

Figs. 20 to 23 show the test results for 2 CFC-and 2 CFC/AFC-cruciforms which exhibit in one plane the same longitudinal stiffness, and in the other plane the same shear stiffness compared to the aluminium cruciforms.

The failure load is about two times as large as with the aluminium cruciforms; at failure load the CFC layers break and the axial force drops abruptly down. Structural integrity is lost with the CFC-elements, but not with hybrid versions. Afterwards a force increase can be observed. The crush work of the CFC-cruciforms differs by about 30%, for the hybrid versions by about 10%. The energy absorption capability lies in the magnitude of the aluminium cruciforms with weight savings of ca. 20-30 %.

Typical for the measured composite force-deflection curves is the fact that they exhibit qualitively similar characteristics compared to the metal cruciforms, though no plastic hinges can be formed. The effect of friction between the fractured composite fragments seems to be comparable to the plastic moment reaction of ductile materials. Thus, in rough approximation, a similar law for the mean crush load can be assumed, unless future empirical or analytical values are contradictory. The test results justify the preliminary assessment for the mean crush load of composite cruciforms similar to the tested elements:

$$P_{m\,calc.} \doteq 10\sqrt{\frac{H}{h}} \cdot P_0 \tag{5.11}$$

with P_0 related to compressive strength.
The deflection at failure load can be approximated from mean modulus of both planes and compressive strength. (CFC: 2.15 mm, test 2.1 mm, CFC/AFC: 2.8 mm, test 3.1 mm).

6. CONCLUDING REMARKS

Compared to other structures with favourable geometrical shapes with respect to energy absorption such as tubes or honeycombs the investigated subfloor cruciform elements show a poor absolute energy absorption capability. Fracture dominated failures which are observed for instance with composite tubular absorbers can result in specific energies up to 100 kJ/kg. Aluminium as well as composite cruciforms show instability dominated failure modes caused by the specified geometrical shapes. Improvements of the energy absorption capability are therefore rather limited, and aluminium as well as composite material selection has relatively low influence on the absolute energy absorption. Therefore, cruciform design optimizations should primarily focus on peak failure load reduction and improvements concerning the crush force efficiency.

Hybrid composite cruciforms demonstrate their effectiveness with respect to post crush structural integrity and energy absorption compared to pure CFC-elements. Aluminium cruciforms provide structural int ..ity caused by the nature of the material.

Multiple notched concepts with aluminium and composite cruciforms intended for peak failure load reduction are unfavourable and result in lower energy absorption performance. Single notch aluminium cruciforms and hybrid composite elements with corrugated edge joints are satisfactory "minor modification" design variants and provide the best results of the test series.

For a composite subfloor structure it can be concluded that compared to an aluminium subfloor an adequate absolute energy absorption can be achieved without additional energy absorbing elements taking into account the reduced structural mass of a composite fuselage and assuming the same maximum take-off weight of the aircraft.

The main topic in practice-directed crush prediction is the availability of quick and simply working empirical or analytical approximation methods in order to predict failure loads as a measure for occuring decelerations on vehicle occupants, and the level of the mean crush loads as a measure for the overall energy absorption capability of a structure. The research efforts towards exact simulation of detailed force-deflection curves is useful for the understanding of acting physical mechanisms in

crush collapse, but is for practical applications not of primary importance. As test reproducibility is possible concerning failure loads within 10 %, and 30% concerning energy absorption, approximate calculation methods are adequate rendering results in the same error limits. It was pointed out that by attention paid to structure specific failure modes and configuration peculiarities an acceptable prediction accuracy of force-deflection behaviour is possible.

The ongoing programme will be focused on further experimental and analytical investigations to improve crashworthy designs of aircraft subfloor structures. Aluminium and composite sub-element (boxes, stiffened plates, angle elements) crush tests will be continued with the aim to create a data base of their crush behaviour and to evaluate analytical approaches for crush force-deflection predictions. Experiments will be extended to dynamic crushing, and the overall crash response of subfloor assemblages will be determined by numerical hybrid crash simulations where the sub-element crush data will be used as inputs for nonlinear structural behaviour.

REFERENCES

/1/ Military Standard Light Fixed-and Rotary-Wing Aircraft Crashworthiness. MIL - STD - 1290 (AV), January 25, 1974

/2/ COLTMAN, J.W.; BOLUKBASI, A.O.; LAANANEN, D.H. Analysis of Rotorcraft Crash Dynamics for Development of Improved Crashworthiness Design Criteria. DOT/FAA/CT -85/11, Final Report, June 1985.

/3/ CRONKHITE, J.D.; BERRY, V.L. Crashworthy Airframe Design Concepts-Fabrication and Testing. NASA CR - 3603, Final Report, Sept. 1982.

/4/ FARLEY, G.L. Crash Energy Absorbing Subfloor Beam Structure. Journal of the American Helicopter Society, Oct. 1987, Vol. 32, No. 4.

/5/ SEN, J.K. Designing for a Crashworthy All-Composite Helicopter Fuselage. Journal of the American Helicopter Society, April 1987, Vol. 32, No. 2.

/6/ KINDERVATER, C.M.; BANNERMAN, D.C. Crashworthiness Investigations of Composite Aircraft Subfloor Beam Sections. Int. Conference on Structural Impact and Crashworthiness, Imperial College, July 1984.

/7/ KÖRBER, U. Stauchversuche an Strukturelementen aus dem Unterboden-bereich von Luftfahrzeugen. Internal Report, DFVLR-Stuttgart, Institute for Structures and Design. IB 435 87/16 (1987).

/8/ BECKER, H.; GERHARD, G. Handbooks of Structural Stability. NACA TN 3781-3785, 1957.

/9/ NEAL, B.G. The Plastic Methods of Structural Analysis. Chapman and Hall, London, New York, 1981.

/10/ MURRAY, N.W. The Static Approach to Plastic Collapse and Energy Dissipation in Some Thin-Walled Steel Structures. In: Structural Crashworthiness (Ed.N. Jones and T. Wierzbiecki) Butterworths, 1983.

/11/ HAYDUCK, R.J., WIERZBIECKI, T. Extensional Collapse Modes of Structural Members. NASA Conf. Proc. 2245 (1982).

/12/ WIERZBIECKI, T. Crushing Behaviour of Plate Intersections. In: Structural Crashworthiness, Butterworths, 1983.

KINETIC ENERGY DISSIPATED BY FUSELAGE CRUSHING THROUGH STOPPING DISTANCE δ

OCCUPANT DECELERATED TO REST BY ENERGY ABSORPTION IN LANDING GEAR, FUSELAGE CRUSHING, AND SEATS

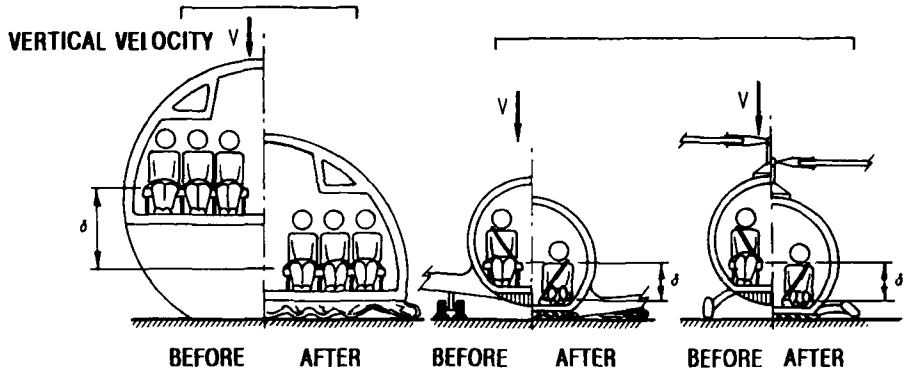

FIG. 1 ENERGY ABSORPTION CONCEPT OF VARIOUS AIRCRAFT

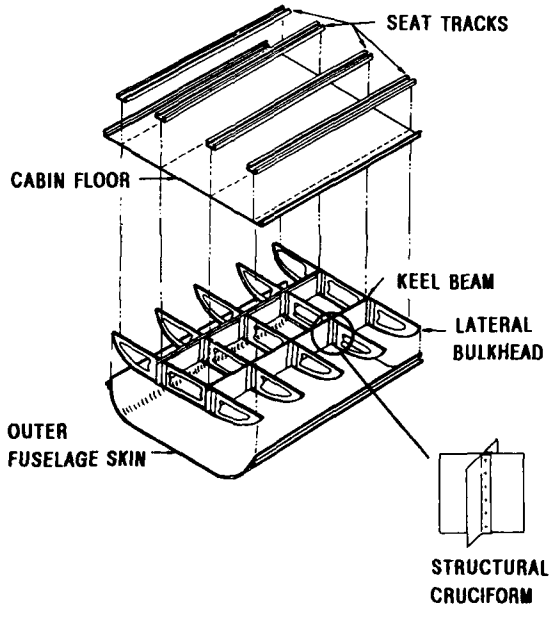

FIG. 2 TYPICAL SUBFLOOR STRUCTURAL ASSEMBLAGE / 3 /

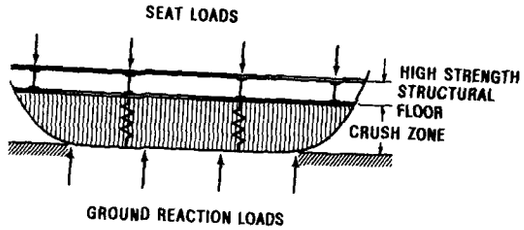

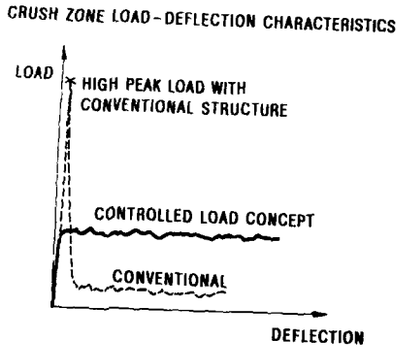

FIG. 3 LOWER FUSELAGE DESIGN PHILOSOPHY / 3 /

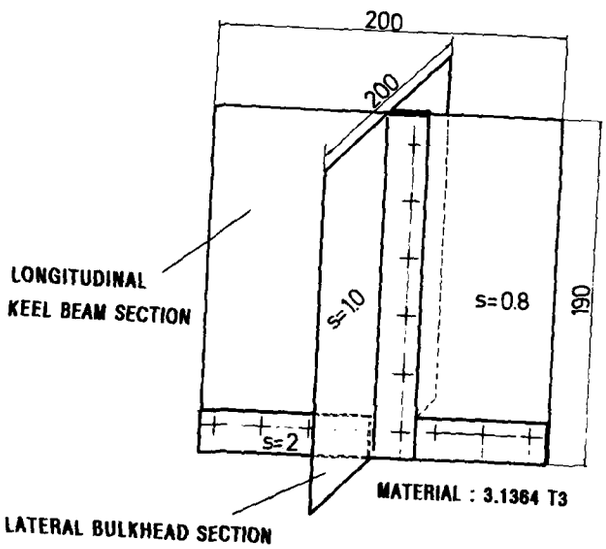

FIG. 4 ALUMINIUM BASELINE STRUCTURAL CRUCIFORM (AL)

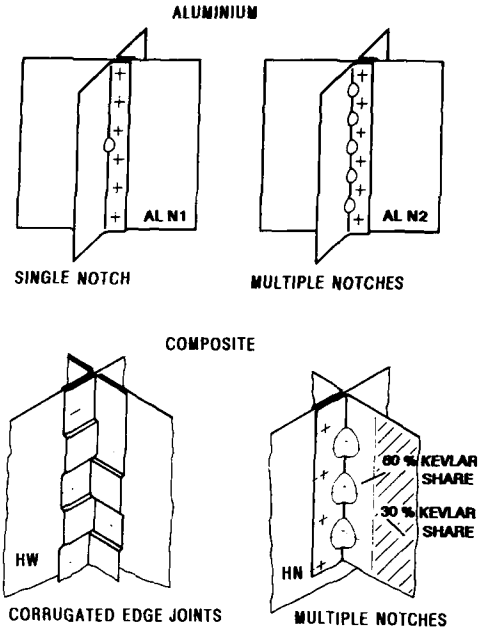

FIG. 5 CRUCIFORM DESIGN VARIANTS

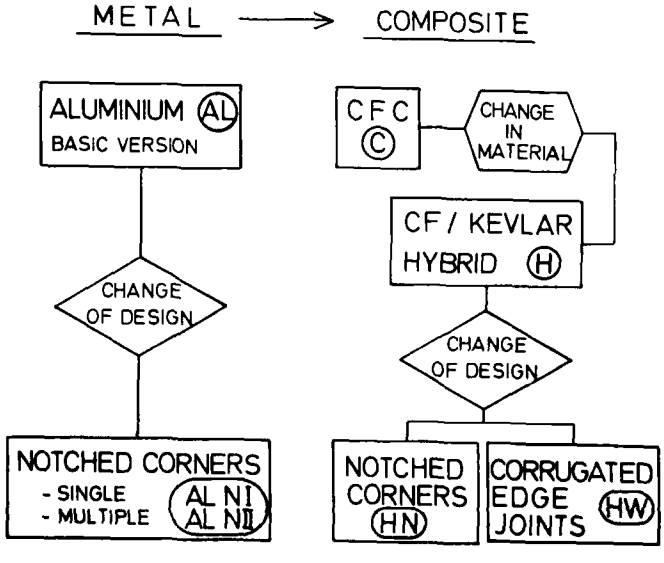

FIG. 6 CRUCIFORM CRUSH TEST PROGRAMME

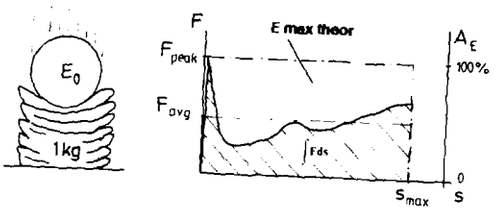

MASS SPECIFIC ABSORBED ENERGY :

$$E_{sp} = \frac{E_{abs}}{m} \quad [kJ/kg] \quad \text{with} \quad E_{abs} = \int_{s} F(s)\,ds$$

LOAD UNIFORMITY :

$$LU = \frac{F_{peak}}{F_{avg}} \qquad [/] \qquad \text{with } F_{avg} = \frac{E_{abs}}{s_{max}}$$

CRUSH FORCE EFFICIENCY :

$$A_E = \frac{1}{LU} = \frac{F_{avg}}{F_{peak}} = \frac{E_{abs}}{E_{max\ theor}} \cdot 100 \qquad [\%]$$

INITIAL COMPRESSION STIFFNESS :

$$K_{Test} = \frac{\Delta F_{peak}}{\Delta s_{peak}} = \frac{F_{(0.8\,F_{peak})} - F_{(0.3\,F_{peak})}}{s_{(0.8\,F_{peak})} - s_{(0.3\,F_{peak})}}$$

FIG. 7 CRUSH BEHAVIOUR VALUATION CRITERIA

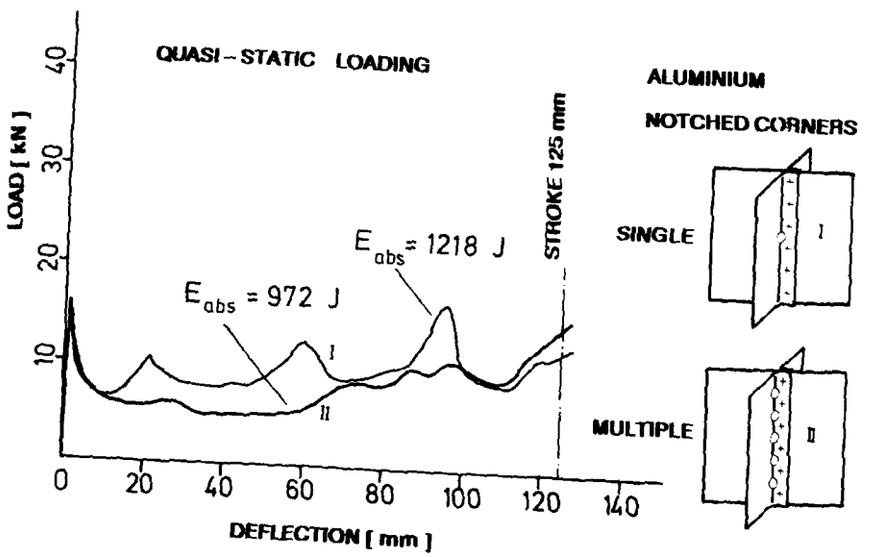

FIG. 8 LOAD – DEFLECTION – CURVES OF ALUMINIUM NOTCHED CORNER CRUCIFORMS (ALN)

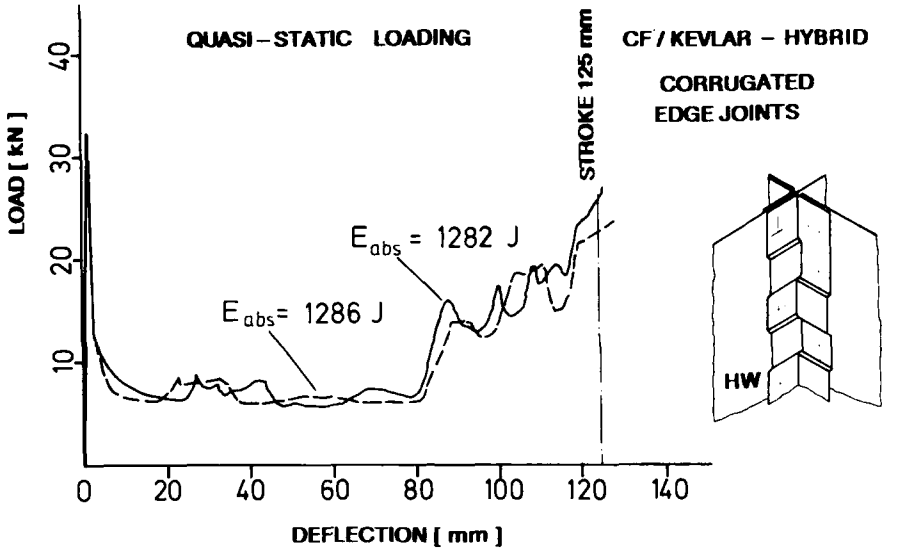

FIG. 9 LOAD-DEFLECTION-CURVES OF HYBRID COMPOSITE CORRUGATED EDGE JOINT CRUCIFORMS (HW)

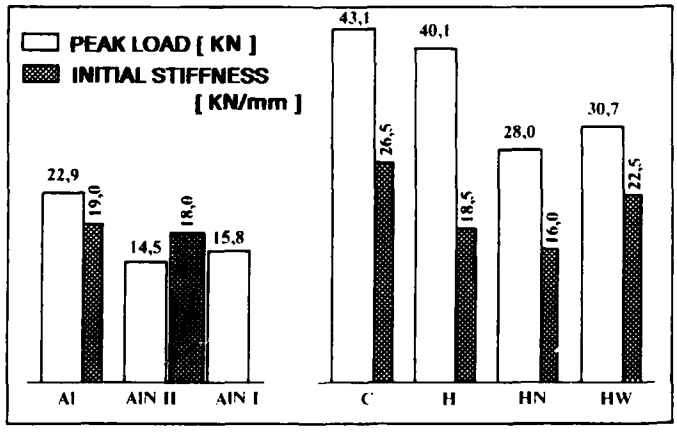

FIG. 10 PEAK FAILURE LOADS AND INITIAL STIFFNESSES

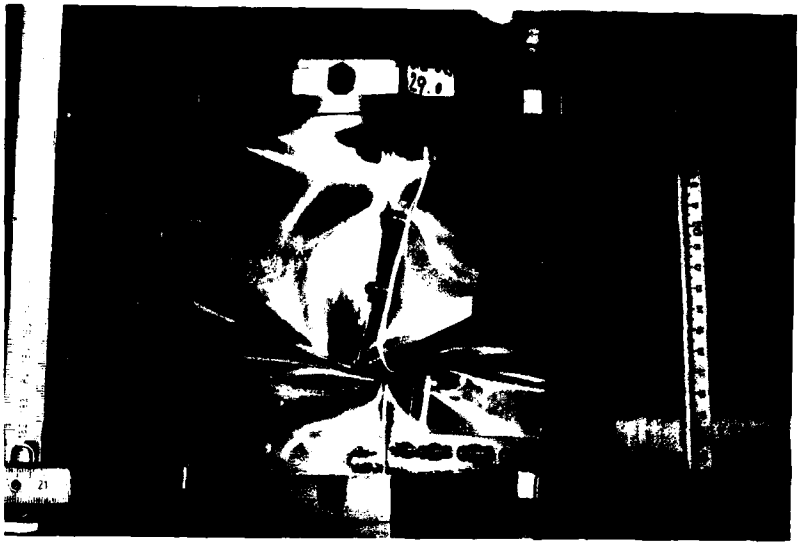

FIG. 11 FAILURE MODE OF ALUMINIUM BASELINE CRUCIFORM (AL)

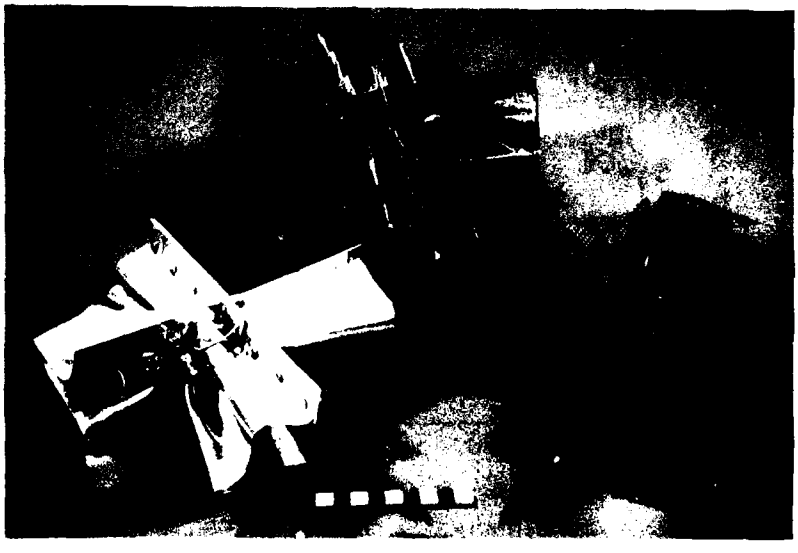

FIG. 12 CRUSHED ALUMINIUM AND COMPOSITE CRUCIFORMS

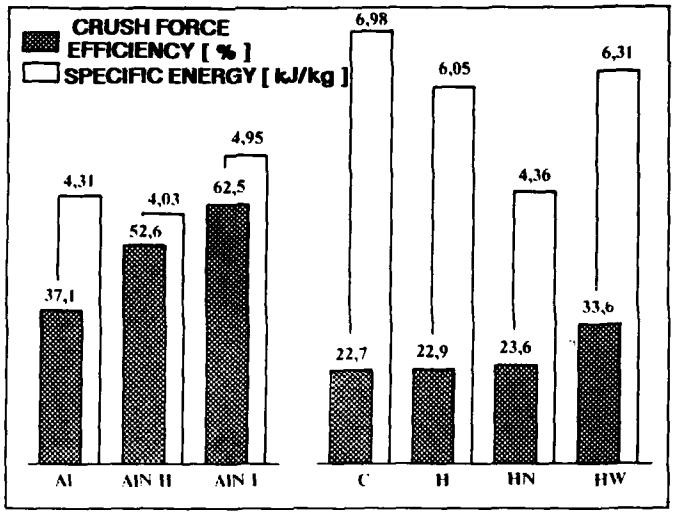

FIG. 13 SPECIFIC ENERGIES AND CRUSH FORCE EFFICIENCIES

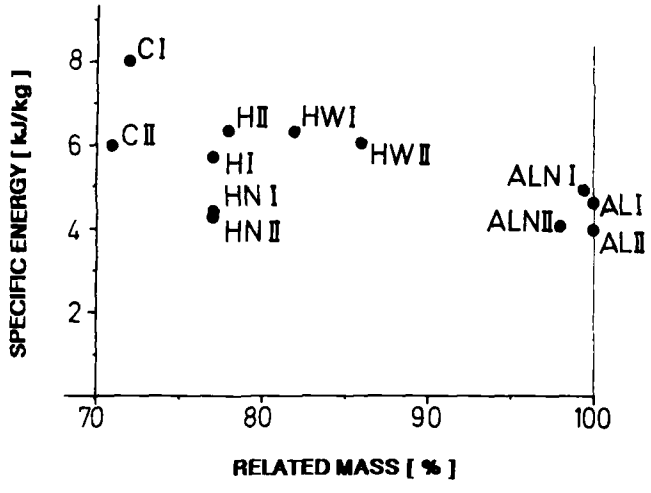

FIG. 14 SPECIFIC ENERGIES VERSUS RELATED MASSES

COMPONENT	F_{peak} [kN]	E_{abs} [J]	F_{avg} [kN]	E_{sp} [kJ/kg]	K_{test} [kN/mm]	LOAD UNIFORMITY	CRUSH FORCE EFFICIENCY [%]	RELATED MASS AL = 100 %	STRUCTURAL INTEGRITY
AL	22,9	1885	8,5	4,31	19,0	2,7	37,1	100	YES
ALN I	15,8	1218	9,7	4,95	18,0	1,6	62,5	100	YES
ALN II	14,5	972	7,8	4,03	18,0	1,9	52,6	88	YES
C	43,1	1230	9,8	5,98	26,5	4,4	22,7	72	NONE
H	40,1	1156	9,2	6,05	18,5	4,4	22,9	78	YES
HN	28,0	824	6,6	4,38	18,0	4,2	23,6	77	PARTLY
HW	38,7	1284	10,3	6,31	22,5	3,0	33,6	84	PARTLY

TABLE I : CRUSH AND ENERGY ABSORPTION BEHAVIOUR OF CRUCIFORMS - STROKE 125 MM

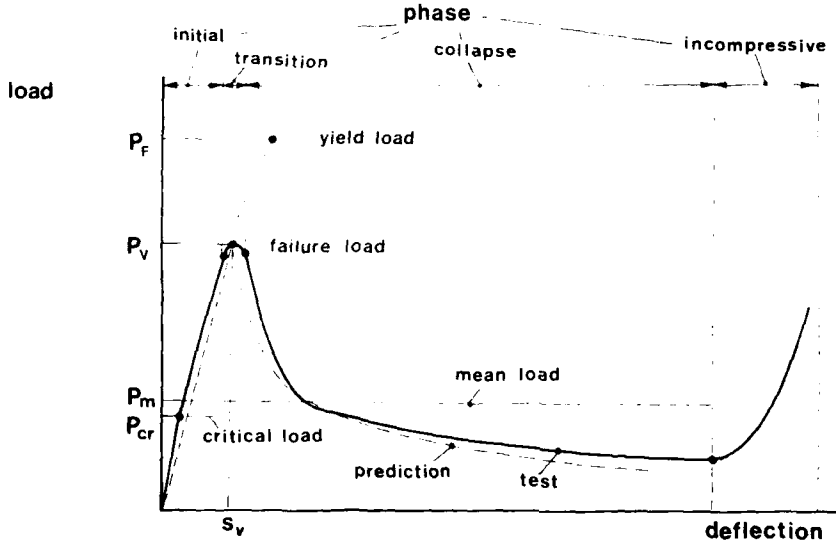

FIG. 15 CHARACTERISTIC PHASES OF CRUSH LOAD-DEFLECTION-CURVES

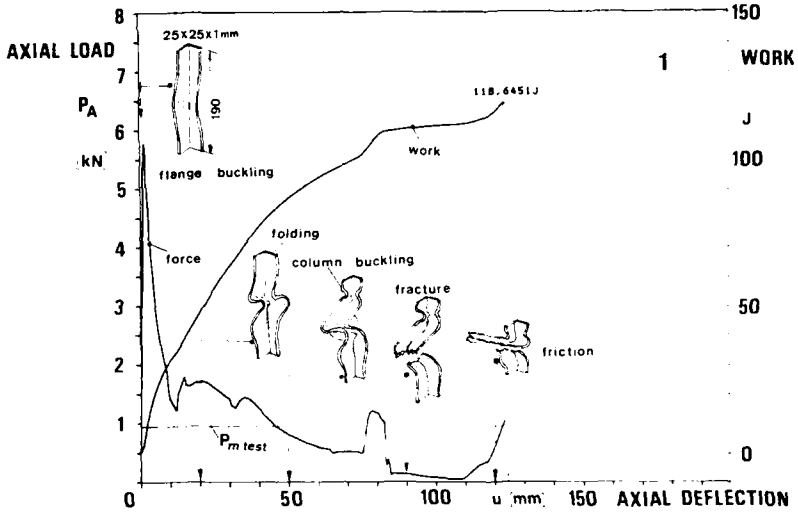

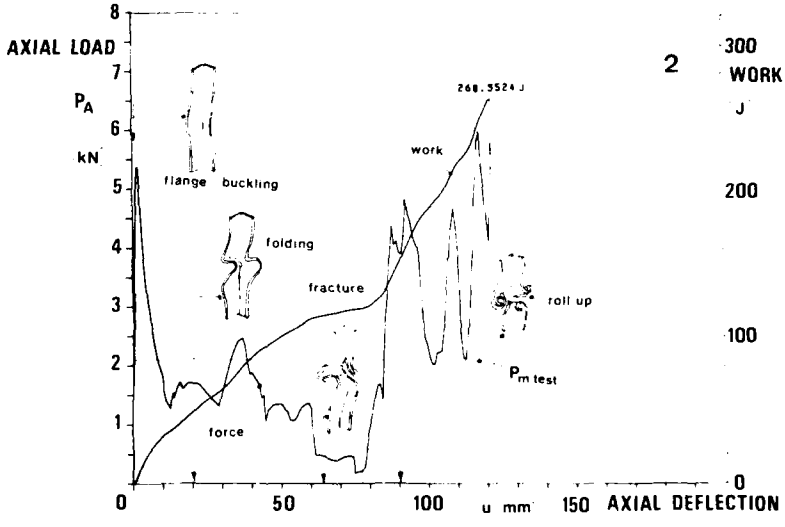

FIG. 16. DIFFERENT FAILURE MODES OF EQUAL ALUMINIUM ANGLES

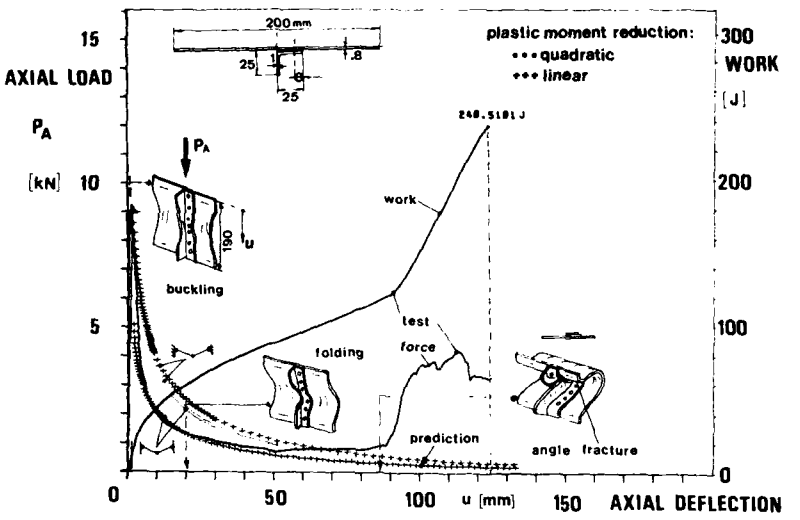

FIG. 17 ALUMINIUM-ANGLE-STIFFENED PANEL
TEST AND PREDICTION FOR DIFFERENT POST FAILURE BEHAVIOUR

	failure load		stress			mod.
	test	calc.	yield / compr.	crit	failure	E
	kN		N/mm²			kN/mm²
Al	9.2	6.5 (9.0)	235	12.5	50.4	70
Al 1	22.8	22	"	"	73.1	"
Al 2	22.8					
CFC 1	43	44.9	H 390	18.9	104.4	H 44.3
CFC 2	44		W 380			W 28.5
CFC/AFC 1	41	38.5	H 220	16.1	85.1	H 43.7
CFC/AFC 2	39		W 440			W 19.5

TABLE 2 COMPARISON OF MEASURED AND CALCULATED FAILURE LOADS

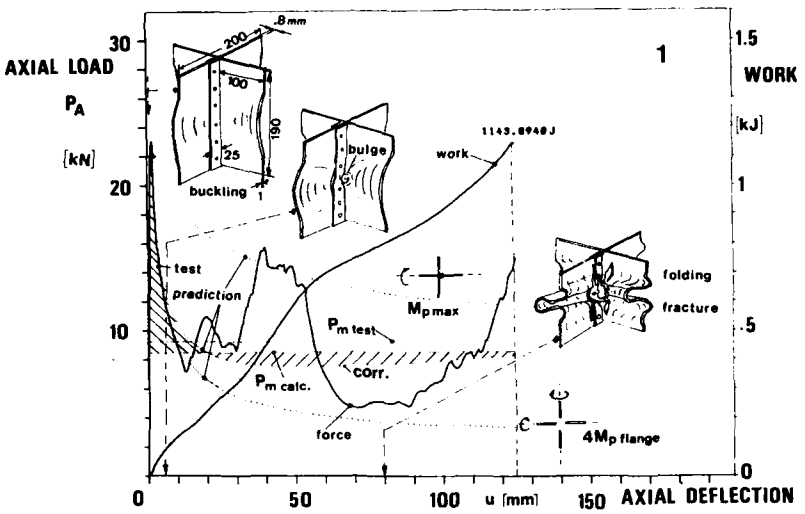

FIG. 18 ALUMINIUM CRUCIFORM NO. 1
TEST AND PREDICTION FOR DIFFERENT PLASTIC MOMENTS AND *CORRECTION FOR PRESCRIBED MEAN CRUSH LOADS*

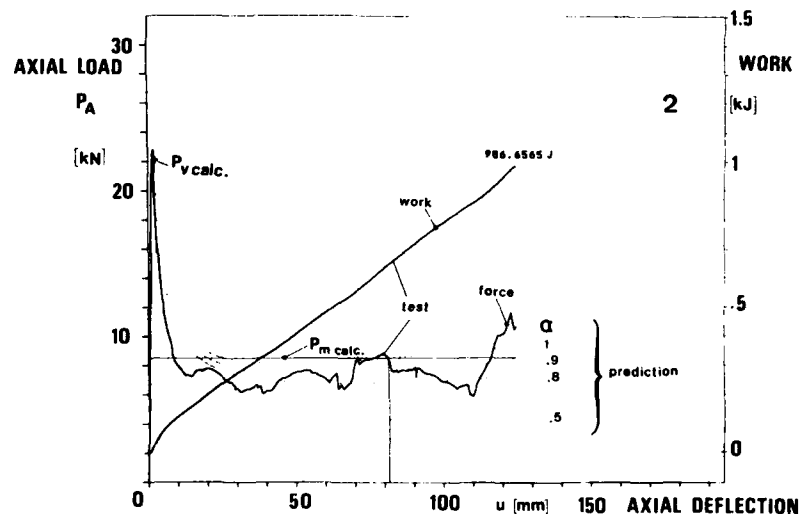

FIG. 19 ALUMINIUM CRUCIFORM NO. 2 – INFLUENCE OF SCALING FACTOR α

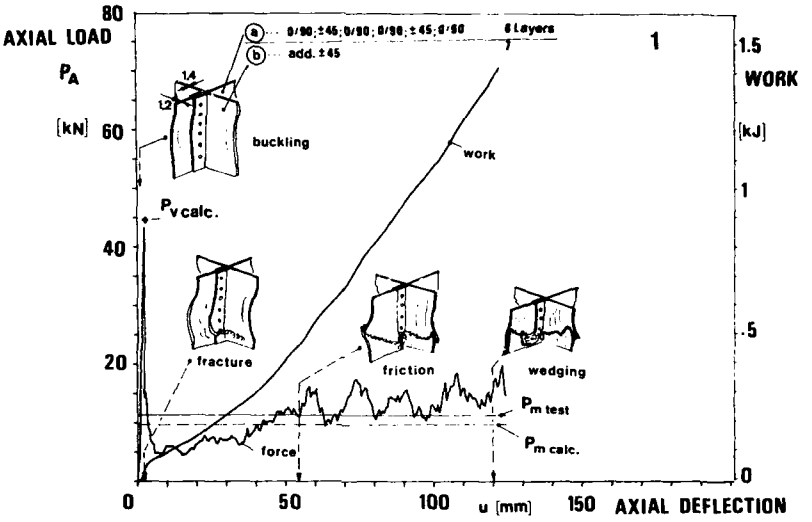

FIG. 20 CFC-CRUCIFORM NO. 1 - COMPARISON OF MEASURED AND CALCULATED MEAN CRUSH LOADS

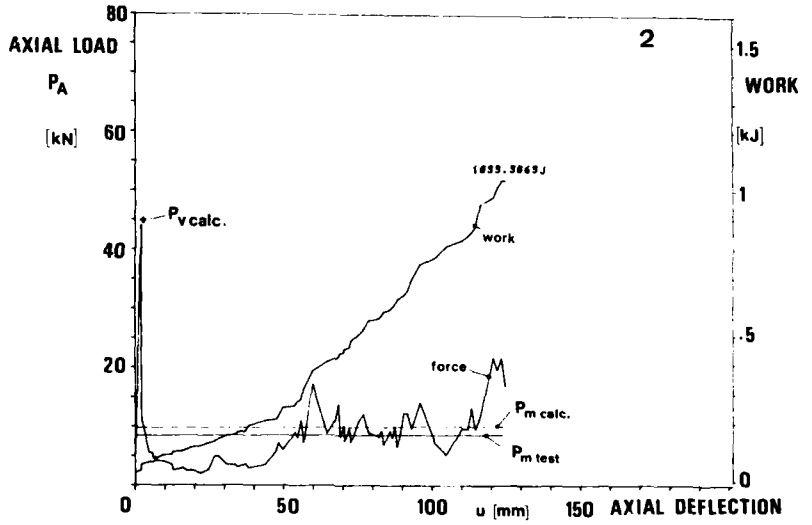

FIG. 21 CFC-CRUCIFORM NO. 2

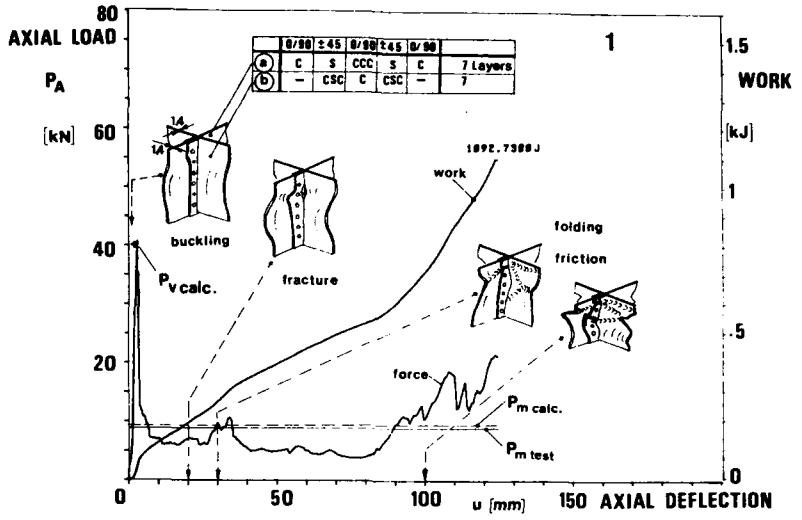

FIG. 22 CFC/AFC HYBRID CRUCIFORM NO. 1
COMPARISON OF MEASURED AND CALCULATED MEAN CRUSH LOADS

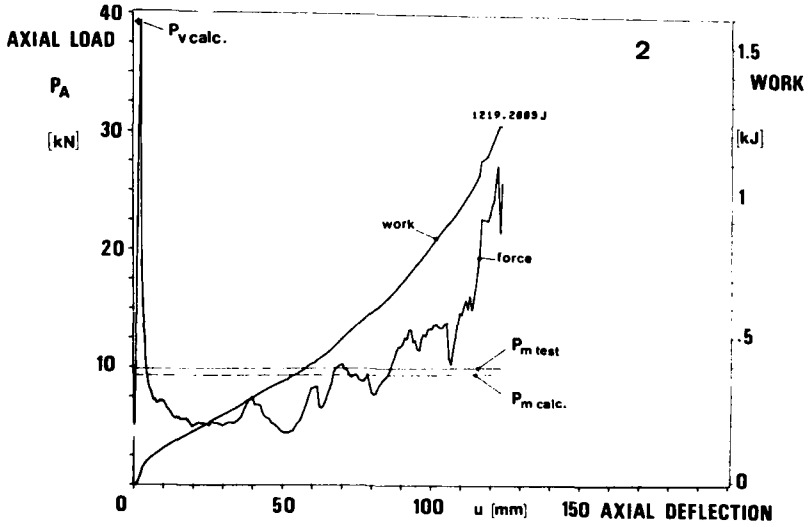

FIG. 23 CFC/AFC HYBRID CRUCIFORM NO. 2

Méthode et Moyens d'essais d'écrasement au sol au Centre d'Essais Aéronautique de Toulouse Application aux Hélicoptères SA 341 et AS 332

par

René Guinot
Chef du laboratoire
d'Essais de Crash au CEAT
23, Henri Guillaumet
31056 Toulouse Cedex

-RESUME

Cette note est une présentation des divers moyens d'essais du CEAT qui ont été développés pour étudier le comportement au "crash" des hélicoptères; SA 341 Gazelle; AS 332 Super-Puma.

-INTRODUCTION

Le développement des études menées en France dans le domaine du comportement au "crash" des hélicoptères, sous l'initiative du Service Technique des Programmes Aéronautiques et de la Direction des Recherches Etudes et Techniques, a conduit les autorités à rechercher les moyens de valider des solutions technologiques et des modèles de calculs pour la mise au point de nouveaux systèmes.

La réalisation des essais, confiée principalement au Centre d'Essais Aéronautique de Toulouse (établissement dépendant du Ministère de la Défense), a conduit ce dernier à se doter de moyens spécifiques adaptés à l'exécution de cette tâche.

Le plus grand nombre d'essais ont été effectués pour valider la protection au "crash" de l'hélicoptère AS 332 SUPER-PUMA jusqu'à des vitesses verticales de 10,2 m/s qui correspondent à 85% des accidents auxquels on peut survivre.

Cette garantie de protection a été obtenue par le développement et la mise au point:
- d'un atterrisseur à haute absorption d'énergie
- de renforcement plancher
- de réservoirs carburant anticrash
- des sièges pilote troupe et troisième homme

Des installations ont été modifiées ou conçues spécialement pour ces essais.

1- MOYENS D'ESSAIS

1-1-AIRE DE CHUTE VERTICALE DE RESERVOIRS

Ces essais sont effectués sur une aire de chute bétonnée à l'intérieur du hall d'essais statiques. La hauteur de chute disponible est de 20 mètres. Le largage est effectué à l'aide d'un crochet électrique.

Principaux résultats :
- Résistance dynamique supérieure de 15% à la résistance statique
- Gain de masse de 40% sur l'ancienne conception
- Validation du modèle de calcul

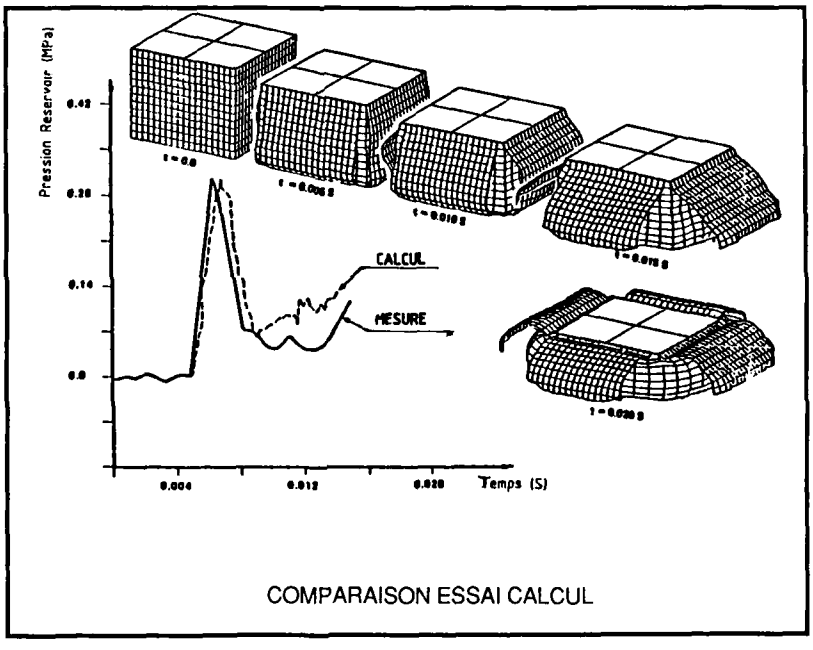

COMPARAISON ESSAI CALCUL

1-2-BANC D'ACCELERATION

Les performances de l'installation ont été choisies de façon à satisfaire aux recommandations de la norme Mil STD 1290 en ce qui concerne le plancher des appareils (95% des accidents avec survivants possibles se produisent pour des vitesses inférieures à 12,8 m/s et conduisent à des accélérations inférieures à 48g).

La structure (ou l'équipement) à essayer est fixée au chariot par l'intermédiaire d'un bâti, orienté de façon à obtenir la direction de l'accélération recherchée. Ce chariot mobile sur des rails est guidé latéralement par des galets sur une distance maximale de 15 mètres.

La masse du chariot est d'environ 500 kg et la masse embarquée peut elle aussi atteindre 500 kg.

a - Mise en vitesse

La mise en vitesse est réalisée à l'aide d'un vérin hydraulique exerçant un effort de traction sur un câble métallique fixé sous le chariot. Un moufle hydraulique permet de multiplier par dix le déplacement du chariot. Le vérin est associé à un ensemble d'asservissement en déplacement qui impose au chariot une accélération linéaire croissante, ce qui assure une tension du câble pendant toute la phase de mise en vitesse. Avant l'impact, le câble est dissocié du chariot et la vitesse d'impact recherchée est contrôlée par des cellules photoélectriques et des détecteurs de proximité.

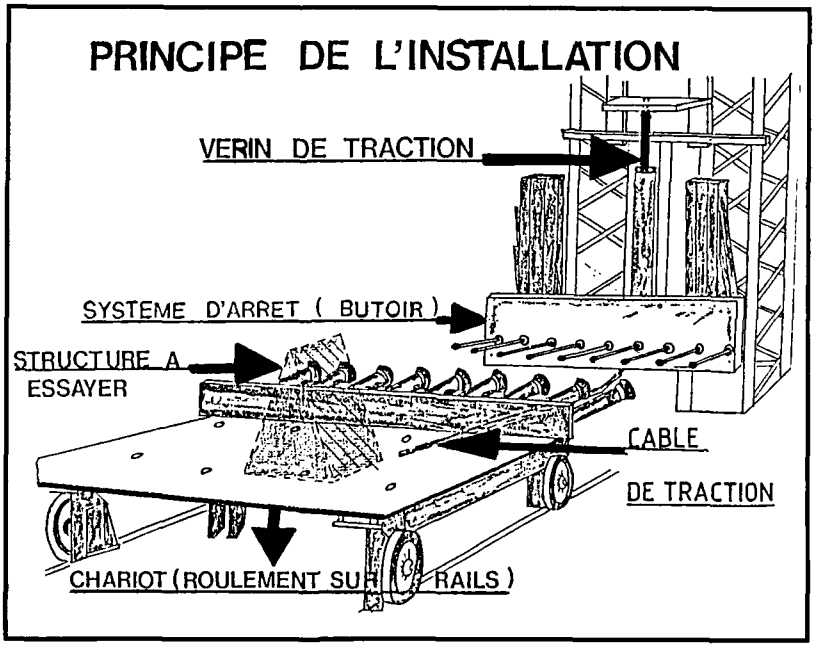

b - Décélération

Le freinage du chariot est réalisé sur un butoir muni de tiges métalliques équipées d'olives de section calibrée à leur extrémité.

Le chariot comprend à l'avant des tubes métalliques à l'intérieur desquels sont inclus des cylindres en polyuréthanne de section tronconique. La décélération est produite par le laminage des cylindres en polyuréthanne par les olives calibrées. Le profil de décélération triangulaire recherché est obtenu en modifiant le nombre et la longueur des tubes, le diamètre des olives et la dureté du polyuréthanne.

c - Exemple de résultat

Cette exemple montre l'atténuation des accélérations ressenties au niveau du thorax par le système d'absorption d'énergie.

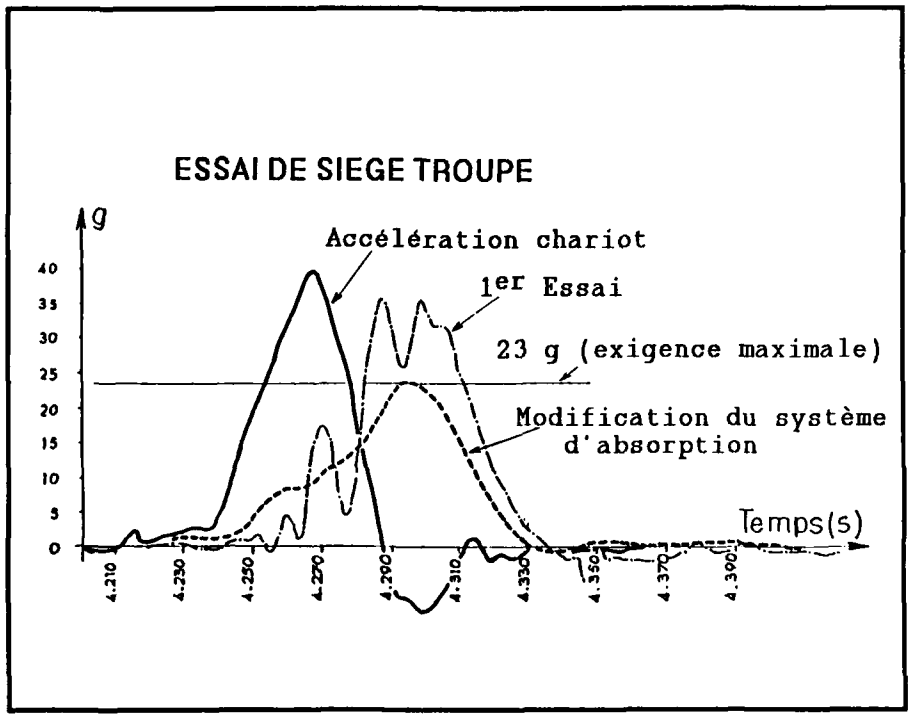

1-3-AIRE DE "crash" CELLULES

Ces installations permettent de faire subir à une cellule un essai de chute dans des conditions de vitesses verticales et horizontales imposées qui simulent des conditions réelles de "crash".

L'évolution des installations a suivi celle des demandes

1-3-1 Première installation

Une première installation a été réalisée à l'intérieur du hall d'essais statiques afin d'effectuer les premiers essais de chute verticale.

- essai partiel d'un fond de structure SA 341 Gazelle
- essai de "crash" d'une cellule complète SA 341 Gazelle
- essai de "crash" d'une cellule complète AS 332 Super Puma

1-3-2 Deuxième installation

De 1982 à 1984 un portique sur une aire d'essai extérieure a permis de réaliser des essais de chute avec des performances en vitesse verticales et horizontales plus élevées.

Les caractéristiques de cette installation sont les suivantes:

- masse maximale de la structure : 8000 kg
- vitesses maximales de chute Vx=16 m/s
  Vz= 18 m/s
- possibilité d'imposer l'assiette d'impact

La mise en vitesse de la cellule est produite par un système de quatre câbles de guidage fixés à leur extrémité inférieure à la structure et par leur extrémité supérieure par l'avant du portique. Un câble de largage fixé sur la partie arrière du portique permet la mise à hauteur de chute désirée. La mise à feu d'un dispositif pyrotechnique entraîne la coupure de ce dernier câble et provoque la chute de la cellule suivant un mouvement pendulaire. En jouant sur la hauteur de chute et sur la longueur des câbles on peut obtenir les conditions de vitesse demandées. Pour s'assurer à l'arrivée au sol que la cellule n'est plus sollicitée par les câbles, ceux-ci sont coupés par des dispositifs pyrotechniques déclenchés par un détecteur de hauteur.

1-3-3 Troisième installation

Cette installation a été terminée fin 1987. Le principe de mise en vitesse est identique à la précédente. Les améliorations ont porté sur les performances et la facilité de mise en oeuvre.

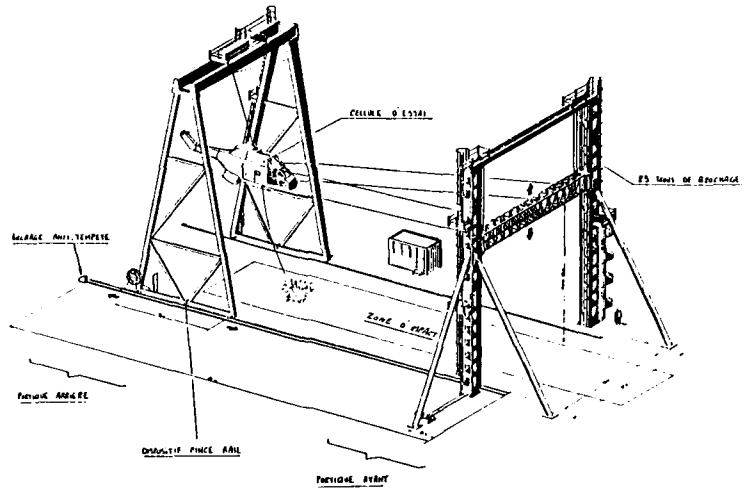

TROISIEME INSTALLATION

Les caractéristiques de cette installation sont les suivantes:
- masse maximale de la structure : 25 000 kg
- vitesses maximales de chute Vx= 17 m/s
  Vz= 21 m/s
- possibilité d'imposer l'assiette d'impact
- aire d'impact de même constitution que la piste d'atterrissage de l'aéroport de Toulouse Blagnac

Ces caractéristiques permettront d'effectuer des essais sur tous types de fuselages d'avions civils (C 160 Transall, Airbus, Falcon).

Principaux résultats:
- Valider les modèles de calcul
- Valider les profils de décélérations subis par les sièges et les occupants
- Valider les efforts au niveau des attaches du train et dans les réservoirs

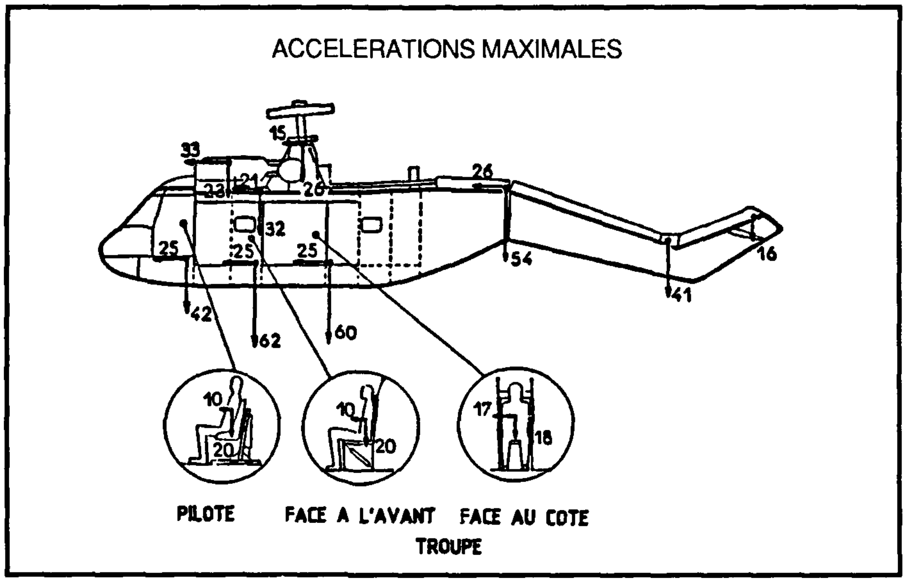
ACCELERATIONS MAXIMALES
33
15
21
23
26
26
25
32
25
25
54
16
41
42
62
60
10
20
10
20
17
18
PILOTE
FACE A L'AVANT
FACE AU COTE
TROUPE

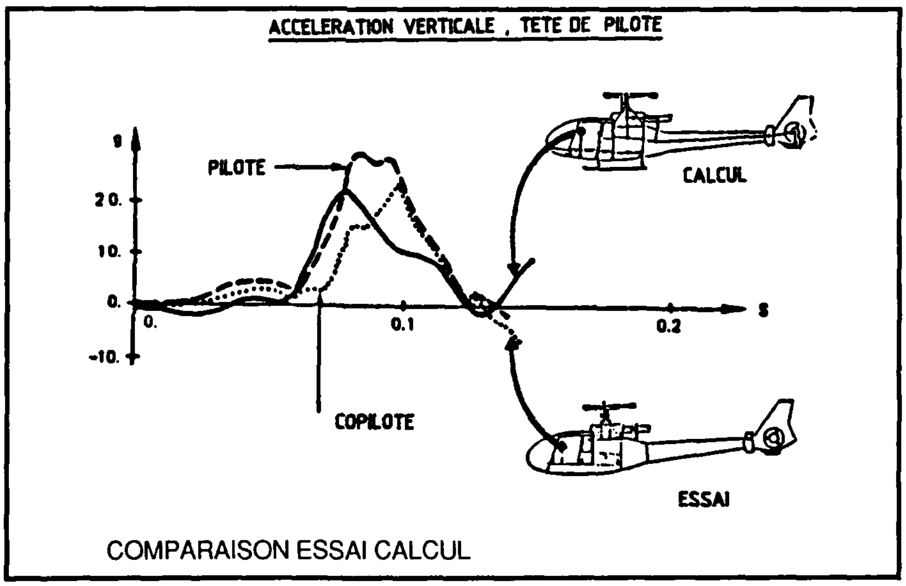
ACCELERATION VERTICALE , TETE DE PILOTE
g
PILOTE
20.
10.
0.
-10.
0.
0.1
0.2
s
CALCUL
COPILOTE
ESSAI
COMPARAISON ESSAI CALCUL

1-4 - MACHINE LATECOERE

Le laboratoire d'essais dynamiques d'atterrisseur dispose d'une gamme de quatre machines qui permettent de simuler des atterrissages avec des masses réduites de 450 kg à 50 000 kg et bientôt 100 000 kg. La machine Latécoère a été conçue pour assurer les essais de qualification dans les conditions d'atterrissage normal, et de "crash" léger (vitesse d'impact entre quatre et six mètres par seconde). Les paramètres simulés sont la masse réduite de l'appareil, l'assiette à l'atterrissage, la vitesse verticale d'impact, la vitesse horizontale et la portance.

Les performances de cette machine sont les suivantes :
- vitesse verticale maximale 6 m/s
- vitesse horizontale maximale simulée par rotation du volant 100 m/s
- masse maximale en mouvement 15 000 kg
- effort vertical maximum 45 000 daN

L'atterrisseur est fixé à la masse en mouvement par l'intermédiaire d'un bâti dynamométrique capable de mesurer les efforts aux attaches dans toutes les directions.

1-5- TOBOGGAN

Cette machine a été conçue pour assurer les essais de qualification dans les conditions de "crash" sévère. Pour des vitesses d'impact dépassant 6 m/s, la machine Latécoère ne peut plus être utilisée. Or l'atterrisseur du Super Puma est conçu pour fonctionner partiellement jusqu'à des vitesses d'impact de 10m/s ("crash sévère"). Dans ce cas l'atterrisseur absorbe une énergie correspondant à 5 m/s, soit le quart de l'énergie d'impact.

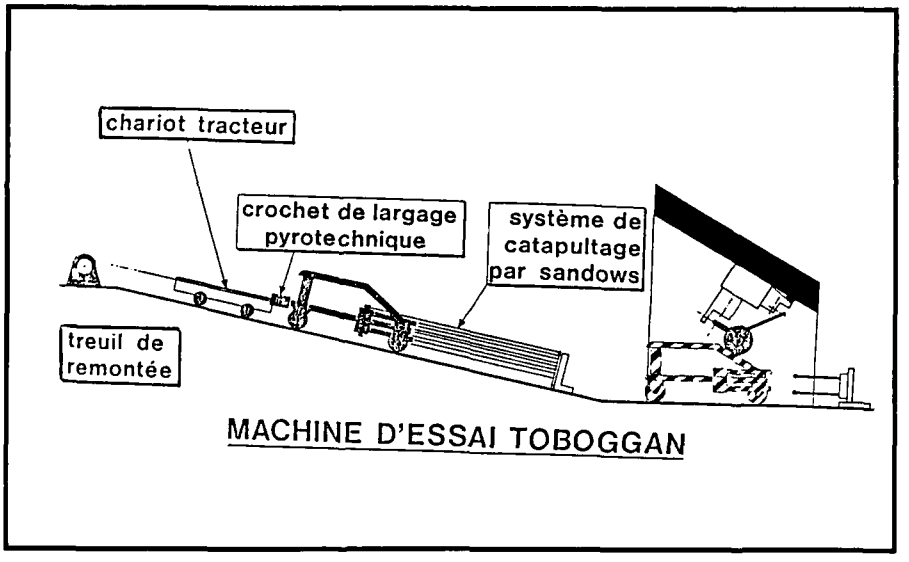

MACHINE D'ESSAI TOBOGGAN

Pour permettre la mise au point du train dans cette configuration sans détériorer entièrement l'éprouvette à chaque essai, une installation a été adaptée pour exposer le train à des conditions réalistes d'impact (masse et vitesse verticale de 10 m/s simulées) mais en absorbant par un moyen annexe la part d'énergie reprise par la structure.

Le train est relié par des attaches à un bâti fixe incliné de trente degrés par rapport au sol. Les conditions de "crash" sont simulées par l'impact d'un chariot, animé d'une vitesse V, sur le train. Le chariot est muni d'un bâti comportant une partie horizontale et une partie inclinée parallèle au bâti du train. L'impact est fait sur un plan incliné qui reproduit une vitesse verticale de V/2 et horizontale de $V\sqrt{3}/2$. Le chariot est catapulté sur le plan incliné à la vitesse de 20 m/s pour simuler une vitesse verticale de 10m/s.

Le catapultage est obtenu par des sandows tendus au moyen d'un treuil et d'un chariot tracteur libérant une énergie élastique importante au moment du largage par un crochet pyrotechnique. L'accélération initiale du chariot peut atteindre 5 g. Le dénivellé (5,70m) permet d'obtenir le supplément de vitesse. Le bâti incliné monté sur le chariot est calculé pour que l'amortisseur atteigne sa course maximale lorsque la roue est située au sommet du plan incliné et roule alors sans effort sur la partie horizontale. L'énergie restante du chariot est absorbée par un butoir muni de tiges métalliques avec des olives calibrées. Ces tiges s'enfoncent dans des cylindres en polyuréthanne inclus dans des tubes métalliques fixés à l'avant du chariot (même principe que pour le banc d'accélération).

2 - MOYENS DE MESURE

2.1. MATERIELS :

2.1.1. Accéléromètres :

Type : il s'agit d'accéléromètres piézo-résistifs.

Gammes : ±10 à ± 250 g pour les accéléromètres structures,

Ecart de linéarité inférieur à ± 0.4 % de l'Etendue de Mesure (E.M.),
Précision d'étalonnage meilleure que ± 1 % de l' E.M,
Bande passante à ± 10 % : 0 à 2500 Hz.
Nombre d'accéléromètres disponibles : 90 (y compris les accéléromètres mannequins, voir ci-dessous),

2.1.2. Mannequins anthropomorphiques :

Actuellement, 3 mannequins sont utilisés. Il s'agit d'un mannequin "Alderson type VIP-50" et de deux mannequins ONSER distribués par la société Sereme. Ils sont équipés chacun de 3 accéléromètres triaxiaux de

± 100 g (tête, thorax et coccyx). Ces mannequins ne sont pas actuellement prévus pour mesurer les efforts dans les fémurs ou dans la colonne vertébrale.

2.1.3. Jauges :

Il peut s'agir de jauges simples, doubles ou de rosettes 3 directions.

Les jauges peuvent être montées en 1/2 pont ou en pont complet. Ces ponts peuvent faire l'objet d'un étalonnage.

2.1.4. Amplificateurs de mesures :

Ecart de linéarité : ± 0.1% de l'E.M,
Bande passante : 10 kHz.
Nombre : 128.

2.1.5. Acquisition et numérisation :

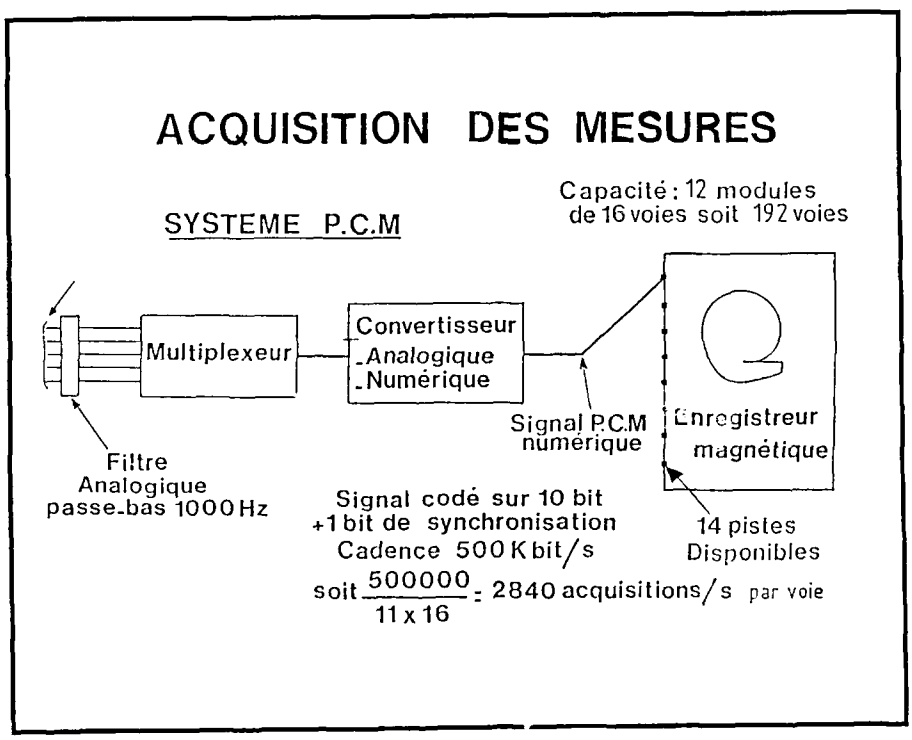

a/ Matériel actuellement en service :

*Fréquence d'échantillonnage : 2,8 kHz,
*numérisation sur 10 bits,
*128 voies de mesure.
*présence d'un filtre anti-repliement passe-bas 1000 Hz d'ordre 7 (voir courbe planche 1).

b/ Matériel en cours d'achat :

Ce matériel vise à équiper le banc d'accélération horizontal en vue de la réalisation d'essais de "crash" de sièges d'avions ou d'hélicoptères.

*fréquence d'échantillonnage : 8 kHz (possibilité de réalisation de filtres numériques de fréquence de coupure plus élevée : nouvelles recommandations en essais de "crash" de sièges),
*numérisation sur 12 bits (meilleure précision : possibilité de réalisation correcte d'essais à faible vitesse d'impact),
*80 voies de mesures,
*possibilités de calculs spécifiques et d'éditions de résultats sur le site dans de meilleurs délais.

c/ Evolution du matériel :

L'utilisation et l'expérience acquise sur ce type de matériel doit permettre à terme de se doter d'un système comportant un plus grand nombre de voies de mesures. Les dépouillements pourront être adaptés au besoin des essais de cellules complètes et à l'analyse des structures.

2.2 . DEPOUILLEMENTS :

2.2.1. Tracés :

a) définition d'une méthode de détection de l'impact;
b) traçage des résultats à partir de l'origine des axes;
c) filtrages numériques effectués en fonction de la recommandation SAE J211 pour les essais de sièges.
d) élimination des parasites de natures mécanique et électro-magnétique.

a/ Définition d'une méthode de détection de l'impact:

L'instant de l'impact peut être déterminé en analysant après traçage avec effet loupe, les résultats d'un accéléromètre pris comme référence. Cet instant est défini comme étant l'intersection de la ligne moyenne de l'évolution de l'accéléromètre avant l'impact, avec la ligne moyenne de la première évolution significative (ou front de montée)

extrapolée vers l'origine (voir planche 2, sans effet loupe et planche 3, avec effet loupe).

L'instant d'impact est déterminé manuellement pour chaque essai.

b/ Traçage des résultats à partir de l'origine des axes:

La synchronisation de tous les tracés est assurée. Le traçage des événements significatifs a lieu à partir de l'origine des axes, cependant, une visualisation de l'évolution des paramètres est donnée à partir d'un instant situé 50 millisecondes avant l'impact.

c/ Méthodes de filtrage :

Pour les essais de "crash" de sièges et l'analyse des accéléromètres structures, sièges ou mannequins, la recommandation SAE J211 préconise l'utilisation de gabarits de filtrage : "classe 60, 180, 600 et 1000" (la classe est sensiblement égale à la fréquence de coupure du filtre).

Pour satisfaire cette demande, une technique de filtrage numérique qui présente l'intérêt de conserver l'intégrale a été mise en place (nom du programme C.E.A.T : "NTRIF").

Comme vu au paragraphe 2.1.5/a, un filtre 1000 Hz est en place en amont du multiplexeur, il interdit l'emploi des filtres numériques "classe 600" et "classe 1000".

Le filtre "classe 60" employé est un filtre Butterworth d'ordre 3 "aller et retour" , sa bande à - 6 dB est de 150 Hz (voir courbe planche 4).

Le filtre "classe 180" est un filtre de Bessel d'ordre 3 "aller et retour", sa bande passante à - 6 dB est de 450 Hz (voir courbe planche 5).

La recommandation SAE J211 préconise également la nature du filtrage en fonction des paramètres :

- accélérations chariot et siège : "classe 60"
- efforts et contraintes : "classe 600"
- accélérations tête mannequin : "classe 1000"
- autres accélérations mannequin : "classe 180".

Ainsi, seuls les paramètres chariot, siège et accélérations mannequins (autres que l'accélération tête) sont filtrés comme demandés; les autres paramètres sont tracés en mesures brutes (c'est-à-dire toujours filtrés par le filtre analogique 1000 Hz).

On peut noter que l'utilisation des matériels en cours d'achat (fréquence d'échantillonnage 8 kHz, 2.1.5/b) permettra d'appliquer intégralement les termes de la recommandation SAE J211 en matière de filtrage.

Pour les paramètres des essais à vitesse nominale, il est choisi de filtrer de la façon suivante :

- accéléromètres chariot/siège en "classe 60",
- accéléromètres mannequin en "classe 180",
- efforts en "classe 180",
- jauges en "classe 180",
- résultantes efforts en "classe 180",
- sommes des efforts en "classe 180".

Cependant, pour le calcul du "Head Injuries Criterion" (H.I.C.) (Critère de blessure à la tête) les mesures brutes (seulement filtrées par le filtre analogique 1000Hz) sont prises en compte. C'est pourquoi les résultantes accélération sont tracées en mesures brutes.

Par ailleurs, pour les essais de calibration, (effectués à vitesse plus faible), l'amplitude des paramètres à enregistrer est peu importante, les capteurs sont cependant choisis pour réaliser immédiatement après, dans de bonnes conditions, des essais à vitesse nominale. Il en est de même pour le réglage des gains des amplificateurs de mesures.

Il s'ensuit, dans ce cas, un mauvais rapport signal sur bruit : les tracés sont difficiles à exploiter.

Pour faciliter l'exploitation des résultats, les signaux de tous les capteurs, pour les essais de calibration ont été tracés après un filtrage numérique (Butterworth ordre 3, fréquence de coupure 30 Hz, voir planche 6). On peut, par comparaison, assimiler ce filtre à un "classe 12".

Les résultantes et les sommes des efforts ont été filtrées avant traçage avec ce même filtre.

Les résultantes des accélérations sont, comme pour le cas des essais à vitesse nominale, tracées en mesures brutes.

On donne planches 7 et 8, des exemples de résultats de capteurs : les évolutions des mesures brutes et filtrées sont superposées.

2.2.2. Résultats numériques :

On distingue trois tableaux :

a/ Valeurs crêtes des mesures de chaque capteur :

Ce tableau (voir exemple planche 9) donne la valeur des maximums positif et négatif ("+peak") et ("-peak") en regard des instants correspondants ("T"). Ces résultats sont exprimés dans l'unité choisie rappelée dans la colonne unité ("unit"). Ces valeurs crêtes ont été déterminées à partir des mesures filtrées comme indiqué au paragraphe 2.2.1/c.

c/ Valeurs crêtes des combinaisons de résultats de plusieurs capteurs :

Ce tableau (voir exemple planche n° 10) donne, les valeurs pour les résultats composés.

On distingue trois types de résultats composés :

* Accélérations résultantes : il s'agit des valeurs crêtes du module de la résultante des accélérations. Elles sont données en regard du temps correspondant, et sont calculées à partir des mesures des accéléromètres triaxiaux de la tête, du thorax et du bassin du mannequin. Les mesures sont brutes, seulement filtrées par le filtre anti-repliement analogique 1000 Hz.

* Efforts résultants : il s'agit d'une façon analogue, des valeurs crêtes du module des efforts. Ces efforts sont mesurés à partir des capteurs de force triaxiaux supportant le siège en quatre points. Avant le calcul des résultantes, les mesures sont filtrées comme indiqué au paragraphe 2.2.1/c ("classe 180" pour les essais à vitesse nominale et "classe 12" pour les essais de calibration).

* Sommes des efforts : il s'agit ici, à partir des indications des mêmes capteurs de force, des sommes selon l'axe des X, des Y et des Z. Avant le calcul des sommes, les mesures sont filtrées comme indiqué au paragraphe 2.2.1/c ("classe 180" pour les essais à vitesse nominale et "classe 12" pour les essais de calibration).

2.2.3. Valeurs du H.I.C. (Critère de blessure à la tête) :

Ces valeurs sont calculées à partir des mesures brutes (filtres analogiques 1000 Hz).

La formule retenue pour effectuer le calcul du H.I.C. est la suivante :

$$H.I.C. = MAX \left\{ (t2-t1) * \left(\frac{1}{(t2-t1)} \int_{t1}^{t2} a(t)\, dt \right)^{2,5} \right\}$$

t2 et t1 délimitent la durée du phénomène pour lequel un calcul de H.I.C. est effectué.

a(t) est la valeur instantanée de l'accélération résultante en "g".

L'optimisation est recherchée sur toute la durée du phénomène : ici, 1 seconde.

La valeur de t1 varie de 1/2840 seconde (période d'échantillonnage) jusqu'à 1 seconde.

La valeur de t2 varie de telle sorte que (t2-t1) ne varie que de 1/2840 seconde jusqu'à 50 millisecondes.

Toutes les valeurs que le H.I.C. est susceptible de prendre (environ 400 000) sont ainsi calculées.

Seule, la valeur maximale est retenue. Cette valeur est donnée en regard des deux instants t1 et t2 correspondants (voir exemple planche 10).

2.3 . PRISES DE VUES :

Deux caméras rapides à 400 images/s sont utilisées pour analyser le comportement de l'éprouvette lors de l'impact.

De plus, des caméras supplémentaires peuvent être mises en place afin d'effectuer la trajectographie de certains points de l'éprouvette et d'obtenir avec précision leur déplacement au cours de la chute et pendant l'impact.

3- PRESENTATION DES ESSAIS REALISES

3-1- Essais de Gazelle SA 341

En 1977, l'essai de "crash" d'une cellule SA 341 Gazelle a été effectué afin:

- d'étudier la survie des passagers et la tenue de la structure
- d'obtenir des informations permettant l'étude d'un modèle de calcul du comportement des structures d'hélicoptères lors d'un "crash".

Les vitesses horizontale et verticale au moment de l'impact étaient égales à 6 m/s, soit une vitesse résultante de 8,4 m/s. Les dommages modérés subis par la cellule ont permis son emploi pour un second essai de "crash" global afin d'évaluer la capacité résiduelle d'absorption d'énergie par écrasement de la structure. Cette deuxième chute a consisté en un impact symétrique à plat avec vitesse verticale de 10,5 m/s.

3-1- Essais de Super Puma SA 332

Dans un premier temps des essais partiels ont été effectués sur les quatre composants principaux participant à la protection au "crash": la structure inférieure, les réservoirs, le train d'atterrissage et les sièges.

Puis un essai de "crash" sévère a été réalisé sur une cellule complète de Puma rendue conforme à celle du Super Puma (après renforcements structuraux, équipée de tous les dispositifs anticrash sauf le train). Pour tenir compte de l'absence du train qui absorbe 25% de l'énergie à l'impact les conditions d'essai ont été ramenées à 10 m/s en vitesse verticale avec une vitesse horizontale de 5,6 m/s.

L'essai a été effectué en juin 1978 sur la première installation d'essai de "crash". Les moyens cinématographiques comportaient une importante installation d'éclairage et de prise de vues : 20 caméras de vitesse comprises entre 24 et 800 images par seconde ont été utilisées, dont deux étaient embarquées à bord de la cellule.

L'installation de mesure comportait plusieurs enregistreurs rapides; 170 voies ont été enregistrées et concernaient des mesures de contraintes , d'accélérations sur la structure et les mannequins, de pressions et de déplacements.

Cet essai a permis de constater le comportement satisfaisant de la structure et notamment la résistance du plancher mécanique, ainsi que la conformité entre résultats et prévisions.

Les accélérations subies par les mannequins, se situent dans le domaine supportable du diagramme de Webb et la déformation de la structure est compatible avec la survie des passagers.

4- CONCLUSION

Depuis le lancement en France des études concernant la protection au "crash" des hélicoptères, le CEAT a investi un potentiel important pour se doter de moyens permettant d'étudier tous les phénomènes structuraux qui interviennent lors du "crash".

Les méthodes qu'il a mises au point et les moyens d'essais développés récemment (troisième aire de "crash", modernisation du banc d'accélération) pourront être d'une aide considérable dans le développement d'hélicoptères futurs et la certification au "crash" des avions civils.

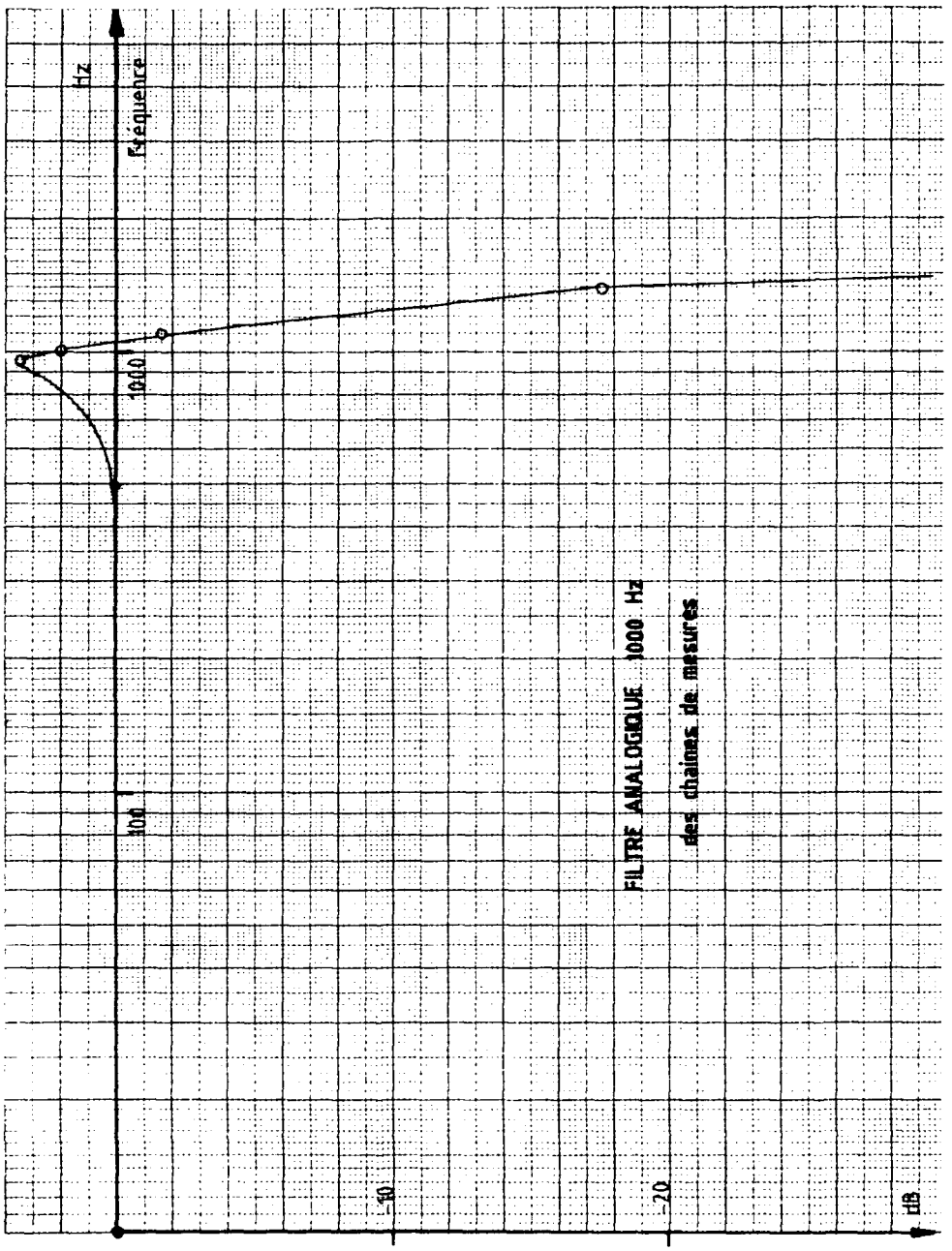

FILTRE D'ENTREE ANALOGIQUE

PLANCHE 1

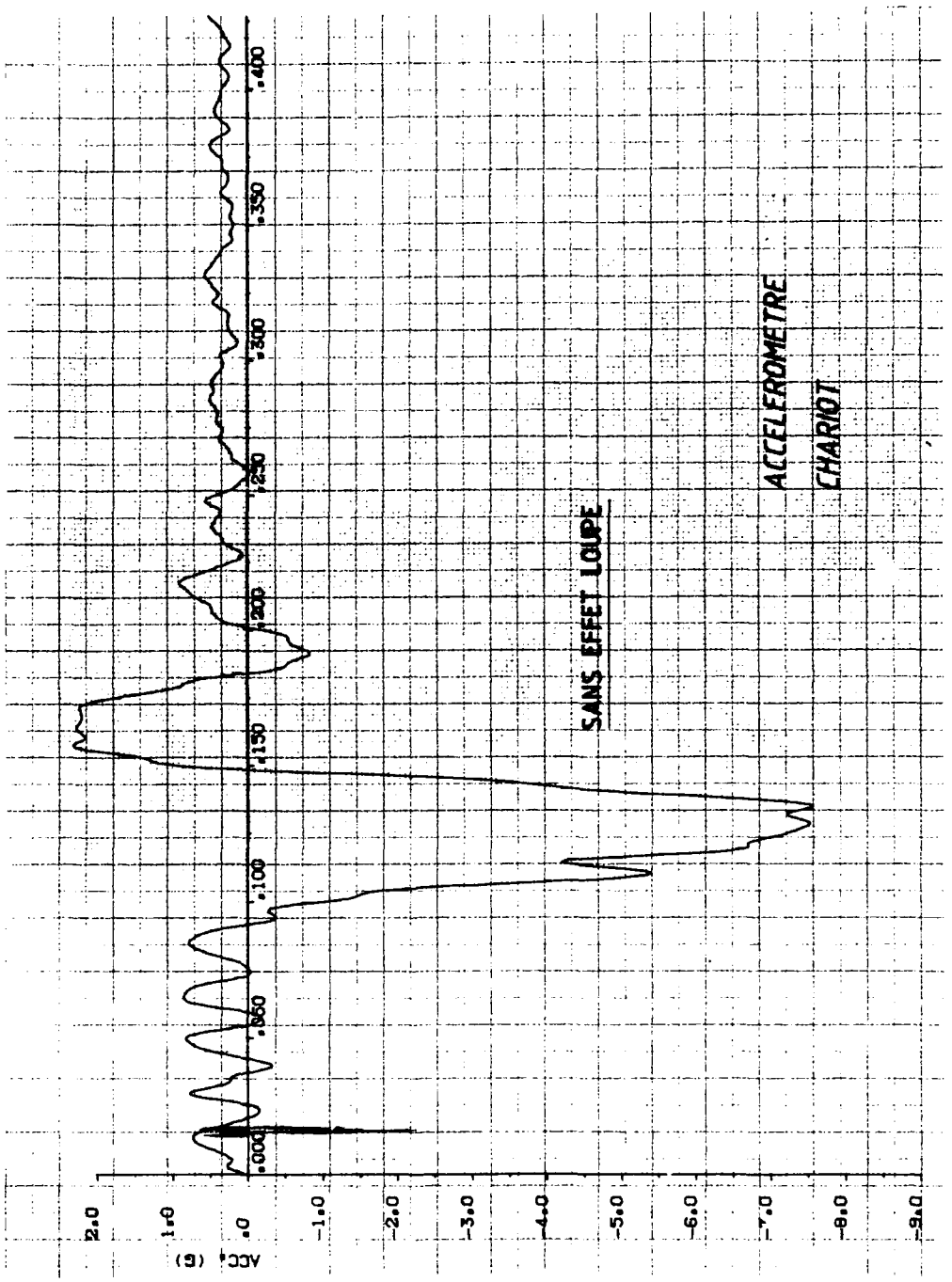

DETECTION DU POINT D'IMPACT

PLANCHE 2

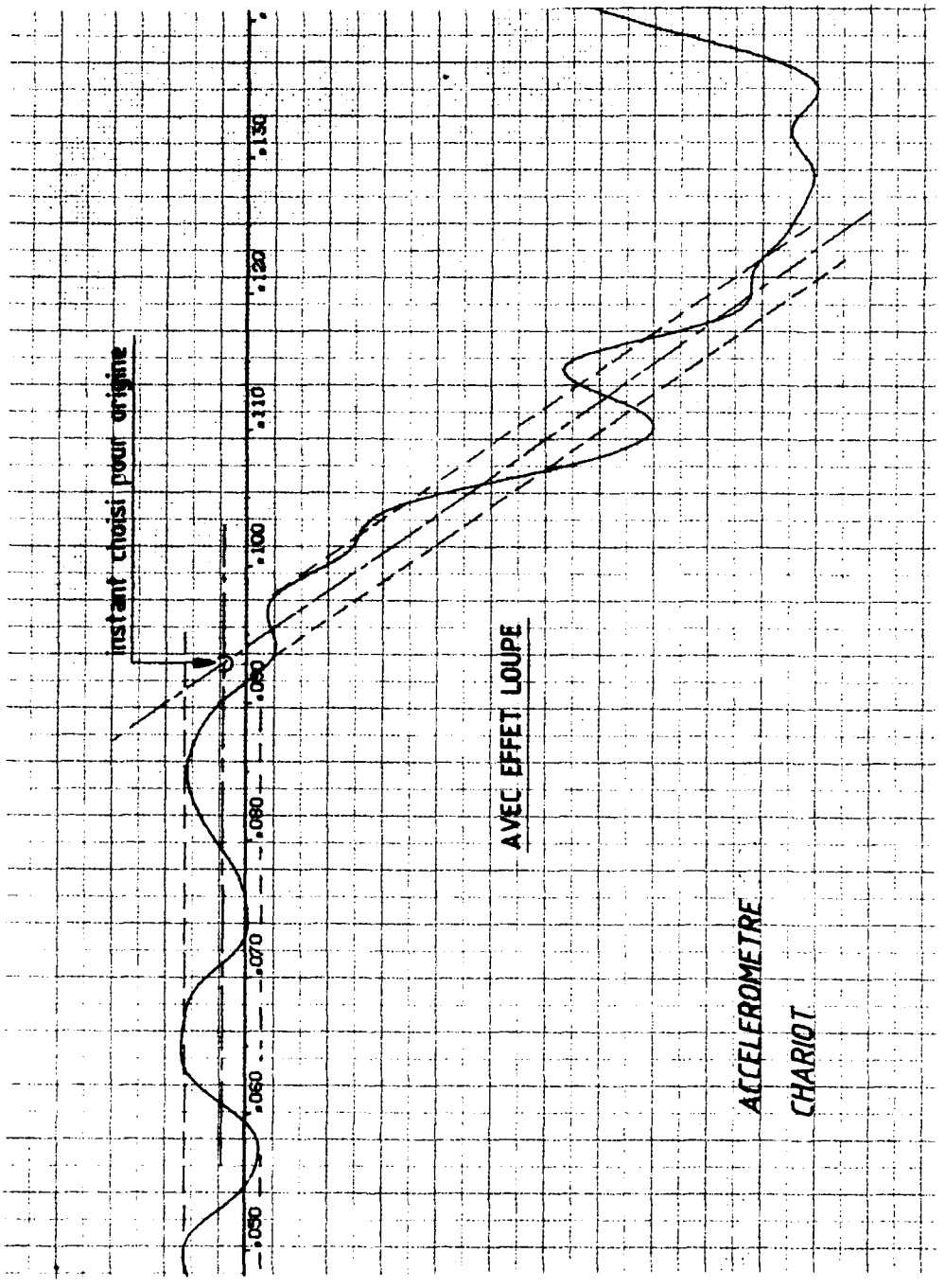

DETERMINATION DU POINT D'IMPACT

PLANCHE 3

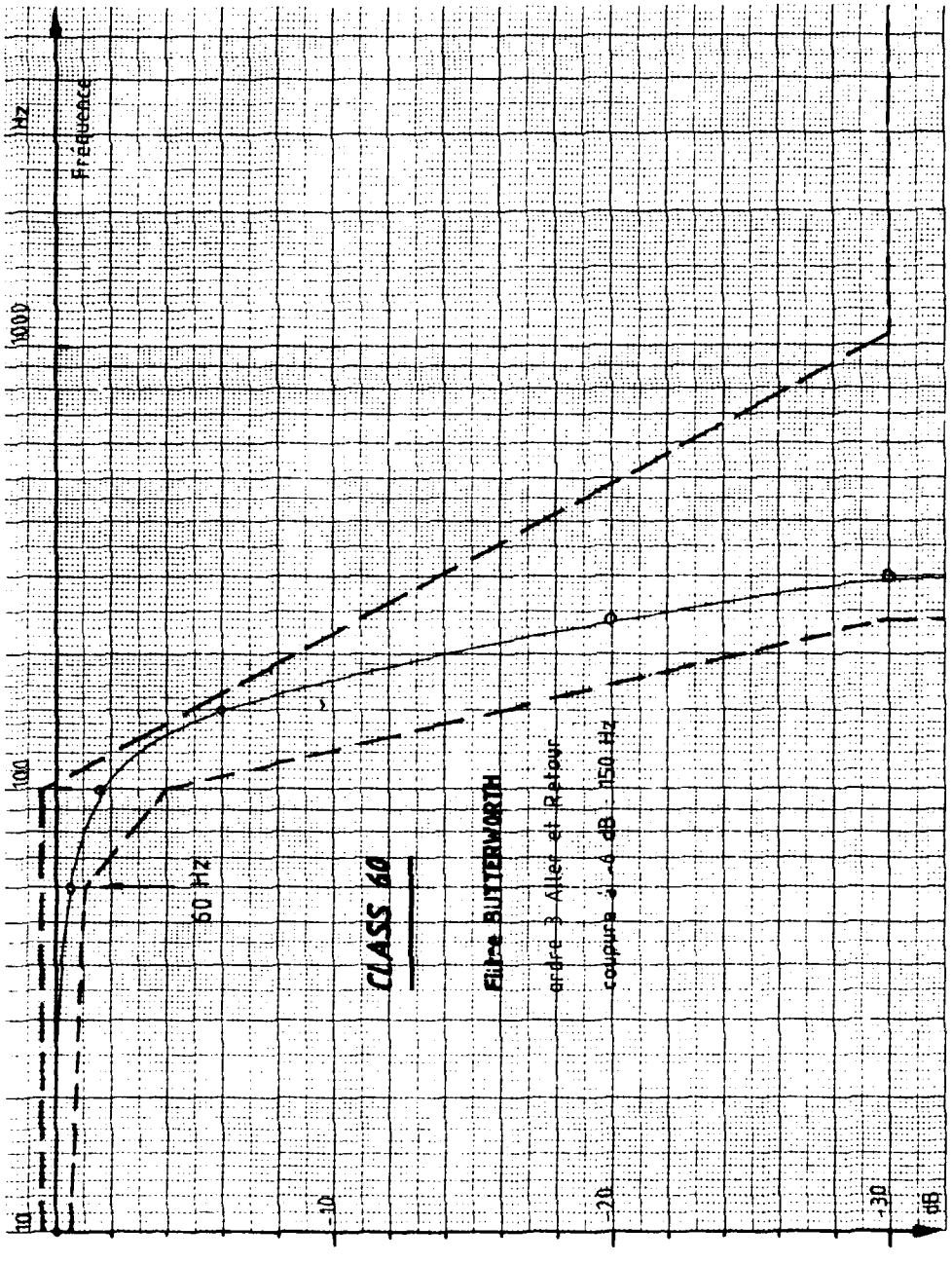

COURBE DE REPONSE FILTRE CLASSE 60

PLANCHE 4

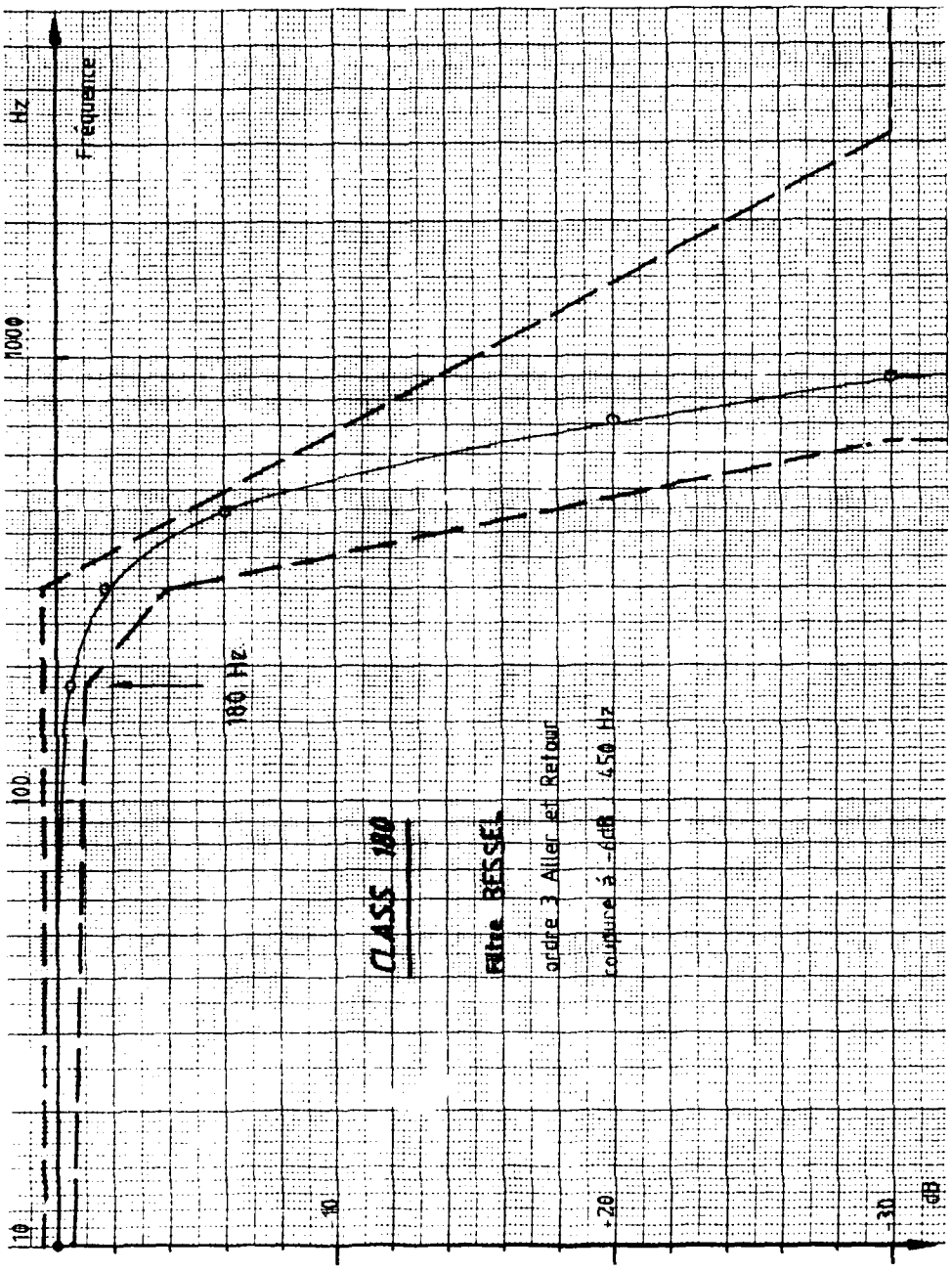

COURBE DE REPONSE FILTRE CLASSE 180

PLANCHE 5

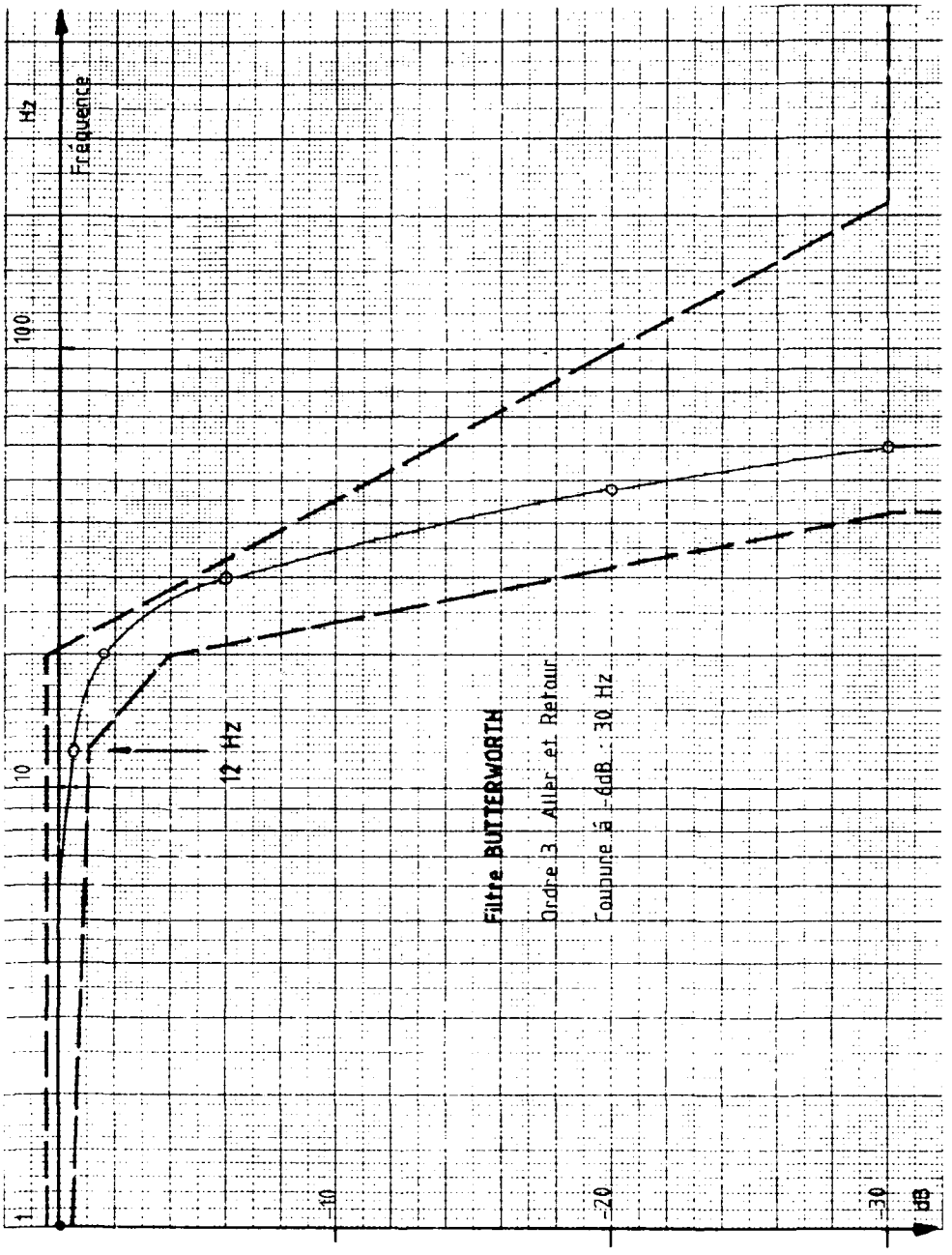

COURBE DE REPONSE FILTRE CLASSE 12

PLANCHE 6

SUPERPOSITION DES MESURES FILTREES ET NON FILTREES

PLANCHE 7

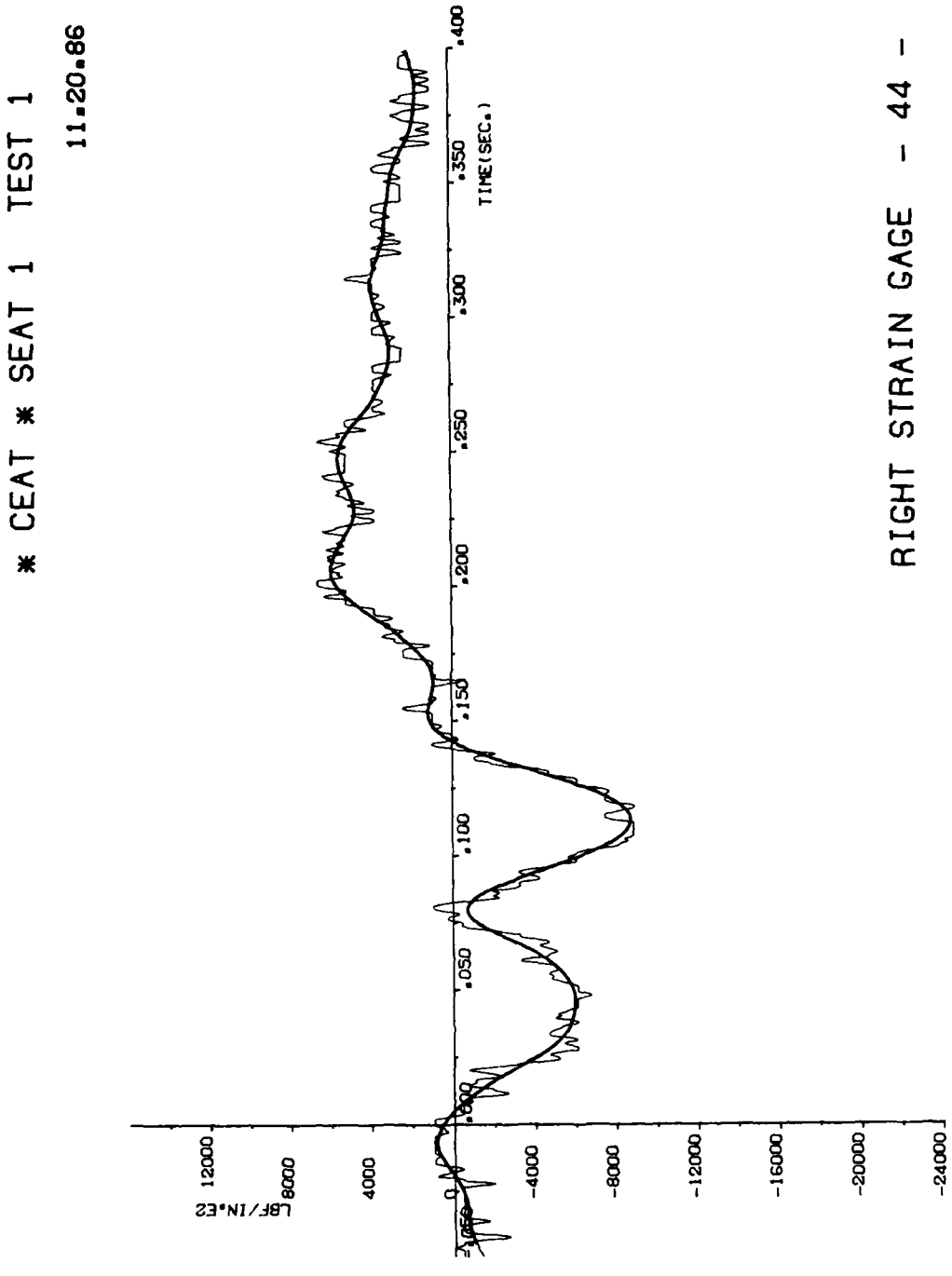

SUPERPOSITION DES MESURES FILTREES ET NON FILTREES

PLANCHE 8

NAME	UNIT	+PEAK	T	-PEAK	T
SEAT ACCELERATION X.....	ACC. (G)	2.23	.0676	-7.66	.031
SEAT ACCELERATION Y.....	ACC. (G)	1.62	.0303	-.60	.070
SEAT ACCELERATION Z.....	ACC. (G)	.84	.0292	-.29	.086
RIGHT SLED ACCELERATION - 1 - ..	ACC. (G)	2.31	.0680	-7.90	.032
RIGHT SLED ACCELERATION - 2 - ..	ACC. (G)	2.32	.0680	-7.90	.032
MIDDLE OCCUPANT PELVIS ACCEL Y ..	ACC. (G)	1.03	.0694	-.22	.101
MIDDLE OCCUPANT PELVIS ACCEL Z ..	ACC. (G)	2.23	.0764	-.38	.146
LEFT OCCUPANT HEAD ACCEL. X ..	ACC. (G)	2.74	.8292	-3.08	.223
LEFT OCCUPANT HEAD ACCEL. Y ..	ACC. (G)	1.44	.1866	-.64	.274
LEFT OCCUPANT HEAD ACCEL. Z ..	ACC. (G)	.64	.0884	-1.62	.165
LEFT OCCUPANT CHEST ACCEL. X ..	ACC. (G)	1.39	.8412	-1.61	.096
LEFT OCCUPANT CHEST ACCEL. Y ..	ACC. (G)	.75	.0750	-.23	.458
LEFT OCCUPANT CHEST ACCEL. Z ..	ACC. (G)	1.17	.0894	-.87	.162
LEFT OCCUPANT PELVIS ACCEL. X ..	ACC. (G)	.46	.1553	-1.66	.111
LEFT OCCUPANT PELVIS ACCEL. Y ..	ACC. (G)	1.13	.0655	-.57	.204
LEFT OCCUPANT PELVIS ACCEL. Z ..	ACC. (G)	3.56	.0996	-.76	.207
RIGHT OCCUPANT HEAD ACCEL. X ..	ACC. (G)	1.32	.1032	-2.48	.192
RIGHT OCCUPANT HEAD ACCEL. Y ..	ACC. (G)	1.10	.1792	-.83	.458
RIGHT OCCUPANT HEAD ACCEL. Z ..	ACC. (G)	1.20	.0592	-2.54	.136
RIGHT OCCUPANT CHEST ACCEL. X ..	ACC. (G)	-.12	.0116	-1.32	.452
RIGHT OCCUPANT CHEST ACCEL. Y ..	ACC. (G)	.63	.2088	-.41	.441
RIGHT OCCUPANT CHEST ACCEL. Z ..	ACC. (G)	1.53	.0775	-1.39	.139
RIGHT OCCUPANT PELVIS ACCEL. X ..	ACC. (G)	.44	.1380	-2.25	.095
RIGHT OCCUPANT PELVIS ACCEL. Y ..	ACC. (G)	1.12	.0644	-.30	.229
RIGHT OCCUPANT PELVIS ACCEL. Z ..	ACC. (G)	2.82	.0852	-.59	.155
MIDDLE OCCUPANT HEAD ACCEL. X ..	ACC. (G)	2.21	.0905	-3.09	.162
MIDDLE OCCUPANT HEAD ACCEL. Y ..	ACC. (G)	.83	.1194	-.74	.415
MIDDLE OCCUPANT HEAD ACCEL. Z ..	ACC. (G)	.66	.0580	-3.67	.128
MIDDLE OCCUPANT CHEST ACCEL. X ..	ACC. (G)	.04	.0000	-2.15	.213
DLE OCCUPANT CHEST ACCEL. Y ..	ACC. (G)	.35	.0704	-.54	.371
DLE OCCUPANT CHEST ACCEL. Z ..	ACC. (G)	1.20	.0743	-1.48	.145
DLE OCCUPANT PELVIS ACCEL. X ..	ACC. (G)	.82	.2032	-5.60	.069
T FRONT LEG - X -.....	FORCE(LBF)	276.25	.0387	-51.17	.175
T FRONT LEG - Y -.....	FORCE(LBF)	13.69	.4711	-157.08	.114
T FRONT LEG - Z -.....	FORCE(LBF)	159.11	.8430	-747.47	.086
T FRONT LEG - X -.....	FORCE(LBF)	196.01	.0412	-14.78	.134

TABLEAU DES PICS DES MESURES

PLANCHE 9

* CEAT * SEAT 1 TEST 1 11.20.86

PEAK LOADS

NAME	UNIT	+PEAK	(T)	-PEAK	(T)
RIGHT OCCUPANT HEAD ACCELERATION RESULTANT	ACC. (G)	3.56	.1863		
MIDDLE OCCUPANT HEAD ACCELERATION RESULTANT....	ACC. (G)	4.45	.1489		
LEFT OCCUPANT HEAD ACCELERATION RESULTANT.....	ACC. (G)	3.44	.2194		
RIGHT OCCUPANT CHEST ACCELERATION RESULTANT....	ACC. (G)	6.21	.1306		
MIDDLE OCCUPANT CHEST ACCELERATION RESULTANT ..	ACC. (G)	2.43	.2077		
LEFT OCCUPANT CHEST ACCELERATION RESULTANT	ACC. (G)	2.39	.1155		
RIGHT OCCUPANT PELVIS ACCELERATION RESULTANT ..	ACC. (G)	4.07	.0799		
MIDDLE OCCUPANT PELVIS ACCELERATION RESULTANT..	ACC. (G)	6.07	.0683		
LEFT OCCUPANT PELVIS ACCELERATION RESULTANT....	ACC. (G)	4.05	.0954		
LEFT FRONT LEG RESULTANT	FORCE(LBF)	794.72	.0866		
RIGHT FRONT LEG RESULTANT.....	FORCE(LBF)	1003.17	.0729		
RIGHT REAR LEG RESULTANT	FORCE(LBF)	676.33	.0754		
LEFT REAR LEG RESULTAT	FORCE(LBF)	889.18	.1004		
X SUM	FORCE(LBF)	916.49	.0387	-85.16	.865
Y SUM	FORCE(LBF)	101.94	.2120	-444.83	.043
Z SUM	FORCE(LBF)	230.56	.1958	-251.47	.087

HIC VALUES

RIGHT OCCUPANT HEAD ACCELERATION RESULTANT	HIC= .8	T1= .1616 (S)	T2= .2116 (S)
MIDDLE OCCUPANT HEAD ACCELERATION RESULTANT	HIC= 1.5	T1= .1222 (S)	T2= .1722 (S)
LEFT OCCUPANT HEAD ACCELERATION RESULTANT	HIC= .8	T1= .1458 (S)	T2= .1958 (S)

PLANCHE 10

TABLEAU DES PICS DES COMBINAISONS

ETUDE NUMERIQUE ET EXPERIMENTALE DU COMPORTEMENT AU CRASH DES HELICOPTERES ET DES AVIONS

F. DUPRIEZ, P. GEOFFROY, J.L. PETITNIOT, T. VOHY

ONERA - IMFL
5, Boulevard Paul Painlevé
59000 - LILLE
FRANCE

RESUME

Après un rappel sur les objectifs (survie des passagers et intégrité de l'habitacle) et sur le choix des méthodes numériques et expérimentales (méthode des éléments finis, essais sur maquettes structuralement représentatives), les points suivants sont abordés :

- similitude structurale du comportement mécanique global et validation des règles de construction des modèles sur des sous-structures élémentaires,
- étude expérimentale du crash d'un hélicoptère tombant en autorotation, définition de la structure de la maquette et comparaison sur un essai effectué en vraie grandeur,
- étude expérimentale du retournement des avions légers à l'atterrissage sur sol mou, analyse des risques et approche d'un modèle de sol,
- étude numérique du comportement de structures métalliques à l'écrasement, méthodes d'analyses développées à partir de macro ou super-éléments finis dans le domaine du flambement élasto-plastique, application à un élément de raidisseur et à une sous-structure d'avion de type commercial, comparaison avec l'essai sur maquette,
- perspectives futures.

1. INTRODUCTION

Le décrochage en autorotation des hélicoptères, l'atterrissage forcé sur piste, train rentré, d'avions de transport ou celui d'avions légers, avec ou sans train, sur terrain hostile, posent au stade de la conception le problème de la survie de l'équipage et des passagers.

Les principaux facteurs de mortalité sont l'incendie, les dommages corporels irreversibles dus à des niveaux d'accélérations trop élevés pendant des temps trop longs, la déformation ou la destruction de l'habitacle.

Ces deux derniers facteurs sont directement reliés au comportement élastoplastique de la structure pendant l'impact.

Pour étudier ce comportement structural, trois principales techniques d'analyse se distinguent :

- l'essai en vraie grandeur de la structure ou d'un composant principal. Dans ce domaine citons, en France, l'essai du fond de barque de l'hélicoptère Gazelle SA341 [1] et, récemment aux Etats Unis, les essais de largage de tronçons de fuselage [2] et l'essai de crash d'un Boeing 720 téléguidé [3] , [4] ,
- l'essai sur maquette à échelle réduite, structuralement représentative en similitude de la structure grandeur, de composants principaux ou secondaires de structures. Dans cette voie expérimentale, citons les travaux effectués à l'I.M.F.L. concernant l'étude, la réalisation et les essais de maquettes à échelle 1/3 du fond de barque de l'hélicoptère Gazelle SA341 [5] , [6], [7], [8] et de maquettes d'éléments de fuselage arrière de gros avions de transports [9], [10]. Dans ce domaine se trouvent également les études de comportement au retournement des avions légers, atterrissant sur des terres de labour, sur maquettes à échelle 1/7 en similitude de vol libre de Froude,
- la troisième direction d'étude est la simulation numérique de la réponse de la structure ou de sous-ensembles, lors de l'impact. Dans cette direction, deux techniques numériques distinctes apparaissent. La première technique est une méthode hybride qui associe les aspects numériques et expérimentaux. La structure est décomposée en sous-ensembles qui sont représentés soit par des éléments de ressort, soit par des poutres non-linéaires associées à des masses ponctuelles. L'un des programmes de calcul fondés sur cette méthode est le code de calcul KRASH [11], [12]. La deuxième technique numérique est la méthode de calcul par éléments finis où l'ensemble structural étudié est représenté par des éléments de type poutre, coque, etc... Pour analyser les phénomènes complexes de ruine intervenant durant l'écrasement (grands déplacements, grandes déformations, contacts ...), des programmes de calcul non-linéaire spécifiques se sont développés. Parmi ces codes, nous pouvons citer notamment les logiciels de calcul DYCAST [13] (NASA et GRUMMAN) et PAM-CRASH [14] (E.S.I.).

Ce document concerne les essais sur maquettes et l'approche numérique.

2. CONCEPTION DES MAQUETTES EN SIMILITUDE STRUCTURALE

2.1. REGLES DE SIMILITUDE

Ces règles sont élaborées à partir des considérations physiques suivantes :

- sous des déplacements relatifs identiques, entre la structure et la maquette, les champs des déformations et des contraintes doivent être conservés pour aborder de façon similaire le domaine plastique,
- le domaine plastique doit être atteint pour les mêmes contraintes et déformations et son évolution doit être identique,
- le rapport des forces d'inertie aux forces élastiques, paramètres principaux de la phase correspondant au premier impact, doit être conservé localement.

Les points 1 et 2 impliquent l'utilisation des mêmes matériaux donc conservation de E, ρ et ν , s'il s'agit de métaux, avec :

E module d' young,
ρ masse volumique,
ν coefficient de Poisson.

Si L est une grandeur caractéristique de la structure maquette, le point 1 implique que $\left[\frac{F}{L^2}\right] = 1$ et $\left[\frac{F L^2}{E I}\right] = 1$ soit $\left[\frac{I}{L^4}\right] = 1$

Ceci entraîne que pour avoir la même répartition des déformations et des contraintes dans l'espace, la structure maquette doit être une réplique exacte de la structure réelle. Comme la répartition de masse doit être conservée localement : $\left[\frac{M}{\rho L^3}\right] = 1$. Le point 3 implique que $\left[\frac{MV^2}{F L}\right] = 1$

avec M masse,
V vitesse d'impact.

Ceci conduit à $[V^2] = 1$; la vitesse d'impact doit être conservée. L'ensemble des rapports de similitude est défini dans le tableau 1.

Pour la représentation d'un sol semblable à l'aire d'essai en grandeur, les règles de similitude appliquées reposent sur la conservation de l'énergie de pénétration. La reconstitution du sol respecte également la similitude géométrique de la granulométrie.

L'application du critère de contrainte de cisaillement maximale a permis de définir l'épaisseur minimale du massif pour éviter toute interférence du dièdre de rupture avec la dalle rigide sur laquelle a été créé le massif [7].

2.2. VARIABLES NON REPRESENTEES DANS LA SIMILITUDE STRUCTURALE

La similitude adoptée conduit à travailler sous une accélération augmentée dans le facteur d'échelle, une constante de temps réduite dans le rapport d'échelle et un facteur d'intensité de contrainte Kc réduit dans la racine de ce même rapport.

Les conséquences du non respect des termes d'accélération de pesanteur sont en général peu importantes en ce qui concerne la phase du premier contact avec le sol. A ce stade, les forces d'inertie sont en effet prépondérantes vis-à-vis des forces de gravité. Par contre, la phase de rebond et de glissement n'est pas représentée et les conditions géométriques initiales du 2ème impact peuvent être modifiées tout en présentant un niveau d'énergie semblable. En ce qui concerne le comportement visco-élastique, l'utilisation de matériaux identiques à ceux utilisés à l'échelle 1 occasionne dans le cas d'un essai dynamique, le non respect de la relation contrainte - déformation à deux niveaux.

Si l'on considère l'influence de la vitesse d'allongement relatif $\dot{\epsilon} = \frac{\partial \epsilon}{\partial t}$ sur les contraintes σ , on montre que : $\log_{10}\left(\frac{\sigma_m}{\sigma_p}\right) = n \log_{10}\left(\frac{\dot{\epsilon}_m}{\dot{\epsilon}_p}\right)$

les indices m et p désignant respectivement la structure maquette et la structure à échelle 1. Pour de nombreux métaux, $n \sim 0{,}01$ ce qui conduit pour le choix d'une échelle au 1/3 à $\sigma_m/\sigma_p \sim 1{,}01$. Pour cette échelle, les valeurs des contraintes dans la structure seront donc, dans les mêmes conditions d'impact, de 1 % supérieures à celle existant réellement dans la structure en grandeur. L'essai sera donc pessimiste, ce qui va dans le sens de la sécurité.

La deuxième remarque concerne la limite élastique qui peut évoluer fortement en fonction de la vitesse de déformation (cas extrême présenté par les aciers doux). Ceci implique que la plastification sera atteinte plus tard sur maquette. Cet aspect est optimiste pour l'essai sur maquette.

Le développement des déchirures, caractérisé par la conservation du facteur d'intensité de contrainte K_c , quantifiant l'apparition et la propagation de fissures jusqu'à rupture n'est pas fidèlement reproduit. Ce facteur qui dépend de la nature du matériau, de l'épaisseur de voile et de la vitesse de déformation augmente en-dessous d'une certaine épaisseur alors que la similitude voudrait le voir diminuer dans la racine carrée de l'échelle.

Ainsi l'amplitude des déchirures et des ruptures constatées sur maquette sera donc a priori inférieure à celle des désordres relevés sur la structure réelle. Dans le cas des structures aéronautiques de faible épaisseur, l'emploi d'un facteur d'échelle raisonnable permet d'amoindrir l'influence de ce paramètre pour une estimation réaliste des dégâts.

2.3. CONTRAINTES TECHNOLOGIQUES LIEES A LA FABRICATION

Les capacités de fabrication définissent l'échelle minimale de représentation d'une structure prototype. Les limites technologiques conduisent à une épaisseur minimale de 0,2 mm pour les peaux obtenues par usinage chimique avec la garantie d'une précision meilleure que 5 %.

Les influences sur les propriétés mécaniques de la rugosité, meilleure que R_a = 2 µm et de la porosité inhérentes au processus d'usinage chimique, n'ont pas fait l'objet d'investigation. Le pliage et l'étirage contrôlé des feuilles pour la réalisation des cadres ainsi que l'usinage des raidisseurs et des cornières n'ont pas posé de difficultés particulières en dehors de la création d'un outillage spécifique.

Le diamètre minimal admissible des rivets, n'occasionnant pas d'amorce de rupture lors de la formation de la bouterolle, a été trouvé égal à 0,8 mm.

Ces deux limites ainsi que la recherche d'un rapport qualité/prix raisonnable ont conduit au choix d'une échelle comprise entre le 1/3, pour la plupart des cas, et le 1/10è, pour des structures d'aéronefs de dimensions importantes.

Les alliages légers utilisés A-U4G (2017), A-U4G1 (2024) ou A-U4G1/A5 pour les revêtements et A-U2G (2117) ou A-U4G (2017) pour les rivets, sont de qualité aéronautique.

Le traitement thermique consistant en une trempe à l'air est scrupuleusement reproduit. Dans le cas des réalisations futures de structures maquette en matériaux composites, deux voies sont à explorer pour représenter le comportement élastique, tout en conservant le même caractère d'anisotropie que la structure réelle et les mêmes limites élastiques :

- une réduction du nombre de plis dans le facteur d'échelle. Deux possibilités sont offertes : agir sur l'orientation des plis et/ou jouer sur le taux volumique de renfort,

- l'emploi de préimprégnés d'épaisseur dans le rapport du facteur d'échelle. Le choix de l'échelle 1/3 peut en effet autoriser cette éventualité, la fabrication de préimprégnés d'épaisseur 75µ, environ le 1/3 de l'épaisseur des plis couramment utilisés, étant délicate mais pas utopique.

2.4. EXEMPLES D'EXPERIMENTATION SUR MAQUETTES

Ce paragraphe présente deux expérimentations réalisées sur maquettes à échelle 1/3 dans le cadre du comportement au crash des hélicoptères :

- l'étude du comportement de caissons métalliques couramment rencontrés dans l'ossature inférieure des hélicoptères,

- l'étude du crash d'un fond de barque complet d'hélicoptère.

Les résultats qui sont obtenus sont comparés aux mesures effectuées sur cellules en vraie grandeur au Centre d'Essais Aéronautiques de TOULOUSE (C.E.A.T).

2.4.1. Structures en caisson raidi

Ces structures en alliage d'aluminium A-U4G et de section parallélépipédique sont constituées par l'assemblage de quatre panneaux raidis (Photo 1).

L'influence de la modélisation des liaisons (rivetée, vissée, collée et mixte), de quelques variantes de fabrication et des conditions d'essais (bridage ou non), résumées dans le tableau 2, a été examinée. Les essais de compression ont été effectués en quasi statique à la vitesse de 5mm/minute. Les mesures relevées en continu concernent l'effort d'écrasement et la hauteur correspondante ainsi que quelques mesures locales de déformation au niveau des raidisseurs. L'évolution des déformées et la chronologie des ruptures successives a été fixée par caméras.

On note une bonne concordance de la courbe charge-déplacement des essais maquette avec les essais échelle 1 avec cependant une tendance générale à minimiser l'énergie absorbée notamment après 30 % d'écrasement (fig. 1). Cette concordance valide le mode de construction qui a été ensuite appliqué à une structure complexe de fond de barque.

2.4.2. Crash de fond de barque d'hélicoptère

La structure étudiée est la partie inférieure de l'hélicoptère Gazelle SA341 dont un essai a été effectué en grandeur réelle au C.E.A.T. (Photo 2). Deux exemplaires de cette structure complexe ont été fabriqués à échelle 1/3 en modélisant de façon précise les éléments structuraux pour obtenir une reproductibilité correcte des phénomènes sur le modèle réduit comme l'a montré l'expérience acquise lors des tests sur les caissons raidis.

La maquette se compose principalement de cadres en tôle d'alliages d'aluminium, usinés chimiquement, pliés, découpés et rivetés, assemblés par des pièces de liaison et des profilés usinés dans la masse pour former le squelette (Photo 3). Des revêtements raidis réalisent l'habillage extérieur et les planchers de référence - en nid d'abeille - sont vissés sur le squelette. Le pupitre de commande et les supports de la batterie qui contribuent à la tenue de l'ensemble du caisson ont été également reproduits. Les masses de la batterie, des pilote et copilote, des passagers et du réservoir ont été représentées par des lests d'aciers, reliés par des biellettes d'effort à un treillis de cornières fixé sur les cadres principaux de l'ossature.

Les essais dynamiques d'écrasement ont été accomplis à la vitesse verticale d'impact de 8 m/s par lâcher de la maquette. Le précalage en assiette a été corrigé de l'influence des forces aérodynamiques pour représenter l'assiette réelle de la structure à l'impact. La reproduction de la consistance du sol par damages progressifs a été contrôlée au pénétromètre dynamique. L'instrumentation de mesure embarquée et reliée au sol par un câble était composée d'accéléromètres disposés en divers points des planchers et sur les lests, et de de jauges de déformation collées sur les biellettes.

L'instrumentation extérieure à la maquette comprenait 3 caméras (2 caméras grande vitesse calées à 1500 images/s et une caméra 200 images/s) et une barrière optique à faisceaux laser mesurant la vitesse moyenne sur une chute de 0,1 m juste avant l'impact. L'impression simultanée du top de largage de la maquette sur les films des deux caméras et sur les deux enregistreurs magnétiques permet la datation des évènements. Les caméras disposent également d'une horloge interne pouvant réaliser le marquage du film toutes les millisecondes.

Les courbes accélérométriques obtenues sur maquette pour les lests, présentent une bonne concordance avec celles obtenues par le CAT (fig.2). En ce qui concerne le plancher, les courbesexpérimentales sont en général plus douces pour la maquette que pour le prototype échelle 1, la rigidité et les termes d'amortissement des liaisons entre plancher et ossature ne pouvant pas être représentés avec suffisamment de finesse. Les courbes d'effort sont très similaires avec une dispersion plus faible que pour les courbes d'accélération.

La morphologie des dégâts sur maquette et sur prototype est très comparable (Photos 2 et 4). Une analyse photogrammétrique restituant les déformations sur la forme de courbes iso-niveau a été effectuée par les services de l'E.T.C.A. En parallèle, un relevé de la géométrie de l'empreinte laissée sur le sol a été effectué par un moulage de plâtre.

2.5. INTERVALLE DE CONFIANCE, COUT ET DELAI DES ESSAIS SUR MAQUETTES

La moyenne des écarts entre les résultats de l'essai échelle 1 et des essais à l'échelle 1/3 se situe autour de 15 % avec un écart maximal d'environ 30 %. Ces valeurs montrent que la simulation d'un crash par un essai sur maquette à échelle réduite est réalisable. Les écarts de mesures sont principalement liés au caractère aléatoire des effondrements qui sont très sensibles aux conditions initiales.

La confrontation calcul-essais a d'autre part montré qu'il était illusoire d'espérer obtenir un écart inférieur à 20 %. Les études sur maquette sont donc tout à fait utilisables comme outil de prévision et de vérification, notamment au niveau de la phase de conception d'un prototype.

Le coût des essais et plus précisément de la maquette, est naturellement fonction de la complexité du prototype à représenter, du degré de simplification admissible et de l'échelle adoptée, l'influence de ces deux derniers paramètres s'imbriquant.

Les postes financiers à prendre en compte pour l'établissement du coût peuvent se décomposer en trois :

- la préparation des données de fabrication,
- la fabrication de la maquette,
- l'essai et l'analyse.

Le premier poste représente souvent la moitié du coût total au stade de l'avant-projet. Dans le cas de la réalisation d'une maquette sophistiquée comme celle relative à un fond de barque d'hélicoptère, le coût de l'essai sur maquette avec réalisation de la maquette est compris entre le tiers et la moitié du coût du même essai à échelle 1 en prenant une structure de série.

3. TURN OVER DES AVIONS LEGERS

L'éventualité d'une panne de moteur ou d'un incident en vol sur un avion léger monomoteur pose le problème de l'atterrissage d'urgence sur des terrains non préparés. Différents comptesrendus d'accident montrent que dans la plupart des cas d'atterrissage en détresse, sur des sols à faible consistance ou détrempés, l'avion capote, puis monte en pylône et se retourne.

Le phénomène de retournement pose le problème de la protection du pilote et de ses passagers vis-à-vis de l'écrasement de la verrière de l'avion.

Les travaux décrits ci-après ont pour objectif de présenter les moyens utilisés pour l'étude du retournement ainsi que les différents résultats expérimentaux qui permettront d'aboutir à un concept de protection.

L'approche proposée concerne d'une part, la recherche d'une modélisation, à l'aide d'essais sur maquette libre et sur un sol représentatif en similitude, et d'autre part, la réalisation d'un programme de calcul utilisant une représentation analytique du mouvement.

3.1. ETUDE EXPERIMENTALE

La phase expérimentale a été initiée par une étude du parc des avions légers utilisés dans les différents Aéroclubs Français de manière à permettre la détermination d'une enveloppe des paramètres massiques et géométriques et de choisir un avion de référence (MS 880 Rallye) qui sera retenu durant toute la campagne d'essais [17] .

Afin d'étudier à échelle réduite le comportement au retournement de l'avion M S 880 Rallye et de quelques variantes massiques et géométriques, une maquette de type "Mécano" a été construite (Photo 5). L'échelle de représentation en similitude est fixée à 1/7.

La similitude employée est la similitude de Froude qui permet la conservation du rapport des forces de pesanteur aux forces d'inertie et donc de simuler correctement la phase de retournement de l'avion, considéré comme un corps rigide.

Le choix des matériaux utilisés dans la construction de la maquette a été guidé par la nécessité de réaliser un ensemble de masse inférieure à 2,5 kg et par le souci de représentativité de la répartition de masse.

L'instrumentation embarquée est composée de deux accéléromètres à axes de mesure verticaux, répartis de part et d'autre du centre d'inertie et d'un accéléromètre à axe de mesure horizontal placé au centre d'inertie (Photo 6). La masse de la maquette étant faible et utilisée en quasi-totalité pour la structure, l'instrumentation embarquée a été limitée aux seuls moyens précités. La mesure des paramètres géométriques et cinétiques a été réalisée par des moyens de mesure au sol (figure 3).

Le choix d'un sol représentatif a été abordé par la recherche d'une configuration de terrains pouvant amener au retournement. La caractérisation des différents types de sols susceptibles d'être rencontrés a été étudiée sous l'aspect de la conservation des énergies de pénétration verticale dans la puissance quatrième de l'échelle. La qualification en grandeur et à échelle réduite est réalisée à l'aide d'un pénétromètre dynamique (Photo 7). Des essais ont été effectués avec cet appareil sur différents types de terrains (terres de labour, terrain gazonné, ...) et ont permis de définir une enveloppe d'enfoncements pénétrométriques.

Quatre types de terrains, dont les énergies de pénétration sont comprises entre 350 Joules/m et 1400 Joules/m ont été retenus dans le cadre de cette étude. Ces sols ont été représentés en similitude par différents mélanges de sable de Seine et de terre tamisée (figure 4). Un dispositif de pesée de sol permettant la mesure du diagramme d'efforts de frottement longitudinal $F_x = f(temps)$ a également été utilisé pour les essais (figure 5).

3.2. ETUDE NUMERIQUE

Un modèle de calcul, utilisant les équations issues du principe fondamental de la Dynamique et du théorème du moment dynamique, est proposé. Il a pour objet de décrire en bidimensionnel le comportement en retournement d'un avion léger à partir de l'ensemble des conditions géométriques, massiques (masse, centrage, inertie, géométrie des trains...) et cinétiques (vitesse d'approche, vitesse angulaire, ...) et du diagramme d'efforts de frottement longitudinal $F_x = f(temps)$ (figure 6).

Ce modèle de calcul est développé en considérant, comme hypothèse que l'avion est indéformable au cours du retournement et que l'étude dynamique du mouvement se ramène à une étude de corps rigide.

Une schématisation du sol permettant de s'affranchir de l'introduction du diagramme d'efforts de frottement longitudinal $F_x = f(temps)$ est en développement. L'architecture du programme ainsi que son articulation vis-à-vis de la phase expérimentale sont définies en figure 7.

3.3. RESULTATS EXPERIMENTAUX ET NUMERIQUES

Les différents essais réalisés sur maquette et sur différents types de sols en similitude ont permis de dégager un certain nombre de résultats qui permettent d'aborder la protection du pilote et des passagers vis-à-vis des niveaux d'accélération rencontrés au cours du retournement et de l'écrasement de la verrière [18] .

Parmi ces résultats, on peut citer principalement :

- Les essais de retournement réalisés sur un sol représentatif d'une terre de labour (350 Joules/m en grandeur) ont montré la possibilité de représentation à échelle réduite du phénomène de retournement (figure 8). Ces résultats expérimentaux sont confirmés par les différents comptes rendus d'accidents, qui montrent que le retournement survient dans tous les cas d'atterrissage forcés sur ce type de sol (figure 9).

De plus, la bonne cohérence entre les distances d'arrêt obtenues expérimentalement et celles relevées dans les différents comptes rendus d'accidents a permis de valider également ce type de sol du point de vue énergétique, en longitudinal (figure 10).

- Les niveaux d'accélérations verticales maximum obtenus au moment de l'impact de l'avion sur le sol (dans le cadre d'une approche en difficulté avec décrochage à environ 1 m du sol) sont de l'ordre de 85 m/s² au centre d'inertie. Suivant l'axe longitudinal, les niveaux d'accélérations maximum enregistrés sont d'environ 120 m/s². Ils mettent en évidence l'importance de baudriers de protection pour le maintien du pilote et des passagers en cas de décélération longitudinale importante (figure 11).

- Les essais réalisés montrent que dans toutes les configurations étudiées, les temps d'application des niveaux d'accélération sont compris entre 0,010 et 0,030 seconde (accélérations verticales), 0,015 et 0,045 seconde (accélérations horizontales) et ne mettent donc pas en jeu la vie du pilote et des passagers au cours du mouvement de retournement (courbes de WEBB et EIBAND, figure 12).

- Les essais réalisés sur différents types de sols définissent une enveloppe des valeurs maximales de vitesses angulaires de l'avion au moment de l'impact de la verrière (figure 13). La valeur de 135°/s, correspondant à la vitesse angulaire de l'avion au moment de l'impact de la verrière, semble apparaître comme une première valeur de référence pour aborder les études de qualification mécanique de la verrière.

- D'une manière générale, les avions à trains classiques sont moins sensibles au retournement que les avions à trains tricycles (figure 14) mais sont par contre plus vulnérables vis-à-vis du phénomène de montée en pylône.

- Le passage d'un obstacle en relief ou en creux à une vitesse proche de la vitesse d'atterrissage provoque un affaissement des trains mais n'engendre pas le retournement ou la montée en pylône.

- La détermination du diagramme d'efforts de frottement en longitudinal $F_x = f(\text{temps})$, obtenue par introduction dans le modèle de calcul des diagrammes d'accélérations longitudinales, verticales, angulaires, montre une bonne cohérence vis-à-vis des mesures réalisées à l'aide du dispositif de pesée de sol (figure 15).

- L'ensemble des mesures expérimentales ainsi acquises permet de remonter à un modèle de sol applicable, cas par cas, à chaque type d'avion. Ce travail est prévu.

4. METHODES D'ANALYSE NUMERIQUE

Pour analyser le problème du comportement structural d'un avion s'écrasant avec une vitesse de l'ordre de 5 m/s environ, l'IMF Lille, en collaboration avec Engineering System International (E.S.I.) propose une méthodologie d'approche originale, reposant principalement sur deux concepts.

- le premier concept repose sur la décomposition de l'avion subissant un crash en deux zones (figure 16) :

  . la première zone correspond à la partie de l'avion qui absorbe peu d'énergie lors du crash. Dans la modélisation mathématique, le comportement structural statique de cette zone est supposé linéaire et dans le domaine dynamique temporel, seules les forces d'inertie sont considérées (forces de pesanteur négligées),

  . la deuxième zone est la partie inférieure du fuselage arrière de l'avion où se produit l'écrasement. Cette partie inférieure est constituée principalement d'un assemblage métallique de cadres circulaires raidis, de biellettes latérales de reprise d'efforts, d'un plancher soute et d'un plancher passager (figure 17). C'est cet ensemble structural qui absorbe en très grande partie l'énergie cinétique de vitesse verticale. Parallèlement à l'absorption d'énergie, des phénomènes physiques non linéaires complexes se produisent durant l'écrasement. Des grands déplacements cinématiques, des grandes déformations plastiques des composants, des contacts non linéaires et également des déchirures apparaissent.

- le deuxième concept de la méthodologie définie par l'IMF Lille est de développer et de mettre en oeuvre des modèles de calcul éléments finis permettant de modéliser le comportement statique pré et post flambement dans le domaine élastoplastique d'éléments de cadre métallique raidis avec un nombre relativement faible de degrés de liberté. Au niveau des hypothèses des lois de comportement des métaux, il est supposé que les déformations structurales ne dépendent que de l'énergie cinétique au moment de l'impact et non de la vitesse d'impact. Dans ce cas, un essai d'écrasement quasi-statique d'une maquette à échelle réduite, conduira à des modes de ruine identiques à ceux d'une structure en vraie grandeur. Compte tenu de la répétition des sections du fuselage arrière, il suffit de développer des modèles éléments finis sur un seul élément de cadre raidi et ensuite de les appliquer pour l'étude complète du fuselage arrière et ceci, pour un coût faible en temps machine.

  Parallèlement à ces travaux de modélisation, des essais sur maquettes à échelle réduite et structuralement semblables ont été effectués afin de constituer une banque de données expérimentales et de valider les modèles éléments finis et les méthodes d'analyse [9], [10], [15], [16], [19], [20].

4.1. MODELES MACRO ET SUPER ELEMENTS FINIS

Les modèles éléments finis développés sont soit des macro-éléments finis, soit des superéléments spécifiques. L'approche par macro-éléments consiste à utiliser des éléments finis classiques (poutre, coque ...) dont les propriétés mécaniques sont déterminées afin qu'un maillage peu dense traduise correctement le comportement non linéaire de la structure. Les propriétés mécaniques recherchées peuvent être le module d'Young, la limite élastique, ...

Quant à l'approche par superéléments, elle fait appel à des éléments finis de dimension géométrique importante qui incluent des lois de comportement analytiques et spécifiques dont les propriétés sont également recherchées. La figure 18 montre une loi type de comportement non-linéaire force-déplacement. On peut noter la réponse linéaire élastique caractérisée par le paramètre E_1, la charge limite (Pic 1), une première réponse de post-flambement (E_2) et un post flambement lointain (E_3).

Pour chacune des deux approches, les propriétés mécaniques des macro-éléments ou des superéléments sont ajustées en calibrant après plusieurs itérations la réponse élastique, la charge limite et la réponse post-flambement de la structure métallique à celle d'une solution cible connue. Cette solution cible peut être soit une réponse numérique obtenue à partir d'une modélisation fine de la composante étudiée, soit une réponse expérimentale obtenue à partir de mesures effectuées sur des maquettes de composants à échelle réduite. D'autres critères peuvent être retenus dont notamment l'énergie absorbée par la structure.

4.2. APPLICATION A UNE POUTRE

Dans un souci de validité, les méthodes d'analyse par macro-éléments et par super-éléments finis ont concerné l'analyse numérique non-linéaire quasi statique d'une poutre métallique (acier). Cette poutre mince de section rectangulaire est soumise à une force latérale à l'extrémité supérieure et encastrée à l'extrémité inférieure (figure 19), les dimensions géométriques sont les suivantes :

- aire de la section : $60 \times 60\ 10^{-3}\ m^2$
- épaisseur : $1\ 10^{-3}\ m$
- longueur : $500\ 10^{-3} m$

Une étude du comportement élastoplastique de la poutre est effectuée avec une discrétisation fine, comprenant 472 éléments de coque mince (figure 19). La figure 19 montre la courbe charge-déplacement F - W du point d'application de la force (point A), obtenue avec le maillage fin. L'évolution de la déformation de la poutre pour différentes valeurs du déplacement W du point A, est présentée sur la figure 20. L'apparition d'une rotule plastique près de l'encastrement et l'ouverture de l'arête caractérisent le mode de ruine complexe de la poutre. La modélisation du comportement élastoplastique de la poutre par la méthode des macro-éléments finis, est entreprise.

La discrétisation considérée est un maillage à 21 éléments de coque mince (figure 21). Dans ce modèle, les propriétés mécaniques que l'on cherche à ajuster pour obtenir la réponse numérique calculée avec le maillage fin, sont d'une part le module d'Young de la structure et d'autre part, la limite élastique de la cornière et des plaques. Quelques analyses non linéaires de la poutre ont suffi pour déterminer (ou ajuster) ces propriétés mécaniques. La courbe charge-déplacement du point A, obtenue avec le modèle macro-éléments, est présentée sur la figure 22, ainsi que la courbe obtenue avec le maillage fin. On constate que la charge limite de flambement et le comportement plastique post-flambement calculés avec le modèle macro-éléments, concordent de façon satisfaisante avec ceux déterminés par le maillage fin.

La même étude a été entreprise en appliquant la technique des superéléments finis. La poutre est discrétisée avec un seul superélément de coque mince et de quatre éléments quadrilatères classiques de coque mince (figure 23). La loi de comportement du superélément fini correspond à celle décrite sur la figure 18. Le rôle de cette loi, incluse dans la formulation de l'élément, est de modéliser du mieux que possible le comportement non-linéaire élastoplastique de la poutre. Les noeuds B et C sont articulés.

Les valeurs des caractéristiques mécaniques (E_1, E_2, E_3, P_1 et P_2) de la loi de comportement sont déterminées après quelques itérations en calibrant la courbe charge-déplacement du point A calculée avec le modèle, à celle obtenue avec la discrétisation fine. La figure 24 montre les deux courbes force-déplacement.

En conclusion de cette application dans le domaine non linéaire structural, la technique des superéléments finis tente de remplacer une composante entière par un élément fini spécialement conçu pour modéliser un comportement post-flambement typique tandis que l'approche macro-éléments tente de remplacer cette composante par un maillage simple.

En outre, il convient d'ajouter que le maillage en superéléments doit contenir les traits topologiques principaux de la composante étudiée, si l'on veut que le modèle conduise aux modes de ruine réels. En ce qui concerne les lois de comportement des super-éléments, il suffit de les créer une fois. Pour analyser différents comportements non-linéaires, seuls les paramètres de ces lois seront à ajuster. A l'inverse, la technique par macro-éléments nécessite de réeffectuer des maillages lors d'analyses de comportements non-linéaires différents. L'utilisation de cette méthode apparaît donc moins efficace pour l'analyse de problèmes non-linéaires, vis-à-vis de la méthode superéléments finis.

5. CONCLUSION ET PERSPECTIVES

Actuellement pour des structures métalliques en alliages légers, les règles de construction de maquettes structuralement représentatives des comportements élastiques et plastiques d'un aéronef sont bien définies et les résultats d'essais de crash sont transposables en similitude directe.

Les coûts de réalisation de ces maquettes, dont l'échelle est comprise entre le 1/3 et le 1/10 (pour des gros avions de transport) sont très nettement inférieurs à ceux d'une cellule de série. L'utilisation de ce type de maquette présente un avantage certain au stade de la conception de la tenue au crash de structures aéronautiques.

Dans le cas du retournement des avions légers, en combinant les études de comportement cinématique sur maquette de vol libre et ensuite les études de réponse structurale à isovitesse sur maquette (avec des échelles plus grandes), l'étude complète de la sauvegarde d'un habitacle et des niveaux accélérométriques subis par les passagers est possible et réaliste. Pour ce problème, la transposition des résultats des essais peut se faire également en similitude directe.

Le développement des techniques de calcul par macro ou superéléments finis montre qu'il est pensable de représenter, dans le domaine non-linéaire en grands déplacements et grandes déformations, des structures complexes répétitives par une schématisation comportant un faible nombre de degrés de liberté et bien adaptée au modèle cible. A cette schématisation du problème crash, il reste à déterminer un modèle de masse représentatif pour qu'une modélisation non-linéaire dynamique de cadres de fuselage métalliques soit effectuée.

L'extension future de ces méthodes d'analyse concernera les études des comportements statiques et dynamiques de cellules d'aéronefs en matériaux composites à matrice organique (carbone, kevlar, verre - epoxy).

REFERENCES

[1] "Essais locaux complémentaires à l'essai global de crash du SA 341 Gazelle. Essai d'écrasement du bas de structure"
CEAT, 9 Février 1978 - P.V. n° 7 668 600

[2] R. HAYDUK, S. WILLIAMS, "Vertical Drop test of a transport fuselage section located forward of the wing"
NASA TM 85679, NTS, Springfield, VA, August 1983

[3] H.G. Mc COMB Jr., R.G. THOMSON and R.J. HAYDUK "Structural Dynamics Research in a Full-Scale Transport Aircraft Crash Test"
Journal of Aircraft, July 1987, Vol. 24, n°7

[4] E.L. FASANELLA, E. WIDMAYER and M.P. ROBINSON "Structural Analysis of the controlled impact demonstration of a jet transport airplane"
Journal of Aircraft, 1987, Vol. 24, n°7

[5] X. de la SERVETTE, F. DUPRIEZ "Etude sur maquette de la résistance au crash d'hélicoptères"
Rapport IMFL, 23.12.1978

[6] M. DESCHAMPS "Dossier de construction des maquettes de fond de barque de l'hélicoptère SA 341 à l'échelle 1/3"
Rapport IMFL, 20.12.1979

[7] F. DUPRIEZ, J.L. PETITNIOT "Essais de crash sur maquettes à l'échelle 1/3 du fond de barque de l'hélicoptère SA 341"
Rapport IMFL, 28.01.1980

[8] J. MENS "Etude du crash de structures d'hélicoptères sur maquette à échelle réduite"
AEROSPATIALE, 15.11.1980

[9] J.L. PETITNIOT, F. DUPRIEZ "Etude expérimentale de la déformation dans les domaines élastique et plastique de la zone d'impact du crash d'un avion de transport"
IMFL, 02.12.1981, Rapport n° 81/53

[10] J.L. PETITNIOT, P. GEOFFROY "Etude expérimentale des déformations élastiques et plastiques de la zone d'impact du crash d'un avion de transport"
IMFL, 18.05.1984, Rapport n° 84/23

[11] M.A. GAMMON,"KRASH User's Manual"
California Company, Feb. 1979, FAA-RD-77-189, vol. I, II, III, Lockheed

[12] G. WITTLIN "Analysis of aircraft dynamic behaviour in a crash environment, in Proc. Twenty-Third Structures, Structural Dynamics and Materials Conf."
New Orleans, 1982, AIAA/ASME/ASCE/AHS, p. 316

[13] H. ARMEN, A. PIFKO, H. LEVINE "Non linear finite element techniques for aircraft crash analysis, Aircraft Crashworthiness, University"
Press of Virginia, 1975, 548 - pp. 517-548

[14] E. HAUG, J.M. LOCCI, F. ARNAUDEAU, PAM-NL "A General finite element program for the non-linear thermomechanical analysis of structures" 5th Int. Conf. on structural Mechanics in reactor technology"
Berlin, August 1979, Section M1/3

[15] J.L. PETITNIOT, J. FABIS "Etude expérimentale de la déformation dans les domaines élastique et plastique de la zone d'impact du crash d'un avion de transport"
IMFL, 25.09.1984, Rapport n° 84/41

[16] J.L. PETITNIOT, J. FABIS "Etude dynamique d'une maquette structuralement représentative d'un élément de fuselage, d'un avion de transport"
IMFL, 16.11.1983, Rapport n° 83/48

[17] T. VOHY, J.L. PETITNIOT "Atterrissage forcé des avions légers. Retournement-Définition de l'étude expérimentale et méthodes de calcul envisagées"
IMFL, 29.07.86, Rapport n° 86/33

[18] T. VOHY, L. BUCHANIEK "Atterrissage forcé des avions légers. Retournement-Première phase d'étude expérimentale"
IMFL, 22.12.1986, Rapport n° 86/71

[19] P. GEOFFROY "Crash des avions sur piste - Développement d'un superélément pour l'analyse non linéaire d'une poutre"
IMFL, 15.12.1987, Rapport n° 87/56

Tableau 1

RAPPORTS de SIMILITUDE

	DIMENSIONS	RAPPORTS	VALEURS n = 1/3
.LONGUEUR	L	$n < 1$	0,3333
.POIDS	M	n^3	0,03704
.TEMPS	T	n	0,3333
.MASSE VOLUMIQUE	ML^{-3}	1	
.MODULE ELASTIQUE	$ML^{-1}T^{-2}$	1	
.CONTRAINTE	$ML^{-1}T^{-2}$	1	
.ALLONGEMENT RELATIF	1	1	
.VITESSE	LT^{-1}	1	
.ACCÉLERATION LINEAIRE	LT^{-2}	n^{-1}	3
.FORCE	MLT^{-2}	n^2	0,1111
.ENERGIE ABSORBEE	ML^2T^{-2}	n^3	0,03704
.CONSTANTE DE VITESSE D'ALLONGEMENT	T	n	0,3333
.FACTEUR D'INTENSITE DE CONTRAINTE Kc	$ML^{-1/2}T^{-2}$	$n^{1/2}$	0,5773

Tableau 2

INFLUENCE DE LA MODELISATION DES LIAISONS

RAIDISSEURS EQUIVALENTS	≡ EQUIVALENT
EXTREMITES BISEAUTEES	• 2017 A RIVETS • REDONDANTE EN ACIER
BRIDAGE	BRIDAGE, CAISSON, PLATES • BRIDE • NON BRIDE
JOINT	• CAISSON DE REF. RAIDISSEURS EN Z NON BISEAUTES. RIVETS 2117 • RIVETS EQUIVALENTS EN 2017 A ($Re_{0,2}$ et R_r) • BOULONNERIE ACIER AVEC $Re_{0,2}$ EQUIVALENTE • BOULONNERIE REDONDANTE EN ACIER
COLLAGE	ENTRE PANNEAUX ET RAIDISSEURS EN Z — ZONE DE COLLAGE ENTRE AILES DES EQUERRES ET PANNEAUX — ZONE DE COLLAGE

Figure 1

COMPARAISON DES RESULTATS D'ESSAIS

SUR MAQUETTES Ech. 1/3 ET EN VRAIE GRANDEUR

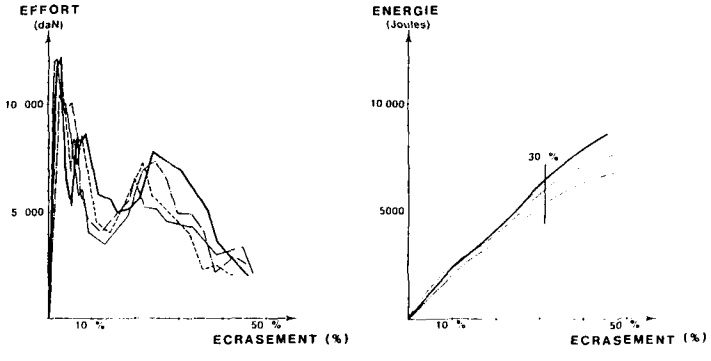

LIAISONS RIVETEES

—— VRAIE GRANDEUR

MAQUETTES

Figure 2

COMPARAISON DES ESSAIS MAQUETTE Ech. 1/3 ET EN VRAIE GRANDEUR

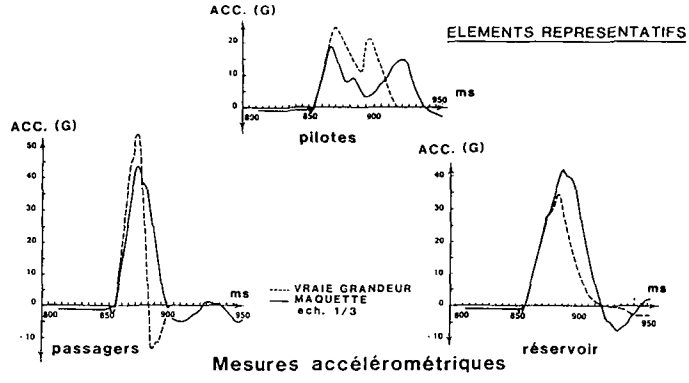

Mesures accélérométriques

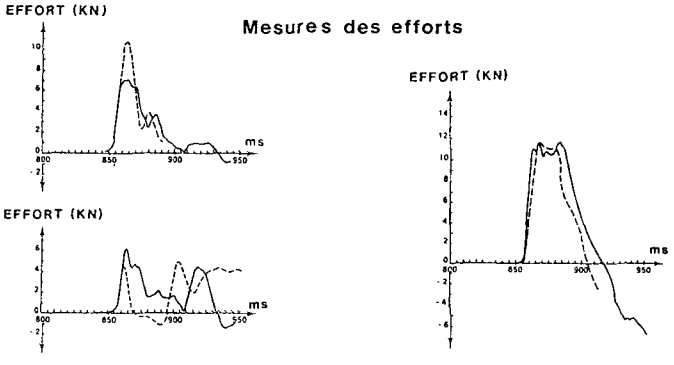

Mesures des efforts

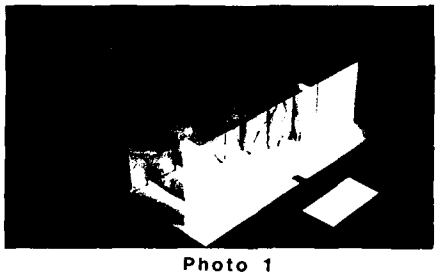

Photo 1

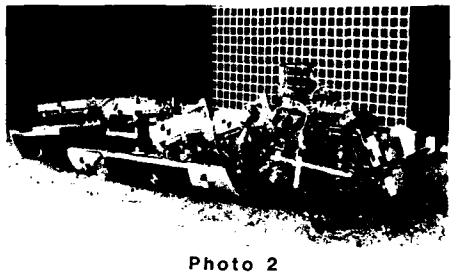

Photo 2

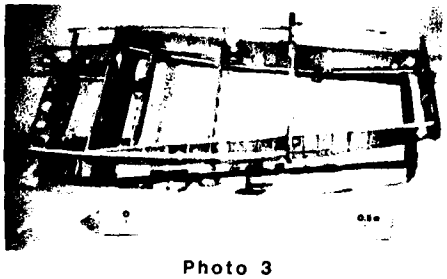

Photo 3

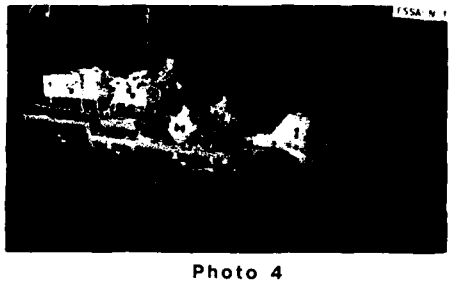

Photo 4

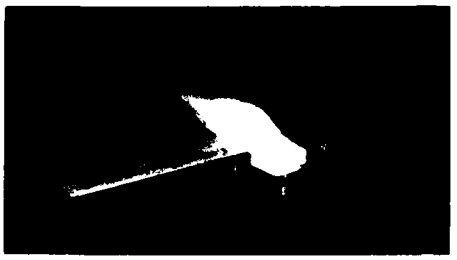

Photo 5

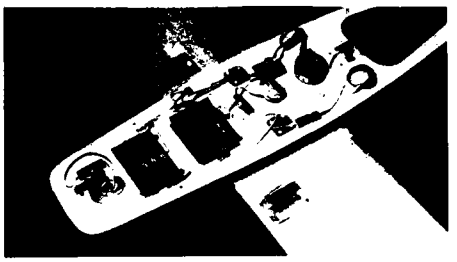

Photo 6

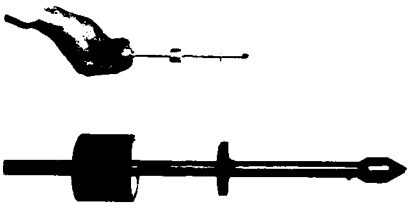

Photo 7

Figure 3

Instrumentation de l'installation d'essai

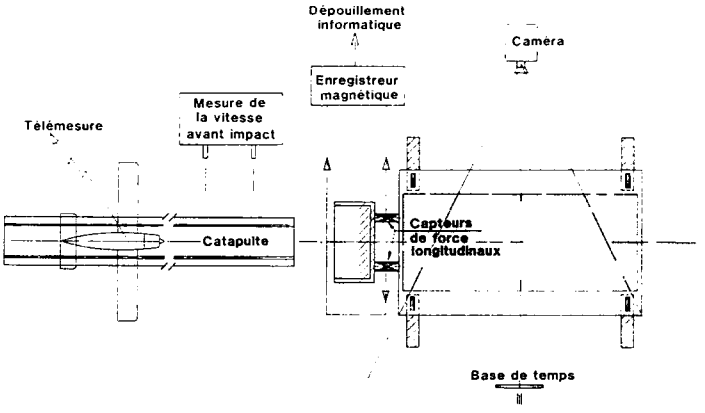

Figure 4

Sols retenus dans le cadre de l'étude

Type de Sol	Energie de pénétration en Vertical (J/m)	Matériaux utilisés pour la représentation à l'Echelle Réduite
Terre de Labour	350	Sable de Seine
		Terre Tamisée
Piste d'atterrissage en Herbe	700 < E < 1400	Terre Tamisée
Terrain en Herbe détrempé	550	50 % Sable de Seine 50 % Terre Tamisée

Figure 5

Dispositif de pesée de sol en longitudinal

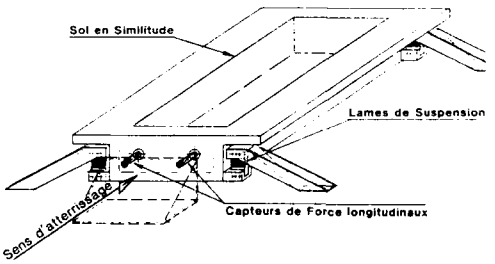

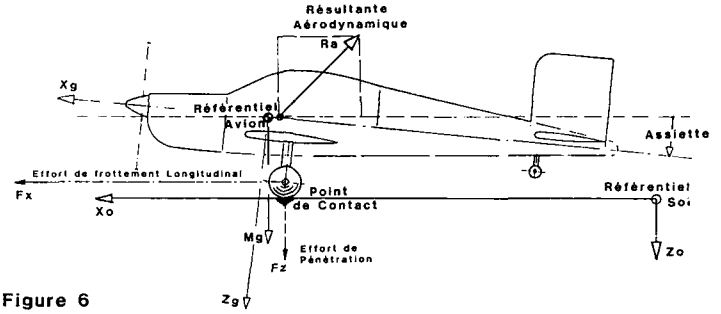

Figure 6

Efforts pris en compte dans le cadre de l'Etude Numérique du Retournement

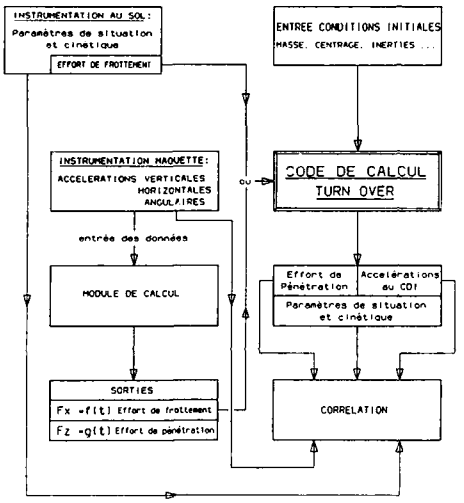

Figure 7 Articulation du programme vis à vis de la phase expérimentale

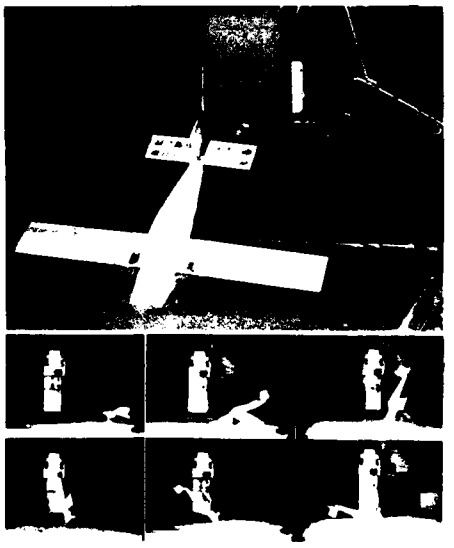

Figure 8

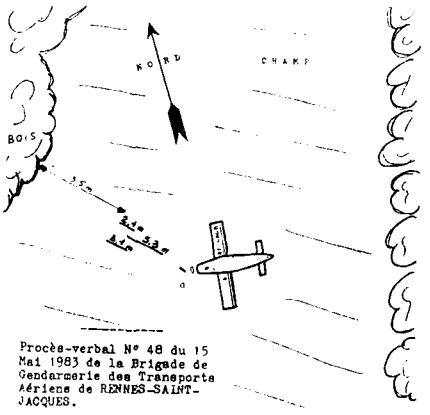

Procès-verbal N° 48 du 15 Mai 1983 de la Brigade de Gendarmerie des Transports Aériens de RENNES-SAINT-JACQUES.

Figure 9 Compte rendu d'accident de l'avion Rallye F-GDGB

	Avion F-GDGB	Essais sur maquette et sol en similitude
Distance de pénétration Train Arrière	2,1 m < D < 3,1 m	2,8 m
Distance de pénétration Train Avant	5,3 m	4,9 m

Figure 10 **Comparaison des distances de pénétration des trains dans le sol**
- **Compte rendu d'accident de l'avion F-GDGB**
- **Essais sur maquette représentative et sol à 350 Joules/mètre**

Configuration de sol / Type d'avion	Terre de labour 350 J/m (Sable de Seine)	
	Accélération Verticale	Accélération Longitudinale
Train Tricycle	40 ➪ 45	65 ➪ 70
Train Tricycle Maquette allourdie	55	70 ➪ 85
Train Tricycle Maquette allourdie Avec variation de Centrage et d'Inertie	85	120
Train Classique Maquette allourdie	40	60 ➪ 70
Train Classique	40 ➪ 45	60 ➪ 70

Figure 11

Accélérations mesurées (m/s²)

à l'impact du train de l'avion

sur le sol.

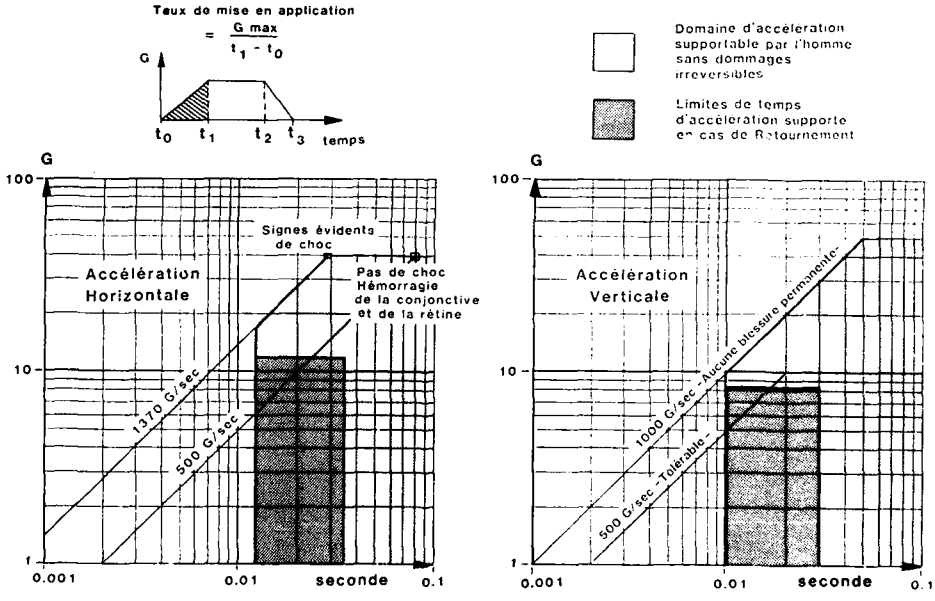

Figure 12 Taux d'accélération horizontal et vertical supportable par l'individu
(Courbes de WEBB et EIBAND)

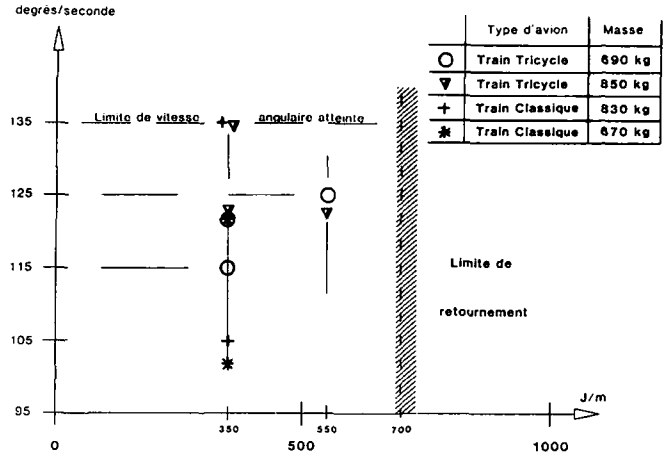

Figure 13 Enveloppe des vitesses angulaires atteintes à l'impact de la verrière en fonction de l'énergie de pénétration en verticale.

Types de sols / Avions	350 J/m Sable de Seine	350 J/m Terre Tamisée	550 J/m Sable de Seine + Terre Tamisée	700 ← 1400 J/m
Train Tricycle (M= 690 kg)	115	120	125	Pas de Retournement
Train Tricycle Maquette allourdie (M= 850 kg)	122	135	122	Pas de Retournement
Train Classique Maquette allourdie (M= 830 kg)	105	135	Pylone	Pas de Retournement
Train Classique (M= 670 kg)	100	120	Pas de Retournement	Pas de Retournement

Figure 14 Vitesses angulaires moyennes (en degrés/seconde) atteintes à l'impact de la verrière en fonction des caractéristiques géométriques.

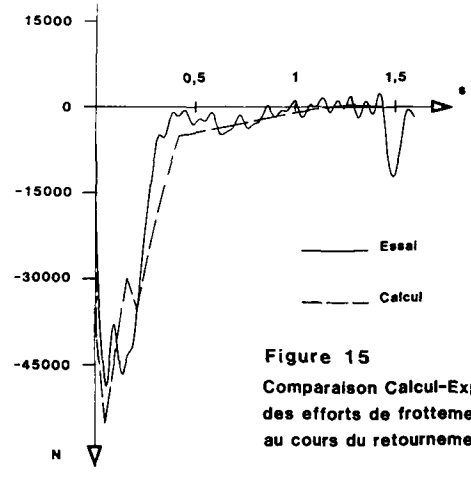

Figure 15
Comparaison Calcul-Expérience des efforts de frottement longitudinaux au cours du retournement

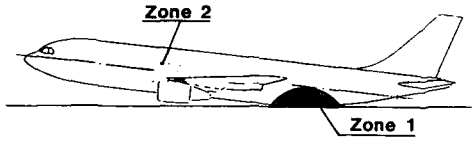

Figure 16

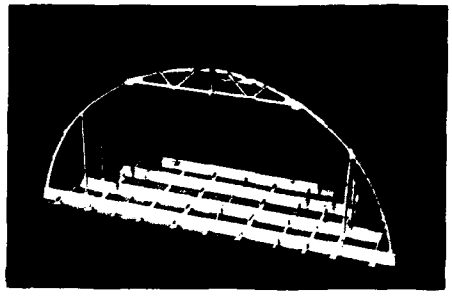

Figure 17

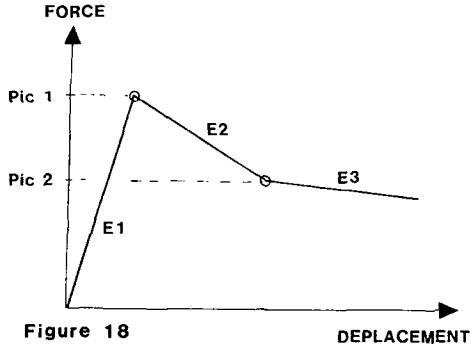

Figure 18

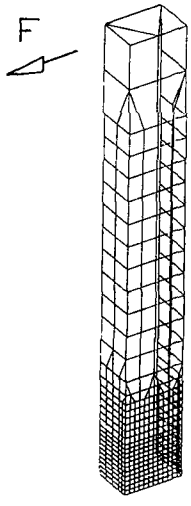

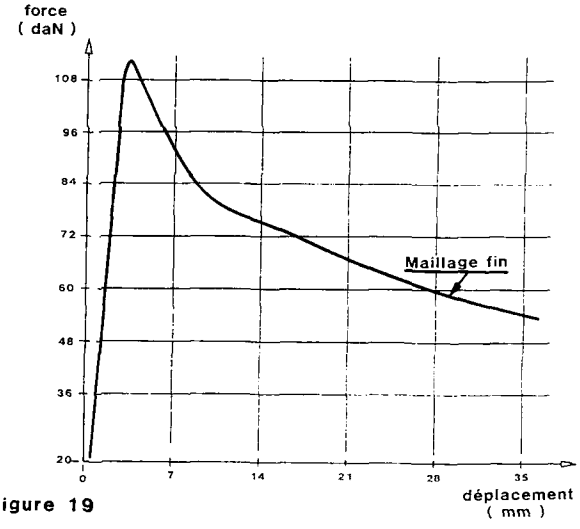

Figure 19

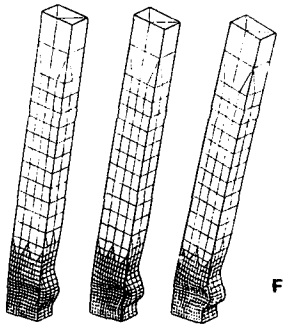

Figure 20

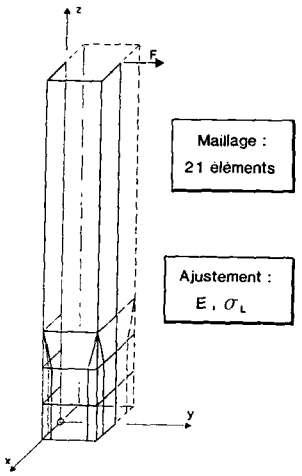

Figure 21

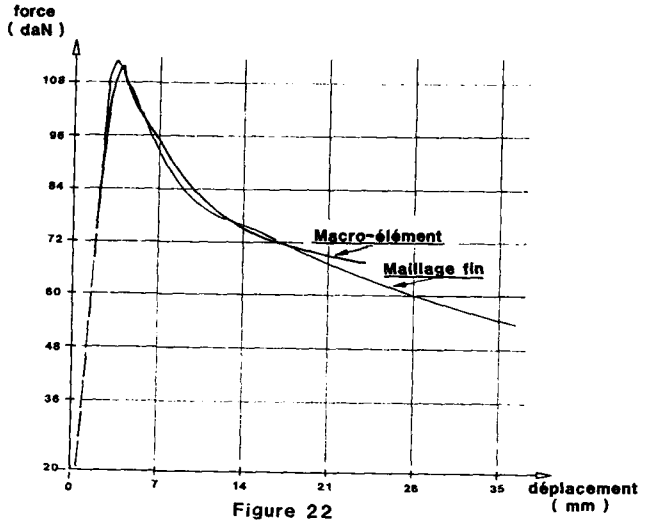

Figure 22

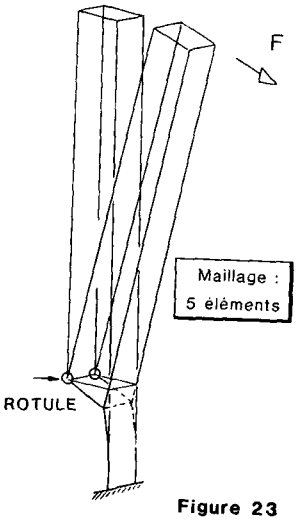

Figure 23

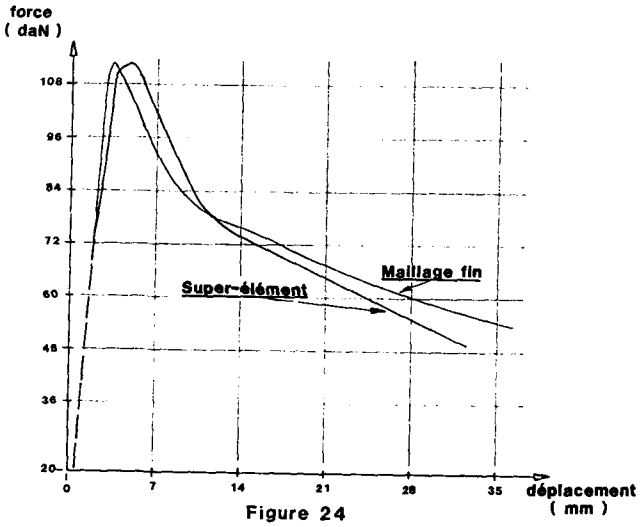

Figure 24

STUDY OF

THE DYNAMIC BEHAVIOUR OF STIFFENED COMPOSITE FUSELAGE SHELL STRUCTURES

by

J. S. Hansen and R. C. Tennyson
University of Toronto Institute for Aerospace Studies
4925 Dufferin Street
Downsview, Ontario, Canada
M3H 5T6

Summary

This report presents an overview of the development of a computer model for analysing the crash response of stiffened composite fuselage structures together with the experimental validation program. Using a finite element formulation based on Reissner/Mindlin plate theories, the numerical model can treat stiffened laminated shell buckling, large deflections, nonlinear material behaviour and element failure. Numerical results are presented for several "test cases", although experimental comparisons are not yet available. Details on the design and construction of our first prototype composite fuselage model are also provided together with a description of the crash test facility.

1. INTRODUCTION

Polymer based composite materials are rapidly replacing metals in the construction of civil and military fixed wing and rotary wing aircraft. Much of this material substitution is driven by the desire to reduce weight, thus increasing payload and fuel economy. For military aircraft, additional benefits accrue in the form of improved performance and reduction of radar cross-section (i.e., stealth technology). Using the design opportunities now available with composite structures also permits structural and aeroelastic optimization, again leading to lower specific weight, higher specific strength and stiffness systems. More recently, aircraft designers are now looking toward composite "smart structures" where optoelectronic sensors and fiber optic grids in the laminates can be incorporated during the manufacturing stage. Such sensor systems can provide real-time structural integrity monitors, damage detectors and flight-worthiness information. There is no doubt that industry is indeed moving in the direction of composite aircraft and rotorcraft when one considers the prototypes that have already been manufactured and the material usage projections illustrated in Figs. 1 and 2. Although military aircraft tend to exploit technology to the fullest, it is only a matter of time when the same technology is utilized by the civil aviation industry as well.

One of the major problems associated with composite fuselage structures is their ability to absorb impact damage. It is well known that carbon reinforced matrices of the thermoset type are indeed brittle in nature and sub-surface delamination and cracking are common even for relatively low levels of impact. More recently of course, thermoplastic resins with substantially higher impact toughness are now available (e.g., PEEK) and permit composite structures to be manufactured that will be superior in terms of their impact behaviour. Clearly it is imperative at this stage in the evolution of composite airframes that crashworthiness be incorporated into the design. From the military point of view it is essential for performance and survivability. In the civil and commercial marketplace, these factors are of equal concern, but the additional necessity of aircraft certification places the onus on the manufacturer to demonstrate performance and reliability compliance.

The objective of crashworthiness design is to determine a minimum weight system at an acceptable cost which provides the highest probability of occupant survival with minimal injuries in a prescribed crash environment. Such design features must necessarily consider the aircraft structure, fuel systems, seat restraints, human tolerance levels and the crash environment (i.e., hard landing, plowing, snow or water). However, the major design requirement is to maintain structural integrity of the cabin-fuselage and acceptable seat loading by ensuring that sufficient ability to absorb energy exists, which thus reduces decelerative forces on the occupants and hazardous large masses (i.e., high wing aircraft), and that a protective shell be maintained around the occupied area during a crash. The need to provide for post-crash emergency egress through operative exits is also an important requirement of structural crashworthiness design.

The development of a comprehensive computer analysis is essential to the aircraft design team for evaluating and optimizing the crashworthiness of the aircraft structures, particularly during the early design phases. Designing a crash-resistant structure and seat configuration necessitates an understanding of the behaviour of a complex structure deforming under various impact loads. Testing of full scale aircraft or scale models is extremely expensive and difficult. Consequently, the experimental approach alone is undesirable. Computer techniques are needed which adequately consider large deflections, nonlinear material response, local buckling and post-buckling behaviour, as well as isolated component fractures. From an economic view, it is desirable to develop the simplest feasible mathematical model representation of the actual structure, while maintaining an acceptable level of accuracy. The cost restrictions place constraints on the total number of degrees of freedom that can be retained in the model, the number of elements that may exhibit material and/or structural nonlinearity, and the number of times the system stiffness matrix can be re-assembled, inverted, and/or transformed in a dynamic analysis.

The following report briefly describes the development of a finite-element computer model for stiffened composite fuselage structures and outlines the experimental program involving the construction and testing of composite fuselage models. The interested reader can refer to Ref. 3 for a description of earlier work by the authors on stiffened metallic fuselages.

2. DEVELOPMENT OF COMPUTER MODEL

Code Characteristics

The present finite element code has been developed specifically for the analysis of impulsively loaded shell and plate structures of arbitrary material construction. The formulation is based on Reissner-Mindlin plate theory and allows full nonlinear geometric and material effects and considers homogeneous isotropic and laminated composite materials. In addition, isotropic and/or composite stringers and ribs can be included. A range of implicit time integration schemes are accessible to the user including the Wilson-θ, Newmark-β and α methods. These techniques permit the integration of the dynamics equations using relatively large time steps while ensuring an accurate and stable numerical solution. Failure and yielding analyses are provided as appropriate for both metallic and composite material systems. For composite materials, the user has the option of specifying either a maximum stress, maximum strain or quadratic tensor polynomial failure criterion. A failure analysis can be performed as an integral part of the response calculation or through the use of a post-processor.

Element Formulation

The following provides a brief overview of the element formulation. More details may be obtained from Refs. 5 and 6.

Application of the finite element method to problems of this nature requires solution of the semi-discretized motion equation

$$M\underline{a} + N(\underline{d}) = \underline{F}(t) \tag{1}$$

In this equation M is the mass matrix while $\underline{a}$, $\underline{v}$, $\underline{d}$ and $\underline{F}(t)$ are the acceleration, displacement and force vectors respectively. The third term, $N(\underline{d})$, is the internal force or stiffness term which is nonlinear in the displacements.

In the formulation it was desired that the element possess the capability of dealing with all combinations of thick/thin and shallow/deep shells, including plates, and at the same time allow nonlinear strain-displacement relations and elasto-plastic material behaviour and the modelling of composite materials. To accomplish this, an element based on Reissner[7] or Mindlin[8] plate theory was developed.

The use of a Reissner or a Mindlin type of plate theory in finite element formulations for plates and shells is well established and has been shown to give good results for thin to moderately thick configurations. This approach has the advantage that independent displacement and rotation trial functions may be used and that these functions need only be C^0 continuous.

The present element is formulated in shell coordinates. Thus, an accurate geometic representation is achieved which overcomes the difficulties that approximations to the geometry can produce.[9] Correspondingly, the following nonlinear strain-displacement relations were utilized.

$$\varepsilon_{xx} = \frac{1}{\alpha}\left[\frac{\partial u}{\partial x} + \frac{v}{\beta}\frac{\partial \alpha}{\partial y} + w\frac{\partial \alpha}{\partial z}\right] + \frac{1}{2}\left(\frac{1}{\alpha}\frac{\partial w}{\partial x}\right)^2 \tag{2}$$

$$\varepsilon_{yy} = \frac{1}{\beta}\left[\frac{\partial v}{\partial y} + \frac{u}{\alpha}\frac{\partial \beta}{\partial x} + w\frac{\partial \beta}{\partial z}\right] + \frac{1}{2}\left(\frac{1}{\beta}\frac{\partial w}{\partial y}\right)^2 \tag{3}$$

$$\gamma_{xy} = \left[\frac{1}{\beta}\frac{\partial u}{\partial y} + \frac{1}{\alpha}\frac{\partial v}{\partial x} - \frac{v}{\alpha\beta}\frac{\partial \beta}{\partial x} - \frac{u}{\alpha\beta}\frac{\partial \alpha}{\partial y}\right] + \frac{1}{2}\left(\frac{1}{\alpha\beta}\frac{\partial w}{\partial x}\frac{\partial w}{\partial y}\right) \tag{4}$$

$$\gamma_{yz} = \left[\frac{\partial v}{\partial z} + \frac{1}{\beta}\frac{\partial w}{\partial y} - \frac{v}{\beta}\frac{\partial \beta}{\partial z}\right] \tag{5}$$

$$\gamma_{zx} = \left[\frac{\partial u}{\partial z} + \frac{1}{\alpha}\frac{\partial w}{\partial x} - \frac{u}{\alpha}\frac{\partial \alpha}{\partial z}\right] \tag{6}$$

Here (x, y, z) are orthogonal curvilinear coordinates such that x and y lie at the mid-surface of the shell, and z is normal to the mid-surface (Fig. 3). The tangential displacements, u and v, are in the x and y directions respectively, w is the normal displacement while α and β are the Lamé coefficients. The normal strain ε_{zz} has not been included in the above equations in anticipation of the requirements of the Reissner-Mindlin formulation which follows.

The Lamé coefficients are defined by $\alpha = A(1+zC_x)$ and $\beta = B(1+zC_y)$ and the curvatures C_x and C_y are defined as the reciprocals of the principal radii of curvature, that is $C_x = 1/R_x$, $C_y = 1/R_y$.

In order that the present results not be restricted to thin or shallow shells, the factors $1/\alpha$ and $1/\beta$ in Eqs. 2-6 are expanded in binomial series that are subsequently truncated to the terms of $O(z^2)$.

In order to treat moderately thick shells it is necessary to include the transverse shear stresses τ_{zy} and τ_{zx} in the strain energy while at the same time taking σ_{zz} to be negligible. It has been shown[11] that, when the effect of transverse shear is included in a plate analysis, the normal deflection and rotation measure that is most convenient to use is a weighted average of the normal deflection over the thickness of the plate and "a pair of rotation variables that are, equivalent but not identical with the components of change of slope of the normal to the undeformed middle surface".[7] With this in mind, the spatial dependence of the displacements is represented in the form

$$u(x,y,z) = \bar{u}(x,y) + z\psi_x(x,y) \tag{7}$$

$$v(x,y,z) = \bar{v}(x,y) + z\psi_y(x,y) \tag{8}$$

$$w(x,y,z) = \bar{w}(x,y) \tag{9}$$

where for $\bar{u}$ and $\bar{v}$ the superposed bar indicates the displacement evaluated at the mid-surface and, as indicated above $\bar{w}$, ϕ_x and ϕ_y are the measures of normal displacement and rotation. These five displacements and rotations are the nodal degrees of freedom associated with each node in the finite element model (see Fig. 3).

The strain-displacement relations can be expressed as[1]

$$\underset{\sim}{\varepsilon}^0 = \left(B_L + \frac{1}{2} B_N\right) \underset{\sim}{d} = B_T \underset{\sim}{d} \tag{10}$$

where the displacement vector $\underset{\sim}{d}^T = (\bar{u}, \bar{v}, \bar{w}, \phi_x, \phi_y)$ and the strain vector $\underset{\sim}{\varepsilon}^{0T} = (\varepsilon_{xx}, \varepsilon_{yy}, \gamma_{xy}, \gamma_{yz}, \gamma_{zx})$. The operator B_L is the linear part of the strain-displacement operator and arises from the terms in square brackets [ ] in Eqs. (2)-(5) while B_N is the nonlinear part of the operator that arises from the terms in parentheses ( ) in Eqs. (2)-(4).

Constitutive Relation

The constitutive relation for a lamina, including transverse shear terms is given by (Fig. 4),

$$\begin{bmatrix} \sigma_{xx} \\ \sigma_{yy} \\ \tau_{xy} \\ \hline \tau_{yz} \\ \tau_{zx} \end{bmatrix} = \left[\begin{array}{ccc:cc} \bar{Q}_{11} & \bar{Q}_{12} & \bar{Q}_{13} & 0 & 0 \\ \bar{Q}_{21} & \bar{Q}_{22} & \bar{Q}_{23} & 0 & 0 \\ \bar{Q}_{31} & \bar{Q}_{32} & \bar{Q}_{33} & 0 & 0 \\ \hline 0 & 0 & 0 & \bar{Q}_{44} & \bar{Q}_{45} \\ 0 & 0 & 0 & \bar{Q}_{54} & \bar{Q}_{55} \end{array}\right] \begin{bmatrix} \varepsilon_{xx} \\ \varepsilon_{yy} \\ \gamma_{xy} \\ \gamma_{yz} \\ \gamma_{zx} \end{bmatrix} \tag{11}$$

or, in terms of membrane (m) and transverse (s) components

$$\begin{bmatrix} \underset{\sim}{\sigma}_m \\ \underset{\sim}{\sigma}_s \end{bmatrix} = \begin{bmatrix} \bar{Q}_m & 0 \\ 0 & \bar{Q}_s \end{bmatrix} \begin{bmatrix} \underset{\sim}{\varepsilon}_m \\ \underset{\sim}{\varepsilon}_s \end{bmatrix} \tag{12}$$

or $\underset{\sim}{\sigma} = D'\underset{\sim}{\varepsilon}$. After integrating through the laminate thickness* (Fig. 5), the stress and moment resultants are given by,

$$\begin{bmatrix} \underset{\sim}{N} \\ \underset{\sim}{Q} \end{bmatrix} = \begin{bmatrix} N_{xx} \\ N_{yy} \\ N_{xy} \\ \hline Q_{yz} \\ Q_{zx} \end{bmatrix} \triangleq \int_{-h/2}^{h/2} \begin{bmatrix} \sigma_{xx} \\ \sigma_{yy} \\ \tau_{xy} \\ \hline \tau_{yz} \\ \tau_{zx} \end{bmatrix} dz \tag{13}$$

*Integration through the finite element thickness takes place in the code, described later.

$$\underset{\sim}{M} = \begin{bmatrix} M_{xx} \\ M_{yy} \\ M_{xy} \end{bmatrix} \triangleq \int_{-h/2}^{h/2} z \begin{bmatrix} \sigma_{xx} \\ \sigma_{yy} \\ \tau_{xy} \end{bmatrix} dz \tag{14}$$

If one re-writes the in-plane strains in the form

$$\underset{\sim}{\varepsilon}_m = \underset{\sim}{\varepsilon}^0 + z\underset{\sim}{K}^0$$

where $\underset{\sim}{\varepsilon}^0$ and $\underset{\sim}{K}^0$ are the midsurface strains and curvatures, respectively, the stress and moment resultants take the form

$$\begin{bmatrix} \underset{\sim}{N} \\ \underset{\sim}{Q} \\ \underset{\sim}{M} \end{bmatrix} = \begin{bmatrix} A & 0 & B \\ 0 & G & 0 \\ B & 0 & D \end{bmatrix} \begin{bmatrix} \underset{\sim}{\varepsilon}^0 \\ \underset{\sim}{\varepsilon}_s \\ \underset{\sim}{K}^0 \end{bmatrix} \tag{15}$$

where

$$(A, B, D) \triangleq \int_{-h/2}^{h/2} (1, z, z^2)\, \bar{Q}_m dz \tag{16}$$

and

$$G \triangleq \int_{-h/2}^{h/2} \bar{Q}_s dz \tag{17}$$

Furthermore, shear correction factors (κ_{ij}) can be incorported in the matrix 'G' in the form,

$$G = \begin{bmatrix} \kappa_{11}^2 G_{11} & \kappa_{12}^2 G_{12} \\ \kappa_{12}^2 G_{21} & \kappa_{22}^2 G_{22} \end{bmatrix} \tag{18}$$

It should be noted that various expressions can be used for these shear correction factors,[12] but results presented in this report indicate little difference based on the varying assumptions.

Mass/Stiffness Matrices and Consistent Force Vector

The equilibrium equations were obtained through the application of the principle of virtual work. Specifically,

$$\int_V \delta\underset{\sim}{d}^T \rho\, \ddot{\underset{\sim}{d}}\, dV + \int_V [B_T \delta\underset{\sim}{d}]^T\, \underset{\sim}{\sigma}\, dV - \int_V \delta\underset{\sim}{d}^T\, \underset{\sim}{b}\, dV - \sum_i \int_{A_i} \delta\underset{\sim}{d}^T\, \underset{\sim}{S}_i\, dA_i = 0 \tag{19}$$

where $\delta\underset{\sim}{d}$ is the vector of virtual displacements, $\underset{\sim}{b}$ is the vector of applied body forces, $\underset{\sim}{S}_i$ represents the surface traction applied to one of the domain surfaces A_i. For a general shell the volume element $dV = \alpha\beta dxdydz$.

The inertial force term of Eq. (1) arises from the first term of Eq. (19) which can be expressed as

$$\int_A \delta\underset{\sim}{d}\, \tau\, \ddot{\underset{\sim}{d}}\, AB\, dxdy \tag{20}$$

after integration through the thickness of the element, where τ is the inertia matrix. For isotropic homogeneous materials and for laminated composites in which every ply has the same density, τ takes the form

$$\tau = \begin{bmatrix} \rho h + \frac{\rho h^3 C_x C_y}{12} & 0 & 0 & \frac{\rho h^3}{12}(C_x + C_y) & 0 \\ 0 & \rho h + \frac{\rho h^3 C_x C_y}{12} & 0 & 0 & \frac{\rho h^3}{12}(C_x + C_y) \\ 0 & 0 & \rho h + \frac{\rho h^3 C_x C_y}{12} & 0 & 0 \\ \frac{\rho h^3}{12}(C_x + C_y) & 0 & 0 & \frac{\rho h^3}{12} & 0 \\ 0 & \frac{\rho h^3}{12}(C_x + C_y) & 0 & 0 & \frac{\rho h^3}{12} \end{bmatrix} \tag{21}$$

For arbitrary layered materials, τ will be more complicated; it is evaluated in the code by an exact integration through the thickness of the element.

Upon discretizing the displacements using bicubic Lagrange polynomials and integrating using fourth order Gauss quadrature in both the x and y directions, the consistent mass matrix is obtained.

For the second term of Eq. (19) it may be shown that

$$\delta(B_T \underset{\sim}{d}) = (B_L + B_N)\delta\underset{\sim}{d} \tag{22}$$

and consequently the second term of Eq. (19) yields

$$\int_V [B_T\ \delta\underset{\sim}{d}]^T \underset{\sim}{\sigma}\, dV = \delta\underset{\sim}{d} \left[\int_V (B_L + B_N)^T D' (B_L + \frac{1}{2} B_N) dV \right] \underset{\sim}{d} \tag{23}$$

In Eq. (23), D' is the constitutive relation which may represent either the properties of an isotropic or a layered composite material (see Eq. 12). It is to be noted that for isotropic materials D' can take the form of an elasto-plastic material including strain-hardening effects. For this situation, the element thickness is divided into a user specified number of layers to allow plastic growth at any location through the thickness. This provides the internal force term of Eq. (1) as (with $dV = \alpha\beta dxdydz$)

$$N(\underset{\sim}{d}) = \left[\int\int\int (B_L + B_N)^T D' (B_L + \frac{1}{2} B_N) \alpha\beta dxdydz \right] \underset{\sim}{d} \tag{24}$$

For both the isotropic and composite materials, exact integration through the thickness is used.

As in the case of the mass matrix, the displacements are modelled using bicubic Lagrange polynomials and integration is accomplished using fourth order Gauss quadrature. This calculation yields the internal force term or the nonlinear stiffness matrix.

The final term in Eq. (19) yields the consistent force vector. For illustrative purposes only, a normal pressure acting on an x-y surface is demonstrated, but other surface tractions are treated in an analogous manner. For notational convenience the applied normal surface load is given in vector form such that $\underset{\sim}{S}_z = [0,0,P_z,0,0]^T$ and therefore the virtual work associated with such a load is

$$\delta W = \int_A \delta\underset{\sim}{d}^T \underset{\sim}{S}_z\, dA = \int_{A_e} \delta\underset{\sim}{d}_e^T N^T \underset{\sim}{S}_z dA_e \tag{25}$$

where the subscript e implies element and the matrix of basis functions N, relates the discrete nodal variables to the continuous displacement field. For an x-y surface of an arbitrary shell $dA = \alpha\beta dxdy$ and the element consistent force vector is

$$\underset{\sim}{F}_e = \iint N^T \underset{\sim}{S}_z \alpha(Z_a)\, \beta(Z_a) dxdy \tag{26}$$

where Z_a is the value of z for the surface at which the load is applied.

Note that for a plate or shallow shell the force is considered to be applied to the mid-surface but for shells with significant curvature it is important to designate the surface to which the lod is applied.

Stringer and Rib Stiffness

In the present code, composite and metallic stiffener elements have been developed using a Timoshenko beam model. This approach has been adopted since the Timoshenko beam can be considered as a one-dimensional version of the Reissner-Mindlin plate theory and thus compatibility of the plate and stiffener is ensured. Details of the development may be found in Ref. 12.

3. NUMERICAL TEST CASE RESULTS

To assess the influence of the various shear correction factors, a simply supported laminated plate subjected to a static sine wave lateral pressure was first investigated (see Fig. 6). Comparison with Whitney's[14] solution is shown together with finite element solutions obtained using various shear correction factors, as noted in Fig. 6. In all cases the finite element results lie above Whitney's curve. The best agreement is obtained using the shear correction factors due to Reissner,[7] with some discrepancy apparent using the results of Bert[15] and Vinson.[16]

The response of a composite spherical cap subject to a centre-point load was also investigated. The shell geometry and material properties are presented in Fig. 7 where comparison is made to the analytical solution of Reddy.[17] The shear correction factors used in the finite element formulation were those due to Reissner[7] and Bert.[15] Quarter symmetry was utilized in the model and two meshes were employed, a single element and a four element (2×2) mesh. The results reported in Fig. 7 indicate that the solution achieved with the shear correction factors derived from Bert will converge to a solution which is significantly different from that determined by Reddy. However, the results obtained when Reissner's shear correction factor is used appear to be converging towards the analytical result. While Reddy indicates the presence of shear correction factors in his formulation there is no indication of the values he used so that the disagreement may be due to differences in the shear correction factors used in each formulation.

The nonlinear geometry formulation was investigated by means of a simply supported circular arch (homogeneous isotropic material) with a central point load as shown in Fig. 8. Keeping the chord of the arch constant, the effect of changing the radius of curvature was investigated. Based on the results of Sabir and Lock,[18] the radii chosen for the tet cases were R = 800 in. and 400 in. The first of these is too large to allow buckling of the arch (Fig. 9) but the second case (Fig. 10) demonstrated severe buckling. Note that this problem has been restricted to symmetric buckling and that half-symmetry has been utilized in the finite element models. It can be seen that the finite element solutions have converged to the analytical results[19] with only two elements.

The behaviour of orthogonally stiffened plates is usually treated by an "equivalent plate" model with a modified bending stiffness.[20-22] This approach is commonly regarded as a "smeared" analysis because the contribution of the stiffeners to the overall structural response is distributed or smeared over the whole plate. Consequently, the global response is recovered reasonably well but not the local response. This situation makes comparison difficult but the following example is included in order to give some indication of how well the finite element results compare with the smeared analysis approach. Bares'[22] solution was chosen for comparison purposes.

Since no analytical results were available for a stiffened laminated plate, the example shown in Fig. 11 was used (homogeneous, isotropic). The stiffener and plate geometry together with material properties are also presented in Fig. 11. Quarter symmetry and six elements were utilized in the finite element model with the result that the finite element method underpredicted the centre displacement by 12.7% as compared to Bares. Insofar as the two methods of achieving the answer are completely different, this level of disagreement is considered reasonable.

Dynamic loading of an isotropic circular cylinder was also analysed (see Ref. 23 for details). A nine element mesh of elements was selected such that over the quarter of the cylinder modelled there were three elements in each direction (Fig. 12). The distribution of the elements in the axial (x) direction was uniform with each element covering 1/3 of the cylinder semi-length. In the circumferential (y) direction the elements are proportioned so that the forward 60% of the circumference is covered by two elements and the remaining element spans the aft 40% of the cylinder. This nonuniform spacing was adopted so that a row of nodes would coincide with the 90° point on the cylinder and in addition it provided a more refined discretization over the forward section of the cylinder where the most severe deformations were expected. The finite element model is illustrated in Fig. 12 where the node numbers are indicated by Arabic numerals and the element numbers by Roman numerals. The origin of the x-y shell coordinate system is located at node number 1. Note that the 3×3 mesh had 500 degrees of freedom.

To illustrate the code capabilities, deformed shapes of the cylinder are shown in Fig. 13 after various times from the initiation of the impact loading. Complete details on the numerical model and calculations can be found in Ref. 23. Suffice it to say that this code can determine transient displacements, velocities and accelerations.

At this point in time, numerical results are also being generated for a laminated composite circular cylinder subjected to lateral impact loading. The corresponding dynamic displacements and accelerations will be determined for various asymmetric impact conditions. These results will then be compared to test data. Finally, it is anticipated that the computer model can then be applied to analyse the stiffened composite fuselage model described later in this report. The test model has been constructed and will undergo static and low energy impact loads to provide a basis of comparison for the numerical predictions. If this phase of the program is successful, then flight impact tests will be conducted using the crash facility described in the following sections.

4. EXPERIMENTAL PROGRAM

Crash Test Facility

To provide fuselage models with both forward and vertical velocity components at impact, a pendulum gantry was constructed over a large (12.2 × 3.7m) reinforced concrete pad. This facility was used to simulate a 'free flight' crash test condition and is depicted in the schematic of Fig. 14. The fuselage specimen is suspended from the top pivot point of the gantry by a rigid swing arm which was drawn back above the impact surface with a pullback cable (Fig. 15). Also, a fuselage mounting

fixture is attached to the rigid swing arm by a pyrotechnic bolt tension separator. During a test, the fuselage is released from the pullback cable which permits the model to swing, pendulum style, over the impact surface. Then, the fuselage mounting fixture is separated from the swing arm by the pyrotechnic device at a predetermined angle of incidence. An umbilical cable remains attached to the fuselage for data acquisition throughout the duration of the test. Separation of the fuselage occurs when the rigid swing arm passes through a laser beam, thus triggering the firing of the pyrotechnic separator. Should the pyrotechnic device not fire, the fuselage would continue to swing through, and then back and forth in a pendulum motion over the impact surface. The height of the fuselage above the impact surface at release determines the vertical impact velocity whereas the horizontal velocity component is governed by the amount of fuselage pullback required to raise the model's centre of mass above the desired separation point. The maximum forward velocity that can currently be achieved in this facility is approximately 8 ms^{-1}. The desired pitch angle at separation is set by the adjustment of four cables which connect the mounting fixture to a point on the rigid swing arm just below the separation point. A consequence of this pendulum swing technique is the creation of a large upward pitch rate about the model's centre of mass which must be taken into consideration before testing to obtain the desired pitch angle at surface impact. A barrier was also constructed and placed at the end of the pad to prevent damage to cameras and other surrounding apparatus. Data acquisition from a crash test is accomplished by photography using 16 mm low and high speed cameras, and by onboard strain gauges and accelerometers.

Earlier work by the authors involving metal fuselage models is described in Ref. 3. Figure 16 shows a crash test sequence using such a model (1m diameter × 2.3m length).

Composite Fuselage Model

To provide comparative crash data with the metal fuselage test results, a composite fuselage model of 1m diameter × 2m length was constructed. The first prototype described below was constructed without stringers and subfloor, but was reinforced with twelve light-rib frames and two main load frames for a high wing configuration. The wing load was simulated by attaching 'dead' weights to a rigid mounting fixture which was bolted to both of these interior main frames. This particular geometry was necessary to properly locate the mass centroid and provide the required pitch moment of inertia.

Woven Kevlar® prepreg was used to fabricate the fuselage model instead of unidirectional prepreg since it was found to be easier to cut, handle and lay-up over tools of complex curvatures. One advantage of unidirectional prepreg is that it can be tailored to defined load paths but when these loads are not fully defined, the quasi-isotropic nature of the woven prepreg can be used. Woven prepreg also offers improvements in impact resistance over non-woven structures. The skin material used was Fiberite prepreg MXM-7714/Kevlar49. The 7714 prepreg system was designed specifically for the aircraft industry. It has excellent drape and tack, and adheres well to the tool during lay-up. The prepreg can be cured either in an autoclave, an oven with a vacuum bag, or by pressing techniques. A laminate stacking sequence of 0/90/0 (0° corresponding to the warp fibre along the fuselage length) was used because it produced a shell with a greater axial/hoop stiffness ratio. The higher axial stiffness was required since there were no stringers incorporated in this composite shell and the rib frames provide the transverse stiffness for the fuselage. Fiberite HMF-133/48 woven graphite/epoxy prepreg was selected for the fabrication of the light-ribs and main load-carrying frames.

For the high wing configuration, the four attachments for the wing load are positioned on the two main frames. Reinforced laminated sandwich construction was used for the main frames to eliminate local buckling and failure, details of which can be found in Ref. 24.

A hollow cylindrical wooden mandrel (or tool) was constructed as shown in Fig. 17. The mold was fabricated from two identical structures which were joined together along a plane 3° off the mold horizontal axis (Fig. 18) to provide ease of separation. Each of the segments were made from wood and epoxy, connected together by a steel shaft and plywood end plates. The mold surface was constructed with marine plywood which could be readily shaped to a circular contour and layered with Hysol R9-2039 resin/HD 3404 hardener. Figure 19 shows the Kevlar® skin wrapped in the mold ready for the autoclave. This particular prepreg was cured at 45 psi and 260°F at McDonnell Douglas of Canada in Malton, Ontario. The final stiffened fuselage model with the high wing load fixture is shown on the crash pad in Fig. 20. No flight impact tests have yet been conducted pending a numerical analysis of the model for given load conditions. Clearly, a non-destructive test program must precede a final crash test to optimize the amount of test data that one can obtain from such an expensive test article.

5. ACKNOWLEDGEMENTS

This research was partly funded by the Canadian Defence Research Establishment Suffield, Ralston, Alberta, under Contract No. 03SU.97702-1-3777 and the Natural Sciences and Engineering Research Council of Canada under Grant No. A-2783.

REFERENCES

1. Wilson, D., "Advanced Polymer Composites for High Temperature Applications", Proc. 15th Congress of ICAS, London, Sept. 1986.

2. Plaice, E., "Airframe Manufacturing Using Non-Metals", World Aerospace Profile 1986, Sterling Publications Ltd., London, 1986.

3. Tennyson, R. C. and Hansen, J. S., "Study of the Crash Behaviour of Aircraft Fuselage Structures", Chapter 8, Structural Crashworthiness, Eds. N. Jones and T. Wierzbicki, Butterworths Pub., London, 1983.

4. Heppler, G. R. and Hansen, J. S., "Time Integration of the Equations of Motion of a Structural System Including Damping", AIAA Journal, Vol. 21, No. 9, pp. 1301-1309, Sept. 1983.

5. Heppler, G. R. and Hansen, J. S., "A Mindlin Element for Thick and Deep Shells", Computer Methods in Applied Mechanics and Engineering, V. 54, No. 1, pp. 21-47, Jan. 1986.

6. Hansen, J. S. and Heppler, G. R., "A Mindlin Shell Element which Satisfies Rigid Body Requirements", AIAA Journal, Vol. 23, No. 2, pp. 288-295, Feb. 1985.

7. Reissner, E., "The Effect of Transverse Shear Deformation on the Bending of Elastic Plates", Journal of Applied Mechanics, 67, A69-A77, 1945.

8. Mindlin, R. D., "Influence of Rotary Inertia and Shear on Flexural Motions of Elastic Plates", Journal of Applied Mechanics, 18, pp. 31-38, 1958.

9. Ashwell, D. G. and Gallagher, R. H. (Eds.), "Finite Elements for Thin Shells and Curved Members", John Wiley and Sons, London, 1976.

10. Langhaar, H. L., "Energy Methods in Applied Mechanics", John Wiley and Sons, New York, 1962.

11. Vlasov, V. Z., "General Theory of Shells and Its Applications to Engineering" (Translation), NASA TT F-99, 1964.

12. Hansen, J. S. and Heppler, G. R., "Development of a Finite Element Capability for the Analysis of Structural Systems Subjected to a Blast Environment - Phase II. Beams and Composite Material Shells", Final Report, submitted to Defence Research Establishment Suffield, Ralston, Alberta, Canada, Contract No. 8SG-84-00095, July 1986.

13. Hansen, J. S. and Heppler, G. R., "Development of a Finite Element Capability for the Analysis of Structural Systems Subjected to a Blast Environment", Final Report, submitted to Defence Research Establishment Suffield, Ralston, Alberta, Canada, Contract No. 03SU.977021-3777, Sept. 1984.

14. Whitney, J. M., "The Effect of Transverse Shear Deformation on the Bending of Laminated Plates", J. Comp. Mater. pp. 534-547, July 3, 1969.

15. Bert, Charles W., "Simplified Analysis of Static Shear Factors for Beams of Nonhomogeneous Cross Section", J. Comp. Mater. 9, pp. 525-529, Oct. 1973.

16. Vinson, Jack R. and Chou, Tsu Wei, "Composite Materials and Their Use in Structures", John Wiley and Sons, New York, Halstead Press, 1975.

17. Reddy, N. N., "Exact Solutions of Moderately Thick Laminated Shells", J. Eng. Mech. (ASCE), 110, No. 5, pp. 794-809, 1984.

18. Sabir, A. B. and Lock, A. C., "Large Deflexion, Geometrically Nonlinear Finite Element Analysis of Circular Arches", Int. J. Mech. Sci. 15, pp. 37-47, 1973.

19. Schreyer, Howard L. and Masur, Ernest F., "Buckling of Shallow Arches", J. Eng. Mech. (ASCE), EM4, 92, pp. 1-19, Aug. 1966.

20. Huffington, N. J. Jr., "Theoretical Determination of Rigidity Properties of Orthogonally Stiffened Plates", J. Appl. Mech. 23, pp. 15-20, March 1956.

21. Hoppmann, W. H. and Huffington, N. J. Jr., "A Study of Orthogonally Stiffened Plates", J. Appl. Mech. 23, pp. 343-350, Sept. 1956.

22. Bares, Richard, "Tables for the Analysis of Plates, Slabs and Diaphragms Based on Elastic Theory", Translated by Carel van Amerogen, 2nd Edition, Bauverlag, Wiesbaden, 1971.

23. Heppler, G. R., "On the Analysis of Shell Structures Subjectd to Blast Environment: A Finite Element Approach", University of Toronto Institute for Aerospace Studies, Report No. 302, Feb. 1986.

24. Johnston, J., "Design and Fabrication of a Scaled Composite Fuselage Section", University of Toronto, M.A.Sc. Thesis, 1984.

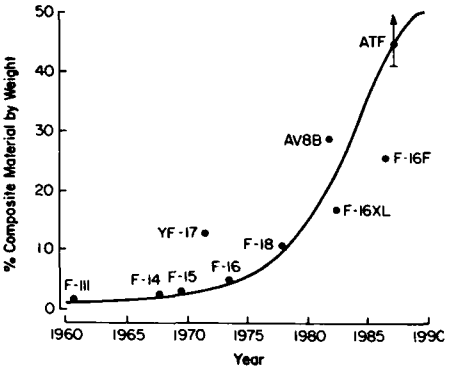

Fig. 1 Composite Usage in Military Aircraft (Ref 1)

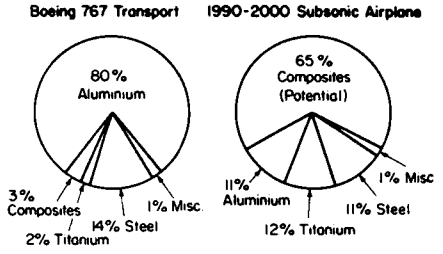

Fig. 2 MATERIALS WEIGHT DISTRIBUTION IN ADVANCED TECHNOLOGY TRANSPORT AIRCRAFT (Ref. 2)

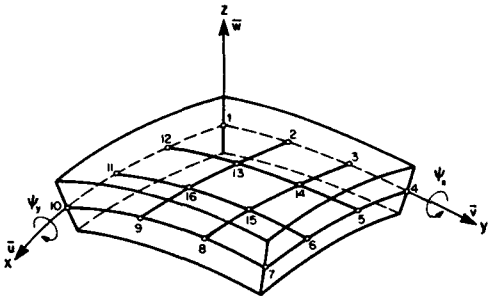

Fig. 3 Element Geometry and Model Degrees of Freedom

Fig. 4 A Composite Material Lamina

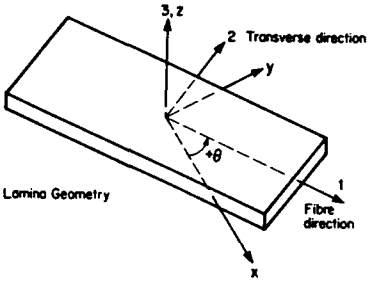

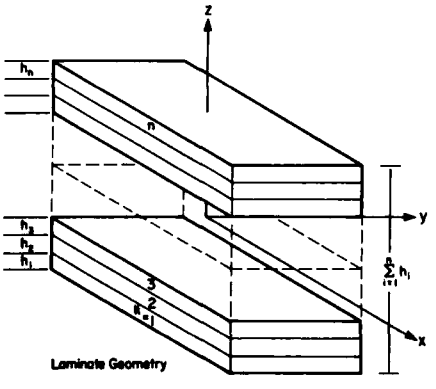

Fig. 5 Laminate Coordinate Frames

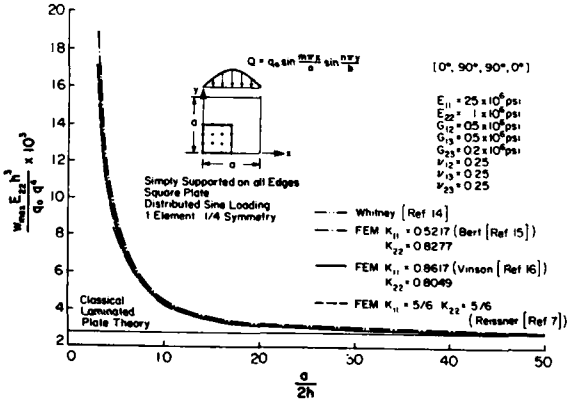

Fig. 6 Double Sine Wave Loading of a Simply Supported Square Plate

SEGMENT OF A SPHERE UNDER A POINT LOAD

$\theta = 0.05$ $\quad P = 100$ $\quad E_{11} = 2.5 \times 10^6$

$A = 0.1$ $\quad E_{22} = 1 \times 10^6$

$\frac{A}{h} = 10$ $\quad G_{12} = 0.5 \times 10^6$

$\frac{R}{A} = 10$ $\quad G_{13} = 0.5 \times 10^6$

$G_{23} = 0.2 \times 10^6$

$\nu_{12} = 0.25$

$\nu_{13} = 0.25$

$\nu_{23} = 0.25$

LAY UP [0,90,90,0]

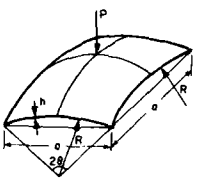

$\bar{w} = \frac{\bar{w} h^3 E_{22}}{Pa^2} \times 10^2$

$\bar{w}_{EXACT} = 5.0186$, J. N. REDDY (Ref 7)

MESH	K_{11}^2	K_{22}^2	$\bar{w}$	%
1 x 1	0.7205	0.5952 (Ref 15)	5.09856	1.6
1 x 1	5/6	5/6 (Ref 7)	4.3623	-13.1
2 x 2	0.7205	0.5952 (Ref 15)	5.59340	11.5
2 x 2	5/6	5/6 (Ref 7)	4.75456	-5.3

Fig. 7 Centre Point Loading of a Square Planform Spherical Cap

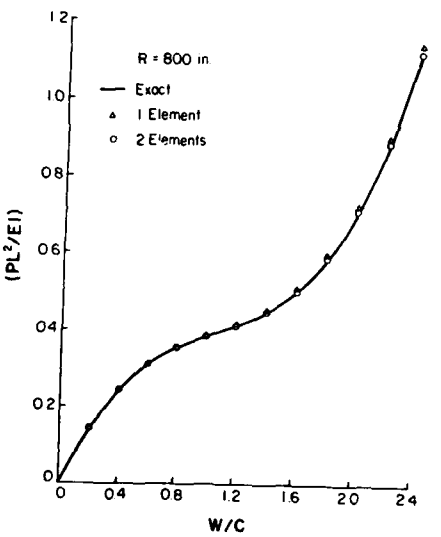

Fig. 9 Simply Supported Circular Arch : R = 800 in. Load-Deflection Response

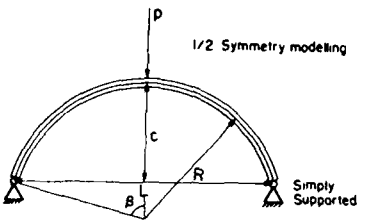

L = 100 in
R = 800," 400," 250"
I = 1/12 in⁴

E = 10^7 psi
ν = 0.3

Fig. 8 Simply Supported Circular Arch : Geometry

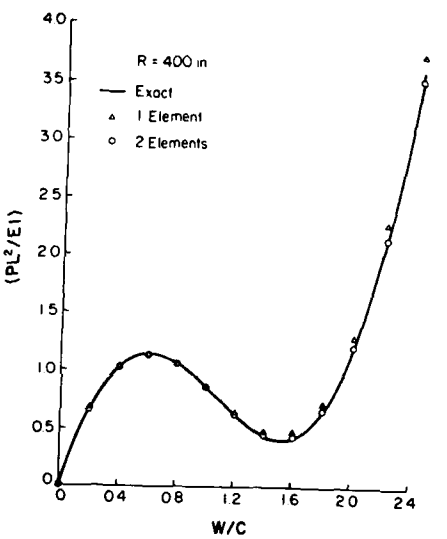

Fig. 10 Simply Supported Circular Arch : R = 400 in. Load-Deflection Results

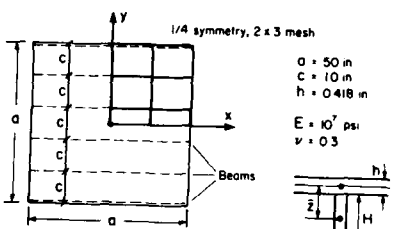

Simply Supported on ALL EDGES
Uniform Load Q = 1 psi

H = 1 in
B = 0.125 in
z̄ = -0.709 in

Analytical Centre point deflection = 0.308 in
Bares, Ref 22

Finite Element Centre point deflection = 0.269 in $\quad \Delta\% = -12.7\%$

Fig. 11 Beam Stiffened Plate Test Geometry

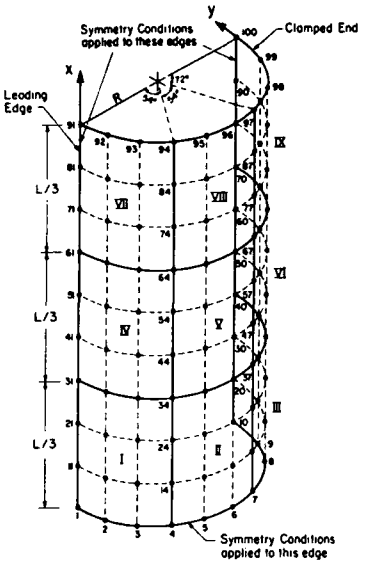

Fig. 12 Cylinder Finite Element Model

Fig 13 Isotropic Cylinder Subjected to Lateral Impact Loading (Ref. 23)

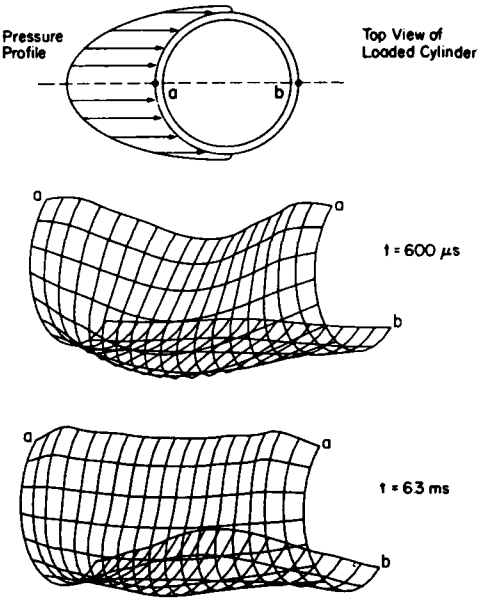

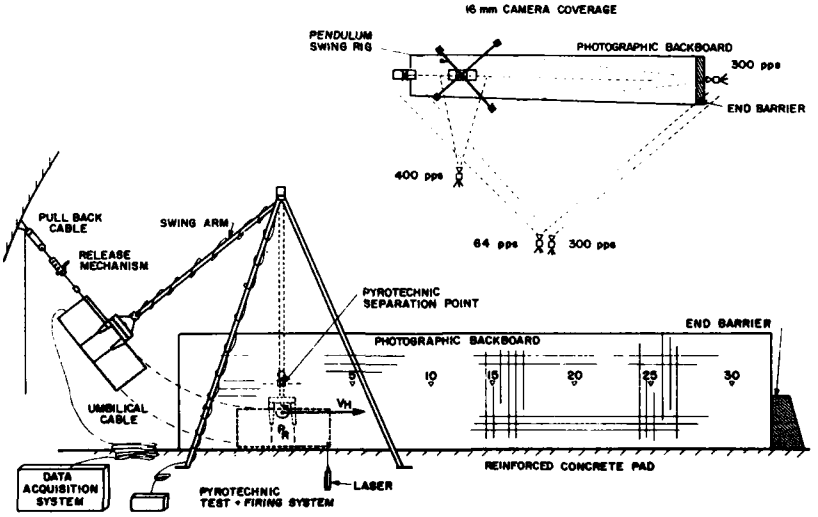

Fig. 14 Schematic of pendulum gantry for free flight tests

Fig. 15 Fuselage Model Suspended on Pendulum Gantry

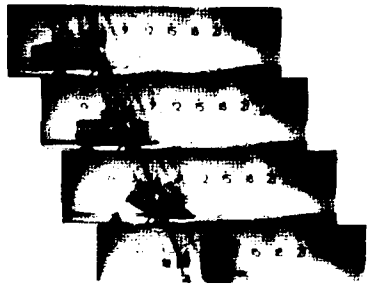

Fig. 16 High Speed Photographs of Model Crash Test

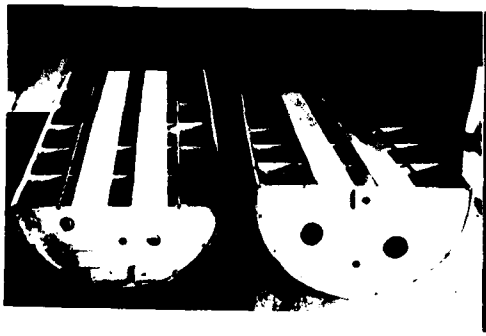

Fig. 17 Split Mold for Manufacturing Composite Fuselage

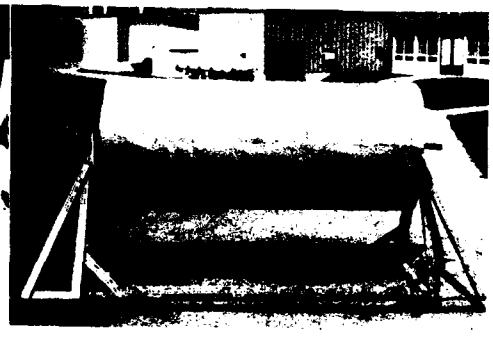

Fig. 18 Assembled Cylindrical Mold

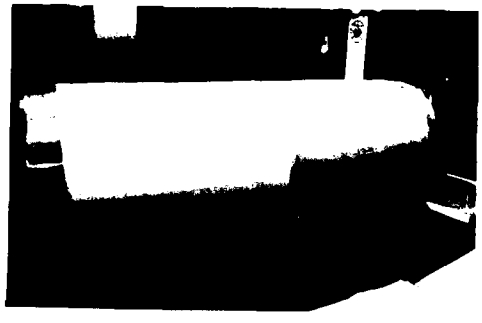

Fig. 19 Kevlar prepreg on Mold

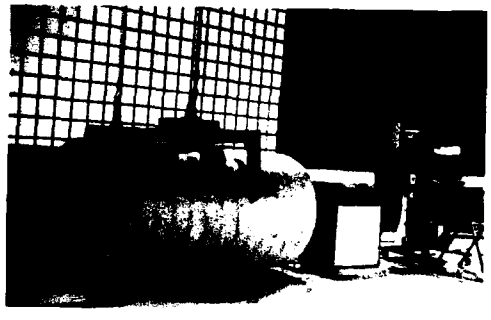

Fig. 20 Stiffened Composite Fuselage with High Wing Load Fixture

TRANSPORT AIRPLANE CRASH SIMULATION, VALIDATION AND APPLICATION TO CRASH DESIGN CRITERIA

G. Wittlin
LOCKHEED AERONAUTICAL SYSTEMS COMPANY
BURBANK, CALIFORNIA

C. Caiafa
CRASHWORTHINESS BRANCH CHIEF
FAA TECHNICAL CENTER, ATLANTIC CITY, N. J.

ABSTRACT

This paper presents a brief description of the evolutionary development of program KRASH to its most recent release, KRASH85, and provides some background to delineate various program features as well as to illustrate the range of aircraft configurations and impact conditions for which the program has been validated.

The application of program KRASH to analyze the structural crash dynamics behavior of a narrow-body commercial jet transport airplane used in the FAA/NASA conducted Controlled Impact Demonstration (CID) test is discussed in this paper. A description of the modeling along with comparative results between test and analyses is provided. Included in the correlation effort are acceleration time histories, sequence of impact events, fuselage crush distribution, wing and fuselage bending moment distributions, and estimates of moment and shear strength levels.

The results of the transport airplane correlation effort is used in a subsequent parametric study to formulate a crash design velocity envelope. The flow diagram provided describes the sequence of this effort and the manner in which analytical and experimental data are integrated. Parametric analyses, section test and full-scale crash test results are utilized and presented in the form of acceleration time histories at the cabin floor. The dynamic pulse parameters, namely velocity change, duration of excitation and peak acceleration amplitude, are related to potential seat dynamic test requirements. The transport crash design envelope, along with additional available data, is used to assess the effect of airplane size on floor acceleration pulses in a survivable crash environment.

The most recent applications of KRASH, under FAA sponsorship, are discussed. Included are the approaches being used to assess; floor pulses as a function of airplane size, various fuselage auxiliary fuel tank installation concepts subjected to a crash environment, the use of composites in lieu of metals, and soil/water impact considerations.

INTRODUCTION

The decade of the 1980's has seen significant progress in application of analytical modeling programs for the assessment of aircraft structural crash dynamics behavior. This is particularly true for rotary-wing aircraft as evidenced by the numerous papers on the subject of analytical modeling presented at the annual meeting of the 1986 American Helicopter Society (AHS) (Reference 1). Program KRASH was the main topic presented in many of the papers at that AHS meeting. The development of program KRASH evolved over a period of time and sequence of applications, aided by numerous planned crash tests of different aircraft configurations and a large independent user community. This paper, while briefly touching on the KRASH development, emphasizes the most recent application of the program to narrow-body jet transport aircraft. A joint FAA/NASA program (Reference 2) involving airframe section drop tests, a full-scale airplane ('Laurinburg') drop test and a Controlled Impact Demonstration (CID) test provided the framework by which analytical modeling of the structure dynamic behavior of transport category airplanes in a survivable crash environment could be enhanced, validated and applied. Correlation of the CID with analytical modeling has shown a degree of success, as can be noted in recent publications (References 3, 4). This paper, in addition to showing the KRASH correlation with the CID test, describes post-CID applications of KRASH. In this latter study, the validated KRASH model results in conjunction with airframe section and full-scale airplane test data are used to develop a survivable crash design envelope for transport category aircraft. The paper also briefly describes the ongoing FAA crash dynamics research effort and discusses several current areas of interest.

PROGRAM KRASH

Program KRASH is referred to as a "hybrid" modeling technique because it approximates large regions of structure in a simplified manner and provides for the use of experimental data. The program was developed in three steps as depicted in Figure 1. The initial step in the development of the program was for the application to helicopters (Reference 5). Subsequently, the program's capability was extended to light fixed-wing airplanes (References 6 and 7) and most recently to transport category aircraft (Reference 8). The three stages of program release are referred to as KRASH, KRASH79 and KRASH85. As might be expected, each release provides additional features and updates the previous version. A comparison of the pertinent features of the three KRASH versions is shown in Table 1. During the course of program development comparisons were made between test and analytical results, both by Lockheed and independent users. Table 2 provides a partial list of aircraft configurations and test conditions, for which correlation has been performed. The following is a partial list of the operations that KRASH can perform:

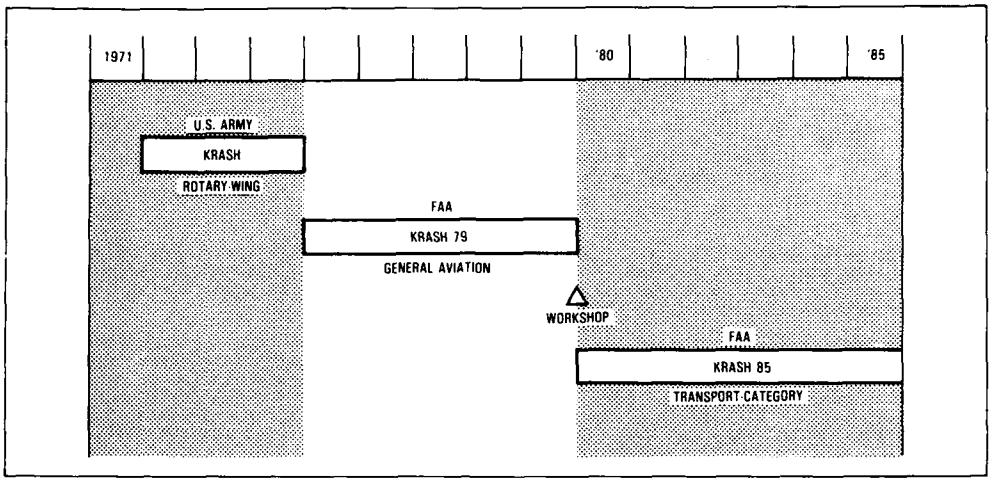

FIGURE 1. KRASH DEVELOPMENT 1971-1985

TABLE 1. COMPARISON OF PERTINENT PROGRAM FEATURES

FEATURES	KRASH	KRASH 79	KRASH 85
1. ENERGY DISTRIBUTION	YES	YES*	YES**
2. ELEMENT RUPTURE	YES	YES*	YES*
3. INJURY CRITERIA (DRI)[a]	YES	YES*	YES
4. PLOT CAPABILITY SUMMARIES	YES	YES	YES**
5. VOLUME PENETRATION	YES	YES	YES
6. PLASTIC HINGE ALGORITHM	NO	YES	YES*
7. SHOCK STRUT	NO	YES	YES
8. FLEXIBLE AND/OR SLOPED TERRAIN	NO	YES	YES
9. ACCELERATION PULSE EXCITATION	NO	YES	YES
10. UNSYMMETRICAL BEAM REPRESENTATION	NO	YES	YES
11. STANDARD MATERIAL PROPERTIES	NO	YES	YES
12. EXTERNAL SPRING DAMPING	NO	YES	YES
13. MASS LOCATION PLOTS	NO	YES	YES
14. PRE-AND POST-DATA PROCESSING	NO	YES	YES
15. RESTART CAPABILITY	NO	YES	YES
16. SYMMETRICAL MODEL CAPABILITY	NO	YES	YES
17. CG FORCE MOTIONHISTORY	NO	YES	YES*
18. VOLUME CHANGE CALCULATIONS	NO	YES	YES
19. STANDARD NONLINEAR CURVES	NO	5	6
20. STIFFNESS REDUCTION FEATURE (KR)[b] APPLICABLE TO DAMPING	NO	NO	YES
21. COMBINED FAILURE LOAD (LIC)[c]	NO	NO	YES
22. INITIAL BALANCE-NASTRAN	NO	NO	YES
23. TIRE VERTICAL SPRING	NO	NO	YES
24. ARBITRARY MASS NUMBERING	NO	NO	YES
25. EXTERNAL FORCE LOADING	NO	NO	YES
26. OLEO METERING PIN	NO	NO	YES
27. ADDITION OF DESCRIPTIVE NAMES TO IDENTIFY INPUT DATA	NO	NO	YES

*ENHANCED ONE LEVEL, **ENHANCED TWO LEVELS

[a]DYNAMIC RESPONSE INDEX [b]STIFFNESS REDUCTION FACTOR [c]LOAD INTERACTION CURVE

TABLE 2. KRASH EXPERIMENTAL VERIFICATION

AIRCRAFT	GROSS WEIGHT (Kg)	IMPACT VELOCITIES (M/SEC) VERTICAL	LONGITUDINAL	LATERAL	(REFERENCE)
ROTARY WING					
UTILITY TYPE	3909	7.0	–	5.6	5
CARGO TYPE	11045	12.8	8.3	–	25
MULTI-PURPOSE	1727	6.0	6.0	–	26
MULTI-PURPOSE	1645	10.0	–	–	26
COMPOSITE SUBSTRUCTURE	1605	9.1	–	–	9
COMPOSITE SUBSTRUCTURE	1605	8.6	–	3.1	9
LIGHT-FIXED-WING					
SINGLE-ENGINE, HIGH-WING	1091	14.0	21.3	–	6
SINGLE-ENGINE, HIGH-WING	1091	6.7	21.7	–	6
SINGLE-ENGINE, HIGH-WING	1091	14.9	21.3	–	6
SINGLE-ENGINE, HIGH-WING*	1091	13.1	21.2	–	6
TWIN-ENGINE, LOW-WING SUBSTRUCTURE	248	8.4	–	–	24
TRANSPORT					
MEDIUM SIZE*	72272	5.5	52.4	–	14
MEDIUM SIZE	88636	5.3	79.2	–	18

*TEST PERFORMED ON SOIL; ALL OTHER TESTS ON RIGID SURFACE.

- Correlation with crash test data (Reference 1)
- Showing compliance with crash design requirements, e.g. MIL-STD-1290 (References 9, 10)
- Modeling composite fuselage structure (References 9 and 10)
- Determining incremental weight increase versus crashworthiness level tradeoff (Reference 11)
- Performing landing gear simulation (Reference 12)
- Assessing the use of advanced composite materials in transport airplane lower fuselage design (Reference 13)
- Modeling occupant/seat systems (Reference 14)
- Evaluating car-barrier impacts (Reference 15)

An extensive listing of recent applications of KRASH can be found in Reference 1. A detailed summary of the chronological development of KRASH is found in Reference 3.

CID CORRELATION

The CID test of a narrow-body jet transport airplane was performed on December 1, 1984, at the NASA Dryden Dry Lake Bed, Edwards AFB, California. The planned impact conditions are compared to the actual conditions in Table 3. The CID crash from initial wing contact to subsequent fuselage impact with the ground is shown in Figure 2. Peak ground impact responses were developed within 500 msec. after initial fuselage ground impact (occurs 400 msec. after initial left wing impact-Figure 2) and prior to contact with any ground obstructions. Only the first 900 msec. post-impact of the CID test are pertinent to the analytical methodology program. The pre-CID test effort consisted of the development of two KRASH airplane models and several frame section models. The frame section model results were compared with section drop test data and the results were used to improve the KRASH stick and expanded models, Figures 3 and 4 respectively. A 24-mass, 23-beam element full stick model, Figure 3, provides overall response and is useful in assessing fuselage and wing structural integrity, lower fuselage crush, and floor accelerations. Despite its simplicity, this model is particularly effective for impacts where the airframe low frequency modes are expected to predominate, as was the case in the CID test. The expanded 48-mass, 137-beam model, Figure 4, is potentially more suitable for detail localized behavior, a situation that was difficult to assess for the CID test

TABLE 3. COMPARISON OF CID TEST PLANNED AND ACTUAL IMPACT CONDITIONS

	PLANNED	ACTUAL*
SINK RATE, M/SEC	$5.18^{+0.91}_{-0.61}$	**5.27**
GROSS WEIGHT, KG	79545-88636	**87447**
GLIDE PATH, DEGREES	3 3 TO 4 0	3 5
ATTITUDE, DEGREES	1 ± 1 (NOSE UP)	0
LONGITUDINAL VELOCITY, KNTS	150^{+5}_{-5}	151.5
ROLL, DEGREES	0 ± 1	−13**
YAW, DEGREES	0 ± 1	−13***

*IMPACTED ON LEFT WING OUTBOARD ENGINE. INITIAL CONTACT ON FUSELAGE WAS AT FOLLOWING **CONDITIONS: 4.3 M/SEC SINK SPEED, NOSE-DOWN ATTITUDE (0-2.0 DEGREES), FORWARD** VELOCITY 150 KNTS. CONTACTED FUSELAGE (BS 360 - 460) REGION.

** LEFT WING DOWN
*** NOSE LEFT

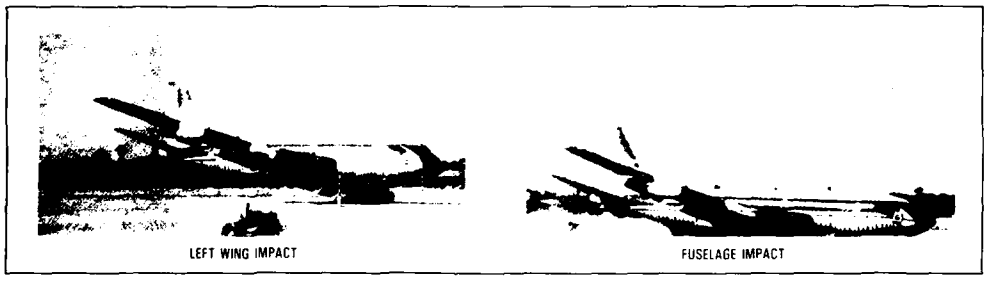

FIGURE 2. CID IMPACT SEQUENCE

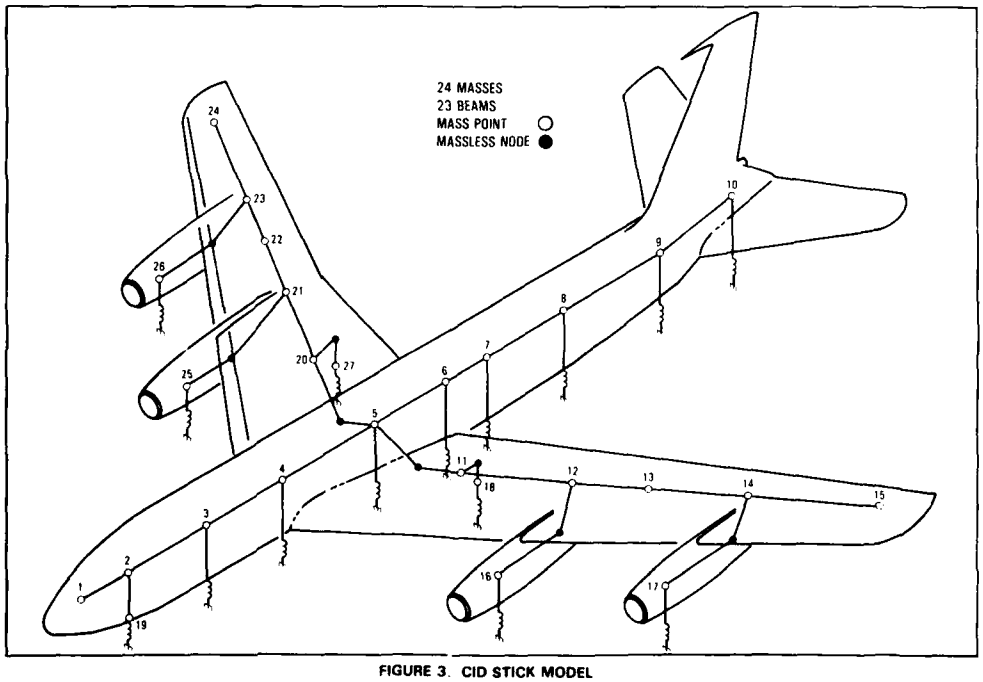

FIGURE 3. CID STICK MODEL

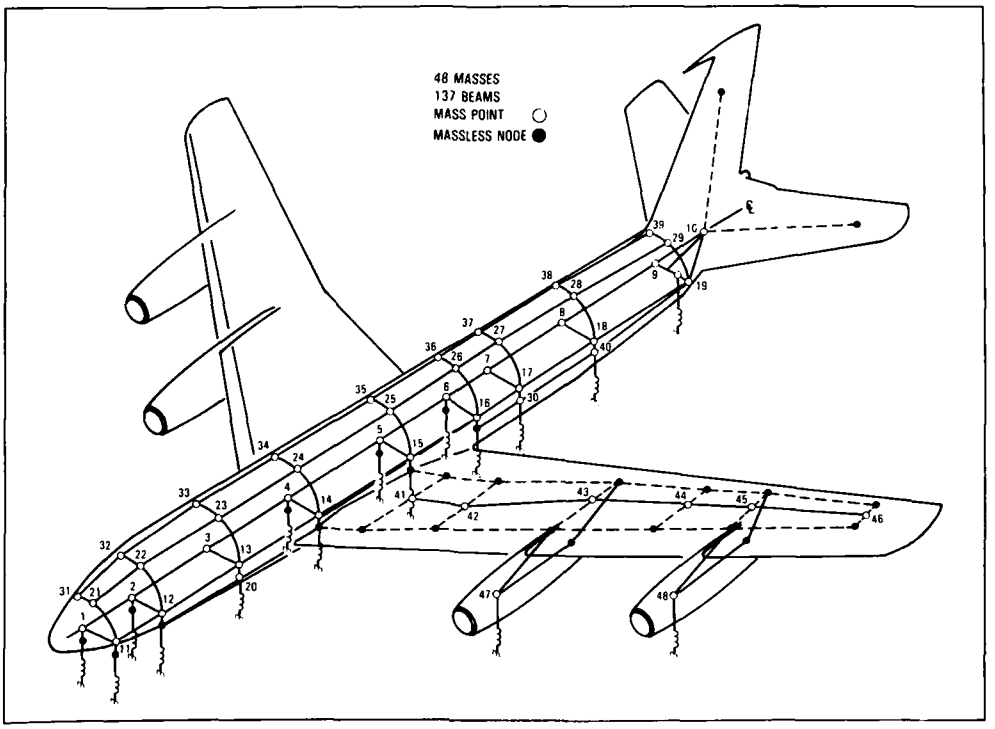

FIGURE 4. CID EXPANDED MODEL

due to the post-impact fire. The pre-CID effort is described, in detail, in Reference 16 and portions of which have been previously presented at a prior AGARD meeting (Reference 17).

The comparison of analysis results with CID test data was performed for two conditions using the stick model; (Figure 3).

- Partial Sequence - Symmetrical impact on forward fuselage at a reduced sink speed 4.27 m/sec, -2° nose down, 0° roll and yaw.
- Complete Sequence - Unsymmetrical impact on left wing engine no. 1, initial sink speed 5.27 m/sec, +1° nose up, 13° roll and yaw.

The primary emphasis of the analysis was to determine cabin floor responses which were then used to evaluate dynamic seat testing criteria. A comparison of results of the two impact sequences is provided in Table 4. A comparison of the peak vertical accelerations on the fuselage are provided in Figure 5.

Considering the unsymmetrical case, the initial impact on the number 1 engine does not produce significant fuselage responses. As the aircraft settles down and impacts the forward portion of the fuselage the impact forces increase significantly. Thus fuselage impact results in greater impact forces and for this reason the previous condition was considered a symmetrical fuselage impact.

In addition to the peak vertical acceleration comparisons, the correlation between CID modeling and test results included comparisons of:

- Lateral and longitudinal direction accelerations (Figure 6)
- Moment distributions along the fuselage and wing (Figures 7, 8)
- Acceleration time histories (Figure 9)

The test and analysis results both showed relatively low longitudinal and lateral accelerations as was expected based on the pre-CID analyses. The analysis results at the forward fuselage are somewhat lower that anticipated. This difference is attributed to the representation of the forward region of the fuselage where the nose-gear bulkhead support structure is located. This structural representation was changed during the post-CID parametric study described later in this paper. In general, one can anticipate the longitudinal and lateral accelerations to be related to vertical peaks by the factor associated with the ground coefficient of friction which is 0.35 for the nonyielding rigid surface.

TABLE 4. COMPARISON OF UNSYMMETRICAL IMPACT SEQUENCE: ANALYSIS VERSUS TEST

	ANALYSIS RESULTS	TEST DATA
INITIAL FUSELAGE CONTACT		
MASS NO.	2	2-3
TIME (SEC)(1)	.432	.400
FUSELAGE CONTACT VELOCITY, M/SEC	4.19	4.27
ENGINE NO. 2 CONTACT		
TIME (SEC)(1)	.083	.080

(1) AFTER ENGINE NO. 1 INITIAL GROUND CONTACT

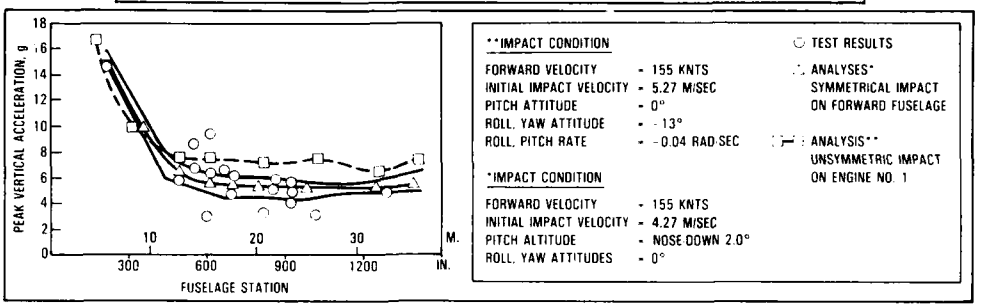

FIGURE 5. PEAK FUSELAGE ACCELERATION DISTRIBUTION OBTAINED FROM KRASH ANALYSIS AND CID TEST DATA

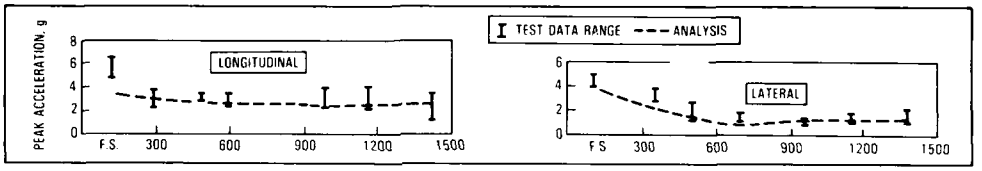

FIGURE 6. COMPARISON OF TEST VERSUS ANALYSIS RESULTS – LONGITUDINAL AND LATERAL ACCELERATIONS, COMPLETE SEQUENCE ANALYSIS

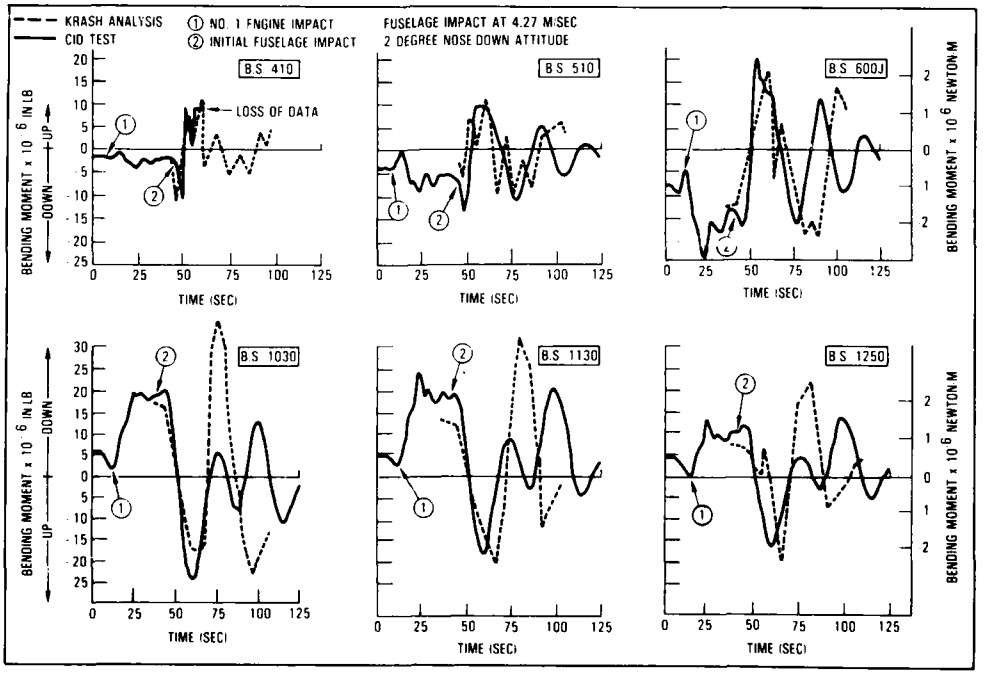

FIGURE 7. KRASH VERSUS CID TEST RESULTS, FUSELAGE BENDING MOMENT DISTRIBUTION

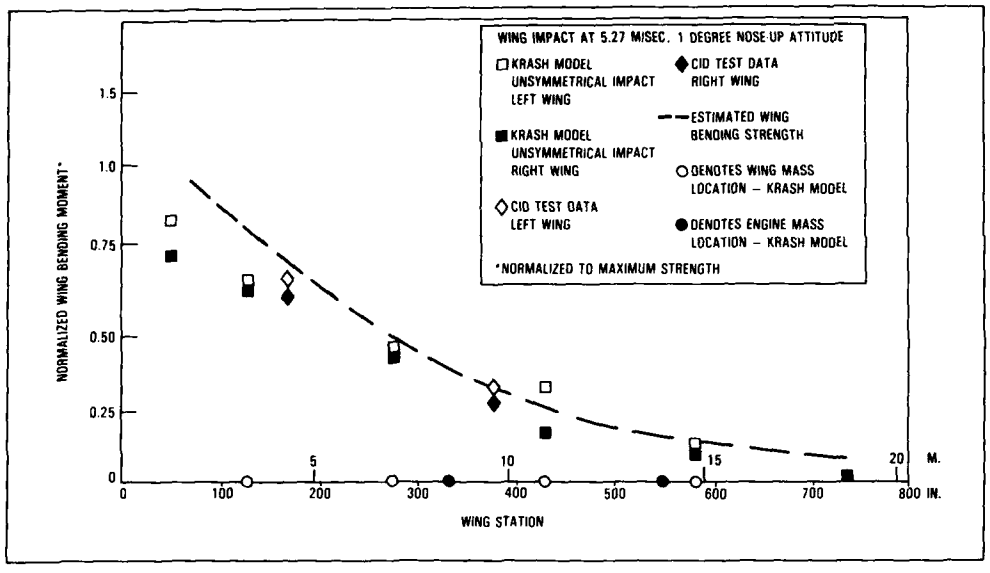

FIGURE 8. COMPARISON OF TEST AND ANALYSIS RESULTS, WING BENDING MOMENT DISTRIBUTION

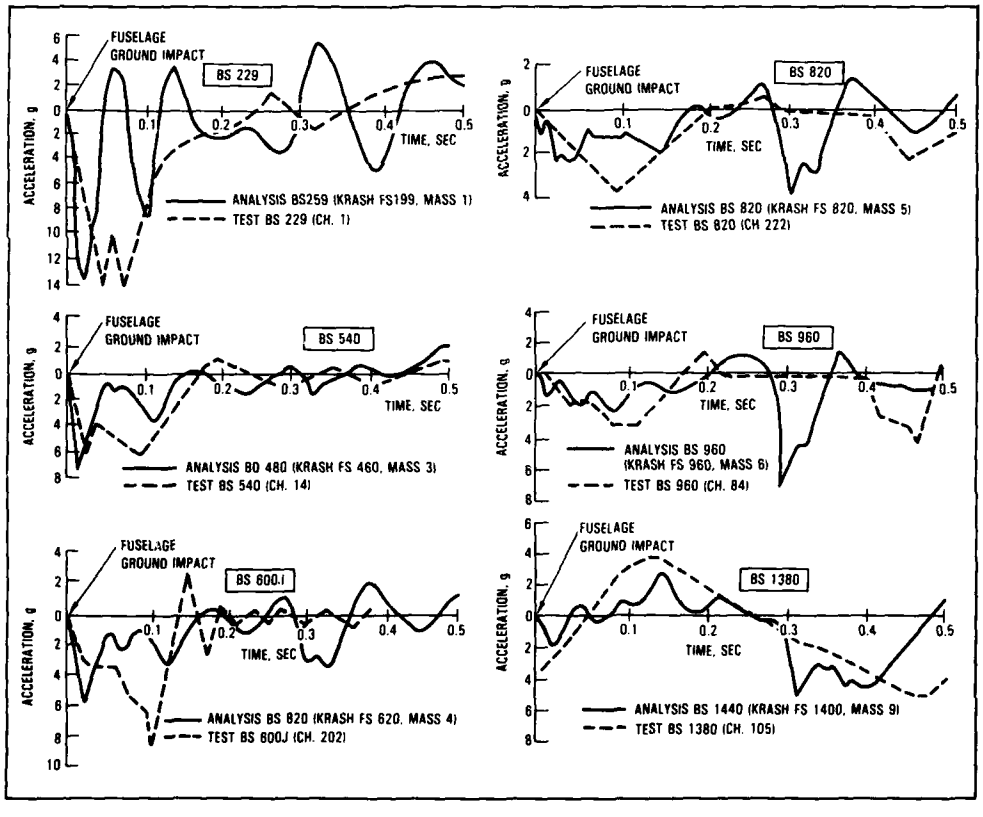

FIGURE 9. VERTICAL ACCELERATION RESPONSE, KRASH VERSUS CID TEST DATA. STICK MODEL – FUSELAGE GROUND IMPACT AT 4.27 M/SEC

The comparisons of the moment responses along the fuselage and wings are shown in Figures 7 and 8, respectively. The analysis to obtain the fuselage moments is initiated at fuselage impact and assumes an initial moment distribution at that time, representative of what is noted in Figure 7. Differences between the CID measured data and analytically developed fuselage data (moments) is partially attributable to the inability to represent the actual aerodynamic time history throughout the crash sequence of the mathematical model. The aerodynamic loading was represented by externally applied forces. The magnitude of the fuselage bending moments, obtained by analysis, although generally higher than the measured responses, do not exceed the estimated strength of the fuselage and, thus the impact results in loads which are within the structural integrity envelope of the airframe. The wing bending moment comparison was performed for the unsymmetrical impact initiated on the left wing engine. This type of impact is probably more severe for the wing and associated wing-related fuel containment concerns than for a symmetrical impact at the same sink rate. The comparison of results suggest the wing responses are close to the estimated bending strength of the wing. The one data point discontinuity on the left wing, at wing station 420, could be associated with the manner in which the KRASH model treats the engine to wing attachment. The apparent marginal strength that the wing exhibits might indicate that the 13-degree roll angle is close to the limit for wing fuel containment at the CID impact conditions. If this is the case, the CID test results would be consistent with previous study results provided in Reference 34. The analysis, based on shear load versus estimated strength, showed that the highest potential for wing failure is located on the left wing outboard of the number one engine, which actually failed at the initial wing-low impact.

The vertical acceleration time histories along the fuselage resulting from a 4.27 m/sec fuselage impact are shown in Figure 9, for both the KRASH analysis and CID test. The initial test and analysis peak amplitudes, at the forward-most regions of the fuselage, exhibit similar response characteristics (amplitude and frequency). The acceleration response from the mid to the aft-fuselage tends to show more deviation between analysis and test results than does the comparison near the impact points. The deviation is more evident for the secondary response which occurs at 400 milliseconds after the forward fuselage impacts the ground. However, the test data shows that the further the response measurement point is from the initial impact point, the lower the associated amplitude. While the percentage difference between test and analysis values at the mid to aft-fuselage region may be relatively large, the actual amplitude difference is somewhere between 1g to 3g. Furthermore, the test data exhibits scatter as noted in Figure 5.

The KRASH correlation stick model was also used to compare results between the planned and actual conditions as shown in Figure 10. The engines do not crush as much in the symmetrical impact as the initial contact with ground is made at FS1000. For the unsymmetrical impact, the airplane hits the ground initially on the No. 1 engine and then contacts the No. 2 engine $\approx$ 80 milliseconds later before impacting the ground at the forward fuselage location (FS300 - FS460) $\approx$ 400 milliseconds after the No. 1 engine ground contact. The symmetrical model results generally shows higher acceleration peaks from the mid-fuselage (FS820) and aft than the unsymmetrical model since the initial contact is on the fuselage. Substantially more crushing is obtained during the symmetrical impact. For reference the drop test crush results of a 5.18 m/sec sink speed pre-CID drop test of a similar airplane configuration, commonly referred to as the "Laurinburg" test, is shown. The Load Interactive Curve (LIC) ratios, which are used as an indication of airframe strength relate to fuselage shear bending moment strength capability. The curves are normalized to estimated failure loads so that LIC >1.0 indicates the potential for exceeding airframe structural integrity. Both the symmetrical and unsymmetrical impacts indicate no airframe failure should be experienced at the prescribed impact conditions. Also shown in Figure 10 are the predicted pre-CID KRASH results. The pre-CID predictions were generally higher and indicated possible exceedance of mid-fuselage strength. The post-CID analyses have revised engine crush and aerodynamic loading distribution characteristics which account for the differences between the pre- and post-analyses results.

POST-CID PARAMETRIC STUDIES

Subsequent to the correlation effort the validated KRASH stick model was utilized to perform a series of analytical runs to determine the envelope of airframe structural integrity. The flow diagram for this effort is shown in Figure 11. This phase involved several iterations as a result of the input of additional data during the effort. The initial analyses were performed for the air-to-ground (gears retracted) scenario followed by the ground-to-ground scenario, also with gears retracted. The KRASH results from the ground-to-ground analyses indicated a need to refine the nose-gear bulkhead representation. Subsequently this refinement was made using existing available test data (Reference 19). The KRASH model was revised as noted in Figure 12 and a new set of results were obtained. In addition to the two scenarios initially investigated, air-to-ground (gears extended) and longitudinal-only impacts were also analyzed. The latter analysis was aided with the use of existing available cylindrical axial crush test data, also obtained from Reference 19. The analytical results yielded vertical, longitudinal and combined vertical-longitudinal pulses. The analyses results, along with the full-scale L-1649, DC-7 and CID (References 20, 21, 22) and fuselage section test data, were then used to formulate crash design velocity envelopes.

For air-to-ground analyses the following assumptions apply:

- Impact directly on fuselage; no engine crush involved
- Symmetrical impact; no roll or yaw angle

- No initial external loading; i.e., no aerodynamic forces
- Limit is airframe structural integrity as measured by Load Interaction Curve, (LIC≤1.0)
- Maximum crush before restiffening occurs is:

  0.254-meter wing center section FS620-820

  0.457-meter wing MLG aft bulkhead, FS960

  0.610-meter fuselage frame sections, FS300, 460, 1040, 1240

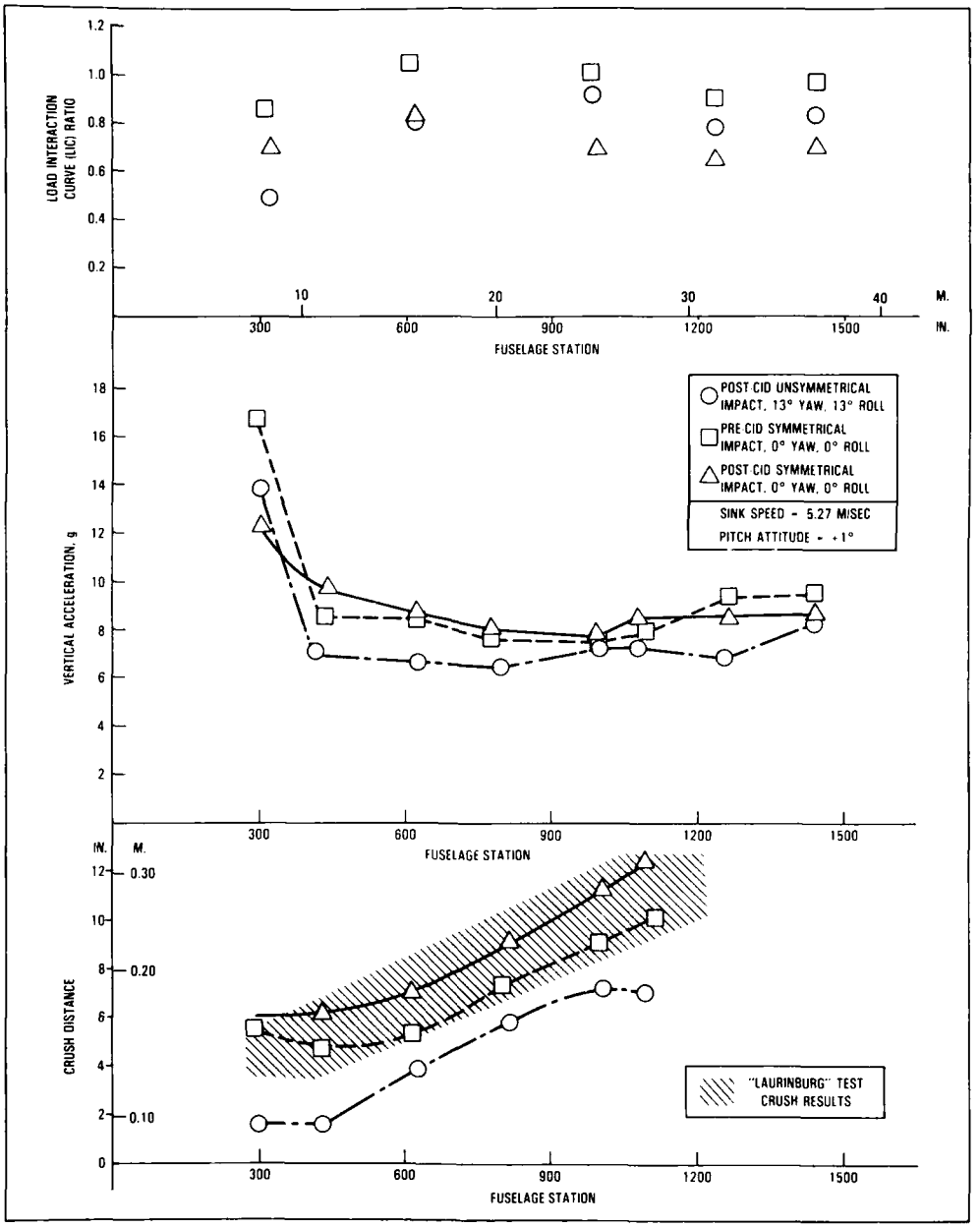

FIGURE 10. SYMMETRICAL VERSUS UNSYMMETRICAL IMPACT AT 5.27 M/SEC SINK SPEED, +1° NOSE UP ATTITUDE WITH ENGINES ON

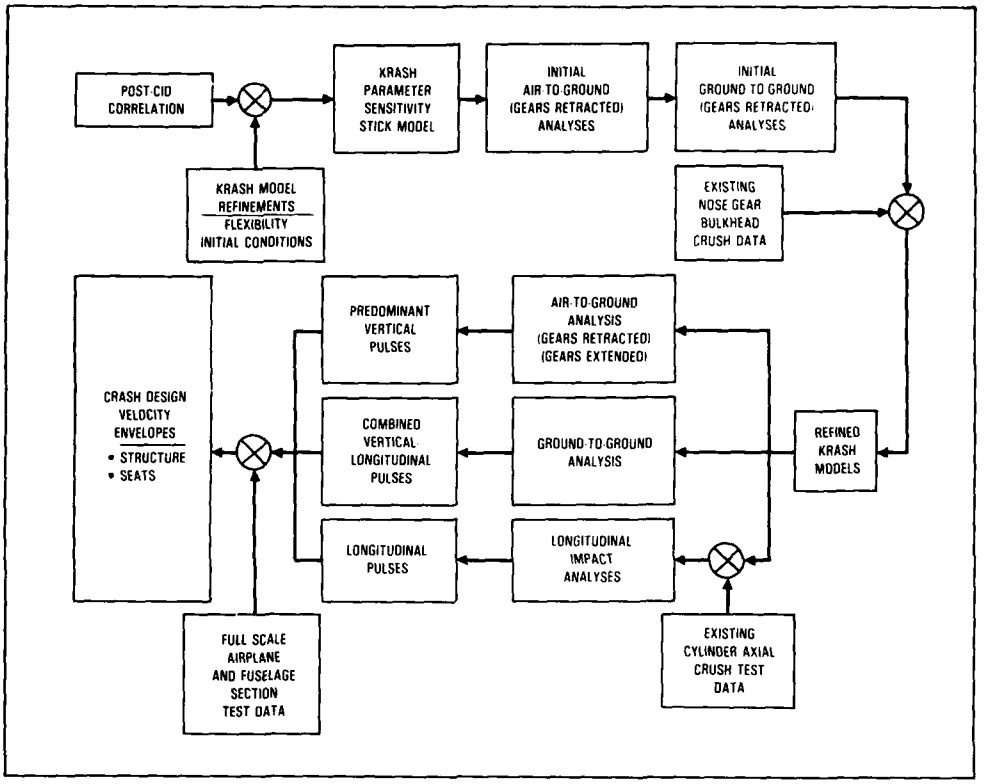

FIGURE 11. PARAMETRIC SENSITIVITY ANALYSES PROGRAM FLOW DIAGRAM

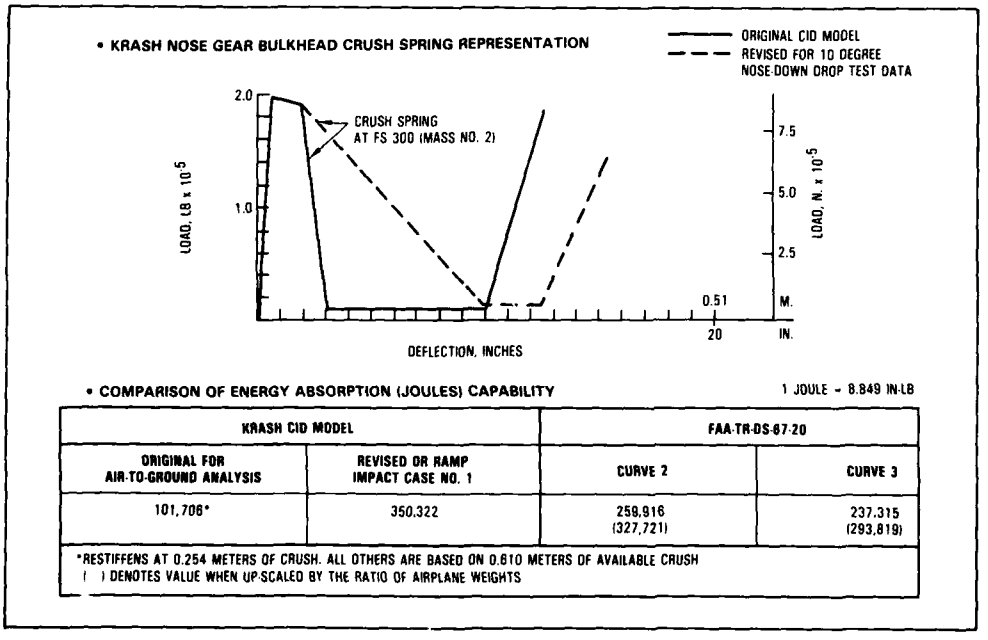

• COMPARISON OF ENERGY ABSORPTION (JOULES) CAPABILITY

1 JOULE = 8.849 IN-LB

KRASH CID MODEL		FAA-TR-DS-67-20	
ORIGINAL FOR AIR-TO-GROUND ANALYSIS	REVISED OR RAMP IMPACT CASE NO. 1	CURVE 2	CURVE 3
101,706*	350,322	259,916 (327,721)	237,315 (293,819)

*RESTIFFENS AT 0.254 METERS OF CRUSH. ALL OTHERS ARE BASED ON 0.610 METERS OF AVAILABLE CRUSH
( ) DENOTES VALUE WHEN UP-SCALED BY THE RATIO OF AIRPLANE WEIGHTS

FIGURE 12. NOSE GEAR BULKHEAD CHARACTERISTICS

A summary of conditions analyzed for the gears-retracted type of impact is shown in Table 5.

TABLE 5. DESCRIPTION OF ANALYSIS: AIR-TO-GROUND IMPACT CONDITIONS

CONDITION NO	AIRPLANE INITIAL SINK SPEED M/SEC	PITCH ATTITUDE DEGREES	INITIAL LIFT	ENGINE GROUND CONTACT	FORWARD VELOCITY COMPONENT (155 KTS)	REVISED NOSE GEAR BULKHEAD CRUSH
1	6.7	0	NO	YES	YES	YES
2	6.7	-1	NO	YES	YES	YES
3	6.1	-1	NO	YES	YES	YES
4	5.3	-1	NO	YES	YES	YES
5	5.3	-1	YES	YES	YES	YES
6	6.7	0	NO	NO	NO	YES
7	6.7	0	NO	NO	YES	YES
8	6.1	0	NO	NO	YES	NO
9	6.1	0	NO	NO	YES	YES
10	4.6	6	NO	NO	YES	YES
11	4.6	-6	NO	NO	YES	YES
12	4.6	6	NO	NO	YES	NO
13	4.6	-6	NO	NO	YES	NO

For the air-to-ground, gears-extended analyses the following three conditions were determined to be approximately the level at which fuselage structural integrity would be exceeded:

1. Sink speed = 5.49 m/sec, Pitch attitude = -6 degrees
2. Sink speed = 6.10 m/sec, Pitch attitude = 0 degrees
3. Sink speed = 5.49 m/sec, Pitch attitude = +6 degrees

For all these runs the assumptions of zero lift force, forward velocity = 79.85 m/sec and ground coefficient (μ) = .35 applied. Main and nose gear failure loads, based on airplane design loads were used as criteria for failure.

The KRASH analyses results were compared to previous air-to-ground impact analysis reported in Reference 19. The models exercised in the CID and Reference 19 models are shown in Figure 13, and the results compared in Table 6. The differences between the two sets of results are readily explained by the fuselage crush representation used in each analysis. The CID representation is believed to be more plausible since the load-deflection characteristics obtained from that analysis were obtained from supporting tests designed to provide just that kind of data. Figure 14 shows a comparison of airplane initial impact velocity versus pitch attitude at the limit of airframe integrity developed from the two analyses.

Figure 15 shows a comparison of the fuselage underside crush for the 'Laurinburg' test the CID test and the parametric analysis results. The latter is based on the revised nose-gear bulkhead representation and encompasses the maximum amplitude for pitch attitudes of -6 (nose-down), 0, and +6 (nose-up) degrees. The analyses results, provided in Figure 15, suggests that in a survivable crash wherein the fuselage structural integrity is maintained the fuselage will crush more than was measured in either the 'Laurinburg' or CID tests.

For the air-to-ground impact conditions the magnitude of longitudinal pulses are relatively low in relation to the magnitude of the vertical pulses. To obtain combined longitudinal-vertical pulses ground-to-ground (ramp) impact analyses were performed. Included in these ramp analyses were the following conditions, which are representative of References 20 and 21 test conditions:

	Ramp (degrees)	ENV* (m/sec)	forward velocity (m/sec)	Reference
1.	6	5.64	53.90	20
2.	20	11.50	33.50	20
3.	8	10.00	71.60	21
*ENV = (sink speed) X (sine of the slope of the ramp)				

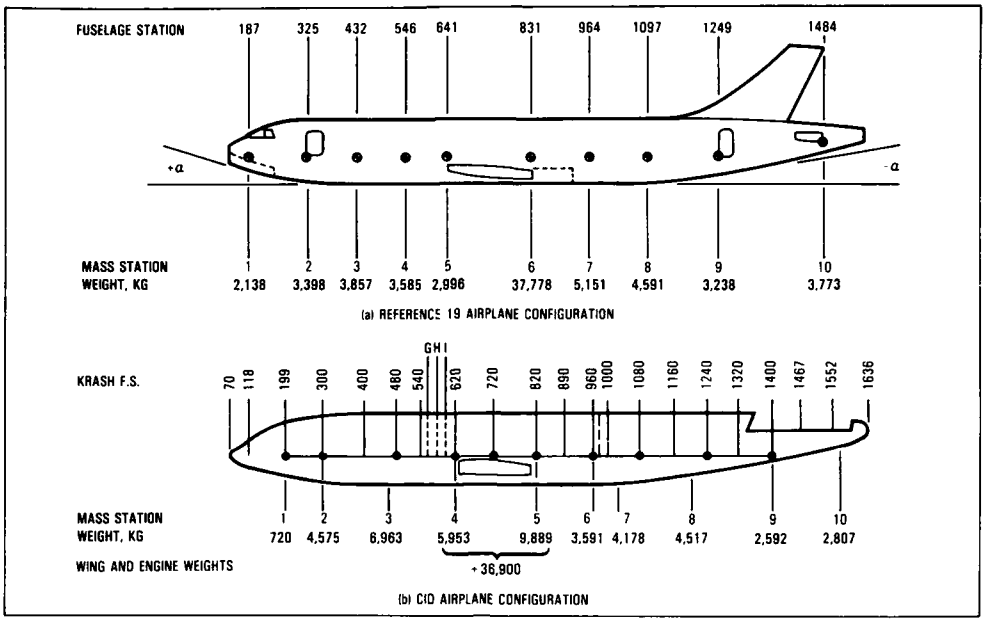

FIGURE 13. COMPARISON OF AIRPLANE CONFIGURATIONS

TABLE 6. COMPARISON OF ANALYSIS RESULTS, SINK SPEED = 4.57 M/SEC, 0-DEGREE PITCH ATTITUDE

FUSELAGE STATION		PEAK VERTICAL ACCELERATION, g		LIC RATIOS		CRUSH DISTANCE, M.	
REFERENCE 2	CID	REFERENCE 19	CID	REFERENCE 19	CID	REFERENCE 19	CID
325	300/350	10	9	0.70	0.55	0.254	0.193
432	450	--	--	0.67	0.55	0.254	0.163
546	540	--	--	0.65	0.52	0.279	0.160
641(a)	620(a)	10	10.5	0.67	0.48(a)	0.279	0.160
831(a)	820(a)	--	--	0.42	0.57(a)	0.406	0.170
964(a)	960(a)	--	--	0.45	0.56	0.381	0.236 (c)
1097	1040/1090	8	9.9	0.46	0.68	0.864	0.246 (c)
1249	1210/1240	--	--	0.60	0.49	0.813	0.036 (c)

(a) BULKHEAD CRUSHING
(b) AVG. OF TWO VALUES
(c) MAX. VALUE OCCURS AT END OF ANALYSIS

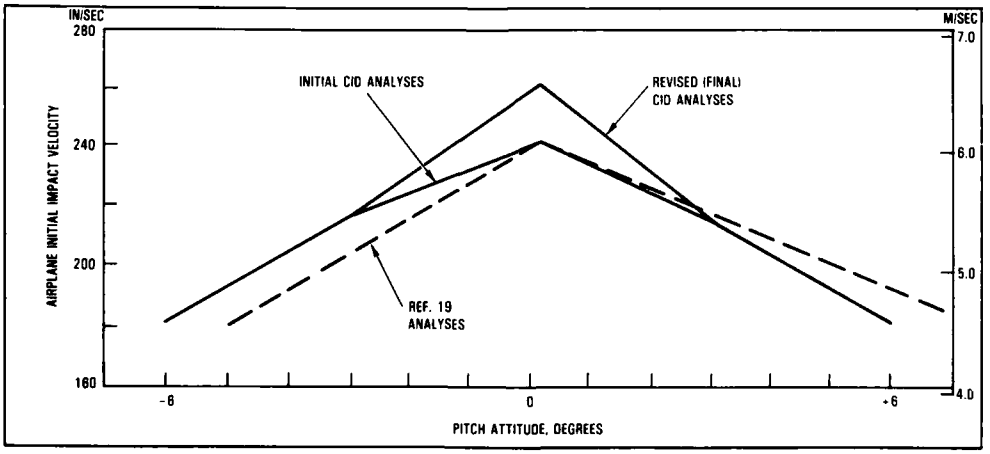

FIGURE 14. AIRPLANE IMPACT VELOCITY VERSUS PITCH ATTITUDE, AIR-TO-GROUND SCENARIO

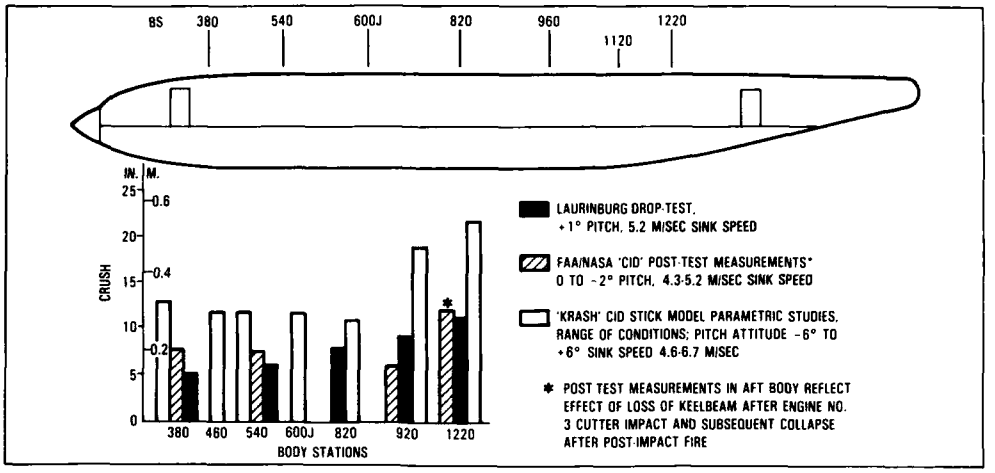

FIGURE 15. FUSELAGE CRUSH COMPARISON; LAURINBURG, CID AND KRASH PARAMETRIC STUDY

The assessment of the fuselage failure modes experienced during the tests described in References 20 and 21 versus that obtained by analysis of the CID test article via LIC curves, showed good agreement.

The measured acceleration pulses obtained from References 20 and 21 data were integrated and along with airframe test data, were used to obtain triangular pulse velocity change-acceleration-rise time relationship which are plotted in Figures 16 and 17 for the longitudinal and vertical directions, respectively. The data presented in Figure 16 and 17 illustrates that typically high accelerations are associated with short durations and that the trend is for a decrease in amplitude as the duration of the pulse increases. The plotted data show that the pulses in the passenger cabin of a transport aircraft can vary substantially, but are generally associated with a change of velocity at or below 9.14 m/sec, without fuselage strength (shell bending, shear) being exceeded. Higher velocity changes may be experienced at the nose section, forward of the passenger cabin. The initial 6-degree ramp impact of the L-1649 occurs with an ENV $\approx$ 5.64 m/sec and experiences no fuselage break. The second impact onto a 20-degree ramp occurs with an ENV $\approx$11.5 m/sec and the airplane experiences two fuselage breaks (Figure 18). The longitudinal acceleration histories (Figure 19) at the cockpit (FS195) and passenger mid-fuselage (FS685) locations for these two impacts illustrate the following:

- The peak acceleration at FS195 is approximately 20g for both impacts, despite the fact that the longitudinal velocity change is $\approx$ 30 percent higher for the more severe impact.
- At FS685 the acceleration response shapes are similar and the magnitudes are nearly equal, despite the higher velocity change in the latter impact.
- The higher velocity change for the more severe impact is accompanied by a a longer pulse time duration, not necessarily a higher "g".

The analyses for the air-to-ground and ground-to-ground scenarios were similarly plotted as triangular pulses showing the acceleration-time-velocity change relationships. As part of the parametric study the affect of additional crush distance in critical bulkhead regions was investigated. The results, which are plotted in Figure 20, show that the added crush distance, if it were available, would allow the airplane to impact at a higher initial sink speed before realizing a fuselage break (LIC > 1.0). However, the increased crush tends to produce lower accelerations and longer pulse durations. At some point the physical constraints of the location of the "hard points" (i.e. aft pressure bulkhead) limits the amount of crush that can be achieved. When the hard point is encountered severe failure-inducing loading is generated. The analysis showed that for the CID configuration, the aft pressure bulkhead (FS1400) contacts the ground for a sink speed of 7.62 m/sec and flat pitch attitude (zero-degrees). An increase in the sink speed to 8.38 m/sec definitely produces failure loads in the analysis.

The analyses to determine longitudinal forces, which could result in passenger cabin failure loads, was performed using the model shown in Figure 21. The crush behavior of the forward fuselage was obtained from cylinder axial collapse tests described in Reference 19. The load-deflection behavior of the nonlinear beams was based on model axial compressive stiffness and failure loads. Three variations each in the behavior of both the fuselage crush and nonlinear beam characteristics were included in the analyses, so that the response throughout the fuselage could be ascertained as a function of relative stiffness and failure levels in the regions both adjacent and downstream of the impact location. The study was then performed for a range of impact velocities from 6.1 m/sec to 15.2 m/sec. The airframe strength exceedance as a function of the

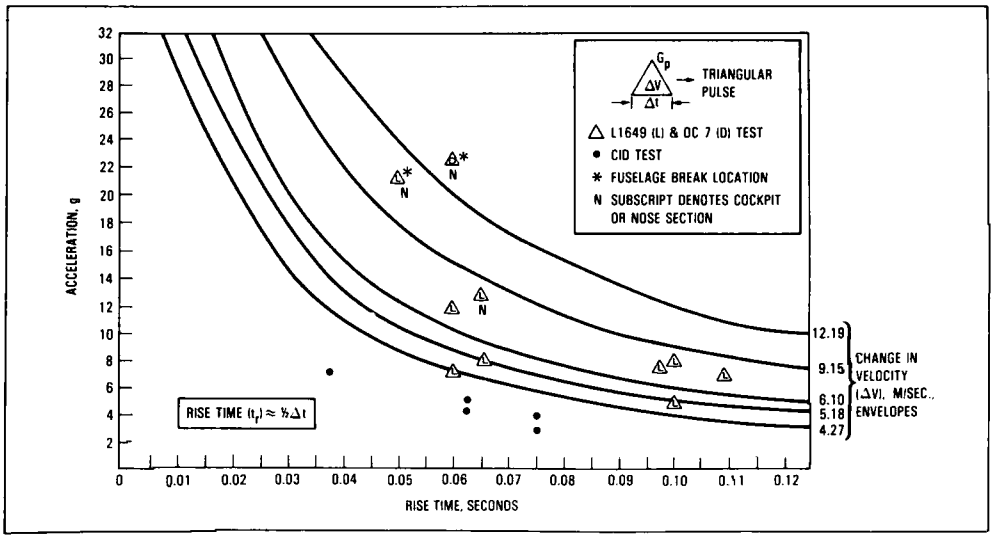

FIGURE 16. SUMMARY OF MEASURED LONGITUDINAL PULSES

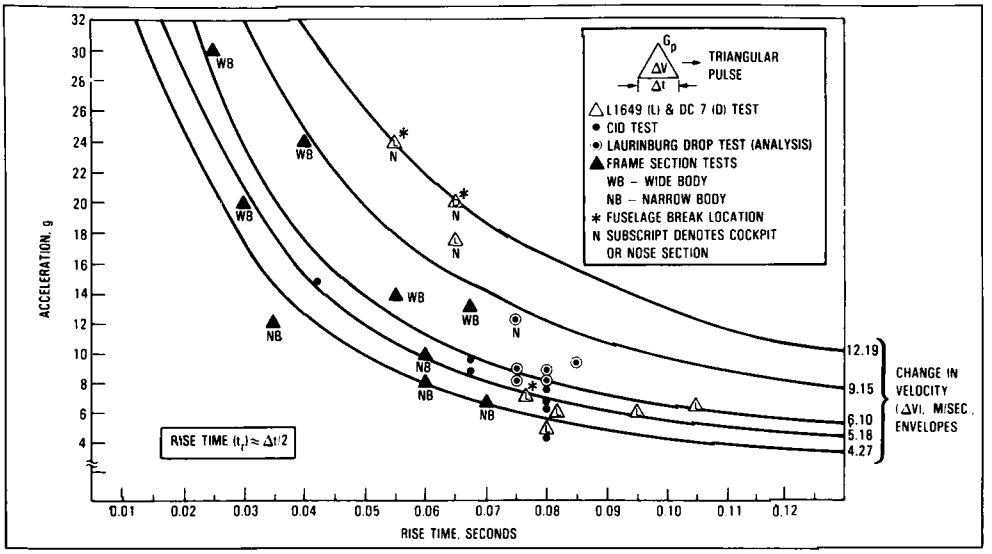

FIGURE 17. SUMMARY OF MEASURED VERTICAL PULSES

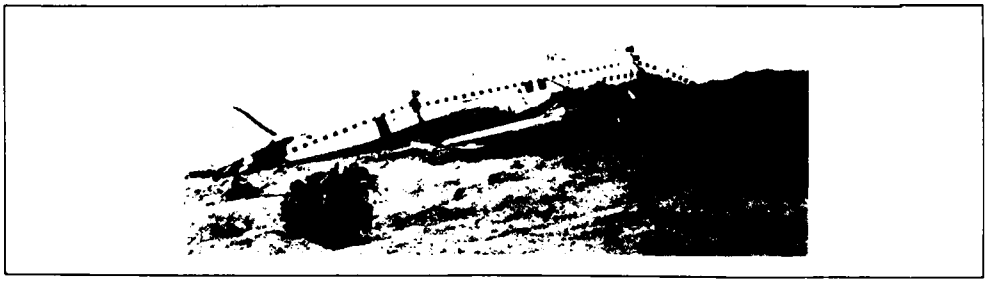

FIGURE 18. L-1649 WRECKAGE SHOWS TWO FUSELAGE BREAKS

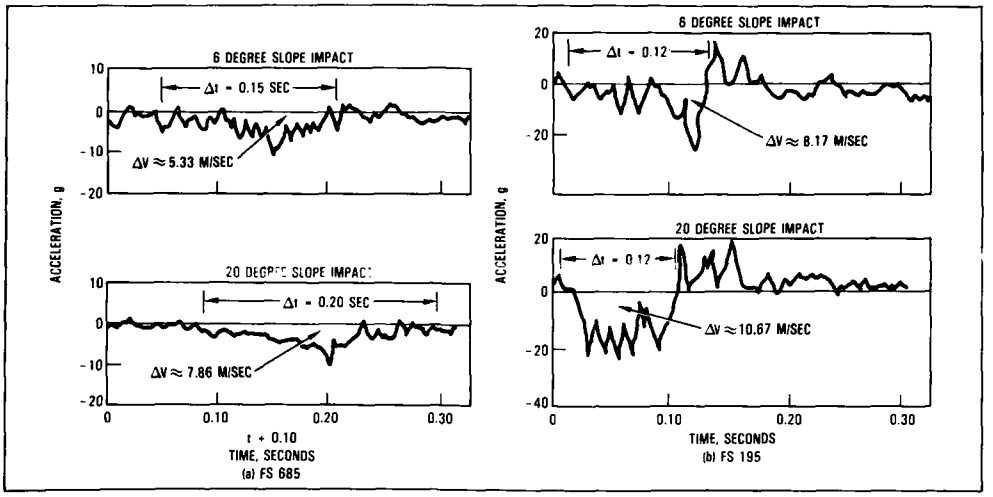

FIGURE 19. L-1649 MEASURED LONGITUDINAL PULSES AT TWO LOCATIONS AND FOR TWO IMPACT CONDITIONS

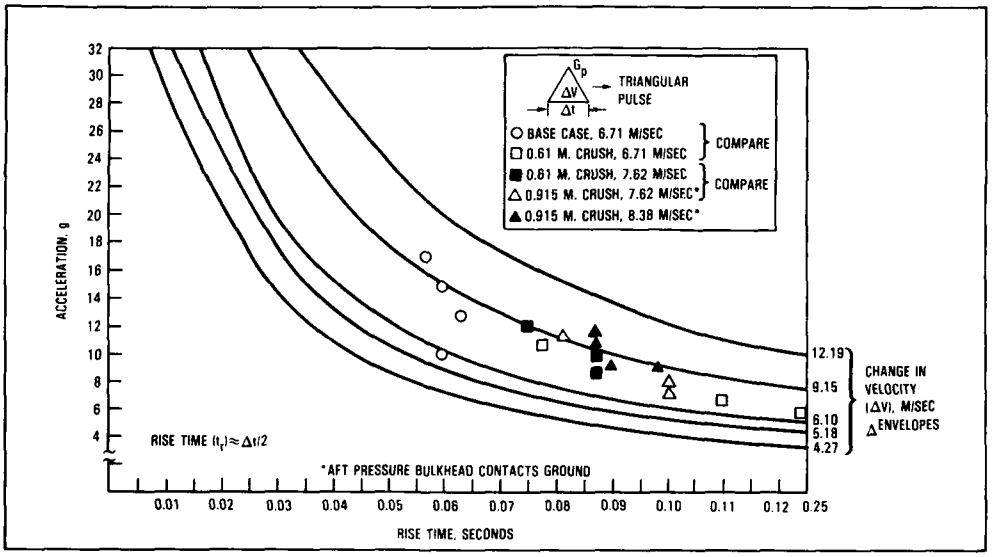

FIGURE 20. ANALYTICALLY OBTAINED VERTICAL PULSES, AIR-TO-GROUND IMPACT-CRUSH VARIATION

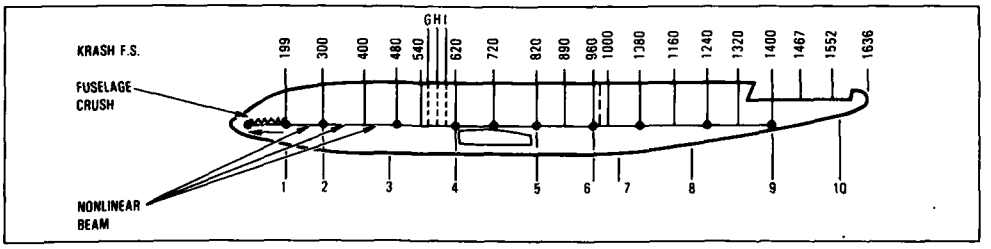

FIGURE 21. KRASH MODEL FOR FORWARD IMPACT INTO A 90 DEGREE WALL

longitudinal impact velocity determined by KRASH analyses suggests that at around a 9.14 m/sec impact the passenger cabin region stays intact. However, at higher velocities there is potential for cabin failures depending on the collapse or failure modes of the structure.

The results of the parametric study involves analyses and test data which were used to formulate the vertical velocity change versus longitudinal velocity change envelopes shown in Figure 22. This data is representative of a triangular pulse with a rise time (t_r) between .075 seconds and .100 seconds. Figure 22 displays analysis and test data points and defines both the airframe structural integrity and the floor induced passenger seat dynamic pulse envelopes. The seat dynamic pulse envelope is higher than the structural integrity envelope and accounts for rotational and rebound effects. The seat pulse represents floor responses anticipated in a survivable accident which is defined as the limit of fuselage strength. A dynamic test requirement for seats could be higher than the airframe pulse envelope provided the seat reaction loads, produced by the pulse, do not exceed floor-airframe design strength.

Tables 7 and 8 provide a summary of test and analysis conditions that were integrated into the development of the envelopes depicted in Figure 22. Table 7 shows the vertical pulse related data, while Table 8 shows both the longitudinal-only and combined longitudinal-vertical pulse-related data. A comprehensive description of the parametric analyses, using the CID airplane as a representative transport category airplane, is presented in Reference 23.

FAA CRASH DYNAMICS PROGRAM

The CID correlation and post-CID parametric study results, presented in prior sections of this paper, represent a segment of a much broader FAA Crash Dynamics research program. Figure 23 chronicles this continuing effort during the decade of the 80's. From Figure 23, it can be observed that while several phases of the program have been completed, others are in progress and some will be initiated shortly. The parametric studies illustrate the application of validated analytical methodology to develop a crash design envelope for transport category aircraft. FAA sponsored research is expanding the test data base and applying state-of-the-art methodology in other areas including:

- Size Effects - Crash design envelopes for a range of aircraft categories and configurations
- Fuel Containment - Crash Design Considerations for Fuselage Auxiliary Fuel Systems
- Composite and/or Advanced Materials - Crash Design Considerations
- Water/Soil Impact Design Considerations

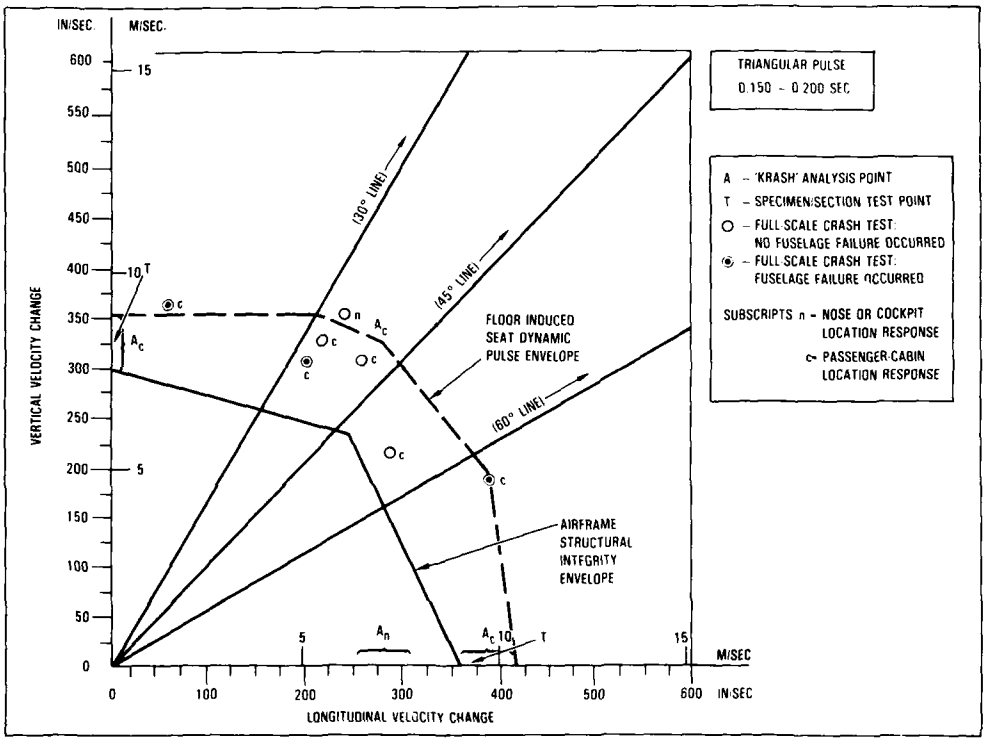

FIGURE 22. VELOCITY ENVELOPES FOR TRANSPORT CATEGORY AIRPLANES

TABLE 7. SUMMARY OF FLOOR VERTICAL RESPONSE PULSES

DESCRIPTION	IMPACT SINK SPEED, M/SEC	FLOOR TRIANGULAR PULSE RANGE					
		LONGITUDINAL			VERTICAL		
		AMPL. g	Δt SEC	ΔV M/SEC	AMPL. g	Δt SEC	ΔV M/SEC
TEST							
• CID A/P (AIR-TO-GROUND)	4.27-4.57	–	–	–	6-8	0.13-0.20	4.59-6.89
• NARROW-BODY SECTION – VERTICAL DROP, 0.46M CRUSH	6.10	–	–	–	8-10	0.11-0.13	5.58-6.56
• NARROW-BODY SECTION – VERTICAL DROP, 0.61M-0.71M CRUSH	10.67	–	–	–	12-14	0.15-0.18	10.83-12.47
AIRPLANE ANALYSES							
• LAURINBURG (+1° PITCH)	5.18	–	–	–	8-10	0.14-0.16	5.58-6.56
• AIR-TO-GROUND (GEARS RETRACTED, 0° PITCH, 0.46M CRUSH)	6.71**	–	–	–	10-13	0.13-0.14	7.22-8.53
• AIR-TO-GROUND (GEARS EXTENDED, 0° PITCH, 18" CRUSH)	6.10**	–	–	–	8-11	0.14-0.18	6.56-9.84
• AIR-TO-GROUND (GEARS RETRACTED, 0° PITCH, 0.61M-0.915M CRUSH	7.62-8.38**	–	–	–	8-12	0.15-0.20	8.20-9.84

*FUSELAGE IMPACT, -2° PITCH **FUSELAGE BREAK OR STRENGTH EXCEEDANCE

TABLE 8. SUMMARY OF FLOOR LONGITUDINAL AND COMBINED LONGITUDINAL/VERTICAL RESPONSE PULSES

DESCRIPTION	IMPACT SINK SPEED, M/SEC	FLOOR TRIANGULAR PULSE RANGE					
		LONGITUDINAL			VERTICAL		
		AMPL. g	Δt SEC	ΔV M/SEC	AMPL. g	Δt SEC	ΔV M/SEC
TEST							
• L-1649 A/P (6° SLOPE)	5.64	8-10	0.12-0.20	4.59-9.51	5-10	0.15-0.20	4.57-7.55
• L-1649 A/P (20° SLOPE)	11.50**	5-10	0.20-0.22	5.25-8.86	5-10	0.15-0.20	4.57-8.20
• AXIAL CYLINDER SECTION – LONGITUDINAL CRUSH	–	12	0.15	9.84	–	–	–
AIRPLANE ANALYSES							
• GROUND-TO-GROUND (6° RAMP)	5.64	8	0.11-0.14	4.59-5.58	6-9	0.08-0.11	3.28-4.57
• GROUND-TO-GROUND (20° RAMP)	7.62**	5-8	0.16-0.21	5.58-8.53	6-8	0.11-0.16	4.59-6.56
• GROUND-TO-GROUND (20° RAMP)	11.50**	8	0.11-0.14	4.59-5.58	14	0.10	7.22
• GROUND-TO-GROUND (8° RAMP)	9.97**	8-14	0.05-0.06	3.28-5.47	20	0.09	9.84
• 90° WALL – LONGITUDINAL	–	8-10	0.20-0.24	9.84	–	–	–

*FUSELAGE IMPACT, -2° PITCH **FUSELAGE BREAK OR STRENGTH EXCEEDANCE

Size Effects

The development of the crash design envelopes described earlier apply to transport category airplanes. This category encompasses a range of gross take-off weights from a minimum of 5,682 kg to as much as 318,182 kg. Consequently, the concern for how the floor crash pulse could vary as a function of airplane size led to a preliminary investigation of this effect. The FAA/NASA studies (References 27-31) were coordinated with the parametric analysis results described in Reference 23. A simplified approximate expression was used which related crush energy dissipation to the kinetic energy to be absorbed. The velocity-crush distance-peak acceleration triangular pulse relationship is plotted in Figures 24 and 25, for the vertical and longitudinal directions, respectively. For the vertical direction impact, Figure 24, one can ascertain that for smaller aircraft, such as the light-weight general aviation airplanes, that if the maximum available below floor space were crushed uniformly and completely (100 percent efficiency) then a velocity change of 7.92 m/sec, a peak acceleration of 26g and a triangular pulse of .063 seconds duration might be appropriate. For larger aircraft, the data suggests lower peak g's, higher velocity changes and a longer pulse duration. The transport catagory airplane parametric study results discussed earlier showed that this trend prevails as additional crush is provided. The parametric study results also show that for the CID airplane configuration the crush distribution along the fuselage varies from 0.31 meters to 0.56 meters (Figure 14) before contact with stiff structure occurs (e.g. bulkhead) and produces sufficiently high loads to exceed airframe strength. Thus, the narrow-body section data point for an impact velocity of $\approx$ 10.67 m/sec (Reference 29) which is performed for a soft

frame and not restrained by airplane bulkheads produces a crush distance which in a crash is most likely not realizeable. For the CID configuration 0.56 meters at the aft fuselage represents approximately 30 percent of the total depth below the passenger floor in that region. Thus, the larger transports, while providing more crush distance than the smaller airplanes, do not allow for total use of the available crush space. Estimates of available crush distance as a function of airplane size are shown in Figure 24.

Figure 25 presents crush, velocity change and peak acceleration response relationships along with supporting analysis and test data for the longitudinal direction pulse. Included in this figure are similar reference data as shown in Figure 24, but for the longitudinal direction. The crush zones for various categories of aircraft for this direction are not as well defined as underfloor space is for the vertical direction. The impact of light-fixed wing aircraft into a soil terrain (References 6, 32, 33) indicates extensive forward fuselage crush is experienced for the smaller aircraft in a

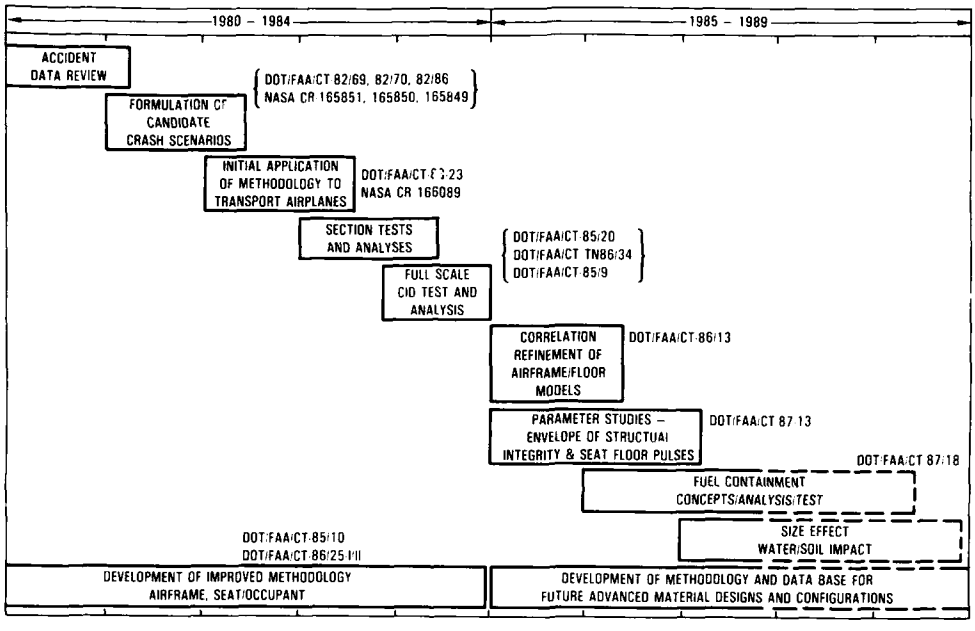

FIGURE 23. IMPACT DYNAMICS PROGRAM, 1980 – 1989

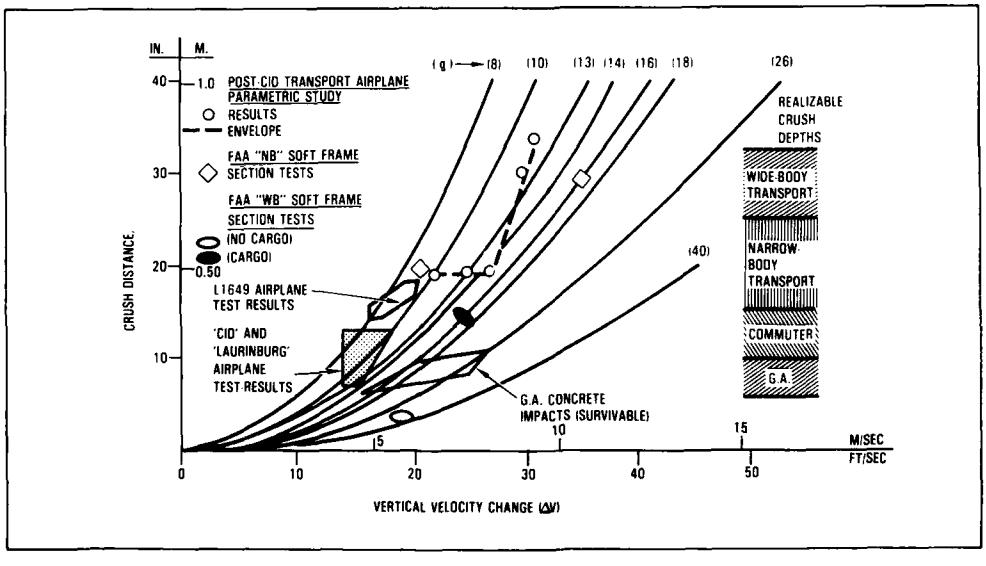

FIGURE 24. CRUSH, VELOCITY CHANGE AND PEAK ACCELERATION RELATIONSHIP-VERTICAL DIRECTION TRIANGULAR PULSE

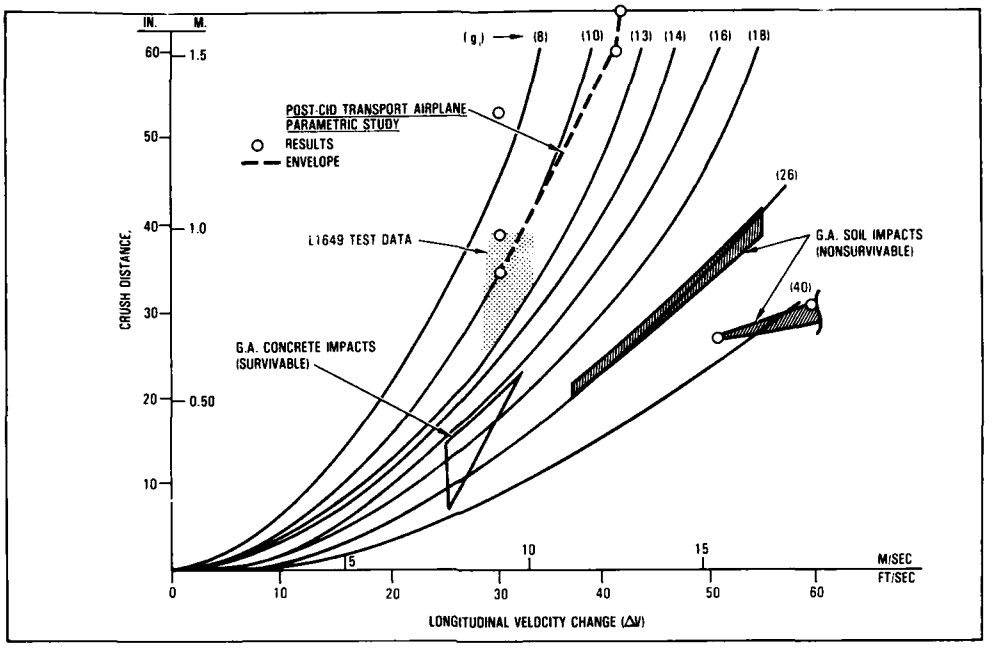

FIGURE 25. CRUSH, VELOCITY CHANGE AND PEAK ACCELERATION RELATIONSHIP – LONGITUDINAL DIRECTION TRIANGULAR PULSE

nonsurvivable crash. The crush term in Figure 25 can include seat stroke and ground displacement in addition to fuselage collapse when addressing test data. The parametric study results based on the narrow-body CID airplane configuration indicate substantial fuselage crush could occur forward of the passenger compartment. *The aforementioned* results, depicting size effects on crash design criteria, is being explored further in current FAA efforts directed toward commuter airplane crash design criteria.

Fuselage Mounted Auxiliary Fuel Tanks

In another related crash design effort an investigation into "fuel containment concepts" is being performed under FAA sponsorship. The initial phase of this study, reported in Reference 35, shows that the use of crash-resistant fuselage auxiliary fuel tanks may have a more advantageous benefit to cost trade-off than wing fuel structure modifications and/or wing fuel crash-resistant systems. As part of the Phase II study the dynamic response of fuselage auxiliary fuel tank system installations are being investigated. These concepts include:

1. Bladder cells fitted in the lower fuselage
2. a) Conformable tank mounted to both passenger and cargo floors e.g. wide-body aircraft

   b) Conformable tank mounted to passenger floor and to fuselage frame e.g. narrow-body
3. Cylindrical tanks mounted to cargo floor

Each of these concepts are being modeled with KRASH to depict attachment loads and mass accelerations, as well as absolute and relative displacements for fore-aft loads and vertical impact loads under dynamic impact loading conditions.

Composite Designs for Crash Dynamics

A third consideration in the development of crash design criteria is the manner in which designs of composite material in lieu of metals influence dynamic response and load transfer behavior. In the last several years the use of advanced materials, including composites, has accelerated. The biggest strides have been made with military rotorcraft. References 36-39 report on crash analysis fuselage designs which incorporate composite materials. In all of these studies, program KRASH is the tool with which the analytical study is performed. The purpose of these studies are, generally, to show trade-off between response levels and designs and/or design requirements. These studies point out that; composite materials offer significant benefits over metallic structures in reducing weight and cost as well as improved corrosion resistance. However, composite materials exhibit low strain-to-failure compared to such metals as 2024 aluminum, a ductile metal

that can tolerate rather large strains, deform plastically and absorb a considerable amount of energy in the nonlinear region without fracture. Because of this difference between composites and metals, crash energy absorption with composites must come from innovative design to augment the lower material stress-strain behavior of the composites.

Taking into consideration the findings from rotary-wing composites studies, the FAA's approach in the assessment of crash design compatibility of composites in "lieu of" metals is as follows:

1. The energy absorption capability of the structure to be affected by the impact loading must be determined.

   Tests conducted by the FAA Technical Center and supporting analyses, described in Reference 16, illustrate the manner in which current structure can be evaluated so as to establish guidelines for replacement structure. Briefly, this approach consisted of analyzing the structural behavior of a wide-body airplane during a crash impact using program KRASH for specified impact conditions, to determine the response and crushing distribution along the fuselage. This analysis is then followed by a more detailed analysis of the frame segments wherein critical responses can occur. Several section tests and analysis, as-sequenced in Figure 26, were performed for this purpose. The FAA conducted two widebody section drop tests. The first consisted of lightly loaded (2,273 kg) section without cargo (6.1 m/sec impact velocity) and the second of a more densely loaded (4,909 kg) section with cargo (7.62 m/sec impact velocity). The post-test results shown in Figure 27, vividly demonstrate the crush behavior associated with both specimens. The lightly loaded structure crushed approximately 0.05 meters while the latter crushed as much as 0.36 meters. The comparative passenger floor responses are approximately 35g peak acceleration, .040 sec; pulse duration and 16g peak acceleration, .100 sec. pulse duration, respectively.

2. The combination of composite material's behavior and designs must exhibit equal or better energy absorption than the metals which they replace.

   There are several parameters which can be used as measures of performance for comparing composites with metals, as illustrated in Figure 28. The parameters are specific energy, which donsiders energy and weight; load uniformity which indicates the relationship between peak and average force; stroke ratio, which provides a measure of effective use of material; energy dissipation density, which also indicates the degree of effectiveness in absorbing energy; ratio of dynamic to static forces, which reflects a material property such as strain rate which could influence behavior under dynamic loading; and crush stress, which is related to the forces and area involved in the loading. As one could surmise, these parameters can be interrelated. The results of the recent 'composite' related study for transport category airframe structure (reference 40) illustrated the manner in which designs and material behavior affect these various parameters.

3. The failure mode and energy absorption of a composite design must meet design criteria requirements and may not be feasible on a one-to-one substitution basis.

   This premise is borne out by the results from the study described in reference 40 which illustrated how the details of design with composites can influence results insofar as failure mode and energy absorption are concerned.

Water/Soil Interaction Design Considerations

Much of the crash dynamics research, whether it be for metallic or composite designs, has been performed considering the impact surface to be rigid. For resilient soil and water impact the underfloor structure can be loaded differently than for rigid surfaces. In soil and water impacts from crash loads can be distributed over the underfloor skins. The potential for a skin rupture exists which could minimize the effectiveness of crushable beams and frames. The effect of soil scoop and with it increased longitudinal loads, as was demonstrated in some earlier general aviation crash tests is also a concern. The development of crashworthy design concepts, which would be beneficial in soil/water impacts, will be enhanced with improved analytical methodology. With this in mind, the FAA has initiated effort to identify additional KRASH code modifications directed at addressing structure-ground interaction load transfer mechanisms. This effort could expand to include tests of shapes/configurations into resilient yielding surfaces.

SUMMARY

The FAA and NASA developed a joint structural crash dynamics program which provided the framework for improved methodology. While the R&D program is still ongoing, several significant milestones have been successfully completed. Section drop tests of narrow-body airplane and wide-body airplane frames, as well as a full-scale drop test of a complete test article ('Laurinburg') and a remotely piloted airplane crash test (CID) have been performed, along with supporting analyses. The validation of analytical modeling of the CID, using an improved KRASH85 code, was followed by a parametric study in which airframe integrity as a function of a velocity and attitude profile was investigated. The results of this parametric study, which included KRASH85 analyses, combined with additional available test data, were used to establish both structure and seat dynamic test crash design velocity envelopes. The application of analytical methodology to the establishment of crash design criteria provides opportunities to expand crash design and compliance procedures to a broad segment of aircraft configurations. As is noted in the

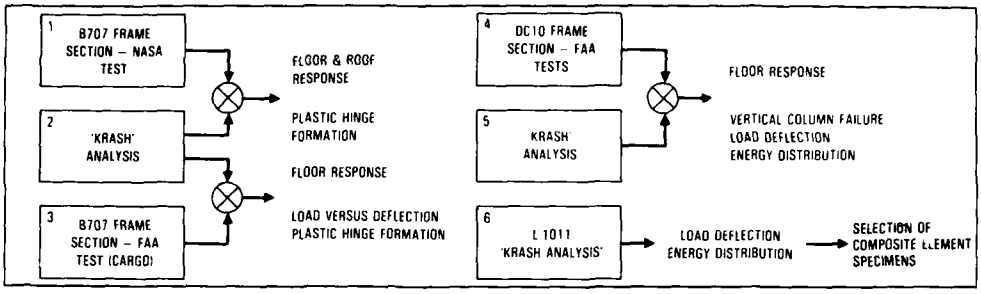

FIGURE 26. FRAME SECTION ANALYSES AND TESTS

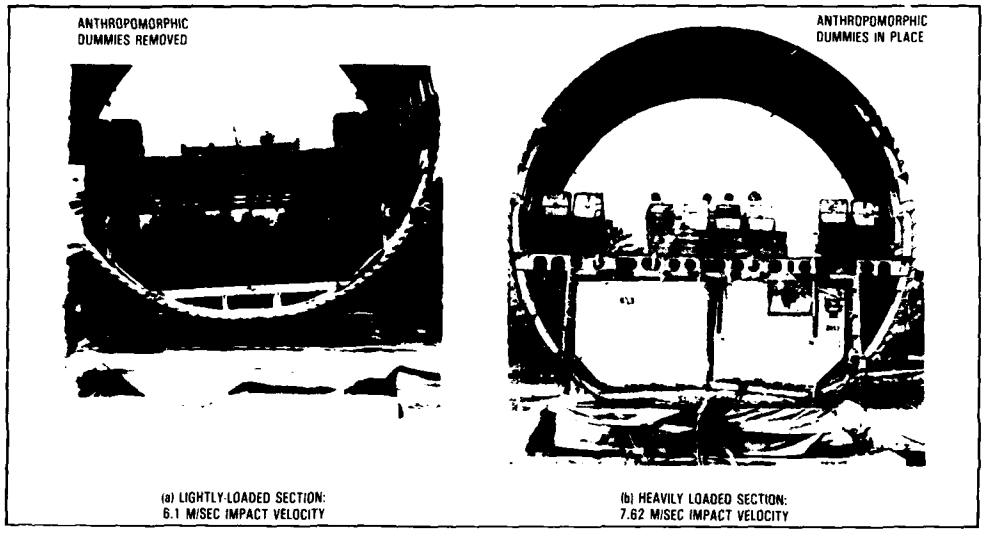

FIGURE 27. WIDE-BODY FRAME SECTION POST-TEST RESULTS

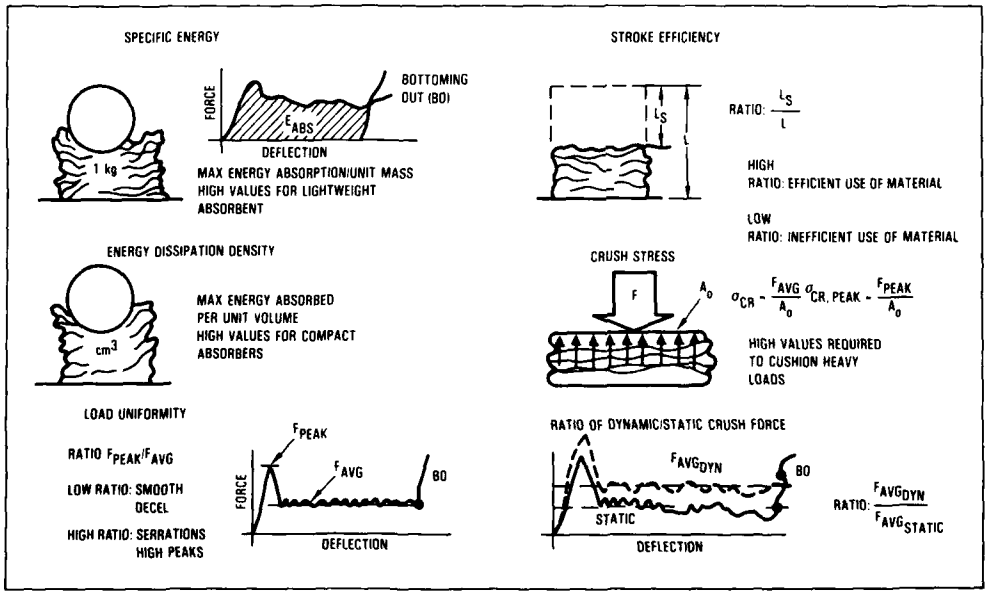

FIGURE 28. ENERGY ABSORPTION TERMS

paper, the application of state-of-the-art analysis complimented by test data enables an assessment of composite material usage in lieu of metal structure in a crash impact sensitive region. The procedure outlined in the paper highlights the key measurement parameters that have to be considered. While preliminary in some respects, the procedures described herein provide the initial application of the FAA/NASA fostered methodology developed to crash design criteria.

The effort to expand the data base and enhance methodology capability is an ongoing effort. Areas that are being addressed include; different sizes and configurations, fuel containment, composites and/or advanced materials, and impacts into resilient yielding surfaces, such as soil and water.

ACKNOWLEDGEMENTS

The authors wish to express their appreciation for the support provided by many individuals and organizations. In particular we would like to acknowledge the cooperative spirit of the late Dr. Bob Thomson of the NASA Langley Impact Dynamics Facility. Also Larry Neri, the FAA Technical center program manager of the many KRASH related studies. A special acknowledgement is due to Max Gamon and Bill LaBarge of Lockheed for their part in the development of program KRASH, which has made possible the many applications that have been described in this paper.

REFERENCES

1. American Helicopter Society, National Specialist's Meeting on Crashworthy Design of Rotorcraft, Atlanta, Ga., April 7-9, 1986.

2. Thomson, R.G., Caiafa, C., "Designing for Aircraft Structural Crashworthiness," AIAA-81-0803, AIAA/SAE/ASCE/ATRIF/TRB 1981 International Conference, May 26-28, Atlantic City, NJ.

3. Wittlin, G., "Program KRASH, the Evolution of an Analytical Tool to Evaluate Aircraft Structural Crash Dynamics Response," AHS Meeting , Atlanta, Ga. April 1986.

4. Fasanella, E.L., Widmayer, E., Robinson, M.P., "Structural Analysis of the Controlled Impact Demonstration of a Jet Transport Airplane," AIAA Paper No. 86-0939 CP, San Antonio, Texas, May 1986.

5. Wittlin, G. and Gamon, M.A., "Experimental Program for the Development of Improved Helicopter Structural Crashworthiness Analytical and Design Techniques," USAAMRLDL-TR-72-72, Volumes I and II, May 1973.

6. Wittlin, G. and Gamon, M.A., Full-Scale Crash Test Experimental Verification of a Method of Analysis for General Aviation Airplane Structural Crashworthiness," FAA Report FAA-RD-77-188, February 1978.

7. Gamon, M.A., Wittlin, G., La Barge, W.L., "General Aviation Airplane Structural Crashworthiness User's Manual Volumes I, II, III, Theory - Input-Output, Techniques, Applications and Related Design Information," FAA- RD-77-189 I,II (Revised), III, September 1979.

8. Gamon, M.A., Wittlin, G., and La Barge, W.L., "KRASH85 User's Guide - Input/Output Format," DOT/FAA/CT-85/10, May 1985.

9. Cronkhite, J.D. and Berry, V.L., "Investigation of the Crash Impact Characteristics of Helicopter Composite Structures," USAAVRADCOM-TR-82-D-14, February 1983.

10. Carnell, B.P., Pramanik, M., "ACAP Crashworthiness Analysis by KRASH," AHS Meeting, March 1983, Philadelphia, PA.

11. Sen, J.K., Votaw, M.W., Downer, G.R., "Influences of Two Landing Gear Designs on Helicopter Crashworthiness and Weights," Hughes Helicopters, Inc., AHS Meeting, May 1985, Ft. Worth, Texas

12. Pramanik, M., "Landing Gear Performance Simulation by KRASH Program," AHS Meeting, April 1986, Atlanta Ga.

13. Jackson, A. C., Wittlin, G., Balena, F. J., Transport Composite Fuselage Technology - *Impact Dynamics and Acoustic Transmission*" - AFWAL-TR-85-3094, Proceedings of the Seventh Conference on Fibrous Composites in Structural Design, June 1985.

14. Wittlin, G., and Lackey, D., "Analytical Modeling of Transport Aircraft Crash Scenarios to Obtain Floor Pulses," FAA Report DOT/FAA/CT-83/23, NASA CR 1666089, April 1983.

15. Discussions with Dr. M. Sadeghi and Dr. A. Walton, Cranfield Institute of Technology, March 1987.

16. Wittlin, G., and La Barge, W.L., "KRASH Dynamics Analytical Modeling - Transport Airplane Controlled Impact Demonstration Test," DOT/FAA/CT-85/9, May 1985 (Revised March 1986).

17. AGARD Report No. 737, "Crashworthiness of Airframes - Transport Aircraft Structural Crash Dynamics Analysis and Test," 61st Meeting of the Structures and Materials Panel of AGARD in Oberammergau, Germany 8-13 September 1985.

18. Wittlin, G., "KRASH Analysis Correlation - Transport Airplane Controlled Impact Demonstration Test," DOT/FAA/CT-86/13, December 1986.

19. Greer D. L., et al, "Design Study and Model Structures Test Program to Improve Fuselage Crashworthiness," FAA Technical Report DS-67-20, October 1967.

20. Reed, W.H., et. al., "Full-Scale Dynamic Crash Test of a Lockheed Constellation Model 1649 Aircraft," FAA Technical Report ADS-38, Washington, D.C., October 1965.

21. Reed, W.H., et. al.: "Full-Scale Dynamic Crash Test of a Douglas DC-7 Aircraft" FAA Technical Report ADS-37, Washington, DC, October 1965.

22. Johnson, D., Garodz, L., "Crashworthiness Experiment Summary, Full-Scale Transport Controlled Impact Program," DOT/FAA/CT-85/20, June 1986.

23. Wittlin, G., La Barge, W.L., "KRASH Parametric Sensitivity Study - Transport Category Airplanes," DOT/FAA/CT-87/13, December 1987.

24. Hayduk, R.J., Thomson, R.G., Wittlin, G. and Kamat, M.P., "Nonlinear Structural Crash Dynamics Analysis," SAE paper 790588, April 1979.

25. Badrinath, Y.V., "Simulation Correlation and Analysis of Structural Response of a CH-47-A to Crash Impact," USARTL-TR-78-24, August 1978.

26. Mens, J., "Survey of Crashworthiness Achievements on Aerospatiale Helicopters," 41st Annual Forum, American Helicopter Society, Fort Worth, Texas, May 1985.

27. "B707 Fuselage Drop Test Report," Calspan Report No. 7252-1, March 1984.

28. Hayduk R., Williams S., "Vertical Drop Test of a Transport Fuselage Section Located Forward of the Wing," NASA Tech Memo 85679, August 1983.

29. Johnson D., Wilson A., "Vertical Drop Test of a Transport Airframe Section," DOT/FAA/CT-TN 86/34, October 1986.

30. "DC-10 Fuselage Drop Test Report," Calspan Report No. 7251-1, September 1984.

31. DC-10 Drop Test No. 2, FAA Technical Center Preliminary Data.

32. Castle C.B., Alfaro-Bou E., "Crash Tests of Three Identical Low-Wing Single Engine Airplanes," NASA Technical paper 2190, September 1983.

33. Vaughan Jr. V., Hayduk R., "Crash Tests of four Identical High-Wing single-engine airplanes," NASA Technical Paper 1699, August 1980.

34. Nissley P.M., Heid, T.C. "Structural Design For Fuel Containment Under Survivable Crash Conditions," FAA-TR-ADS-19, August 1964.

35. Wittlin G., "Fuel Containment Concepts - Transport Category Airplanes," DOT/FAA/CT 87/18, November 1987.

36. Sen, J.K., "Designing for a Crashworthy All-Composite Helicopter Fuselage," AHS, Philadelphia, PA, May 1984.

37. Logan, A.H., Votaw, M. W., "The Hughes Integrated Approach to Helicopter Crashworthiness - Past, Present and Future, AHS, Ft. Worth, Texas, May 1985.

38. Sen, J.K., and Votaw, M.W., "Skin Wing Design for a Crashworthy Composite Fuselage for the Hughes 500E Helicopter," AHS, Ft. Worth, Texas, May 1985.

39. Cronkhite, J.D., "Design of Airframe Structures for Crash Impact," AHS, Atlanta, Ga., April 1986.

40. Jackson, A.C., et. al., "Transport Composite Fuselage Transmission," NASA CR 4035, December 1986.

CRASHWORTHINESS OF AIRCRAFT STRUCTURES

by

W. Jarzab, R. Schwarz
Industrieanlagen-Betriebsgesellschaft
Einsteinstraße 20, 8012 Ottobrunn
Federal Republic of Germany

SUMMARY

Modern analytical models and their numerical realizations have become powerful tools in nonlinear crash analysis. Crash simulation has to consider advanced nonlinear constitutive equations and sophisticated formulations of the contact problem. The refinement of discretisation and the treatment of geometrical complex structures requires highly developed hardware like the vector processor.

Topics discussed are the material modeling of impact loaded composite structures, the main features of an explicit crash code and the results of two calculations simulating the drop test of a B707-section. Finally the possibilities of a specific interface between a crash code based on the finite element method like ANCS and a program like KRASH85 are outlined in detail.

1. INTRODUCTION

In order to move ahead the knowledge about the structural response of crash loaded aircraft systems and to establish adequate prediction methods the development, application and verification of crash codes was of main importance in aircraft and automotive industry during the last years. It has been proven to be useful to apply analytical, numerical and experimental tools in combination. Especially for the modeling of dynamically loaded structures and the crashworthy design of components an experimental data base is undispensable. Vice versa the numerical analysis will support the experimental investigations and reduce the number and cost of tests (ref./1/-/3/). It should be mentioned that for scientific and economical reasons the numerical analysis of crash loaded aircraft components seems to be more valuable and promising than the analysis of complete airframes. A deeper knowledge of crash loaded metallic and composite components will be of main importance for the engineer and will support the research of complex structures consisting of already investigated substructures.

2. NONLINEAR MATERIAL MODELING

The nonlinear field theories of continuum mechanics developed and extended during the last 30 years permit the description of metallic and nonmetallic materials taking into account geometrical and physical nonlinearities and the dissipative behavior as well. The analytical modeling of nonmetallic composite materials is realized by specific constitutive equations of finite anisotropic elasticity and nonlinear viscoelasticity in order to approximate the elastic and dissipative phenomena of laminates. Figure 1 shows a hysteresis of a nonlinear incompressible viscoelastic material which is comparable with certain resins. The chosen constitutive equation is a generalization of Haupt's material model (ref. /4/). Under a static preloading of 80.24 N a harmonic displacement excitation with an amplitude of 0.5 mm and a frequency of 25 Hz is applied to the specimen. The dynamic stiffness and the loss factor are calculated to 20 N/mm resp. 9.62 degrees. The calculation of the energy dissipation, characterized by the area of the hysteresis yields 4.83 N mm. As dynamic stiffness and loss factor are increasing with frequency and static preloading the viscoelastic material will dissipate more energy in the high than in the low frequency range. In connec-

tion with the elastic stiffness of the fibre material the whole composite structure will absorbe a quantity of kinetic energy under reduced deformations.

The constitutive equations of anisotropic elasticity and nonlinear visoelasticity are implemented in a layer-sublayer-element which takes into account the shear deformation behavior of laminates due to the theoretical approach of J.N. Reddy. Further applications of this model to other types of composites will prove the admissibility of the separation into an elastic and a viscoelastic part. It should be mentioned that the classical rheological models of viscoelasticity have a limited qualification to describe the main nonlinear effects of resins. The main reasons for that are the reduced consideration of deformation history and the linear basic assumptions of these constitutive laws.

The material failure behavior - consideration of delamination and fibre cracks - is described by empirical models which are compatible with continuum mechanics and allow a direct approach to experimental results. The shear strength of the laminate is the main base of that description. However further analytical and experimental investigations concerning fracture mechanics for composites are necessary to establish more general models and to evaluate all appearing failure modes.

3. CRASH CODE ANCS

The crash code ANCS (Advanced Numerical Crash Simulation) is an explicit Lagrangian code with a linear and sequential program structure, portable on standard computers, vector and array processors as well. The main features are (ref./5/-/8/):

- keyword directed input;
- explicit time integration based on the central difference scheme;
- direct element formulations based on nonlinear strain analysis (e.g. Green-Lagrangian strain tensor, Almansi-Eulerian strain tensor);
- nonlinear material modeling (finite isotropic and anisotropic elasticity, dynamic plasticity, nonlinear viscoelasticity, viscoplasticity);
- material failure package (empirical and statistical models);
- contact processor based on a generalized master slave concept (modeling of geometrical arbitrary contact problems);
- adapted postprocessing;

The first verifications of ANCS were concentrated on the numerical simulation of frontal car crash and the investigation of crash loaded box beams with geometrical imperfections. Figure 2 shows the typical failure behavior of a complex box beam. ANCS allows an evaluation of all geometrical and physical state variables. Local stress and strain concentrations, the global and local energy absorption and the induced contact forces can be studied in detail. In consequence the engineer will find valuable informations of a nearly "crash optimized structure" and define necessary experiments. The same approach will be performed in the near future for specific aircraft subfloor sections and crucial forms.

4. NUMERICAL SIMULATION OF DROP TESTS

For a real B707 aircraft section two numerical simulations of a drop test, comparable with the experimental investigations of FAA (ref./9/-/11/) were performed using the code ANCS. The first finite element model corresponds to the KRASH85 model. The ANCS data base (figure 3) is characterized by

- 15 MINDLIN-REISSNER shell elements,
- 32 nodal points,
- 2 master planes, 14 slave points and
- an impact velocity of 6.096 m/s.

The calculation of cross sectional parameters and stiffness values was done in analogy to /10/.

The time step was chosen in the range of 10^{-5} s and the simulation was performed in the time range $0 < t < 230$ ms. The obtained numerical results (figures 4-10) show a sufficient correlation with the KRASH85 simulation /10/. At t=155 ms the turning back point is reached and the structure is pushed back from the rigid target wall by elastic rebound (figure 8). Figure 10 shows the transformation of kinetic energy into work of deformation. At t=230 ms approximately 90 % of the kinetic energy is absorbed by the aircraft structure.

The second more complex finite element model (figure 11) takes into account the local stiffened structural parts and consists of

- 656 MINDLIN-REISSNER shell elements,
- 625 nodal points,
- 209 master planes, 200 slave points.

The time step was chosen in the range of 10^{-6} s and the simulation was performed in the time range $0 < t < 95$ ms. The results of the numerical simulation are plotted in figures 12-25. The influence of the real physical stiffness parameters based on the continuum mechanical model is in comparison to the simple finite element model clearly to be seen in the deformation history (figures 12-17). Especially the local cross sectional failure and the reduction of stiffness during the crash process is evident. The obtained transients of displacements, velocities, accelerations, contact forces and kinetic energy show a sufficient correlation with the first simulation performed with ANCS, the simulation performed with KRASH85 and the experimental investigation.

The presented results of two drop test simulations show that ANCS is an adequate software tool for the crashworthiness analysis of aircraft structures. The code ran stable during the whole calculation and a consistency with known numerical and experimental data was achieved. Of further interest will be the recently started investigations of aircraft frames with modified components in order to improve the crashworthiness behavior of the whole structure and to get local structural zones characterized by a "maximized energy absorption capacity".

5. CONCLUSIONS

The explicit Lagrangian crash code ANCS allows detailed investigations of impact loaded aircraft structures. The main advantages of ANCS contrary to experimental testing are the detailed description of strain/stress history, contact forces, local and global energy absorption and the modeling of folding mechanisms. However, up to now the elapsed CPU time on vector computers and the resulting costs are a slight disadvantage of the numerical approach. Further development activities will reduce these costs and the numerical simulation will become a real and promising alternative to very expensive experiments.

The main acitivities at IABG now are concentrated on advanced composite material modeling, superelements and the consideration of vector processor features. Benchmarks on different hardware systems (e.g. VP-200, CRAY-XMP, CONVEX-C1) were performed in order to optimize the code and to improve the portability of ANCS. Another important subject of IABG activities is the creation of a specific interface between ANCS and KRASH85. Crash loaded aircraft components (e.g. crucial forms, whole subfloor sections) will be investigated applying ANCS. The results - e.g. crash loading deflection curves and local cross sectional failure data - will be the input for KRASH85 (ref./9/-/12/) which then should be applied to a whole aircraft section consisting of the already investigated subcomponents by using ANCS. This way of research will save computer costs and will give all relevant technical informations to

the engineer. Modifications of the KRASH85 model will be realized easily substituting only a reduced set of input data. The presented approach will be realized as an item of an existing MoU between FAA and BMFT.

REFERENCES

/1/ Giavotto, V., Crash Simulation Models and Interaction with Experiments, AGARD Report No.737, April 1986

/2/ Poth, A., Scharpf, F., Application of Nonlinear FE/FD-Methods for Support of Structural Tests, AGARD Report No.736, April 1986

/3/ Poth, A., Scharpf, F., Impact Damage Effects and Computational Methods, AGARD Report No.729, February 1986

/4/ Jarzab, W., Advanced Numerical Visco-elastodynamical Simulation, IABG Report, Ottobrunn, 1988

/5/ Jarzab, W., Mathematical Modeling and Applications in Crash Analysis, Proceedings of the International Conference of Supercomputer Applications in the Automotive Industry, Suppl., Zurich, October 1986

/6/ Jarzab, W., Bretz, G., Schwarz, R., Numerical Simulation and Experimental Validation in Crashworthiness Applications, Structural Design and Crashworthiness of Automobiles (Eds. T.K.S. Murthy, C.A. Brebbia), Springer-Verlag, Berlin-Heidelberg-New York, 1987, pg. 1-16

/7/ Bretz, G., Jarzab, W., Raasch, I., Berechnung des frontalen Crashvorganges bei einer heckangetriebenen Limousine, VDI-Berichte No. 613 (Ed. D. Radaj), VDI-Verlag, Düsseldorf, 1986, pg. 507-525

/8/ Jarzab W., Schwarz, R., Numerical Simulation in Crashworthiness and Structural Impact Applications, Proceedings of the Summer Computer Simulation Conference, Montreal, 1987

/9/ Wittlin, G., Transport Aircraft Structural Crash Dynamics Analysis and Tests, AGARD Report No.737, April 1986

/10/ Hienstorfer, W.G., Erweiterungen zum Rechencode KRASH85, DFVLR Report, Stuttgart, December 1986

/11/ Georgi, H., Parameteruntersuchungen zum Krash-Rechencode an einem 5-Massen-Testgerät, DFVLR Report, No. IB 435-85/18, Stuttgart, November 1985

/12/ Gamon, M., Wittlin, G., LaBarge, B., KRASH85 User's Guide - Input/Output Format, FAA Report, DOT/FAA/CT-85/10, Atlantic City, March 1986

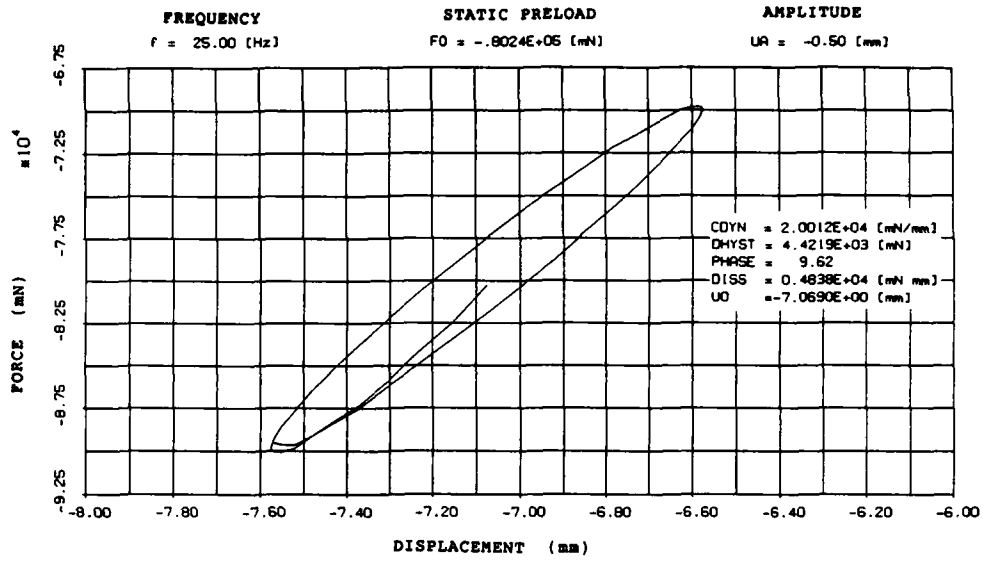

Figure 1. Viscoelastic Hysteresis of a Dissipative Structure.

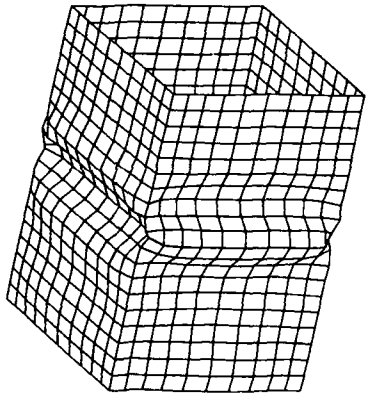

Figure 2. Local Folding Zone of a Box Beam.

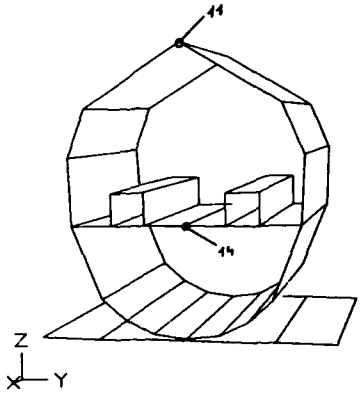

Figure 3. Reduced Finite Element Model of a B707 Section.

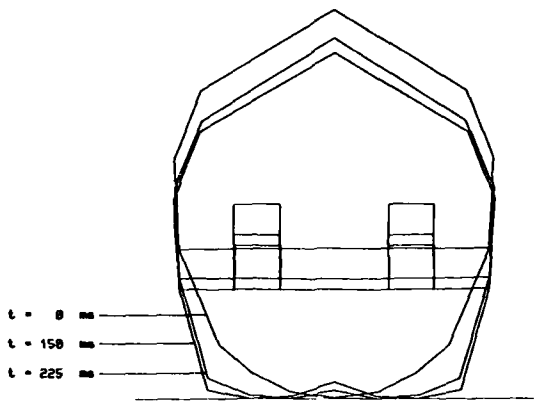

Figure 4. Deformation History of a B707 Drop Test.

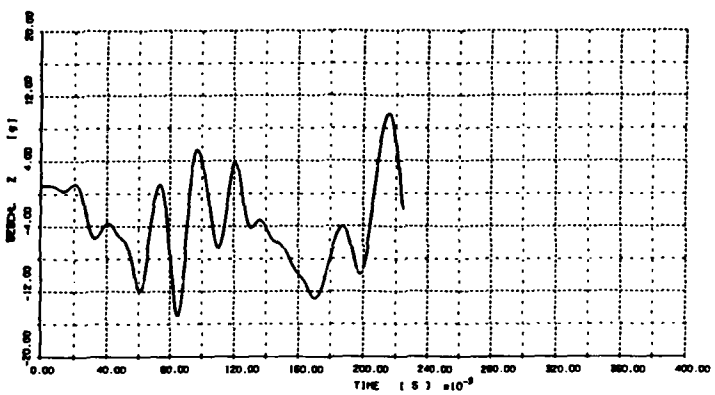

Figure 5. Vertical Acceleration at Nodal Point 11.

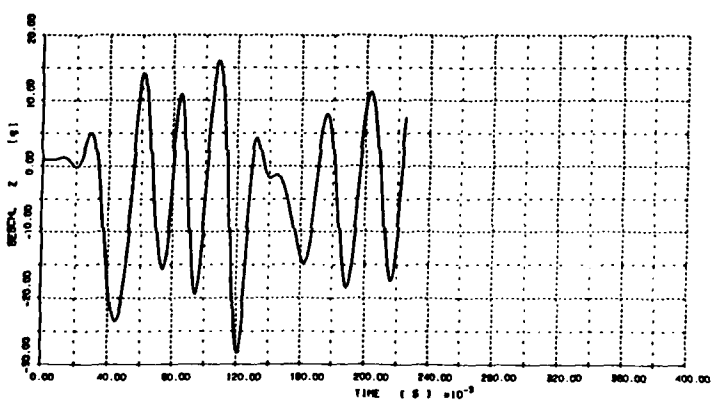

Figure 6. Vertical Acceleration at Nodal Point 14.

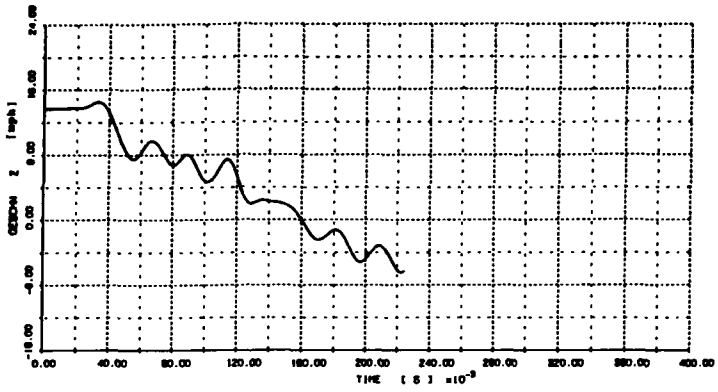

Figure 7. Vertical Velocity at Nodal Point 14.

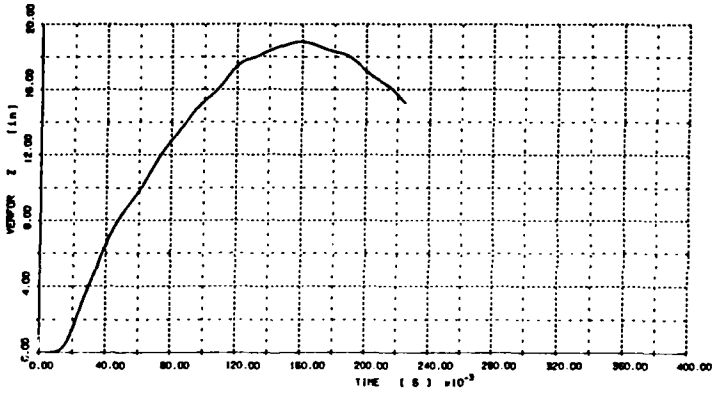

Figure 8. Vertical Displacement at Nodal Point 14.

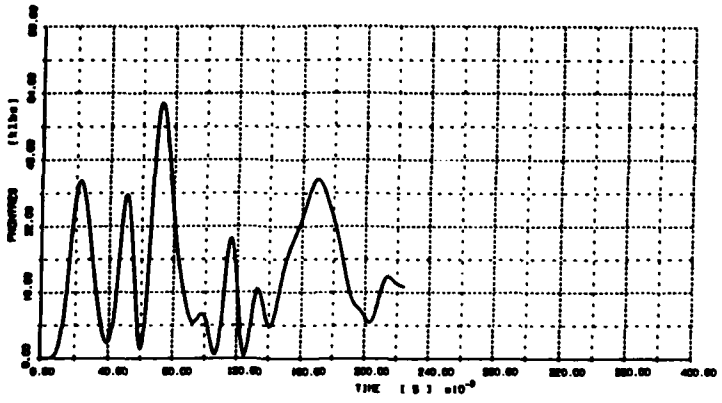

Figure 9. Contact Force.

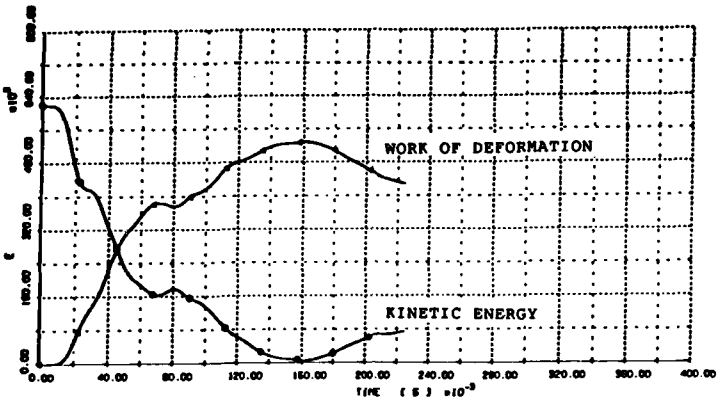

Figure 10. Kinetic Energy versus Work of Deformation.

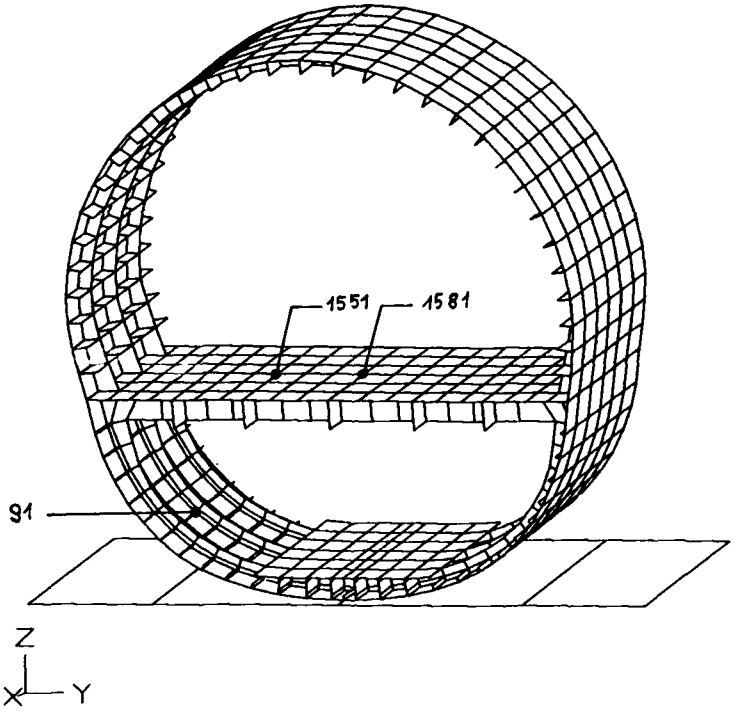

Figure 11. Complex Finite Element Model of a B707 Section.

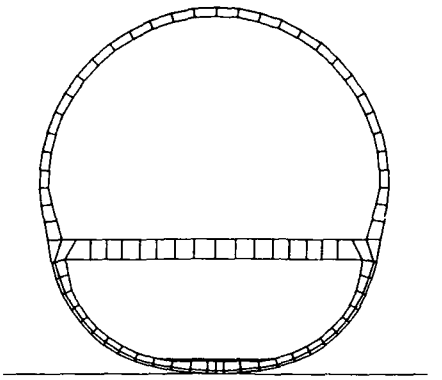

Figure 12. Undeformed Structure at t = 0 ms.

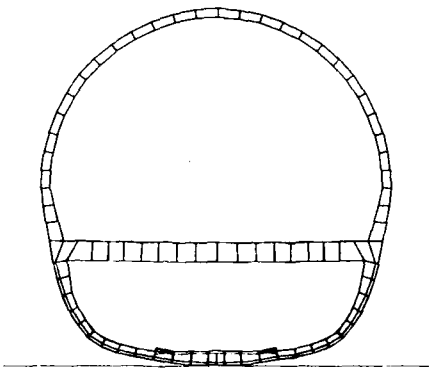

Figure 13. Structural Deformation at t = 20 ms.

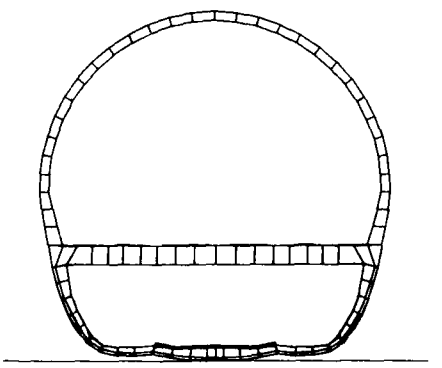

Figure 14. Structural Deformation at t = 40 ms.

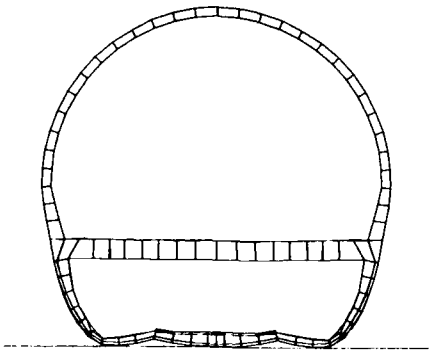

Figure 15. Structural Deformation at t = 60 ms.

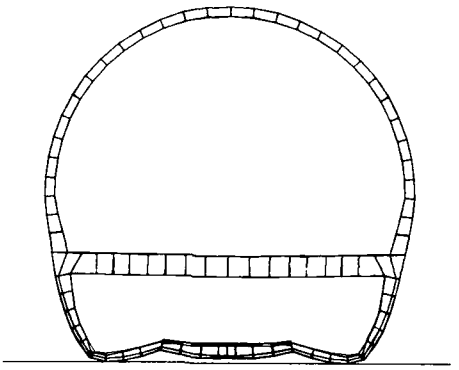

Figure 16. Structural Deformation at t = 80 ms.

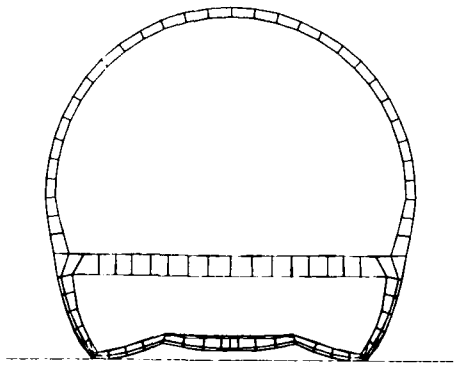

Figure 17. Structural Deformation at t = 96 ms.

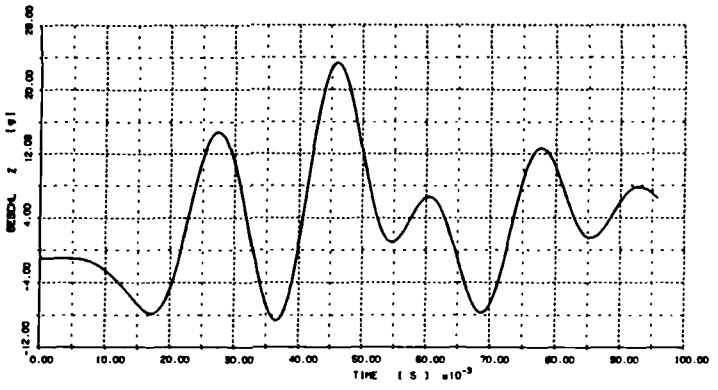

Figure 18. Vertical Acceleration at Nodal Point 91.

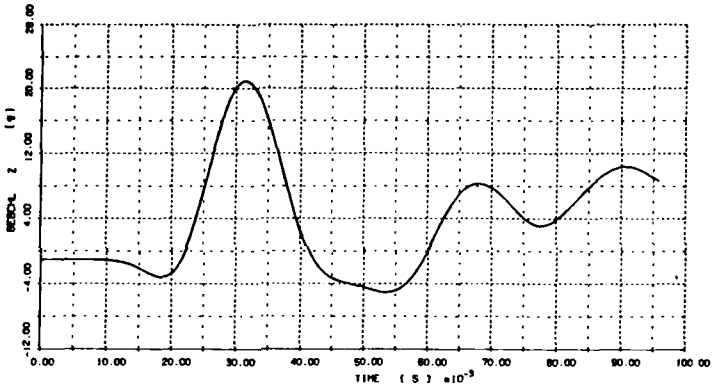

Figure 19. Vertical Velocity at Nodal Point 1551.

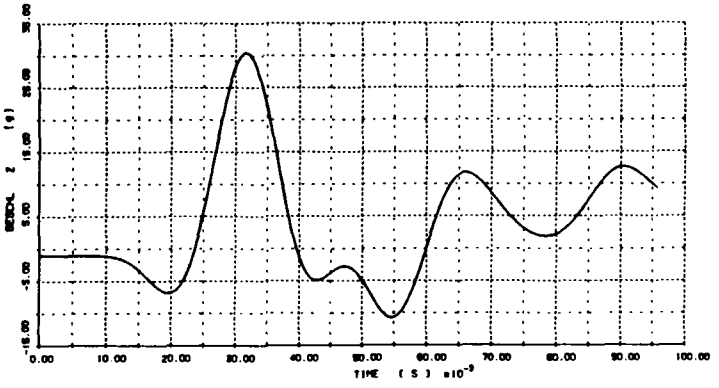

Figure 20. Vertical Acceleration at Nodal Point 1581.

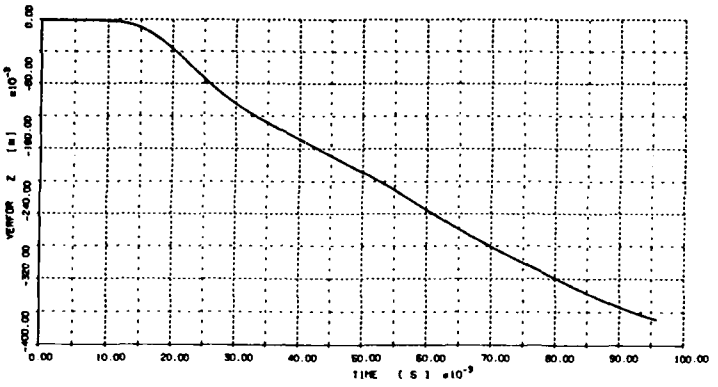

Figure 21. Vertical Displacement at Nodal Point 1581.

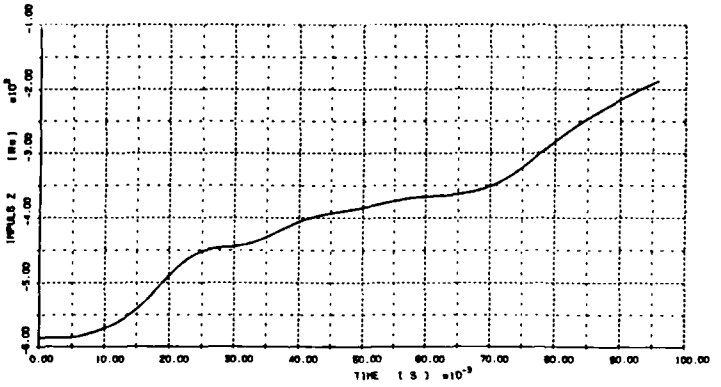

Figure 22. Vertical Momentum.

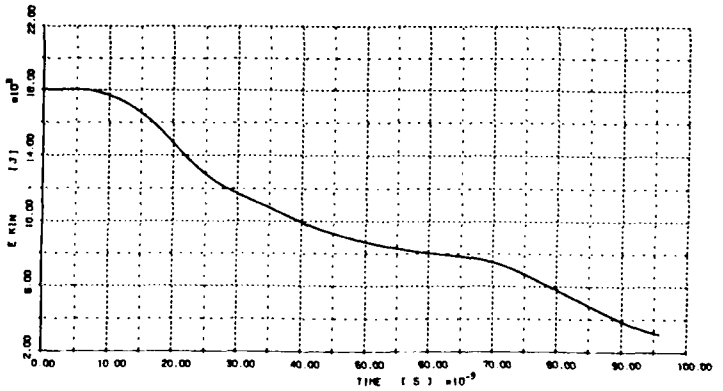

Figure 23. Kinetic Energy.

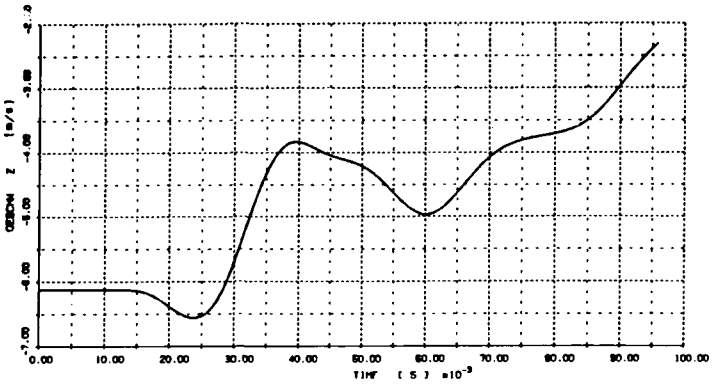

Figure 24. Vertical Velocity at Nodal Point 1581.

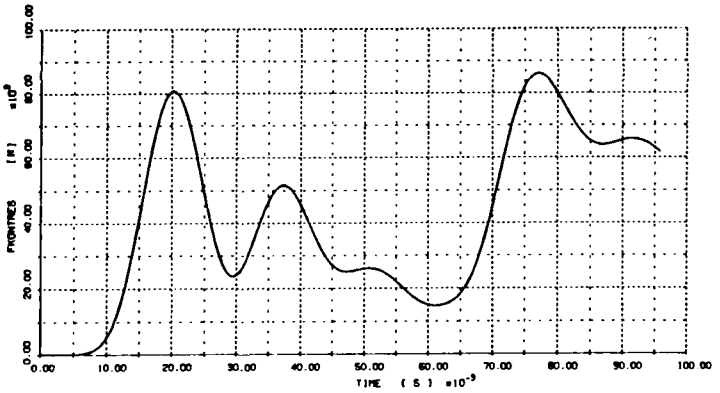

Figure 25. Contact Force.

Crash Simulation and Verification for Metallic, Sandwich and Laminate Structures

AUTHORS D. Ulrich and A. K. Pickett
E S I GmbH, Frankfurter Str. 13 - 15, D-6236 Eschborn
West Germany

E. Haug and J. Bianchini
E S I S.A., 20, Rue Saarinen - Silic 270, F-94578 Rungis Cedex
France

Abstract

This paper outlines some of the research for crash simulation of structures using metallic and composite construction recently undertaken at ESI. Several current areas of interest are reviewed including helicopter stiffened panel construction, automotive structures and, on a micro level, the compressive failure analysis of Carbon-Epoxy test coupons. In each study a specialized Finite Element code is used.

The dynamic buckling behaviour of panels stiffened with 'Z' sections are simulated numerically. The various components are connected using specially developed 'rivet' elements that fail at a prescribed load and are intended to produce a controlled collapse mode. These panels form the lower structure of a helicopter frame which also houses a flexible membrane fuel compartment. The effect of this internal Hydrostatic loading is also represented during the crash event. Some preliminary dynamic investigations for failure predictions of honeycomb core panels are also discussed.

Verification of these numerical procedures with experimental behaviour is an important issue. The Automotive industry has well defined experimental test procedures which provide an excellent standard to assess and validate numerical results. Considerable recent work in this area has provided a better understanding of the accuracy and limitations of these analyses.

The progressive failure analysis of Carbon-Epoxy fibre test coupons loaded in compression and in bending are undertaken using the ESI program PAM-FISS. The material model uses a novel BI-PHASE concept in which the constituent matrix and fibre materials have independent mechanical and failure criteria.

1 Introduction

This paper outlines several recent studies conducted by ESI which use numerical methods to investigate the crashworthiness of various metallic structures and failure study of composite materials. The studies presented are loaded either dynamically with a medium impact velocity or, quasi-statically, with a low velocity in which inertia effects are negligible. The work uses three specialized finite element codes namely, PAM-NL and PAM-CRASH for metallic structures and PAM-FISS for composite materials which are briefly described in

the following section.

The first studies investigate numerically the buckling behaviour of stiffened panels which are used to form part of a helicopter lower frame structure. Each panel is constructed of Aluminium sheeting and stiffened with 'Z' shaped reinforcement. These panels then form a box section which is interconnected with rivets through right angled members. The box section must have light weight, high energy absorbtion with a stable progressive collapse which, in addition, must serve as a protective skin to a flexible fuel tank.

An alternative to the stiffened panel construction is the honeycomb core sandwich panel which may be designed to have the desirable progressive collapse characteristics by introducing deliberate imperfections. Some preliminary studies are presented which numerically simulate this structure.

The second studies concern crashworthiness analysis of automotive structures. Over the past two years numerous studies have been conducted using PAM-CRASH and the technique is now established in many car companies as a part of their overall design process. The topic of verification using numerical crash simulation techniques is aptly discussed in this area where established standards and a wide range of experimental test data is available.

The third, and final studies, consider the failure of Carbon-Epoxy fabric test pieces loaded in compression and in bending. The material model used is "heterogeneous" BI-PHASE with an elasto-plastic matrix and elasto-brittle fibres. The discontinuous nature of the composite in the thickness direction is represented using a multi-layered finite element mesh. The simulation allows fibre buckling in compression zones and fibre failure in tensile zones with matrix plastification.

2 Numerical Methods

The explicit PAM-CRASH and implicit PAM-NL and PAM-FISS finite element codes each use a very different solution strategy and are each specialized for a particular class of problems. Some explanation and general remarks concerning these programs is first appropriate.

- PAM$^+$-NL: This is an implicit, general purpose, three dimensional finite element program specifically for the static and dynamic collapse analysis of shell structures (1). It is mainly used for quasi-static or low velocity crash problems where the inertia effects are negligible. The thin plate and shell elements used are based on the Clough-Felippa-Sharifi element (2) with a total Lagrangian formulation and 3 to 5 integration points through the thickness (multi-layered approach). The conventional or modified Newton Raphson iteration method is used to obtain convergence of the nonlinear equations at each load increment.
- PAM$^+$-CRASH: This is a three dimensional finite element code for analysing the large deformation dynamic response of inelastic solids. It uses an explicit method (3) whereby successive solutions are obtained at small timesteps of the order 1 μs during the simulation. The timesteps must be smaller than a critical value (4) for stability and, perhaps, one hundred thousand cycles are not unusual for large problems. Spatial discretization may use a variety of elements including solid, Belytschko thin shell (5) and various bar or beam elements. A wide variety of material laws are available to

represent elastic, non linear and possible failure conditions. Other features include moving or stationary rigid walls and definition of internal impact surfaces.

- PAM+-FISS: This is a nonlinear fracture mechanics and stress analysis code (6). It allows arbitary three dimensional geometries with either static, dynamic or thermal loading. Impact, contact and interface sliding may also be defined. The specialized fracture mechanics options allow:
  - A detailed study of areas of stress concentration via locally refined meshes.
  - Crack propagation and delamination fronts which may proceed independent of the mesh orientation. This necessitates evaluation of the criteria for propagation at each element during each load increment.
  - Automatic evaluation and selection from several toughness criteria: K (stress intensity factor), J (Rice Integral), G (total or partial strain energy release rate), D-R (damage over a critical distance).

  The material model used is BI-PHASE in which the constituent materials of the composite are treated separately. This will be more fully described later.

These programs may be linked to a common interactive graphics pre and postprocessor which allows the various input data to be generated or results data to be interpreted.

3 Case Studies on a Helicopter Lower Frame Structure

In general the crashworthiness design of a helicopter requires the structure to absorb impact energy whilst maintaining a necessary survival volume for the occupants. In particular the helicopter lower frame, that part below the occupants, must be designed to have a controlled collapse and restrict acceleration levels to tolerable limits at the passenger position. It must also be lightweight and serve other operational functions.

This lower structure typically consists of box type volumes formed by panels which are stiffened using 'Z' and angle sections. The components are usually riveted together. The following numerical studies consider the crashworthiness of the vertical side panels which are stiffened using 'Z' sections. A schematic interpretation of the problem is shown in Figure 1.

+ PAM - Programs in advanced mechanics developed by ESI.

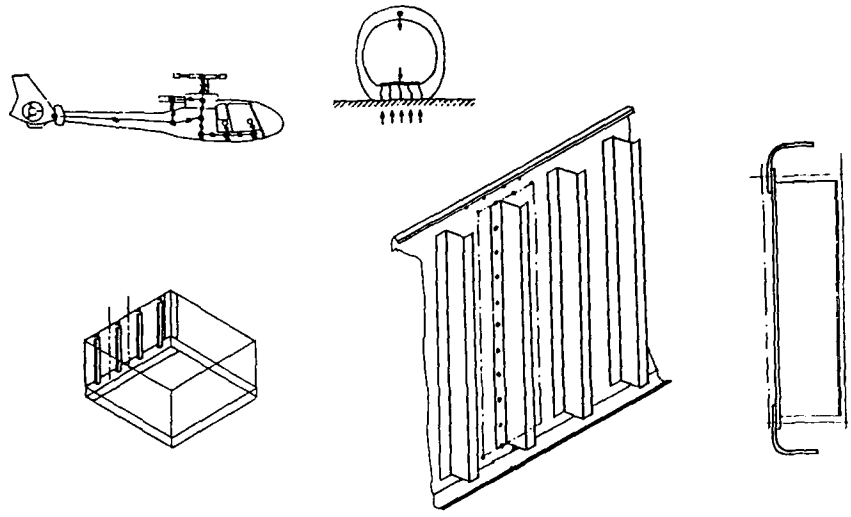

Fig. 1 - Overview of the Stiffened Panel Concept

3.1 Quasi-Static Study of the Stiffened Panel

An initial numerical study of the stiffened panel concept considered a slice of the panel with one attached stiffener. Quasi-static (*low rate of loading*) experimental results were available for this section and, therefore, to have a correct comparison between numerical and experimental methods the PAM-NL code was first chosen.

Due to the crash the panel is subject to compressive forces from loads transmitted by the upper and lower horizontal plates. The initially right angled corner plates are seen in Figure 2 to unfold and transfer a variable eccentric buckling load to the vertical panel. This failure was observed to be more gradual and at a lower value than predicted by analytical formulae.

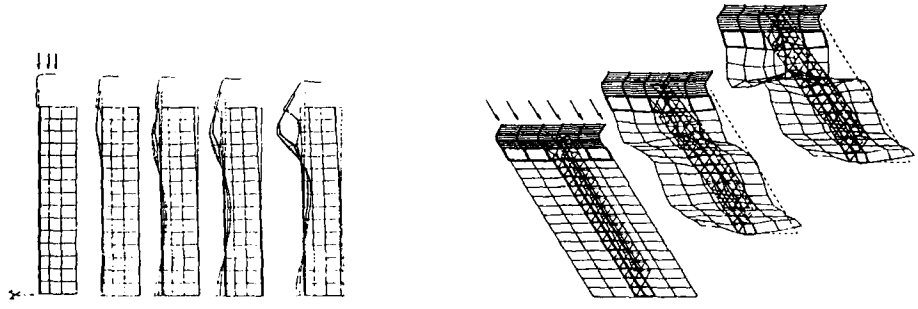

Fig. 2 - Crushing and Deformation Mode of the Slice of Panel with Attached Stiffener

The peak force transmitted through the section is limited by the first rivet failure. Thereafter, the post peak behaviour is controlled by progressive "unbuttoning" failure of the rivets which dictate the collapse of the members.

The incremental collapse force-displacement curves for numerical and experimental crushing of the panels were found to be in close agreement Fig. 3.

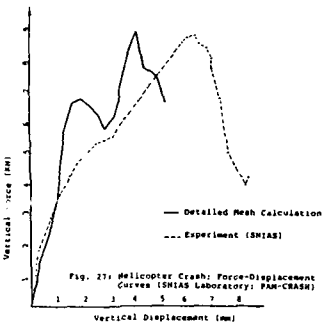

Fig. 3 - Experimental and Numerical Results for the Single Section Panel Study.

3.2 Dynamic Study of the Stiffened Panel

The dynamic behaviour of a similar panel with two attached 'Z' stiffeners was then undertaken using the PAM-CRASH code. The general arrangement of loading and the finite element mesh used are shown in Figure 4. Hydrostatic loading from the internal fuel compartment was also applied as a time-dependent pressure. Previous experimental and numerical studies of the flexible fuel tank (7) have quantified this lateral pressure.

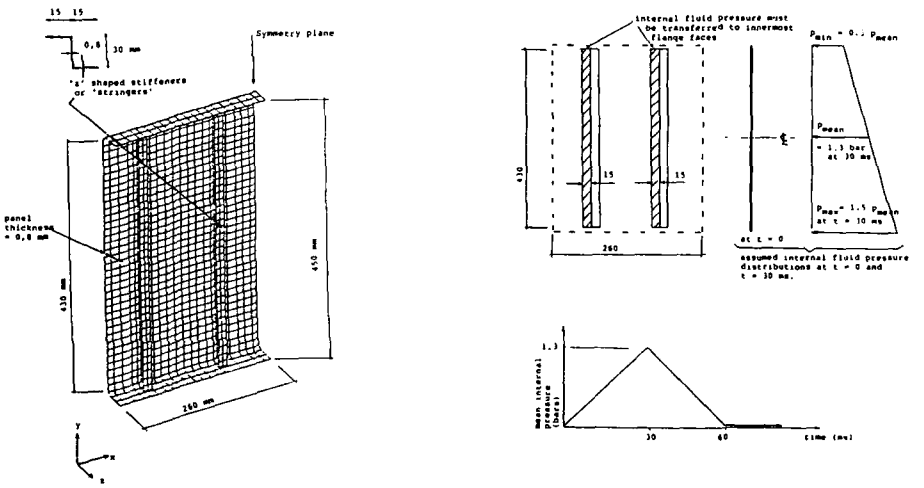

Fig. 4 - Loading, Boundary Conditions and the Finite Element Mesh used for the Dynamic (PAM-CRASH) Study of a Stiffened Panel.

For a correct representation of loading, the vertical crushing velocities from full scale experimental tests, or a more complete numerical model, would have to be available. Unfortunately at this early design stage they were unknown. However the object of this study was to compare with experimental sub component tests (8) which were subject to symmetric quasi-static loading. Therefore, as a compromise, symmetric moving rigid walls top and bottom were applied to give a realistic constant closing velocity of 10 m/sec. This helped provide understanding of the dynamic behaviour of the panel and the influence of the riveted connection system, yet some verification was still possible with the available limited experimental tests.

The 'rivet' elements provided connection by enforcing translational displacements between adjacent nodes of the panel and stiffener. Each rivet transfers a normal tensile force component F_T and tangential shear force component F_s. The following simple failure criteria is invoked to decide connectivity.

$$\left[\frac{F_T}{T_R}\right]^{a1} + \left[\frac{F_S}{S_R}\right]^{a2} \leq 1 \quad \text{for the no failure condition (nodal connectivity maintained)}$$

where:

T_R = dynamic failure force of rivet in tension
S_R = dynamic failure force of rivet in shear.

Graphically, these conditions are interpreted in Fig. 5.

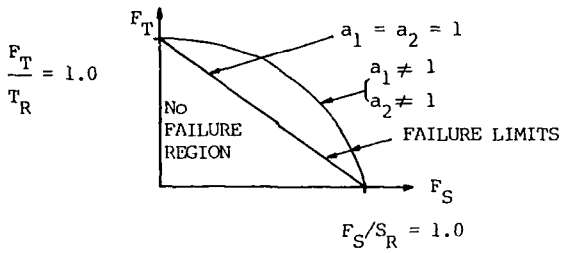

Fig. 5 - Failure Criteria used for the PAM-CRASH Rivet Elements.

For these studies the exponential values $a_1 = a_2 = 1$ were used. Clearly an improved study would first decide these values from experimental testing of specimens with various load combinations. Also, the effects of bending on rivet failure remains to be established. Penetration of the panel and stiffener is prevented by specifying internal impact surfaces.

Fig. 6 shows deformation modes for the dynamic study and some graphical results of the impact behaviour and energy absorbtion. Also given are the sequence of locations and times (ms) at which the rivets break.

The lateral thrust from the internal hydrostatic pressure was found to reduce the total energy absorption capacity by some 60 % when compared to a simulation with only vertical loading . All rivets were observed to fail before 18.2 ms.

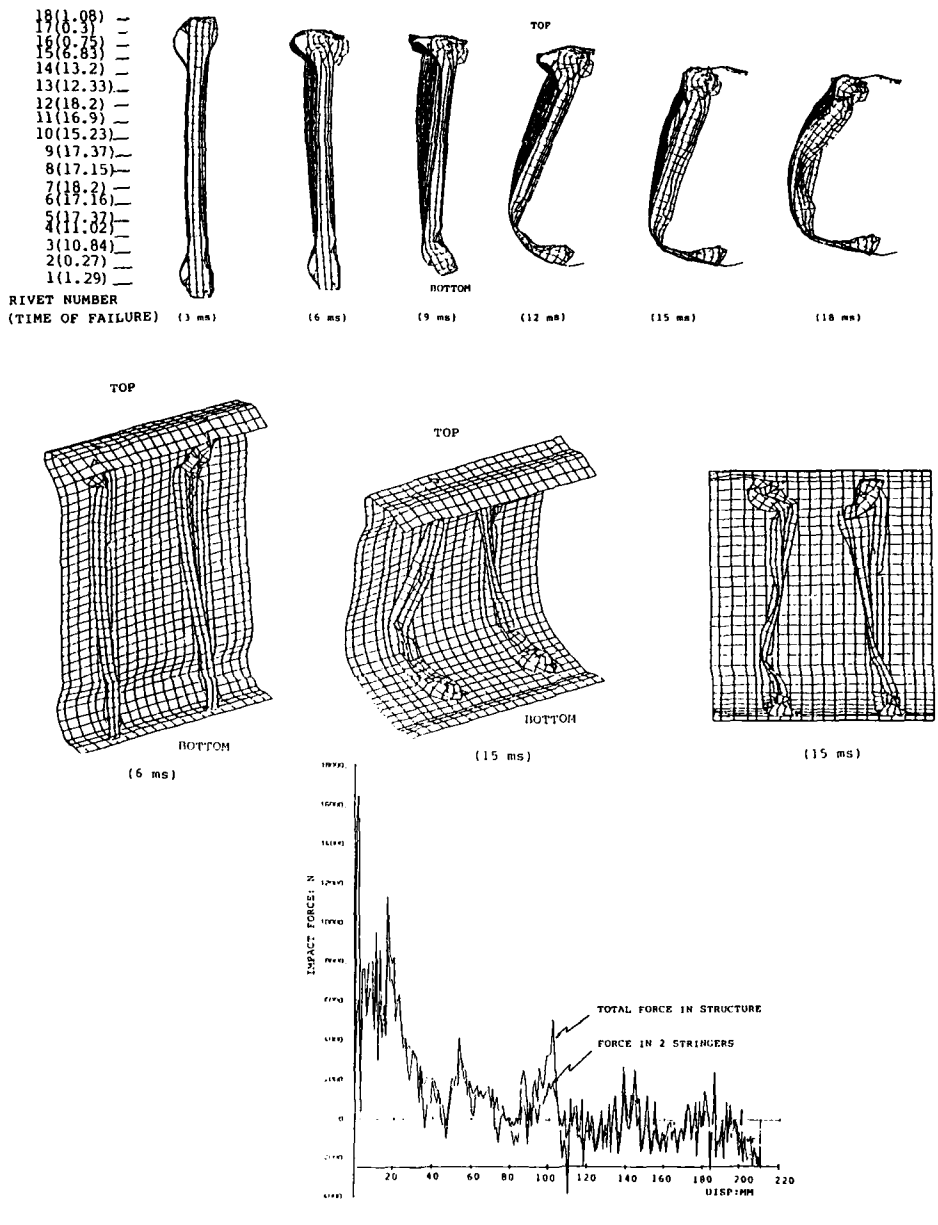

Fig. 6 - Results from PAM-CRASH Dynamic Study of a Stiffened Panel.

3.3 Dynamic Impact of Complete Structure-Fuel Tank System

A complete three dimensional study of the box section with internal fluid interaction was performed with the PAM-CRASH code. This necessitated a relatively coarse finite element mesh in which the stiffened 'Z' sections were approximated using an equivalent shell thickness determined by calibration from earlier studies on isolated panels. The internal fuel with flexible membrane produces a strong lateral thrust to the panel from pressure waves generated at impact. The fuel volume was modelled using solid elements and impact surfaces were defined for the fluid panel interaction. Figure 7 shows the excellent correlation between numerical and experimental results which were obtained.

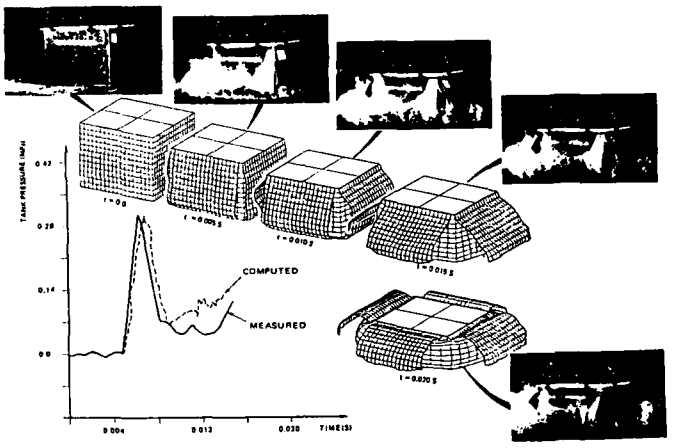

Fig. 7 - 14 ms Dynamic Impact of Structure-Fuel Tank System.

4 Preliminary Studies of Honeycomb Sandwich Panels

An attractive construction alternative to the stiffened panel are Honeycomb core sandwich panels. These can be designed to have desirable energy absorption characteristics by introducing deliberate imperfections. An example compressive test coupon is shown in Figure 8.

Figure 9 depicts the load transfer mechanism at an imperfection region with compressive loading. Clearly a successful numerical simulation of this component will require an accurate material representation for the highly orthotropic Honeycomb core.

Preliminary analyses have been made using the PAM-CRASH code for this simulation. The outer aluminium skin is readily modelled with elasto-plastic shell elements. The highly orthotropic core was discretized using nonlinear bars for through-the-thickness properties

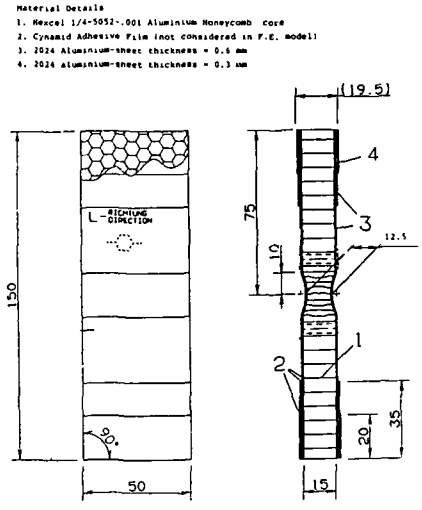

Fig. 8 - Example of Compressive Test Coupon with Imperfection for a Honeycomb Core Sandwich Panel.

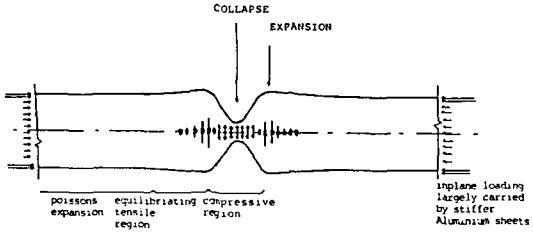

Fig. 9 - A Simplified View of the Internal Stresses Developed in the Compressively Loaded Sandwich Panel.

and solid "brick" elements to represent shear properties of the core.

Numerical simulation and experimental results of force carried by the panel vs. time and the deformation modes are shown in Figure 10. From these results it appears that the deformation modes are in reasonable agreement, although the numerical force values are consistently too low. It is thought that deficiencies in representing the core material with the currently available PAM-CRASH elements are responsible and further work is required to improve this aspect.

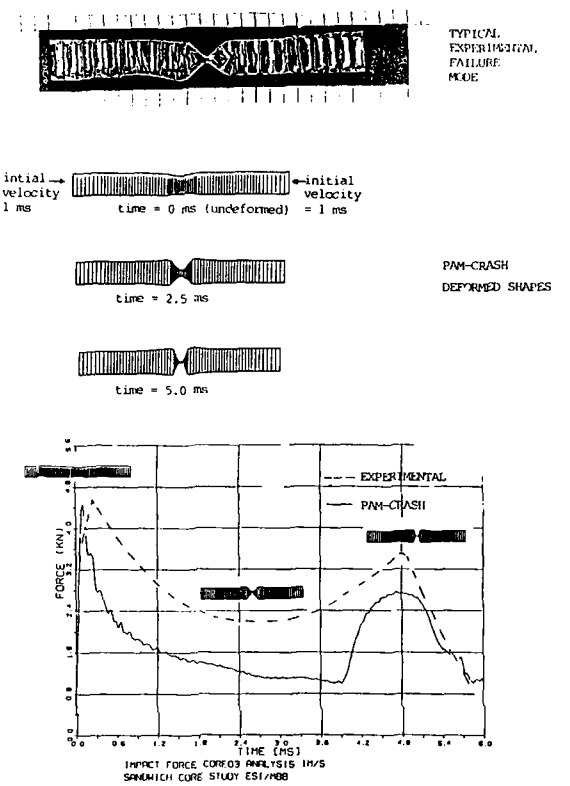

Fig. 10 - Comparison of Dynamic (PAM-CRASH) and Experimental Results for the Sandwich Panel

5 Verification and Crashworthiness Studies for Automotive Components

Over the past two years numerical simulation has become an accepted method for the verification and crashworthiness asessment of automotive structures. The technique is now sufficiently established that many companies have integrated crashworthiness simulation of components in their design process and, in some cases, have performed full model crash simulation prior to the availability of experimental prototype tests. The following illustrate

two examples made at component level and of a full car crash simulation.

5.1 Dynamic Simulation of a Frontal Car Component

Figure 11 shows a typical example of a frontal assembly consisting of an upper and lower rail with several cross members.

The engineering goals of this study were the following:

- Obtain the barrier load vs. time curve.
- Obtain forces transmitted through several beam cross sections, in particular obtain the forces transmitted to the carriage by the upper and lower beams respectively.
- Obtain the global failure modes.
- Obtain energy absorption and global deceleration of the structure.
- In a parametric study, investigate influences of small design changes such as thickness variations, introduction of holes, notches and reinforcements.

The finite element mesh used consisted of approximately 2,000 shell elements and required less than one hour CPU on a CRAY XMP for 35 ms of crash. Also given in Figure 11 are sample results of the study which include deformation shapes and impact force at the wall vs. time. The numerical results for impact force at the wall and forces through the main rails were in close agreement with experimental test results.

5.2 Dynamic Frontal Impact Simulation of Full Car

The following study investigates crashworthiness of the Citröen BX of the PSA (Peugeot S.A.) group. The finite element mesh used for this purpose is shown in Figure 12. A total of 7,900 thin shell elements were used and carefully distributed in order to minimize computing requirements and allow accurate representation of all important geometries and capture the impact buckling modes. The engineering objectives of the simulation were the following:

- Check the accuracy of the impact force with the experimental results.
- Check the accuracy of the simulation with regard to the damage modes of each structural member, the main parts being: front rails, engine and gearbox support structure, steering wheel support structure and passenger cabin floor.
- Check the accuracy of the simulation with regard to the contact kinematics within the engine compartment.
- Check the accuracy of the velocity and acceleration time histories at the joint of rocker and B-Pillar.
- Check the force transmissions through the side members.
- Check the force transmissions between engine and dash.

Some example results of deformation modes and barrier impact force are included in Figure 12. In general the numerical deformation modes were close to reality, with the barrier impact force also showing a good agreement. The observed time shift between numerical

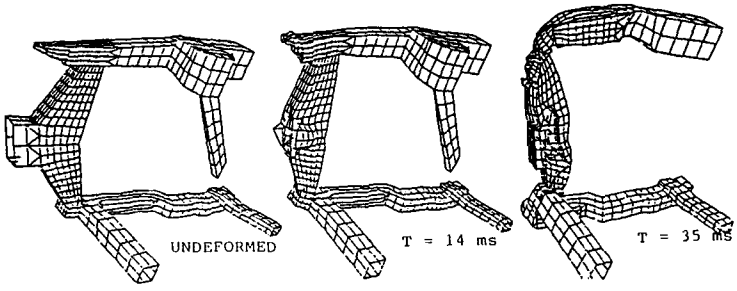

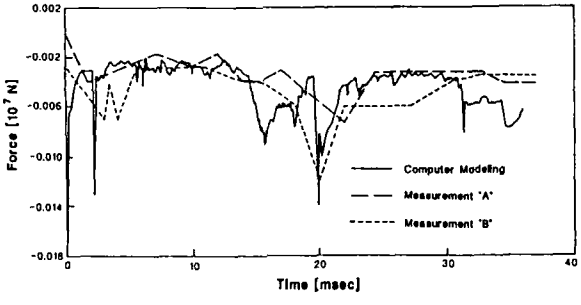

Impact Force versus Time for the Frontal Car Assembly

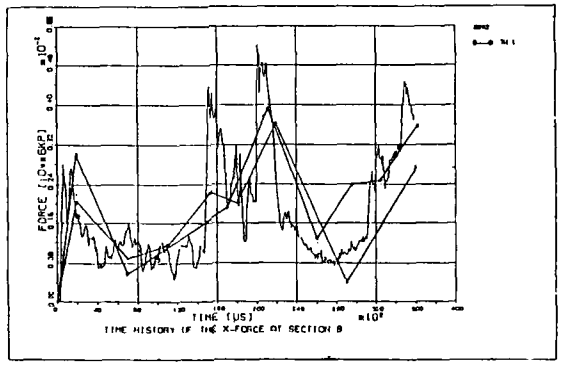

Forces Transmitted through Upper and Lower Rail for Frontal Car Assembly

Fig. 11 - The Finite Element Mesh and Sample PAM-CRASH Numerical Results for the Frontal Car Component

and experimental impact force curves is due to approximations in the numerical model, namely, use of a perfectly rigid wall, internal structural connections being assumed perfect and only approximate representation of the bumper and its support.

6 Numerical Study of Compression and Fibre Buckling in Composites

The merits of using fibre matrix materials in many structural applications are now well recognized (9). However, to obtain full advantage of these materials a meaningful design process must permit an acceptable degree of internal damage within the composite, such as matrix plastification and microcracking, or delamination between layers. Typically matrix microcracking may initiate at 20 % of ultimate load with first fibre failure occuring at 40 % of ultimate load. Use of these load levels as a design criteria would negate the benefits of these materials and lead to an overly conservative structure.

This section presents a numerical approach using the finite element method to simulate and automatically follow the various damage modes which occur in composite fabric loaded in compression. The numerical model is first calibrated with experimental tests and then exploited to help gain an insight to the nature of the failure modes, from which acceptable damage and permissible stress values for the composite may determined to be used in the design process.

The numerical method uses the PAM-FISS program with a specialized element having a BI-PHASE material law. The BI-PHASE material allows separate rheological laws for the elasto-plastic or fracturing matrix and the elasto-brittle fibres. Its justification is logical when considering the failure mechanism of undirectional composite materials. At low load levels, less than 20 % of the ultimate, the composite is a fully bonded material which obeys traditional continuum mechanics. However, with increased loading fibre and matrix damage tend to progress independently within the two constituents which then obey independent mechanical and failure criteria. The BI-PHASE approach conveniently enables each material to be treated separately.

The BI-PHASE element stiffness is derived by superimposing the matrix (composite minus fibre but including voids) and the unidirectional fibre phases. Each phase being assigned different rheological laws (Fig. 13). Upon loading, stresses are calculated for each phase, and damage criteria (matrix cracking, matrix slipping and fibre rupture) appropriate to each phase are tested and may then propagate independently. A multidirectional laminate is modelled by stacking through the thickness several such elements with fibres orientated in the warp and weft directions. Studies have shown the fabric weave must be realistically modelled as shown in Fig. 13 in order to obtain correct linear stiffness and help induce the correct local fibre buckling in the composite.

Compressive bending stresses in the composite may favor local fibre buckling which, in turn, will impose local high stress in the matrix with possible plastic or fracture failure. Thereafter the fibres will be less confined leading to local buckling and increased curvature with reduction of fibre forces and load capacity of the section. Subsequently some redistribution of stresses at the critical section will occur and, for example, in bending tests some tensile fibres will rupture due to overstressing. This will then lead to further load transfer to the previously undamaged compression zone. This cyclic process repeats until

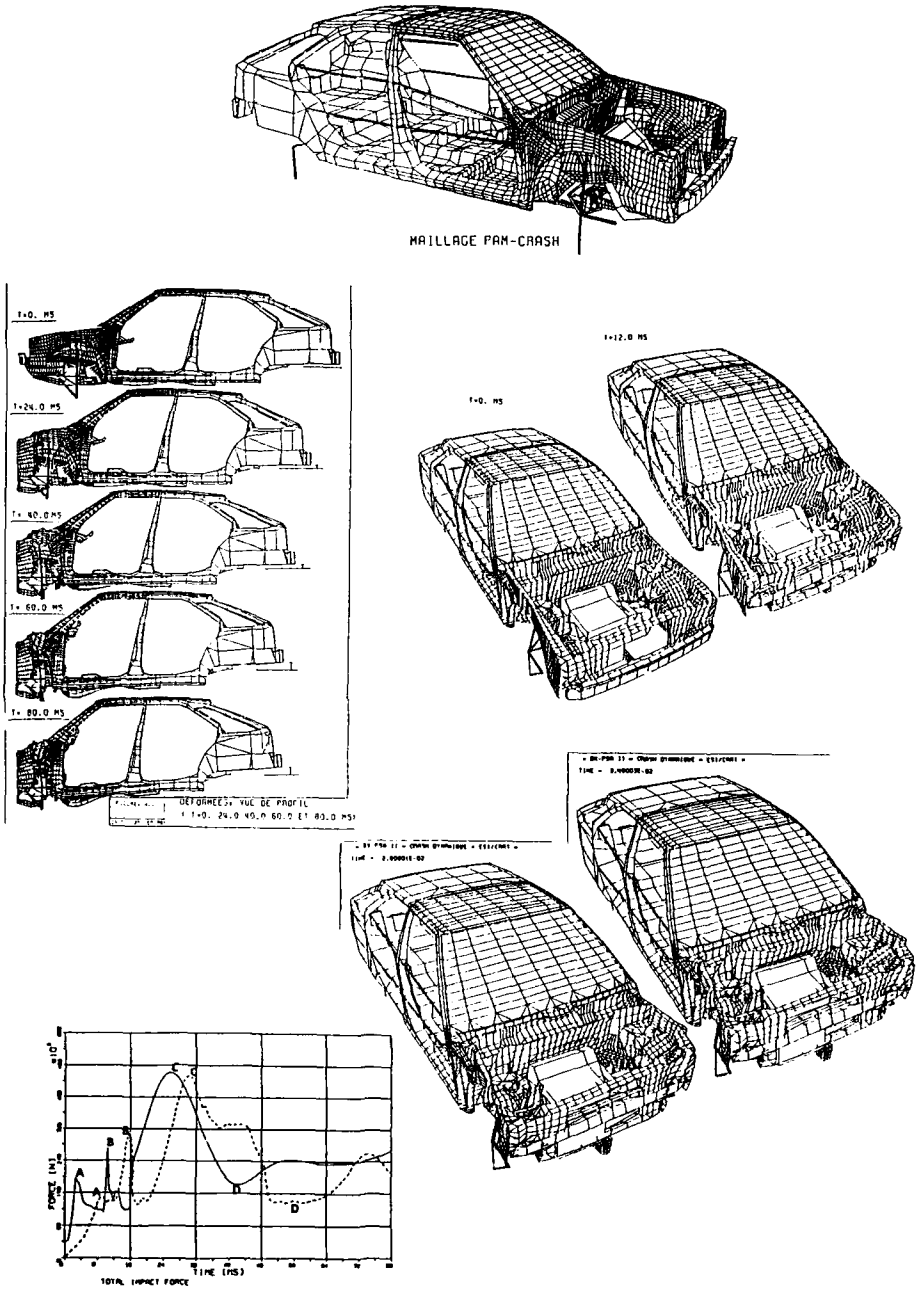

Fig. 12 - The Finite Element Mesh and Sample PAM-CRASH Numerical Results for the BX Full Car Study.

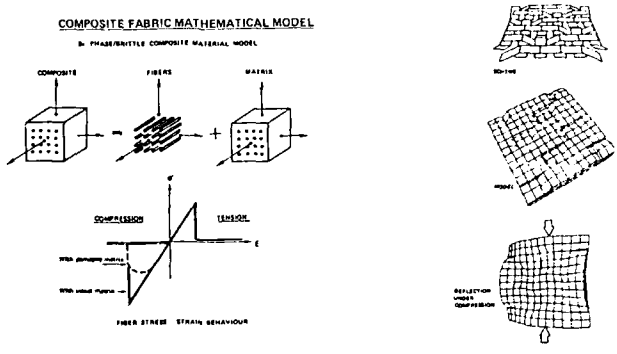

Fig. 13 - The BI-PHASE Material Model

ultimate failure of the section.

6.1 Compression Test of Composite

Figure 14 shows details of the finite element mesh used for this study and the results obtained. It is seen that a balanced (50 % warp - 50 % weft) layup of 3 equivalent layers is used. This idealization and the mechanical properties used correspond to an experimental test which used *Carbon-Epoxy Satin 5 Fabric* -G803M10 Brochier.

The experimental and analytical axial force vs. axial overall strain curves are in good agreement and the local fibre buckling near the warp-weft intersection is clearly visible. The results have been achieved by best calibrating the matrix elastic limit to 16 N/mm^2 and using a true fibre stress of 3000 N/mm^2. The fibre volume fraction was 0.47.

6.2 Bending Test of Composite

The previous compression test specimen was also loaded as a simple beam as shown in Figure 15. A similar mesh and identical mechanical properties were used.

Results for the analysis are also present in Figure 15. The calculated plastic strain contours of the matrix phase are plotted on the upper surface of each of the three layers and show a tenfold increase when one of the compressive threads buckle.

The experimental and the calculated transverse load vs. transverse (midspan) displacement curves are compared. The failure in bending is interpreted as a succession of compressive fibre buckling due to matrix yielding and tensile fibre ruptures due to subsequent stress redistributions.

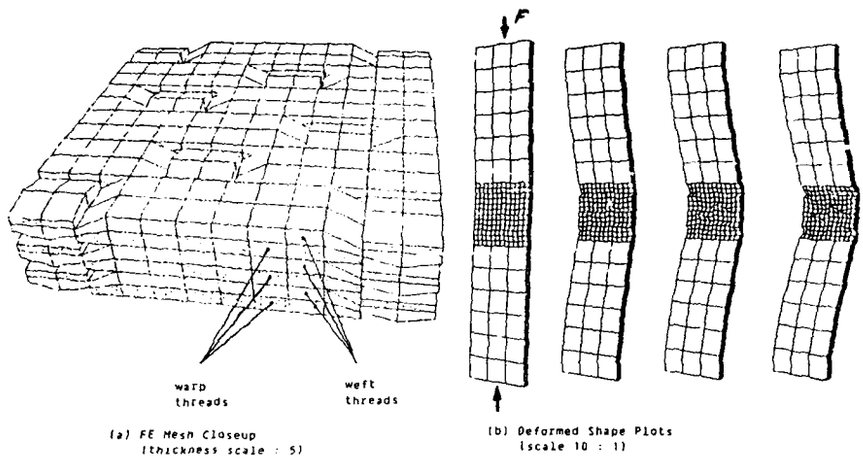

(a) FE Mesh Closeup
(thickness scale : 5)

(b) Deformed Shape Plots
(scale 10 : 1)

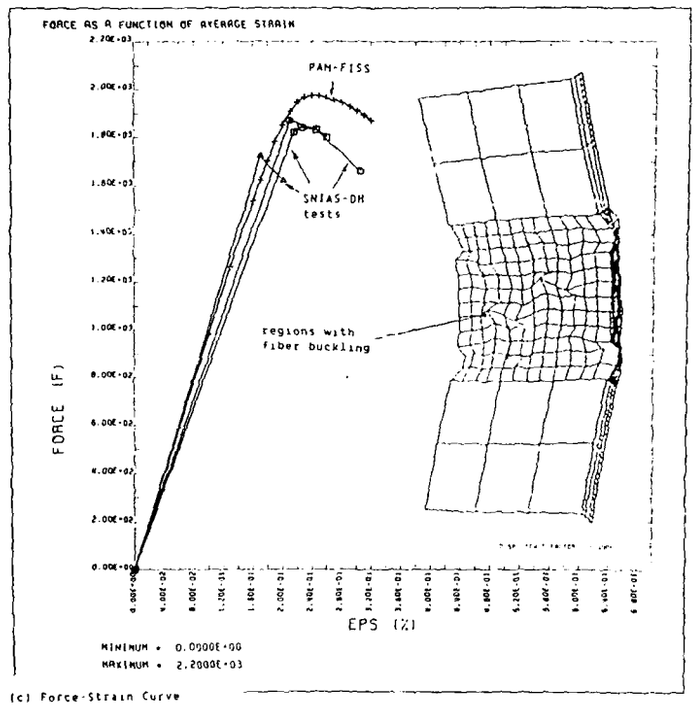

(c) Force-Strain Curve

Fig. 14 - Carbon Epoxy Satin 5 "G803 M10 Brochier"
Equilibrate Tissue (3 layers) Compression Test

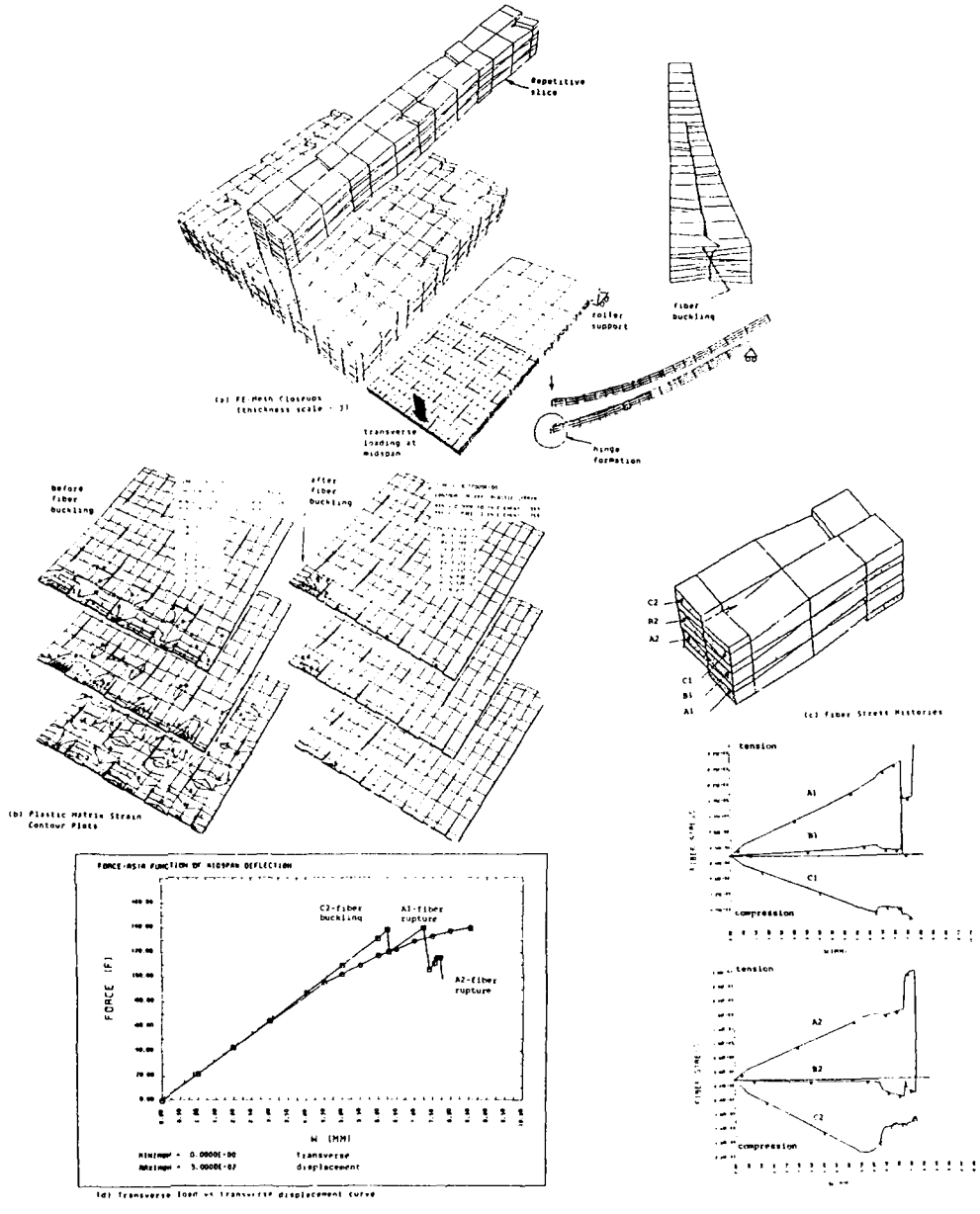

Fig. 15 - Carbon Epoxy Satin 1 "G827 M10 Brochier" Unidirectional Tissue (3 layers) Bending Test.

7 Conclusions

A cost effective and successful design process should incorporate numerical simulation techniques if desired crashworthiness objectives are to be achieved. Where possible, experimental tests should be available to verify the numerical procedures. The simulation may then be used with confidence to provide detailed information usually unavailable in the test, or extrapolated to undertake parametric studies.

The simulation of metallic structures for crashworthiness is now widely accepted and used in industry as demonstrated by several automotive examples presented. However, the dynamic failure analysis of Honeycomb core and composite materials is still at a research stage and some promising approaches have been proposed.

8 References

1. SMIRT Paper - E. Haug et al. - Engineering System International, "PAM-NL A General Finite Element Program for the Nonlinear Thermomechanical Analysis of Structures", 5th Int. Conf. on Structural Mechanics in Reactor Technology, Berlin, Section M1/3, August 1979.
2. AIAA Paper - P. Sharifi, "Non-Linear Buckling Analysis of Composite Shells", AIAA Journal, Vol 13, No 6, pp 729-734 - June 1978
3. Structural Crashworthiness Publications; E. Haug et al. - Engineering System International, "Static and Dynamic Finite Element Analysis of Structural Crashworthiness in the Automotive and Aerospace Industries", Chapter 7: eds. N. Jones and T. Wierzbicki, Butterworths, London, 1983.
4. Ed T. Belytschko and T. Hughs, "Computational Methods for transient analysis", Pub Elsevier Science Publishers B.V., The Netherlands, 1983 pp 41
5. T. Belytschko and B. H. Hsieh, "Nonlinear Transient Finite Element Analysis with convected coordinates", Int. J. Num. Methods in Eng. 7, 255 - 271, 1973
6. "PAM-FISS" A specialized Finite Element Code for Fracture Mechanics Analyses, Ref. 4/85. ESI SA
7. J. Mens and J. C. Bianchini, "Computing Codes for Development of Helicopter Crashworthy Structures and Test Substuntiation", presented at the AIIS/NAI, International Seminar, November 6-8, 1985 Nanjing, China
8. MBB/ESI (ESI Project No. 86-263)
9. L. Hollaway, "Composite Materials in Structures", University of Surrey Press, UK, 1976

9 Acknowledgements

The helicopter studies have been carried out under an MBB contract with Mr. Frese and under an AEROSPATIALE contract with Mr. M. Mens. The automotive studies cited in collaboration with SAAB-SCANIA Sweden and Citröen-Peugeot France res
The investigations on composites were also conducted under an AEROSPATIALE contract with Mr. Mens. Both AEROSPATIALE contracts were financed by DRET/SDR/G8 (French Ministry of Defence) under its technical representative Mr. M. Grellier. The authors gratefully acknowledge all the contributions received.

PREDICTING CRASH PERFORMANCE

by D. Parsons PhD BSc, Director
and A. Belfield PhD BSc CEng MIMechE, Principal Analyst
H.W. Structures Ltd. Pembroke House, 11 Northlands Pavement, Pitsea,
Essex SS13 3DU, England.

ABSTRACT

In the past, aircraft have been designed with high structural integrity such that crash situations can be avoided, i.e. aircraft have been designed for crash avoidance and not crashworthiness. There is considerable effort now being devoted to the study of aircraft crashworthiness. Clearly, it is only in relatively low speed impacts that design considerations may be effective. In this area, H.W. Structures and the automotive environment in general have built up a wealth of experience.

This paper discusses how this experience may be applied to aircraft structures. Analytical techniques for prediction of the behaviour of the structure and its occupants are examined.

INTRODUCTION

Aircraft are normally designed with high structural integrity in order to withstand in-service loads. These loads, although due to a variety of conditions, e.g. aerodynamic, landing, etc., do not include any crash loading. Effort is now being devoted to the study of aircraft impacts. There are two principal reasons. The first and most obvious is to reduce the number of injuries and deaths caused by aircraft impacts. An impact at only 4.5 m/s (10 mph) is sufficient to cause injuries to occupants[1]. Secondly, by careful design there may be a reduction in the repair costs following a low speed impact.

It is in the area of low speed impacts that technology can be read across from the automotive industry. H.W. Structures operate in this field. In common with most modern structures, the automobile relies heavily upon analysis to provide an efficient structure.

It was the advent of legislation for improved vehicle safety that significantly influenced automobile design. In aircraft design there is no current legislation regarding crashworthiness requirements. It is the designers, not the legislators, that are directly introducing crashworthiness considerations.

In the automotive field, full scale prototype testing is an expensive activity and has a significant effect on prototype build volumes and timing of whole programmes. Obviously extensive full scale prototype testing of aircraft is out of the question. This implies that the numerical simulation of an impact is the only practical way of evaluating an aircraft's crashworthiness. Confidence in this predictive approach is vital. It is by using the experience gained in evaluating automobile impacts that confidence in the analysis techniques may be found.

AIRFRAME IN-SERVICE LOADS

Before the structural integrity of any aircraft can be evaluated, the external loads acting on the structure must be known. The determination of these loads is normally evaluated by specialist groups of engineers. This normally involves extensive knowledge of aerodynamics. In general, the magnitude of the in-flight forces are dependent on the velocity and acceleration of the aircraft. Therefore the function of an aircraft determines, to some extent, the loads which may be applied. E.g., for a military aircraft, the limiting factor may be the pilot's capacity to withstand inertia forces, whereas for a passenger aircraft the above factor is obviously too harsh. What is necessary to transport the passengers safely and in comfort predominates.

The external loads on civil aircraft may be summarised as follows:

1) In flight loads
2) Landing loads
3) Take off loads
4) Engine loads
5) Special loads

The purpose of this paper is to examine what may be analysed for

6) Crash loads.

AIRFRAME CRASHWORTHINESS

Information is available concerning the survivability of conventional aircraft occupants in a crash situation. This data[2] is shown in Figure 1. As may be seen if the vertical component of velocity is above 12 m/s (27 mph) or the horizontal component above 18 m/s (40 mph) then the survivability of occupants is marginal.

Furthermore, for a direct head-on impact into a rigid barrier the equation of motion may be approximated to

$$v \frac{dv}{dx} = \frac{F}{Mc + k(l-x)} \qquad (1)$$

where v is the velocity of the aircraft
x is the crushed length
l is the initial length
k is the mass per unit length of fuselage
Mc is the concentrated mass at the wings (fuel, engines, etc.)
and F is the average crushing strength of the aircraft.

Integrating (1) leads to

$$\left(\frac{v}{v_0}\right)^2 = 1 - \frac{2F}{kv_0^2} \log \left(1-\frac{x}{L}\right) \qquad (2)$$

where v_0 is the original aircraft speed

and $$L = l + \frac{Mc}{k} \qquad (3)$$

These equations applied to a typical large passenger aircraft lead to Figures 2 and 3. In deriving these figures, the following was assumed:

Original length	=	60 m
Concentrated Mass	=	85,000 kg
Position of the conc. Mass from front of aircraft	=	28 m
Mass/Unit length of fuselage	=	1333 kg/m
Average Crushing Force	=	1 MN

From Figure 2, if the original speed is greater than 85 m/s (190 mph), then all the kinetic energy is not absorbed even if the aircraft is completely crushed. Impacts at velocities greater than this imply that the aircraft is likely to be totally destroyed by the excess energy.

Even if impact speeds are low enough such that the energy is absorbed, the deceleration levels are likely to be so high that seat fittings, cargo tiedowns, etc. will tear out. Passengers and containers will then be catapulted forward.

This type of analysis is a gross over-simplification, e.g. no spreading out of the fuselage is included. However, it does indicate that high speed impacts are probably not worth analysing in terms of occupant survivability.

For a low-medium speed impact (such as in a take off or landing accident), the finite element simulation does not have to be so detailed that it models the stresses in the highly deformed areas. It is only the overall behaviour that needs to be predicted. The model has to be able to:-

i) simulate the crushing behaviour

ii) have the ability to absorb the energy

iii) transmit the accelerations to the undeformed part of the structure

i.e. when the speed of impact is much less than the speed of the stress wave passing through the structure, the area of contact is not so important. This implies that simulation techniques currently used within the motor industry can be utilised.

It is the rapid development in computer technology and finite element packages such as DYNA3D, ABAQUS, PAMCRASH, etc. which have allowed such simulation of an impact to become practicable.

Figure 4 shows a typical hybrid finite element model of a vehicle under front impact. This model also contains masses, non-linear springs and dashpots as well as beam and shell elements. This level of model gives good results for the overall behaviour of the vehicle. The analysis used the non-linear dynamic capabilities of ABAQUS[3]. Figure 5 shows a similar model for a helicopter impact. Even for such an apparently simple model, experience is required to get good results. This approach has been discussed at a previous AGARD MEETING[4].

For more detailed analyses, such as those required to simulate the local crush behaviour of a member, the model would consist mainly of shell and/or solid elements. Either DYNA3D or ABAQUS would be used to achieve a solution. For large non-linear models a finite element package which utilises vector processing and an explicit time integration scheme is beneficial in terms of processing cost. H.W. Structures would normally only run such detailed models for individual components. The results of these analyses are then incorporated into the overall model.

OCCUPANT ANALYSIS

Occupant protection may be aided without any analysis being undertaken. The occupants' deceleration in both intensity and duration should be minimised. Hazards e.g. projections, equipment, cargo, etc. should be removed from the occupant's environment. Cargo and equipment tiedowns should be sufficiently strong so as not to fail in survivable accident cases.

In low speed impacts, probably the greatest hazard to the occupants are post-crash hazards, e.g. fire, smoke, toxic fumes from foams, etc.

Many of the above points may be addressed by engineering judgement. For example, in order to reduce occupant deceleration the following may be undertaken:

- Introduce crumple zones into the aircraft
- Have a structural cell for the passengers and cabin crews.
- Ensure scooping of soil/earth is minimised by designing the fuselage to skid.
- Suspend all seats from the ceiling or fuselage sides and not mount them on the floor.
- Introduce full harness belts for all passengers.
    - Use energy absorbing seats.
    - Modify seat positions, e.g. revise to rearward facing.

A major occupant environment hazard which may be improved is the seat or more precisely the back of the seat in front. A friendly interaction between the occupant and seatback is sought.

In general, there are four major factors in transporting any fragile object in a container. These points apply equally to the aerospace as to the automotive field.

1. The container must not spill its contents or collapse in on its contents.
2. The objects should be held securely within the container to stop secondary impact.
3. The means of securing the objects must transfer the forces to strong parts of the container.
4. The container must be designed to spread the impact loads and have properties which spread the deceleration time.

Clearly, this is a simplification of the problems in occupant analysis. H.W. Structures use an occupant kinematic program MADYMO[6] to evaluate points 2 and 3 above. MADYMO is a commercially available computer program specifically designed for crash victim simulation. Human beings can be represented mathematically by considering the body as a system of rigid elements linked by rotational and/or translational joints. The behaviour of the system is calculated by solution of the equations of motion.

MADYMO models comprise rigid body and surface elements, non-linear springs, dashpots and gaps. The specific use for crash simulation has led to the establishment of verified data sets representing the dummies. The surface interactions between the dummy and the rest of the vehicle including any restraint system have to be specified. It is in the specification of these interaction forces that actual test results or assumed data is required. Valid assumptions can only be developed with experience. In practice, modelling usually requires the geometries and stiffnesses of the seat and occupant environment to be accurately known.

Figure 6 shows a three dimensional model[9] set up to simulate an occupant in an aircraft seat. The seat and belt stiffnesses were estimated from previously correlated automotive crash victim simulations. The deceleration pulse applied to the system was again derived from the automotive field - the deceleration experienced by the driver in a 30 mph front impact. In an automobile under this deceleration, legal safety requirements in the USA (FMVSS 208) require the dummy to have a HIC (Head Injury Criterion) value of less than 1000. This is the value over which a typical human being will not survive. The head acceleration time history from this example is shown in Figure 7 and a HIC level over five times the FMVSS requirement is implied. This is mainly due to two factors - the hard seat backs normally found in aircraft and the presence of a lap belt only. The same analysis with an equivalent automotive three point belt reduces the HIC level by a factor of 3.

Figures 8 and 9 show kinematic plots of the two analyses. The introduction of the three point belt dramatically alters the kinematics of the dummy. In this case, the dummy just hits his head against the front seat-back, so a friendly interface is not as important. Although this example is a simple one, it shows the capabilities of MADYMO. These capabilities, when used correctly, can be extremely powerful in determining and optimising the kinematics of any occupants.

CONCLUSIONS

Aircraft differ substantially in design usage and number of occupants, and so no single crash simulation technique may be applicable. The outlined techniques would have to be adapted for each individual class of aircraft, although for light aircraft and helicopters they seem ideally suited.

In the automotive field there are approximately ten times the number of people injured than killed, whereas in the aerospace environment there is only half the number of people injured as killed. Although aircraft crashworthiness will not reduce this number of accidents, its use will change the ratio between the number of injuries to fatalities.

Design/analysis can be directed towards improved safety. An example is the new standard being proposed for aircraft seats[8]. Seats currently approved to FAA standards are required to separately meet inertia forces of - 9g in a forward direction, 4.5g down, 2g up and 1.5g sideways. The UK Civil Aviation Authority propose to increase these to any combined loads with an overall 9g limit. Proposals also include more severe testing to take into account dynamic loads and floor deformation.

In the automotive field when a new product is released, there may be 200 prototypes which are tested and/or destroyed. In the aircraft environment, where production costs are high and volumes low, there may only be six prototypes - and these should not fail. This implies that analytical techniques are heavily relied upon - so expertise is paramount. H.W. Structures foresee an opportunity for the aerospace industry to capitalise on the considerable crashworthiness experience within the automotive field. This experience is as yet, untapped by the aerospace industry.

REFERENCES

1. SWEARINGHAM JJ, General Aviation Structures Directly Responsible for Trauma in Crash Decelerations 1971 (Department of Transportation, Federal Aviation Administration, Office of Aviation Medicine, Washington DC)

2. JOHNSON W and MAMALIS AG, Crashworthiness of Vehicles. Mechanical Engineering Publications Ltd., London 1978.

3. HIBBITT, KARLSSON & SORENSEN INC., ABAQUS User's Manual, Providence, Rhode Island 1985

4. PARSONS D - Predictive Analysis and its Role in Structural Approval - A Crashworthiness Perspective. AGARD Structures & Material Panel Meeting, Turkey 1987

5. JONES N and WIERZBICKI T - Structural Crashworthiness, Butterworths & Co. 1983

6. MADYMO Users Manual, TNO Road-Vehicles Research Institute, The Hague, 1986

7. ROARK R and YOUNG W - Formulas of Stress and Strain, McGraw Hill, 1975

8. WARREN DV, Airworthiness Division, Civil Aviation Authority, AEROSPACE Magazine - December 1987

9. Report HW1115, MADPOST Post Processor for MADYMO 2D and 3D programs, H.W. Structures Ltd, February 1987

FIGURE. 1.

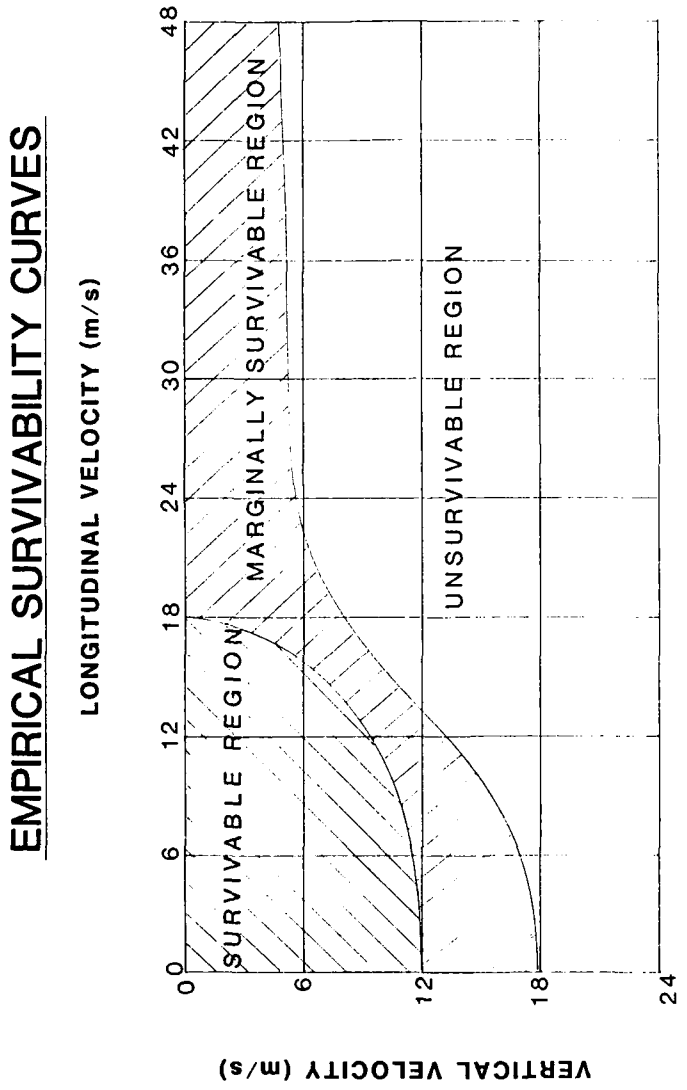
EMPIRICAL SURVIVABILITY CURVES
LONGITUDINAL VELOCITY (m/s)
VERTICAL VELOCITY (m/s)
0
6
12
18
24
30
36
42
48
SURVIVABLE REGION
MARGINALLY SURVIVABLE REGION
UNSURVIVABLE REGION

FIGURE 2

AIRCRAFT IMPACT INTO A RIGID BARRIER

VELOCITY VS CRUSH DISTANCE

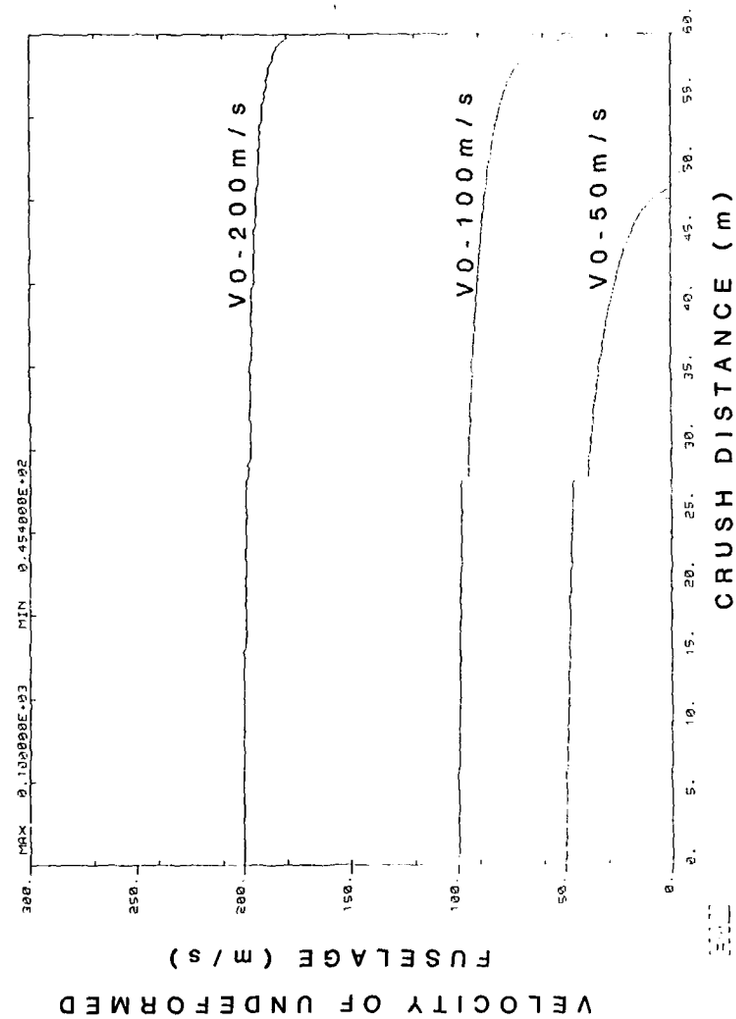

FIGURE 3

AIRCRAFT IMPACT INTO A RIGID BARRIER

ACCELERATION VS CRUSH DISTANCE

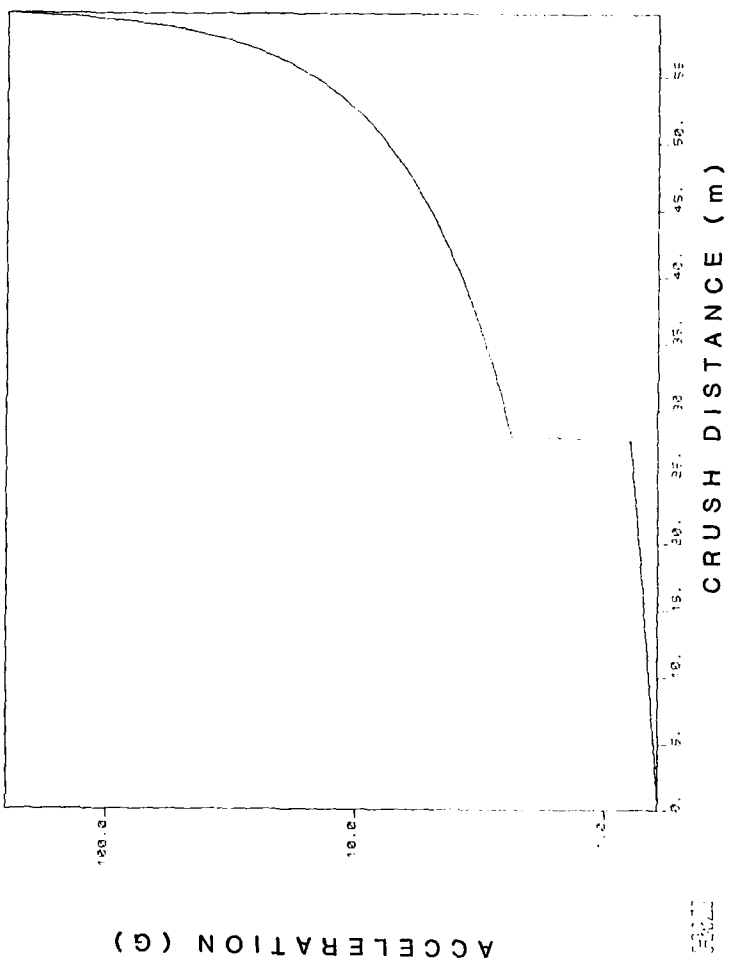

FIGURE 4

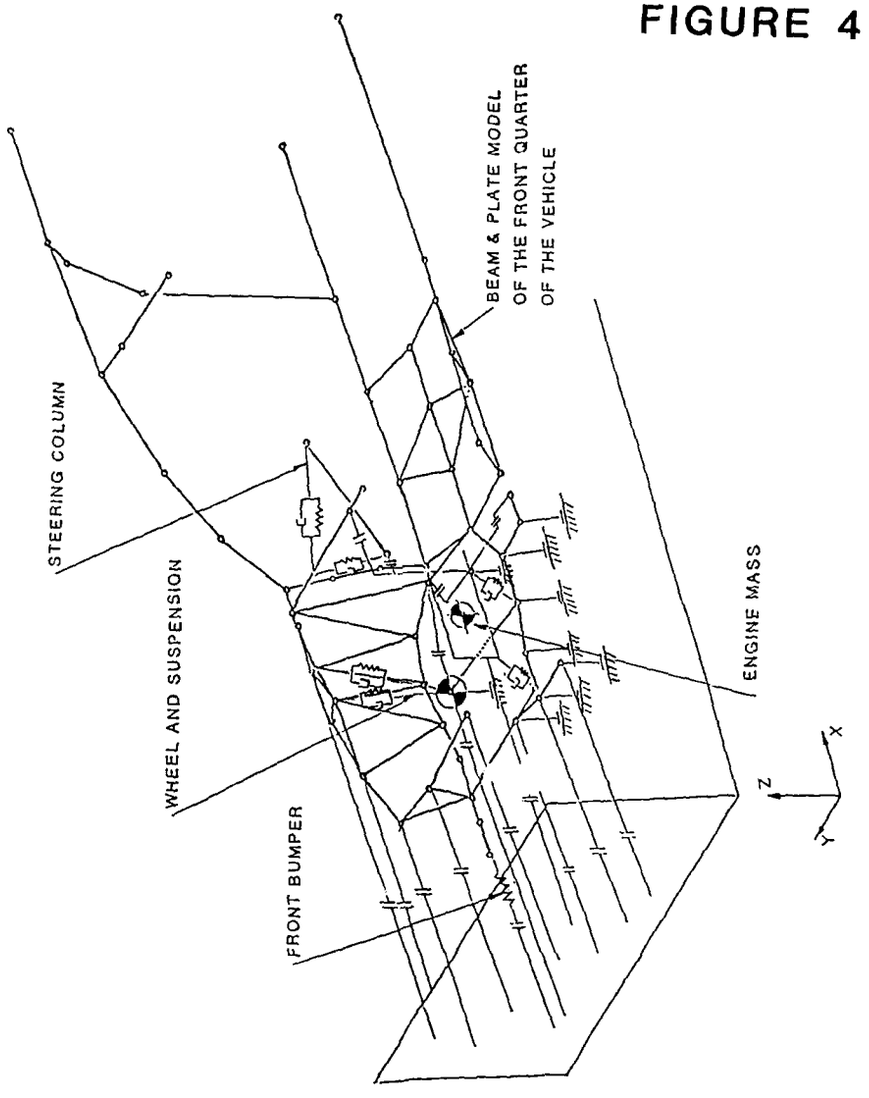

HYBRID MODEL FOR NON LINEAR DYNAMIC ANALYSIS

OF FRONTAL BARRIER

FIGURE 5

BEAM AND PLATE HALF MODEL

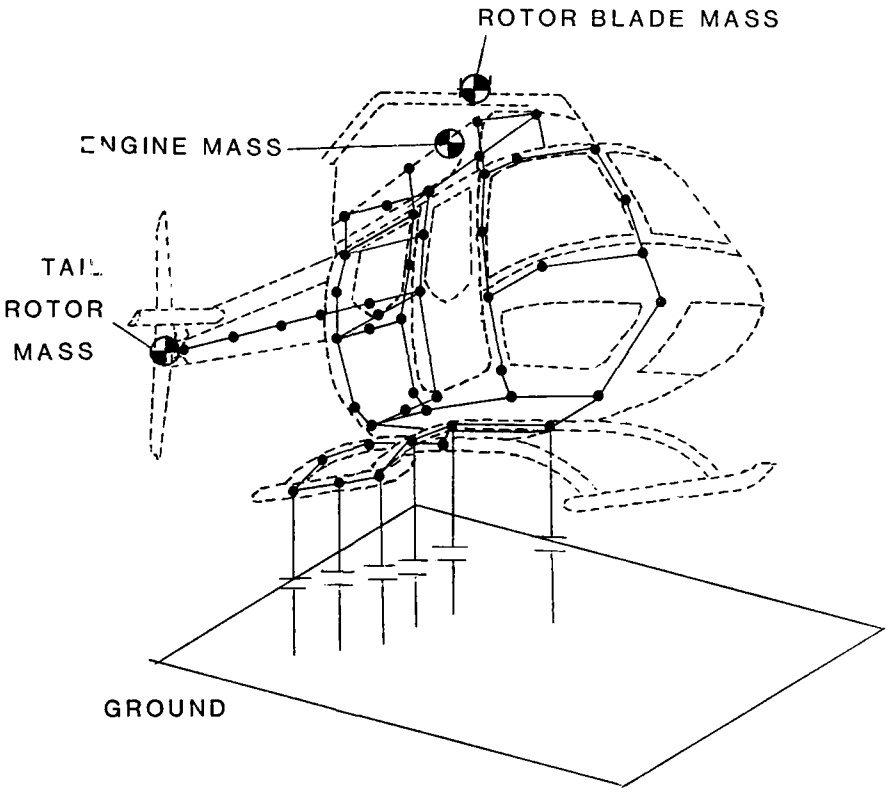

HYBRID MODEL FOR NON LINEAR DYNAMIC ANALYSIS

FIGURE 6

THREE DIMENSIONAL OCCUPANT MODEL

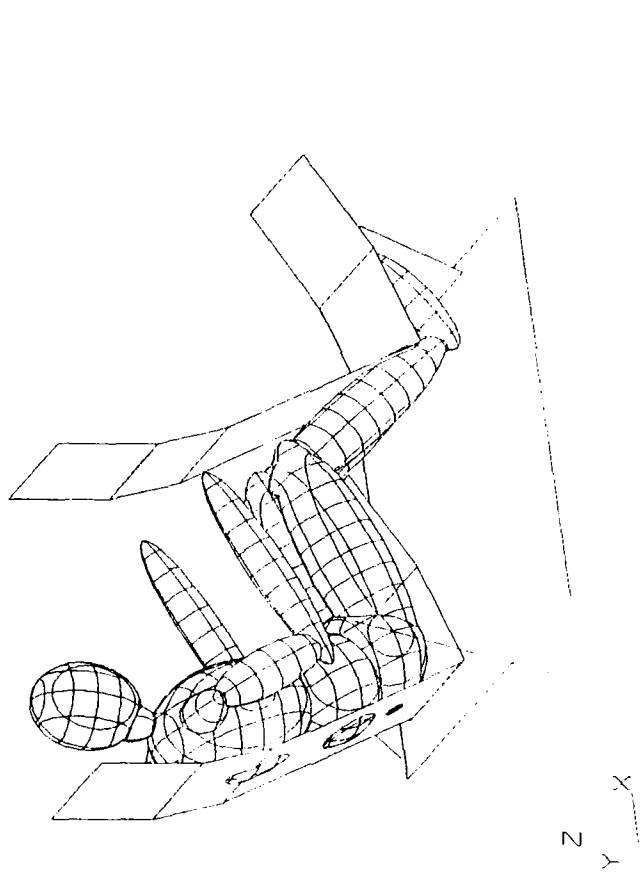

FIGURE 7

HEAD ACCELERATION VS TIME HISTORY PLOT

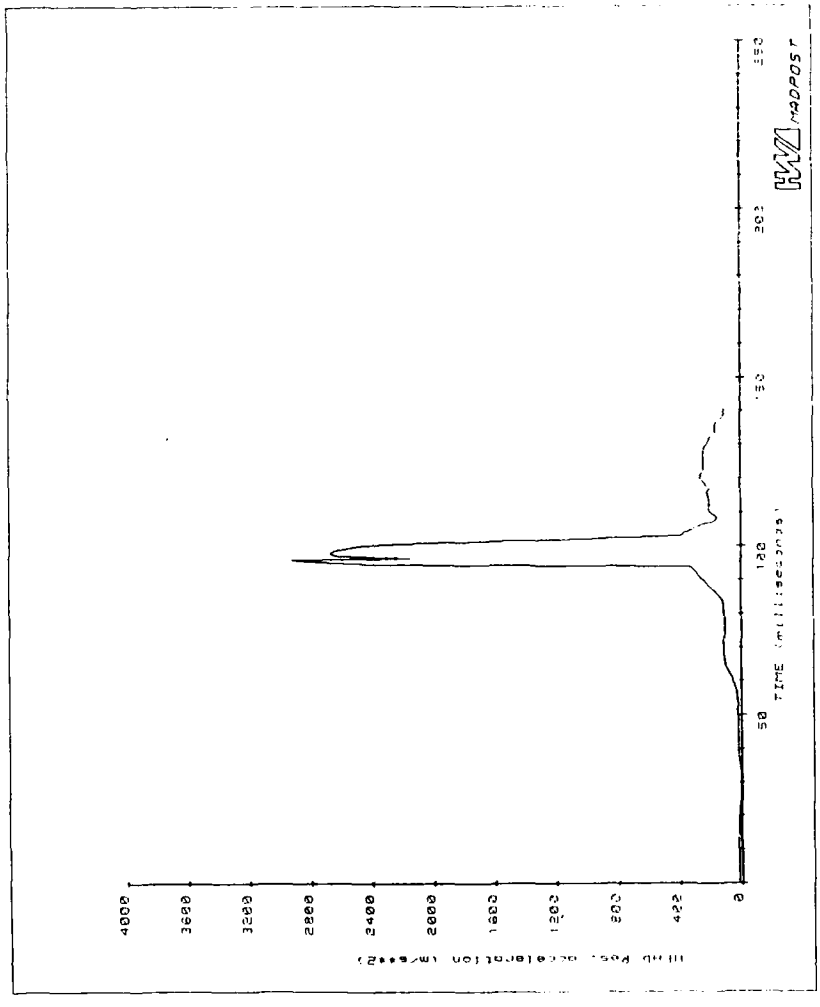

FIGURE 8

CRASH SEQUENCE PLOT OF OCCUPANT

WITH LAPBELT

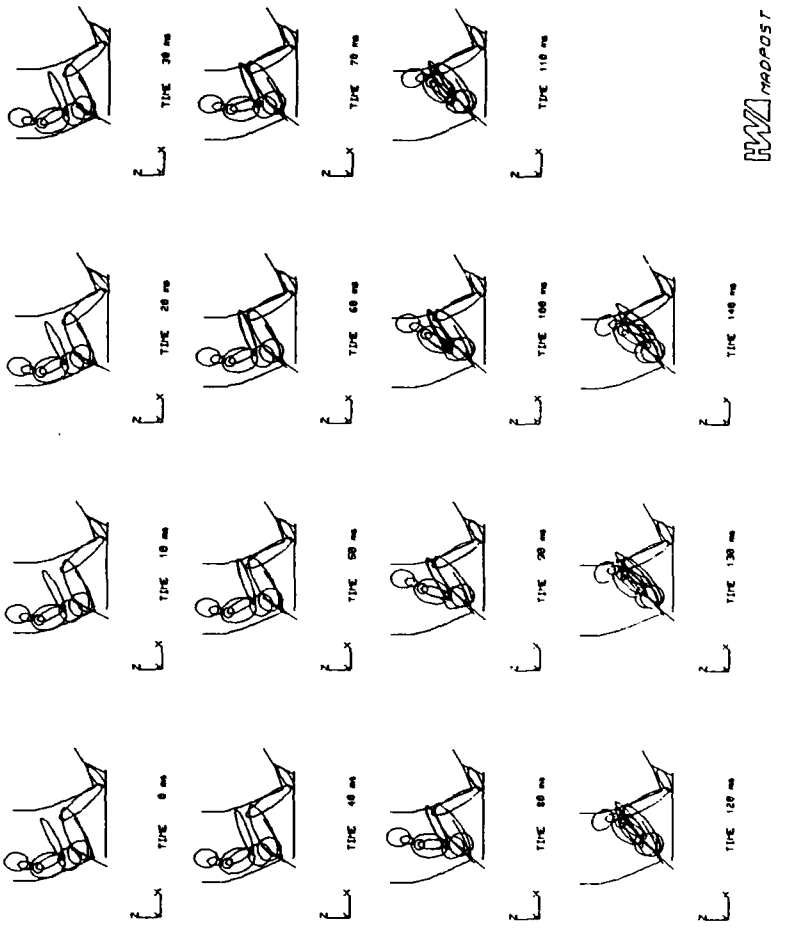

FIGURE 9

CRASH SEQUENCE PLOT OF OCCUPANT

WITH 3PT BELT

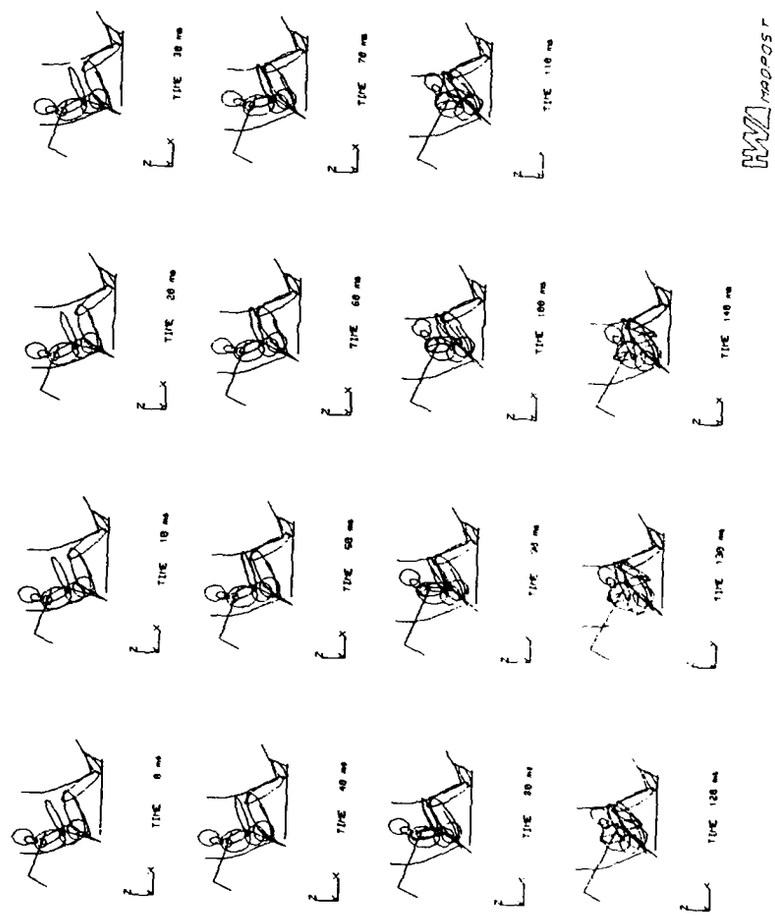

HUMAN CRASHWORTHINESS AND CRASH LOAD LIMITS

Henning E. von Gierke, Dr Eng, Ints Kaleps, PhD, and James W. Brinkley
Biodynamics and Bioengineering Division
Harry G. Armstrong Aerospace Medical Research Laboratory
Wright-Patterson Air Force Base, Ohio 45433-6573

SUMMARY

The assessment of the hazard to a crewmember in a potential aircraft crash requires information about human tolerance to mechanical forces, a method for the identification and evaluation of the contributing factors to potential injury in a crash and a means of estimating the environmental forces on an occupant and the resultant responses of the occupant. Results of research in the US Air Force in these three areas are discussed. Specifically, 1) the rationale for and formulation of a dynamic response six degree-of-freedom whole body impact tolerance specification. 2) a detailed head-spine structural mechanics and a vehicle occupant gross motion rigid body dynamics model and their areas of applicability in crash analysis, and 3) features of the newly developed US Air Force Advanced Dynamic Anthropomorphic Manikin (ADAM) are discussed. It is suggested that a comprehensive method for injury risk assessment for any system must consider all three areas.

LIST OF SYMBOLS

$\ddot{\delta}$	- acceleration of the dynamic response model mass relative to acceleration input point.
$\dot{\delta}$	- relative velocity between the input point and the model mass.
δ	- compression of the model spring.
ζ	- damping coefficient ratio.
DR	- dynamic response of the model.
ω_n	- undamped natural frequency of the model.
$\ddot{s}$	- seat acceleration component along the pertinent axis.
g	- acceleration due to gravity.
DRX	- dynamic response computed from the X axis acceleration component.
DRY	- dynamic response computed from the Y axis acceleration component.
DRZ	- dynamic response computed from the Z axis acceleration component.

I. INTRODUCTION

The ultimate effectiveness of the crashworthiness of an aircraft is its ability to protect the aircraft occupant. Various measures of an aircraft's structural integrity can be made, but the final measure is the state of the crewmember after the crash. This state primarily depends on two factors: the level of exposure to mechanical forces experienced by the crewmember and the crewmember's susceptibility to injury due to such exposure. The first requires the specifications of such conditions as whole body accelerations and localized impact forces on the body and the second requires the specification of the criteria for tolerance to such accelerations and forces.

In this report some of the latest advances in methods for injury potential assessment developed by the US Air Force are discussed. These include criteria for whole body tolerance to acceleration, analytical methods for predicting human body responses to various mechanical force exposures and the development of a highly sophisticated manikin.

II. SIX-DEGREE-OF-FREEDOM ACCELERATION EXPOSURE LIMITS

The current method for assessing the risk hazard associated with whole body acceleration and which takes into account the dynamic character of the body's response was developed by Stech (Ref. 1) and is known as the Dynamic Response Index (DRI). It idealizes the human response as that of a mass supported by parallel elastic spring and damper elements which respectively represent the upper body mass and the lumbar/thoracic spine. This model was originally developed to provide an injury risk assessment for aircrew members being ejected from aircraft and its applicability was strictly limited to longitudinal spinal accelerations. While this model was developed to address ejection problems, it also was applicable to other situations where the body primarily experienced abrupt vertical accelerations as, for example, in helicopter crashes.

This model has recently been generalized to also include fore-aft and lateral responses as well as an added rotational tolerance mechanism (Ref. 2). The approach taken has included the following assumptions and steps:

1. Use of the same dynamic model for all three orthogonal body axes.

2. Assignment of an injury-risk level for each axis.

3. Assumption of independent responses along each orthogonal axis.

4. Evaluation of the injury risk level assumptions using existing data from impact tests including ones with acceleration vectors off the orthogonal axes, ejection seat test data, and studies with mathematical models.

5. Assignment of angular acceleration limits based on the effects of their translational acceleration components.

The equations that describe the dynamic response along each major axis are given in the following equations:

$$\ddot{\delta} + 2\zeta\dot{\omega}_n\delta + \omega_n 2\delta = \ddot{s}$$

and

$$DR(t) = \frac{\omega_n 2\delta(t)}{g}$$

The axes are taken so that the +Z acceleration acts from foot to head and a +X acceleration acts from back to front.

Each of the dynamic response models, other than for the +Z axis, were developed by the same procedure. First, the experimental acceleration-time histories from tests with volunteer subjects were approximated with a half-sine pulse where feasible. The test data, which were measured on the test fixtures that transmitted the acceleration to the subjects in whole-body impact tests, were obtained from numerous reports published by US Air Force and Navy investigators and Department of Defense contractors. The approximations were established by fitting the peak acceleration and the time to the acceleration peak (rise time) with a half-sine pulse. This procedure yielded relatively good fits for the majority of the data. However, the fit was not good where the experimental acceleration pulse shape was actually more trapezoidal, as in some of Stapp's early tests (Ref. 3) or where the acceleration-time history was irregular. In such instances, the procedure used was to fit only the initial portion of the pulse; this approach provided a conservative estimate since the energy of the fitted half-sine pulse was always less than that contained in the actual data. Second, a model response curve was calculated which was descriptive of the higher acceleration data points where, in many cases, subjective tolerance limits of injuries had been identified by the original investigators. The curve was derived by computing the peak response of a single-degree-of-freedom model to half-sine acceleration pulses of varying durations. To select the natural frequency and the damping coefficient ratio for each axis, the natural frequency and the damping coefficient ratio of the model were adjusted until the shape of the peak response to the half-sine acceleration pulse matched available human response data. The results of no-injurious acceleration exposures of volunteer subjects were also considered to verify the frequency response and damping characteristics of the model. Verification was accomplished by study of the relationships between the acceleration input conditions and the measured responses of the test subjects, e.g., acceleration of body segments, displacement of body segments, restraint harness loads, and forces measured between the seat structure and the test subject.

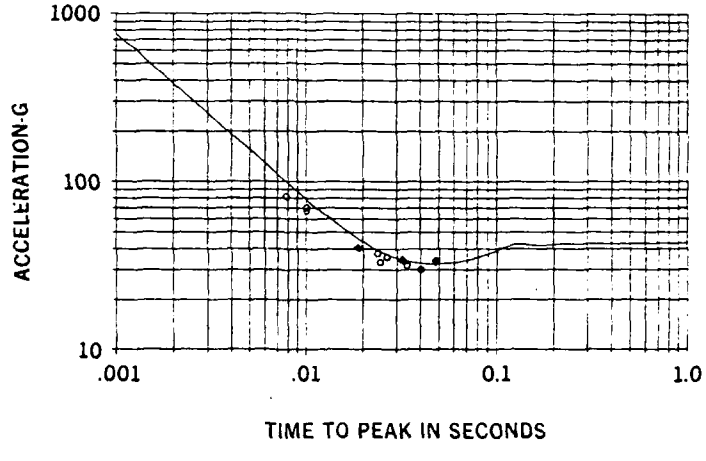

Figure 1 Model Response Curve for +X Axis Half-Sine Acceleration Pulses

Figure 1 shows the model response curve initially fitted to data collected from experiments conducted with the acceleration vector directed primarily along the +X axis. Tests resulting in injury (spinal fractures) or potentially serious sequelae (cardiovascular shock) are designated by the black symbols. The curve was derived from the responses of a mathematical model with a natural frequency of 62.8 rad/sec and a damping coefficient ratio of 0.2. Each of the models that have been developed presumes a specific restraining system consisting of a lap belt, crotch strap, and double shoulder strap configuration.

Figure 2 shows the derived curve and data points for -X axis impacts. The available data points do not demonstrate that the human body can tolerate higher acceleration levels as the duration of the acceleration pulse is decreased. However, this appeared to be a reasonable approximation on the basis of data from tests with animal subjects and analysis of physical responses of volunteer test subjects. A further refinement of the model coefficients was made based on transfer function calculation relating test seat and occupant chest accelerations. The results of 11 tests conducted at a level of 10G (impact velocity of 30.5 ft/sec) were analyzed. The mean natural frequency was found to be 64.2 rad/sec (SD = 6.0) and the mean damping coefficient was 0.23 (SD = 0.07).

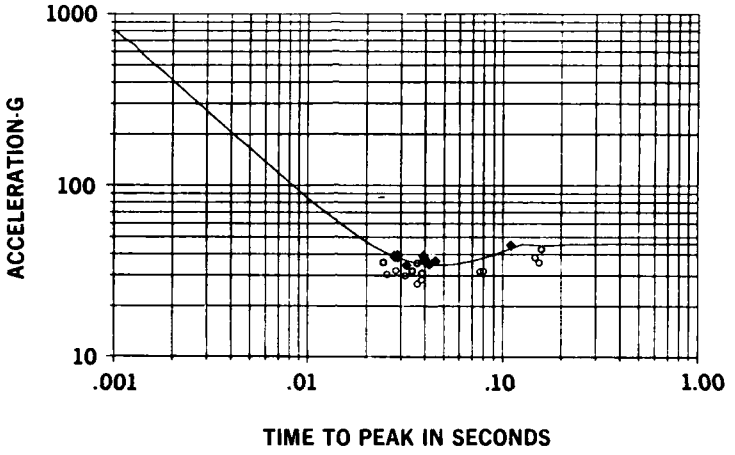

Figure 2 -X Axis Acceleration Response Curve

The injury-risk levels for the +Z axis were assigned by using the 50, 5, and 0.5-percent probability of spinal injury from the injury probability distribution for the DRI reported in reference 4. These injury risk levels are characterized as high, moderate, and low with respective DR values of 22.8, 18 and 15.2, as shown in Figure 3. A 50-percent probability of injury was selected as the highest spinal injury rate

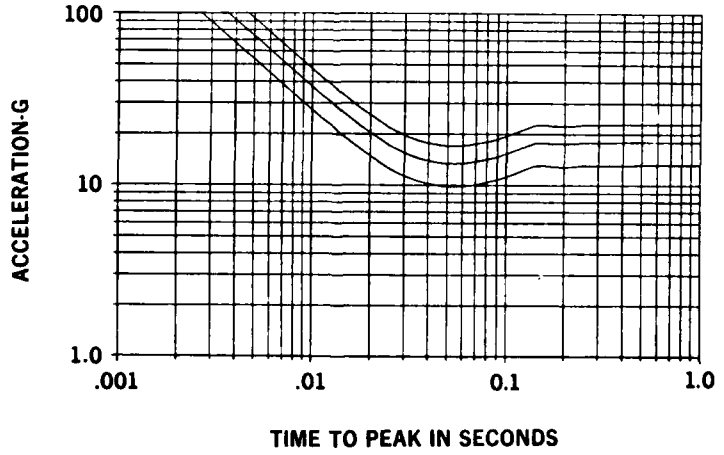

Figure 3 Injury Risk Levels for +Z Axis Half-Sine Acceleration Pulses

acceptable in the system design for two reasons. First, it is the highest spinal injury rate that has been observed for any USAF ejection seat. Second, this level was judged to be the maximum allowable considering that multiple exposures would be likely subsequent to the catapult acceleration, i.e., rocket acceleration, parachute-opening shock, and ground landing impact. The moderate-risk level corresponds to the level used in current USAF ejection-seat design (ref. 5) and is at a mid-point between the high and low levels. The low-risk level corresponds to acceleration conditions used routinely without incident in tests with volunteers conducted by the USAF.

Figure 4 illustrates the injury-risk levels assigned for the -X axis. The DR limit values are 46, 35, and 28.

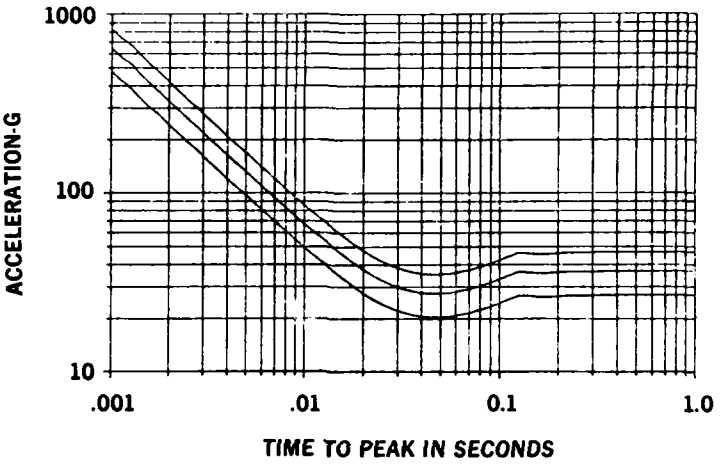

Figure 4 Injury Risk Levels for -X Axis Half-Sine Acceleration Pulses

The methodology used to establish the risk levels produced higher statistical confidence in its application of the +/-X and +Z axes than in its application of the +/-Y and -Z axes since more data are available to define the higher-risk levels. The data used to define the risk levels for the Y axis did not permit the assignment of high-risk levels with an adequate degree of confidence since clear evidence of injury has not been observed under laboratory conditions. The Y-axis model was initially assigned the same coefficients as the X-axis model (ref. 6). But the injury risk levels were lowered to correspond to the levels judged reasonable on the basis of available human test data. A transfer function analysis technique has been used to provide coefficients for the Y-axis model. Using data from 8-G impact tests with 13 volunteers, a mean natural frequency of 58.0 rad/sec (SD = 1.7) was derived. The damping coefficient was 0.09 (SD = 0.04). DR limit values, which have been estimated, are 22, 17, and 14.

The human test data available for the -Z axis, are also limited; however, the acceleration-time histories that have been used in non-injurious tests with volunteers span a relatively large range of time durations. The low-risk level was assigned on the basis of injury-free laboratory tests with volunteer subjects. The moderate level was selected on the basis of previous downward-ejection catapult acceleration limits, and the upper bounds of the available data from tests with heavily restrained subjects were used to establish the high-risk limits although injuries were not observed. The available data were not sufficient to do more than provide a rough approximation of the frequency response range of a model that would be descriptive of human dynamic response to -Z axis acceleration inputs. Since the +Z axis model was in that range, the natural frequency and damping coefficient for the +Z axis model were selected for the -Z axis acceleration limit model. The DR limit values which were selected are 15, 12, and 9.

While the individual orthogonal axes responses were assumed to be independent, a combined risk assessment in the form of an ellipsoidal envelope is proposed. It can be expressed in the following form:

$$\left[\left(\frac{DRX(t)}{DRX_L}\right)^2 + \left(\frac{DRY(t)}{DRY_L}\right)^2 + \left(\frac{DRZ(t)}{DRZ_L}\right)^2\right]^{1/2} \leq 1.0$$

where the suffix L denotes the limiting value for the assigned risk value.

The task of providing criteria for bounding allowable angular acceleration has been a problem that has required an assessment from first principles since no precedent exists. There is very little data available on human tolerance to angular acceleration and velocity. Translational accelerations and angular rates have been measured in only one test where a volunteer was exposed to the combined translational and high-level angular accelerations that may be associated with ejection seat operation (ref. 7). The approach selected to limit the angular acceleration is based on the hypothesis that the injuries associated with angular acceleration are directly related to local linear accelerations. This hypothesis has some support based on the experimental findings of Tarkov (ref. 8) and Weiss et al (ref. 9). Thus, the tangential and, to a greater degree, the centripetal acceleration must be considered. Payne has recommended that assessment of the effects of angular acceleration be accomplished by applying to the injury models the net linear acceleration due to whole body translational acceleration plus the local linear acceleration due to body rotation at a body center point. In the application of this method a body center point that is 18.2 in. up and 3.4 in. forward from the seat reference point (the intersection of the planes of the seat, seatback, and the mid-sagittal plane of the seat occupant) was chosen.

III. PREDICTIVE MODELS

The most desirable form for tolerance criteria is one that is specified in terms of external to the body variables. For example, the acceleration of the seat, the impact velocity of an aircraft or the height of a fall can be used to estimate the likelihood of an injury. Unfortunately most injuries associated with aircraft operations do not lend themselves to such simple approaches because the exposure conditions are usually more complicated and better resolution between exposure conditions and injury consequences is needed.

This may be illustrated by considering the case of a helicopter crash in which the net crash deceleration and ground impact velocity may be reasonably estimated, but the degree of anticipated injury can be substantially modified depending on whether the helicopter was equiped with an energy absorbing seat, the seat stayed rigidly attached, the crewmember was in an upright position at time of impact, the harness functioned properly in restraining the crewmember and the aircraft structure was sufficiently deformed to interact with the crewmember. Obviously all these factors complicate an injury potential assessment and in a given crash event any one of them may be the causative factor in an injury or fatality.

While no current method exists that can factor in all such eventualities and provide a meaningful absolute injury probability prediction, analytical models are being developed that can assess the relative effects of system designs, procedures and crash conditions.

One such model has been developed by the USAF to predict stresses developed in the spine due to abrupt accelerations applied to the torso (Ref. 10). This is a three dimensional, discrete model of the human spine, torso and head developed for the purpose of evaluating mechanical response in pilot ejection. It was developed in sufficient generality to be applicable to other body impact problems, such as occupant response in aircraft crashes and arbitrary loads on the head-spine structure.

A graphical representation of the Head-Spine model structure is shown in Figure 5. The anatomy is modeled by a collection of rigid bodies, which represent skeletal segments such as the vertebrae, pelvis, head and ribs, interconnected by deformable elements, which represent ligaments, cartilageneous joints, viscera, and connective tissues. Techniques for representing other aspects of the environment, such as harnesses and the seat geometry, are also included. The model is valid for large displacements of the spine and treats material nonlinearities.

The basic model is modular in format, so that various components may be omitted or replaced by simplified representations. Thus, while the complete model is rather complex and involves substantial computational effort, various simplified models are available that are quite effective in duplicating the response of the complete model within a range of conditions.

Various conditions can be studied using the model, including different acceleration pulses, harness configurations and elasticities, seat geometries and initial spinal postures. Predictions include spinal deformation, local stresses and a thoracic/lumbar compression fracture probability. The latter prediction is based on the predictive calculation of vertebral body stresses during a dynamic exposure event and the comparison of these stresses to measured strength properties of human vertebral bodies (Ref. 11).

The injury prediction is given in terms of an Injury Potential Function which is obtained by dividing the maximum predicted stress at each vertebral level by the corresponding vertebral level mean failure stress. An example of the Injury Potential Function for a fully upright and tightly restrained individual is shown in Figure 6. Four levels of vertically applied acceleration ranging from 14 to 20 g's are considered. A bi-model response is observed with peaks at T8 and L3. The steep increase of the curves at T4 is probably not realistic because of the relatively unstable response of the upper thoracic and cervical spine structure. The higher probability of injury predicted in the middle thoracic region than the lumbar region, which is the more common region for spinal compression fractures, illustrates the model's capability to examine the effects

of varying conditions. In this case it showed that a highly upright seated position and restricted column bending due to very tight torso restraint may move the most likely site of spinal injury up the spine.

Another model adapted by the USAF to study gross human body dynamics is the Articulated Total Body (ATB) model (Ref. 12). This model is a derivative of the Crash Victim Simulator (Ref. 13) originally developed to study road vehicle occupant motion during crashes. The model is totally three-dimensional and its analysis method is based on coupled rigid body dynamics. Its standard configuration, consisting of 15 segments and 14 joints, as shown in Figure 7.

A graphical depiction of the model is shown in Figure 8 where the segments are depicted by ellipsoidal surfaces. The graphical display can be presented from any direction and distance and its image projected through a point. Such a graphical display allows direct comparison to video images as well as being a convenient means for examining body position and motion relative to support and potentially interacting structures.

The modeled body structure is assumed to be passive in that muscle forces do not act. The dynamic response of the body can be induced by interactions with the seat and harness system or windblast, gravitational or local contact forces acting on the segments. In addition to the graphical depiction of body motion, the linear and angular displacements, velocities and accelerations of all segments, the forces and moments in all joints, the points on segments and forces of contact and the loads in the harness system are predicted.

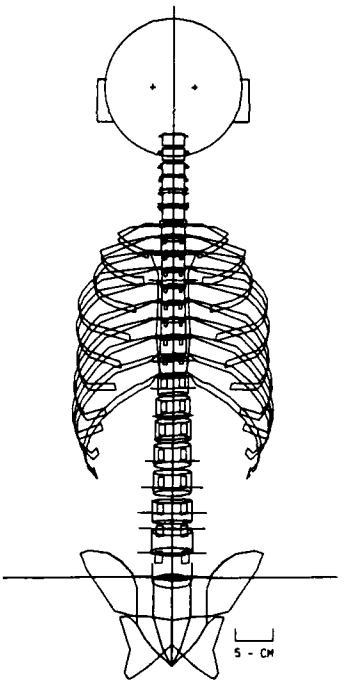

Figure 5 Graphical Representation of the Head-Spine Model

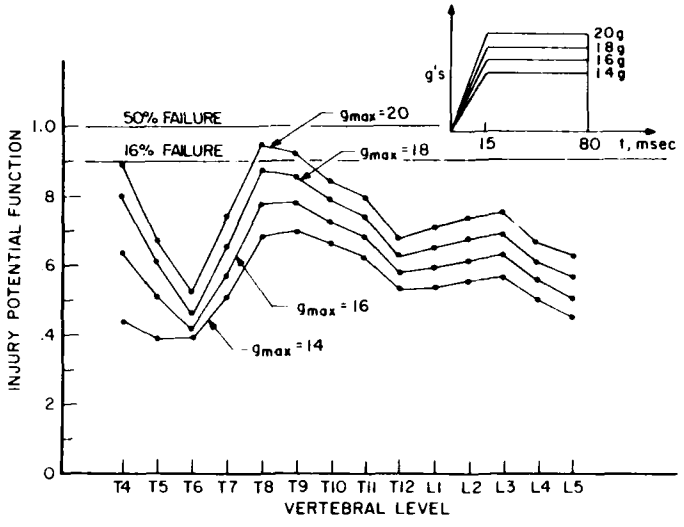

Figure 6 Injury Potential Function from Head-Spine Model in Upright and Highly Restrained Posture for Gz Impacts

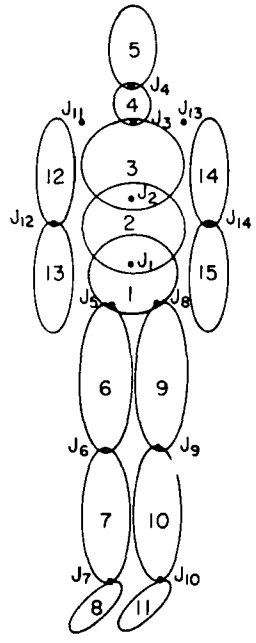

Figure 7 ATB Model Segment and Joint Configuration

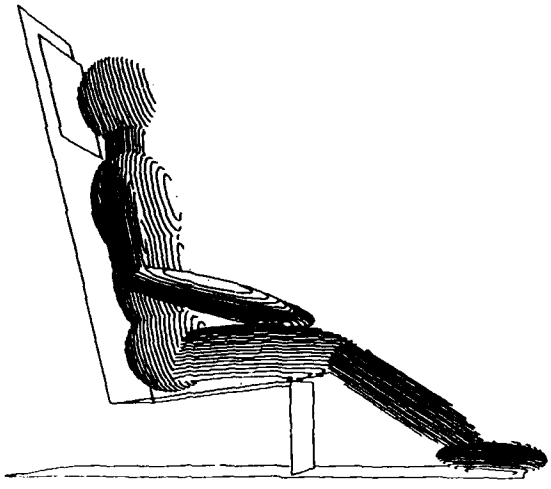

Figure 8 Graphical Representation of the Articulated Total Body Model

Various data bases for different size males, females and children (Ref. 14), as well as the Part 572 dummy (Ref. 15) and the Hybrid III dummy (Ref. 16) have been developed. These allow a broad choice of occupant sizes and can be used to investigate effects on dynamic response of size variation.

Human response validation (Ref. 17) and dummy response validations (Ref. 18) have been made with the model. Additionally a number of simulations have been performed with excellent agreement between predicted and observed responses (Ref. 19 and 20).

The ATB model is an excellent tool for clearance or body trajectory prediction. The model was used to investigate child motion in an automobile during panic braking and subsequent impact (Ref. 21). Three child sizes and seven different initial positions were chosen. In Figure 9 a child initially facing forward experiences a .5G vehicle deceleration while his feet have a .25 seat friction coefficient. In Figure 10 a child in the same initial position experiences a .7G vehicle deceleration while his feet have a

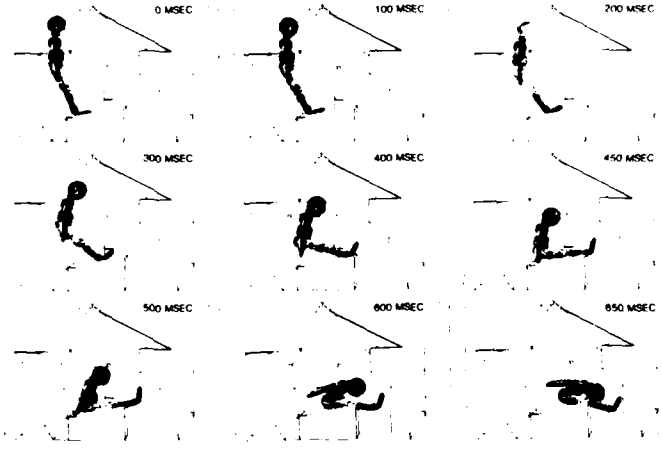

Figure 9 Two-and-One-Half-Year-Old Child Motion During .50 G Panic Braking Deceleration with .25 Seat Friction Coefficient

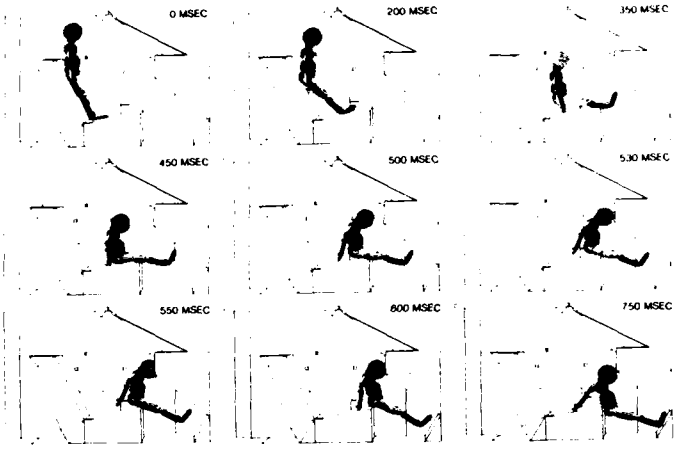

Figure 10 Two-and-One-Half-Year-Old Child Motion During .70 G Panic Braking Deceleration with .20 Seat Friction Coefficient

.20 seat friction coefficient. In the first case the motion is relatively benign with the child not contacting the dash and coming to rest on the front part of the seat. A 20 percent reduction in the seat friction coefficient, combined with an increase in vehicle deceleration from .5G to .7G, substantially modified the resultant body motion leading to a significant head impact with the dash and final body location on the vehicle's floor.

The above simulations are only two of over 160 that were performed in which various conditions and parameters were varied, but they illustrate the ease of examining the relative effects of such changes. The model has also been used in a number of internal USAF studies to look at body motion and clearances of limbs during escape from aircraft.

IV. ADVANCED MANIKIN DEVELOPMENT

The use of mechanical human surrogates or dummies is becoming a more common and relevant approach for assessing the safety of crash protection systems and procedures. Early dummies were developed to provide inertial loading similar to that of the human body and were primarily used to test the proper operation of harnesses, seat structures and ejection seats. In these tests the concern was with the response of the equipment as affected by the inertial effects of the human body. Typical dummies used for such applications were developed by Sierra and Alderson in the 1950s primarily to provide human-like ballast for ejection seats. While their overall mass distribution properties were quite good, their joint mobility and body flexibility were highly limited. This resulted in a highly rigid response to external forces and internal dynamic measurements that did not compare well to human responses for similar exposures (Ref. 22).

A new generation of dummies was developed in the 1960s and 1970s, primarily driven by increased emphasis on road motor vehicle safety. The most common of these is the Hybrid II dummy originally developed by General Motors and adopted by the National Highway Traffic Safety Administration as the standard automotive safety compliance testing dummy. This dummy, most commonly known as the Part 572 dummy from its documentation designation, had considerably improved human-like fidelity and was designed to provide internal response measures that could be correlated to equivalent human responses and possibly, likelihood of injury. Several other dummies were developed in the United States, Great Britain and Sweden in this same time period that attempted to improve response characteristics, but none achieved the degree of standard acceptance as had the Part 572 dummy. In the late 1970s General Motors developed the Hybrid III, which had improved bio-fidelity and instrumentation capability over the Hybrid II.

This evolutionary process did improve the state-of-the-art in dummy design sophistication, biofidelity and response measurement capability. Most of it, however, was directed at road vehicle safety design considerations with considerable emphasis on chest and head impact responses, horizontal plane impact events and testing under highly controlled conditions.

Attempts to use these types of dummies in aerospace environments led to the identification of a number of shortcomings. These included the lack of a proper dynamic longitudinal spinal axis response, which is the predominant loading direction for aircraft related force exposures. Standard data retrieval by means of an umbilical cord limiting freedom of dummy motion and requiring a separate data acquisition system. Durability sufficient only to withstand relatively low forces compared to those encountered in aircraft crashes or escape from aircraft.

To address these shortfalls, the US Air Force has pursued the development of an Advanced Dynamic Anthropomorphic Manikin (ADAM) to be used in the testing of escape systems and various protection systems and procedures (Ref. 23). This effort, initiated in 1981 has resulted in the production of a small and a large male prototype manikin. These manikin sizes are based on an Air Force male aviator anthropometric survey conducted in 1967 (Ref. 24) with the specific dimensions and inertial properties taken from US tri-service recommendations (Ref. 25). The small ADAM whith full skin covering is shown in Figure 11. The small ADAM with upper torso, right arm and right leg skins removed to show the mechanical structure, battery storage compartment in upper leg and the instrumentation package located in the thorax, is shown in Figure 12. Also shown in Figure 12 is a head mounted antenna used for data transmission.

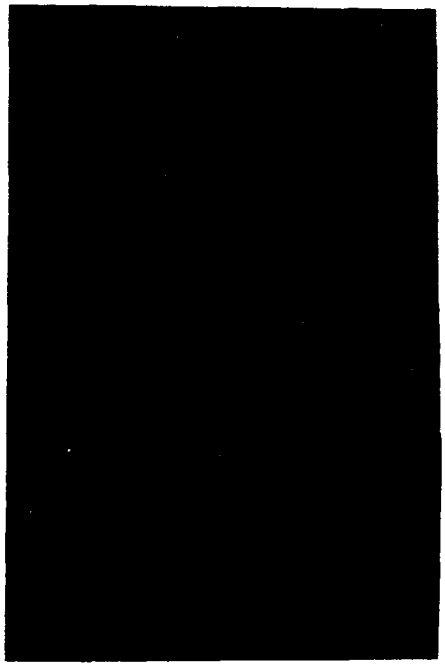

Figure 11 Small ADAM with Full Skin Covering

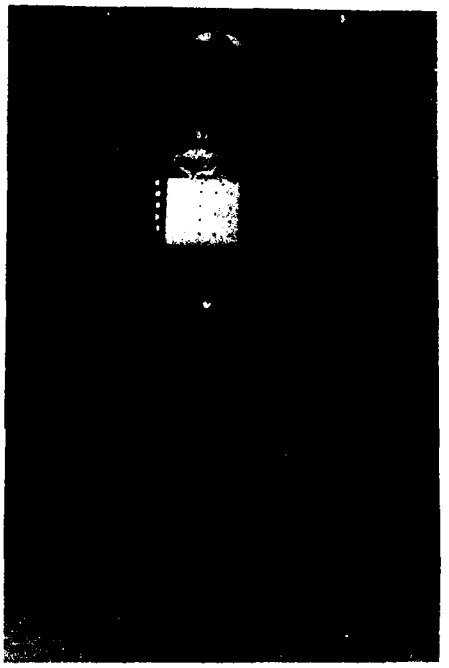

Figure 12 Small ADAM with Skins Partially Removed to Show Mechanical Structure and Instrument Package in Thorax

The design for this manikin stresses faithful human joint articulation and torso axial deformation to properly reflect the mass shifts and limb motion, as well as dynamic spinal compression, that an actual crewmember would experience during a whole body impact. All the joints with the exception of the neck and spine, are single or compound revolute joints with precisely defined axes orientations, joint stops with soft snubbers, adjustable friction pads and position sensing potentiometers. These features can be seen in Figures 13 and 14 which are the knee and shoulder joints respectively. The axial spine element is a combined spring and hydraulic damping element which is tuned to provide longitudinal impact response with a natural resonance in the 10 to 12 Hz range. Re-tuning may be accomplished by spring replacement and use of different viscosity hydraulic fluid. Below the axially deforming spinal element is a universal joint that allows for yaw motion and flexural and lateral bending. This compound articulation is approximately in the lumbar anatomical region and provides the only bending articulation in the torso. The total spine structure is shown in Figure 15.

Figure 13 ADAM Knee Joint Showing Flexure and Torsion Articulations, Friction Pads and Wire Connections to Fosition Measuring Potentiometers

Figure 14 ADAM Shoulder Joint Showing Multiple Revolute Articulations

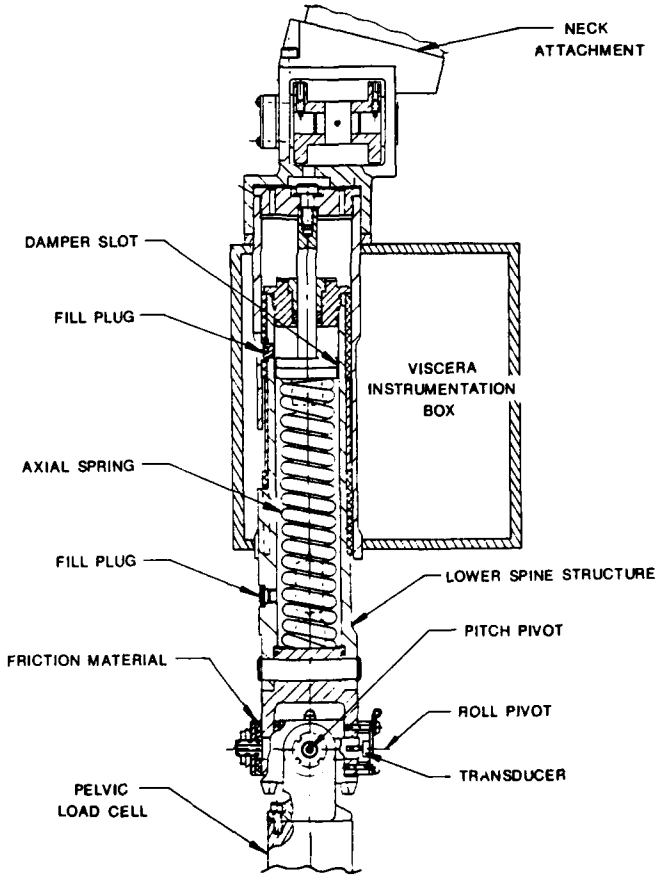

Figure 15 ADAM Spine

The durability of the manikins was specified in terms of a violent exposure environment in which they must be able to operate without any functional degradation. This environment is the ejection into a 700 KEAS wind stream, in an ejection seat with unrestrained limbs for the large manikin and restrained arms and legs for the small manikin. They must also be able to sustain 45G impact loads in the Gx, Gy and Gz directions without functional degradation or permanent structural damage.

The standard Hybrid III dummy head and neck are used, but, as opposed to the Hybrid III design, the head skin covering extends over the neck as can be seen in Figure 11.

The total instrumentation and data acquisition system for ADAM is a substantial advancement over any other current manikin. The system is located in the thorax, is computer controlled and, in its standard configuration, can collect 128 channels of data at 1000 samples/channel-sec and store up to 4 seconds of data as well as telemeter this data in real time to a ground station. The system configuration can be modified by an operator, through computer input, to change the number of channels, the sampling rate and the filter bandwidths. The circuit board configuration, from a rear view, is shown in Figure 16.

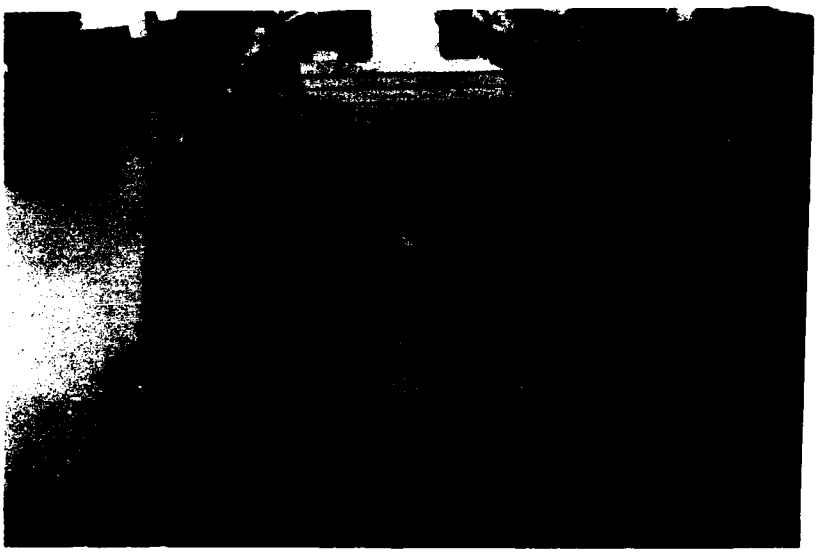

Figure 16 ADAM Instrumentation Package with Rear Access Panel Removed

The availability of 128 channels allows extensive monitoring of the manikin's responses as well as collection of external data. ADAM has been designed for measurement of three orthogonal acceleration components in the head, thorax and pelvis; six force and moment components both between the head and the top of the neck and between the lumbar spine and the pelvis; and the position of all revolute joints. Additionally, load cells are located at the joints in the lower legs to measure torsional moments. The instrumentation system provides for signal conditioning, analog to digital data conversion and pre and post data collection calibration for all of these transducer channels. A listing of these transducer channels, including ones for internal temperature and parachute riser loads, are presented in Table 1. The other channels may be used for additional ADAM sensors or to collect external information.

TABLE 1
ADAM TRANSDUCER CHANNELS

1	Left Hip Abduction/Adduction Position
2	Right Hip Abduction/Adduction Position
3	Left Hip Flexion Position
4	Right Hip Flexion Position
5	Left Hip Medial/Lateral Position
6	Right Hip Medial/Lateral Position
7	Left Knee Flexion Position
8	Right Knee Flexion Position
9	Left Knee Medial/Lateral Position
10	Right Knee Medial/Lateral Position
11	Left Shoulder Arm-Joint Abduction/Adduction Position
12	Right Shoulder Arm-Joint Abduction/Adduction Position
13	Left Shoulder Thoracic-Joint Abduction/Adduction Position
14	Right Shoulder Thoracic-Joint Abduction/Adduction Position
15	Left Shoulder Flexion/Extension Position
16	Right Shoulder Flexion/Extension Position
17	Left Shoulder Medial Lateral Position
18	Right Shoulder Medial/Lateral Position
19	Left Arm Raising/Lowering Position
20	Right Arm Raising/Lowring Position
21	Left Elbow Flexion Position
22	Right Elbow Flexion Position
23	Left Forearm Supination/Pronation Position
24	Right Forearm Supination/Pronation Position
25	Left Lower Leg Torque
26	Right Lower Leg Torque
27-32	Neck Forces and Moments (6 axis)
33-38	Lumbar Forces and Moments (6 axis)
39-41	Head Accelertion (triaxial)
42-44	Head Rotation Rate (3 rate sensors)
45-47	Chest Acceleration (triaxial)
48-50	Pelvis Acceleration (triaxial)
51-52	Parachute Loads, Right and Left Risers
53	Temperature Measurement
54-58	Lumbar Position
59	Viscera Position
60	Viscera Acceleration
61	Sternoclavicular Elevation/Depression Position
62	Sternoclavicular Pronation/Retraction Position

V. CONCLUSIONS

It is suggested that a comprehensive assessment of injury potential in a crash or other exposure to violent mechanical forces requires a broad based methodology including direct injury prediction based on environmental conditions; analytical or modeling approaches that an provide interpolative, extrapolative and sensitivity information; and the use of mechanical surrogates that can provide direct measures of what the human body would experience in a given environment.

The direct tolerance criteria, while usually the easiest to use, often have limited utility because they apply to very specific modes and mechanisms of injury. For example, the DRI as specified for evaluating allowable ejection seat accelerations (Ref. 5) is only applicable to Z axis accelerations and is strictly based on observed spinal compression fractures as the injury mechanism.

Analytical methods and models can provide a means of relating a general body exposure to a specific susceptible body structure and, given the appropriate strength properties of the local structure, allow prediction of failure/injury of that particular structure. From an engineering point this is a straight forward process; however, in application it can be difficult due to the large variability in biological material properties, the structural complexity of the human body and the generally unknown extent of active muscle participation. Where the modeling methodology is particularly useful is in relative assessments of system design changes, procedure modifications and operation condition variations. The assessments are made on the basis of predicted changes in local stresses, deformations and accelerations; external contact and harness forces; maximum ranges of limb motion; and amount of clearance between body segments and structural elements.

To define the exposure environment, tests must be conducted that, as closely as possible, replicate the anticipated operational conditions. This not only requires that the vehicle or occupants external environment is properly controlled, but that the occupant be an appropriate surrogate for a crewmember. The ADAM has been designed not only to provide correct reactive loads into the harness, seat and any other interactive structures, but to also be sufficiently internally biofidelic so that its internal response measures may be related to equivalent human responses under the same exposure conditions. While substantial validation still needs to be performed, the biofidelity and extensive response measurement capability of ADAM should make it a powerful tool for the safety assessment of aircraft, subsystems and procedures.

REFERENCES

1. Stech, E.L. and Payne, P.R., Frost Engineering Development Corporation, "Dynamic Models of the Human Body," November 1969, AAMRL Technical Report 66-157, AD 701383.

2. Brinkley, J.W., Air Force Aerospace Medical Research Laboratory, Wright-Patterson Air Force Base, "Acceleration Exposure Limits for Escape System Advanced Development," SAFE Journal, Volume 15, Number 2, Summer Quarter - 1985, Pages 10-16.

3. Stapp, J.P., Aero Medical Laboratory, Wright Air Development Center, "Human Exposures to Linear Deceleration, Part I: Preliminary Survey of Aft-Facing Seat Position," 1949, AF Technical Report 5915, Part I.

4. Brinkley, J.W. and Shaffer, J.T., Aerospace Medical Research Laboratory, Wright-Patterson Air Force Base, "Dynamic Simulation Techniques for the Design of Escape Systems: Current Applications and Future Air Force Requirements," Symposium on Biodynamic Models and Their Applications, 1971, AMRL-TR-71-29.

5. Military Specification (USAF), "Seat System: Upward Ejection, Aircraft, General Specification for," 1972, MIL-S-9479B.

6. Brinkley, J.W., "Personnel Protection Concepts for Advanced Escape System Design," Human Factors Considerations in High Performance Aircraft, AGARD Conference Proceedings, 1984, Pages 61 to 6-12.

7. Belytschko, T., Schwer, L. and Schultz, A., Department of Materials Engineering, University of Illinois at Chicago Circle, "A Model for Analytic Investigation of Three Dimensional Spine-Head Dynamics," April 1976, AMRL-TR-76-10.

8. Belytschko, T. and Privitzer, E., Department of Materials Engineering, University of Illinois at Chicago Circle, "Refinement and Validation of a Three-Dimensional Head-Spine Model," August 1978, AMRL-TR-78-7.

9. Fleck, J.T. and Butler, F.E., Calspan Corporation, "Development of an Improved Computer Model of the Human Body and Extremity Dynamics," July 1975, AMRL-TR-75-14.

10. Clarke, N.P., "Biodynamic Response to Supersonic Ejection," Aerospace Medicine, Volume 34, Number 12, 1963, Pages 1089-1094.

11. Tarasov, V.M., "Human Endurance of Impact Angular Accelerations," Aviation and Space Medicine, ed. V.V. Parin, 1969, Volume 2, Moscow (NASA TT-F-4, 565).

12. Weiss, H.S., Edelberg, R., Charland, P.V. and Rosenbaum, J.I., Wright-Patterson Air Force Base, "The Physiology of Simple Tumbling," Part 2, Human Studies, 1954, WADC Technical Report 53-139.

13. Fleck, J.T. and Butler, F.E., Calspan Corporation, "An Improved Three-Dimensional Computer Simulation of Motor Vehicle Crash Victims," July 1974, Report Nos. DOT-HS-801507 through 510, Volumes 1-4.

14. Baughman, L.D, Calspan Corporation, "Development of an Interactive Computer Program to Produce Body Descriptive Data (GEBOD)," July 1983, Report No. AFAMRL-TR-83-058, NTIS No. AD-A133-720.

15. Fleck, J.T., Butler, F.E. and DeLeys, N.J., Calspan Corporation, "Validation of the Crash Victim Simulator," 1982, Report Nos. DOT-HS-806-279 through 282, Volumes 1-4, NTIS No. PC E99, PB86-212420.

16. Kaleps, I., White, R.P., Jr., Beecher, R.M., Whitestone, J. and Obergefell, L.A., Armstrong Aerospace Medical Research Laboratory, Wright-Patterson Air Force Base, "Measurement of Hybrid III Dummy Properties and Analytical Simulation Data Base Development," February 1988, AAMRL-TR-88-05.

17. Kaleps, I., "Prediction of Whole-Body Response to Impact Forces in Flight Environments," AGARD Conference Proceedings No. 253, Models and Analogues for the Evaluation of Human Biodynamic Response, Performance and Protection, published June 1979, Pages A1-1 to A1-13.

18. Obergefell, L.A., Kaleps, I. and Steele, S., Armstrong Aerospace Medical Research Laboratory, Wright-Patterson Air Force Base, "Part 572 and Hybrid III Dummy Comparison Sled Test Simulations," 1988, SAE Paper No. 880639.

19. Kaleps, I., Obergefell, L.A. and Ryerson, J.R., Armstrong Aerospace Medical Research Laboratory, Wright-Patterson Air Force Base, "Simulation of Restrained Occupant Dynamics During Vehicle Rollover," June 1986, DOT HS 807 049 Final Report.

20. Obergefell, L.A., Kaleps, I. and Johnson, A.K., "Prediction of an Occupant's Motion During Rollover Crashes," SAE The Engineering Resource for Advancing Mobility, SAE Technical Paper Series, October 1986, Thirtieth Stapp Car Crash Conference, San Diego, California.

21. Kaleps, I. and Marcus, J.H., "Predictions of Child Motion During Panic Braking and Impact," SAE The Engineering Resource for Advancing Mobility, SAE Technical Paper Series, October 1982, Twenty-Sixth Stapp Car Crash Conference, Ann Arbor, Michigan.

22. Coermann, R.R., "Comparison of the Dynamic Characteristics of Dummies, Animals and Man," Impact Acceleration Stress--Publication 977, National Academy of Sciences, National Research Council, Pages 173-184.

23. Rasmussen, R.R. and Kalpes, I., "The USAF Advanced Dynamic Anthropomorphic Manikin - ADAM," 1987, Proceedings of the 24th Annual Symposium SAFE Association, Pages 88-91.

24. Staff of Anthropology Research Project, Webb Associates, "Anthropometric Source Book, Volume II: A Handbook of Anthropometric Data," July 1978, NASA Reference Publication 1024.

25. "Anthropometry and Mass Distribution for Human Analogues, Volume I: Military Male Aviators," 1987, to be published as a US Military Tri-Services Report.

Requirements and Criteria for the Passive Safety of Automobiles

Prof. Dr.-Ing. R. Weißner
Volkswagen AG, Research and Development, 3180 Wolfsburg
Germany

Summary

Success has been achieved in the last 17 years in increasing traffic safety. The number of people killed has dropped dramatically despite a considerable increase in the number of vehicles involved.

The following deals with the passive safety requirements imposed on passenger vehicles and with technical concepts designed to satisfy these requirements.

The interpretation of the functions

- Speed/time function for a head-on vehicle collision
- Occupant acceleration as a function of forward displacement

leads to the definition of the basic demands to be made of an occupant restraint system:

- Occupant restraint system should come into action quickly following start of vehicle deceleration with a view to minimizing occupant acceleration with the same throw-forward distance, i.e. the system response time should be as short as possible.
- Only slight occupant deceleration, i.e. biomechanically tolerable limits must not be exceeded due to the mechanical load.
- With a view to achieving the highest possible usage quota, the system must afford adequate comfort when not in action.

Use can be made, for example, of belt force limiters to reduce the forces acting on the occupant during the restraint process.

A belt lock-up or belt pre-tensioners can be used to limit to occupant throw-forward distance.

Numerous measures have to be taken to make a restraint system comfortable. Belt height adjustment, for example, provides an individual adaptation of the belt position.

An important safety feature - which is often underestimated in terms of its contribution to safety - is the seat plus head restraint. The seat has a considerable influence on the effectiveness of the entire system both in the event of a head-on collision and in the case of a rear end collision.

If it is assumed that there is good correlation between the load values measured with dummies and the real risk of injury for a person involved in an accident, the possible benefit of any safety measure can be forecast.

This is a necessary prerequisite for cost/benefit analyses.

Some 50 % of the people who die each year in the Federal Republic of Germany as a result of the injuries they have sustained are cyclists, motor cyclists and pedestrians.

The efforts to improve passive safety must also include this group of road users.

It is to be hoped that the number of people who sustain serious injuries or even lose their lives as result of a traffic accident will continue to drop in the future. This goal will be attained if all those involved - namely vehicle manufacturers, road users and legislators - sustain their efforts to increase road traffic safety.

Requirements and Criteria for the Passive Safety of Automobiles

Success has been achieved in the last 17 years in increasing traffic safety. The number of people killed has dropped dramatically despite a considerable increase in the number of vehicles involved (Fig. 1).

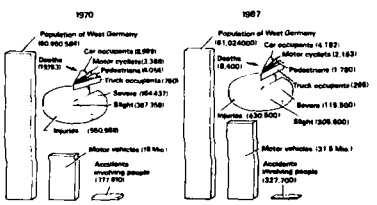

Fig. 1:
Accident statistics

The following deals with the passive safety requirements imposed on passenger vehicles (Fig. 2) and with technical concepts designed to satisfy these requirements.

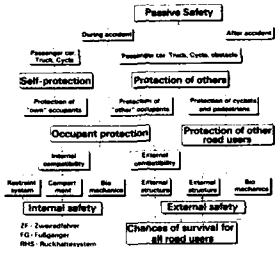

Fig. 2:
Passive safety requirements

The interpretation of the graphs

- Speed/time function for a head-on vehicle collision (Fig. 3),

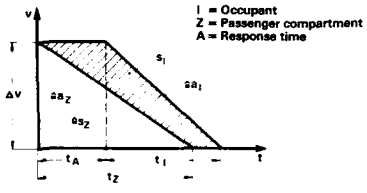

Fig. 3:
Speed/time graph for a head-on vehicle collision

- Distance occupants are thrown forwards as a function of occupant acceleration (Fig. 4) and

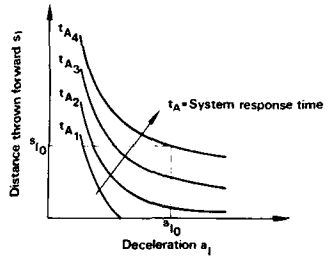

Fig. 4:
Distance occupants are thrown forwards as a function of occupant acceleration

- Occupant acceleration as a function of system response time (Fig. 5)

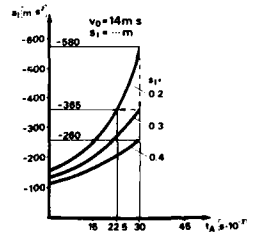

$t_A = f(s_L)$

t_A s·10⁻³	s_L cm
0	0
5	0.31
10	1.25
15	2.81
20	5
26	7.81
30	11.25
38	15.31
40	20
45	25.31

Fig. 5:
Occupant acceleration as a function of system response times

leads to the definition of the basic demands to be made of an occupant restraint system:

- Occupant restraint system should come into action quickly following start of vehicle deceleration *with a view to minimizing occupant acceleration with the same throw-forward distance, i.e. the* system response time t_A should be as short as possible.
- Only slight occupant deceleration a_I, i.e. biomechanically tolerable limits must not be exceeded due to the mechanical load.
- With a view to achieving the highest possible usage quota, the system must afford adequate comfort when not in action.

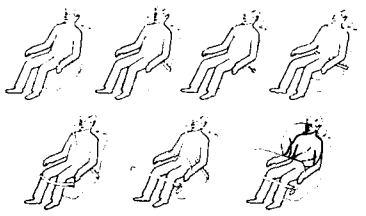

Fig. 6:
Occupant restraint system

Use can be made, for example, of belt force limiters to reduce the forces acting on the occupant during the restraint process. Some force limiter designs are shown in Fig. 7.

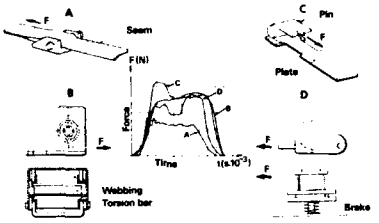

Fig. 7
Belt force limiter

A belt lock-up (Fig. 8) or belt pre-tensioners (Figs. 9, 10, 11) can be used to limit to occupant throw-forward distance.

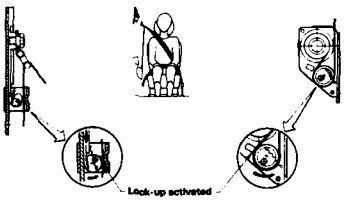

Fig. 8:
Belt lock-up

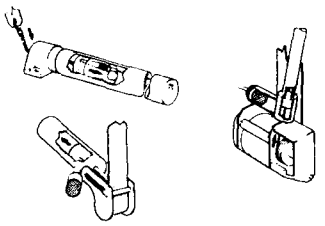

Fig. 9
Belt pre-tensioner (Pyrotechnic actuation)

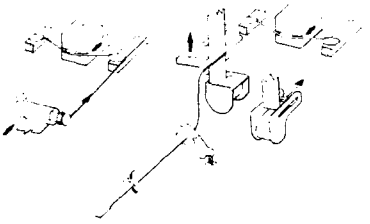

Fig. 10:
Belt pre-tensioner (Mechanical actuation)

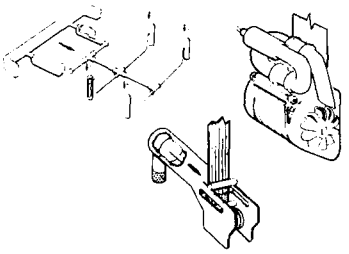

Fig. 11:
Belt pre-tensioner (Hydraulic actuation)

Numerous measures have to be taken to make a restraint system comfortable. Belt height adjustment, for example, makes for individual adaptation of the belt position (Fig. 12).

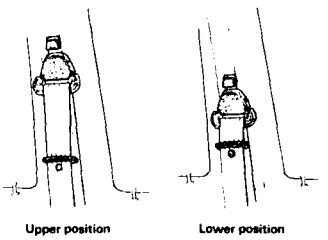

Fig. 12:
Belt height adjustment

An important safety feature - which is often underestimated in terms of its contribution to safety - is the seat plus head restraint (Fig. 13). The seat has a considerable influence on the effectiveness of the entire system both in the event of a head-on collision and in the case of a rear end collision. Fig. 14 shows, for example, occupant movement during a rear end collision. The effectiveness of a head restraint is clearly apparent.

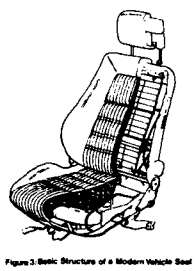

Figure 3: Basic Structure of a Modern Vehicle Seat

Fig. 13:
Structure of a car seat

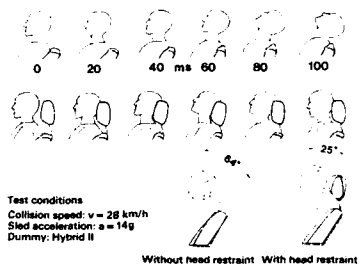

Fig. 14:
Head movement during rear end collision

The effectiveness of occupant protection systems is assessed on the basic of compliance with protection criteria (Fig. 15).

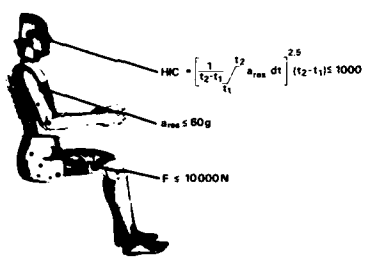

Fig. 15:
Protection criteria

Compliance with such protection criteria is substantiated by way of measurements taken with dummies during a vehicle collision. The correlation of these protection criteria with the real risk of injury is however unclear at present. as a bridge between medicine and vehicle technology, biomechanics helps to fill this gap (Fig. 16).

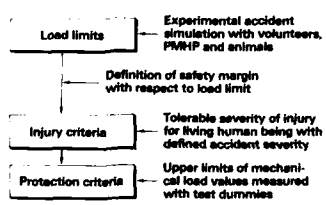

Fig. 16:
Aims of biomechanics

If it is assumed that there is good correlation between the load values measured with dummies and the real risk of injury for a person involved in an accident, the possible benefit of any safety measure can be forecast (Fig. 17).

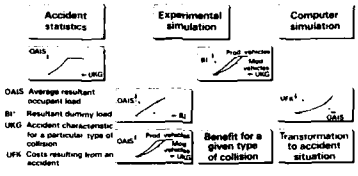

Fig. 17:
Determination of benefit

This is a necessary prerequisite for cost/benefit analyses.

Some 50 % of the people who die each year in the Federal Republic of Germany as a result of the injuries they have sustained are "external road users", i. e. motor cyclists and pedestrians (Fig. 18).

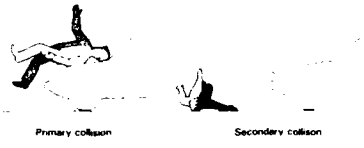

Fig. 18
Vehicle/Pedestrian collison

The efforts to improve passive safety must also include this group of road users.

It is to be hoped that the number of people who sustain serious injuries or even lose their lives as result of a traffic accident will continue to drop in the future. This goal will be attained if all those involved - namely vehicle manufacturers, road users and legislators - sustain their efforts to increase road traffic safety.

MADYMO CRASH VICTIM SIMULATIONS: A FLIGHT SAFETY APPLICATION

by
J. Wismans and J.A. Griffioen
TNO Road-Vehicles Research Institute
P.O. Box 237
2600 AE Delft
The Netherlands

SUMMARY

MADYMO is a computer program for two- or three-dimensional simulation of human body gross motions. The program has been developed particularly for crash analyses. In the past years the program has been applied and validated extensively for vehicle safety research. In this paper an application is described in the field of flight safety: the simulation of a space shuttle crew escape system.

INTRODUCTION

In the field of flight safety research the simulation of human body response and injuries resulting from abrupt acceleration changes and impacts is of vital importance to evaluate and improve restraint systems, crash safety devices and emergency escape systems. Most of this work is done by means of experiments using instrumented dummies, human cadavers and occasionally also animals and volunteers. Due to the rapid developments both in computer hardware and software it is expected that whole-body response computer models will be applied more and more in this field.

Examples of whole-body response programs used for aircraft safety problems are the Articulated Total Body (ATB) model [1] and the Seat-Occupant-Light-Aircraft (SOM-LA) model [2]. Both models are three-dimensional. The SOM-LA model has a fixed number of segments: 12, while in the ATB model an arbitrary number of segments can be specified. The ATB model is based on the CAL 3D crash victim simulation model. Several modifications were introduced, e.g. the capability to apply aerodynamic forces to the human body. The SOM-LA model was developed particularly for light aircraft crashworthiness design studies. The seat in this model is represented by a finite element model. A third program used for study of flight safety problems is the UCIN model. This program was applied e.g. to study parachutist dynamics [3].

The objective of this paper is two-fold: to summarize briefly the most important characteristics of the MADYMO Crash Victim Simulation Program and to illustrate the use of MADYMO in a flight safety environment by means of a recent simulation which was conducted by the TNO Road-Vehicles Research Institute. In addition some examples of applications of MADYMO in vehicle safety research will be addressed briefly.

MADYMO: GENERAL INTRODUCTION

The development of the MADYMO program package started in the mid seventies. The program performs time history simulations for systems of rigid bodies connected by joints in either two-or three-dimensional inertial space. Each of these bodies may be in force-interaction with any of the other bodies or with the environment. The program is based on rigid body dynamics using Lagrange equations. Fig. 1 shows examples of systems of rigid bodies with various types of force interaction. The systems of rigid bodies in MADYMO are so-called tree structures, also often referred to as open loop systems.

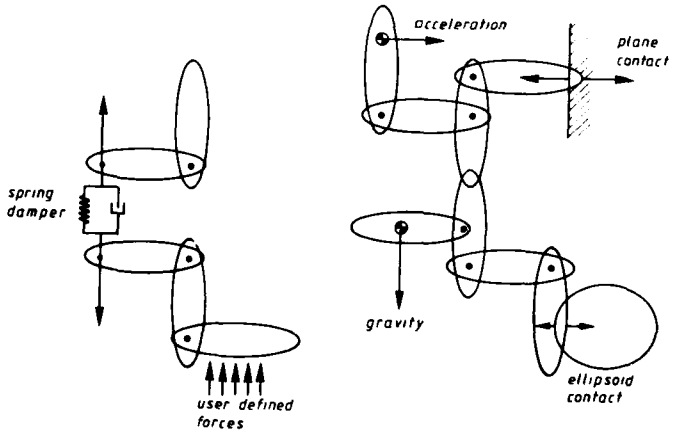

Fig. 1 Examples of tree structures with force interactions.

Standard calculation modules are available in MADYMO for the following force-interactions: geometric contacts, belt restraint systems, spring-dampers, gravitation and acceleration fields, etc. For special force-interactions like e.g. wind-blast the user can develop a user-defined module which can be linked to the general program. To create a MADYMO input dataset the user defines simply the number of systems and bodies in each system, the geometry, the centre of gravity, mass and rotational inertia for each body, properties of the joints, properties of force-interactions and the initial conditions of the systems. He can also specify which output results are required from the simulation.

The program performs the simulation by automatically generating and solving the set of non-linear equations of motion and predicting the condition of the system for one time step further. This process is repeated until the end time of the simulation is reached. Two methods are available in MADYMO to solve the equations of motion. The first method is a fourth-order Runge-Kutta method with a fixed time step and the second a fifth-order Runge-Kutta Merson method with variable time step.

A description of the theoretical background and the features of the current MADYMO version (i.e. version 4.2 to be released in 1988) is provided in refs. [4, 5]. For a general treatment of rigid body dynamics theory refer to Wittenburg [6]. In the next section a brief summary of the most important MADYMO features will be presented followed by some typical examples of applications of the program in vehicle safety research.

SUMMARY OF MOST IMPORTANT MADYMO CAPABILITIES

- MADYMO consists of two separate programs: MADYMO 2D and MADYMO 3D for two- and three-dimensional simulations respectively. Both programs offer broadly similar features. MADYMO 2D allows a more economical solution in case of planar motions.
- The standard program dimensioning allows up to 30 tree structures and 60 rigid bodies to be simulated.
- The rigid bodies are connected by hinge joints (2D) or ball and socket joints (3D).
- Prescription of acceleration fields and spatial motions as functions of time.
- Non-linear spring-damper elements and point-restraints.
- Up to 10 belt restraint systems with several belt segments can be defined. Slip, slack and pretension can be specified for each belt segment. Belt material can be characterized by means of non-linear force-elongation functions and hysteresis. To each of the belt systems a retractor with film spool effect can be connected (time, acceleration- or webbing sensitive).
- For contact interactions, planes, ellipses (2D) and ellipsoids (3D) can be connected to the rigid bodies and the environment. Higher order ellipses (2D) or ellipsoids (3D) can be used for edge contact problems. Prescription of contact surface motion is possible, e.g. to simulate intrusion.
- Non-linear elastic properties, viscous damping, hysteresis and dry friction can be specified for the joint and contact models.
- Specification of spatial orientations by means of direction cosine matrices, rotation angles or screw axes (3D).
- Separate principal moments of inertia and joint coordinate systems (3D) can be introduced.
- Simple input data structure by means of keyword identifiers.
- User-controlled generation of output quantities such as:
  - acceleration and velocity time histories
  - forces and torques
  - (relative) displacements
  - injury parameters.
- Peak values of the time histories are produced in tabular form offering the user a quick and efficient overview of the simulation results.
- A graphics program is available which produces three-dimensional projections of planes and ellipsoids with the option of hidden lines, contour lines, viewpoint selection, etc.
- Animation of simulation results is possible with special graphical devices.

EXAMPLES OF APPLICATIONS IN AUTOMOTIVE SAFETY

Many studies conducted in the past have proven the validity of MADYMO results in the area of vehicle impact research. Fig. 2 summarizes two typical examples of a vehicle occupant in a crash. The first example concerns the simulation of the Hybrid III dummy in a frontal impact test. The Hybrid III dummy is generally considered to be the most advanced crash test dummy for frontal vehicle impacts available today. The MADYMO 3D database developed for this dummy consists of 15 segments. The model was based on measurements conducted by the Biodynamics & Bioengineering division of the Harry G. Armstrong Aerospace Med. Res. Lab., Wright Patterson Airforce Base in Ohio, USA. Results of model simulations have been compared with sled tests at three impact severity levels conducted by Ford Motor Co. [8]. Details of the dummy model database, the simulations and the validation efforts are given in ref. [9].

The second example is a simulation of a Part 572 dummy in a lateral collision. This simulation was a reconstruction of a real world accident between a Peugeot 405 (stationary) impacted on the side (impact angle 70°) by another Peugeot 405 at a velocity of approximately 75 km/h. For this accident several experimental reconstructions were conducted by the Lab. of Phys. and Biom. Peugeot S.A./Renault. The mathematical simulation was limited to the interaction between the occupant in the struck vehicle (a Part 572 dummy) and the inside structure of the vehicle. The displacement (intrusion) of the struck door was used as model input.

The example shown in Fig. 3 is a simulation of a cyclist impacted from the side by a vehicle front. The model presented is divided into three separate systems: one for the dummy (nine bodies), one for the bicycle (one body) and one for the vehicle (one body). For details on this simulation and the corresponding verification tests see ref. [10].

Other examples of the use of MADYMO in the past are for instance child-restraint system simulations, human body segment models for the neck and thorax, simulation of wheelchair occupants and several computer aided design studies. In ref. [11] some of these simulations are described in detail.

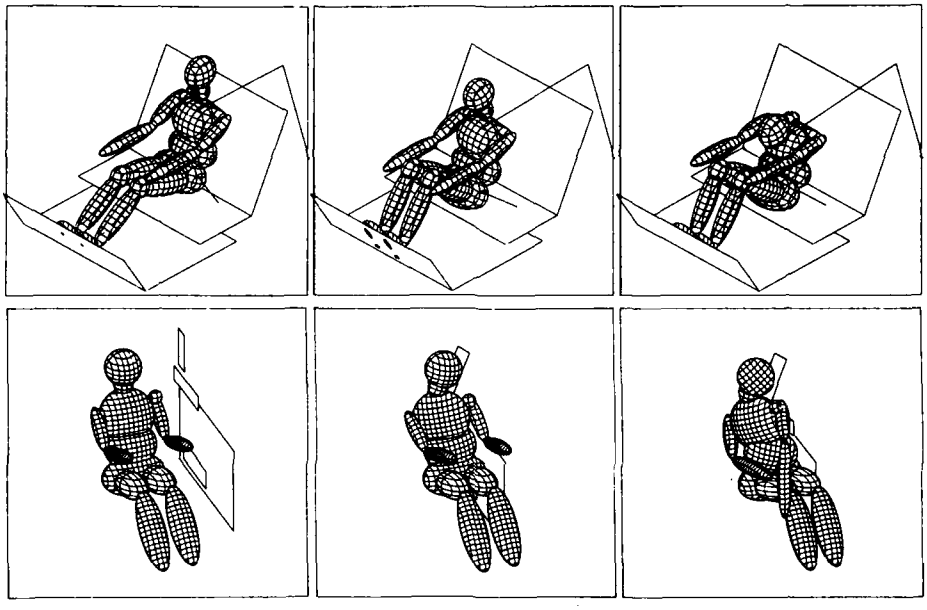

Fig. 2 Vehicle occupant simulations.

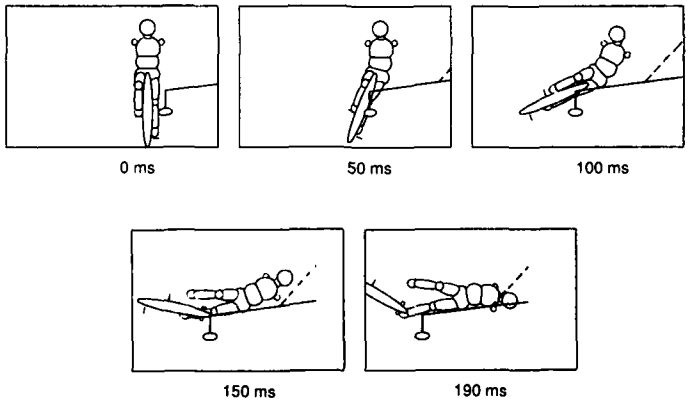

Fig. 3 Simulation of a cyclist impact.

A FLIGHT SAFETY APPLICATION

The simulation to be presented here was carried out to illustrate the potential of the MADYMO program for simulations of the human body in a flight environment. In contrast to many of the MADYMO applications in vehicle safety problems no experimental results were available at the time of our simulations (beginning of 1987) for proper model validation.

The simulation concerns the in-flight escape of a space shuttle crew member. One of the potential methods evaluated by NASA to obtain a safe escape from the space shuttle made use of a tractor rocket escape system. The astronaut is laying backwards on a horizontal ramp with his feet placed on a vertical foot plate. A small hatch at the side of the space shuttle is available for the escape. The crew member harness system is connected to the tractor rocket by means of an elastic rope further referred to as pendant line.

The MADYMO 3D program was used for this simulation. The crew member model is a 13 segment system representing a 50th percentile person. Anthropometry, mass distribution and joint properties are all based on the Part 572 Hybrid II dummy, i.e. a crash dummy developed especially for vehicle crash tests. Aerodynamical forces on the crew member are described by an acceleration field. The tractor rocket is simulated by one segment. The propulsion force on the rocket is estimated and prescribed in the input file. The pendant line is simulated by a spring element with estimated elastic and damping properties. The space shuttle is represented by a number of contact planes to study the contact interaction with the astronaut.

Fig. 4 illustrates the initial position of the crew member shortly before escape. The hatch opening of the space shuttle is indicated by a fine grid.

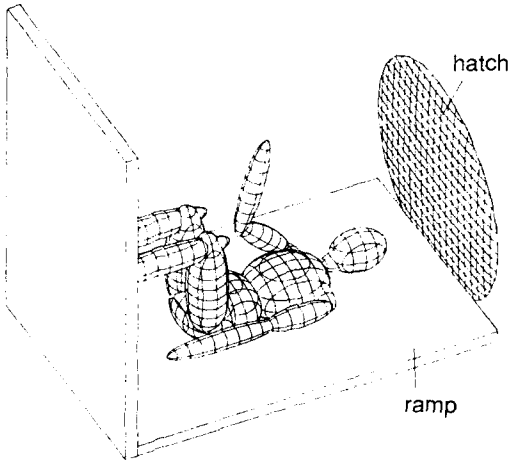

Fig. 4 Initial position of astronaut in simulation model.

After ejection of the tractor rocket the pendant line will become stretched and the crew member is pulled through the hatch opening. The MADYMO simulation presented here was conducted during 1.2 sec. Results of the predicted crew member kinematics are shown in Fig. 5.

Fig. 6 illustrates some of the resulting body accelerations as function of time. Results are presented for the chest, head and pelvis acceleration (time zero is ignition of tractor rocket). Peak accelerations appear to be near 13 g in this simulation.

DISCUSSION

The objective of this paper was to review briefly the present status of the MADYMO Crash Victim Simulation Program and to illustrate its use in a flight safety environment. The example presented concerned the ejection of a crew member from a space shuttle using a tractor rocket. Since significant parameters in this simulation like aerodynamic forces on the human body, rocket propulsion and pendant line material characteristics all were estimated, the present simulation does not need to be in agreement with experimental test results. The example is presented here for illustrative purposes only.

Results presented in this paper include kinematics and body accelerations. Other results like tension force in the pendant line, contact forces on the human body, injury parameters, angular accelerations and velocities are available for analysis too. A graphical terminal is used at the TNO Road-Vehicles Research Institute offering the kinematics to be visualized in real-time animation which contributes significantly to the interpretation of the model results.

Possible applications of the presented model (or an improved model with e.g. more realistic aerodynamic force-interactions and a more detailed human neck model) include:

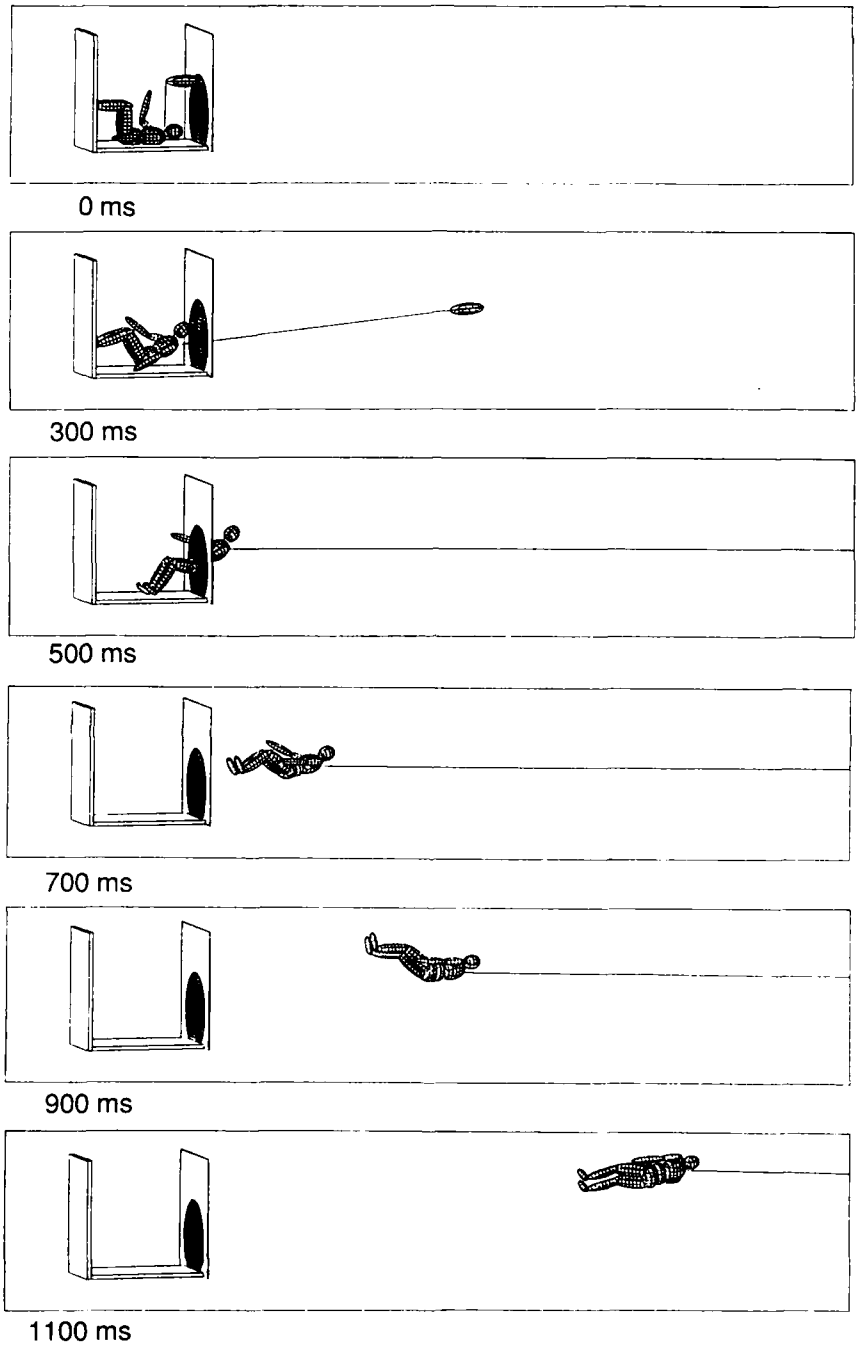

Fig. 5 Astronaut motion predicted by computer simulation.

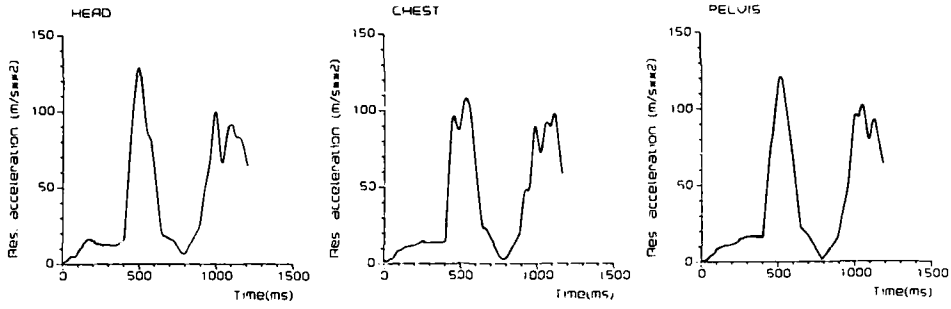

Fig. 6 Resultant acceleration time-histories of head, chest and pelvis.

- analysis of the effect of body size and initial position;
- optimal design of the tractor rocket and pendant line;
- analysis of the attachment between pendant line and crew member harness system;
- evaluation of the effect of ramp and pull angle;
- design of the hatch opening (padding!) to minimize the possible contact interaction with the astronaut;
- simulation (and validation) of laboratory tests and extension of experimental results to real conditions.

The presented example indicates that this type of mathematical simulation also could be applied successfully to study the human body response in other types of flight related impact problems or flight situations where the human body is exposed to sudden acceleration changes like e.g. helicopter crashes, ejection seat design or parachutist dynamics.

REFERENCES

1. Kaleps, I.: "Prediction of whole-body response to impact forces in flight environments", AGARD conference proceedings, No. 253, Paris, (1978).

2. Laananen, D.H.: "Mathematical simulation for crashworthy Aircraft Seat Design", J. Aircraft, Vol. 15, No. 9, Sept. (1978).

3. Huston, R.L. and Kamman, J.W.: "On parachutist dynamics", J. Biomechanics, Vol. 14, No. 9, 645-652 (1981).

4. Wismans, J., Griffioen, J.A. and J.J. Nieboer: "Use of MADYMO in general impact biomechanics", Symposium on Computational Methods in Bioengineering, ASME Winter Annual Meeting, Chicago, Ill., (1988) (In preparation).

5. "MADYMO User's Manual 3D", Version 4.2, TNO Road-Vehicles Research Institute (1988).

6. Wittenburg, J.: "Dynamics of systems of rigid bodies", B.G. Teubner, Stuttgart, (1977).

7. Kaleps, I.: "Hybrid III Geometrical and Inertial Properties", SAE 880638, SAE Int. Congress & Exposition, Detroit (1988).

8. Prasad, P.: "Sled Testing of Hybrid III", SAE 880637, 1988 SAE Int. Congress & Exposition, Detroit (1988).

9. Wismans, J. and Hermans, J.H.A.: "MADYMO 3D simulations of Hybrid III Dummy Sled Tests", SAE 880645, 1988 SAE Int. Congress & Exposition, Detroit (1988).

10. Janssen, E.G. and Wismans, J.: "Experimental and mathematical simulation of pedestrian-vehicle and cyclist-vehicle accidents", Proceedings of the 10th International Technical Conference on Experimental Safety Vehicles, Oxford (1985).

11. Wismans, J., Hoen, T. and Wittebrood, L.: "Status of the MADYMO Crash Victim Simulation Package 1985", Tenth Int. Conf. on Experimental Safety Vehicles, Oxford, England (1985).

ACKNOWLEDGEMENTS

The suggestion to carry out the space shuttle crew escape simulation and the necessary background information were given by dr. Bill Muzzy of the Naval Biodynamics Laboratory in New Orleans.

CONCEPTION D'UN ENREGISTREUR DE GRANDEURS DYNAMIQUES ET VALIDATION AU COURS D'UN CRASH SIMULE

par

CLERE J.M.* LE BRUN D.**, DOBUA J.**, POIRIER J.L.*

LABORATOIRE DE MEDECINE AEROSPATIALE* - SERVICE METHODES**
CENTRE D'ESSAIS EN VOL - F 91220 - BRETIGNY-sur-Orge

RESUME

La protection des équipages et des passagers au cours des crashs d'aéronefs est redevenue une question d'actualité. Les travaux de recherche, axés essentiellement sur l'interaction structure-siège-occupant, nécessitent actuellement l'utilisation des chaines de mesure avec des transferts d'information par câble ou télémétrie. Cette technique n'étant pas toujours utilisable, le Centre d'Essais en Vol a développé un enregistreur embarquable à déclenchement automatique à l'impact. Il permet l'enregistrement numérique pendant 6 secondes, de façon autonome, de 9 signaux analogiques. Il peut fonctionner en ambiance sévère, choc ou feu.

Il est un des éléments d'une chaîne de mesure comprenant un mannequin anthropomorphique, des accéléromètres, des amplificateurs-démodulateurs de mesure, des batteries, un interface mécanique.

Une expérimentation a été effectuée à Atlantic City aux U.S.A. lors du largage d'un tronçon de DC 10 d'une hauteur de 6 mètres à partir d'un portique.

Cet essai a permis de valider, en situation réelle de crash expérimental, cet enregistreur de nouvelle génération. Ce type d'appareil, d'un volume et d'un poids réduits, pourrait être utilisé comme enregistreur de crash sur les avions de ligne.

1. - INTRODUCTION

Au cours des accidents d'avions commerciaux, il est surprenant de constater dans certains cas, pour les occupants du même aéronef, des blessures légères pour les uns, gravissimes pour d'autres. Ainsi, dans le même avion, des passagers, par un concours de circonstances, peuvent sortir indemnes de l'accident, tandis que leurs voisins de cabine ou de siège y périssent. Le maximum d'informations concernant les circonstances et les effets du crash est nécessaire pour pouvoir mieux analyser la situation et protéger les différents occupants.

Seuls les hélicoptères militaires sont protégés. En effet, à la demande des différentes armées, les hélicoptères bénéficient d'une meilleure protection au crash due à une structure et des sièges adaptés à cette situation. En France, au C.E.A.T. et au C.E.V., les études ont été menées sur hélicoptères SA 330 et 340 ainsi que sur les sièges anticrash SOCEA.

En ce qui concerne les avions commerciaux, seuls les Etats-Unis se sont lancés dans une campagne d'expertise. La Federal Aviation Administration se penche depuis plusieurs années sur ce problème. Elle désire mieux protéger les passagers en imposant aux constructeurs des normes concernant la structure des avions et la structure des sièges. C'est pourquoi elle a entrepris d'évaluer il y a plusieurs années les causes et les circonstances des accidents de l'aviation civile, ainsi que leurs effets sur les structures d'avion, et de ce fait, sur la survie des passagers.

Pour compléter ces études, elle a entrepris d'effectuer une série d'essais en laboratoire sur segments d'avions de ligne largués d'un portique avec des conditions de crash différentes.

Le C.E.V. a pu participer à l'un de ces essais effectué à Atlantic City lors du largage d'un tronçon de DC 10 d'une hauteur de 6 mètres.

Les services officiels français ont été invités à partager cette expérience et à mettre en place un siège équipé d'un mannequin instrumenté. Cette participation ne devant pas interférer avec les mesures et l'autonomie du système américain, il a été demandé de prévoir un ensemble entièrement autonome. Cette chaîne de mesure possède un enregistreur spécifique non destructible par le choc et par le feu, à bande passante élevée et dont la durée d'enregistrement correspond à la durée d'un crash. En effet, après inventaire du matériel d'enregistrement, il n'a pas été trouvé d'enregistreur ayant cette performance.

En plus de cet enregistreur, cette chaîne de mesure comprend :

- un mannequin anthropomorphique ;
- neuf accéléromètres ;
- neuf amplificateurs démodulateurs ;
- un boîtier de protection contenant l'enregistreur numérique à mémoire statique;
- une alimentation électrique par batteries sur le siège ;
- un interface mécanique qui permet de fixer l'enregistreur et les batteries sur le siège ;
- un interface électrique (câble) qui permet d'interconnecter les batteries à l'enregistreur ainsi que les voies de mesure.

Cette chaîne de mesure est destinée à fonctionner aux niveaux d'accélérations susceptibles d'être observés lors de ce crash (inférieurs à 50 G).

Le siège sur lequel est installé le mannequin instrumenté et l'enregistreur est un siège SICMA.

2. - LE MANNEQUIN

L'utilisation d'un mannequin anthropomorphique permet d'effectuer des mesures standardisées et reproductibles, bien que différentes de celles qui peuvent être effectuées ou recueillies sur un corps humain. C'est pourquoi le "NATIONAL HIGHWAY TRAFFIC SAFETY ADMINISTRATION" a édité une norme de fabrication de mannequins anthropomorphiques. Il s'agit de la norme 49 CFR part 572.

Le mannequin ALDERSON HYBRID II correspond à cette norme. Il est composé d'un ensemble d'éléments correspondant à chaque partie du corps humain. Il a été utilisé au cours de cette expérimentation. Il a été conçu pour recevoir des capteurs d'accélération selon les trois axes, au niveau de la tête, du thorax et du bassin.

3. - LES ACCELEROMETRES

Les neuf accéléromètres utilisés sont des accéléromètres ENDEVCO du type 2262-200. Ces accéléromètres sont du type piézorésistif avec une étendue de mesure de plus ou moins 200 G. La tension électrique de sortie est proportionnelle à l'accélération. Cette tension est de 1,4 mV/g. Les normes données par le constructeur sont les suivantes : Leur fréquence de résonnance est de 3600 Hz. La linéarité de leur réponse est assurée à $\pm$ 5 pour cent lors d'un mouvement à 1100 Hz et une température de + 24°C. Il existe une petite dérive liée à la température. Elle est de deux pour cent à une température de 66°C. Le constructeur estime que ces accéléromètres ont une dérive compensée entre - 18°C et + 93°C. Ces capteurs possèdent de sérieuses propriétés de solidité puisqu'ils peuvent être soumis sans destruction à un choc sinusoïdal dont le pic d'accélération est de 2000 G. Enfin, ces accéléromètres ont fait l'objet d'un étalonnage au laboratoire de recherches balistiques et aérodynamiques de VERNON.

4. - LES AMPLIFICATEURS-DEMODULATEURS DE MESURE

Chaque accéléromètre est monté avec un amplificateur. Il s'agit d'amplificateurs de mesures type ABN 30 qui sont des amplificateurs différentiels à courant continu. Les caractéristiques constructeurs sont les suivantes : L'alimentation doit être assurée par une tension de 28 V. La consommation est de 35 mA. Leur gain est réglable de 10 à 100. La bande passante est de 0 à 3000 Hz. Leur linéarité de réponse est donnée à 1 pour mille. Ils sont montés sur une platine à 9 voies AJAX.

5. - ALIMENTATION

L'utilisation d'accumulateurs est rendue nécessaire par l'absence de possibilité de connection électrique avec l'alimentation de bord. Cet ensemble de deux batteries fabriquées par SAFT est spécifique de l'alimentation de télémesures ou de caméra. Ce sont les batteries SAFT SAS 632/80. Ce sont des batteries cadmium-nickel dont la capacité est de 1,6 Ah. Elles sont prévues pour fonctionner dans un environnement relativement sévère, puisque le constructeur a déterminé un domaine d'accélération de $\pm$ 250 m/s· et une température de + 60°C.

6. - DESCRIPTION DE L'ENREGISTREUR

A - INTRODUCTION

Le système développé par le Centre d'Essais en Vol permet de réaliser l'enregistrement de neuf paramètres analogiques sur une mémoire numérique.

Ce matériel est adapté à la mémorisation de phénomènes rapides et de type impulsionnel, lors d'essais en environnement dynamique sévère. Il peut être utilisé

pour toute installation d'essai en vol ou à bord de véhicules terrestres subissant des chocs mécaniques ou thermiques importants.

Cet enregistreur est destiné à conserver en mémoire, après l'essai de crash d'un avion, les niveaux d'accélération subis pendant le choc par un mannequin anthropomorphique. La durée de l'enregistrement correspond à 6 secondes environ.

Le top d'enregistrement est donné par un système de détection automatique. Le système de déclenchement de l'enregistrement est basé sur la détection de l'accélération en X et en Y (détecteur de seuil réglable).

Cet ensemble est entièrement autonome. L'alimentation est fournie par une batterie de 28 volts continu.

La durée de fonctionnement est de 6,5 s.

B - DESCRIPTION

1° Partie Externe

Le système d'acquisition est enfermé dans une enceinte de protection "Feu et Choc" du type A 9854. Cette enceinte a un volume cylindrique de 2,5 litres et pèse 21 kg. Elle est normalement destinée à recevoir l'enregistreur de sécurité (A 20) qui équipe certains aéronefs du C.E.V.

Cette enceinte se présente sous la forme d'un cyclindre muni de quatre pattes permettant sa fixation sur un support plan. L'ouverture se fait sur l'une des bases par un couvercle équipé d'une poignée et de quatre goupilles de verrouillage. Ce couvercle dispose en outre sur sa face externe d'une embase électrique de type 51 à 19 broches mâles (réf. 85102 E 19 P) assurant la liaison du système avec l'alimentation et avec la platine de conditionnement et d'adaptation des capteurs.

2° Partie Interne

La partie électronique, située à l'intérieur du boîtier sous une autre protection plus légère est fixée sous le couvercle. Elle se compose de quatre modules électroniques et de trois modules mémoires.

La première carte comporte trois modules :

- La génération de l'alimentation est régulée à partir de 28 V. $\pm$ 3 volts en :

. + 15 V pour les amplificateurs opérationnels et la détection de début de crash.

. + 5 V pour la logique de commande et le système de conversion analogique-numérique et d'acquisition.

. + 10 V pour les amplificateurs de capteurs d'accélération.

- La logique de commande située, elle-aussi, sur cette carte, est du type T.T.L.

- Le système de détection du début de crash est basé sur quatre voies d'acquisition.

Les trois cartes d'acquisition sont identiques. Elles sont réalisées en circuit double face et possèdent chacune trois entrées analogiques.

Pour chaque voie sont réalisés :

- un adaptateur d'impédance et un système de décodage de tension d'entrée ;

- un correcteur de gain ;

- un filtre passe-bas de deuxième ordre codé à 750 Hz et de - 3 db d'atténuation.

Ensuite sur chaque carte sont réalisés :

- un multiplexeur à trois voies d'entrée ;

- un convertisseur analogique-numérique DAC 847 M.

A chaque carte d'acquisition est associé un module mémoire. Chaque module possède une capacité de 64 K octets. C'est une mémoire statique non volatile de type RAM CMOS ;

Un faisceau câblé assure les liaisons électriques intercartes et la liaison avec le connecteur d'entrée.

C - PRINCIPE DE FONCTIONNEMENT

Le principe est décrit à partir de l'application qui en est faite dans le cadre de l'essai crash. En fait, chacun des paramètres est représenté par une tension d'entrée.

1° - Principe d'enregistrement

Les mesures d'accélération sont faites au niveau du bassin, du thorax et de la tête, selon les trois axes, ce qui représente neuf paramètres.

Il est prévu d'avoir une étendue de mesure selon le type d'expérimentation. Dans notre cas il est de ± 50 G sur tous les axes.

La résolution est de 0,2 g sur les axes X, Y et Z.

Le gain de la chaîne est de 100 mV/g. Le signal est conditionné, multiplexé, converti en valeur numérique puis mémorisé. La chronologie des enregistrements est assurée par une horloge à quartz 10 MHz.

Le codage est réalisé sur 8 bits et la fréquence d'échantillonnage du signal est de 3300 points par seconde sur chaque voie.

Sur chaque mémoire sont gardés les résultats des mesures faites sur les trois axes d'une zône du mannequin.

Ainsi chaque carte d'acquisition associée à un bloc mémoire constitue un module d'entrée. Les trois modules ont un fonctionnement identique et sont indépendants les uns des autres.

Dès la mise sous tension, le module acquiert cycliquement les données présentes sur chacune des trois entrées et les enregistre dans une boucle d'attente occupant les 4096 premiers mots du bloc mémoire.

Cette boucle correspond à un enregistrement du phénomène d'une durée d'environ 0,4 seconde avant le déclenchement. Chaque paramètre est échantillonné toutes les 0,3 ms.

A la détection du seuil à l'adresse 4096 sont stockés :

4 bits d'adresse mémoire de crash ;

2 bits d'adresse de paramètres ;

2 bits d'identification de mémoire (permettant de connaître l'origine des paramètres enregistrés et de recaler les bits d'adresse mémoire).

L'acquisition précise des bits s'effectue en dehors de la prise des paramètres, ceci afin de ne pas éliminer l'acquisition d'un paramètre.

L'enregistrement se poursuit ensuite à la même cadence à partir de la mémoire 4097 jusqu'au remplissage de la mémoire.

Les modules doivent ensuite être déposés et lus sur un lecteur approprié piloté par un micro ordinateur disposant d'une mémoire de capacité suffisante.

2° - Principe de déclenchement de l'enregistrement

Le code de déclenchement est assuré, soit par une impulsion fournie, soit par un système automatique de détection de seuil.

Deux conditions doivent être réalisées simultanément au niveau des capteurs installés, soit au bassin, soit au thorax.

3 g sur l'axe Z pendant 5 ms.

1 g sur l'axe X pendant 5 ms.

D - EXPLOITATION DES RESULTATS

Les mémoires sont, soit traitées directement par un micro ordinateur HEWLET PACKARD, soit enregistrées sur bandes magnétiques en code PCM qui peuvent alors être exploitées par le Service SM/4 du Centre d'Essais en Vol.

7. - ***DESCRIPTION DU SIEGE***

Le siège expérimenté de la marque SICMA équipe les avions AIRBUS. C'est un siège biplace dont le système de fixation à l'avion est adapté au rail de fixation du DC 10. Ce siège, large de 1,006 m, comporte deux poches de 0,430 m ayant un dosseret en coussin et une assise avec un coussin fixé par deux VELCRO longitudinaux sur une plaque métallique. Cette plaque est ajourée par des trous de deux centimètres environ. Sur ce siège sont installés le mannequin anthropomorphique à une place et l'enregistreur et les batteries à une autre. Ce dernier ensemble est fixé par un interface mécanique.

8. - **INTERFACE MECANIQUE**

Elle a été adaptée pour être fixée sur n'importe quel siège. Cette fixation s'effectue, après suppression du coussin, par l'intermédiaire de deux paires de colliers boulonnés sur la plaque. Chacune d'elles enserre les poutres maîtresses du siège, à l'avant et à l'arrière. Ce montage s'effectue sans modification du siège puisque les boulons se glissent dans les trous de la plaque métallique qui supporte le coussin. Ainsi, la fixation du système n'est pas spécifique d'une place et ne nécessite aucun démontage du siège.

9 - **RESULTATS DE L'EXPERIMENTATION**

La chute du tronçon de DC 10 s'est effectuée verticalement sans aucune composante en roulis ou en tangage. Ces résultats concernent les accélérations mesurées au niveau du mannequin.

Nous avons trouvé des variations d'accélération sur l'axe Z mais aussi sur les axes X et Y.

- Axe Z :

D'une manière générale on observe un pic d'accélération de durée limitée suivi d'une accélération plus faible d'une durée beaucoup plus longue.

Après une phase ondulatoire, on note 550 ms après l'impact une nouvelle variation d'accélération positive qui dure 100 ms.

Au niveau du bassin, le premier pic d'accélération se situe aux environs de 30 g, au niveau du thorax autour de 36 g et au niveau de la tête le pic dépasse 40 g.

A la différence du bassin où une accélération négative autour de 4 g seulement est observée, au niveau du thorax et de la tête le pic négatif se situe respectivement à 15 g et 20 g avec un décalage dans le temps de 50 ms.

La deuxième phase d'accélération située 550 ms après l'impact est caractérisée par un niveau plus homogène d'accélération 10 g au niveau du bassin et de la tête et 18 g au niveau du thorax.

- Axe X :

Les variations d'accélération sur cet axe sont plus polymorphes. D'une manière générale les pics d'accélération sont d'abord négatifs, puis positifs, pour ensuite se stabiliser pendant une durée de 400 ms et subir une petite variation 550 ms après l'impact.

Au niveau du bassin on observe un pic d'accélération à - 10 g suivi d'un pic à 10 g.

Au niveau du thorax l'accélération négative dure 20 ms et ne dépasse pas 5 g, l'accélération positive dure 80 ms et atteint 7 g.

Au niveau de la tête, l'accélération négative est importante en temps (100 ms) et en niveau (- 14 g) puis devient positive pour atteindre 20 g.

- Axe Y :

On rencontre sur cet axe des variations d'accélération plus ou moins importantes selon la partie du mannequin considérée.

Au niveau du bassin, l'accélération est du type sinusoïdal avec un pic négatif dépassant 20 g puis un pic positif dépassant 15 g suivi d'un amortissement.

Au niveau du thorax, l'accélération est positive avec un pic à 10 g, puis s'amortit.

Au niveau de la tête, l'accélération est positive, puis négative, mais la période est plus grande et la valeur maximale atteinte est plus faible.

10. - DISCUSSION

Cet essai d'impact, du fait des contraintes expérimentales, ne nous a pas permis de mesurer le niveau d'accélération rencontré sur le plancher, ce qui enlève une précieuse information concernant l'importance de la fonction de transfert du siège. Par conséquent on ne connait pas son facteur d'amortissement. Par ailleurs l'enregistreur a été fixé sur le bâti de l'ensemble du siège. Il risque de transformer dans une certaine mesure sa rigidité et donc de modifier sa fonction de transfert. Les niveaux d'accélération observés au cours de cette expérimentation ne sont peut-être pas ceux qui auraient pu être observés dans une situation expérimentale "plus proche de la réalité".

Les mesures effectuées montrent qu'il y a un transfert d'énergie de l'axe vertical vers les deux autres axes, en particulier l'axe X. Il y a donc eu une modification d'axe dont on peut imputer l'origine non seulement à la structure du tronçon mais aussi au dispositif de réception de crash et surtout au mannequin. Le largage d'un tronçon d'avion à partir d'un portique ne représente pas en effet un crash réel. D'autre part, la position des passagers en cas de crash n'est pas celle du mannequin dans cet essai. Donc nos mesures d'accélération sont assez théoriques.

L'intensité et la durée des accélérations observées selon l'axe Z font penser qu'il y aurait peut-être des fractures osseuses en particulier au niveau du rachis. Si éventuellement il n'y avait pas rupture à la première variation d'accélération, on peut penser qu'une onde de choc entrant en résonance avec la structure du rachis produira ponctuellement des niveaux d'accélérations plus élevés (QUANDIEU 1982) (4).

Les niveaux d'accélération sont sûrement plus intenses que ceux que nous aurions observés dans une situation expérimentale comportant un être humain à part entière (GRAGG 1984) (3).

En ce qui concerne l'axe X, les variations d'accélération sont relativement faibles au niveau du thorax, plus élevées au niveau de la tête. Ceci s'explique par le mouvement de bascule qu'a pu avoir le mannequin au moment de l'impact étant donnée sa position dans le siège. Il apparaît toutefois que les accélérations selon l'axe X sont tolérées à des niveaux plus élevés et donc les risques de fractures osseuses sont faibles malgré les niveaux atteints. En aucun cas on ne peut penser qu'il y ait rupture des viscères.

Les variations d'accélération observées selon l'axe Y et auxquelles on ne s'attendait guère, peuvent avoir deux origines : un balancement du tronçon d'avion lors de l'impact, une différence de rigidité de l'ensemble du siège entre la place droite et la place gauche induite par le support de l'enregistreur.

Cet enregistreur représente un ensemble cohérent et homogène faisant appel à une technologie moderne. Il a non seulement la caractéristique d'être embarquable à bord d'un avion, mais aussi de pouvoir être installé après quelques modifications pour la mesure d'accélérations produites lors des essais d'éjection de siège. De plus, les données d'entrée étant analogiques, il peut être utilisé dans d'autres conditions nécessitant l'acquisition rapide de neuf paramètres. Ces autres conditions sont entre autres celles des études de décompression explosive, telles que nous les rencontrons à bord des avions de combat de haute performance.

Deux enregistreurs similaires ont été décrits par FRISCH G.D. et P.H. (1984) et WHITE et coll. (1984) (1-2-5). Chacun de ces enregistreurs a ses qualités propres. En ce qui concerne celui que nous présentons, il a l'avantage d'être entièrement autonome et à déclenchement automatique. Cela pourrait lui permettre d'être utilisé comme moyen d'enregistrement de phénomènes brefs et aléatoires.

11. - CONCLUSION

Une chaîne de mesure destinée à évaluer les effets des accélérations créés par un crash d'avion a été réalisée. Elle a permis le développement d'un enregistreur de 9 paramètres analogiques sur mémoire numérique statique. Cette chaîne de mesure a pu être testée et validée lors du largage d'un tronçon d'avion.

Elle pourra être utilisée pour obtenir une banque de données sur le comportement des avions et des sièges au crash, vérifiant l'efficacité des sièges normaux, des sièges expérimentaux et des systèmes de retenue existants ou améliorés.

BIBLIOGRAPHIE

1. - FRISCH G.D., FRISCH P.H. - The development of a dynamic response sensing recording system for incorporation into a state-of-the art manikin.
SAFE J. 1984, 14 (1) : 13-19.

2. - FRISCH G.D., WHITLEY Ph.E., FRISCH P.H. - Structural integrity tests of a modified Hybrid III manikin and supporting instrumentation system.
SAFE J. 1985, 15 (2) : 20-29.

3. - GRAGG C.D. - Could anthropometric dummy data be used to predict injury to humans.
SAFE Proceedings, 22nd Annual Symposium, Las Vagas, 1984 : 320-329.

4. - QUANDIEU P., PELLIEUX L., GARNIER B., BORREDON P. - Etude en régime impulsionnel et "in vivo" de la transmissibilité des disques intervertébraux lombaires d'un primate.
AGARD 1982, CP 322 (6) (1-21).

5. - WHITE R.P., WATTERS D.M., SSMIR. - A new approach to acquiring data during an aircraft seat/sled ejection sequence.
SAFE Proceedings, 22nd Annual Symposium. Las Vegas, 1984 : 320-329.

REPORT DOCUMENTATION PAGE

1. Recipient's Reference	2. Originator's Reference	3. Further Reference	4. Security Classification of Document
	AGARD-CP-443	ISBN 92-835-0485-2	UNCLASSIFIED

5. Originator	Advisory Group for Aerospace Research and Development North Atlantic Treaty Organization 7 rue Ancelle, 92200 Neuilly sur Seine, France
6. Title	ENERGY ABSORPTION OF AIRCRAFT STRUCTURES AS AN ASPECT OF CRASHWORTHINESS
7. Presented at	the 66th Meeting of the Structures and Materials Panel of AGARD held in Luxembourg, 1—6 May 1988.

8. Author(s)/Editor(s)	9. Date
Various	December 1988
10. Author's/Editor's Address	**11. Pages**
Various	334

12. Distribution Statement This document is distributed in accordance with AGARD policies and regulations, which are outlined on the Outside Back Covers of all AGARD publications.

13. Keywords/Descriptors

Aviation accidents	Survival
Safety engineering	Airframes
Impact strength	Energy absorption

14. Abstract

Considerable effort has hitherto been devoted to crash avoidance, but relatively little to crash survivability. In certain regimes the risk of accident remains high in some of these, e.g. the low-altitude low-speed regime. There is a strong incentive to increase the prospects for occupant survival through improvements in airframe design. Information about structural behaviour and characteristics under these conditions is very sparse and an exchange of information between the NATO nations is long overdue.

At its sixty-sixth meeting, the Structures and Materials Panel held a conference of Specialists, the aim of which was to stimulate an exchange of experience and development results. A further aim was to act as a focus for the discussion of those novel design philosophies which may be needed to provide the balance between survivability and function. This document contains the papers presented at that Meeting.

AGARD Conference Proceedings No.443
Advisory Group for Aerospace Research and Development, NATO
ENERGY ABSORPTION OF AIRCRAFT STRUCTURES AS AN ASPECT OF CRASHWORTHINESS
Published December 1988
334 pages

Considerable effort has hitherto been devoted to crash avoidance, but relatively little to crash survivability. In certain regimes the risk of accident remains high in some of these, e.g. the low-altitude low-speed regime. There is a strong incentive to increase the prospects for occupant survival through improvements in airframe design. Information about structural behaviour and characteristics under these conditions is very sparse and an

P.T.O

AGARD-CP-443

Aviation accidents
Safety engineering
Impact strength
Survival
Airframes
Energy absorption

AGARD Conference Proceedings No.443
Advisory Group for Aerospace Research and Development, NATO
ENERGY ABSORPTION OF AIRCRAFT STRUCTURES AS AN ASPECT OF CRASHWORTHINESS
Published December 1988
334 pages

Considerable effort has hitherto been devoted to crash avoidance, but relatively little to crash survivability. In certain regimes the risk of accident remains high in some of these, e.g. the low-altitude low-speed regime. There is a strong incentive to increase the prospects for occupant survival through improvements in airframe design. Information about structural behaviour and characteristics under these conditions is very sparse and an

P.T.O

AGARD-CP-443

Aviation accidents
Safety engineering
Impact strength
Survival
Airframes
Energy absorption

AGARD Conference Proceedings No.443
Advisory Group for Aerospace Research and Development, NATO
ENERGY ABSORPTION OF AIRCRAFT STRUCTURES AS AN ASPECT OF CRASHWORTHINESS
Published December 1988
334 pages

Considerable effort has hitherto been devoted to crash avoidance, but relatively little to crash survivability. In certain regimes the risk of accident remains high in some of these, e.g. the low-altitude low-speed regime. There is a strong incentive to increase the prospects for occupant survival through improvements in airframe design. Information about structural behaviour and characteristics under these conditions is very sparse and an

P.T.O

AGARD-CP-443

Aviation accidents
Safety engineering
Impact strength
Survival
Airframes
Energy absorption

AGARD Conference Proceedings No.443
Advisory Group for Aerospace Research and Development, NATO
ENERGY ABSORPTION OF AIRCRAFT STRUCTURES AS AN ASPECT OF CRASHWORTHINESS
Published December 1988
334 pages

Considerable effort has hitherto been devoted to crash avoidance, but relatively little to crash survivability. In certain regimes the risk of accident remains high in some of these, e.g. the low-altitude low-speed regime. There is a strong incentive to increase the prospects for occupant survival through improvements in airframe design. Information about structural behaviour and characteristics under these conditions is very sparse and an

P.T.O

AGARD-CP-443

Aviation accidents
Safety engineering
Impact strength
Survival
Airframes
Energy absorption

exchange of information between the NATO nations is long overdue.

At its sixty-sixth meeting, the Structures and Materials Panel held a conference of Specialists, the aim of which was to stimulate an exchange of experience and development results. A further aim was to act as a focus for the discussion of those novel design philosophies which may be needed to provide the balance between survivability and function. This document contains the papers presented at that Meeting.

Papers presented at the 66th Meeting of the Structures and Materials Panel of AGARD held in Luxembourg, 1—6 May 1988.

ISBN 92-835-0485-2

exchange of information between the NATO nations is long overdue.

At its sixty-sixth meeting, the Structures and Materials Panel held a conference of Specialists, the aim of which was to stimulate an exchange of experience and development results. A further aim was to act as a focus for the discussion of those novel design philosophies which may be needed to provide the balance between survivability and function. This document contains the papers presented at that Meeting.

Papers presented at the 66th Meeting of the Structures and Materials Panel of AGARD held in Luxembourg, 1—6 May 1988.

ISBN 92-835-0485-2

exchange of information between the NATO nations is long overdue.

At its sixty-sixth meeting, the Structures and Materials Panel held a conference of Specialists, the aim of which was to stimulate an exchange of experience and development results. A further aim was to act as a focus for the discussion of those novel design philosophies which may be needed to provide the balance between survivability and function. This document contains the papers presented at that Meeting.

Papers presented at the 66th Meeting of the Structures and Materials Panel of AGARD held in Luxembourg, 1—6 May 1988.

ISBN 92-835-0485-2

exchange of information between the NATO nations is long overdue.

At its sixty-sixth meeting, the Structures and Materials Panel held a conference of Specialists, the aim of which was to stimulate an exchange of experience and development results. A further aim was to act as a focus for the discussion of those novel design philosophies which may be needed to provide the balance between survivability and function. This document contains the papers presented at that Meeting.

Papers presented at the 66th Meeting of the Structures and Materials Panel of AGARD held in Luxembourg, 1—6 May 1988.

ISBN 92-835-0485-2